STUDIES OF ATMOSPHERIC POLLUTANTS IN

URBAN DISTRICTS

by

DOUGLAS RAYMOND MIDDLETON, M. A. CANTAB.

A Thesis presented for the Degree of

Doctor of Philosophy

in

The University of Aston in Birmingham

August 1976

STUDIES OF ATMOSPHERIC POLLUTANTS IN

URBAN DISTRICTS

by

DOUGLAS RAYMOND MIDDLETON, M. A. CANTAB.

A Thesis presented for the Degree of

Doctor of Philosophy

in

The University of Aston in Birmingham

August 1976

SUMMARY

To study pollution near a motorway intersection, concentrations of oxides of nitrogen, carbon monoxide and total hydrocarbons were monitored, and calculated by a generally applicable programme. Road-side dilution was measured.

After calibration by flow and exponential dilution, unattended instruments recorded pollutant concentrations in analogue form. Zeroes and calibrations were measured during visits and automatically. Intersection traffic-flows, and simultaneous weather readings from a nearby airport, were obtained.

The data were stored and manipulated by computer - principles for processing environmental data are suggested. Data, identified by gas, observation type, site, time and date, were calibrated, zero corrected and averaged by an appropriate programme. Similarly, programmes calculated hourly traffic-flows from instantaneous readings of cumulative counters; hourly flows were interpolated from non-hourly counts, to minimise abstraction. For simple usage, input was flexible and accepted missing values; default options included an assumed zero or calibration.

Another programme calculated gaseous pollutant concentrations for any elevated, curved or straight roads from dilution of traffic-emissions. Ordnance Survey map references defined road geometries and axes were rotated downwind. Point-source plumes, from elements stepped along each road, were integrated.

Statistical comparison of calculated with measured concentrations showed a high correlation; the regression coefficients were not unity because of uncertain emissions estimates, errors of measurement and approximations of calculation.

Concentrations at a more distant site were noticeably lower than at the intersection.

A sampling technique was developed to measure concentrations at two separate locations simultaneously using a single analyser: dilution curves calculated by the programme for the motorway and the intersection were compatible with concentration gradients measured in the field.

Concentrations of pollutants at the intersection were related to the traffic-based model, but exact agreement between calculation and field measurement is still hard to achieve, because many variables are involved.

ACKNOWLEDGEMENTS

The work required many arrangements with organisations outside the University so that we could have monitoring sites and traffic-counts around the Motorway Intersection. I am particularly grateful to my Supervisor, Dr J D Butler, who in making these arrangements made all the rest possible.

The project was sponsored by the Transport and Road Research Laboratory of the Department of the Environment, and I would like to thank Mr D M Colwill from the Transport and Road Research Laboratory for his efforts to assist us: he made many visits to discuss the work.

I thank also the many officials representing the City of Birmingham, the Motorway Control Police, the Department of the Environment, and other Public Bodies, who contributed to the provision of facilities needed in the field.

Within the Chemistry Department, I was assisted by the technical staff, of whom Tony, Squadron Leader A S Aldridge, D.F.C., is especially thanked for much moral and physical support in the field. He would say, "Remember you're British!" when trouble struck.

To my friends, my thanks for their patience - Suru Patel, who whilst also working for the Degree always made time to listen or offer advice, and Phyllis and Christopher Gilford who in leading the

folk dance group gave me many friends, including Penny, my fiancee.

Finally I am grateful for the opportunity to work on a problem related to the common good, for, as the Poet suggests ...

"We dance
to a whispered voice
overheard by the soul
undertook by heart
and you may know it
if you may know it ..."

.... from .... " Be ",
by Neil Diamond (Stonebridge Music, 1973)
for the Sound Track (CBS 69047) of the film

" Jonathan Livingstone Seagull ",

a parable on perfection and life by
Richard Bach.

Published by Turnstone Press, 1972 and Pan Books, 1973.

To Mother,

thanks, and with love.

STUDIES OF ATMOSPHERIC POLLUTANTS IN URBAN DISTRICTS

CONTENTS

Page No

Page No

LIST OF FIGURES

Figure	Description	Page No

LIST OF TABLES

ABBREVIATIONS

M6) A38(M))	Major roads (see Figure 1.1)
NO	Nitric Oxide
NO_2	Nitrogen Dioxide
NO_x	($NO + NO_2$ in unknown proportions)
CO	Carbon Monoxide
HC	Total Hydrocarbons, measured as methane
12A	Analyser for Oxides of Nitrogen
MGA2	Analyser for Carbon Monoxide
AA521	Analyser for Total Hydrocarbons
ppm	parts per million by volume

CHAPTER 1

INTRODUCTION

1.1 The Problem

The object was to monitor gaseous pollutants around the Midland Links Motorway-Intersection and with this information assess the contribution such an intersection makes to the overall air pollution of the area. The emphasis was on measurement and interpretation of these pollutant levels: the work did not include medical aspects.

The intersection lies four kilometres from the city centre but well within the urban area (Map: Figure 1.1). An elevated and interlocking set of roads join a ground-level roundabout to the local roads, the M6 Motorway and the A38(M) or Aston Expressway (Map: Figure 1.2). The interconnections are flyover or underpass roads so that all turning movements are made without crossings. Elevated roads are largely mounted on pillars; the rest, on mounds. The intersection occupies thirteen hectares of land, and the highest viaduct is twenty four metres above the ground (Williams, 1974).

The observed levels of pollutants depend on many variables. The surrounding area contains sources: other roads at greater distances, chimneys of houses and factories, and Nechells Power Station. There

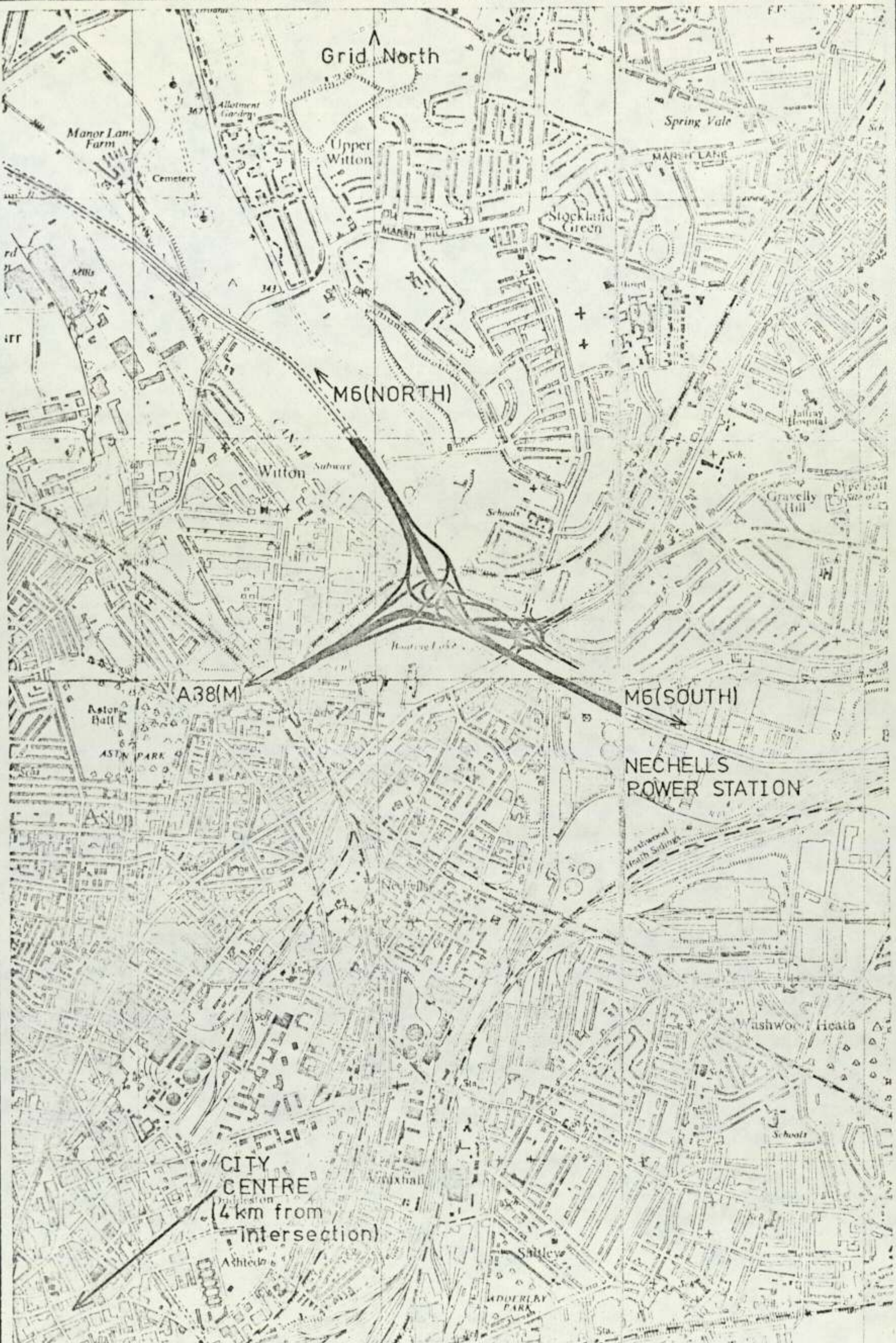

FIGURE 1.1 POSITION AND SURROUNDINGS OF THE MIDLAND LINKS MOTORWAY INTERSECTION (Based on Ordnance Survey)

0 1km

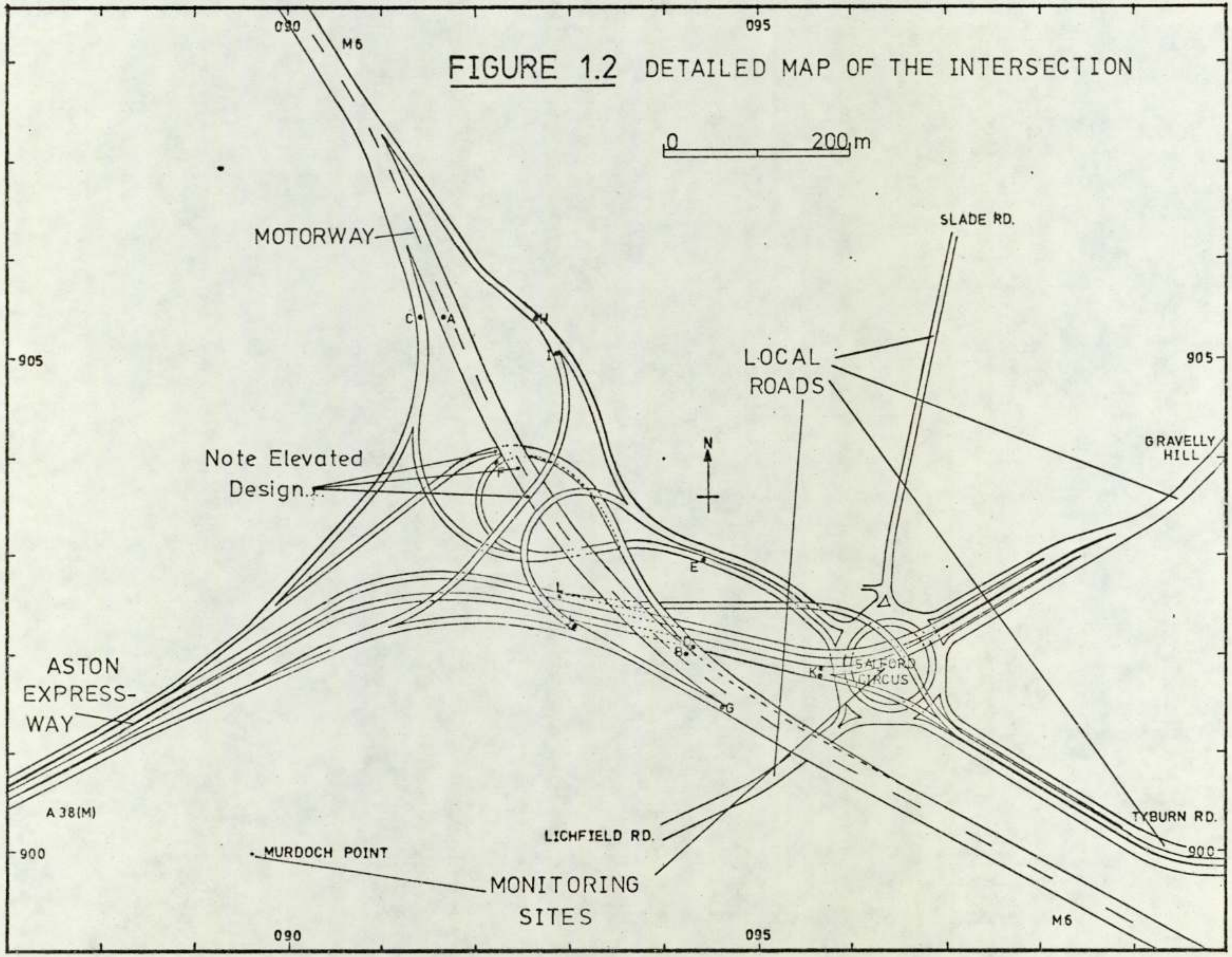

FIGURE 1.2 DETAILED MAP OF THE INTERSECTION

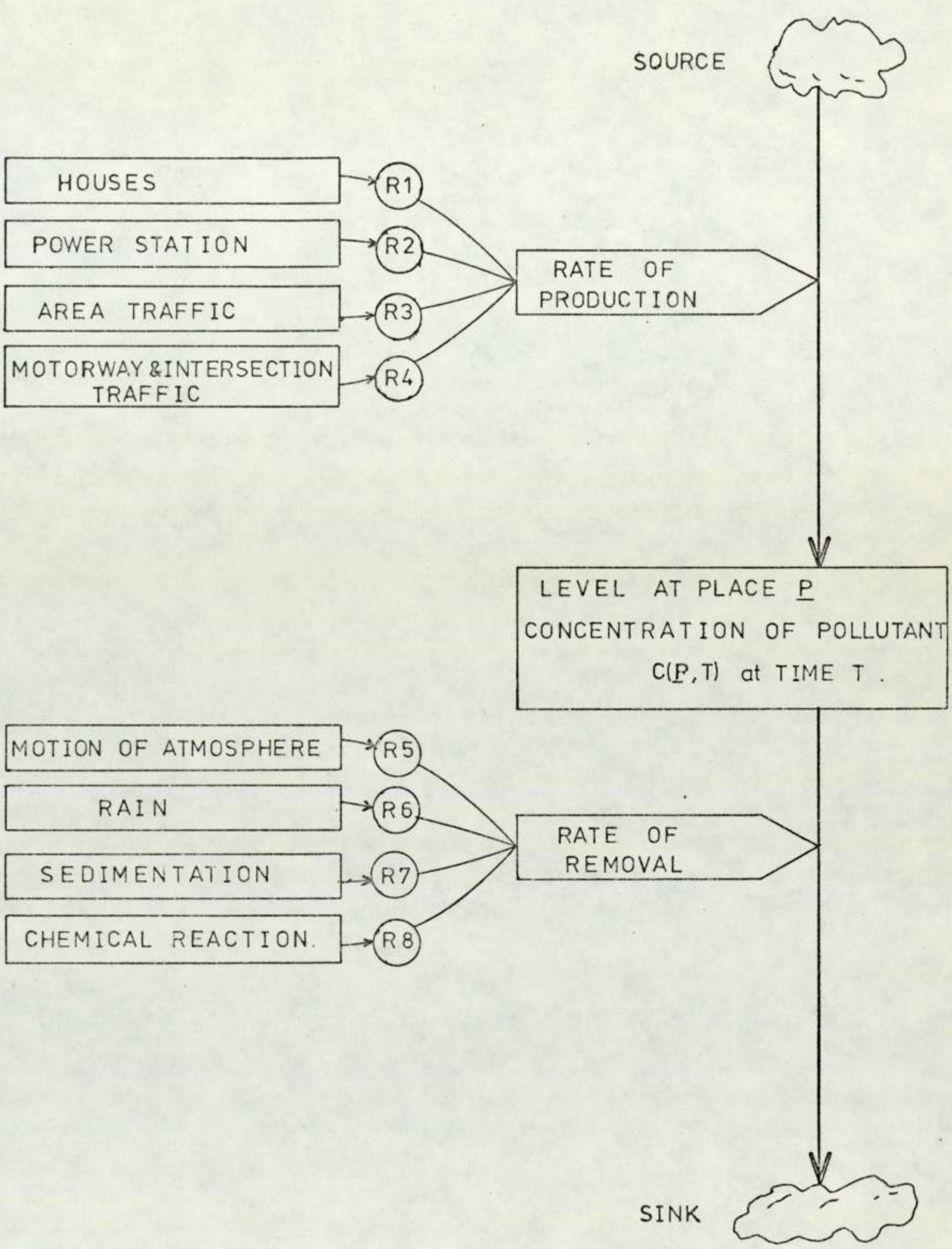

FIGURE 1.3 PROCESSES DETERMINING THE CONCENTRATION OF POLLUTANTS. R1 TO R4 INCREASE C, WHILE R5 TO R8 MAY REDUCE IT. THE PRESENT PROJECT ONLY STUDIED R4 AND R5, AND EACH OF THESE COULD NOT BE CONTROLLED.

is therefore a varying baseline of city pollution to which exhaust gases from the intersection are added. In general terms the wind speed and atmospheric mixing are expected to affect both the size of the background levels and the dilution characteristics of the source whose contribution we are trying to recognise and measure. This makes for a complicated study best described by a diagram (Figure 1.3). As compared to a laboratory experiment the problem is not closed. Traditionally one might vary one variable at a time to see the effects, but here we cannot. The spirit behind the research must be a feeling that each factor is an independent variable affecting the observed pollution levels: the individual effects of each variable have to be acknowledged by the use of their measured values to predict the pollution levels as observed. The rates of emissions and their dilution were the prime variables selected.

Source patterns were partly described using traffic counts while area sources such as houses were ignored. Dilution factors were estimated from weather observations taken at an adjacent airport; this assumed that the meteorological conditions were similar at the airport and in the city.

1.2 Outline of the Work

Following calibration of the instruments much of the work was monitoring in the field. Problems of calibrations and field-work are discussed. Routine monitoring involves large data sets for pollutants, traffic and weather, so computerised data processing as relevant to this type of project is considered. A new experimental technique to help the study of the dilution of plumes is presented. The results from the routine monitoring and this technique are discussed in terms of a Gaussian-plume dilution model. A programme to predict the pollutant levels is described and the predictions compared with field observations.

1.3 Information Available

Routine monitoring for a period at a fixed site needs time and effort. The periods of monitoring time were a compromise between the number of variables measured and the manpower requirements of the instruments used for the analyses. Since the study was designed to investigate pollution from vehicles, carbon monoxide and oxides of nitrogen were the gases of primary interest, but hydrocarbons were added later. A limiting resource was manpower, although the author had help from a technician.

With the three gas analysers and associated equipment the monitoring system had reached a level of complexity at which maintenance problems took up much of the author's time. The data were hourly measurements of NO_x, NO, CO, HC; NO_2 was available as NO_x less NO. Weather readings from Elmdon Airport (10 kilometres from the city centre) were at first hand-copied from the log- book at the airport and later from a line-printer output purchased from the Meteorological Office, Bracknell, Berkshire. There were two counters of traffic: one at Perry Barr covered the whole junction; the other, Salford Circus roundabout (Map: Figure 1.2). Reliable field measurements were made at Salford Circus and at Murdock Point (Map: Figure 1.2). The concentration decay was measured alongside the M6 Motorway away from the junction, and in the heart of the junction.

To calculate the pollution, traffic counts were scaled by literature values of emissions estimates for exhaust gases. The source geometry was represented as lines, curves and circles set in horizontal planes; Gaussian point-source plumes were integrated over this source representation by the trapezium rule. The plumes were defined by empirical curves (Geomet, 1971) according to a modified form of the Pasquill stability categories (Smith, 1972).

1.4 Summary

The following chapters describe the measurement and estimation of parameters believed to influence the levels of pollutants as observed. The problem is not closed since the variables are not under our control: this determines the approach to the problem and the discussion of the results.

CHAPTER 2

INSTRUMENTS USED FOR ROUTINE MONITORING

In the present chapter we describe the principles of operation of the instruments, and the calibration and zero checks as carried out. The following chapter will describe the monitoring sites and how the machines were used; together these chapters will indicate the limitations on the measurements made in the field. We begin with the machines themselves.

2.1 Description of the Instruments[1]

2.1.1 Analyser for Oxides of Nitrogen:-

Thermo Electron Chemiluminescent Model 12A NO-NO_x Analyser (Waltham, Massachusetts, United States of America)

This machine measures both NO and NO_x at eight sensitivities from 1000ppm down to 0.01ppm full scale. It has a negligible interference from water vapour, carbon and sulphur compounds. It is designed for continuous monitoring; the response time is 5 - 7 seconds at 0.25ppm full scale. Accuracy is quoted as $\pm$ 1% on standard gas and $\pm$ 3% on the 0.01ppm scale. Linearity is $\pm$ 1% of full scale.

The NO is measured by the light ($\lambda \sim 600$ - 875nm) emitted from the chemiluminescent reaction (Fontijn et al., 1970).

$$NO + O_3 \longrightarrow NO_2 + O_2 + h\nu$$

Note 1: Notes based upon Manufacturer's Manuals.

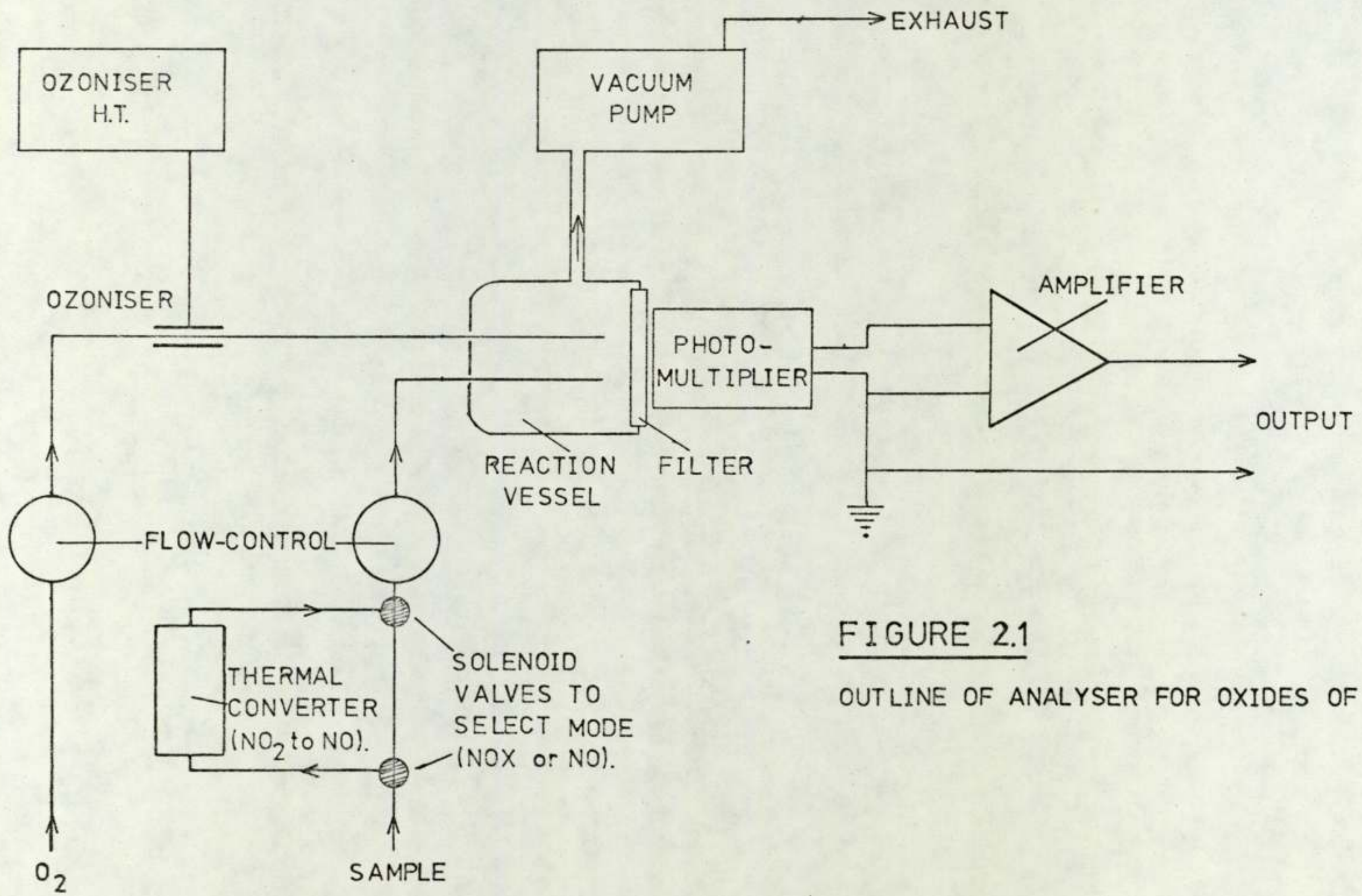

FIGURE 2.1

OUTLINE OF ANALYSER FOR OXIDES OF NITROGEN

An optical filter in front of the photomultiplier makes the response specific to this reaction and therefore to NO. The flow parameters are set up to give a light emission proportional to the NO concentration. NO_x (NO plus NO_2) is measured as the NO produced by thermal pyrolysis of the NO_2 as it passes down a heated (stainless steel) converter. The diagram (Figure 2.1) shows the instrument schematic.

2.1.2 Analyser for Carbon Monoxide:-

Grubb Parsons MGA2 (Newcastle, United Kingdom)

The instrument is analagous to that described in "Am. Conf. Govt. Hygienists", 4th Edition. It has one range 0 - 100ppm. It has no response to water vapour. Atmospheric fluctuations have a negligible effect. The high selectivity to carbon monoxide derives from the use of the characteristic absorption-spectra in the infra-red. The zero point is stabilised by double compensation, and sensitivity is electronically adjusted for temperature drift.

The arrangement is shown in Figure 2.2. Infra-red radiation from the lamp passes alternately through the chopper disc into either the sample vessel(4) or reference vessel(5). The reference does not absorb the IR; it contains N_2. Either beam enters the diffuser(7), and thence the first section(9) of the receiver block(8). The CO in the first section absorbs radiation of wavelengths at the band centres of the CO spectrum. The longer second section(10) absorbs the remainder, which is chiefly from the band flanks. The energy absorbed by the CO in each section produces heating and expansion; the sections

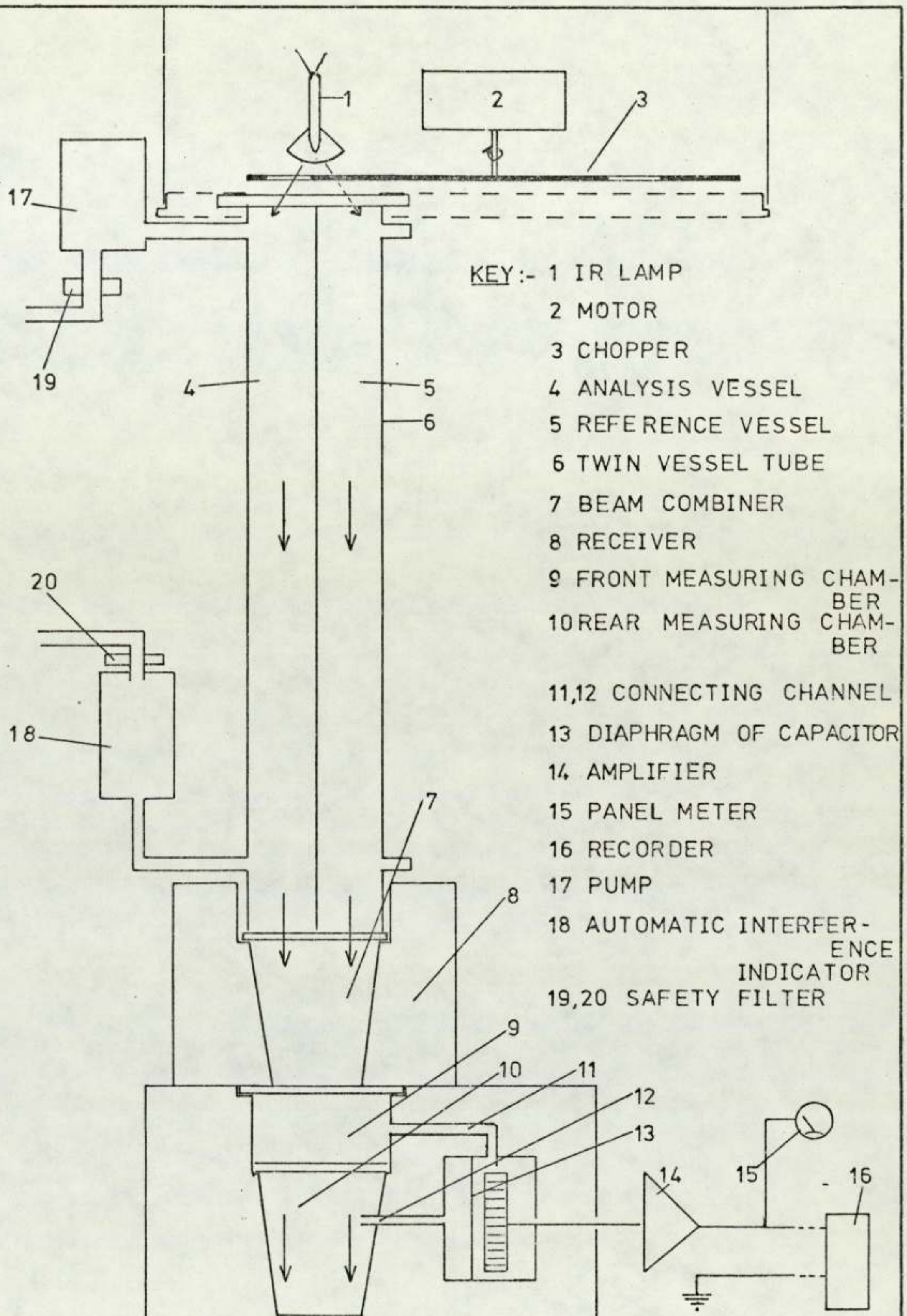

FIGURE 2.2 OUTLINE OF ANALYSER FOR CARBON MONOXIDE

are separated by windows but connected by tubes to the opposite sides of a diaphragm. This moves according to the pressure difference. The geometry and concentration of the CO in each section are arranged to give equilibrium when the sample vessel(4) contains no CO. When there is CO present in the sample, it absorbs band-centre radiation; the first section(9) is affected and the diaphragm moves. In practice the radiation is modulated and the oscillations of the diaphragm measured as capacitance, amplified and displayed as a DC signal.

2.1.3 Analyser for Total Hydrocarbons:-
Analysis Automation Model 521 Total Hydrocarbon Analyser
(Oxford, United Kingdom)

This uses a hydrogen-air flame in a flame ionisation detector to measure total organics. It does not respond to other gases such as CO, CO_2, NO, SO_2 and water vapour. The detector response to molecules of the same carbon number is roughly the same; oxygenated compounds give a smaller response. The instrument has four ranges from 1ppm to 1000ppm methane, and is linear over the range 0 - 1ppm to 0.1% full scale.

The sample is passed into the hydrogen flame; a potential difference is applied between the jet and a collector electrode. The ions normally present give a standing current. When organic compounds (with a CH bond) are present, the ion current increases in proportion to the number of carbon atoms in the flame. The flow rates and cabinet temperature are held constant to maintain steady conditions.

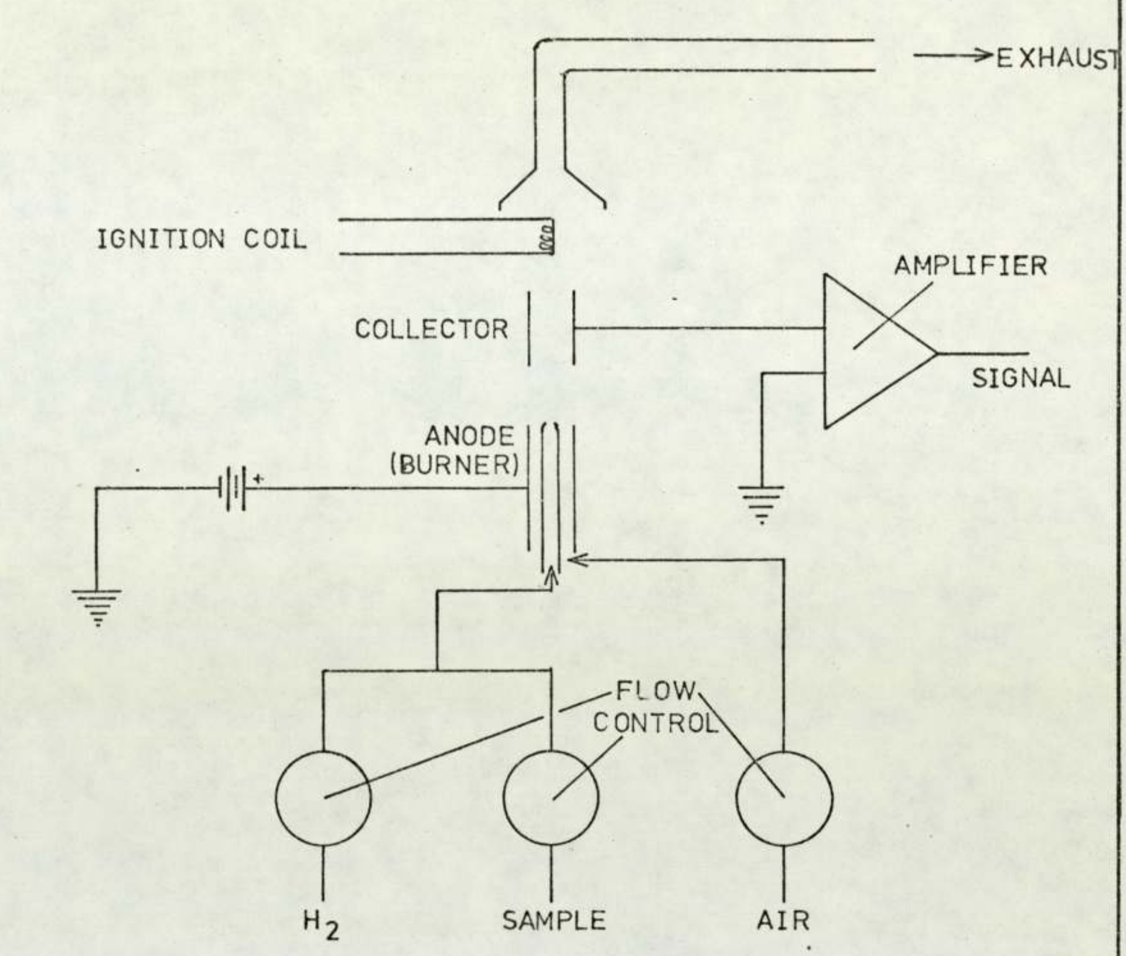

FIGURE 2.3 OUTLINE OF ANALYSER FOR HYDROCARBONS

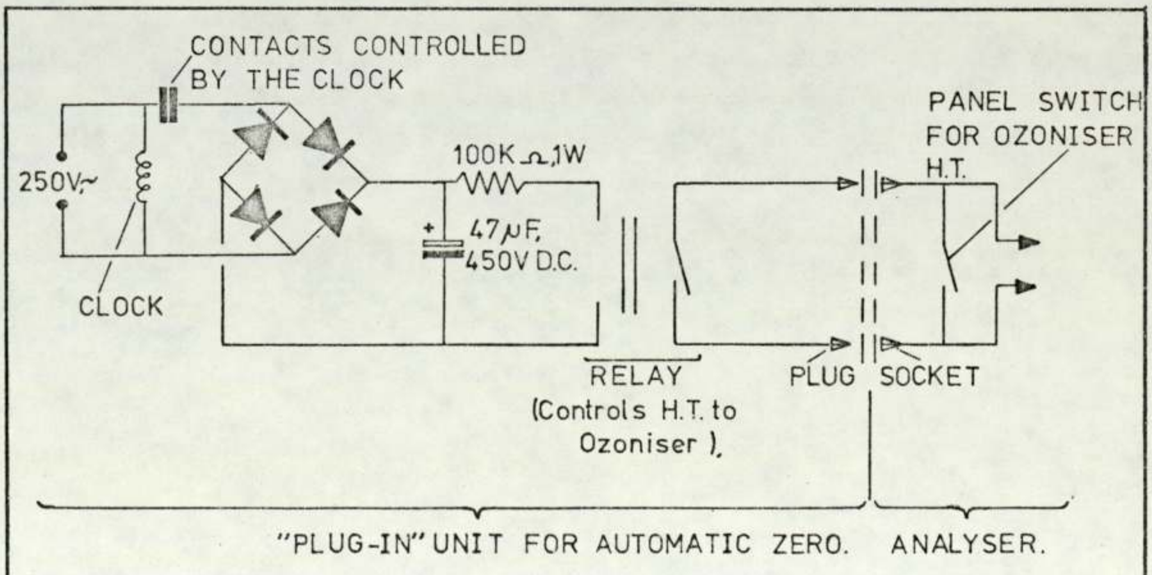

FIGURE 2.4 AUTOMATIC ZERO CHECKER FOR NO/NO_X ANALYSER

Figure 2.3 shows an outline.

2.2 Zero Measurement

2.2.1 NO - NO_x Analyser

The NO - NO_x Analyser was zeroed by switching off the power supply to the ozonator. Production of ozone ceased and the response fell to zero. The zero was that current remaining after subtraction of a standing current from the photomultiplier dark current.

The noise and drift depended on the ambient temperature of the machine and the degree of moisture present in the photomultiplier housing. The latter continually collected water by condensation and caused most of the trouble experienced with this machine. A time clock was wired to switch off the power supply to the ozonator every six hours to give an automatic zero check, (Figure 2.4).

2.2.2 CO Analyser

The CO Analyser was zeroed originally with cylinder N_2. Later a tube of silica gel followed by Hopcalite (Lamb et al., 1920) was used to dry the sample air, and oxidise any CO to CO_2. The CO free air thus gave the zero. A tube of 2.5cm diameter holding 10cm silica gel followed by 8cm Hopcalite gave the same readings on laboratory air as cylinder N_2. It gave consistent results with easy portability in the field.

2.2.3 HC Analyser

The HC Analyser uses a hydrogen/air flame and the sample is injected directly into the fuel line. Zeroes were measured as the ion-current existing in the flame without the passage of sample gas: the sample-pump was simply turned off. The zero had to be taken on the same sensitivity range as that used for monitoring.

2.2.4 Frequency of Zeroes

The NO/NO_x machine was zeroed automatically every six hours. The CO and HC Analysers were zeroed daily as part of the routine checks.

2.3 Calibration Checks

2.3.1 Introduction to the Calibrations

It was decided for convenience that the instruments when on site would be calibrated with mixtures of gas made up in the ppm range. This assumed that such mixtures delivered from cylinders were stable and that the instrument responses were linear. Cylinders of standard gases, as listed in Table 2.1, were purchased from Rank-Precision Industries. They do not necessarily deliver a mixture of composition as prepared since absorption losses and decomposition may occur. Indeed a mixture of 100ppm NO and 100ppm NO_2 in N_2 was unstable: the NO_2 disappeared in a few weeks.

To cross-check the concentrations delivered from the cylinders,

TABLE 2.1

Commercial Gas Mixtures Purchased and Concentration Levels at which Calibrations were Needed

Pollutant	Concentration[1]	Field Sensitivity
NO, NO_2	100ppm $\pm$ 5% NO, in N_2	<1ppm, often <.25ppm
	100ppm $\pm$ 5% NO_2, in N_2	
NO	100ppm $\pm$ 5% NO, in N_2	<1ppm, often <.25ppm
CO	50ppm $\pm$ 5% CO, in N_2	<10ppm
HC	8ppm $\pm$ 5% CH_4, in N_2	<10ppm

Note 1: Generally above field level as harder to prepare and store at lower concentrations.

carbon monoxide and nitric oxide were diluted in N_2 to the ppm level; this required a two-stage process. The commercial mixture was diluted in one step to measure the instrument linearities at sensitivities near to that required in the field. Exponential dilution was used to check the NO/NO_x analyser below 1ppm. The HC Analyser was used as a carbon monoxide analyser to compare the CO and CH_4 standards.

2.3.2 Two-Stage Dilution: CO and NO

Precise dilution by 10^5 times requires careful pressure regulation and flow control (Am. Conf. Govt. Hyg., 4th Edition). A small part of the mixture produced by the first stage (Figure 2.5) was diluted in the second (Figure 2.6), with the surplus led to waste down a capillary. The latter kept the pressure above atmospheric to aid flow control. Micrometer gas-valves (Hoker) were used for fine flow control. The diluent, N_2, was held at a standing pressure in the line from the cylinder regulator to the input control valve. Soap bubbles (Figure 2.6) were injected from the teat and timed; their pressure was measured on the water manometer. The appendix kept the feed line free of surplus soap solution. Wherever possible materials were glass, teflon or stainless steel. Either of the two mixing ranges could be selected using the tap on the first board to change the rotameter in use. The second stage gave a total flow equal to the sample flow of the instrument under test. The flow-meter capacities are listed in Table 2.2. Scatter arising from the use of several rotameters was increased for the oxides of nitrogen work by the lack of a non-corrosive pressure-regulator.

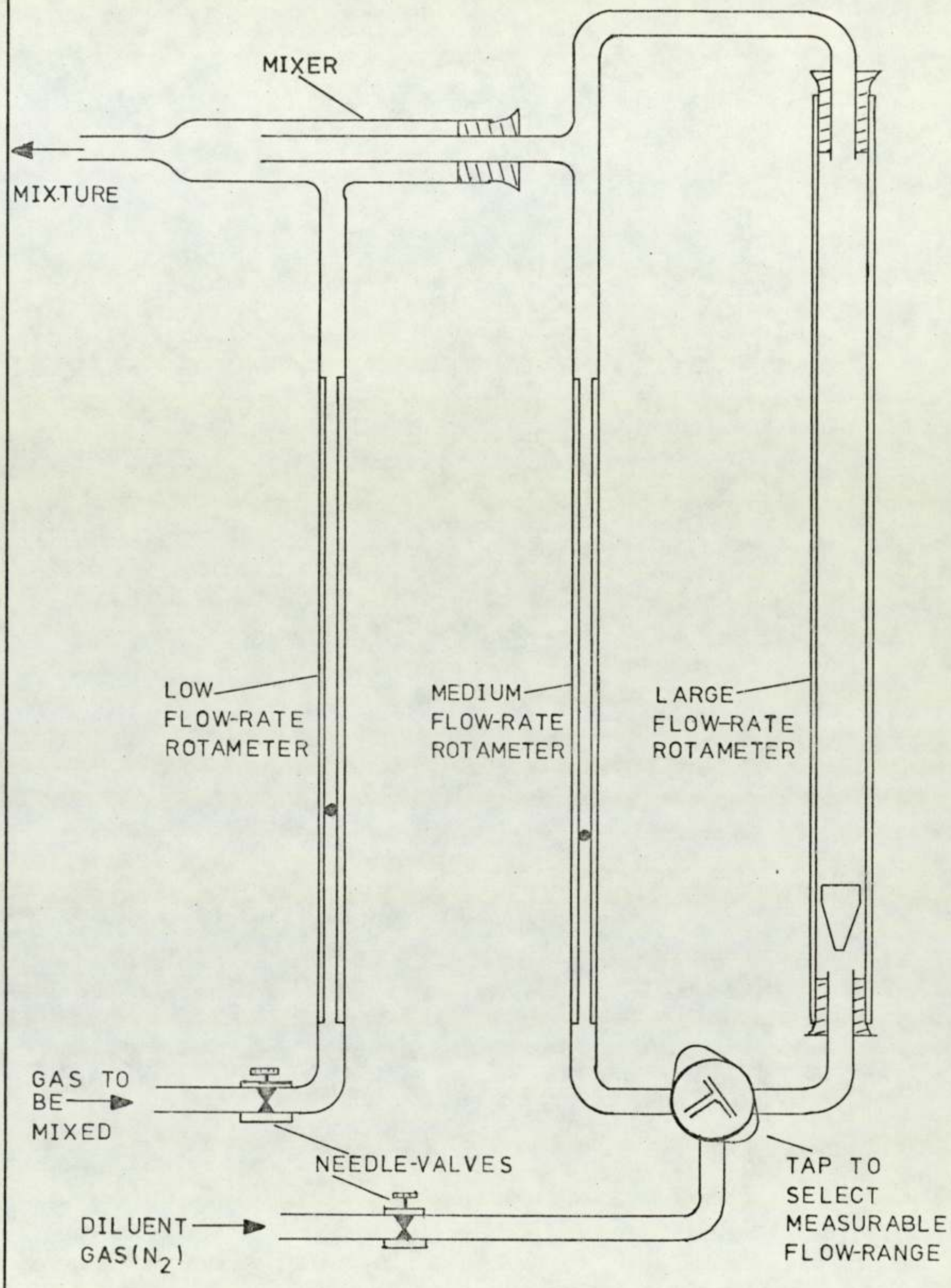

FIGURE 2.5 FIRST-STAGE DILUTION APPARATUS

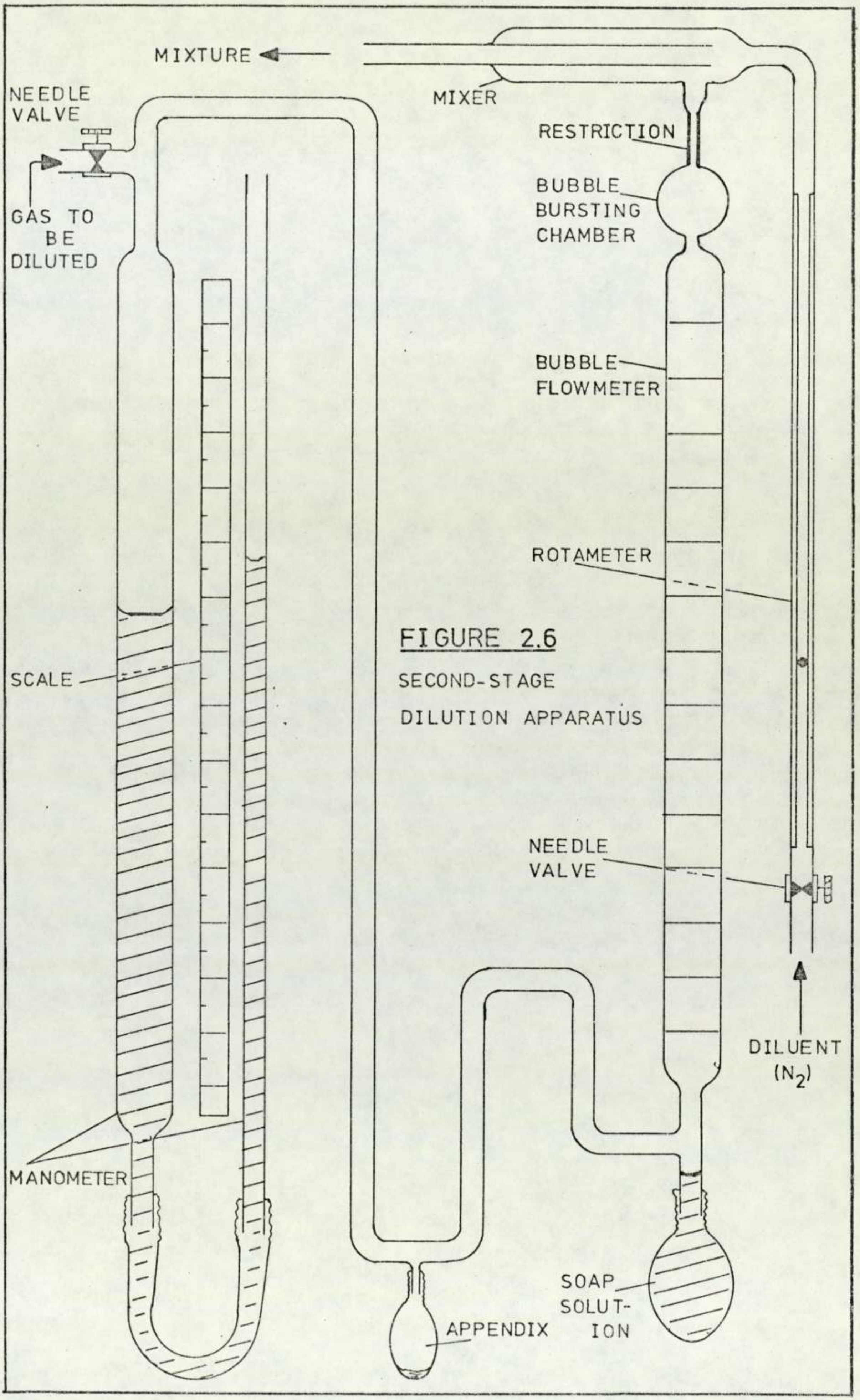

FIGURE 2.6

SECOND-STAGE DILUTION APPARATUS

TABLE 2.2

Flow Meter Capacities

Flowmeter	Flow Range AIR, $ml\,min^{-1}$, STP	Comments
Rotameter[1] (A Glass)	5 - 45	Poor float stability
Rotameter[1] (B St-St)	50 - 450	Good float stability
Rotameter[1] (C St-St)	150 - 1300	Good float stability, covers I2A, MGA2 input
Rotameter[2] (Metric 7P)	1000 - 9000	Good float stability
Bubble meter[3]/Stop-watch	2.4 - 180	Assume absorption into soap solution reaches negligible steady state

Notes 1: Glass Precision Engineering Limited, Hemel Hempstead, Hertfordshire, United Kingdom.

2: Rotameter Manufacturing Company Limited, United Kingdom

3: Constructed from 25ml burette, ~1cm i - d;
Minimum flow depends on bubble life time;
Maximum flow on shortest stop-watch period.

The instruments were calibrated on standard gases (Table 2.1). On analysis by these instruments, the concentration measured in the flow-mixture was lower than expected on the basis of the flows and extent of dilution.

For agreement between instrument analysis of the flow-mixture and the calculated flow-concentration it is necessary that:-

1. Standard gas is correct, so that instrument reads true;
2. Correct calibration of flow-meters so that the calculated concentration derived from the dilution is correct;
3. Absence of leaks and absorption on the walls or in the bubble meter.

The instrument responses were low, with about 10% scatter:-

1. 12A/NO_x was 70% of expected flow-dilution concentration;
2. 12A/NO was 73% of expected flow-dilution concentration;
3. MGA2/CO was 60% of expected flow-dilution concentration.

The low readings imply that:-

1. Instrument reads low: cylinder mixtures were of a higher concentration than as labelled.
2. Incorrect calibration, or error accumulation: reading large and small flows near ends of rotameters.
3. Leaks: not considered significant. Absorption losses should

appear also in the single stage dilution which follows, but the deviations are much smaller, so unlikely.

It is not known which is responsible for the discrepancy, but the important point is that standard gas mixtures as commonly used in air-pollution research are not completely reliable (e.g. disappearance of NO_2 as above), and that to cross-check instruments by dilution of the neat gas requires more sophisticated apparatus than that used here. The work does suggest that the concentrations as reported could be 30 to 40% low. For the field work the instruments were always calibrated on the standard gases because the two-stage dilution was felt to be only a little better than an order-of-magnitude check.

2.3.3 Single-Stage Dilution of ppm level mixtures of CO and NO

Standard gases (Table 2.1) were diluted in the bubble-meter board (Figure 2.6) to check the linearity of the instruments. Within the concentration range covered (1 - 15ppm CO; 0.5 - 10ppm NO), the instruments gave a linear response. Table 2.3 summarises the results (Figures 2.7, 2.8, 2.9).

Rotameters (Linford, 1961) give a volume-flow reading which varies with temperature as $T^{1/2}$, pressure as $P^{-1/2}$ and density of the gas as $\rho^{-1/2}$. The apparatus was used at pressures within 3% of atmospheric pressure. Temperature effects are negligible since the flow-meters were calibrated in the laboratory. Unsteadiness of the float relative to the float height can be 1% at large flows, and exceed 5% at low flows. Allowing for the pressure effect the error is $\sim$3-5 %

TABLE 2.3

One-Stage Dilutions: Discrepancy between the Instruments' Response and the Calculated Concentration (Calculated from the Flow Rates and Standard Gas Composition)

Instrument	Observation Range, ppm	Least Squares Line[1] of Instrument Response to Calculated Concentration m	c	s	Source Gas, ppm in N_2
MODEL I2A/NO	0.07 - 9	0.900	0.0513	0.0513	100ppm,NO + 100ppm,NO_2
MGA2/CO[2]	3 - 15	0.988	-0.058	0.257	50ppm.CO

Note 1: Instrument reading = m.calc-conc + c, with standard deviation s.

Note 2: CO Analyser 0 - 50ppm, as modified for field use (Chapter 3)

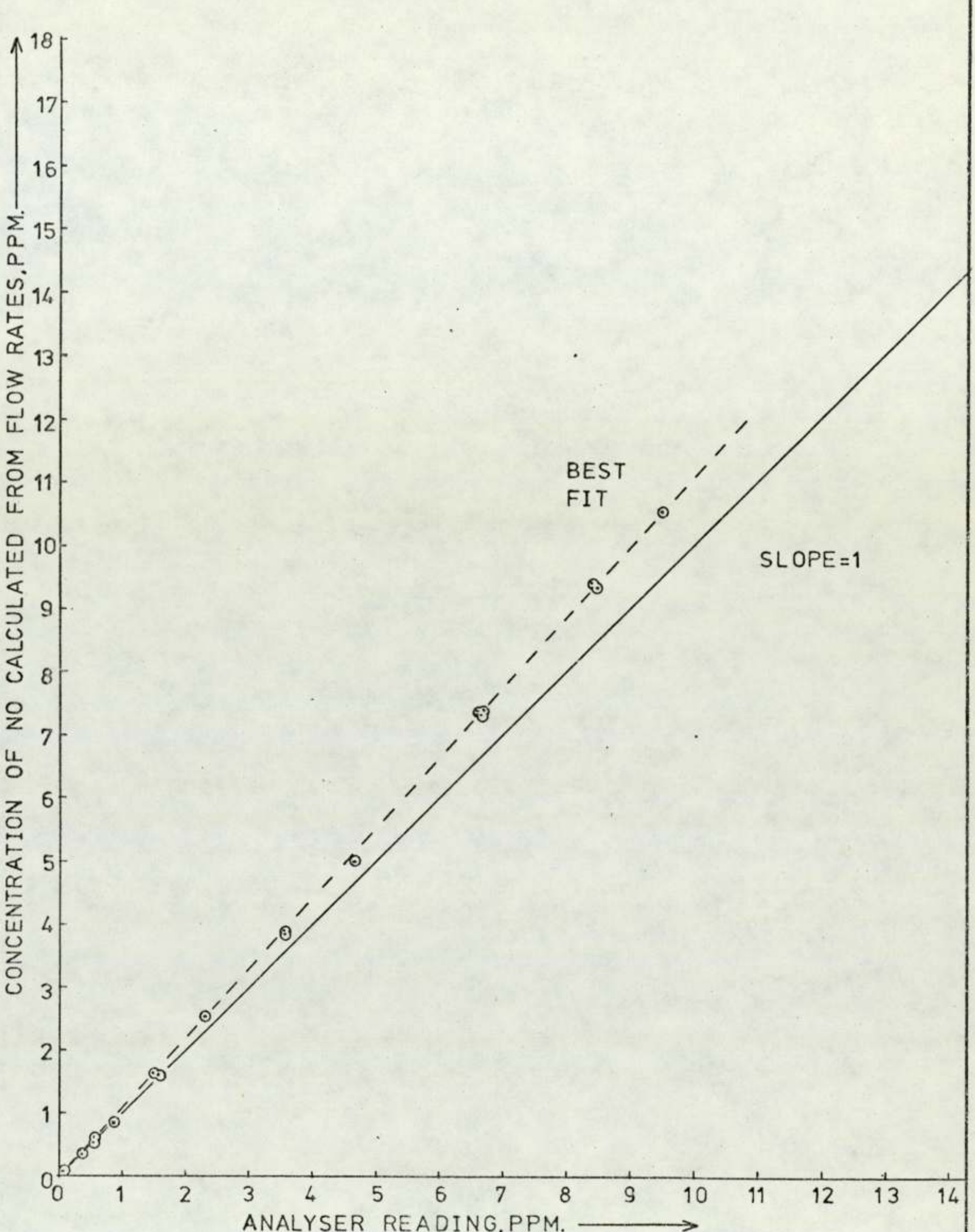

FIGURE 2.7 CHECK OF LINEARITY OF THE OXIDES OF NITROGEN ANALYSER (NO mode) BY SINGLE STAGE DILUTION OF STANDARD GAS (100 ppm NO in N_2)

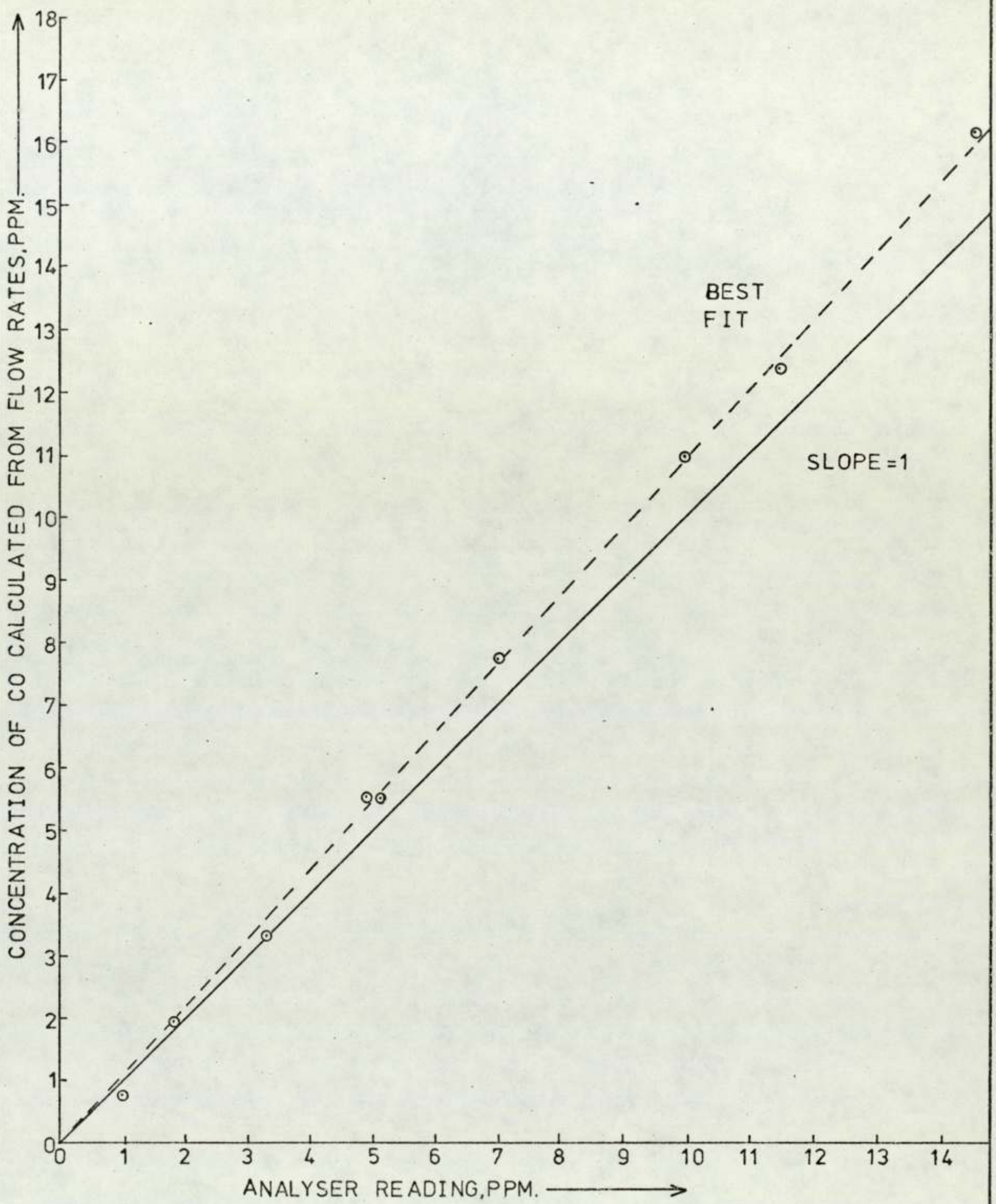

FIGURE 2.8 CHECK OF LINEARITY OF THE CARBON MONOXIDE ANALYSER (0-100 ppm fsd) BY SINGLE STAGE DILUTION OF STANDARD GAS (50 ppm CO in N_2)

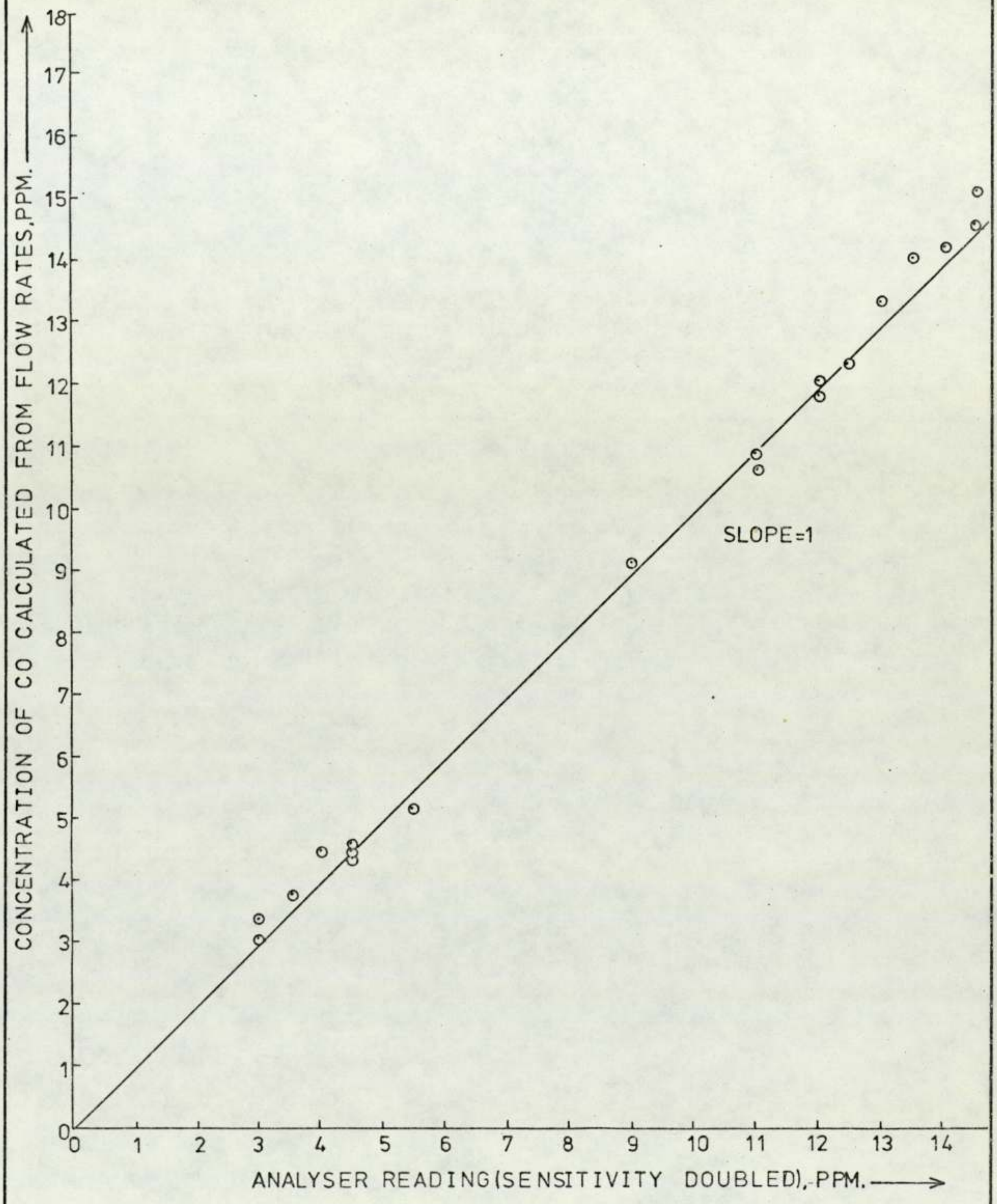

FIGURE 2.9 CHECK OF LINEARITY OF THE CARBON MONOXIDE ANALYSER (0-50ppm fsd), AS USED IN THE FIELD WITH SENSITIVITY DOUBLED, BY SINGLE STAGE DILUTION OF STANDARD GAS (50 ppm CO in N_2)

Thus single-stage dilution has an error of $\sim 5\%$, and two-stage, $\sim 7\%$.

The single-stage dilution showed, for the CO Analyser, good linearity within this scatter: for the NO/NO_x analyser there was a systematic deviation of around 10%; this may be partly due to absorption losses.

2.3.4 Exponential Dilution

When a gas of concentration C_o is passed into a well mixed vessel of volume V and the supply is then suddenly changed to diluent, the concentration C at time t after the start of dilution is:-

$$C = C_o \exp(-Qt/V),$$

(Fontijn et al., 1970), where Q is the volume flow rate. Fontijn et al., found the NO monitor they made was linear from 4.10^{-3}ppm to 100ppm. Figure 2.10 shows a plot of $\log_{10}(C)$ against t, obtained by the dilution of standard gas (Table 2.1) with nitrogen. With perfect mixing and no absorption-desorption effects the graph should be linear. In fact the curvature increases at lower concentrations where the time since dilution began is ten times the time constant V/Q (200 sec as against 180 sec). During one run the mixer was heated: the concentration rose rapidly, consistent with desorption.

The NO/NO_x analyser appears to be linear down to 0.25ppm on the NO mode, and 1ppm on the NO_x mode. The curvature below these levels is thought to arise from the effects (e.g. inadequate mixing and

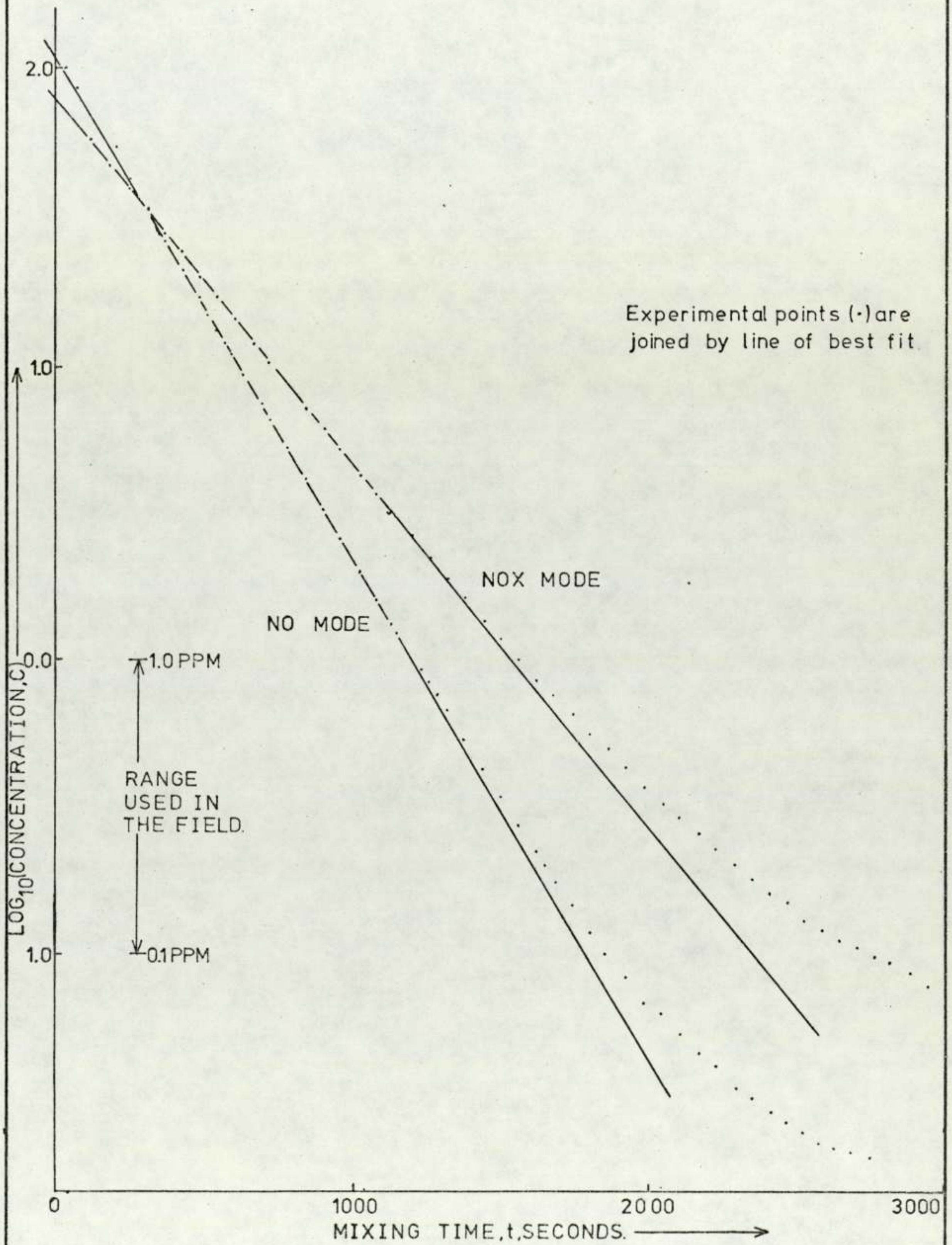

FIGURE 2.10 CHECK OF LINEARITY OF THE OXIDES OF NITROGEN ANALYSER BY EXPONENTIAL DILUTION

absorption-desorption) of the long mixing-time needed to reach that level rather than any non-linearity of the instrument.

2.3.5 Cross-Check of CO and HC Calibrations

The total HC Analyser, purchased later in the project, was calibrated on our own standard (8ppm CH_4 in N_2). Cross-checks with mixtures from Transport and Road Research Laboratory were consistent with a linear response and that our standard was valid.

The HC Analyser was adapted to estimate the carbon monoxide content of the standard (50ppm CO in N_2). A nickel catalyst was inserted in the hydrogen-fuel/sample line before it entered the burner. Hydrogen from the fuel reduced the carbon monoxide present as the mixture passed over the heated catalyst (Porter and Volman, 1962). The results were:-

CO standard over cold catalyst	1ppm
CO standard over hot catalyst	46ppm
CH_4 standard over cold catalyst	7ppm
CH_4 standard over hot catalyst	20ppm

The latter discrepancy is thought to be impurities in the methane standard, since with fuel alone no change with catalyst temperature occurs. The methane standard did not contain carbon monoxide however, for it gave no response on the carbon monoxide analyser.

It was concluded that the methane and carbon monoxide standards were mutually consistent, although the methane standard appeared to have an impurity not normally detected by the FID, unless reduced by the hydrogen over the hot catalyst. This reinforces the earlier comments on the problems experienced with cylinder supplies of standards.

2.4 Summary

Absolute calibration requires careful design with regard to absorption of constituents, flow stability and the measurement of large and small flows before mixing. More sophisticated equipment is now available: the reader is referred to "Am. Conf. Govt. Hygienists", 4th Edition.

Absolute concentrations were checked by dilution of CO and NO down to 5ppm; the standard gases were checked to better than an order of magnitude.

Linearity was within 10% for the NO/NO_x analyser and 5% for the CO Analyser in the ranges 100 - 1 and 50 - 3 ppm, respectively. The commonly used cylinders of standard gases, although used in the field, are felt to be not completely reliable.

CHAPTER 3

FIELD OPERATION OF INSTRUMENTS AND ABSTRACTION OF THE RESULTS

The instruments were left unattended at various sites to record data. We shall discuss the nature of the sites and their effect on both the performance of the instruments and the attention they required. The chart records were abstracted manually and processed by computer. We shall outline the programme to show how this method of unattended field monitoring with manual data abstraction determined the calculations required, and how the results were output to storage ready for later use. These results, together with those calculated from emissions and dilution, will be discussed in Chapter 6.

3.1 Sites Used for Routine Monitoring

The project began with little knowledge of the levels of gaseous pollutants expected. The site at Salford Circus (Map: Figure 3.1) provided a junction monitor while that at Murdoch Point was further away to give a distance effect and a city "background" level. A further site at Slade Road Schools was used but the results were not accurate for technical reasons.

An unattended monitoring site must have:-

1. Security against vandalism;

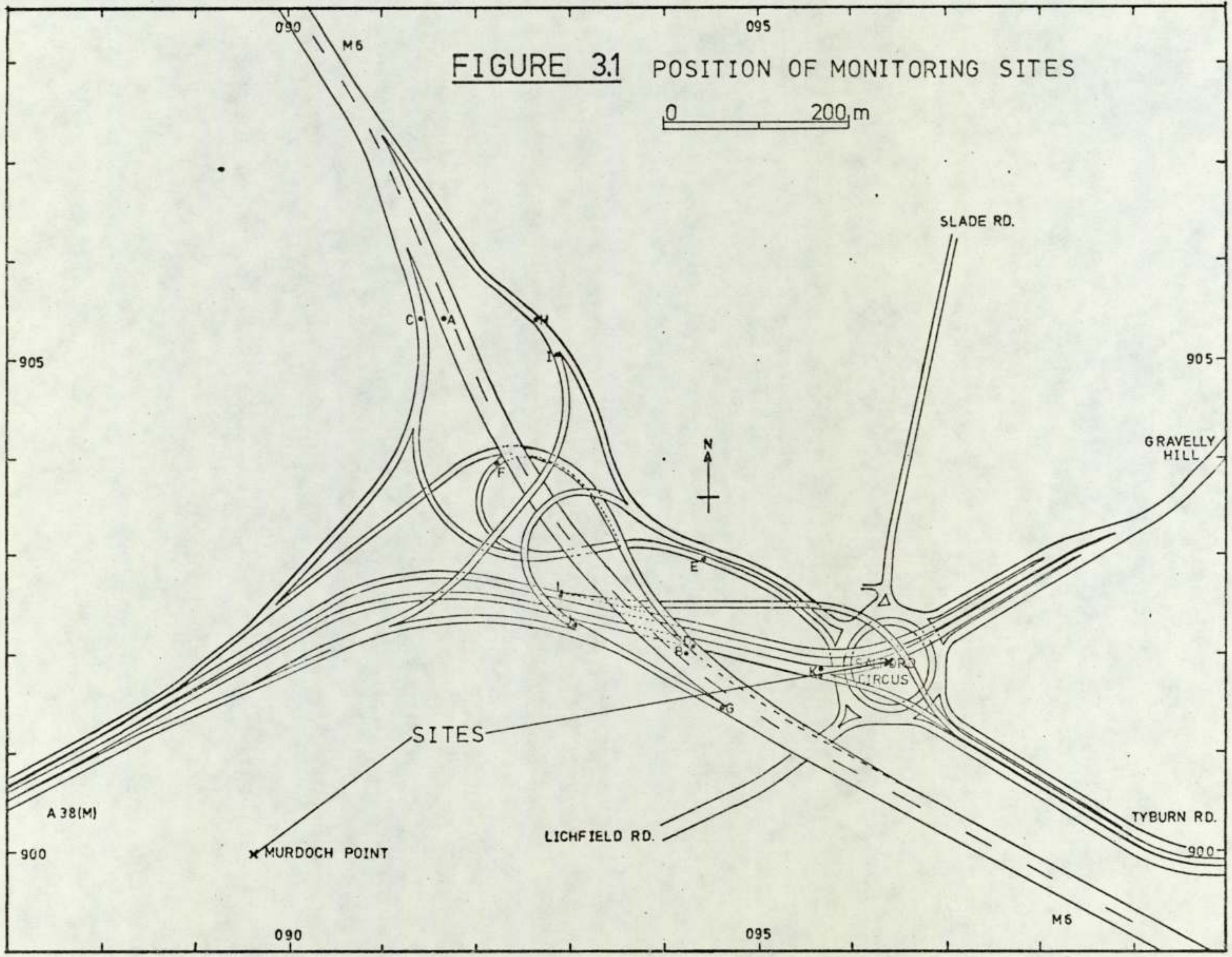

FIGURE 3.1 POSITION OF MONITORING SITES

2. Mains supply;

3. No severe temperature drift to upset instruments.

If the project has a specific source to monitor there should not be interfering sources nearby or the results will be hard to interpret. Buildings of potential use may be privately or publicly owned: in either case special facilities such as lockable doors and mains supplies may be needed; this requires much negotiation with public bodies. The positions available for monitoring are therefore restricted. The choice of sites for monitoring programmes larger than the present project has been analysed theoretically (Bibbero and Young, 1974).

The site at Salford Circus (Map: Figure 3.1) was used as the intersection monitor. It consisted of a triangular room ($\sim$ 9 square feet available) in the public conveniences at the centre of the roundabout. The equipment was installed with the chart recorders on the walls, the cylinders at the back of the room, the NO-NO_x Analyser on the floor, the CO machine on the wall and the HC Analyser on a shelf aloft (Photograph: Figure 3.2). Inlets were mounted on the roof.

The site at Murdoch Point (Map: Figure 3.1) was further from the intersection. It was less satisfactory as a site to study pollution from the Motorway, for there was an interfering chimney in a building between it and the intersection. It was useful as a guide to the pollution levels in air approaching the intersection from the city. The equipment was placed at the top of the building in the winch room ($\sim$ 50 square feet available).

FIGURE 3.2 EQUIPMENT IN THE FIELD

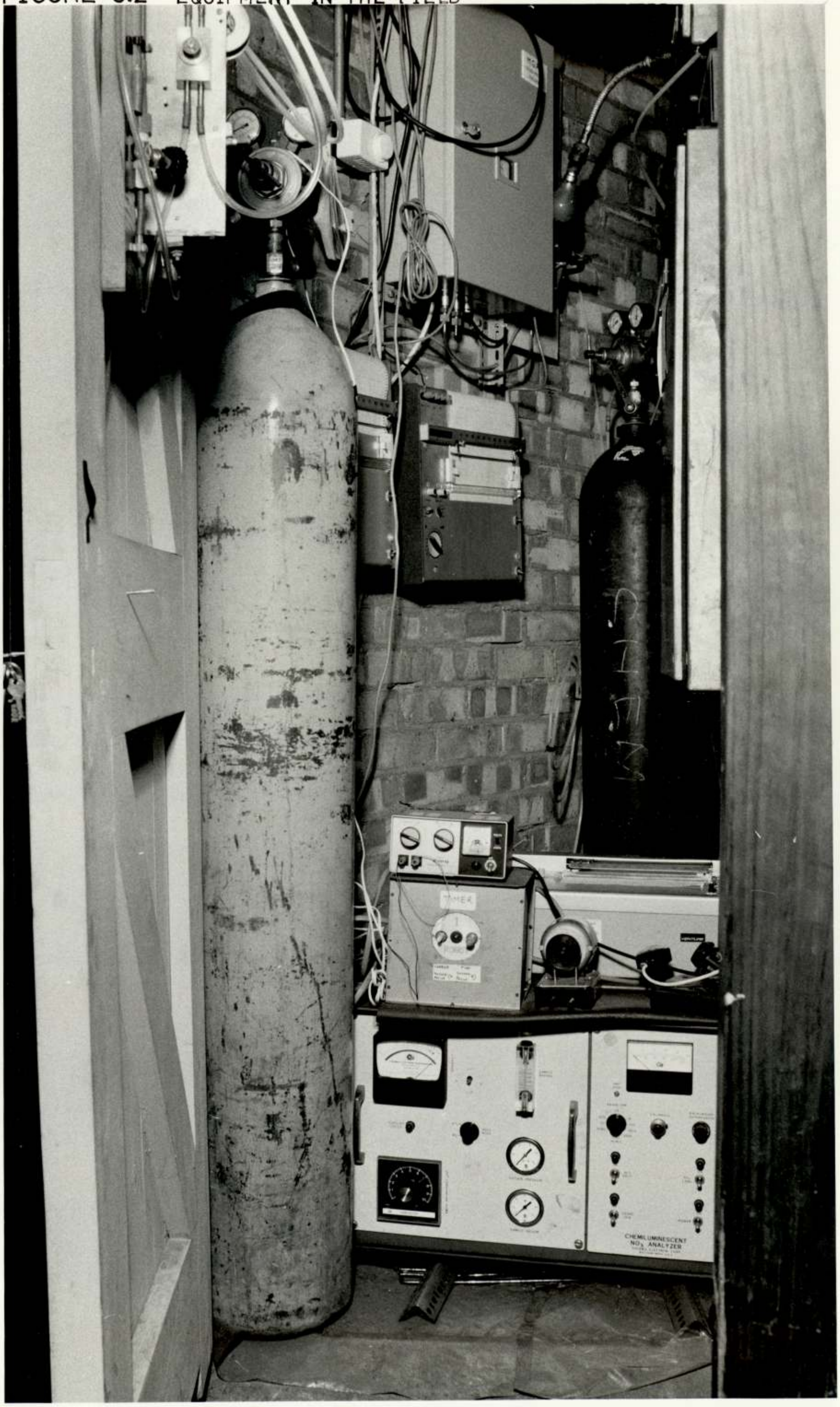

3.2 Method of Operation

Chart recorders were linked to each instrument. A clock was fitted to the NO-NO_x Analyser to switch it alternately from the NO to the NO_x mode and back; the results for each mode were distinguished by colour on a dual pen recorder. During daily visits the charts were labelled and collected, and zero and calibration readings taken. Filters (Whatman 3.7 GF/A) in the gas inlets were changed regularly: sample lines were Teflon for HC and NO_x, and PVC for CO. Experience showed many items might be left undone so a checklist (Table 3.1) was used. The site determined ease of checking: that at Salford Circus was rather cramped while at Murdoch Point space was ample, although a hand winch was needed to lift equipment into the room.

3.3 Field Performance of Instruments

The CO and HC Analysers gave little trouble. The No-NO_x Analyser required constant servicing because there was an unknown source of condensation so that water slowly collected on the photomultiplier tube. This showed itself as noise and spikes in the signal. Intermittant faults such as noise or drift were especially hard to find as they were often only apparent from the charts when the daily visit was made, yet the machine could appear to be satisfactory. Unattended operation increased the fraction of monitoring time during which faults or incomplete data were produced, but it did give periods of continuous data with limited manpower.

The CO Analyser was run on a 0 - 50ppm scale using the chart recorder on a more sensitive scale with load resistors wired as in

TABLE 3.1

Checklist for Routine Monitoring

Chart Recorders	Oxides of Nitrogen Analyser
Paper, ink, pens Electric connections Drive - Speed Sensitivity Recorder zero = instrument zero Chart labelled - date, time, FSD, speed, site, mode, gas **Hydrocarbon Analyser** Chart recorder H_2, Air, sample pressures Cylinder taps on Sample pump on Sample tube connected Gas leaks? Cabinet warm Flame alight Zero: sample off Calibration: standard gas **Carbon Monoxide Analyser** Recorder Sample tube connected Filter clean Cabinet on inside Zero: silica gel/Hopcalite Calibration: standard gas	Chart recorder Mode:- AUTO or NO/NO_x Pens agree with mode NO_x = Red Connections: 10V+ to X1, 10V- to X2, 10mV- to Earth Sample flow NO_x converter on, temperature set Reaction chamber vacuum O_2 cylinder tap on O_2 pressure Gas leaks? O_3 generator: on only if O_2 flowing. If automatic dark current, O_3 generator switch off, and clock plugged in to instrument. Dark current - steady and low Sensitivity Gas filters clean Exhausts connected Calibration: standard gas

Figure 3.3. The sensitivity was not ideal but a further increase was unwarranted because of zero drift. The arrangement gave linear results (Figure 2.9).

Table 3.2 shows the drift experienced with the machines in the field.

3.4 General Requirements for a Programme to Process the Charts

Although the signal varied rapidly (Figures 3.4, 3.5, 3.6, 3.7), analogue smoothing was not used as it would have obscured instrument noise and intermittant faults. To cope with this variance of signal (Table 3.3) a fast chart speed was used (typically 30cm h^{-1} for NO-NO_x; 12cm h^{-1} for CO, HC) and up to 30 points abstracted per hour. The chief task of the programme was to average these, taking due note of zero and calibration readings.

Any given instrument may be run on any sensitivity range even within a week's monitoring. Zeroes and calibrations may be recorded at any, usually irregular, times as demanded by the quality of instrument performance and the available manpower for checking. Various instruments may be out of action at differing times. It follows that the monitoring data must be sorted by time to eliminate incomplete data rows and to identify the appropriate zero and calibration readings from those taken.

Various chart speeds are used for resolution of the finer parts of the trace so any number of observations per hour may be read in and averaged.

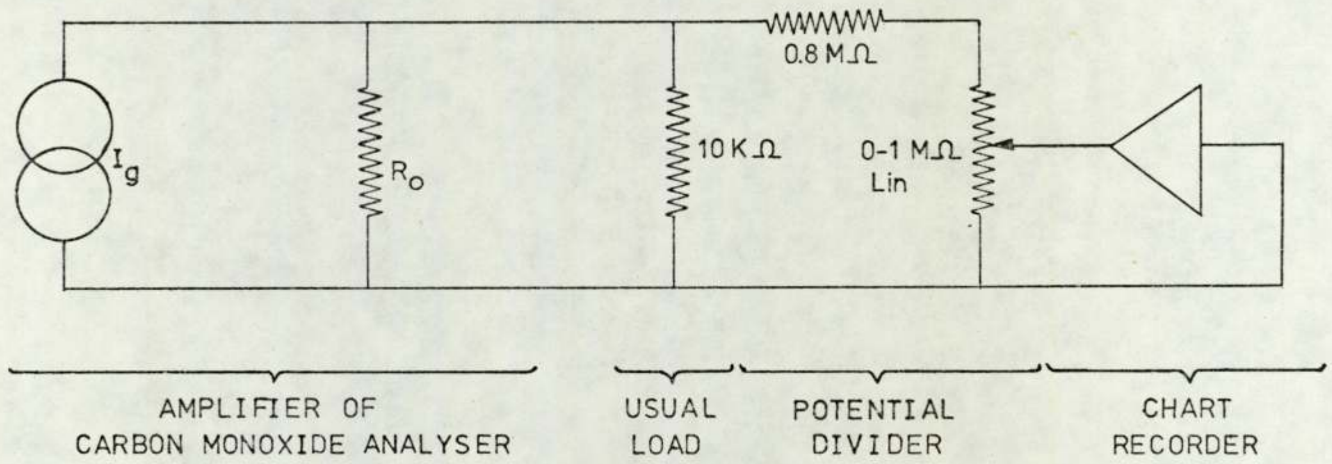

FIGURE 3.3 CIRCUIT TO DOUBLE THE SENSITIVITY OF THE CARBON MONOXIDE ANALYSER

TABLE 3.2

Zero Drift relative to Observed Levels

Gas	Instrument	Zero Drift		Zero Drift ÷ Mean Level		Zero Drift ÷ Maximum Level	
		SC ppm	MP ppm	SC %	MP %	SC %	MP %
NO_x	MODEL I2A	± 0.005	± 0.004	4	15	1	3
NO	MODEL I2A	± 0.005	± 0.004	5	37	1	5
NO_2[2]	MODEL I2A	± 0.010	± 0.008	71	51	12	17
CO	MGA2	± 0.3	± 0.13	10	12	3	4
HC	AA.521	± 0.2	± 0.1	3	2	2	2

Note 1: Salford Circus (SC)

Murdoch Point (MP)

Note 2: NO_2, recorded as (NO_x - NO), shows a larger drift effect because of subtraction.

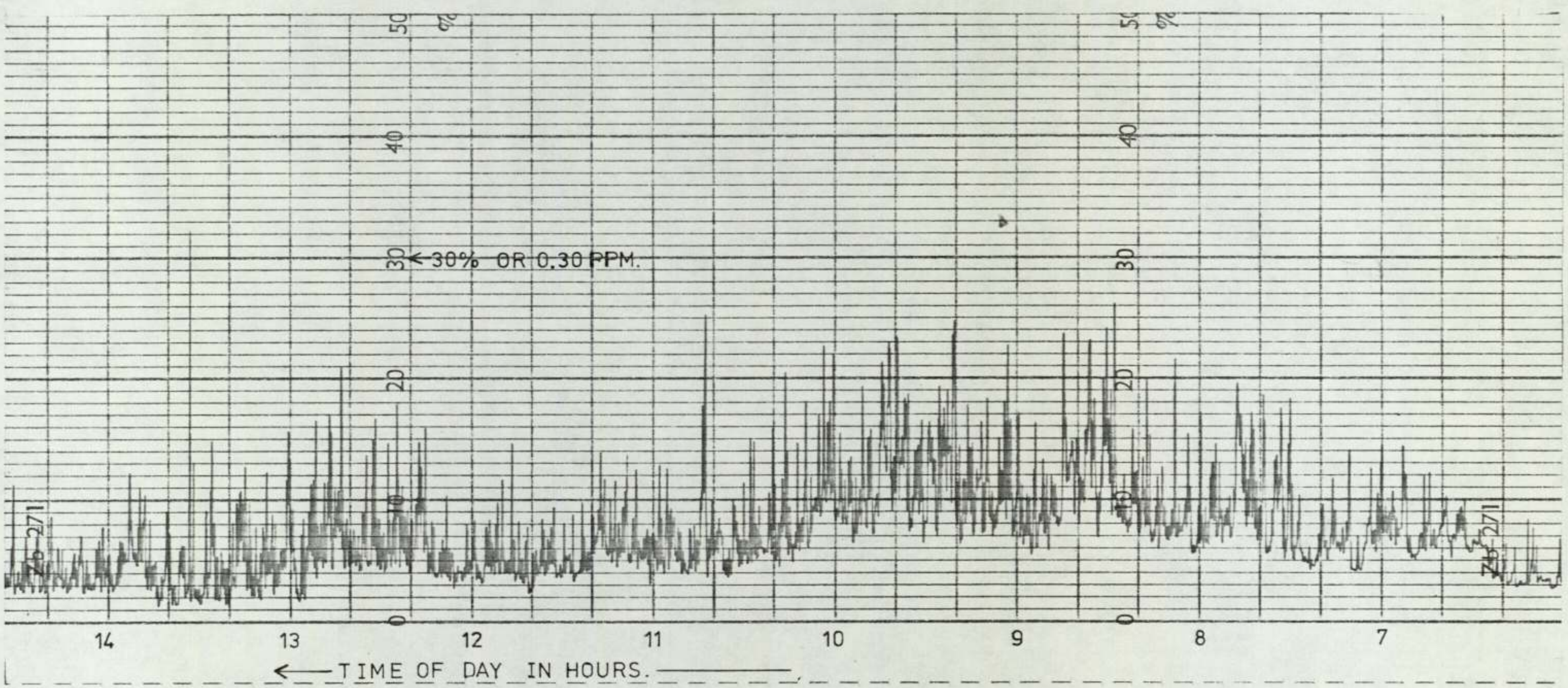

FIGURE 3.4 CHART OF NO_X AS RECORDED ON 17-03-1973 AT SALFORD CIRCUS.

CONDITIONS:- 0-1PPM FSD IS 100% ON CHART; CHART SPEED 3 cm h^{-1}, WHICH IS TOO FAST FOR ACCURATE ABSTRACTION.

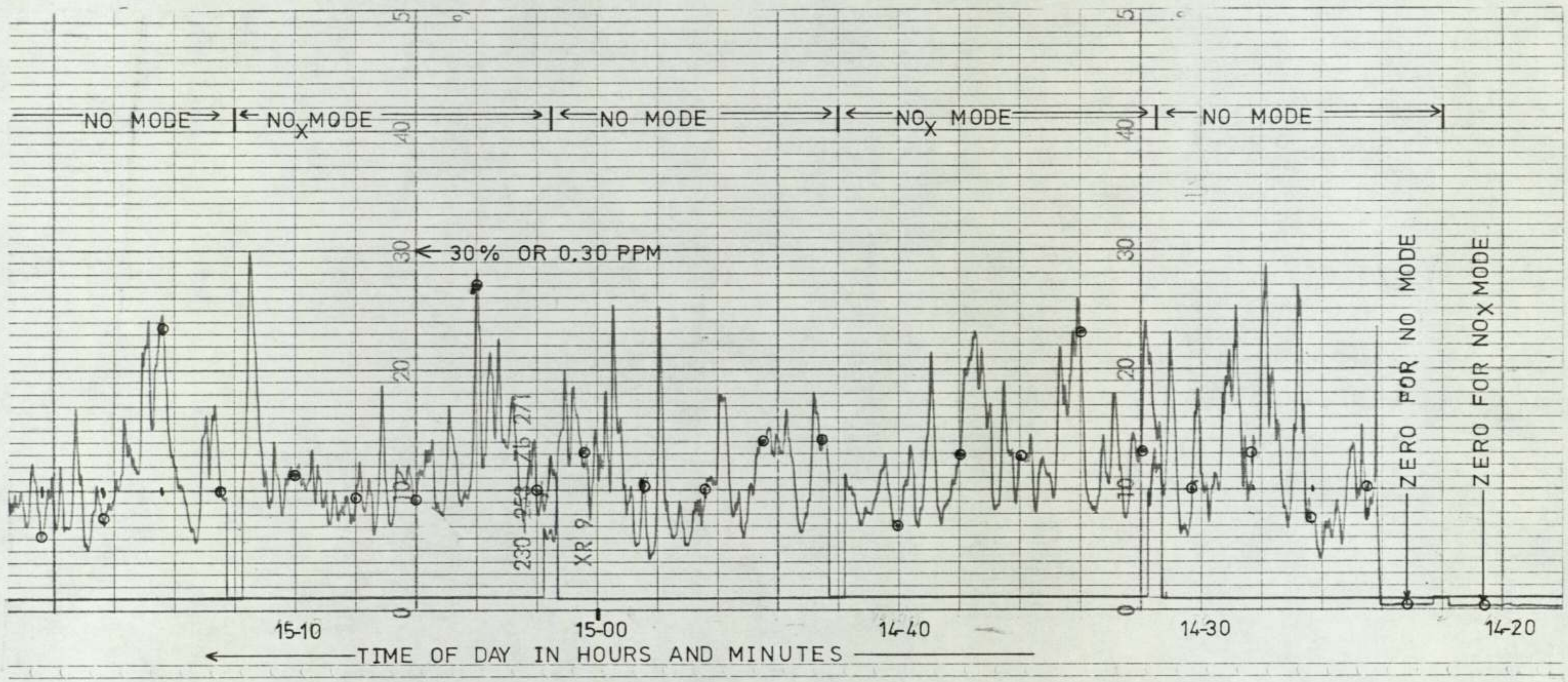

FIGURE 3.5 CHART OF NO AND NO AS RECORDED ON 04 11 1974 AT SALFORD CIRCUS.

CONDITIONS:- 0-1 PPM FSD IS 100% ON CHART; CHART SPEED 30cm h^{-1} AS USED FOR ABSTRACTION.

o SIGNIFIES ABSTRACTED POINT.

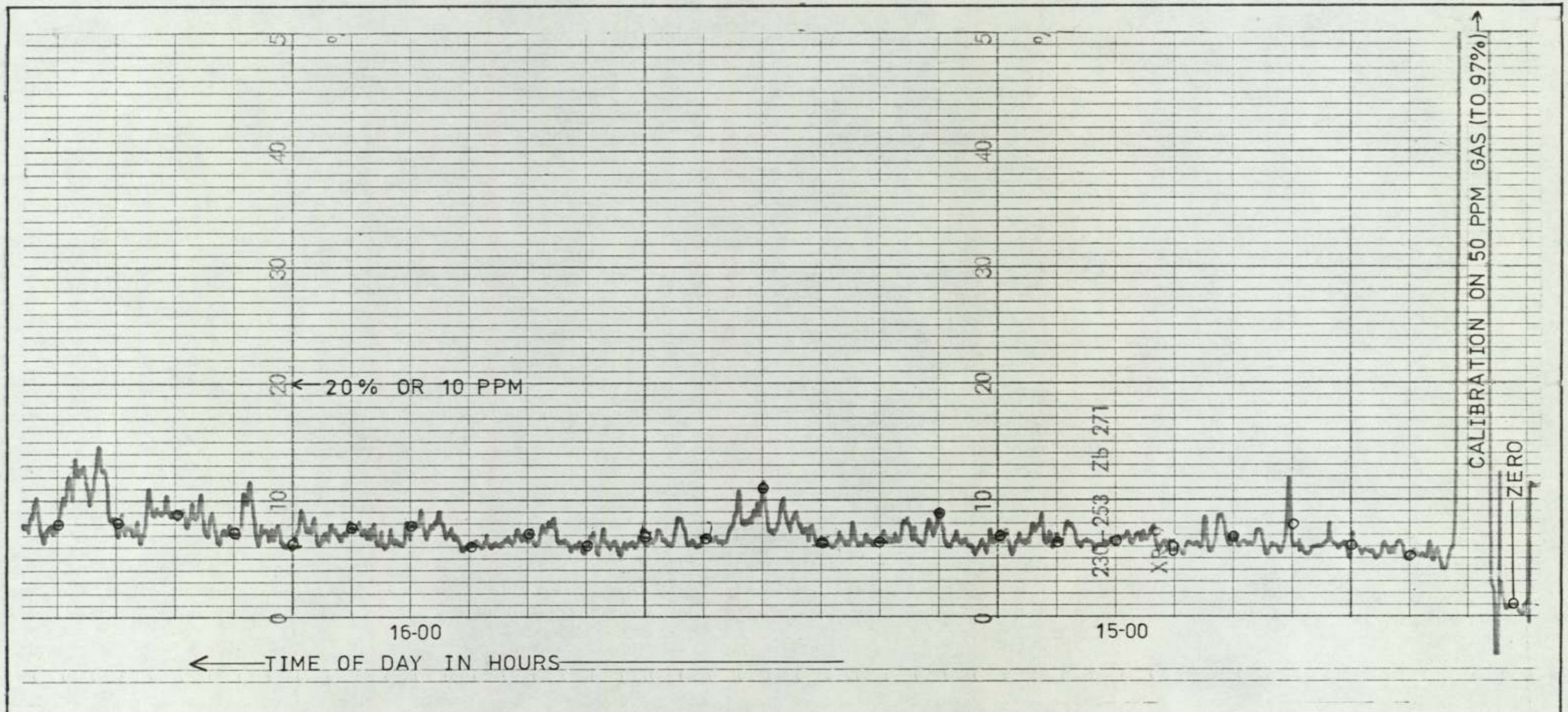

FIGURE 3.6 CHART OF CO AS RECORDED ON 04-11-1974 AT SALFORD CIRCUS.

CONDITIONS:- 0-50 PPM FSD IS 100% ON CHART; CHART SPEED 12 cm h^{-1} AS USED FOR ABSTRACTION.

o SIGNIFIES ABSTRACTED POINT.

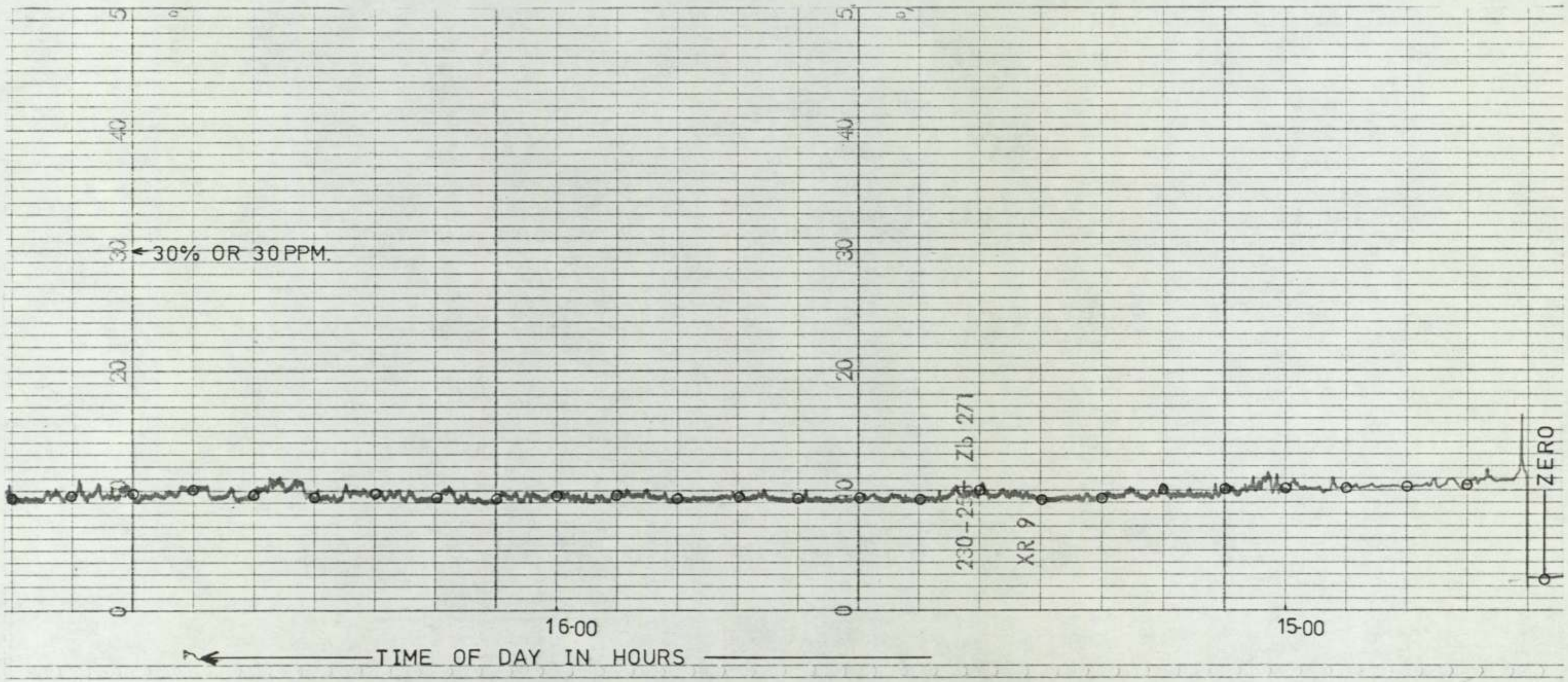

FIGURE 3.7 CHART OF HC AS RECORDED ON 04-11-1974 AT SALFORD CIRCUS.

CONDITIONS:- 0-100 PPM FSD IS 100 % ON CHART ; CHART SPEED IS 12 cm h^{-1} AS USED FOR ABSTRACTION.

o SIGNIFIES ABSTRACTED POINT.

TABLE 3.3

Fluctuations of recorded signal:

Coefficient of variation (standard-deviation ÷ mean)

of points abstracted and averaged to give hourly averages

Gas and sensitivity	NO_x 0 - 1ppm	NO 0 - 1ppm	CO 0 - 50ppm	HC 0 - 100ppm
Coefficient of Variation, %	20 - 60	20 - 60	15 - 25	<5

Data errors are bound to be present: the programme run must not be abortive due to one number being in error. The most serious error would be faulty assignment of whole arrays of data following one invalid entry. This is avoided to some extent by the somewhat lengthy card description of which the first eight columns define the observation uniquely by pollutant, zero/observation/calibration, site, hour, date, month, year, full-scale, observation points. The first two are used to define the subscripts of the arrays, and the time information is used for card sorting and sequence checking. This reduces the number of errors from a faulty data point since array-subscript overflow or a time sequence error will be spotted.

The zero-corrected and calibrated hourly-averages are required for comparisons with prediction results so are sorted into rows and output. In each hourly row is listed the site and time information followed by the levels of each pollutant as hourly averages. For convenience in data processing the traffic counts from Salford Circus are input, sorted and printed along with the pollutant levels.

A fuller description is given in Appendix 1, and example output in Figure 3.9 (details of the input are less important: Figure A1.1 in Appendix 1).

3.5 Use of the Instruments and Programme

We have shown how the instruments were operated and explained the programme used to process the results (Flow Chart: Figure 3.8). Charts were brought back from site and labelled in Greenwich Mean Time. It was necessary to check zeroes for excessive noise or drift, and the charts for timing errors due to power failures. Abstraction was then made. The data were run in sets of forty eight hours (programme maximum was fifty) and the output stored in the ICL 1904S filestore. The results tables were then edited into one file and stored as hourly means of pollutant concentrations. For one week (168 observations) about 16000 numbers would be input and the final table would have about 2000 numbers. Figure 3.9 shows example results and indicates the levels found at Salford Circus and Murdoch Point. The present work will discuss the most reliable results obtained: covering seventeen days or an output of 5000 numbers. Much data of poorer quality was recorded but rejected. In fact the very size of the data base presents a problem of time and the flexible nature of the programme was a great help when abstracting charts. The early work used very slow chart speeds (3cm h^{-1}, cf Figure 3.4): a ruler was drawn through the trace to get an eye-average for the reading. The results were of low accuracy but did indicate a dependence on traffic: Figure 3.10 shows some early results obtained this way. The results (Figure 3.9) from fast chart/programme processing are plotted in Chapter 6. The fast chart speed demanded a programme to ease the work of abstraction but made it feasible to discuss the results in a more sophisticated manner (Chapter 6). There is a problem in this type of project of balancing time for monitoring with that for interpretation. The observed hourly mean concentrations (Figure 3.9) were compared with calculated values so are discussed later (Chapter 6).

FIGURE 3.8 OUTLINE FLOWCHART OF PROGRAMME CHART50 TO AVERAGE, CALIBRATE, ZERO-CORRECT AND SORT ROUTINE-MONITORING CHART-DATA

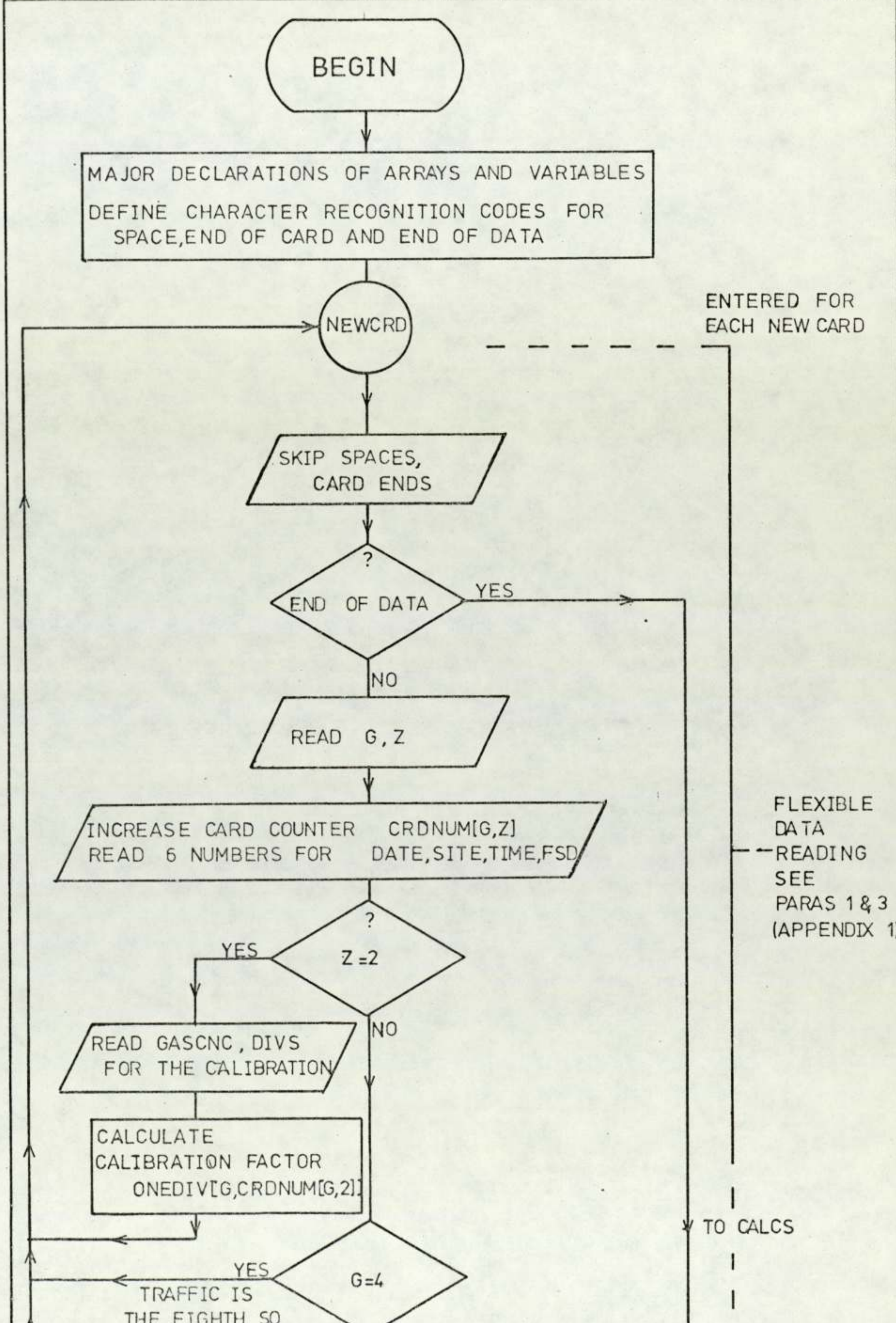

(CONTINUED ON NEXT 7 PAGES)

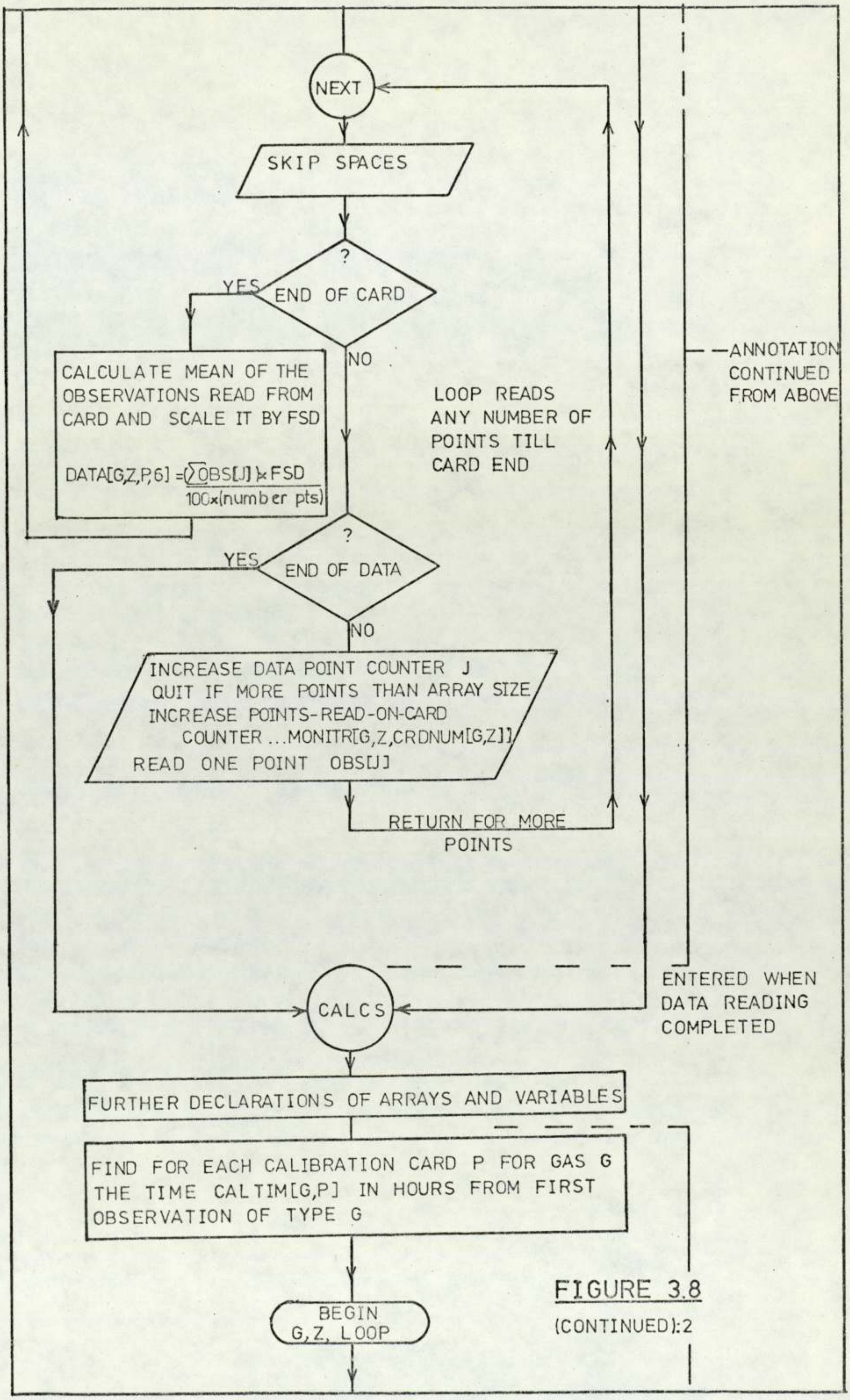

FIGURE 3.8

(CONTINUED):2

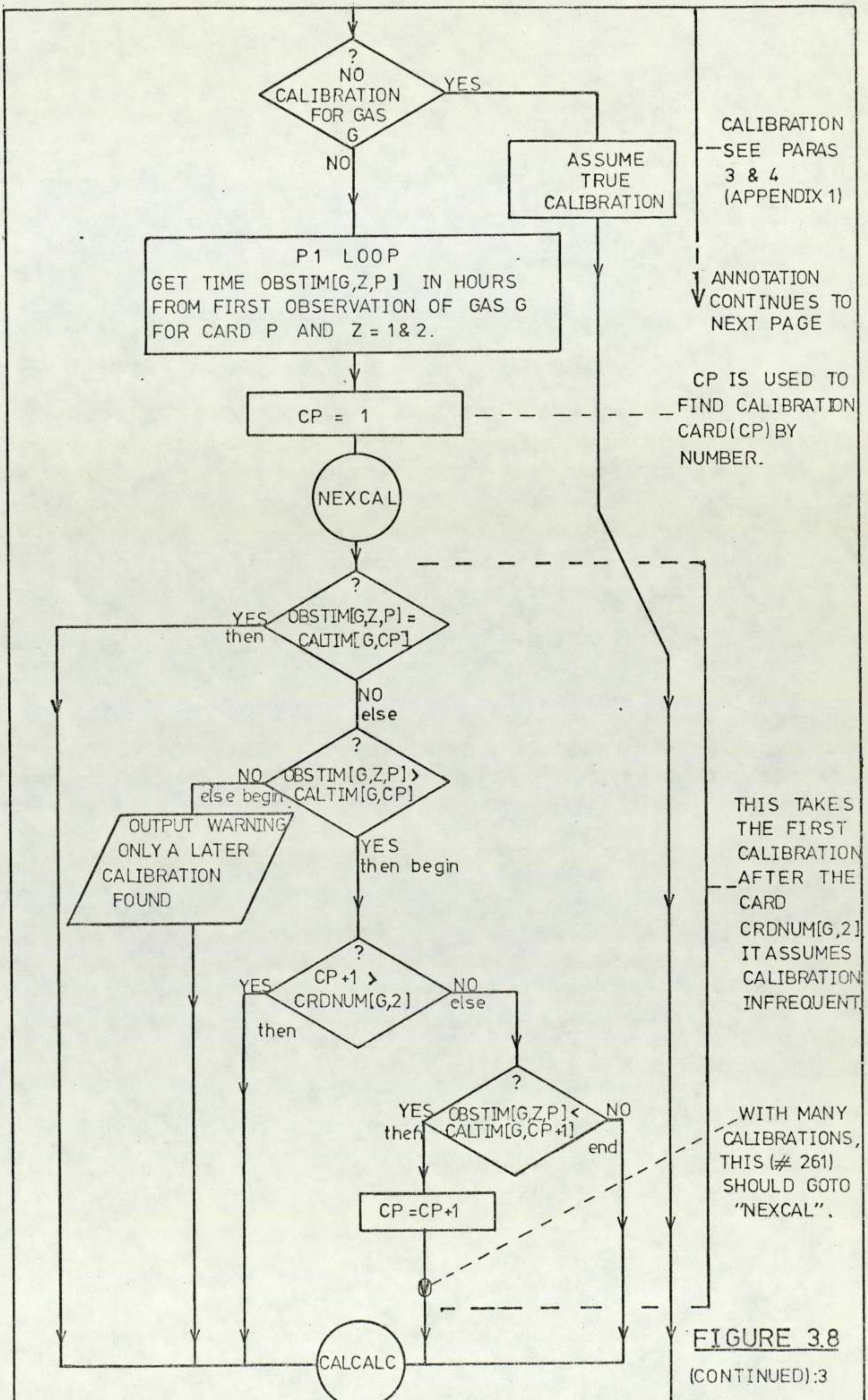

FIGURE 3.8

(CONTINUED):3

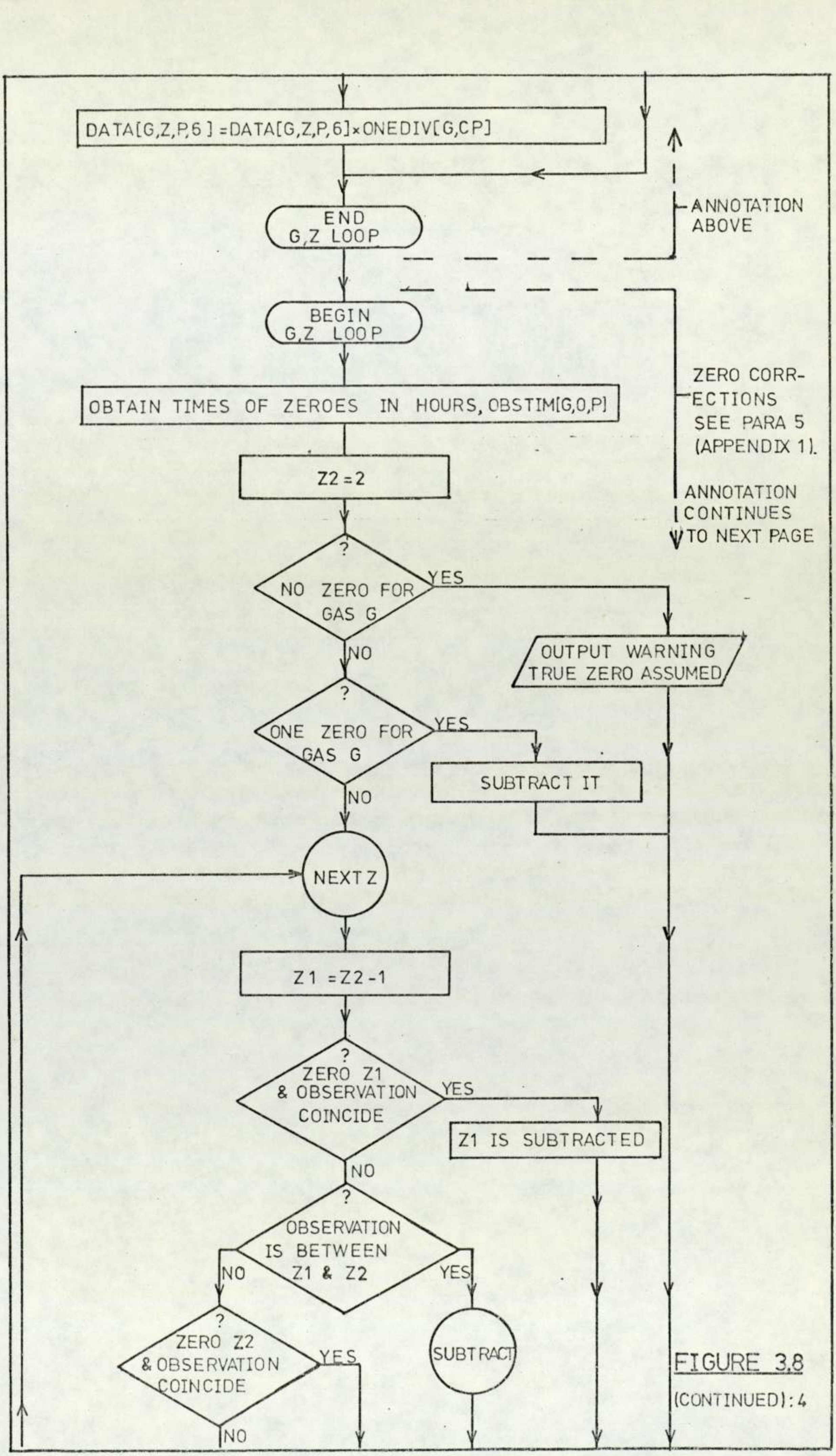

FIGURE 3.8

(CONTINUED): 4

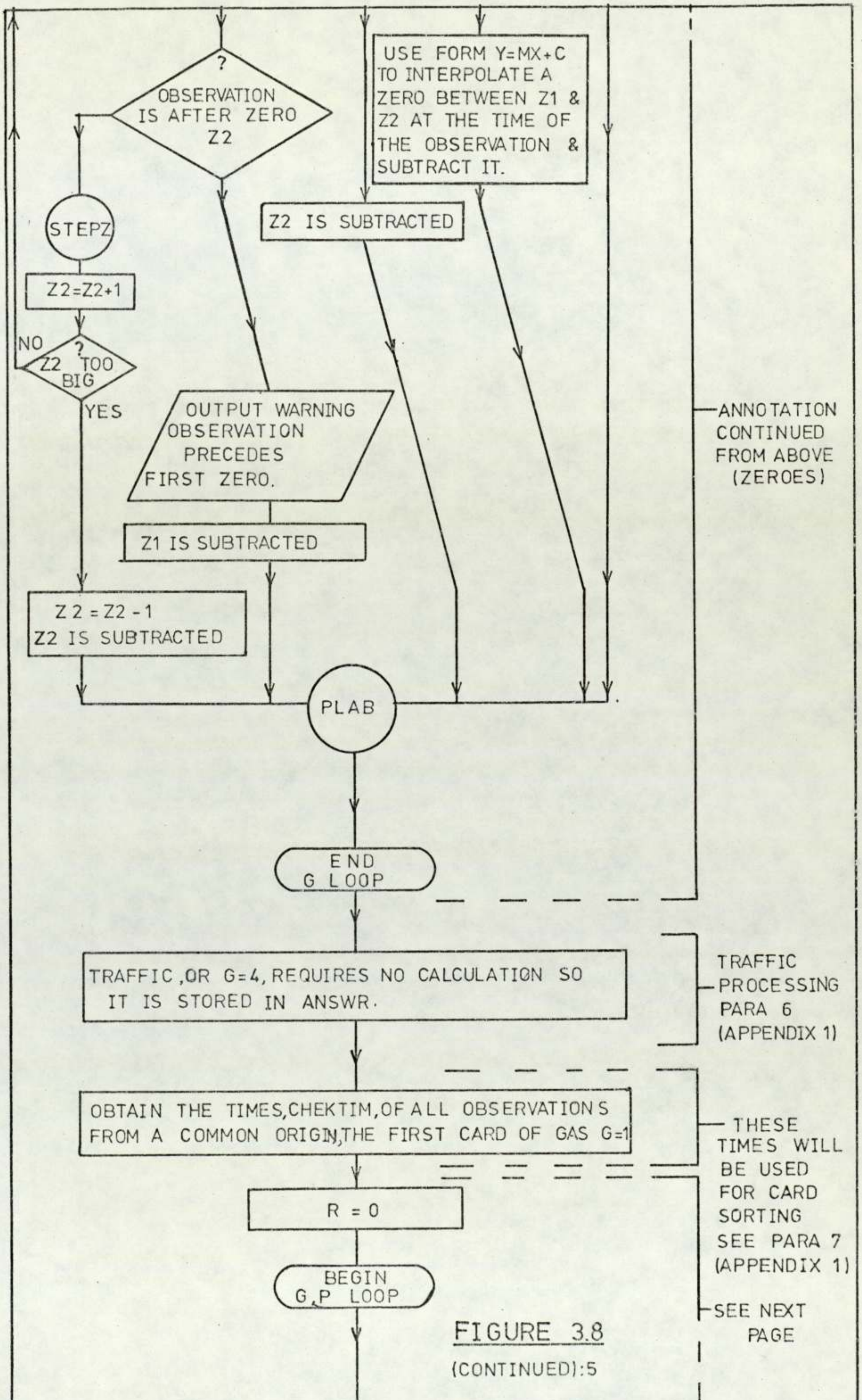

FIGURE 3.8

(CONTINUED):5

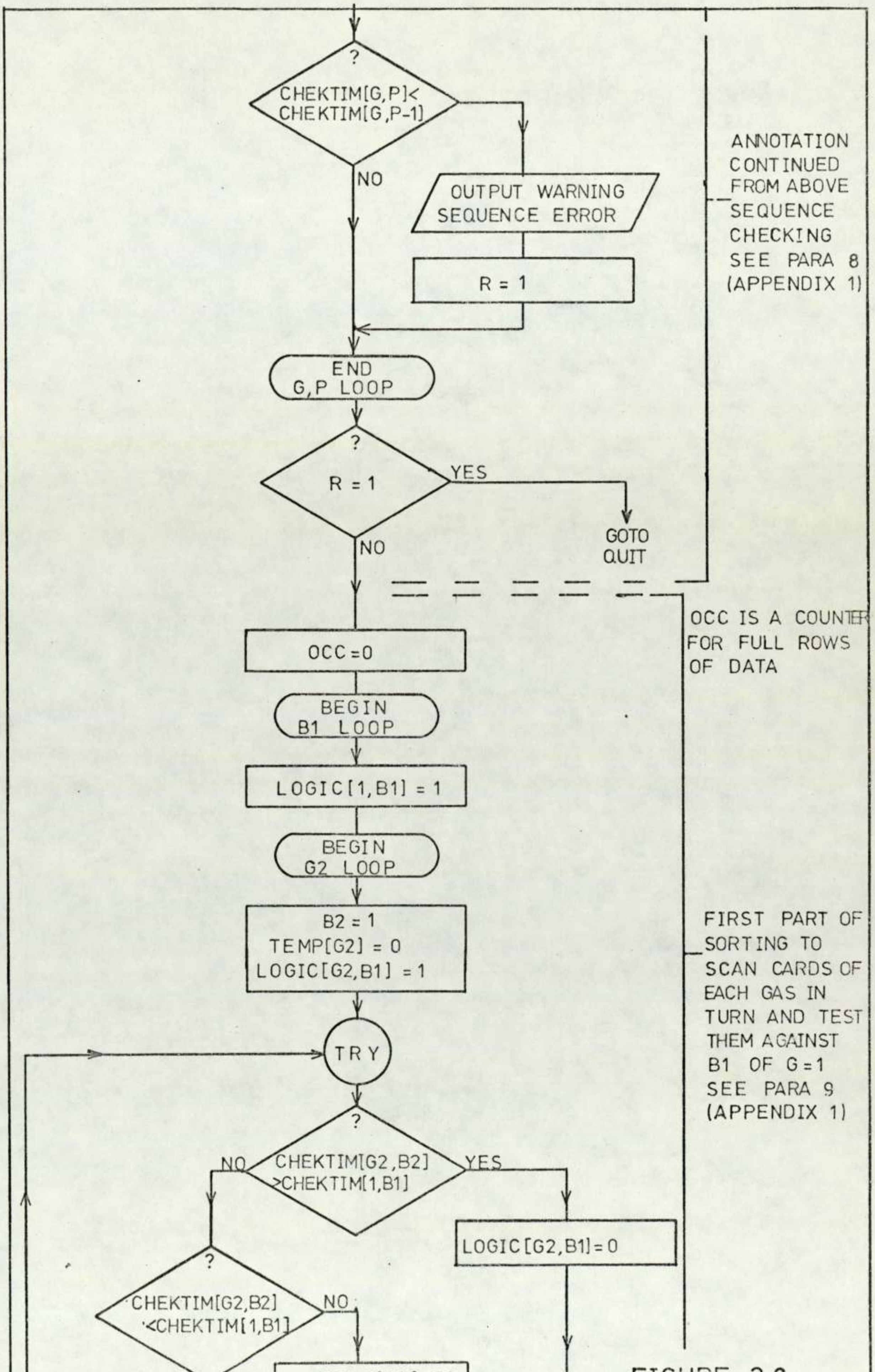

FIGURE 3.8

(CONTINUED): 6

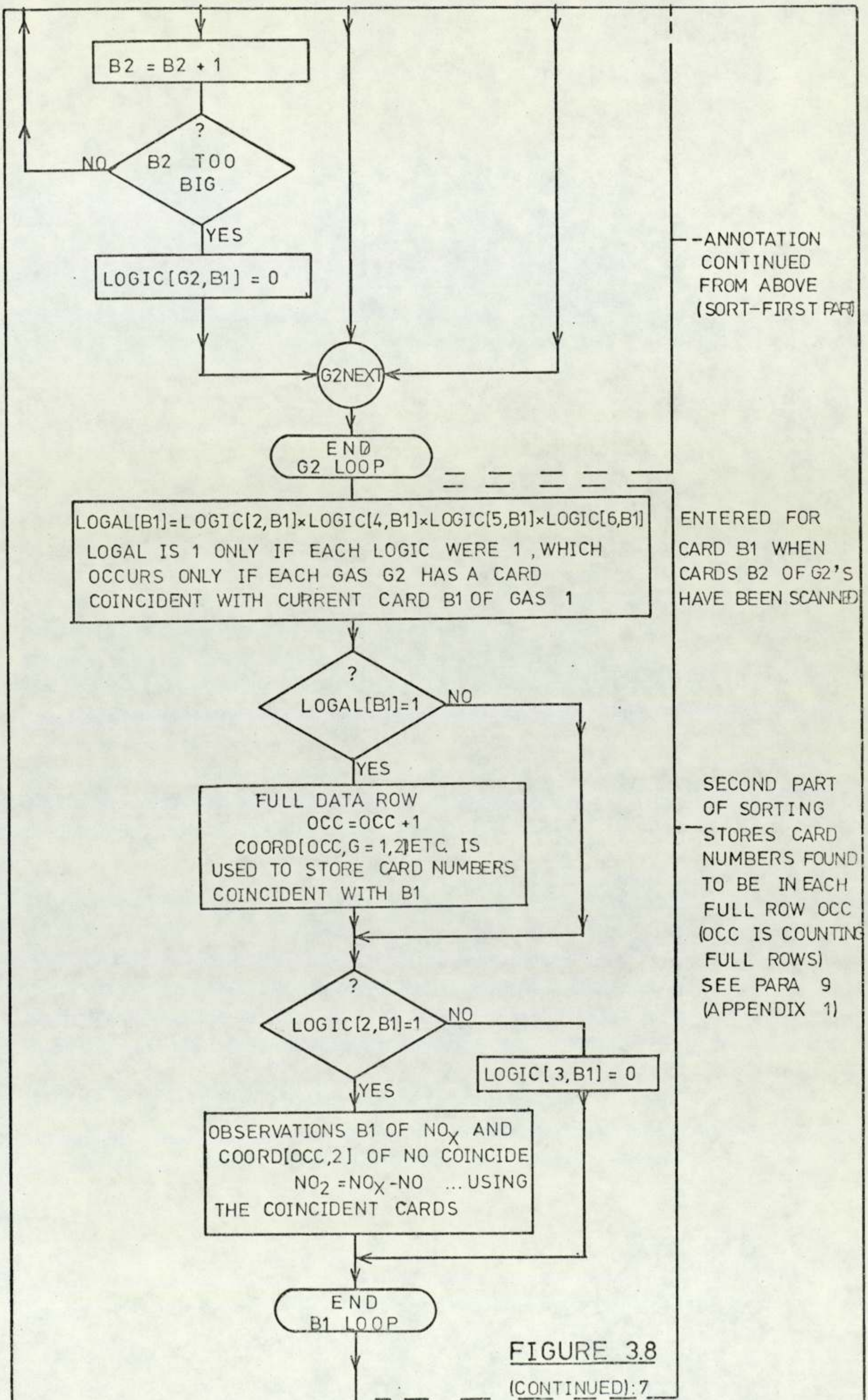

FIGURE 3.8

(CONTINUED): 7

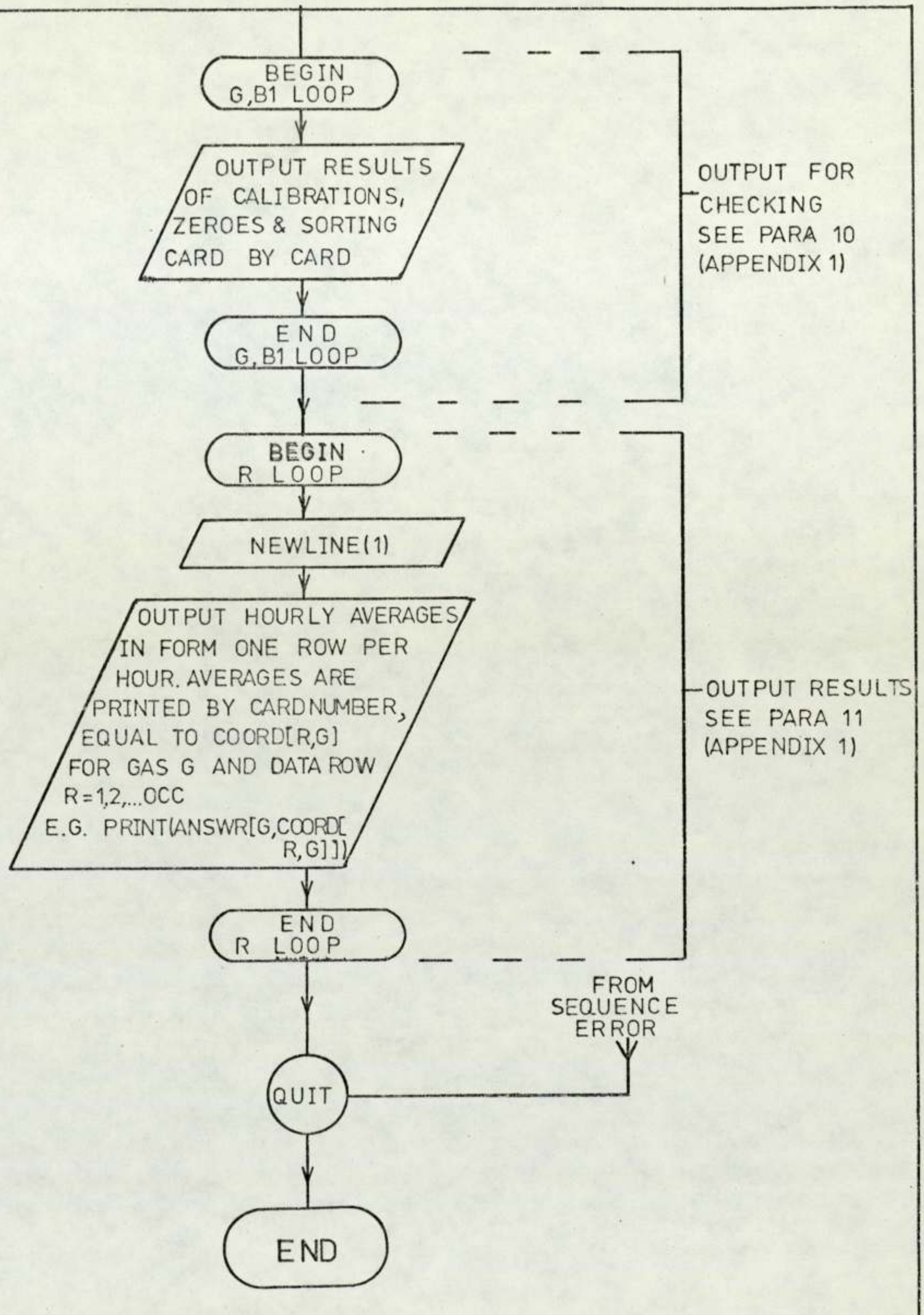

FIGURE 3.8

(CONTINUED-LAST PAGE):8

DOCUMENT [illegible]

ONLY A LATER CALIB FOUND FOR GAS 1 OF OBSN TYPE 0 CALIB CARD NO WAS 1 OBSN CARD NO WAS 1
THE NEXT CALIBN WAS USED
ONLY A LATER CALIB FOUND FOR GAS 2 OF OBSN TYPE 0 CALIB CARD NO WAS 1 OBSN CARD NO WAS 1
THE NEXT CALIBN WAS USED

DATA MEANS AND CHEKTIM

G	Z	SITE	HR	DY	MT	YR	DATAJ5	ANSWR	CHEKTIM
1	1	8	16	14	3	74	0.044	0.039	0
1	1	8	17	14	3	74	0.044	0.040	1

PROGRAM RUNNING COMMENTS

COINCIDENCE RESULTS

G	Z	CARDNO	SITE	HOUR	DAY	MONTH	YEAR	ANSWR	CHEKTIM	COINC NOX CRDNO	NOX TIME
		29									
1	1	1	8	16	14	3	74	0.039	0	1	0
1	1	2	8	17	14	3	74	0.040	1	2	1
1	1	3.	8	18	14	3	74	0.055	2	3	2
1	1	4	8	19	14	3	74	0.056	3	4	3

RESULTS OF CHART ABSTRACTION

SITE 8:-MURDOCH POINT.

YEAR	SITE	HOUR	DAY	MONTH	NITROX	NITICO	NITDIO	TRAFIC	CMONOX	HYDROC
74	8	16	14	3	0.039	0.011	0.028	2301	1.0	6.2
74	8	17	14	3	0.040	0.010	0.030	3358	1.1	6.1
74	8	18	14	3	0.055	0.020	0.035	3556	1.5	6.1
74	8	19	14	3	0.056	0.019	0.037	2225	1.6	6.5
74	8	20	14	3	0.049	0.015	0.034	1546	1.5	6.4
74	8	21	14	3	0.046	0.012	0.034	1268	1.4	6.6
74	8	22	14	3	0.046	0.012	0.034	1167	1.4	6.4
74	8	23	14	3	0.037	0.009	0.028	912	1.0	6.0
74	8	24	14	3	0.036	0.010	0.026	684	1.0	6.0
74	8	1	15	3	0.028	0.007	0.021	373	0.9	5.7
74	8	2	15	3	0.023	0.006	0.017	156	1.0	5.5
74	8	3	15	3	0.019	0.006	0.013	120	1.0	5.3
74	8	4	15	3	0.017	0.005	0.012	75	1.0	5.1
74	8	5	15	3	0.016	0.006	0.010	82	1.0	5.1
74	8	6	15	3	0.018	0.005	0.012	379	1.0	5.0
74	8	7	15	3	0.021	0.006	0.015	1041	1.0	4.9
74	8	8	15	3	0.035	0.012	0.023	2603	1.2	6.2
74	8	9	15	3	0.040	0.014	0.026	2749	1.5	5.4
74	8	10	15	3	0.039	0.017	0.022	2364	1.4	6.4
74	8	11	15	3	0.037	0.014	0.023	2072	1.4	5.6
74	8	12	15	3	0.037	0.013	0.023	2130	1.4	5.5
74	8	17	15	3	0.043	0.022	0.021	3563	2.0	5.9
74	8	18	15	3	0.041	0.013	0.027	3423	2.0	5.6
74	8	19	15	3	0.037	0.015	0.022	2111	1.5	5.5
74	8	20	15	3	0.022	0.007	0.015	1531	1.4	5.3
74	8	21	15	3	0.021	0.006	0.015	1472	1.2	5.7
74	8	22	15	3	0.019	0.006	0.014	1209	1.2	5.5
74	8	23	15	3	0.023	0.005	0.018	1058	1.2	5.6
74	8	24	15	3	0.017	0.005	0.012	578	1.1	5.5

DOCUMENT MEAS1174

SITE 4 :-SALFORD CIRCUS

74	4	13	4	11	0.105	0.108	0.001	2321	3.1	5.8
74	4	14	4	11	0.130	0.122	0.008	2555	3.3	5.9
74	4	16	4	11	0.160	0.126	0.034	2251	3.5	5.7
74	4	17	4	11	0.169	0.142	0.026	3370	3.9	7.0
74	4	18	4	11	0.149	0.135	0.013	3411	3.8	6.7
74	4	19	4	11	0.142	0.153	-0.010	2073	3.2	5.5
74	4	20	4	11	0.131	0.098	0.032	1413	3.4	5.5
74	4	21	4	11	0.114	0.075	0.039	1103	3.0	5.5
74	4	22	4	11	0.102	0.090	0.013	1044	3.3	5.7
74	4	23	4	11	0.080	0.087	-0.007	658	2.5	6.5
74	4	24	4	11	0.089	0.073	0.016	534	2.9	6.5
74	4	1	5	11	0.060	0.043	0.017	276	2.3	6.3
74	4	2	5	11	0.042	0.031	0.011	135	1.9	5.2
74	4	3	5	11	0.050	0.027	0.023	106	1.6	5.2
74	4	4	5	11	0.080	0.053	0.012	53	1.8	5.5
74	4	5	5	11	0.083	0.083	-0.005	78	2.1	5.9
74	4	6	5	11	0.123	0.097	0.026	550	2.2	5.9
74	4	7	5	11	0.193	0.208	-0.015	1036	3.3	7.7
74	4	8	5	11	0.556	0.653	-0.076	2821	10.5	12.1
74	4	9	5	11	0.571	0.573	-0.005	2791	12.1	11.9
74	4	10	5	11	0.340	0.427	-0.037	2324	5.1	9.3
74	4	11	5	11	0.321	0.314	0.005	2101	4.4	8.0
74	4	12	5	11	0.210	0.168	0.042	2144	3.0	7.2
74	4	13	5	11	0.210	0.265	-0.053	2252	3.0	7.1
74	4	14	5	11	0.203	0.179	0.024	2345	3.1	5.5
74	4	15	5	11	0.246	0.216	0.030	2274	2.9	6.6
74	4	16	5	11	0.212	0.195	0.017	2324	2.5	5.7
74	4	17	5	11	0.291	0.322	-0.031	3339	4.5	7.8
74	4	18	5	11	0.306	0.270	0.037	3304	4.8	8.5
74	4	19	5	11	0.257	0.200	0.057	2031	4.0	7.9
74	4	20	5	11	0.165	0.131	0.033	1353	3.0	7.4
74	4	21	5	11	0.133	0.078	0.040	1127	3.0	7.3
74	4	22	5	11	0.129	0.088	0.041	1075	3.0	7.1
74	4	23	5	11	0.114	0.083	0.031	955	2.9	7.1
74	4	24	5	11	0.047	0.051	0.045	[illegible]	2.5	[illegible]

FIGURE 3.9

HOURLY AVERAGES OF ROUTINE MONITORING AS OUTPUT BY CHART50.

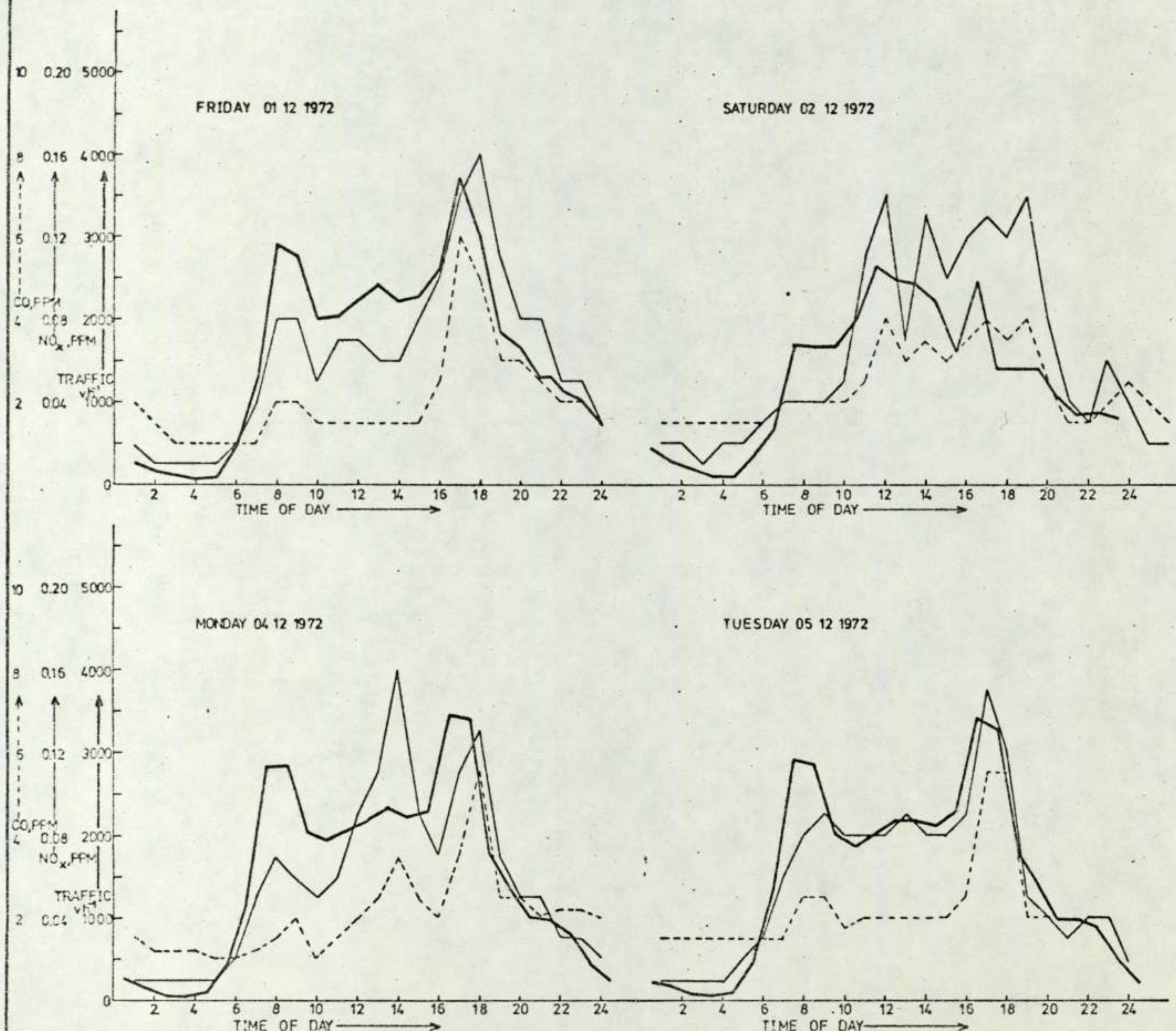

FIGURE 3.10 NO AND CO CONCENTRATIONS RECORDED AT SALFORD CIRCUS BY EYE-AVERAGING OF THE CHART RECORD (3 cm h^{-1}), TOGETHER WITH TRAFFIC ON THE ROUNDABOUT.

(CONTINUED ON NEXT PAGE)

KEY:- ——— TRAFFIC ENTERING SALFORD CIRCUS (vh^{-1})
——— NO_X IN PPM.
- - - - CO IN PPM.

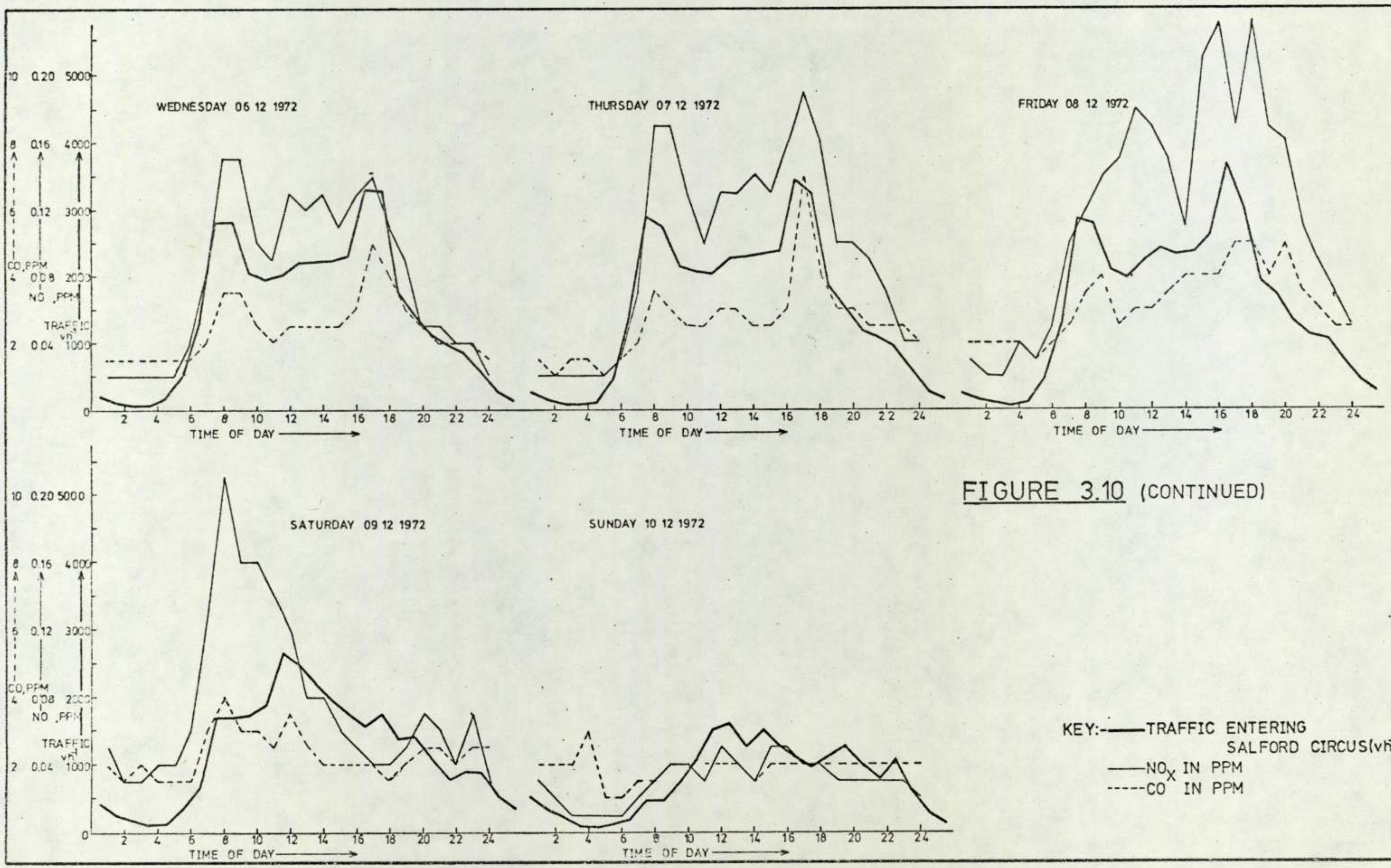

FIGURE 3.10 (CONTINUED)

3.6 Precision and Accuracy of Monitored Results

The hourly mean concentrations are averages of between twelve and fifteen points read from a fluctuating record. The average therefore lacks precision. The effect of the averaging of a finite sample from the hour may be described statistically - the readings are samples from a non-stationary random process (cf Bendat and Piersol, 1966) and have an uncertainty due to the finite number of points. Theoretical aspects of this uncertainty were not considered: in Table 3.3 we summarise the coefficients of variation for some hourly averages. They indicate a large range of signal values. Between twelve and fifteen points were used in a compromise between precision and the amount of chart and work required. This implies in Figures 3.5, 3.6, 3.7 that one point was read at each centimetre of chart.

There was in addition to signal fluctuation an uncertainty due to zero drift (Table 3.2): the effects of this were minimised by the method of operation and by interpolation of zeroes by the programme when subtracting the zero from the recorded average.

Finally each data set is consistent within itself as regards calibration, since the instruments were checked on commercial mixtures, but the data set as a whole may have error in absolute calibration (Chapter 2). We summarise these points in Figure 3.11. With automated data abstraction (e.g. data logger), the limitations on sample size are probably less severe and the effect of signal fluctuation may be considered more fully.

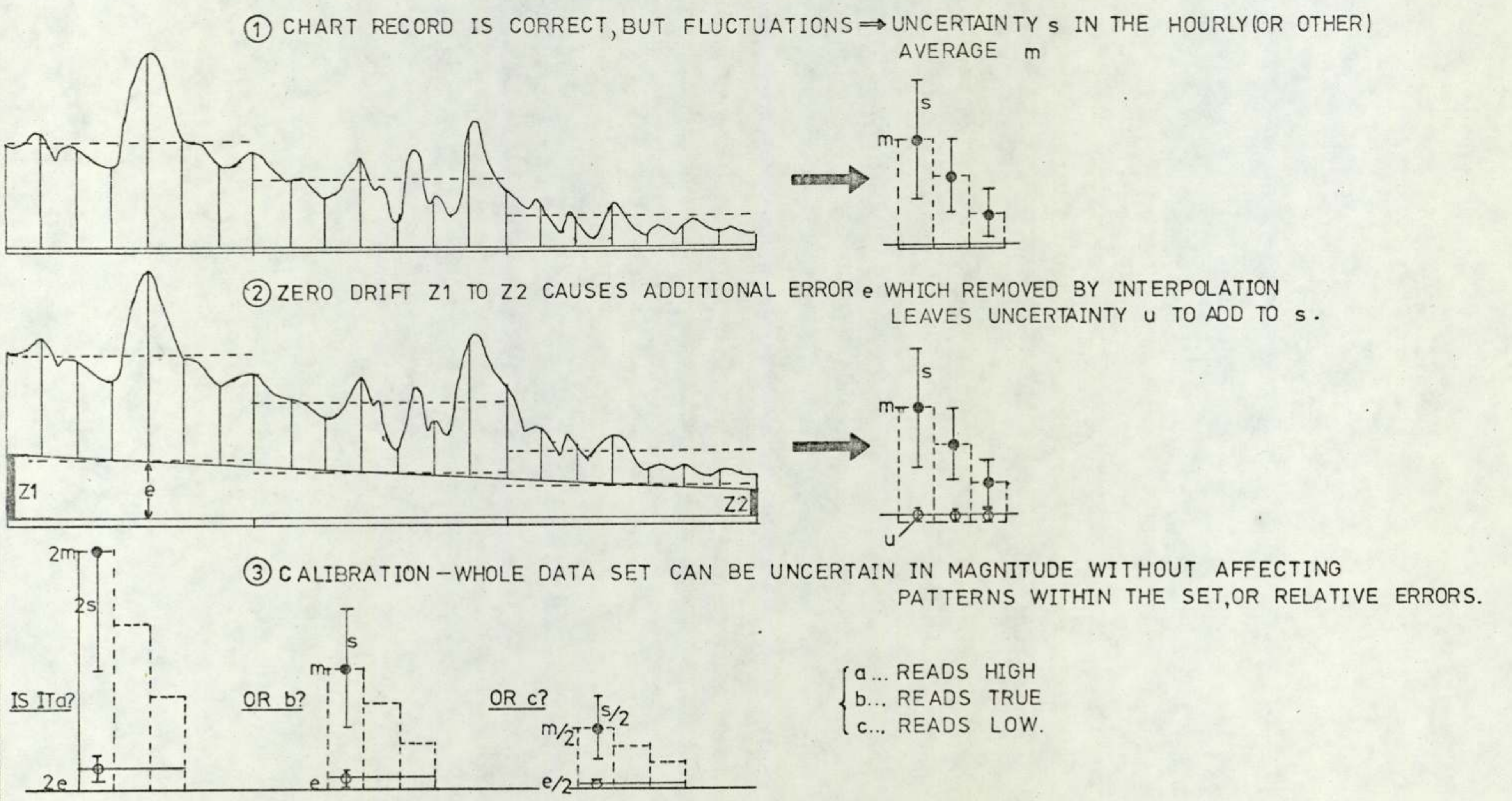

FIGURE 3.11 ERRORS OF ROUTINE MONITORING.

3.7 Summary

The instruments were left operating at permanent sites, enabling other tasks to be performed at the same time. This did mean the choice of distance as a parameter for study was restricted. The levels fluctuated rapidly: as many points as practicable were abstracted to be averaged into hourly means, corrected for calibration and zero drift and stored for later comparison with emissions-based calculations. Typical levels are shown in Figure 3.9, but more detailed discussion follows in Chapter 6.

CHAPTER 4

TRAFFIC COUNTS

The project aimed particularly at assessing the influence of traffic on air quality near the intersection and therefore fairly extensive traffic counts were required. In the present chapter we describe the traffic counting and the principles of the computer programmes used to calculate traffic flows. We estimate the errors associated with the traffic flows. In later chapters we use the traffic flows to help understand the pollutant levels as recorded.

4.1 Traffic Count for the Roundabout (Salford Circus)

The Streeter-Amet equipment has detectors on each entrance to the roundabout (Map: Figure 4.1). The count, summed for an hour, and the time are printed on paper tape. The numbers were abstracted by hand on to coding sheets for card-punching. The counts were hourly traffic flows (without further calculation) for vehicles entering the roundabout; subdivision into journeys around the roundabout was not possible so the flows on each feeder road were not separately available.

4.2 Traffic Count for the Intersection and Motorway

4.2.1 Principle

Sub-surface loops set in the various lanes of the intersection have electrical pulses induced as vehicles pass over them. The loops are

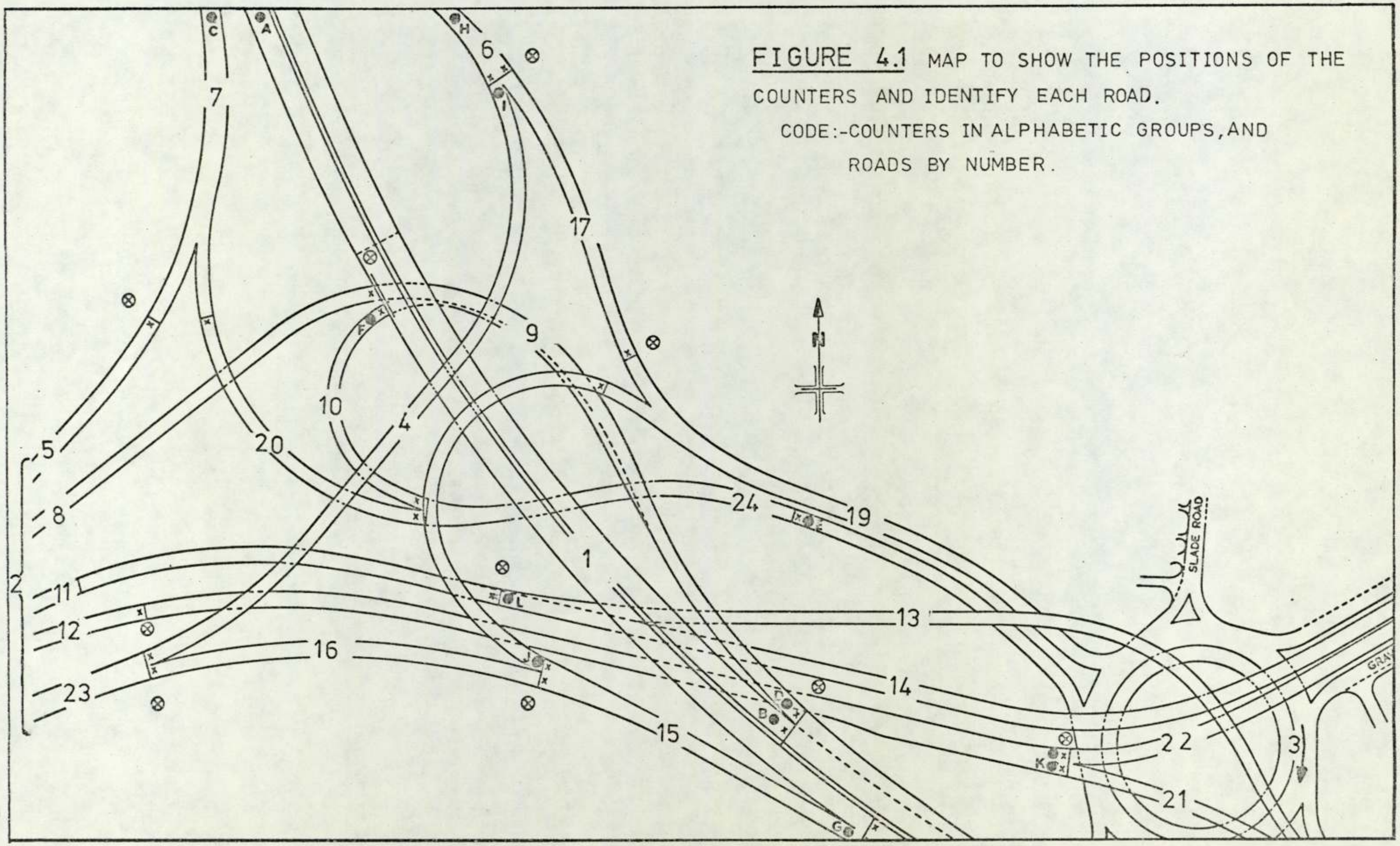

FIGURE 4.1 MAP TO SHOW THE POSITIONS OF THE COUNTERS AND IDENTIFY EACH ROAD.
CODE:-COUNTERS IN ALPHABETIC GROUPS, AND ROADS BY NUMBER.

used by the Motorway Control Police as a flow indicator. For the present project equipment was installed at the Motorway Control Centre (Perry Barr) to monitor twenty eight loops. The loops are in groups identified alphabetically on the map (Figure 4.1). Pulses are summed continuously on electromechanical counters. A camera photographs the array of counters and the face of a continuously running clock at regular intervals: an interval timer creates the period between photographs. Possible periods range from minutes to hours. The traffic-flow is the elapsed count divided by the period.

4.2.2 Drift of Photograph Times

The camera-timer operates by resetting itself at the end of each period. Unfortunately the small, variable errors in the reset accumulate so that the timing drifts away from that desired: hourly-counts photographs can be on the half hours. The clock-face included in the photograph has the exact time at which the photograph was taken, so the traffic counts are recorded over a known period of approximately one hour.

The traffic-flow has a drifting time which bears no simple relationship with on-the-hour measurements made in the rest of the work. This point will reappear in the discussion of errors.

4.2.3 Maintenance: Missing Values

Pulses from the loops are frequency-coded and sent by land-line to the counter at Perry Barr. It was difficult to keep all counters operating simultaneously: the system was sometimes disturbed by engineers working on other equipment. Often at least one counter was not working so missing values exist as a potential data loss, or as an error source if a substitute value is interpolated.

4.2.4 Calibration

The sub-surface loops were installed before the white road-markings; the two do not always coincide exactly. This, together with the variable lane discipline of drivers, means that the counters tend to read high. The closed-circuit television used for surveillance of the intersection by the police was pointed at each lane in turn and a visual count of vehicles was recorded for comparison with the counter value. This gave a set of factors to correct the results from each alphabetic group of counters (Appendices 2, 3).

4.3 Computer Programmes to Calculate Intersection Traffic-Flows

4.3.1 General Requirements

The photograph times are available as year, month, day, day-type (Monday = 1, Tuesday = 2, ... Sunday = 7), hours and minutes. The counts, possibly including missing values, are six-digit cumulative sums. The flow over any loop is the difference between the sums, or counter readings, on the first and second of any pair of photographs, divided by the period. The counter may pass zero during this period.

We require traffic-flows on the various roads of the intersection. A separate listing for the major roads M6 and A38(M) is useful. The flows should run from the hour to the next hour; the time is denoted by the hour ending the period.

Hourly counts are expensive in film and time, and suffer noticeably from timer drift, so twelve-hourly photographs were taken for much of the work. The programme should estimate hourly flows from twelve-hourly ones, using the hourly pattern of traffic-flow.

Four programmes (Table 4.1) were developed in response to these requirements.

4.3.2 Principles of the Traffic Programmes

The programmes perform differing calculations on a common theme so are described together. Fuller details are given in Appendix 2.

Data are read and missing values recognised. The counts are cumulative so the number of vehicles that passed during the time between two adjacent photographs is the difference between the two counts (with allowance for a counter passing zero). If either of the two counter readings is missing this subtraction is not possible: the traffic that passed is interpolated. We suppose that the distribution of traffic over the intersection is constant. Then the relative contributions of each counter to the total of the counters in each row are constant. These relative contributions are RJ [J] for the Jth counter.

From counts C [J] of traffic passing between photographs, $RJ[J] = (C[J]) / (\sum_{J=1}^{28} C[J])$. These RJ [J] were stored in the

TABLE 4.1

Programmes to Process Traffic-Counts

for the Intersection

PROGRAMME	INPUT	OUTPUT
TRRLINTR	Abstracted photographs Including missing values	Counter differences Calibrated counter differences Estimates of missing values M6, A38(M) flows as total and per hour
TRRLRATGEN	Abstracted photographs No missing values	Counter differences Calibrated counter differences M6, A38(M) flows as total and per hour Ratios RJ J of each counter contribution to total count: used in other programmes
TRRLRØFLØ	Abstracted photographs Including missing values Number of roads	Counter differences Calibrated counter differences Estimates of missing values Flows per hour
TRRLBØX	Abstracted photographs Including missing values Number of roads Standard matrix	Counter differences Calibrated counter differences Estimates of missing values Mean flows per hour Interpolated flows per hour

programme as parameters of the counters. In any row where a counter is missing, RJ [J] is summed for those counters which are available. This sum is SIGMAR [I] and it represents what fraction the available counters make to the total twenty eight counter count that would exist were all the counters present. If the full count (i.e. from all twenty eight counters) is T then the total of those counts which are available is

RØWSUM [I] = SIGMAR [I] .T

Thus T is calculated. The missing value would have contributed a fraction RJ [J] to T: the missing elapsed traffic-flow is therefore RJ [J] *T .

The counters tend to read high because of driver lane discipline, so the elapsed traffic is scaled by the calibration factors (Section 4.2.4).

The traffic passing along a given road is counted by several counters: in some cases the flow is only available as the difference between say that entering a road common to two roads and that leaving by a side road. The traffic-flows are therefore printed as the appropriate combination of (calibrated) counter differences (or elapsed traffic) divided by the time period between the two photographs. The programmes produce as output the total traffic and the hourly traffic-flow for A38(M) and M6. In addition, the programme TRRLROFLO gives the hourly elapsed traffic for all roads in the intersection. This used the road labelling of Figure 4.1 and two procedures to set up the complex set of counter combinations required. Figure 4.2

gives an example input. Figure 4.3 gives an example output. The programme TRRLBØX will interpolate hourly flows if the periods between the photographs exceed one hour. It uses the same two procedures as in TRRLROFLO to derive the number of vehicles which passed along each road between the photographs. The latter may have been taken say twelve hours apart: the number of vehicles which passed is subdivided into hourly flows according to the hourly traffic pattern (which reflects the rise and fall with peak periods). The pattern was obtained (using hourly photographs and TRRLROFLO) for all roads for four day-types, (Monday, Friday, Saturday, Sunday with Tuesday, Wednesday, Thursday equivalent to Monday: cf footnote to Table A3.3). Figure 4.3 shows an example for day-type 5.

From the times of the photographs, the times and day-type of each hour occurring between the two photographs are obtained: for each hour the traffic-flow is estimated as the standard count for that hour (and day-type), scaled by the ratio of how much the elapsed count exceeded the sum of those standard counts occurring at the same time (and day-type). This ratio is to allow for differences in the general level of traffic-flow between the date of the standard counts, and the date of the twelve-hour (or other) photographs.

$$\text{FLOW} = (\text{STANDARD COUNT(HOURLY)}) \times \frac{(\text{ACTUAL TWELVE-HOUR COUNT})}{(\text{SUM OF TWELVE STANDARD COUNTS OF SAME TIME, DAY-TYPE AS OCCUR BETWEEN THE TWO PHOTOGRAPHS})}$$

The interpolated flows are printed. Fuller details are given in Appendix 2.

```
DOCUMENT     TRA7974O2
28
74   9    12   4   22   59
145207   578429   981848   427128   945573
908157   797575   601449   507522   165494
711251   916566   879005   024725   198463
793106   212504   580953   245325   064242
409458   567526   377259   805997   411565
845797   924565   487910
74   9    12   4   23   57
145389   578508   981970   427410   945668
908327   797468   601461   607561   165572
711251   914508   879061   024965   198585
793106   212333   580964   255529   064362
409567   567590   377567   804671   411702
845806   924816   487911
74   9    13   5   00   55
145530   578514   982035   427577   945730
908468   797529   601462   607565   165610
711251   916519   879117   025038   198670
793106   212566   580969   255332   064435
409674   567615   377472   807724   411777
845812   924915   487924
74   9    13   5   01   53
145655   578519   982076   427619   945778
908553   797562   601462   607553   165644
711251   914522   879121   025089   198723
793106   212561   580975   255366   064475
409729   567452   377527   809225   411835
845817   924975   487927
74   9    13   5   02   50
145769   578525   982117   427631   945827
908724   797589   601462   607560   165659
711251   914535   879135   025137   198749
793106   212576   580977   255336   064497
409758   567449   377555   810959   411870
845820   925013   487932
74   9    13   5   03   46
145865   578525   982145   427642   945837
908849   797505   601462   607560   165676
711251   916540   879144   025122   198768
793106   212416   580961   255337   064505
409778   567450   377575   810137   411885
845820   925045   487934
74   9    13   5   04   45
145999   578526   982167   427661   945854
909002   797549   601465   607566   165699
711251   914567   879164   025151   198798
793106   212430   580964   255339   064553
409810   567450   377605   810179   411872
845824   925079   487937
74   9    13   5   05   43
146113   578527   982218   427487   945889
909206   797701   601467   607575   165730
711251   914559   879188   025228   198867
793106   212441   580992   255358   064583
409824   567471   377577   810219   411907
845833   925117   487941
74   9    13   5   06   41
146340   578537   982326   427578   945956
909508   797949   601465   507595   165783
711251   914557   879259   025557   198994
793106   212444   581000   255540   064688
410019   567537   377805   810562   411934
845861   925225   487947
74   9    13   5   07   39
146714   578597   982655   427949   946128
909983   794242   601591   507517   165961
711251   915599   879525   025931   199530
793106   212517   581050   255547   065055
410595   567517   378504   810913   412046
845935   925584   487962
74   9    13   5   08   37
147348   578974   983302   424540   946466
910490   795376   601895   607757   165257
711251   914951   880761   027159   200771
793106   213157   581114   255600   065608
412005   569757   379755   811732   412258
846023   925812   488115
74   9    13   5   09   14
147933   579433   984038   427973   945640
910960   799542   602185   607967   166556
711251   917225   881741   025976   201673
793105   213972   581200   255447   066076
413003   567972   380754   812471   412535
846114   927755   488245
```

NUMBER OF PHOTOGRAPHS.

CARD NUMBERING (READ BUT NOT USED)

FIRST PHOTOGRAPH

TAKEN IN 1974, SEPTEMBER, 13, DAYTYPE 5 (FRI), AT 00-55.

COUNTER READINGS ARE CUMULATIVE

BETWEEN 04-46 & 05-43 34 VEHICLES WERE REGISTERED.

FIGURE 4.2 FORMAT OF TRAFFIC-COUNTS FOR INPUT TO THE TRAFFIC PROGRAMMES.

1974	9	13	FRI	0	55	3	5	1				
379	700			56	196		99	121	75	35	75	
305	164	155		155	10		-2	43	12	55	196	
92	92	54		0								
1974	9	13	FRI	1	53	4	5	2				
300	455			9	125		62	76	48	35	48	
235	109	117		117	3		-0	53	3	56	125	
55	55	9		0								
1974	9	13	FRI	2	50	5	5	3				
297	340			15	89		36	62	26	27	26	
168	50	84		84	13		8	21	5	26	89	
30	30	25		0								
1974	9	13	FRI	3	48	6	5	4				
261	154			12	41		33	24	16	6	16	
75	34	38		38	4		2	21	2	23	41	
17	17	14		0								
1974	9	13	FRI	4	46	7	5	5				
331	195			21	63		35	34	29	23	29	
44	59	22		22	6		3	14	3	17	63	
35	35	25		0								
1974	9	13	FRI	5	43	8	5	6				
385	339			30	127		56	38	68	36	68	
52	135	25		26	11		7	26	4	30	127	
78	78	37		0								
1974	9	13	FRI	6	41	9	5	7				
753	705			54	276		123	144	132	61	132	
157	287	78		78	7		2	68	6	74	276	
143	143	55		0								
1974	9	13	FRI	7	39	10	5	8				
1395	2832			289	1031		590	306	524	251	524	
610	1157	305		305	22		8	301	14	313	1031	
383	383	297		0								
1974	9	13	FRI	8	37	11	5	9				
2854	6037			1217	2185		1016	976	1209	432	1209	
949	2395	475		475	230		87	-201	143	-57	2185	
1197	1197	1304		0								
1974	9	13	FRI	9	34	12	5	10				
2939	5453			999	1956		2308	1062	894	434	894	
952	1890	475		476	248		126	1310	122	1432	1956	
945	945	1125		0								
1974	9	13	FRI	10	32	13	5	11				TIME,DATE
2398	3390			323	1272		917	867	405	354	405	ROADS 1-24
773	1010	387		387	133		62	394	72	466	1272	(EXCEPT 3)
305	305	383		0								
1974	9	13	FRI	12	29	15	5	12				
2793	3737			535	1256		942	921	336	390	336	
1019	925	310		310	106		47	407	59	466	1256	
413	413	382		0								
1974	9	13	FRI	13	26	16	5	13				
2700	3579			408	1209		618	918	291	376	291	
1095	839	548		548	100		43	210	57	267	1209	
420	420	450		0								
1974	9	13	FRI	14	25	17	5	14				
2674	3776			460	1235		1014	863	372	359	372	
1081	951	540		540	104		52	334	52	606	1235	
481	481	312		0								
1974	9	13	FRI	15	0	18	5	15				
3265	4100			473	1370		892	1028	342	451	342	
1211	881	606		506	124		56	419	68	487	1370	
440	440	529		0								
1974	9	13	FRI	16	7	19	5	16				
3600	4334			419	1525		886	1193	338	318	338	
1425	926	713		713	122		60	467	62	329	1525	
463	463	479		5								
1974	9	13	FRI	17	7	20	5	17				
4151	6805			478	2268		909	1848	420	947	420	
2505	1038	1253		1253	138		49	431	88	319	2268	
329	329	327		0								
1974	9	13	FRI	18	6	21	5	18				
4151	5405			368	2165		926	1760	386	916	386	
2525	837	1263		1253	103		39	337	64	621	2165	
429	429	406		0								
1974	9	13	FRI	19	6	22	5	19				
3318	3835			310	1115		680	816	299	385	299	
1387	888	693		493	111		70	370	41	412	1115	
444	444	379		0								
1974	9	13	FRI	20	6	23	5	20				
2779	2869			236	821		541	316	305	223	305	
952	874	476		476	110		68	305	42	347	821	
437	437	304		0								
1974	9	13	FRI	21	6	24	5	21				
1944	2325			178	633		391	364	269	143	269	
859	738	429		429	72		45	213	27	240	633	
368	358	225		0								
1974	9	13	FRI	22	5	25	5	22				
1429	1881			124	408		262	262	146	89	146	
659	475	429		429	71		32	138	19	158	408	
238	238	175		0								
1974	9	13	FRI	23	5	26	5	23				
879	1282			86	342		208	221	121	87	121	
489	355	244		244	58		37	124	21	145	342	
162	162	121		0								

FIGURE 4.3 HOURLY TRAFFIC FLOWS AS OUTPUT BY TRRLROFLO AND AS USED TO INTERLATE HOURLY FLOWS (ONLY DAYTYPE 5 SHOWN).

4.3.3 Errors in the Traffic-Flows

We now discuss the errors and attempt to combine them to assess the accuracy of the calculated traffic-flow: fuller details are given in Appendix 3.

1. The sample used to calibrate the counters is not statistically representative but allows some correction to be made. The calibration factors have probable error of say 5% (this estimate is not available directly).

2. Occasional misread or mispunched numbers may escape detection: their effect on the data-set as a whole is probably random, analagous to noise in the information.

3. Missing values as interpolated have errors whose effects vary with the counter-combination, for each road has an error if it uses the missing counter: the error is specific to the road.

4. The traffic-flows of each road are obtained from sums and differences of (inaccurate) counter differences so the errors tend to propagate. The size of the error varies with the number of operations and the sizes of terms: with n functions combined by additions and subtractions (s of them), the error appears to be $\sqrt{n}/(n - s)$ times the typical percentage error in the counter differences (Appendix 3).

5. The time drift of the photographs causes a phase error between the time of the photographs and the integer value of the time

TABLE 4.2

Summary of Errors in the Traffic-Flows

Text Reference to Paragraph in Para. 4.3.3	Process	Error	% Error
1	Correction of systematic lane discipline error	Probable error $\pm 5\%$	5
2	Abstraction of numbers	Noise -	-
3	Missing values Roads 2, 4, 17, 19, 23	Depends on road 2 + 4% 4 + 60% 17 - 40% 19 - 35% 23 + 42%	
4	Propagation by counter combinations. With addition error tends to diminish since random errors sometimes counteract.	Varies as $\sqrt{n}/(n-s)$ n counters; s subtracted. Error typically $\sim \pm 4\%$ from 5% in each counter. Roads in (3) above larger error.	4
5	Timer drift.	Mostly probable error $\sim \pm 10\%$ Friday mornings (0700, 0800) systematic ~ 30% low	10
6	Traffic pattern constant?	Error $\sim \pm 4\%$	4

TABLE 4.2

(Continued)

Summary:-	
Combining 4, 5, 6	Overall error typically ± 18%
Noting 4	Roads 2, 4, 17, 19, 23 systematic
Noting 5	Friday 07.00, 08.00 systematic

used to represent the photograph time. The effect on the traffic-flows is most serious when the traffic-flow changes rapidly with time. For the data used, the error in traffic-flow is usually $\sim \pm 10\%$, since the time drift was usually less than ten minutes from the hour. An exception occurs for the Friday morning rush-hour values of the standard counts, when the values are probably $\sim 30\%$ low.

6. The hourly interpolation relies on the reproducibility of the hourly traffic-pattern. Test data (Appendix 3) suggested that the traffic-pattern was constant to within 4%. The standard counts are therefore an inaccurate sample from a distribution of traffic patterns, so to represent the traffic pattern by these standards counts implies both a random measurement-error (Paragraphs 1 - 5) and a random error from limited sampling (the standard photographs were a limited set). The standard counts probably have error $\sim 14\%$ (Appendix 3). An interpolated count is made using perhaps a twelve-hour count and the standard counts: together the error in the interpolated flow will be $\sim 18\%$. In addition, for roads 2, 4, 17, 19, 23 the error is larger because of the missing counter 13, and on a Friday morning rush-hour the count is probably low by 30%. These points are discussed more fully in Appendix 3, and Table 4.2 summarises these discussions.

4.4 Summary

Traffic entering Salford Circus was counted precisely; the results are available without calculation. They do not give a resolution as to how the traffic is destributed over the roads to and from the roundabout.

Traffic-flows for all roads on the junction were derived as hourly and twelve-hourly counts from the combination of counter differences. Errors arose from poor lane-discipline, drift of the photograph times and missing values. The need to reduce the amount of abstraction and the problem of timer drift ruled out hourly junction-counts on a routine basis: the method of interpolation based on a sample hourly junction count has been discussed.

Estimates of traffic flow were made for all sections of the intersection (except Slade Road, Gravelly Hill, Tyburn Road and Lichfield Road). The propagation of errors has been discussed: it is suggested that the typical error in interpolated hourly counts is 18%, and extreme situations have been described where the error may be much larger. Table 4.2 presents a convenient review. Despite these errors the two counters and the programmes described here gave counts of the traffic over all roads in the intersection and in the roundabout: these in turn made feasible the pollution calculations (Chapter 6) based on emission estimates.

CHAPTER 5

DIFFUSION IN THE ATMOSPHERE

In the introduction we remarked that a major part of the work would be the measurement of pollutants around the junction. This has been described above. We now draw on the literature to show how the dilution of gases emitted into the atmosphere may be estimated numerically: we can then discuss an experiment (Chapter 7) to measure this dilution and a model (Chapter 6) to compare estimates based on emissions and dilution of the levels of pollutants with those recorded. The bulk of this Chapter reviews literature on atmospheric diffusion; the summary discusses those results actually used in the present work.

5.1 Turbulent and Molecular Diffusion

The effects of wind in transporting airborne material and of turbulence in spreading it have long been recognised (e.g. Hewson and Gill, 1944). If the material is not to alter the flow it should behave as part of the fluid: it should have a velocity coincident with the instantaneous flow-velocity at any point. Ideally it should have the same density as the fluid so that buoyancy and settling do not occur (Monin and Yaglom, 1971a).

It is hard to estimate the relative importance of turbulent and molecular diffusion in spreading material: the problem is discussed at greater length in Monin and Yaglom (1971b). They suggest eddy diffusivity is $\sim 10^5 - 10^6$ times greater than the molecular diffusivity and that for practical purposes both molecular diffusion and the interaction between turbulent and molecular diffusion may be neglected relative to turbulent diffusion (Monin and Yaglom, 1971c). This is implicit in many models of air-pollution.

5.2 Semi-empirical equation for turbulent diffusion

By analogy with diffusion from a region of high to low concentration, one can define an eddy diffusivity K so that the flux S is proportional to the gradient of mean concentration C of material in the direction X_i say.

$$\text{i.e.} \qquad S = -K \frac{\partial C}{\partial X_i} \qquad \ldots (5.1)$$

Thus a general equation may be derived for the nett transport of material in and out of a small element by turbulent diffusion and advection by a wind of speed U(Z) (in the X direction). Terms can be included for transport by settling and removal or formation by chemical reaction (Appendix 4). For advection and diffusion,

$$\frac{\partial C}{\partial t} + U(Z)\frac{\partial C}{\partial X} = K_{XX}(Z)\frac{\partial^2 C}{\partial X^2} + K_{YY}(Z)\frac{\partial^2 C}{\partial Y^2} + \frac{\partial}{\partial Z}\left(K_{ZZ}(Z)\frac{\partial C}{\partial Z}\right)$$

This equation (Semi-empirical diffusion equation, Monin and Yaglom, 1971d; K Theory or Gradient-Transfer Theory, Pasquill, 1971) assumes that the flux is proportional to the gradient of concentration. Pasquill (1970) questioned this for it implies that the diffusive spread should be over dimensions larger than all effective eddies and that diffusivity is a function only of position in the flow. Monin and Yaglom (1971e) consider that provided the diffusion time significantly exceeds the Lagrangian integral time scale (which in the atmosphere $\sim$ 1 second) the equation may be used to describe turbulent diffusion.

The semi-empirical theory is useful because it can be applied to inhomogeneous or non-stationary turbulence and because it offers a framework for formulae which frequently occur in discussions of air-pollutant plumes. It can be used for both continuous and instantaneous releases of material.

Two other theories in particular (Statistical Theory and Similarity Theory) have been developed to describe turbulent diffusion but we will not discuss them: we are primarily interested in plume formulae and their limitations. The reader will find a review of all three theories in Pasquill (1971) and in Bibbero and Young (1974).

5.3 Solutions of the Semi-empirical Equation

The semi-empirical diffusion equation (Monin and Yaglom, 1971d) describing advection and turbulent diffusion without losses of material is equation 5.2.

$$\frac{\partial C}{\partial t} + U(Z)\frac{\partial C}{\partial X} = K_{XX}(Z)\frac{\partial^2 C}{\partial X^2} + K_{YY}(Z)\frac{\partial^2 C}{\partial Y^2} + \frac{\partial}{\partial Z}\left(K_{ZZ}(Z)\frac{\partial C}{\partial Z} \right) \qquad \ldots (5.2)$$

Additional terms for losses by settling, reaction or decay can be added (Appendix 4).

To completely define the problem the coefficients U(Z), K(Z) and the boundary conditions must be specified. The boundary conditions are

<u>TABLE 5.1</u>

Analytic Solutions: U,K constant; no settling, no reaction; reflection at $z = o$; $z > o$

Point Source Instantaneous release (Monin & Yaglom, 1971, Eq. 10.89). <u>EQUATION 5.3</u>

$$C(X,Y,Z,t) = \frac{Q}{[4\pi.\Delta t]^{3/2}(K_{xx}K_{yy}K_{zz})^{\frac{1}{2}}} \exp\left(-\frac{[X - u.\Delta t]^2}{4K_{xx}.\Delta t}\right) \exp\left(-\frac{y^2}{4K_{yy}.\Delta t}\right) \left[\exp\left(-\frac{(Z - H)^2}{4K_{zz}.\Delta t}\right) + \exp\left(-\frac{(Z + H)^2}{4K_{zz}.\Delta t}\right) \right] \quad \ldots (5.3)$$

Point Source Continuous release (Monin & Yaglom, 1971, Eq. 10.90). <u>EQUATION 5.4</u>

$$C(X,Y,Z) = \frac{Q}{4\pi X(K_{yy}K_{zz})^{\frac{1}{2}}} \exp\left(-\frac{y^2 \; U}{4K_{yy}.X}\right) \left[\exp\left(-\frac{(Z - H)^2.U}{4K_{zz}.X}\right) + \exp\left(-\frac{(Z + H)^2 \; u}{4K_{zz}.X}\right) \right] \quad \ldots (5.4)$$

TABLE 5.1 (continued)

Line Source Instantaneous release (Drivas & Shair, 1974, Eq. 3) using $K_z = K_x = K$; EQUATION 5.5

$$C(X,Z,t) = \frac{Q}{2\pi K.\Delta t} \exp\left(-\frac{[X - u.\Delta t]^2}{4K.\Delta t}\right)\left[\exp\left(-\frac{(Z-H)^2}{4K.\Delta t}\right) + \exp\left(-\frac{(Z+H)^2}{4K.\Delta t}\right)\right] \quad \ldots (5.5)$$

Line Source Continuous release (Monin & Yaglom, 1971, Eq. 10.91) EQUATION 5.6

$$C(X,Z) = \frac{Q}{2(\pi K_{zz} uX)^{\frac{1}{2}}}\left[\exp\left(-\frac{(Z-H)^2 u}{4K_{zz}.X}\right) + \exp\left(-\frac{(Z+H)^2 u}{4K_{zz}.X}\right)\right] \quad \ldots (5.6)$$

Notes: Travel time Δt; Downwind distance X, Crosswind Y, Vertical Z; Source Q; Eddy diffusivities K; Source at (0,0,H); u=U=windspeed.

usually linear in concentration, having form

$$\chi \frac{\partial C}{\partial n} + \beta C = f(t)$$

for the flow bounded at n with β representing absorption. With $\beta = \infty$, absorption is complete, while $\beta = 0$ corresponds to total reflection. For a flow bounded by solid walls the boundary conditions are homogeneous: $f(t) = 0$. For a flow unbounded in any direction, $f(t) = 0$ and $\beta = \infty$, so that $C \longrightarrow 0$ as $n \longrightarrow \infty$. With instantaneous sources initial conditions on $C(\underline{X},t)$ are used ($\underline{X}$ = position): for continuously active sources the boundary conditions are inhomogeneous with $f(t) \neq 0$.

The ease of solution varies with the problem: we require some perspective on the validity of formulae common in models of air pollution (e.g. the collection of results in Turner, 1970; Bibbero and Young, 1974).

Analytical solutions are available for the case of constant wind speed U and constant diffusivities K_X and K_Y: Table 5.1 presents four results under this condition (constant U, K). The equation 5.4 will be recognised as the Gaussian continuous point source formula (Pasquill, 1961: Section 5.4 below) used to define the functions $\sigma_Z(X)$, $\sigma_Y(Z)$ in the Pasquill category scheme, provided the relationships

$$\sigma_Z = \sqrt{2K_Z t} \quad \text{and} \quad \sigma_Y = \sqrt{2K_Y t} \qquad \ldots (5.7)$$

apply. Then equation 5.4 becomes

$$C(X,Y,Z) = \frac{Q}{2\pi\sigma_Y\sigma_Z U} \exp\left(\frac{-Y^2}{2\sigma_Y^2}\right)\left[\exp\left(\frac{-(Z-H)^2}{2\sigma_Z^2}\right) + \exp\left(\frac{-(Z+H)^2}{2\sigma_Z^2}\right)\right] \ldots (5.8)$$

Experimentally however all four equations (constant U, K: Table 5.1) are unsatisfactory (Monin and Yaglom, 1971f): they do not give at large X the correct dependence of concentration on X. Presumably they are satisfactory at small X though. Monin and Yaglom (1971f) ascribe the discrepancy to the constant U and K: they suggest inclusion of wind shear.

When variable functions U(Z), K(Z) are used in the equation, analytic solution becomes difficult: numerical integration is required although integral moments give some information (Monin and Yaglom, 1971g).

Returning to the equations 5.4, 5.7, 5.8, we note that Hoffert (1972) plots σ_Y and σ_Z in the form $\sigma = \sqrt{X}$ (remember $t \simeq X/U$), showing that the latter is not as in the empirical curves for $\sigma_Z(X)$ and $\sigma_Y(X)$. This discrepancy between $\sigma_Z(X)$, $\sigma_Y(X)$ and $X^{\frac{1}{2}}$ is explained by the discussion in Monin and Yaglom (1971h) suggesting that the simple form $\sigma = \sqrt{2Kt}$ is inadequate when wind shear is included and that the functional relationship between σ, K and t depends on the type of functions U(Z), K(Z) that are assumed. (See also Section 5.6.2: Drivas and Shairs' work). Therefore it seems that the equations in Table 5.1 (constant U, K) are useful formulae provided empirical functions (Section 5.4) of $\sigma(X)$ are used.

When considering long range diffusion, one must also consider the possibility of restricted vertical diffusion. Pasquill (1961) suggested the use of a constant σ_Z when the plume reaches the ceiling. We are dealing with pollutants close to the source and so do not consider this further although it is important in city models (e.g. Johnson et al., 1971).

5.4 Estimation of Plume Standard Deviation to Downwind Distance

Two schemes have been suggested. The first relates plume widths to measured fluctuations of the wind direction (Hay and Pasquill, 1959; Pasquill, 1961) and the second, for when measured fluctuations are unavailable, defines a stability category by wind-speed and solar radiation (Pasquill, 1961); the plume geometry is then defined for each category.

5.4.1 Plume Standard Deviation from Fluctuations of Wind Direction

Hay and Pasquill (1959) assumed that the Lagrangian and Eulerian autocorrelograms were similar in shape but that their integrals decayed to the same value in times whose ratio was β . Knowing β (specified originally by short-range crosswind diffusion and later by the intensity of turbulence (Pasquill, 1971)) one could smooth the wind-fluctuation trace over a time s, such that the spread of material by turbulence could be uniquely related to the measured statistics of the turbulence. Empirical values for β are scattered but 4 is typical (Pasquill, 1961; Monin and Yaglom, 1971i).

Bivanes record vertical and horizontal wind-direction fluctuations with a good time resolution during a sampling time τ . The mean wind speed U and travel distance X are measured to obtain $s = X/\beta U$ for that sample. The traces are smoothed over a moving interval s. The standard deviations for horizontal and vertical wind-direction fluctuations, σ_θ and σ_ϕ (radians) respectively, are then calculated. The plume widths are estimated as $\sigma_Y(X) = X.\sigma_\theta$ and $\sigma_Z(X) = X.\sigma_\phi$, ... (5.9) (Hay and Pasquill, 1959; Pasquill, 1961; Pasquill 1971) for use in the continuous point-source formula (equation 5.8).

Islitzer (1961) used an elevated point-source in a tracer experiment to derive $\sigma_Y(X)$ from the plume concentrations at ground level and σ_θ from a bivane recording. He suggested $\sigma_Y(X) = 0.81.\sigma_\theta.X$, when σ_θ was smoothed over five seconds, with good correlation. With $\sigma_Y(X)$ thus determined he applied the continuity condition to the continuous point-source formula (equation 5.8) to derive $\sigma_Z(X)$. Using the downwind positions of concentration maxima as additional evidence he obtained for the plume

$$\sigma_Y(X) = \frac{1}{1.23} \sigma_\theta.X \quad \text{and} \quad \sigma_Z(X) = \frac{1}{1.23} \sigma_\phi.X$$

Leahey and Halitsky (1973) measured with bivanes the turbulence of the air in the Hudson River valley so as to study possible diffusion without using tracers: they were able to recognise the possible role of inversions in initiating katabatic winds or surges of dense air which may cause large changes in wind direction. They also studied the diurnal changes in turbulence with the break up of inversions at sunrise causing a maximum in horizontal fluctuation then, and the increase in vertical fluctuation during the day, as insolation increased. This is an interesting application of the bivane method to study turbulence as relating to diffusion in a complex site.

5.4.2 Plume Standard Deviation from Stability Categories

Mechanical turbulence arising from wind shear may be increased or decreased by the effects of buoyancy. The former depends on wind speed and surface roughness and the latter on heat transfer to the air from incoming radiation. Hoffert (1972) gives a fuller review of these aspects of stability than we have room for here. Thus the method of Pasquill (1961) as reworked by Gifford (1961) gave curves of plume standard deviation to downwind distance for a continuous point-source release (equation 5.8) in terms of six categories (Table 5.2); the categories were defined by wind speed and insolation (using time of day and cloud cover). These curves have been expressed as power law functions by Geomet (1971) as in Table 5.3 and were used in the present project.

A modified form of the Pasquill stability categories has been described by Smith (1972) and Pasquill (1974) ; a closely related scheme was obtained from M J O Dutton in Department Met 09 of the Meteorological Office as two FØRTRAN subprogrammes.

1. FUNCTIØN MST2 (Z, NCLØUD, NWIND) to derive a value of the stability index MST2 ranging from 1 to 10 for categories A,A-B, B, B-C, C, C-D, D, E, F, or G according to the incoming solar-radiation Z, mwatt cm^{-2} (assuming clear skies), cloud cover NCLOUD, oktas, and wind speed NWIND in knots. The subprogramme is based on Table 5.4. In the present project when the intermediate categories (e.g. A-B) occurred, the average of two curves (A and B) from Table 5.3 were used.

TABLE 5.2

Pasquill Stability Categories (Pasquill, 1961)

Surface wind speed (at 10m) ms^{-1}	Insolation			Night	
	Strong	Moderate	Slight	Thinly over-cast or ≥ 4/8 low cloud	≤3/8 cloud
< 2	A	A - B	B	-	-
2 - 3	A - B	B	C	E	F
3 - 5	B	B - C	C	D	E
5 - 6	C	C - D	D	D	D
> 6	C	D	D	D	D

Note: Bibbero and Young (1974) relate categories to σ_θ for a bivane trace as, approximately, (cf. Section 5.3.1)

A, 25° or 0.436 rad; B, 20° or 0.349 rad;

C, 15° or 0.262 rad; D, 10° or 0.175 rad;

E, 5° or 0.0873 rad; F, 2.5° or 0.0436 rad.

TABLE 5.3

Power Law Functions for Plume Parameters σ_z and σ_y (Geomet, 1971)

Class		σ_y [1]	σ_z [2]							
Geomet	MST2 [3]	a_y	a_x	b_x	$X < X_1$ X_1	a_x	b_x	$X_1 < X < X_2$ X_2	a_x	b_x
A	(1)	0.40	0.125	1.03	250	0.00883	1.51	500	0.000226	2.10
B	(3)	0.295	0.119	0.986	1000	0.0579	1.09	10000	0.0579	1.09
C	(5)	0.200	0.111	0.911	1000	0.111	0.911	10000	0.111	0.911
D	(7)	0.130	0.105	0.827	1000	0.392	0.636	10000	0.948	0.540
E	(8)	0.098	0.100	0.778	1000	0.373	0.587	10000	2.85	0.366

Note 1: $\sigma_y(X) = a_y(X^{0.903})$

Note 2: $\sigma_z(X) = a_x(X^{b_x})$

Note 3: Index MST2 as used in present work

TABLE 5.4

Modified Pasquill Categories: Stability Index MST2 used in present work (Chapter 6)

Wind Speed, kt	Daytime (excluding 1h after sunrise, 1h before sunset) Incoming solar radiation (mW cm^{-2})				Within 1h of sunset or sunrise	Night time[1] Cloud amount (oktas)		
	Strong ≥ 60	Moderate 30-60	Slight ≤ 30	Overcast		0 - 3	4 - 7	8
<4	A	A - B	B	C	D	F or G	F	D
4-6	A - B	B	C	C	D	F	E	D
6-10	B	B - C	C	C	D	E	D	D
10-12	C	C - D	D	D	D	D	D	D
>12	C	D	D	D	D	D	D	D

Note 1: Night was originally defined to include periods of one hour before sunset and after sunrise. These two hours are always categorised here as D.

Note 2: See over.

TABLE 5.4 (continued)

Note 2: Pasquill (1961) said that in light winds on clear nights the vertical spread may be less than for category F, but excluded such cases because the surface plume is unlikely to have any definable travel. They are important from the point of view of the build up of pollution and category G (night time, 0 or 1 okta of cloud, windspeed 0 or 1 kt) was added when coding to derive MST2 was written at the Meteorological Office. Present project used the coding supplied, but (Chapter 6) when MST2 was returned with a value of 8, 9 or 10, for E, F or G respectively, category E (Table 5.3) was used. No calculation was made for zero windspeed.

2. FUNCTIØN SØLR2(NNTIME, NNDAY, NMØNTH, NLAT) to estimate incoming solar radiation Z for clear skies from ten years of data gathered at Cambridge; the subprogramme incorporates a correction for latitude so that it can be applied over latitudes 48N to 60N. SØLR2 is a function of time of day, NNTIME (Greenwich Mean Time; hours and tenths), day of month NNDAY, month NMØNTH and latitude NLAT (degrees and tenths). Figure 5.1 shows the radiation contours from which Z is interpolated; Table 5.5 shows the allowance made in SØLR2 for cloud cover.

Other modified category schemes have been published but these are tied up with studies of urban influences on diffusion as discussed in the next Section.

5.5 Diffusion over Urban Areas

The above descriptions of plume behaviour stem from the open-country predictions for continuous emissions (Pasquill, 1961). Extrapolation to urban areas has been made for convenience in predictions of urban pollution although the surface roughness and thermal properties are different for city and country.

Pasquill (1970) discussed heat-island effects in some detail; he suggested that when predicting air pollution over any terrain two meteorological conditions can be considered:

1. When geostrophic winds exceed 5 ms^{-1}, the airflow is well defined

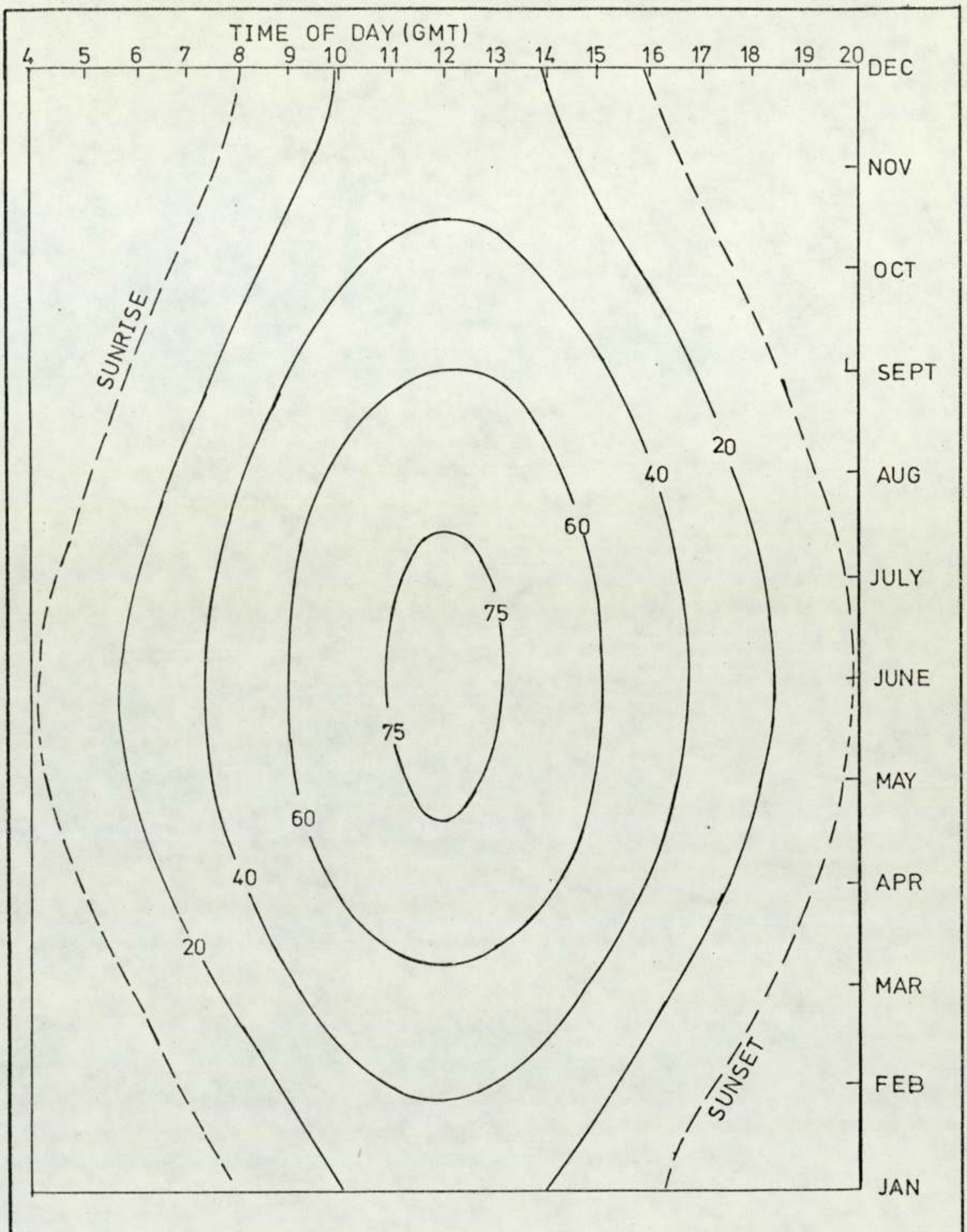

FIGURE 5.1 INCOMING SOLAR RADIATION IN MILLIWATTS PER CM^2 REACHING THE GROUND ON A CLOUDLESS DAY, AS A FUNCTION OF TIME OF DAY AND MONTH. TABLE 5.5 SHOWS CORRECTION FACTORS FOR CLOUDY CONDITIONS. (Information supplied with the punched cards for Functions SOLR2 & MST2 – see Section 5.3.2).
THIS FIGURE IS BASED ON CAMBRIDGE DATA:- FUNCTION SOLR2 HAS A CORRECTION FOR LATITUDE, EXTENDING IT OVER 48N TO 60N.

TABLE 5.5

Reduction of Incoming Solar Radiation by Cloud

Cloud Amount (oktas)	Fraction to Multiply I.S.R.[1]
0	1.07
1	0.89
2	0.81
3	0.76
4	0.72
5	0.67
6	0.59
7	0.45
8	0.23

Note 1: I.S.R. is Incoming Solar Radiation:

See Figure 5.1

and the open-country method can be extended to the city.

2. When light winds occur the flow is not subject to large-scale control.

Comparisons of urban and country diffusion were made by Pooler (1966), McElroy (1969) using tracers in St Louis, United States of America. They measured wind movements with anenometers, bivanes and a radar-tracked tetroon; the tracer plume was sampled at ground-level to give $\sigma_Y(X)$. The continuity equation applied to the continuous point-source formula gave $\sigma_Z(X)$. Indirect (Pasquill type) and direct (gustiness; wind-direction fluctuations from bivanes with conditions of vertical stability by temperature) indices of turbulence were compared with $\sigma_Y(X)$ and $\sigma_Z(X)$ for the tracer plume. These city $\sigma_Y(X)$ and $\sigma_Z(X)$ were similar to the Pasquill curves for open-country provided an initial plume-size similar to that of buildings was used: Pooler (1966) suggested an extra 80m to $\sigma_Y(0)$ and 30m to $\sigma_Z(0)$. Dispersion could be described by the common indices (cf. Pasquill type) although the most detailed one using directional-fluctuations (cf. bivane method of Section 5.4.1) σ_θ and vertical stability (Ri or Richardson number) were the best. Either travel distance, X, or travel time, t, can be used to define the plume: $\sigma_Y(X)$ was better than $\sigma_Y(t)$ while $\sigma_Z(X)$ was comparable to $\sigma_Z(t)$ (this depended on whether it was day or night).

The urban area increased the initial crosswind dispersion though this converged to open-country results at greater distances. Vertical dispersion was significantly enhanced, particularly in stable conditions. Restrictive layers aloft sometimes significantly affected the vertical dispersion and concentrations near the ground.

Following this urban tracer-work, Johnson et al. (1971) found a surface-based inversion often occurred in mornings with low wind-speeds, yet the Pasquill type scheme predicted moderately unstable weather conditions: they suggested an additional time classification (Table 5.6) for early morning and late afternoon cases. They allowed for the enhanced vertical diffusion in the city by an initially finite plume size of σ_Z = 10m at X = 50m for all stabilities. A comparison of initial plume sizes to allow for local roughness is given in Table 5.7.

In view of Pasquill's remarks as to the predictability of air-flow (weather condition 1), we note that Johnson et al. (1971) proposed a helical circulation in street canyons as a function of wind-speed above roof-level. It has been suggested (Calder, 1970) that puff models which follow the trajectories of individual puffs of gas may be useful in calm conditions (where a continuous Gaussian "plume" is undefined) or where local flow effects are important. Such models are more complex (see, for example, Chapters Six and Ten in Stern, 1970); no further discussion will be presented here.

5.6 Line-Source Result for Idealised Road

We have seen above that the continuous point-source (Gaussian) formula, with constant U and K, (equations 5.4, 5.7 and 5.8). conveniently defines plume behaviour when empirical curves for $\sigma_Z(X)$

TABLE 5.6

Alternative Scheme for Stability Index[3] allowing for early morning and late afternoon cases (Given as Table 12 by Johnson et al., 1971)

Surface winds (Knots)	Daytime (SR[1] + 4 hours to SS[1] 3 hours)			Early morning and late afternoon (SR + 1 to SR + 3 and SS - 2 to SS - 1)	Night time SS to SR	
	Strong Insolation	Moderate Insolation	Slight Insolation		⩾5/10 cloud[2]	⩽4/10 cloud[2]
⩽3	1	2	2	4	5	5
3 - 6	1	2	3	4	4	5
6 - 10	2	3	3	4	4	4
10 - 12	3	3	4	4	4	4
⩾13	3	4	4	4	4	4

Note 1: SR = sunrise, SS = sunset

Note 2: Cloud in tenths ...... American publication

Note 3: Johnson et al., (1971) use five stability classes 1 to 5

TABLE 5.7

Estimates of Initial Plume Size

		Initial Size	Reference
Urban Diffusion	Add 80m to σ_y Add 30m to σ_z	σ_y = 80m, σ_z = 30m (all stabilities)	Pooler (1966)
Urban Diffusion	(1) Add 50-60m to σ_y Add 20-30m to σ_z (2) $\sigma_z(0)$ = BH/2.15 $\sigma_y(0)$ = BL/4.3	σ_y = 50-60m, σ_z = 20-30m (all stabilities) Varies with topography BH = Building Height BL = Building Length	McElroy (1969)
Urban Diffusion[1]	Curves for $\sigma_z = ax^b$ Cross at X = 50m	All stabilities σ_z = 10m for $0 \leqslant X \leqslant 50$m	Johnson et al. (1971)
Vehicle Wake[2] (used in present work)	$\sigma_y = 0.13X^{0.903}$ $\sigma_z = a(X+c)^b$ with c = 27m	Neutral stability σ_z = 1.5m at X = 0	Calder (1973)

Note 1: Model extended to include a streets submodel - a more detailed approach to topography than use of an initial plume size (Johnson et al., 1971).

Note 2: Has disadvantage: varies with stability class - see Section 6.2.4, Paragraph 1.

and $\sigma_Y(X)$ are used. We draw on this background to consider the concentration from a road: an integral of the continuous-source Gaussian-plume for a long straight road (Calder, 1973), and a tracer study of SF_6 released from a vehicle travelling crosswind (Drivas and Shair, 1974).

5.6.1 Integral of Continuous-Source Gaussian-Plume Formula Along a Road

Calder (1973) draws on the classic result for an infinite line source to predict the concentration distribution at various wind angles for small enough distances that the road may be regarded as infinitely long. He defines axes as in Figure 5.2, and a general function

$$Cp = Qp.\emptyset\ (x,y) \qquad \ldots (5.10)$$

to define the concentration Cp at the point x, y for a point-source of constant strength Qp at the origin, with a dilution function in general form $\emptyset(x,y)$. With x, x_o, y, t, θ defined in Figure 5.2, we have $x = x_o + t\sin\theta$ and $y = t\cos\theta$. The integral of the point-source concentration along the infinite line parallel to the road (i.e. along BB^1) is

$$D\ (\theta,x_o) = \int_{-\infty}^{+\infty} Qp.\emptyset\ (x_o + t\sin\theta,\ t\cos\theta)\ dt \qquad \ldots (5.11)$$

If the plume is not too wide, the crosswind gradient of concentration is greater than the downwind gradient: over the traverse BB^1 through

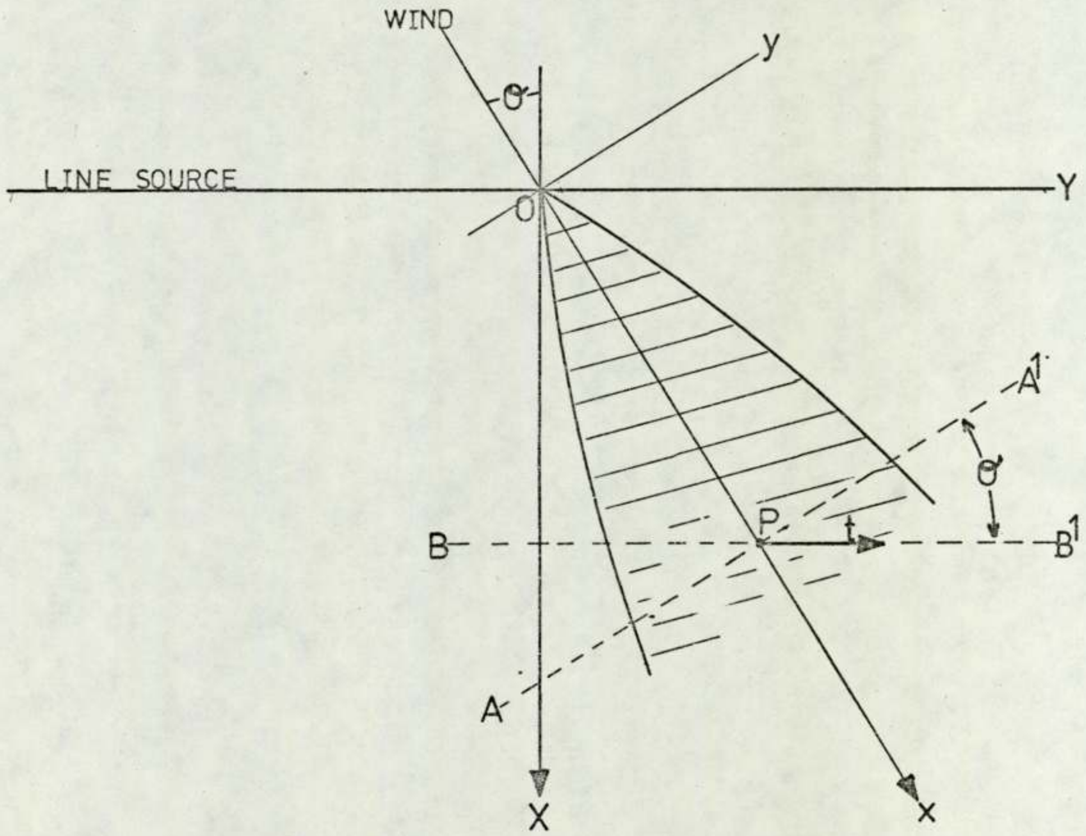

FIGURE 5.2 AXES FOR CALCULATION OF CONCENTRATION DOWNWIND FROM A HIGHWAY, AFTER CALDER, 1973.

the plume, the concentration will vary primarily with perpendicular distance from the plume-axis rather than with distance parallel to the plume-axis. Then $t\sin\theta < x_o$ so

$$D(\theta, x_o) = \int_{-\infty}^{+\infty} Q_p \quad \phi(x_o, t\cos\theta)\, dt \qquad \ldots \quad (5.12)$$

which may be written as $Qp \cdot \frac{\psi(x_o)}{\cos\theta}$, where

$$\psi(x_o) = \int_{-\infty}^{+\infty} \phi(x_o, y) \frac{dy}{\cos\theta} \qquad \ldots \quad (5.13)$$

Consider the line-source distribution as the superposition of infinitesmal point-sources distributed along the line-source, so that Q_p is replaced by the line-source strength Q_L per unit length. Then at the perpendicular distance $X_o = x_o\cos\theta$ from the source, the concentration is

$$C_L(\theta, X_o) = Q_L \frac{\psi(X_o/\cos\theta)}{\cos\theta} \qquad \ldots \quad (5.14)$$

This general result shows the dependence of downwind concentration on wind obliquity θ at perpendicular distance X_o from the source, where $\psi(x_o)$ is as defined above (5.13) for any dilution law $\phi(x, y)$.

Calder (1973) uses the point-source formula (Equation 5.8)

$$\emptyset\ (x,\ y) = \frac{1}{\pi U \sigma_y(x), \sigma_z(x)} \quad \exp\left(- \frac{y^2}{2\sigma_y^2(x)} \right) \exp\left(\frac{-\ H^2}{2\sigma_z^2(x)} \right)$$

for concentration at ground level from a continuous point-source of unit strength at (O, O, H) to derive the exact result

$$C\ (\theta, X_o) = \frac{Q_L}{\pi U} \int_{-\infty}^{\infty} \frac{\exp\left(- \dfrac{t^2 \cos^2 O}{2\sigma_y^2(\lambda)} \right) \ \exp\left(- \dfrac{H^2}{2\sigma_z^2(\lambda)} \right)}{\sigma_y(\lambda)\sigma_z(\lambda)} \, dt$$

... (5.15)

where $\lambda = \left(\dfrac{X_o}{\cos\theta} + t\sin\theta \right)$.

For a perpendicular wind, $\theta = O$,

$$C\ (O, X_o) = \frac{Q_L}{\pi U} \int_{0}^{\infty} \frac{\exp\left(- \dfrac{X_o^{\ 2}}{2\sigma_y^2(\xi)} \right) \ \exp\left(- \dfrac{H^2}{2\sigma_z^2(\xi)} \right)}{\sigma_y(\xi)\sigma_z(\xi)} \, d\xi$$

... (5.16)

These two results must be obtained numerically: an approximate result is

$$C\ (\theta, X_o) = \frac{\sqrt{\left(\dfrac{2}{\pi}\right)}\ Q_L \ \exp\left(- \dfrac{H^2}{2\sigma_z^2(X_o/\cos\theta)} \right)}{U \cos\theta . \sigma_z(X_o/\cos\theta)}$$

... (5.17)

The functions $\sigma_z(x)$ and $\sigma_y(x)$ may be determined as in Section 5.4.

The turbulence from vehicle motion may be considered as causing an initially finite plume so that from the form (after Calder, 1973)

$$\sigma_z(x) = a(x + c)^b,$$

$$\sigma_z(o) = ac^b \qquad \dots \quad (5.18)$$

where a, b may be determined as usual for the Pasquill-Gifford curves (cf Table 5.3) with c = o; c = 27m is used when defining the plume for the road (so that σ_z is 1.5m at x = o). In Table 5.8 we show his predictions for C (θ, X_o) derived from Equations 5.17 and 5.15, together with the functions $\sigma_z(x)$ and $\sigma_y(x)$ as used by him (we return to this in Section 6.3).

The present project used this form with c = 27m and a, b defined from Geomet (1971): Table 5.3.

5.6.2 Tracer Study of Instantaneous Cross-wind Line-source

Drivas and Shair (1974) released SF_6 from a quasi-instantaneous line-source, i.e. in the exhaust of an automobile travelling along a road perpendicular to the downwind sampling direction. Concentrations of the SF_6 cloud were determined as a function of time using a squeeze bottle and electron-capture gas chromatograph. For each concentration-to-time curve they calculated the along-wind standard deviation σ_x, the area under the curve, the average travel time and corresponding average wind velocity using average travel time and downwind distance.

TABLE 5.8

Concentration Estimates of Calder (1973) for Infinite Line Source

(Windspeed 1 ms^{-1}; $Q_L = 1$; wind angle θ;

downwind distance X_o).

Calder's Equation 9 (5.17) and Calder's Equation 12 (5.15)

gave the same results (below)

X_o m	θ = 0°	θ = 15°	θ = 30°	θ = 45°	θ = 60°	θ = 75°
50	0.218	0.221	0.231	0.250	0.282	0.338
100	0.141	0.143	0.148	0.156	0.171	0.197
200	0.085	0.086	0.088	0.092	0.099	0.121
400	0.049	0.050	0.051	0.054	0.061	0.076
800	0.031	0.031	0.032	0.034	0.038	0.048

The Gaussian model equation (Equation 5.7 into Equation 5.5 from Table 5.1) for an instantaneous cross-wind line source,

$$C(X,\ z = o,\ t) = \frac{Q_L}{\pi\,\sigma_x(X,I)\,\sigma_z(X,I)} \exp\left(\frac{-(x - Ut)^2}{2\sigma_x^2(X,I)} \right)$$

(for stability parameters defined for the stability index I as well as downwind distance X), was not a good description of their results when $\sigma_x(X,I)$ and $\sigma_z(X,I)$ were defined from empirical curves.

A transient solution (Equation 5.5, Table 5.1) using eddy coefficient K for the diffusivity was also tested, but it too gave Gaussian curves.

Their experimental curves were, in contrast to these two models, decidedly non-Gaussian in shape. The constant U, K solution with a restrictive inversion-layer aloft and a large initial well-mixed zone (20m x 20m) was considered (as a numerical solution), but this also proved inadequate.

To explain the non-Gaussian concentration profiles and an apparent velocity which increases with height, the effect of wind shear was included (cf. Section 5.2: analytical solution is less easy).

They (Drivas and Shair, 1974) considered two possibilities by the method of integral moments:

1. $U = k_1 \ln z$; $k_z = k_2 z$ which predicts tracer spreading $\sigma_z \sim t$.

2. $U = k_1 z^a$; $k_z = k_2 z^c$ which predicts apparent velocity of tracer $U \sim t^{a/(2-c)}$ and tracer spreading $\sigma_z \sim t^{1 + a/(2-c)}$.

A plot of $\ln\sigma_x$ to $\ln t_{ave}$ for the tracer profiles showed slopes ranging from 1.11 to 1.47, which exceeds the prediction of case 1. A plot of ln U to $\ln t_{ave}$ gave slopes a/(2 - c) of 0.13 to 0.55.

These results are consistent with the observation in Section 5.2 that when U (Z), K (Z) are not constant, the simple relation $\sigma = \sqrt{2Kt}$ (Equation 5.7) no longer applies.

Thus the power-law model ($U = k_1 z^a$; $k_z = k_2 z^c$) accurately predicted the increase with time of both the spread and the apparent plume velocity.

They (Drivas and Shair, 1974) concluded that the Gaussian model arising from a constant U and constant K is less satisfactory: the model based upon the semi-empirical diffusion equation with power-law velocity profile and a power-law vertical eddy diffusivity profile was the most consistent interpretation of their data for an instantaneous cross-wind line source.

5.7 Summary: Application to the Present Work

Although there is some debate as to its generality, the semi-empirical diffusion equation usefully describes practical problems of pollutant dispersal. Terms may be included to allow for losses by settling, absorption at boundaries, chemical reaction or decay. Some common formulae have been listed and the present need for empirical definition of the plume parameters has been described. Given the availability of such functions we have discussed the problem of urban diffusion where vertical mixing is enhanced and the problem of low wind-speed particularly difficult. We have considered the use of the results to describe the ideal case of a long straight road analytically and experimentally.

In subsequent chapters we discuss both the routine monitoring results taken near the intersection and an experiment to measure the concentration distribution from the Motorway. In our analyses we shall use empirical functions for the plume parameters (Table 5.3) with stability categories defined by the parameter MST2 (Table 5.4) and a continuous point source plume (Equation 5.8) with initial size defined by Equation 5.18 where C = 27m. Integration will be made over curved and elevated roads by a computer programme (Chapter 6); no mixing ceiling limit is considered as travel distances were limited. Also, no adjustment of the curves was made for urban effects since there were other uncertainties, particularly in the emissions estimates.

CHAPTER 6

CALCULATION OF POLLUTION CONCENTRATIONS

In this Chapter we describe a computer programme which integrates the point source continuous-plume formula (Equation 5.8) over a simplified three dimensional model of the Motorway intersection. The integral is scaled by the emissions estimate and wind-speed to print an estimated concentration alongside that recorded in the field: the latter are then compared. This comparison is made to assess the combination of road layout, emissions estimate, airport weather readings, stability estimates and plume formula as a pollution level predictor. It therefore brings together (Figure 6.1) various parts of the work already described. The Chapter ends by discussing both the calculated pollution levels and those measured in the field.

6.1 Emissions Estimate

The Equation (5.17) given as Calder's (1973) Equation 9, for the concentration of pollution downwind of a line source will be used to estimate the source strength Q_L. The integral over the Y direction for a perpendicular wind

$$C(0,x_o) = \frac{\sqrt{\frac{2}{\pi}}\; Q_L \exp\left(-\frac{H^2}{2\sigma_z^2(X)}\right)}{U.\sigma_z(X)} \qquad \text{(Equation 5.17 with } \theta = 0)$$

Then C is dimensionally equivalent to $Q_L/(U.\sigma_z)$. Various concentration units may be used in the field when measuring C: related units for Q_L are given in Table 6.1.

FIGURE 6.1 DATA PROCESSING TO COMPARE OBSERVED AND CALCULATED CONCENTRATIONS OF POLLUTANTS

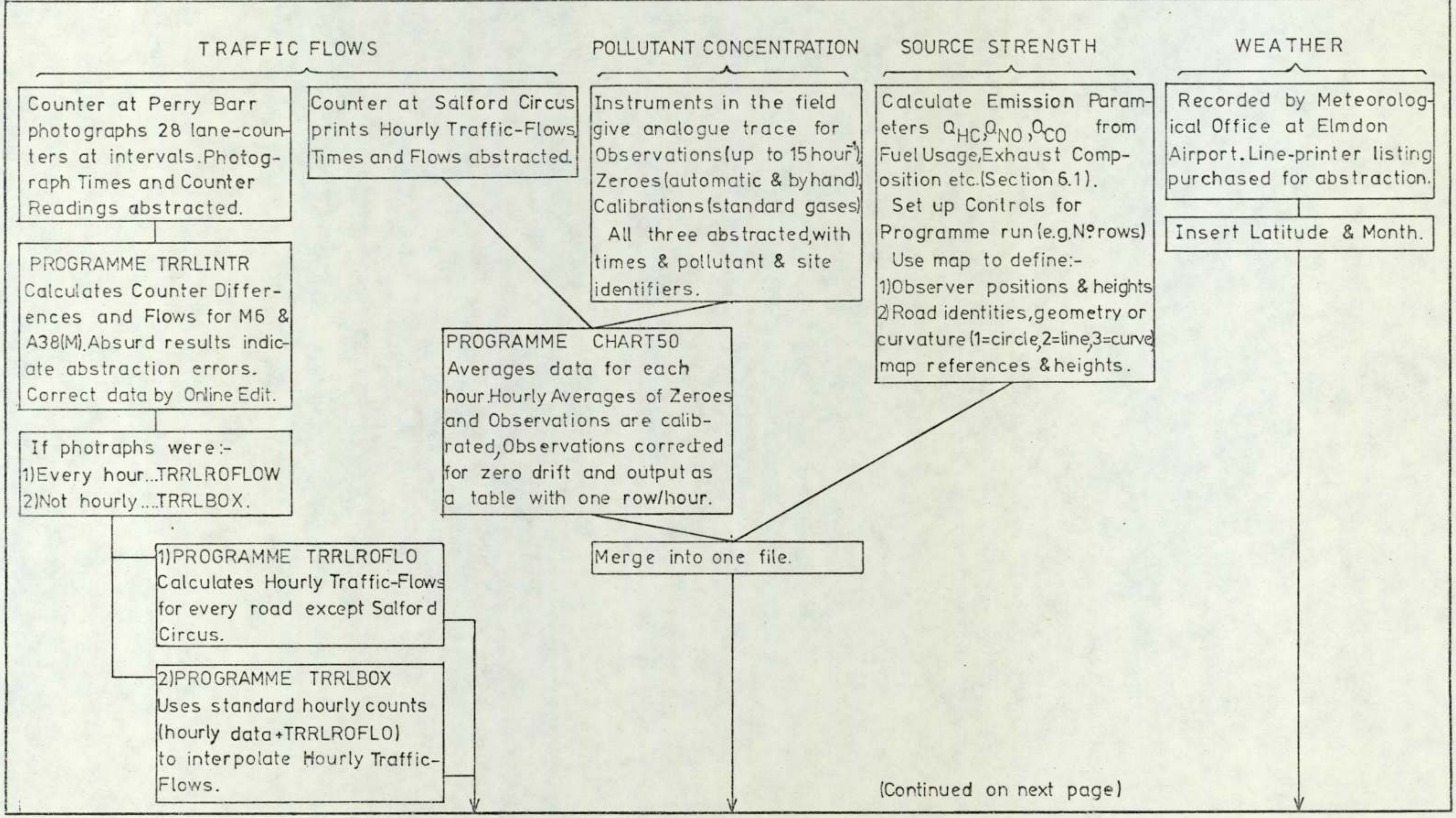

FIGURE 6.1 (CONTINUED)

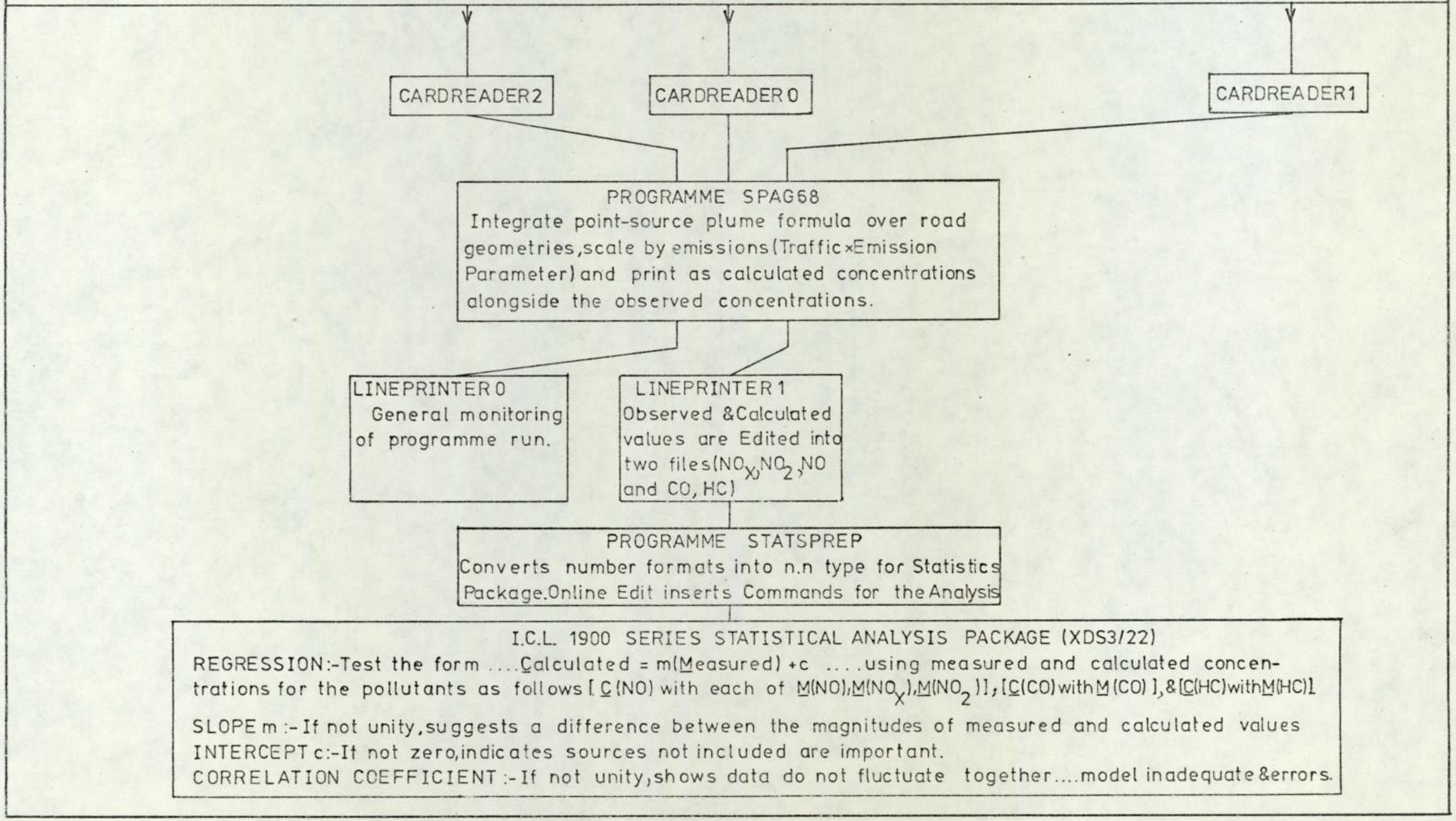

We consider a motorway to be a single line source (unlike Chamberlain, 1974).

Define Q_L = volume emitted per unit length of road per second for whatever traffic is passing. The emissions parameter Qi is the value of Q_L for the gas i emitted by unit traffic flow.

$$Qi = Q_L/T$$

Consider one vehicle:

Fuel consumption = F   l per km road

$\therefore$ Fuel burnt per metre of road = $10^{-6}F^{-1}$ m^3 per m road

Density of fuel = ρ kg m^{-3}

Mass of fuel burnt per metre road = $10^{-6}F^{-1}.\rho$ kg per m road

Stoichiometry of combustion = s air:fuel ratio by mass

$\therefore$ Mass of exhaust gas per metre of road = $10^{-6}F^{-1}.\rho.s$ kg per m road

Density of air = ρA kg m^{-3}

Volume of exhaust gas per metre of road $V_E = 10^{-6}F^{-1}.\rho.s.(\rho A)^{-1}$

m^3 per m road

V_E (m^3 per m road) is the volume of exhaust gas emitted per metre of road when one vehicle travels down the road. If T vehicles travel the road in say one hour (corresponding to a flow T vehicles h^{-1}), the emission per metre of road is V_ET (m^3 per m road) and it occurs for one hour: converting to seconds the emission Q_L(EXH) of exhaust gas in m^3 per metre of road per second for a flow T vehicles h^{-1} is

$$Q_L(EXH) = \frac{V_ET}{3600} = \left(\frac{10^{-6}\ \rho s}{3600(\rho A)F}\right) T \quad m^3s^{-1} \text{ per m road}$$

The exhaust gas contains c ppm by volume of pollutant so

$$Q_L = \left(\frac{c\,\rho s\ 10^{-12}}{3600\,(\rho_A)F}\right) T \quad m^3 s^{-1} \text{ per m road},$$

which in Equation 5.17 will give the concentration in volume-volume ratio. For convenience, we define λ such that

$$Q_L = \lambda.c.T.10^{-6} \qquad \text{"ppm"}\ m^3 s^{-1} \text{ per m road},$$

where

$$\lambda = \frac{\rho s\ 10^{-9}}{3{\cdot}6\ .\rho_A F} \qquad \text{to give concentration in ppm by volume.}$$

Where necessary, subscripts P and D will denote petrol and diesel respectively. In Table 6.2 we give some literature values for the parameters, and in Table 6.3 derive values for Q_L under several engine conditions. Under different conditions very different exhaust gas compositions are produced (cf. Fussel, 1970). In the present work we used the values for half power (Table 6.3) and a traffic mixture of 60% petrol, 40% diesel (manual count at site by J D Butler) to derive emission parameters Q_i as in Table 6.4.

There is some difficulty in arriving at a satisfactory emissions estimate: there may be considerable errors in the values used. The uncertainty for NO could be 100% (for NO, half-load), or in the extreme, 1000%(for CO, half-load). Nevertheless the values in Table 6.4 are used throughout the project - at no time are calculated values "calibrated" using field measurements. Comparisons will be made between pollutant levels calculated from these uncertain emissions estimates and measured in the field: the range of values in Table 6.3 should be remembered.

TABLE 6.1

Dimensions and Units of Concentration C and Source

Strength Q_L for a Line Source (using $Q_L = u\sigma_z C$)

Emission	Dimensions		Example Units	
	C	Q_L	C	Q_L
Mass	$[M][L]^{-3}$	$[M][L]^{-1}[T]^{-1}$	kg m^{-3}	kg $m^{-1}s^{-1}$
Volume	$[L]^3[L]^{-3} = 1$	$[L]^3[L]^{-1}[T]^{-1} = [L]^2[T]^{-1}$	Volume-volume ratio	m^2s^{-1}

TABLE 6.2

Parameters for Fuels and Engines (λ defined so that $Q_L = \lambda CT$ gives calculated concentration in ppm by volume)

Variable		Value	Units	Foot-note	Comments
ρ_A		1.225	kg m^{-3}	1	Air at N.T.P.
ρ	ρ_P	$0.78.10^3$	kg m^{-3}	2	Petrol density
	ρ_D	$0.84.10^3$	kg m^{-3}	3	Diesel density
S	SP	14.5:1	mass ratio	4	Stoichiometry for petrol engine
	SD	25:1	mass ratio	4	Stoichiometry for diesel engine
F	F_P	9	km l^{-1}	5	Petrol vehicle fuel usage
	F_D	5	km l^{-1}	5	Diesel vehicle fuel usage
λ	λ_P	$2.8494.10^{-7}$			Petrol
	λ_D	$9.5238.10^{-7}$			Diesel

Note 1: Handbook of Chemistry and Physics (1970 - 1971) Edition 51 Table F147.
The Chemical Rubber Co.

Continued/......

TABLE 6.2 (continued)

Note 2: Air Pollution Control in Transport Engines (1971) Table 132.3 Institute of Mechanical Engineers, London.

Note 3: Air Pollution Control in Transport Engines (1971) Table 137.1, Institute of Mechanical Engineers, London.

Note 4: Fussel D R (1970) Atmospheric Pollution From Petrol and Diesel Engined Vehicles Petrol Rev 24, 192 - 202.

Note 5: Derwent R G and Stewart H N M (1973) Air Pollution from the Oxides of Nitrogen in the United Kingdom Atmos. Environ. 7, 385 - 401.

TABLE 6.3

Exhaust Concentrations and Line-Source Strengths for Gaseous Pollutants. Concentration c ppm and Traffic Flow T = 1 vehicle h^{-1} are used in Equations $Q_L = (2.8494.10^{-7}Tc)$ for petrol and $Q_L = (9.5238.10^{-7}Tc)$ for Diesel so that Q_L will give calculated downwind concentrations in ppm: see Section 6.1

Gas Engine		FULL LOAD		HALF LOAD		NO LOAD		IDLE	
NO		C	$Qi = Q_L/T$	C	$Qi = Q_L/T$	C	$Qi = Q_L/T$	C	$Qi = Q_L/T$
Petrol	2	6000	$1.7096.10^{-3}$	2000	$5.6988.10^{-4}$	60	$1.7096.10^{-5}$	30	$8.5482.10^{-6}$
	3			1700	$4.8439.10^{-4}$				
	4	1050	$2.9918.10^{-4}$	650	$1.8521.10^{-4}$	20	$5.6988.10^{-6}$	30	$8.5482.10^{-6}$
Diesel	1	921	$8.7714.10^{-4}$	493	$4.6952.10^{-4}$	109	$1.0380.10^{-4}$	119	$1.1333.10^{-4}$
	4	850	$8.0952.10^{-4}$	250	$2.3809.10^{-4}$	30	$2.8571.10^{-5}$	60	$5.7142.10^{-5}$
CO		C	Q_L/T	C	Q_L/T	C	Q_L/T	C	Q_L/T
Petrol	3			6000	$1.7096.10^{-3}$				
	4	30000	$8.5482.10^{-3}$	40000	$1.1397.10^{-2}$	30000	$8.5482.10^{-3}$	70000	$1.9945.10^{-2}$
Diesel	1	2000	$1.9047.10^{-3}$	300	$2.8571.10^{-4}$	300	$2.8571.10^{-4}$	300	$2.8571.10^{-4}$
	4	1000	$9.5238.10^{-4}$						

Continued/......

TABLE 6.3 (continued)

HC		C	Q_L/T	C	Q_L/T	C	Q_L/T	C	Q_L/T
Petrol	3			260	$7.4084.10^{-5}$				
	4	700	$1.9945.10^{-4}$	500	$1.4247.10^{-4}$	4400	$1.2537.10^{-3}$	820	$2.3365.10^{-4}$
Diesel	1	29	$2.7619.10^{-5}$	70	$6.6666.10^{-5}$	90	$8.5714.10^{-5}$	106	$1.0095.10^{-4}$
	4	110	$1.0476.10^{-4}$	55	$5.238.10^{-5}$	160	$1.5238.10^{-4}$	220	$2.0952.10^{-4}$

Note 1: Fussel D R (1970) Atmospheric Pollution from Petrol and Diesel Engined Vehicles Petrol Rev. 24, 192 - 202.

Note 2: Derwent R G and Stewart H N M (1973) Air Pollution from the Oxides of Nitrogen in the United Kingdom, Atmos. Environ., 7, 385 - 401.

Note 3: Fussel D R (1970) Atmospheric Pollution from Petrol and Diesel Engined Vehicles Figure 3 Petrol Rev 24, 192 - 202.

Note 4: Economic and Technical Appraisal of Air Pollution in the United Kingdom PAUM20 (1972) HMSO London

TABLE 6.4

Line-Source-Strength Parameters used in the Present Work (60/40 petrol:diesel; half-power of Table 6.2; values are for unit traffic flow, 1 vehicle $hour^{-1}$; predicted pollutant concentration will be in ppm by volume)

Gas i	Vehicle Type	ppm in exhaust	Emission Parameters Qi: For engine type $Qi = Q_L/T$ in ppm $m^2s^{-1}(vh^{-1})^{-1}$	Emission Parameters Qi: As used $Qi = Q_L/T$ for 0.6P + 0.4D	Emission Parameters Qi: Units ppm in v/v ratio
NO	Petrol	1700	$4.8439.10^{-4}$	$4.7843.10^{-4}$	ppm $m^2s^{-1}(vh^{-1})^{-1}$
	Diesel	493	$4.6952.10^{-4}$		
CO	Petrol	6000	$1.7096.10^{-3}$	$1.1400.10^{-3}$	ppm $m^2s^{-1}(vh^{-1})^{-1}$
	Diesel	300	$2.8571.10^{-4}$		
HC	Petrol	260	$7.4084.10^{-5}$	$7.116.10^{-5}$	ppm $m^2s^{-1}(vh^{-1})^{-1}$
	Diesel	70	$6.6666.10^{-5}$		

6.2 Programme to Calculate Pollution from Roads

6.2.1 Outline

The programme (Flowchart: Figure 6.2) integrates numerically the point source continuous-plume formula (Equation 5.8) by the trapezium rule over a set of elevated, curved roads. Pollution was to be calculated at any observer position; for general application Ordnance Survey eight digit (four East, four North) reference positions were used to define all positions (to the nearest ten metres). The programme distinguishes straight, curved and circular sections of the roads. Roads are represented as horizontal, but can be elevated.

Emissions are read in two parts: the emissions parameter Qi (calculated for the unit traffic-flow in the petrol:diesel ratio normally present: Section 6.1) and the hourly traffic-flow of the road being integrated over. Thus Qi is read once and individual traffic-flows on each contributing road are recognised: no allowance for vehicle speed or road slope is made in the emissions estimate.

The integration step-length is read rather than defined as it can affect integral results. Data for measured field-levels of pollution, weather readings and traffic-flows are read hour by hour from three separate input channels: one integration is performed for each row and the prediction printed alongside the measured result. Additional information is printed on a second output channel separate from the table of calculated results.

FIGURE 6.2 FLOWCHART FOR PROGRAMME TO INTEGRATE A POINT-SOURCE PLUME OVER ELEVATED CURVED ROADS

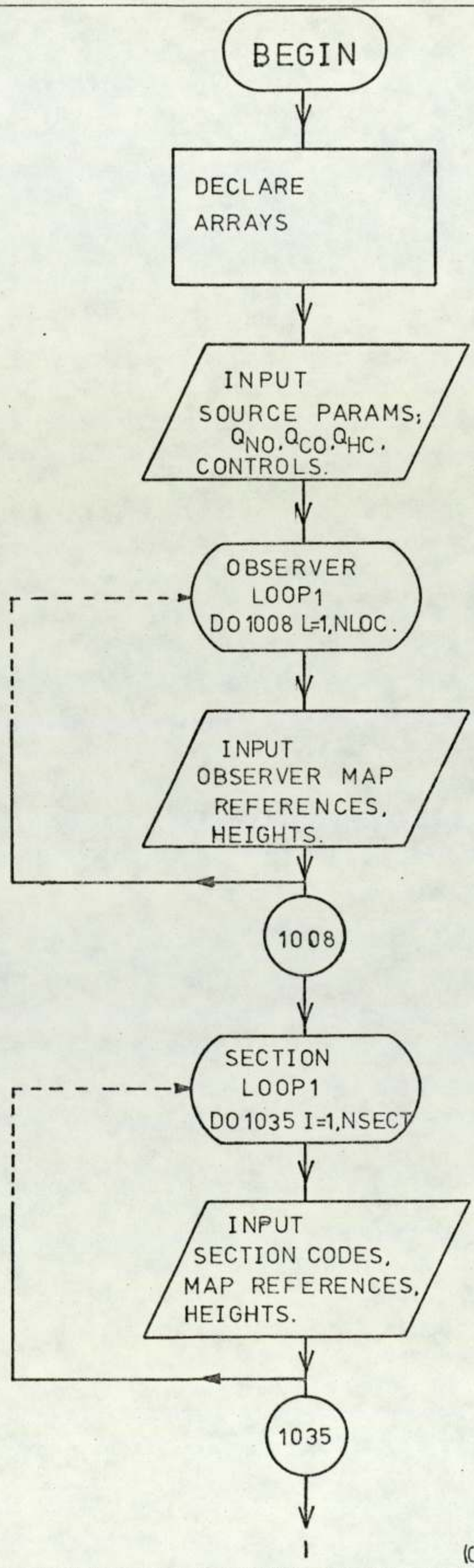

(Continued on next 4 pages):1

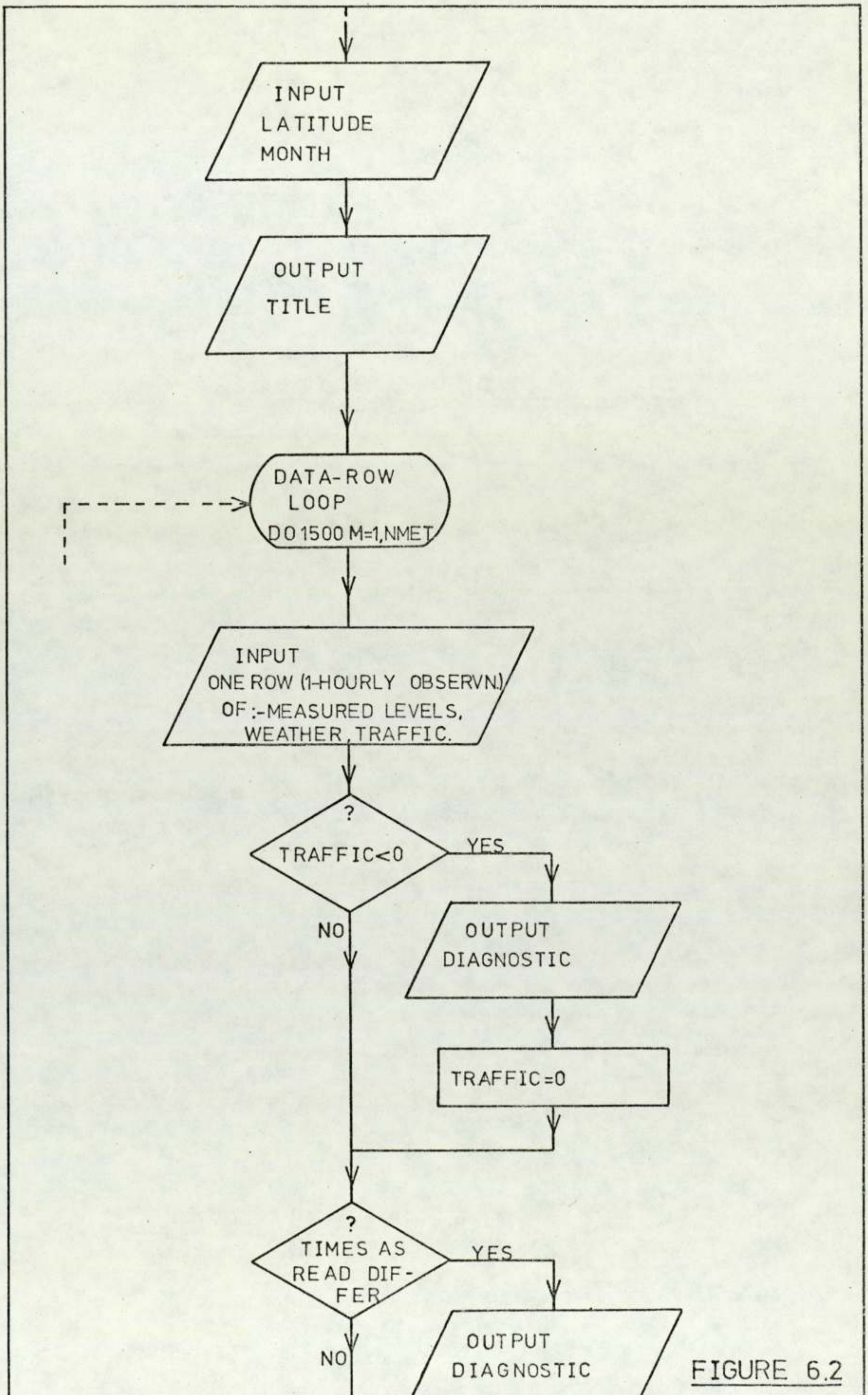

FIGURE 6.2
(CONTINUED):2

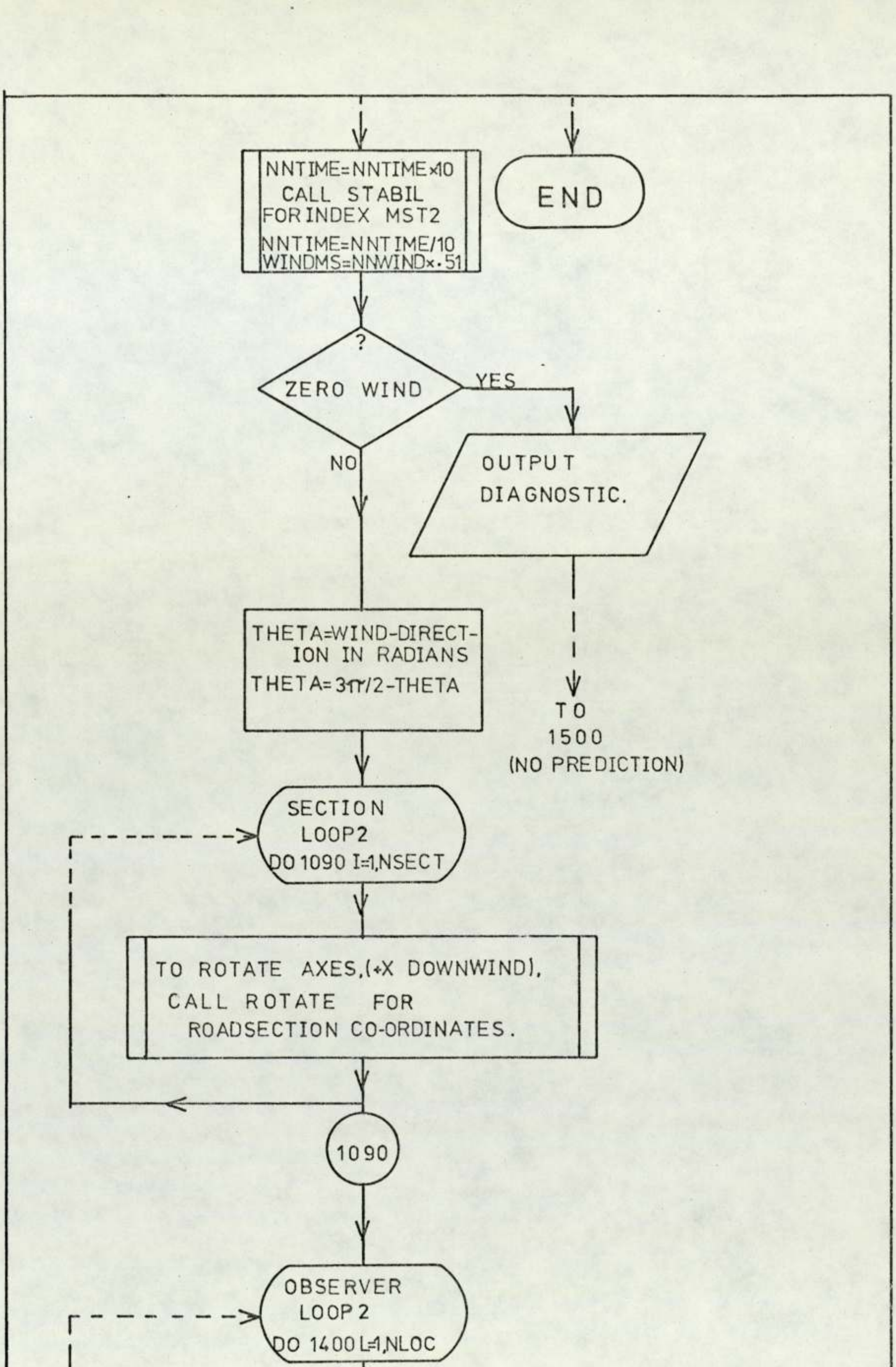

FIGURE 6.2

(CONTINUED):3

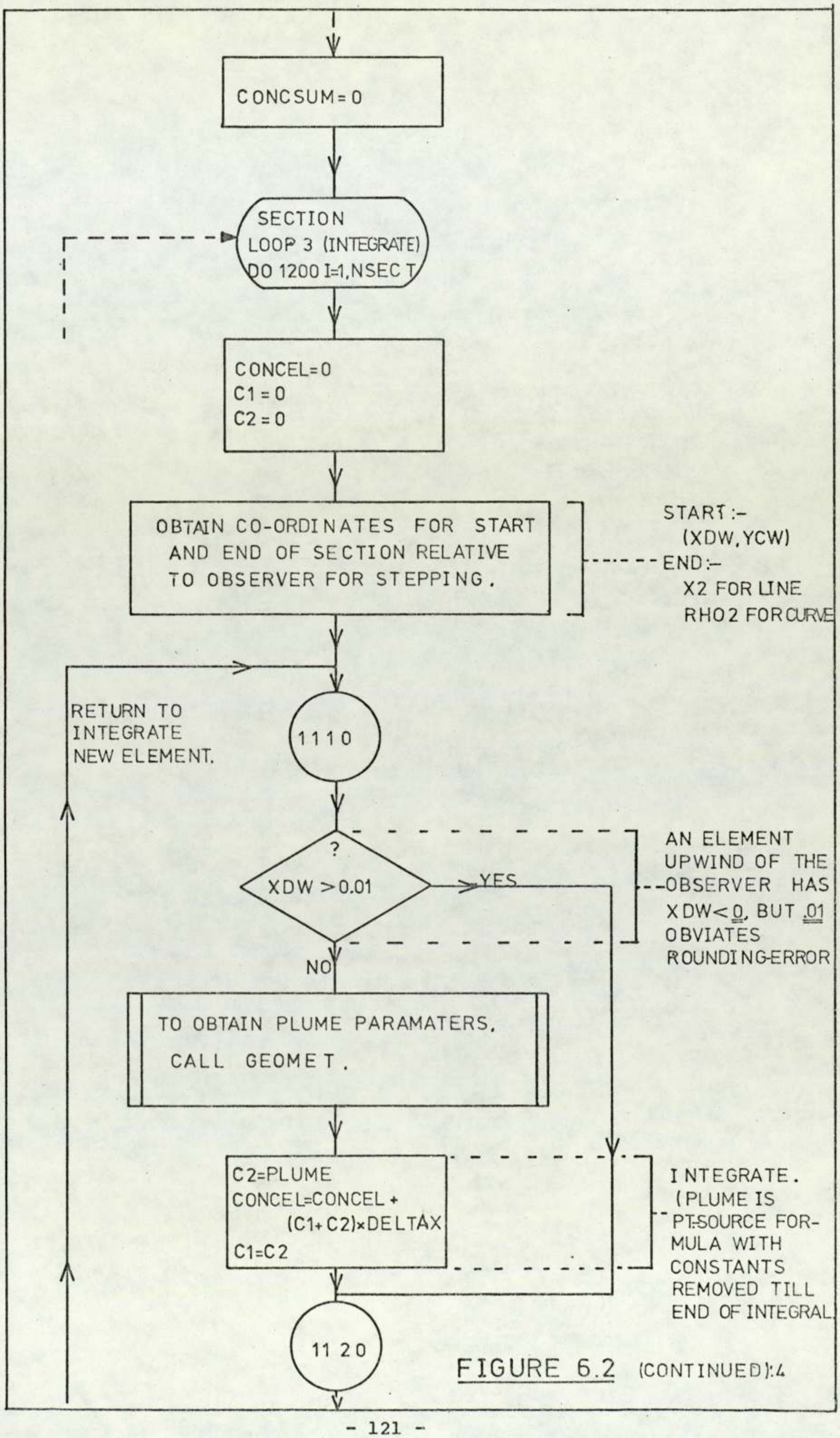

FIGURE 6.2 (CONTINUED):4

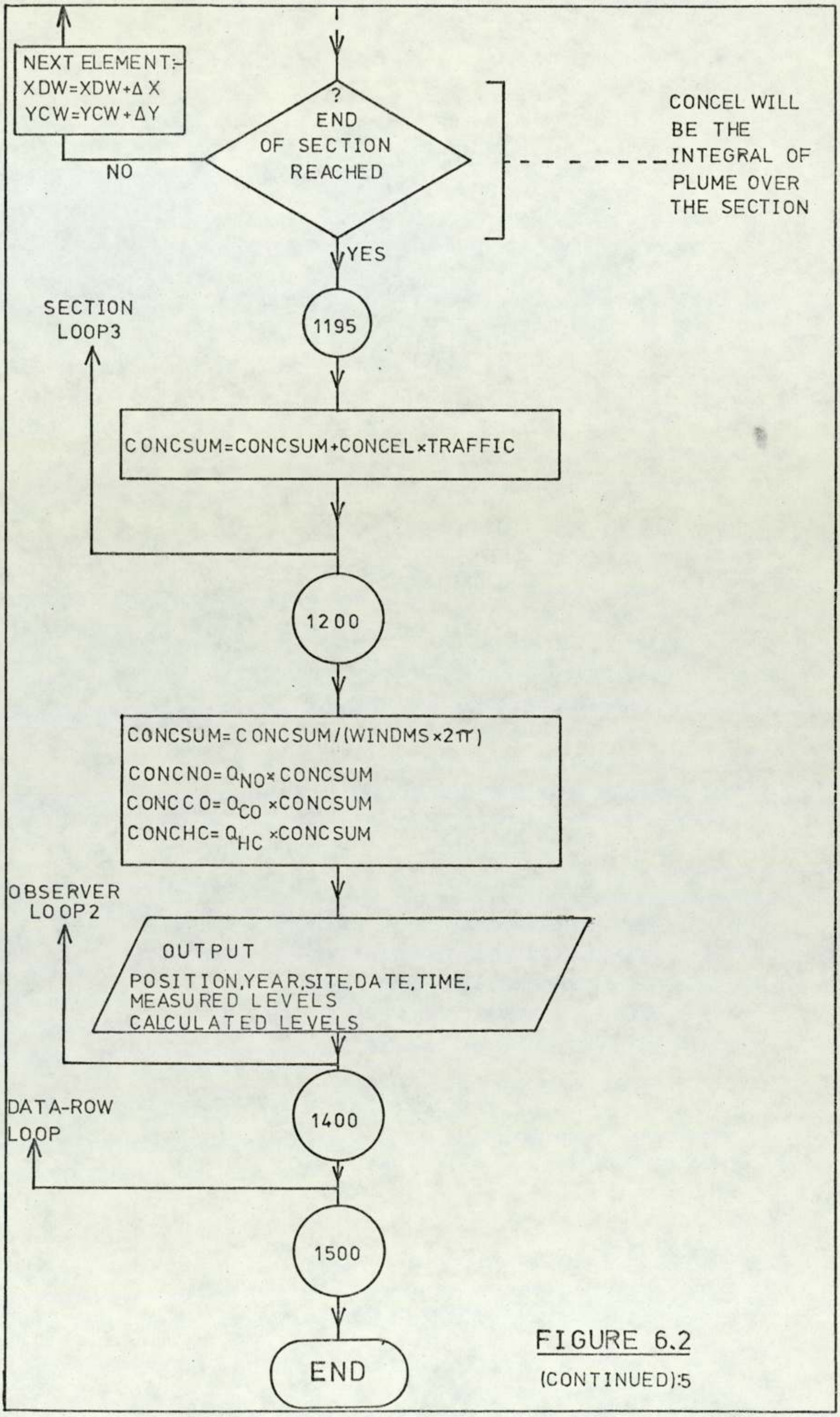

FIGURE 6.2
(CONTINUED):5

```
DOCUMENT    PRED117404                                   INPUT TO CARDREADER0

 0.00047843   0.00114  0.000071116                       EMMISION PARAMETERS Q_NO Q_CO Q_HC
 50  1  43  5  24                                        OBSERVER POSITION (HEIGHT=0)
09649018
01  1 3  09099071   12  09289033  000  09609008  000__CURVE   ]
02  1 2  10008988   12  09609608  000                          ] MAP REFERENCES
03  1 2  09099071   12  08909100  000                 }LINES   ] FOR ROAD POSITIONS
04  2 2  08819012   12  08609000  000                          ] (SECTIONS 6-42
05  3 1  09649018   00     50_________________________CIRCLE  ]         DELETED)
45 23 2  09109022   12  08819011  000
         CURVATURE                   HEIGHT
         ROAD IDENTITY               POSITION
         SECTION NUMBER
 74    4   13    4   11   0.108   0.108   0.001   2321   3.1   5.8
 74    4   14    4   11   0.130   0.122   0.008   2355   3.5   5.9 FIELD OBSERVATIONS.
```

```
DOCUMENT    MET117402                                    INPUT TO CARDREADER1

525  11_____LATITUDE & MONTH
 4  13  350  10  8  900   86   74   60   93   84        0   0 ] WEATHER READINGS
 4  14  350   8  7  700   87   75   60   94   84        0   0 ]
```

```
DOCUMENT    TRARES117403                                 INPUT TO CARDREADER2

  1974    11     4   MON  19   34   13_ _ _TIME & DATE
  2492  2548          203       854      0     921    39    351     39 ] FLOW ON
  1073     1   537    537        99     44    -227    53   -152    854 ] EACH ROAD
     1     1   249      0
  1974    11     4   MON  19   34   14
  2222  2344          183       874      0     816    64    322     64
   916     1   459    459       117     56    -216    60   -147    874
     1     1   235      0
```

```
DOCUMENT    BAC680400                                    OUTPUT TO LINEPRINTER0

  943.6    367.3    751.2 ]
                           ] SOME OF THE CENTRES & RADII CALCULATED FOR
  139.0   -478.8    272.2 ] CURVED SECTIONS
                           ]
  226.4    -65.0    225.0 ]

FIELD   DAY AND HOUR AS READ          4    13                           ]
METDATA DAY AND HOUR AS READ          4    13   350    10    8          ] COMMENTS ON
TRAFFIC DAY AND HOUR AS READ          4    13                           ] DATA READING
                                                                        ]
NEGATIVE TRAFIC FOR I=    17 WAS SET ZERO                               ]
NEGATIVE TRAFIC FOR I=    19 WAS SET ZERO
NEXTELEMENT=   1    1    3XDW  -617.5YCW  -449.6 ]
NEXTELEMENT=   1    1    3XDW  -612.5YCW  -449.3 ] STEPPING OVER ELEMENTS
NEXTELEMENT=   1    1    3XDW  -607.5YCW  -448.9 v
```

```
DOCUMENT    BAC680401                                    OUTPUT TO LINEPRINTER1

                         FIELDWORK AND THEORY
                                    --MEASURED-----------------------------------------CALCULATED-
L=  OBSERVPOSN  YR ST HR DY MT  FIELDNOX    FIELDNO    FIELDNO2     FIELD CO   FIELD HC    PRED NO

 1  964. 9018. 74  4 13  4 11 .1080E 00 .1080E 00 .1000E-02 .3100E 01 .5600E 01 .4570E-01
 1  964. 9018. 74  4 14  4 11 .1300E 00 .1220E 00 .8000E-02 .3500E 01 .5900E 01 .3826E-01
                                                              PRED CO    PREDHC

                                                             .1089E 00 .6793E-02
                                                             .9118E-01 .5688E-02
```

FIGURE 6.3 STRUCTURE OF INPUT AND OUTPUT FOR PROGRAMME SPAG68 TO CALCULATE CONCENTRATIONS OF GASEOUS POLLUTANTS.

Axes are rotated to point positive x in the downwind direction: co-ordinates for the start and end of each section are set up. The programme steps along each section in elements of length as read, and calculates the co-ordinates of the element thus stepped out. If the element is upwind of the observer it contributes to the pollution sum: the downwind distance of the element relative to the observer is negative so that element is included in the summation. Summation proceeds by the trapezium rule. Having summed for that element, the programme finds the next element and repeats until the section of road has been covered. The sum for that section is scaled by the traffic of that section. When all sections have been covered the constants for every section (π, wind-speed, Qi) are included in the sum which becomes the predicted level for print-out.

The plume is defined from empirical curves (Table 5.3) of plume standard deviation $\sigma_y(X)$, $\sigma_z(X)$ as a function of downwind-distance and stability index (Table 5.4). An initially finite plume is used (after Calder, 1973: Section 5.5.1): the distance 27 metres is added to X when calculating $\sigma_y(X)$ and $\sigma_z(X)$, and then subtracted to leave the location of co-ordinates for following elements unchanged. The stability index sub-routine was obtained from the Meteorological Office: Section 5.3.2. It uses cloud cover, wind-speed, time and date to estimate solar radiation and thence stability. Figure 6.3 summarises input and output.

6.2.2 Trigonometry for Road Positions

The curved and elevated structure of the intersection was simplified to lines, curves and circles, each at a particular horizontal level.

This layer structure avoided the need to interpolate heights along sloping sections, although the model could be extended to include this.

In Chapter 4 we described the measurement of traffic counts for each road in the intersection. For the present calculation, each of those roads is broken into sections according to their geometry. Each section has a section number, a road identity number (the same as in Chapter 4) and a curvature parameter. The latter is

1 for a circle (Figure 6.4), when the map-reference for the centre, the radius, and the height are read.

2 for a line (Figure 6.5) when map-references for the two end points, and the height, are read.

3 for a curve (Figure 6.6) when map-references for three points on the curve, and the height, are read:

the sequence is important as a circle is fitted through the three points. The section is defined as an arc of that circle, running from the first to the third point by increasing an angular co-ordinate ρ in the anti-clockwise direction. To define the correct part of the circle the points must be in sequence around the curve, with the most clockwise point first. Figures 6.4, 6.5 and 6.6 describe the trigonometry required to define the layout of the roads and the co-ordinates of small elements stepped out along the roads in steps of variable length Δs.

The prgramme reads the section data for storage by section number according to the curvature parameter (dummy variables are used in the read). Map references are split by the read format into East and North values, and converted to distances in metres from the point 09649018 (a convenient origin on the map in question) to reduce the magnitude of

Map References NS1E,NS1N define the centre at (RCX,RCY)

RCX=(NS1E-0964)×10 metres

RCY=(NS1N-9018)×10 metres

The radius is read as NS2E

RAD=NS2E metres

Axes are then rotated anticlockwise through θ to point the X-axis downwind,using the subroutine ROTATE

CALL ROTATE(θ,RCX,RCY,NCX,NCY) gives new co-ordinates (NCX,NCY) for the centre.

CALL ROTATE(θ,ROBSX,ROBSY,NOBSX,NOBSY) gives new coordinates (NOBSX,NOBSY) for the Observer.

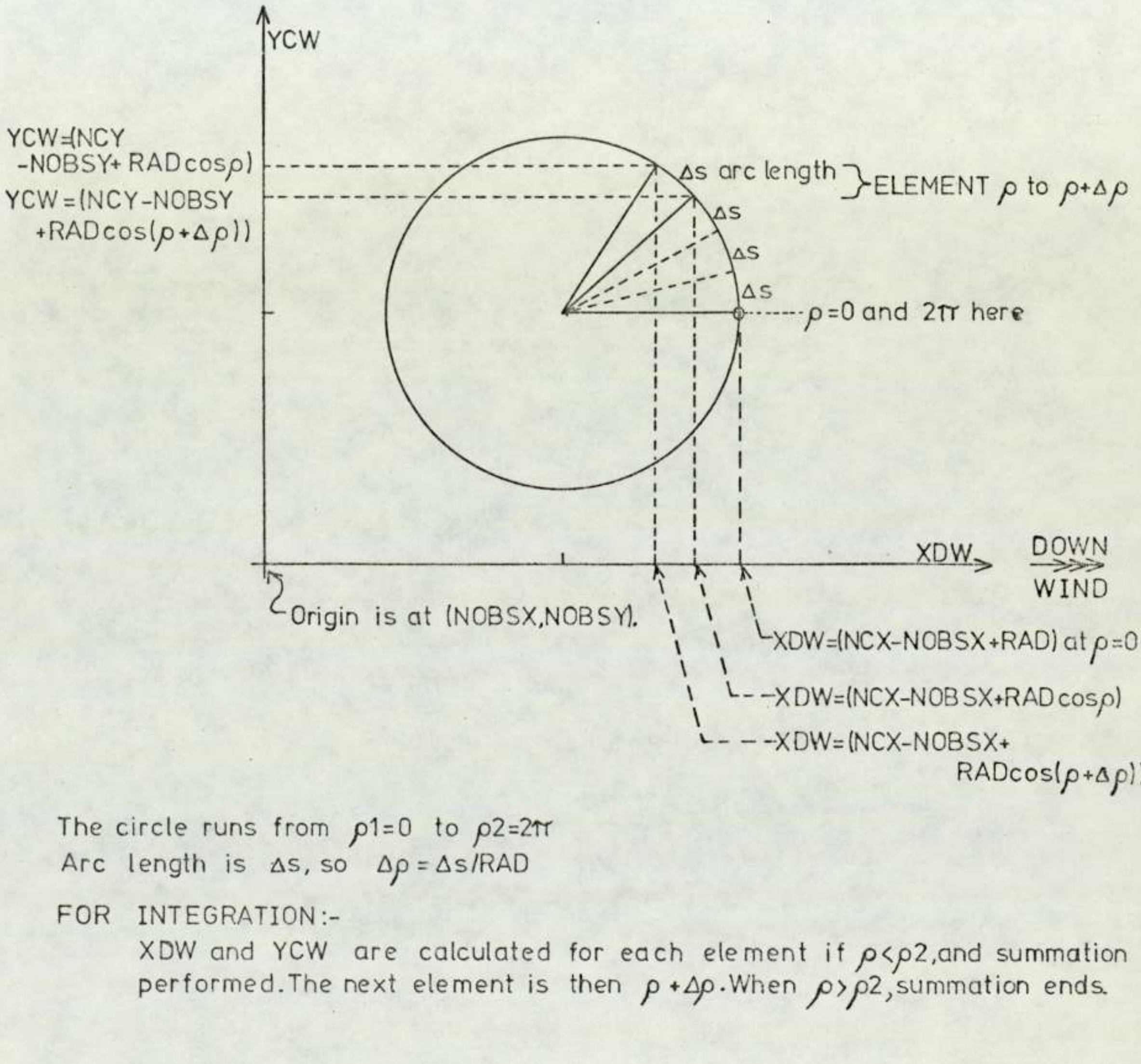

The circle runs from $\rho1=0$ to $\rho2=2\pi$

Arc length is Δs, so $\Delta\rho = \Delta s/RAD$

FOR INTEGRATION:-

XDW and YCW are calculated for each element if $\rho<\rho2$, and summation performed. The next element is then $\rho+\Delta\rho$. When $\rho>\rho2$, summation ends.

FIGURE 6.4 DEFINITION OF TRIGONOMETRY FOR A CIRCULAR ROAD.

Map References NS1E,NS1N and NS2E,NS2N define the start and end of the line

RX1 =(NS1E-0964)×10 metres

RY1 =(NS1N-9018)×10 metres

RX2=(NS2E-0964)×10 metres

RY2=(NS2N-9018)×10 metres

Axes are then rotated anticlockwise through θ to point the X-axis downwind, using the subroutine ROTATE

CALL ROTATE(θ,RX1,RY1,NX1,NY1) gives new co-ordinates (NX1,NY1) for the start of the line.

CALL ROTATE(θ,RX2,RY2,NX2,NY2) gives new co-ordinates (NX2,NY2) for the end of the line.

CALL ROTATE(θ,ROBSX,ROBSY,NOBSX,NOBSY) for the Observer, as in Figure 6.4

Axis rotation may change the size and sign of X-co-ordinates, which in turn would make difficult the recognition of line-start and line-end by a simple magnitude test. Hence the subroutine call...

CALL SHUFEL(NX1,NY1,NX2,NY2) swops NX1 for NX2 and NY1 for NY2 if NX1>NX2

Thus the line runs from (NX1,NY1) to (NX2,NY2), with NX1<NX2.

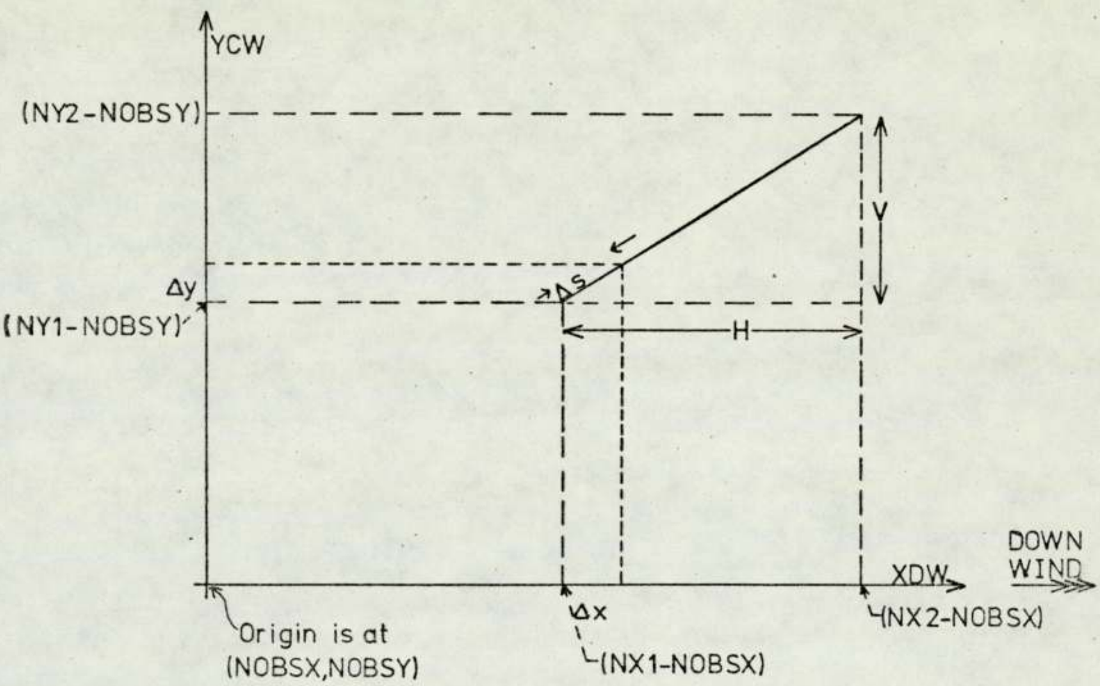

V=NY1-NY2

H=NX1-NX2

G=V/H

Using $Y=GX+C$, $\frac{dY}{dX}=G$, so $\Delta Y=G\Delta X$.

$\Delta s^2=\Delta X^2+\Delta Y^2=\Delta X^2(1+G^2)$

$\Delta X=\Delta s/\sqrt{1+G^2}$

$\Delta Y=G.\Delta X$

FOR INTEGRATION:-

XDW is set to NX1-NOBSX, YCW to NY1-NOBSY and summation occurs if XDW<0 and the end of the road has not been reached.

Next element is XDW+ΔX,YCW+ΔY.

<u>FIGURE 6.5</u> DEFINITION OF TRIGONOMETRY FOR A STRAIGHT ROAD.

Map References NS1E,NS1N: NS2E,NS2N; NS3E,NS3N define three points taken in anticlockwise sequence along the curve with the most clockwise first

RX1=(NS1E-0964)×10 RX2=(NS2E-0964)×10 RX3=NS3E-0964)×10

RY1=(NS1N-9018)×10 RY2=(NS2N-0964)×10 RY3=(NS3N-0964)×10

. . . all in metres.

Centre C and Radius RAD are calculated by subroutine CURVE

CALL CURVE(RX1,RY1,RX2,RY2,RX3,RY3,RAD,RCX,RCY) fits a circle through the three points, having centre (RCX,RCY).

Axes are then rotated anticlocwise through θ to point the X-axis downwind, using the subroutine ROTATE

CALL ROTATE(θ,RX1,RY1,NX1,NY1) gives new co-ordinates (NX1,NY1) for first point.

CALL ROTATE(θ,RCX,RCY,NCX,NCY) gives new co-ordinates (NCX,NCY) for centre.

CALL ROTATE(θ,RX3,RY3,NX3,NY3) gives new co-ordinates (NX3,NY3) for 3rd point.

CALL ROTATE (θ,ROBSX,ROBSY,NOBSX,NOBSY) for the Observer, as in Figure 6.4

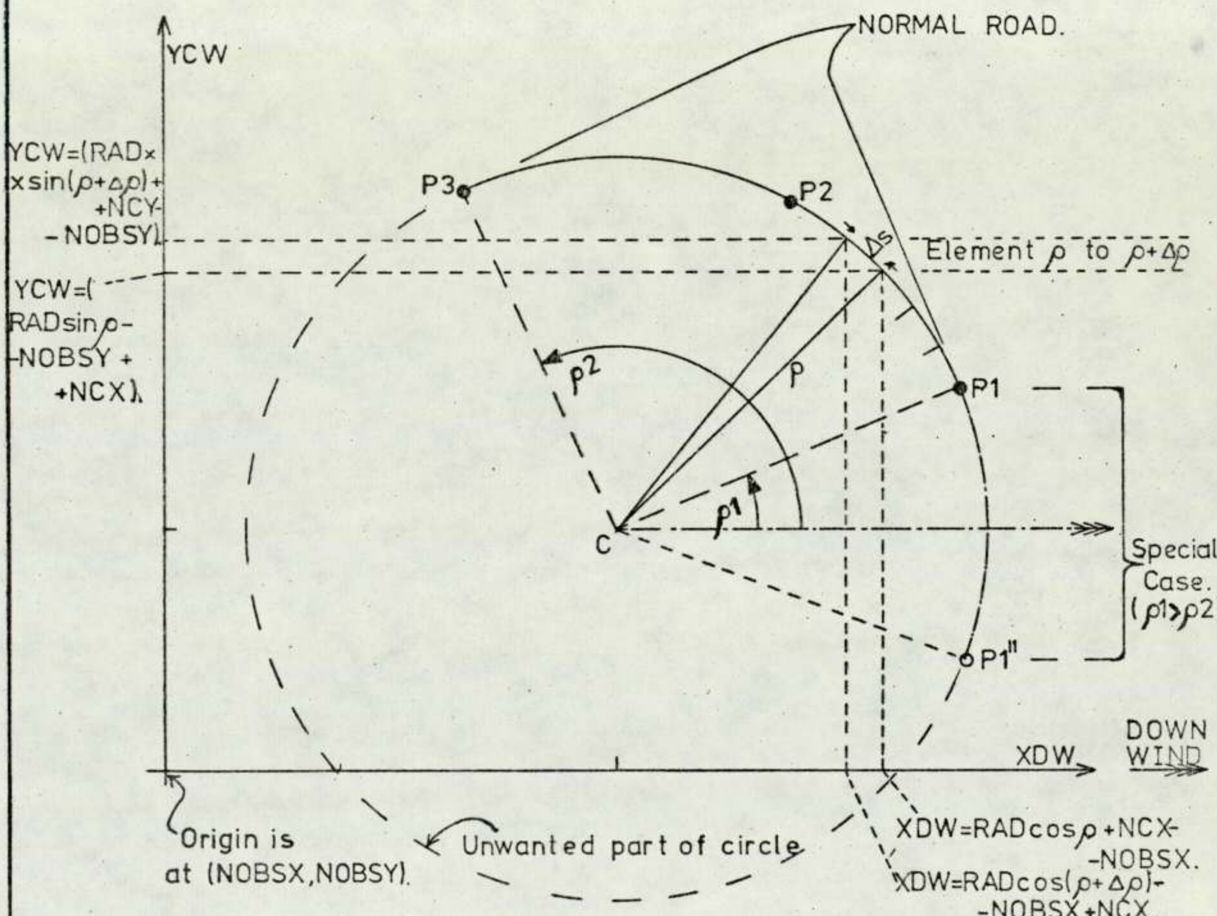

POINTS ARE :- C=(NCX,NCY),P1=(NX1,NY1),P2=(NX2,NY2),P3=(NX3,NY3).

Angular Co-ordinates for P1 and P3 measured about C are $\rho 1$ and $\rho 2$.
SubFunction ARCTAN uses arctangent of the slope of a line to give $\rho 1$ and $\rho 2$ in range 0-2π.
$\rho 1$=ARCTAN(NX1,NY1,NCX,NCY), and $\rho 2$ similarly.

FOR INTEGRATION:-

XDW and YCW are calculated for P1, and the limits of summation are $\rho 1$ & $\rho 2$. A Special Case occurs if the curve is intersected by the Downwind direction, which makes $\rho 1 > \rho 2$ and positive stepping of elements $\Delta\rho$ from $\rho 1$ to $\rho 2$ impossible. Hence if $\rho 1 > \rho 2$, we set $\rho 1 = (\rho 1 - 2\pi)$, which is $< \rho 2$. Then $\rho = \rho 1$. The summation is made for elements $\rho = \rho + \Delta\rho$, until $\rho > \rho 2$.

FIGURE 6.6 DEFINITION OF TRIGONOMETRY FOR A CURVED ROAD.

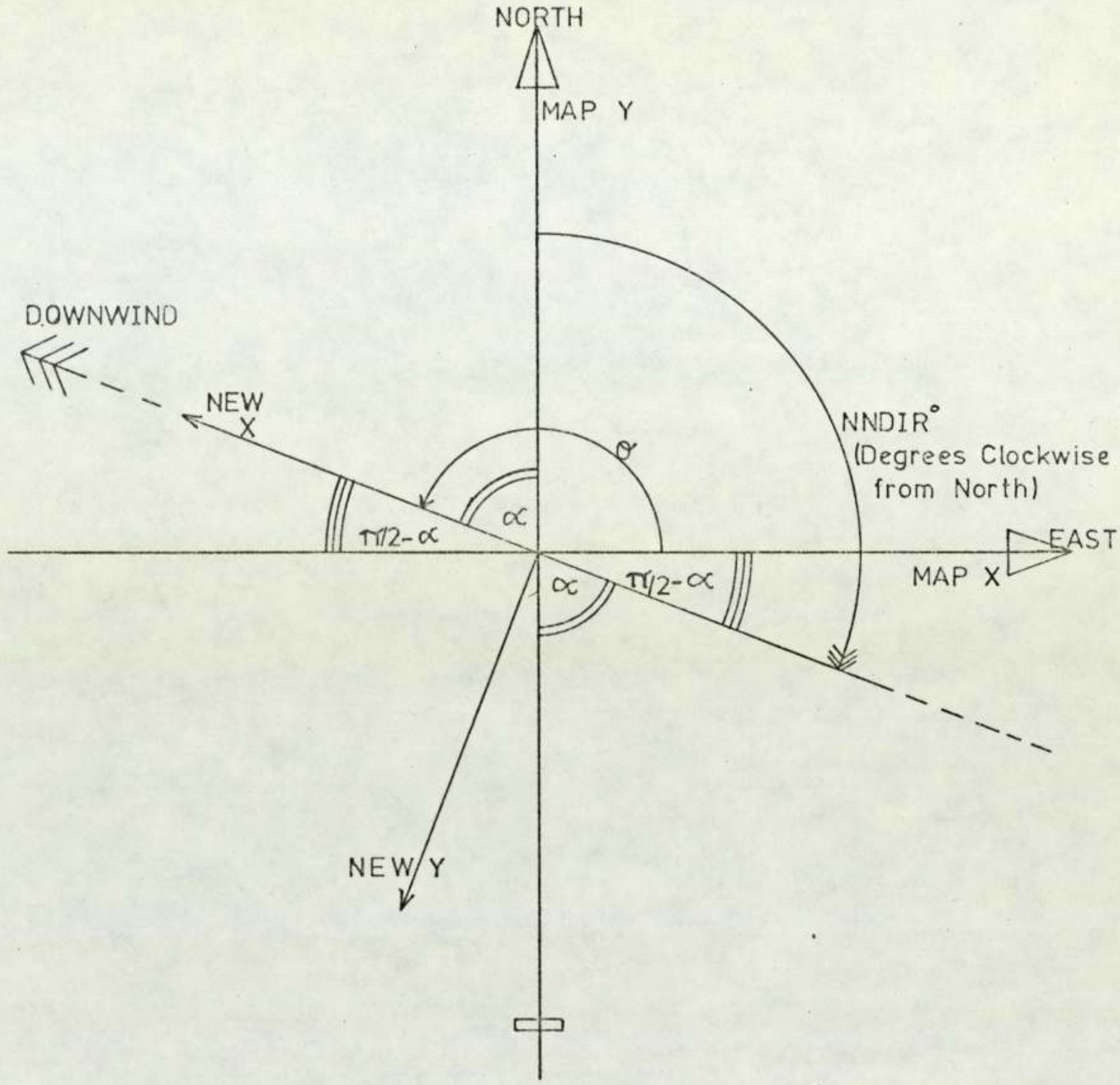

Define $\alpha = \pi - NNDIR \times \pi/180$ radians

Then $\theta = \pi/2 + \alpha$ radians

Whence $\theta = 3\pi/2 - NNDIR \times \pi/180$ radians

Thus the original axes (X=East) are rotated anticlockwise through θ to point X downwind.

FIGURE 6.7 DERIVATION OF THE ANGLE θ FOR AXIS ROTATION.

of numbers. The angle θ (Figure 6.7) is calculated from the wind-direction: the axes are rotated anti-clockwise through θ so that use of the above trigonometry defines the co-ordinates of elements along each road in the downwind and crosswind directions.

6.2.3 Integration of Plume Formula

For each hourly observation, the wind-speed, cloud cover, time and date are used by sub-routine STABIL (Section 5.3.2) to obtain the stability index MST2. If the wind-speed is zero, no integration is performed. One integral is returned for each observer position and each hourly observation.

Integration by the trapezium rule is carried out element by element along each road-section: C1, C2 and CONCEL are zeroed, and initial co-ordinates for the start of the road-section defined as XDW, YCW (downwind and crosswind distances from the observer respectively). If the element is upwind of the observer, XDW < 0 and the element contributes to the summation: sub-routine GEOMET is called to obtain parameters σ_y, σ_z for the point source plume of the element at the observer. The concentration C2 of that plume at the observer is, from Equation 5.8 with $(Qi/2\pi U)$ to be multiplied in later,

$$C2 = \frac{1}{\sigma_y \sigma_z} \exp\left(-\frac{YCW^2}{2\sigma_y^2}\right) \left[\exp\left(\frac{-(Z-H)^2}{2\sigma_z^2}\right) + \exp\left(\frac{-(Z+H)^2}{2\sigma_z^2}\right) \right]$$

where Z, H are the observer and element heights respectively. For the first element, C1 = 0; for later elements, C1 is the value of CZ from the previous element. C1 and C2 are combined by the trapezium rule as

$$CONCEL = CONCEL + \Delta s\frac{(C1 + C2)}{2} = CONCEL + (C1 + C2)DELTAX$$

for a steplength ΔS (read as DELTAS to give DELTAX = $\Delta S/2$). C1 is then set equal to the present C2 ready for the next element, if found. If not found, the end of the road section has been reached: summation of CONCEL ceases and it is scaled by the traffic-flow of that section and added to CONCSM, the sum from previously completed sections. When all sections have been covered, CONCSM is scaled by the constants: (windspeed $.2\pi)^{-1}$ and the appropriate emissions parameter Q_{NO}, Q_{CO} or Q_{HC} for unit traffic-flow per metre of road.

$$CONCNO = Q_{NO} \cdot \frac{CONCSM}{(2\pi . WINDMS)}$$

where WINDMS is the windspeed, ms^{-1}.

CONCCO, CONCHC are derived similarly.

The calculated concentrations CONCNO, CONCCO, CONCHC (ppm) for NO, CO, HC respectively, together with the observer position, time and date are printed alongside the measured levels. This table forms the basis for comparison studies (Section 6.6).

6.2.4 Sub-routines

1. GEOMET (X,MST2,SY,SZ) gives SY = $\sigma_y(X)$ and SZ = $\sigma_z(X)$ for a positive downwind distance X and stability index MST2, by the curves in Table 5.3: these curves (Geomet, 1971) were used since both σ_y and σ_z were needed to integrate the point-source formula (Equation 5.8) over the complex source geometry. For an upwind road, XDW is negative, so the sub-routine is called with arguments (-XDW,MST2,SY,SZ).

Geomet (1971) gave but five classes, while the coding (supplied by Dutton of the Meteorological Office: Section 5.3.2) in subroutine STABIL returns MST2 in the range 1 to 10. We thus defined classes (cf. Pasquill, 1971)

Class	A	AB	B	BC	C	CD	D	E	F	G
MST2	1	2	3	4	5	6	7	8	9	10

This is one area for model development.

No attempt is made to allow for restricted vertical mixing as no mixing heights were available (e.g. see Johnson et al., 1971). After Calder (1973), initial plume sizes were obtained by adding 27m to X before and after using the above formulae for SY, SZ. This parameter requires study: Figure 6.8 gives a resumé for the value of 27m as used. Figure 6.8 shows that $\sigma_X(0)$ and $\sigma_Z(0)$ vary with MST2. This format, i.e. X = X + C, was used following Calder (1973): since the aim was to represent an initially finite wake, a format $\sigma(X) = \sigma(X) + \sigma_C$ might be better, for then σ_C would define wake size independent of stability. This would be of similar format to the suggestions of Pooler (1966): see Section 5.4 and Table 5.7. Urban effects are complex and we go no further save to comment that a thorough study of both formats is needed.

2. SHUFEL (AX,AY,BX,BY) interchanges the co-ordinates of the points A and B if AX exceeds BX. Thus AX is less than BX. For straight-line sections (Figure 6.5) SHUFEL is called to ensure NX1 $<$ NX2, so that addition of ΔX (which is always positive) to XDW always implies positive stepping from P1 to P2: otherwise one might lose

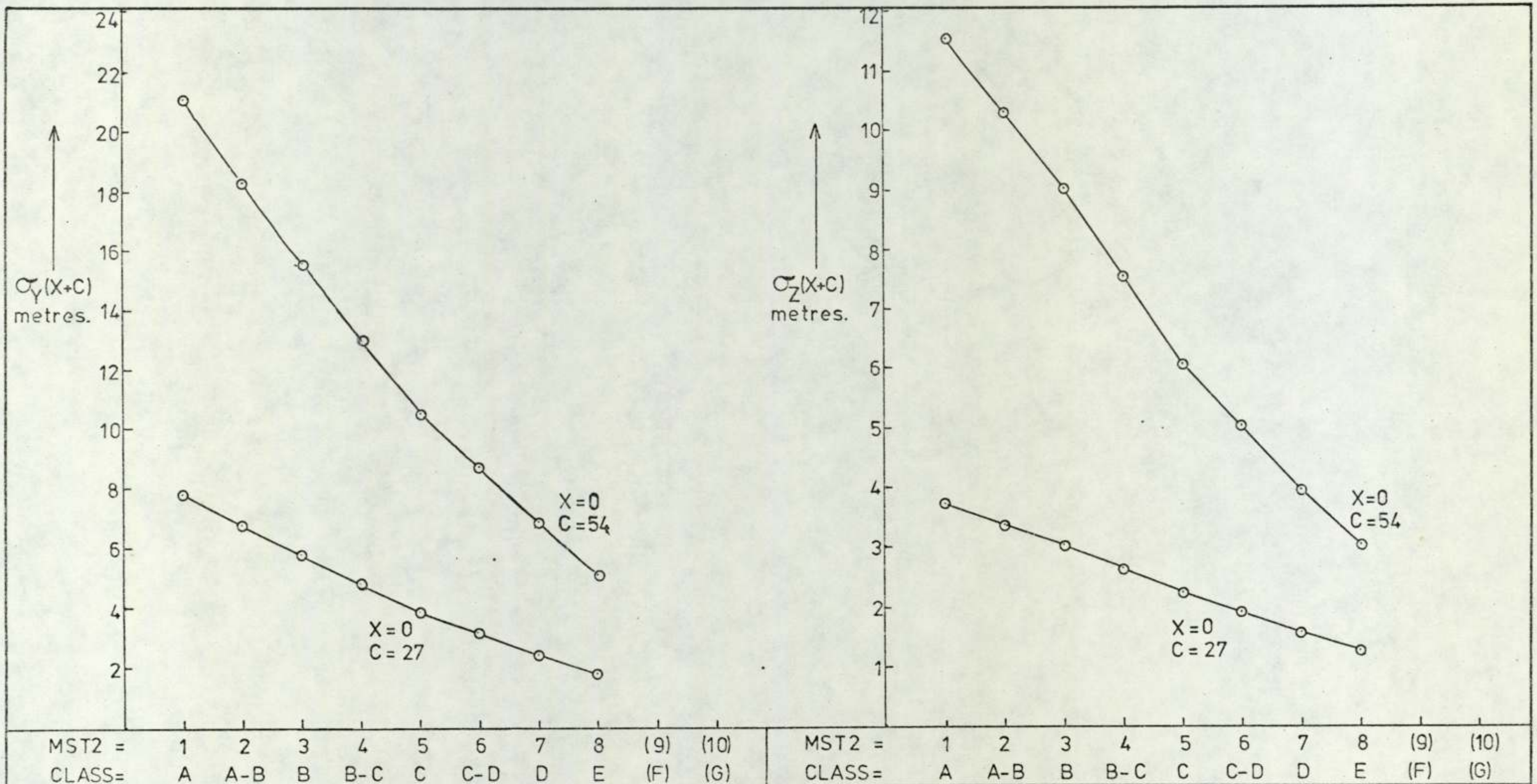

FIGURE 6.8 VARIATION OF INITIAL PLUME SIZE, AS GIVEN BY THE FORM $\sigma(X+C) = a(X+C)^b$ WITH X=0, DUE TO CHANGES IN STABILITY INDEX MST2. THE VALUES SHOWN WERE CALCULATED USING SUBROUTINE GEOMET.

the whole line when testing XDW against the end-point of the line (X2 for P2).

3. ROTATE (θ,X,Y,TX,TY) rotates the X, Y axes by $+\theta$ radians in the anticlockwise direction.

$$TX = X\cos\theta + Y\sin\theta$$

$$TY = -X\sin\theta + Y\cos\theta$$

4. CURVE(X1, Y1,X2,Y2,X3,Y3,R,CX,CY) fits a circle to three points (X1,Y1), (X2,Y2), (X3,Y3) and returns the radius R and centre (CX,CY). To avoid overflow when the Y axis happens to pass through (X1,Y1) and (X2,Y2), if Y1 equals Y2, the points are swopped around. This presupposes that no two points are co-incident, when an error occurs. The swop does not affect co-ordinates outside the sub-routine since X1,Y1, etc., are dummy variables local to the sub-routine.

5. STABIL (NNTIME, NNDAY, NMONTH, NLAT, NCLOUD, NWIND, MST2) returns the stability index MST2 according to the other variables (time, date, month, latitude, cloud cover, windspeed respectively). To match the coding (supplied by Dutton of the Meteorological Office: Section 5.3.2), the time NNTIME must be (hours x 10 + tenths), and the latitude NLAT (degrees x 10 + tenths). NLAT is input in this form; NNTIME is read as the hour, but multiplied by 10 before calling STABIL and divided by 10 afterwards. NWIND is in knots and NCLOUD is in oktas.

6. ARCTAN (X1,Y1,XC,YC) is a real function whose value is the arctangent (0 to 2π) of the gradient of the line (XC,YC) (X1,Y1). The ICL FORTRAN (1900 series) function ATAN(E) gives the arctangent of an expression E in the range $-\pi/2$ to $+\pi/2$. ARCTAN is called to calculate initial and final angular co-ordinates of curved sections (Figure 6.6) for element stepping: the angle is returned increasing in the anticlockwise sense from 0 at the X axis to 2π. Tests on the co-ordinates locate the relevant quadrant and appropriate multiples of $\pi/2$ are added to ATAN(E). Special cases arise at $3\pi/2$ and $\pi/2$, when X1 = XC. If Y1 $<$ YC the angle is $3\pi/2$, otherwise Y1 $>$ YC and the angle is $\pi/2$. By default if X1 = Y1 and Y1 = YC, the result is $3\pi/2$.

6.2.5 Input and Output

During data entry (Figure 6.3) extensive use is made of the ICL FORTRAN (1900 series) free formats (I0 and F0.0) with which spaces and ends of cards are skipped until the number is read. Since fixed formats are also used, care is needed in data preparation.

Input is arranged as follows:

1. Three emission parameters Q_{NO}, Q_{CO}, Q_{HC} (format F0.0). We used values of Q_L/T for 60/40 petrol:diesel mix as in Table 6.4.

2. Integer controls (format I0) to define programme operation. They are a number of hourly observations NMET, number of observer positions NLOC, total number of road sections (several may constitute one road) NSECT, step distance DELTAS in metres, and

number of distinct roads (and of traffic-counts to be read per hourly observation) NROAD.

3. Map references for observer positions entered as eight-digit (format I8: East and North each four-digit) Ordnance Survey references, accurate to nearest ten metres, followed by height to nearest metre.

4. Map references for road sections, in eight-digit Ordnance Survey, preceded by three identifying integers (format I2,I3, I2) for section number, road identity and curvature (equal to 1, 2 or 3: see Section 6.2.2). The road section map references, again in format I8, are each followed by the height in format I5. By default, spaces will be read as zero. At present only the height of the first map reference is used, but the input is general in case height interpolation is to be inserted (e.g. along a curve between the heights of the end-points).

5. NLAT as (degrees x 10 + tenths: 510 = $51^{\circ}\ 0'$) and NMONTH (format I0, I0).

6. Three channel input of field observations, weather readings and traffic counts, in the form of one data row (possibly several cards per row) per hourly observation. Field observations, for comparison purposes, had the time, date and site, followed by levels recorded for NO_x, NO, NO_2 (as NO_x - NO), Streeter Amet traffic flow at Salford Circus, CO and HC. Weather readings had time and date followed by wind-direction (degrees clockwise from North), windspeed (knots) and cloud cover (oktas). The traffic for each road (except road 3, Salford Circus) followed

the time and date. The three inputs used free format as far as possible.

Output is to two channels:

1. General run diagnostics and warnings such as error messages and various calculation results, including the co-ordinates of each element stepped out in the first integration only (Figure 6.9). This information is used for run checking.

2. A table of the levels of pollutant as measured and calculated.

6.3 Programme Accuracy

Calder (1973) gave approximate and exact formulae (Equations 5.15, 5.17) for the integral of the continuous point-source formula (Equation 5.8) over a linear source. The programme (section 6.2) should give the same results.

A special set of data files were set up to give the integral from the programme over finite-length line-sources (unit source-strength) for several distances and wind angles. Roads and observer positions were set up (Figure 6.10) using the usual Ordnance Survey type entry: downwind distance X ranged from 50 to 800m, so the line-source was 10X in length and the elements were in steps of X/10. Similar wind angles and unit wind speed (here 2 knots which is $1.02 ms^{-1}$) as Calder were used. Stability index MST2 was 7, which should give the same plume parameters as used by Calder, but in fact there was a slight difference: sub-routine GEOMET gave slightly different $\sigma_y(X)$ and $\sigma_z(X)$. The

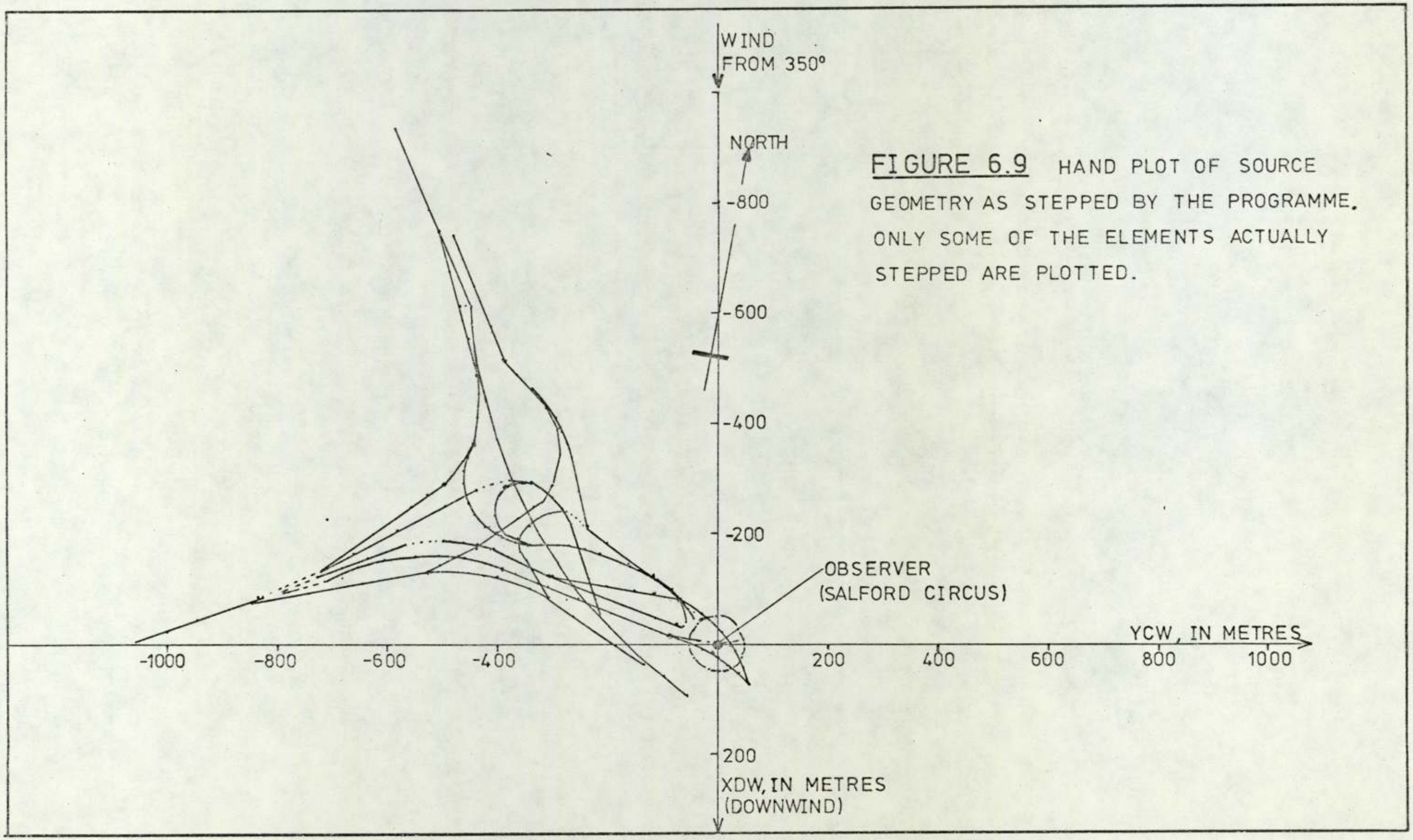

FIGURE 6.9 HAND PLOT OF SOURCE GEOMETRY AS STEPPED BY THE PROGRAMME. ONLY SOME OF THE ELEMENTS ACTUALLY STEPPED ARE PLOTTED.

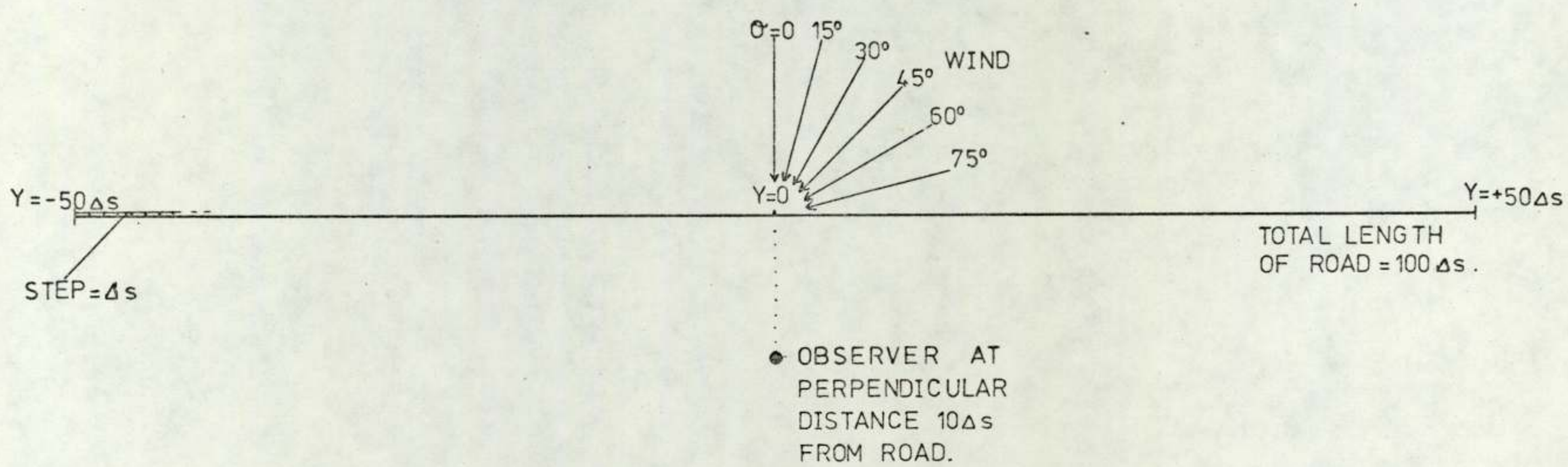

<u>FIGURE 6.10</u> ROAD LAYOUT, OBSERVER POSITION AND WIND DIRECTIONS FOR COMPARING THE VALUES GIVEN BY THE PROGRAMME WITH THOSE OF CALDER(1973).

TABLE 6.5

Comparison of Programme Results with those of Calder (1973)

(Unit Q_L, Observer Height = o, Road Height = o, Class D, 1.02 ms^{-1})

	X_o in m	Wind Direction							s in m	RD in m	σ_z in m
		0^o	15^o	30^o	45^o	60^o	75^o	90^o			
C[1]	50	0.218	0.221	0.231	0.250	0.282	0.338	-	-	-	3.666
P[1]		0.205	0.208	0.219	0.238	0.271	0.260	10^{-2}	5	500	3.813
C	100	0.141	0.143	0.148	0.156	0.171	0.197	-	-	-	5.652
P		0.136	0.137	0.142	0.152	0.168	0.160	10^{-3}	10	1000	5.767
C	200	0.085	0.086	0.088	0.092	0.099	0.121	-	-	-	9.342
P		0.084	0.085	0.087	0.092	0.099	0.095	10^{-3}	20	2000	9.326
C	400	0.049	0.050	0.051	0.054	0.061	0.076	-	-	-	16.13
P		0.050	0.050	0.051	0.054	0.058	0.060	10^{-4}	40	4000	15.73
C	800	0.031	0.031	0.032	0.034	0.038	0.048	-	-	-	26.15
P		0.029	0.029	0.030	0.032	0.036	0.040	10^{-4}	80	8000	27.16

Note 1: C = Calder, P = programme

discrepancy between Calder's integration values and those from the programme are believed to be due to this: Table 6.5 compares the two models. Some discrepancies (e.g. 200m and 75^{o}) may be due to the finite road-length and large wind-angle; the low values at 90^{o} probably reflect this.

6.4 Sensitivity of Calculated Levels

6.4.1 Effect of Step Length

The data file for comparing the programme with Calder (1973) for a downwind distance of 50m was used to study step lengths of 1m, 5m, and 50m. The first two gave practically the same results as Calder (1973) while a 50m step gave values that were higher (Table 6.6). In all work with the programme the step length was set to 5m (to balance accuracy with economy of iteration).

6.4.2 Effect of Heights

Observer and road heights were varied for a downwind distance of 50m (from the same line-source as in Section 6.3), with step length 5m.

In Table 6.7 we summarise these results: they show a very sensitive behaviour with height. The variation is rapid so the logarithm of the ground level concentration is plotted against road height in Figure 6.11. This shows an increasing dependence of the level on height: this is of particular importance at Salford Circus where the monitor is amongst elevated roads. The integral of pollution over the intersection may be very dependent on the heights of the roads that are used. The effect should be less at greater distances though.

TABLE 6.6

Effect of Step Length for 50m Downwind Distance:

Integral Values for Linear Source using Various Steps

and Wind Directions. (1.02 ms^{-1}, Class D, Unit Q_L)

Step, m	θ						
	0^o	15^o	30^o	45^o	60^o	75^o	90^o
1	0.2051	0.2084	0.2188	0.2382	0.2712	0.2579	0.00357
5	0.2051	0.2084	0.2188	0.2382	0.2712	0.2598	0.00373
50	0.623	0.0858	0.0309	0.4137	0.231	0.2787	0.00566

TABLE 6.7

Effect of Road and Observer Heights on Pollutant Levels for Linear Source

(1.02 ms^{-1}, Class D, Observer X_o = 50m, perpendicular wind, unit QL)

Observer height m	Road height, m					
	0	2	5	10	15	25
0	0.2051	0.1788	0.08684	0.006589	$0.8960.10^{-4}$	10^{-10}
5	0.08684	0.09429	0.1059	0.04346	0.003295	10^{-6}
10	0.006589	0.01208	0.04346	0.1026	0.04342	$0.4480.10^{-4}$
15	$0.8960.10^{-4}$	0.0003122	0.003295	0.04342	0.1026	0.003294
20	10^{-6}	$0.1495.10^{-5}$	$0.4480.10^{-4}$	0.003294	0.04342	0.04342
25	10^{-10}	10^{-8}	10^{-6}	$0.4480.10^{-4}$	0.003294	0.1026
30	10^{-14}	10^{-12}	10^{-10}	10^{-6}	$0.4480.10^{-4}$	0.04342
50	10^{-38}	10^{-35}	10^{-31}	10^{-24}	10^{-19}	0.04769
100	0	0	0	0	0	0
200	0	0	0	0	0	0

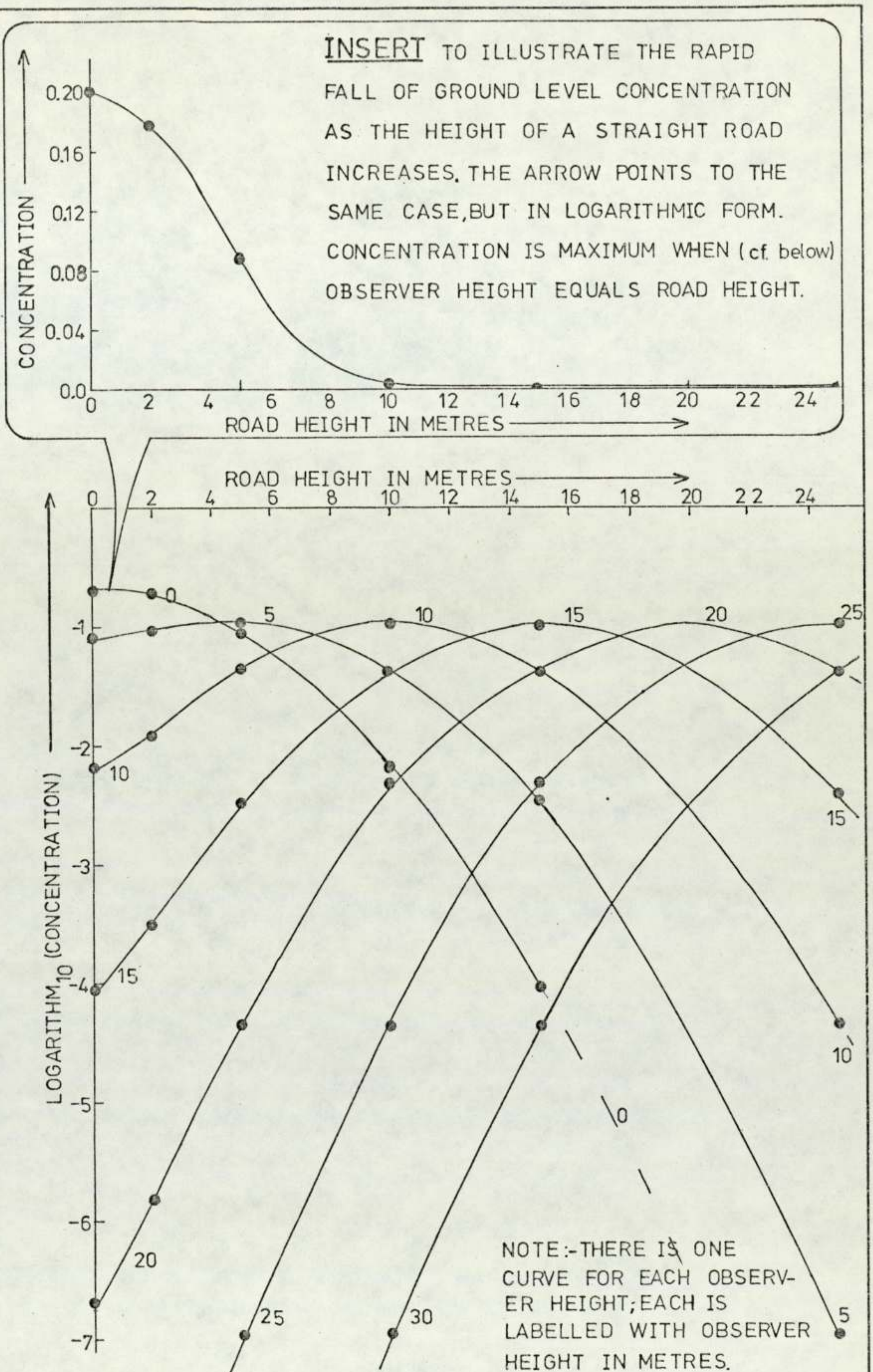

FIGURE 6.11 EFFECT OF ROAD HEIGHT ON DOWNWIND CONCENTRATION FOR SEVERAL OBSERVER HEIGHTS. CONCENTRATION WAS CALCULATED AS VOLUME-VOLUME RATIO USING PROGRAMME SPAG68, DOWNWIND DISTANCE 50m (cf. FIGURE 6.10, $\theta = 0°$), MST2 = 7, Q = 1, U = 2 kt or 1·02 ms^{-1}.

6.4.3 Wind Direction

In the case of a line source, the effect is slight: see Calder (1973) and Table 6.5. The integral runs into problems at large angles because a finite length of road is used.

6.4.4 Windspeed

Predictions vary as U^{-1} (an over-simplification since the choice of MST2 depends on U also).

6.4.5 Sensitivity of Integral over the Intersection

When studying real-life situations there is a problem as to how many combinations of variables should be considered (cf. Geomet, 1971). This study was restricted to predictions at locations outside of and downwind from the intersection (Map: Figure 6.12). A typical set of evening rush-hour traffic was used for all roads: the programme was modified with a special series of DO loops to generate combinations of wind-direction, stability category and wind-speed. Some of the more interesting results are shown in Figure 6.13 to 6.20. These predictions used the emission parameter given in Table 6.4 for NO.

In Figure 6.12 we show the observer positions and the wind directions used in the sensitivity study. Figures 6.13, 6.14 show the downwind concentration curves for a range of stabilities. Roughly speaking, the pollutant concentration varies by about 10 - 20% (Figure 6.14) with unit change in MST2 (although more exactly this depends on which part of the figure is used).

The wind-speed curves (Figure 6.15) reflect the inverse relation

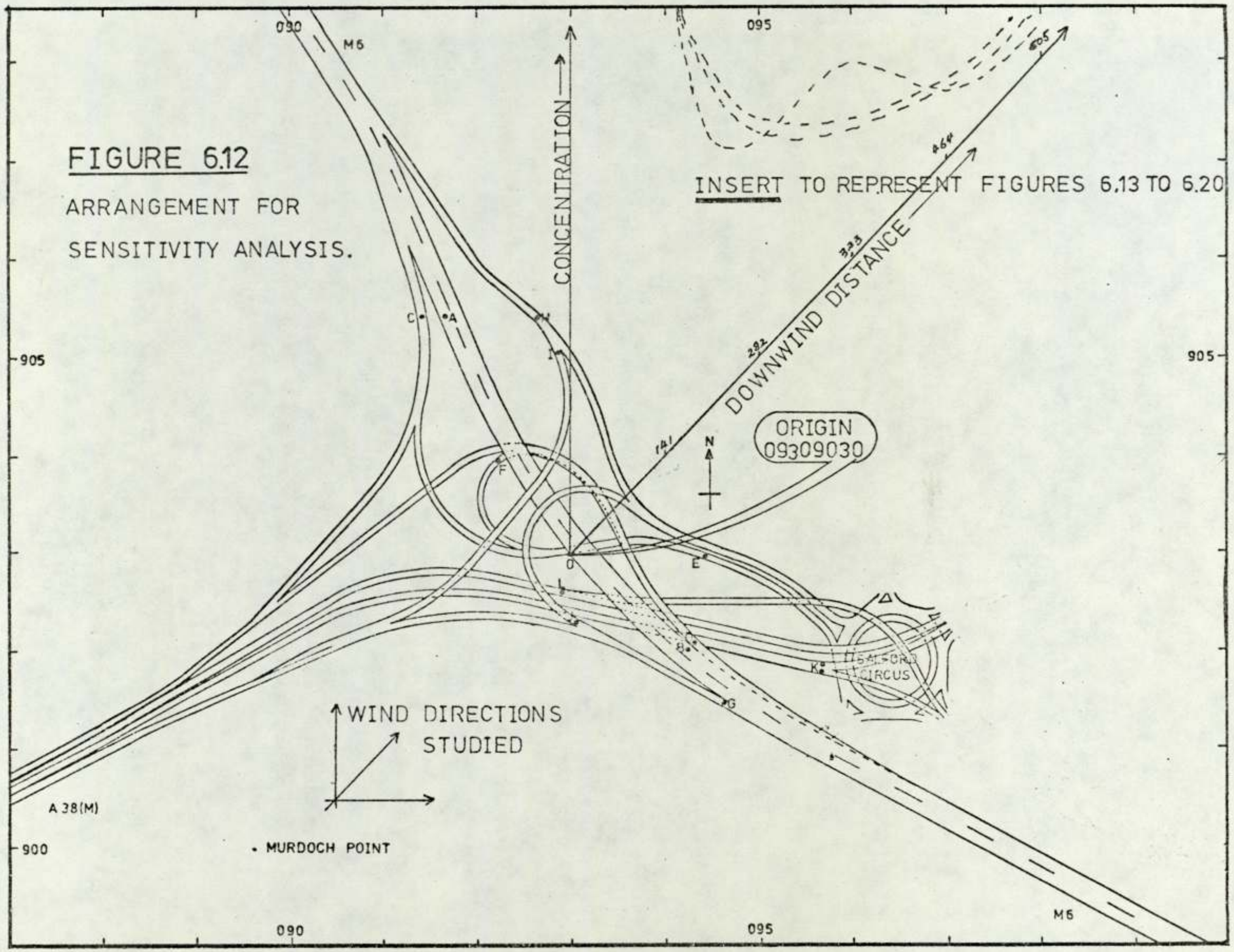

FIGURE 6.12
ARRANGEMENT FOR
SENSITIVITY ANALYSIS.
CONCENTRATION
DOWNWIND DISTANCE
INSERT TO REPRESENT FIGURES 6.13 TO 6.20
ORIGIN
09309030
WIND DIRECTIONS
STUDIED
M6
A 38(M)
MURDOCH POINT
SALFORD
CIRCUS
090
095
905
900

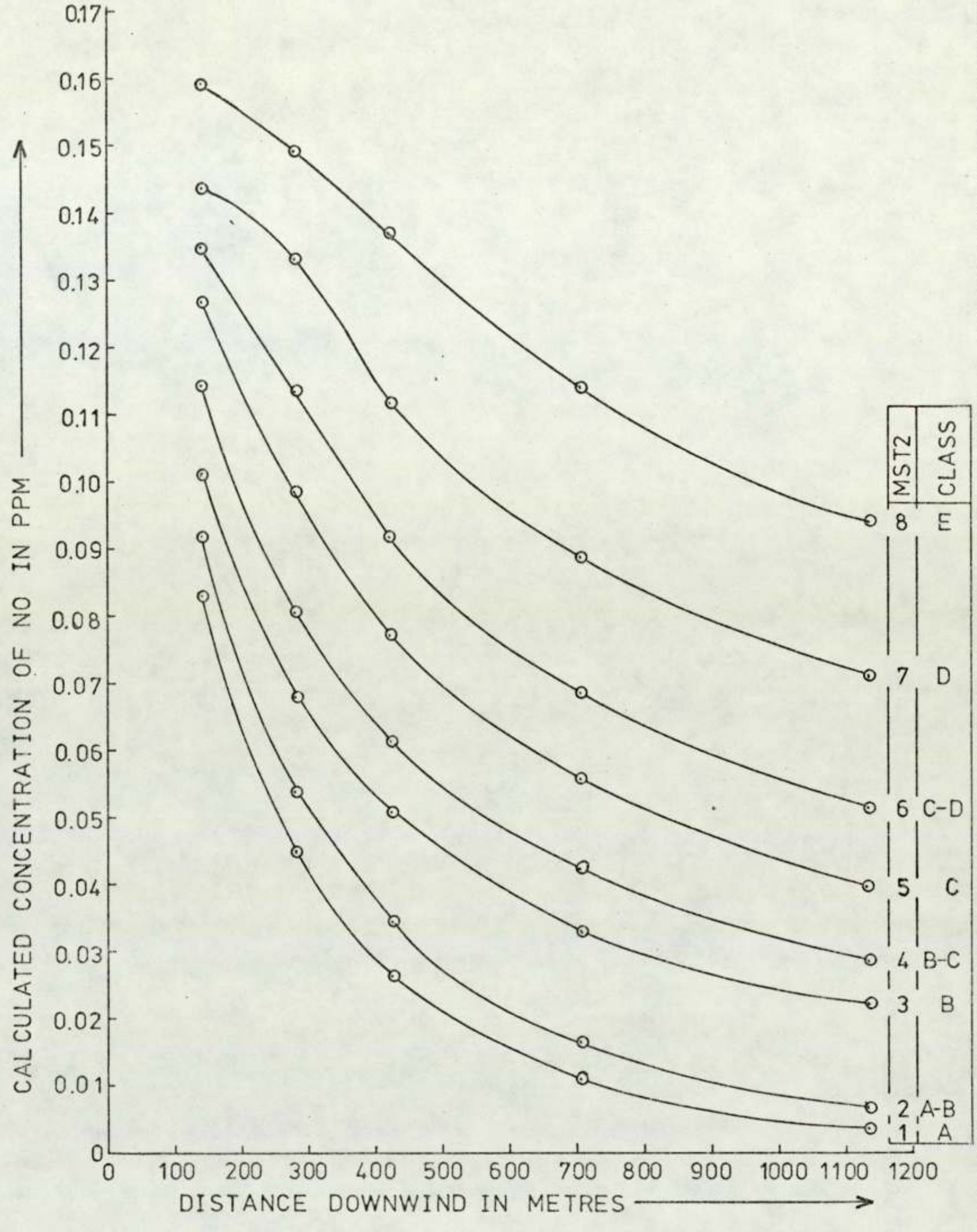

FIGURE 6.13 VARIATION WITH DISTANCE DOWNWIND FROM THE INTERSECTION OF NO CONCENTRATION, CALCULATED FOR STABILITY CLASSES A TO E USING MST2 =1 TO 8.

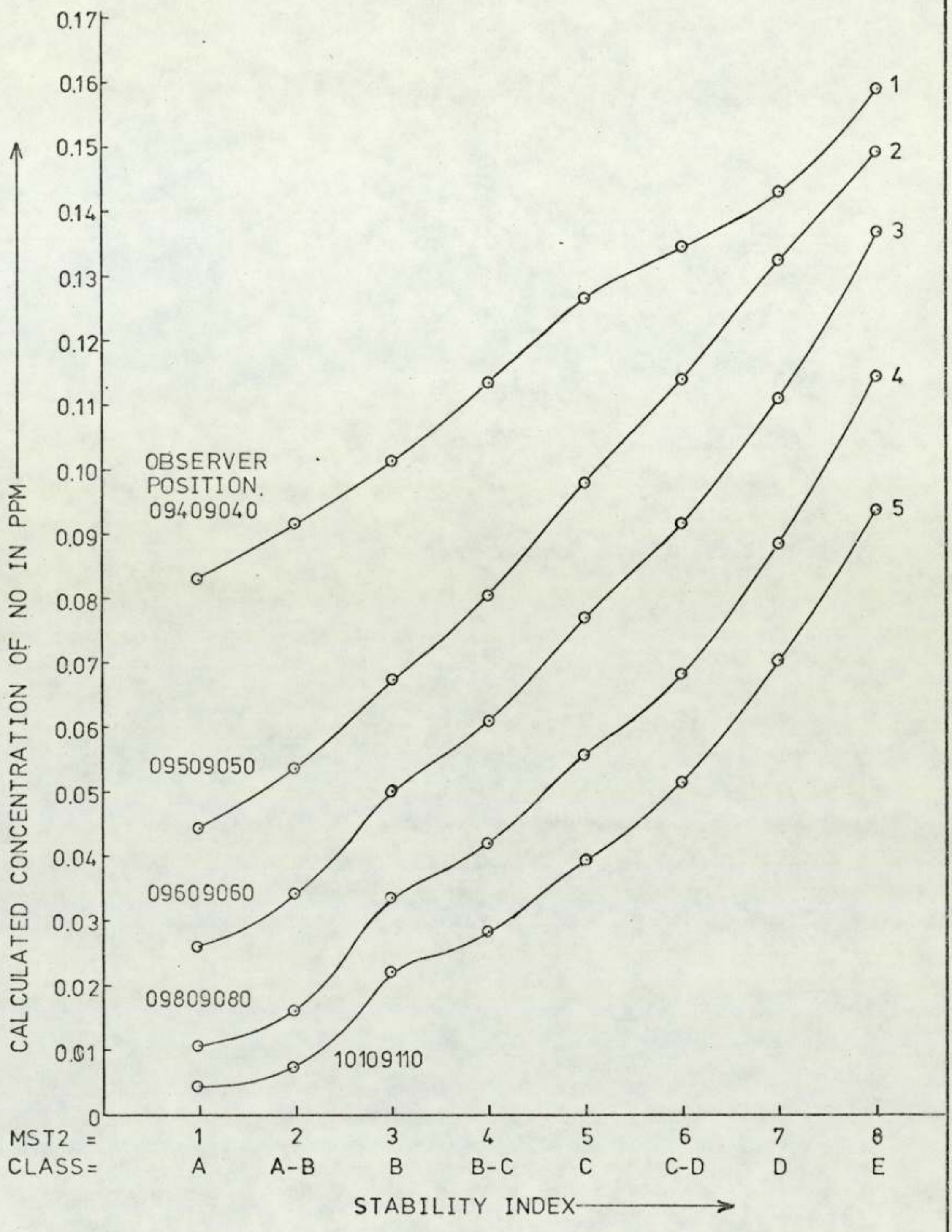

FIGURE 6.14 VARIATION WITH STABILITY INDEX MST2 OF NO CONCENTRATION, CALCULATED FOR SEVERAL DISTANCES DOWNWIND FROM THE INTERSECTION. TIME 17-00

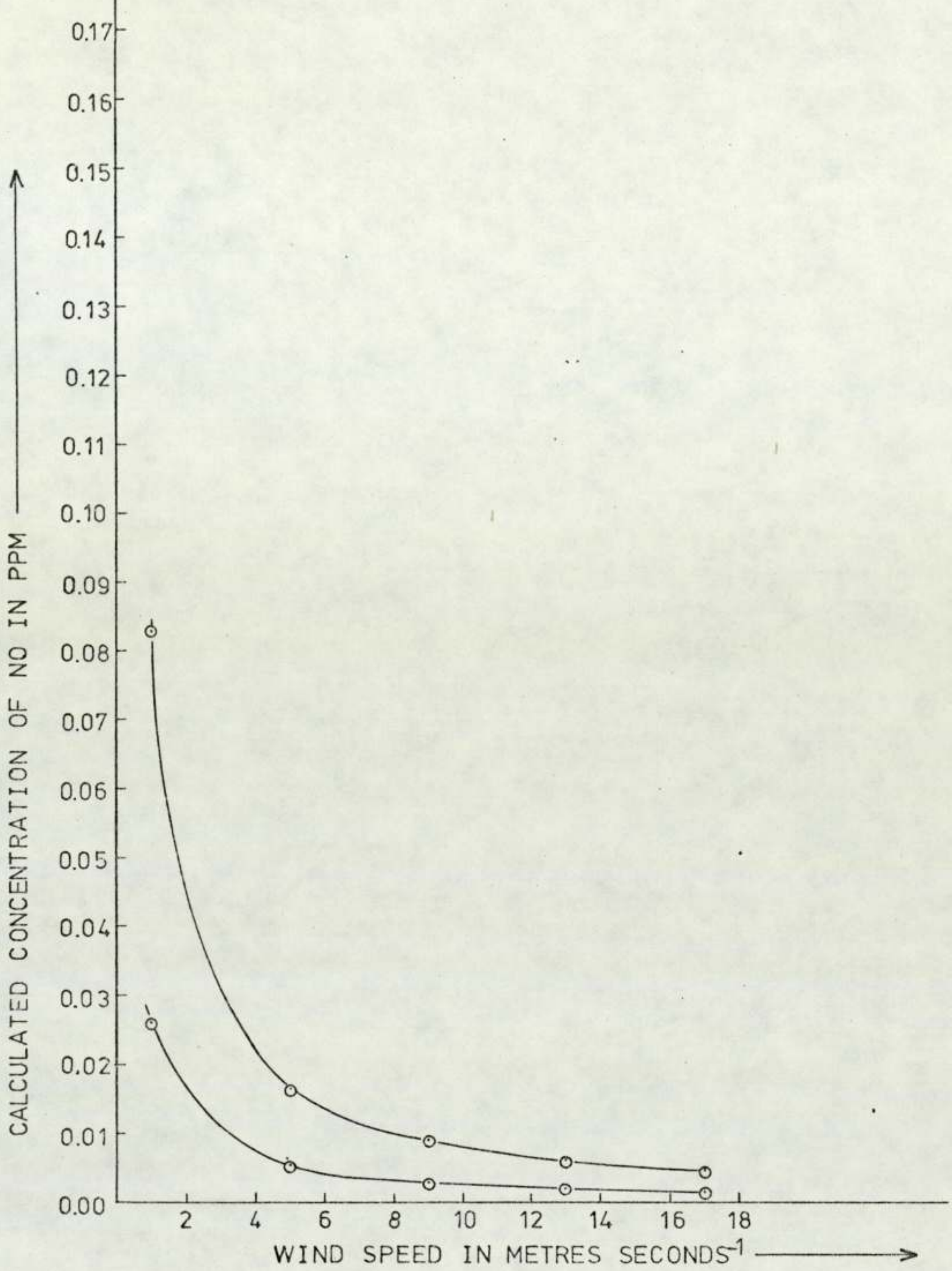

FIGURE 6.15 VARIATION WITH WINDSPEED OF NO CONCENTRATION, CALCULATED FOR TWO DOWNWIND DISTANCES.

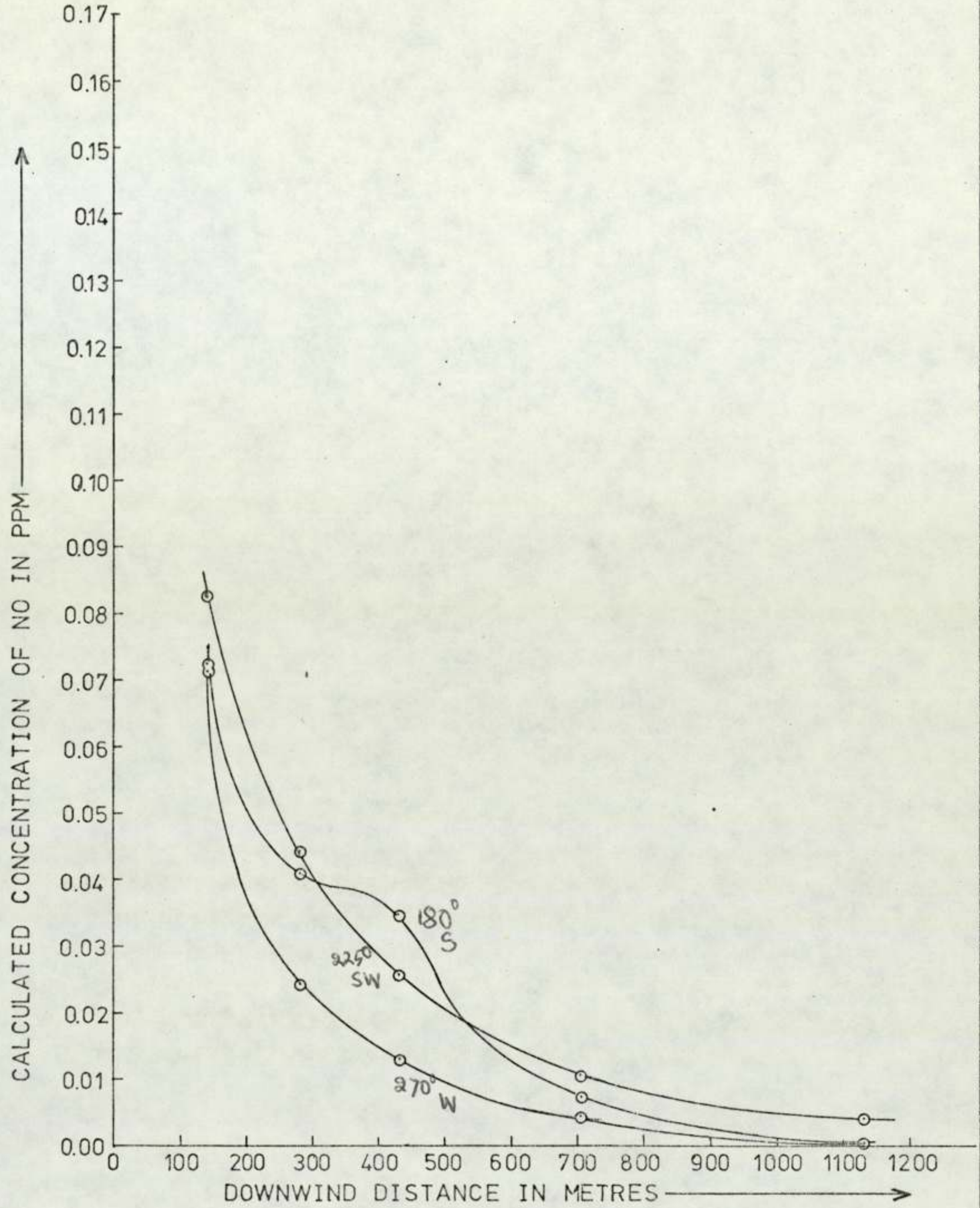

FIGURE 6.16 VARIATION WITH DISTANCE DOWNWIND FROM THE INTERSECTION OF NO CONCENTRATION, CALCULATED FOR THREE WINDDIRECTIONS WITH MST2 =1 (CLASS A).

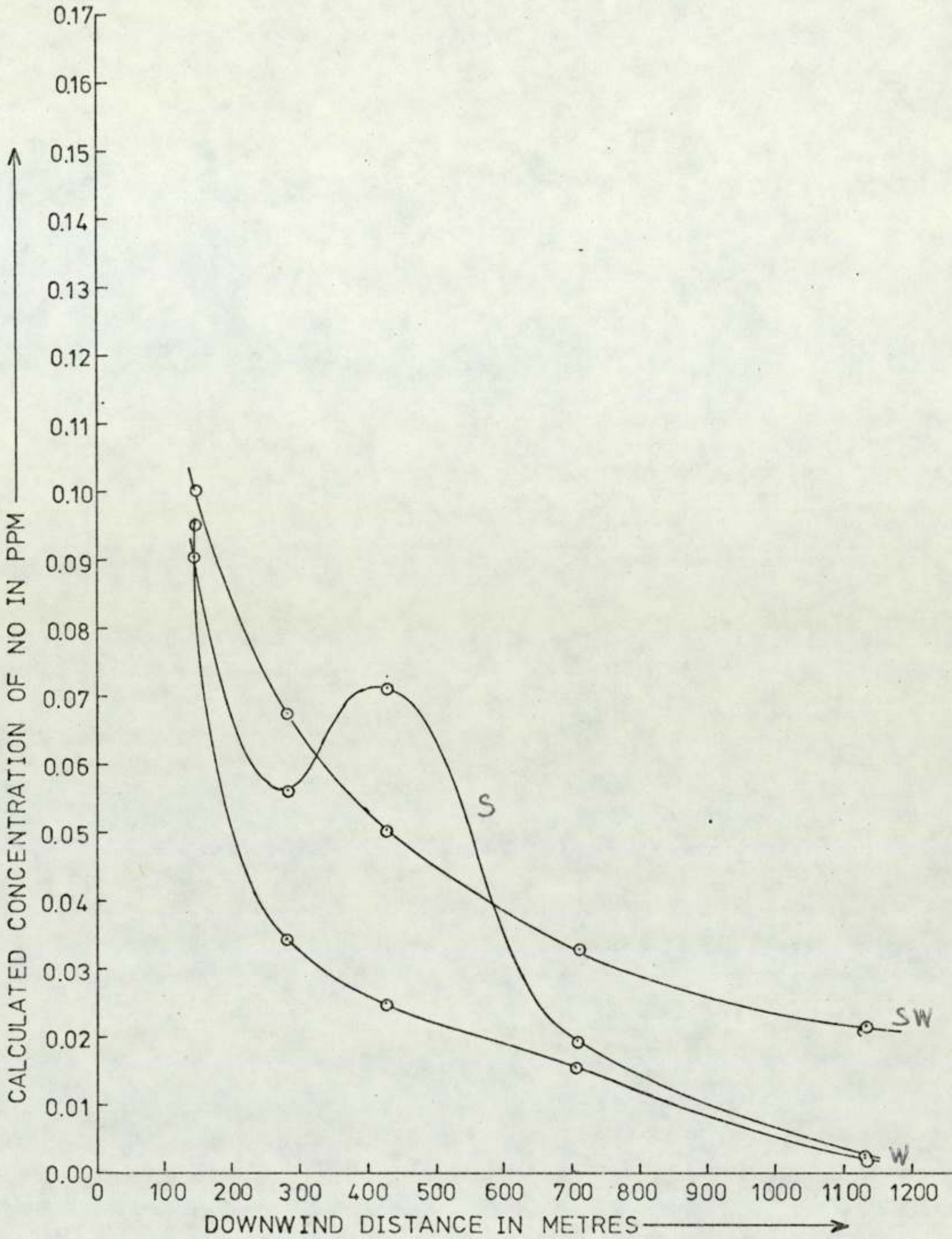

FIGURE 6.17 VARIATION WITH DISTANCE DOWNWIND FROM THE INTERSECTION OF NO CONCENTRATION, CALCULATED FOR THREE WINDDIRECTIONS WITH MST2 = 3 (CLASS B).

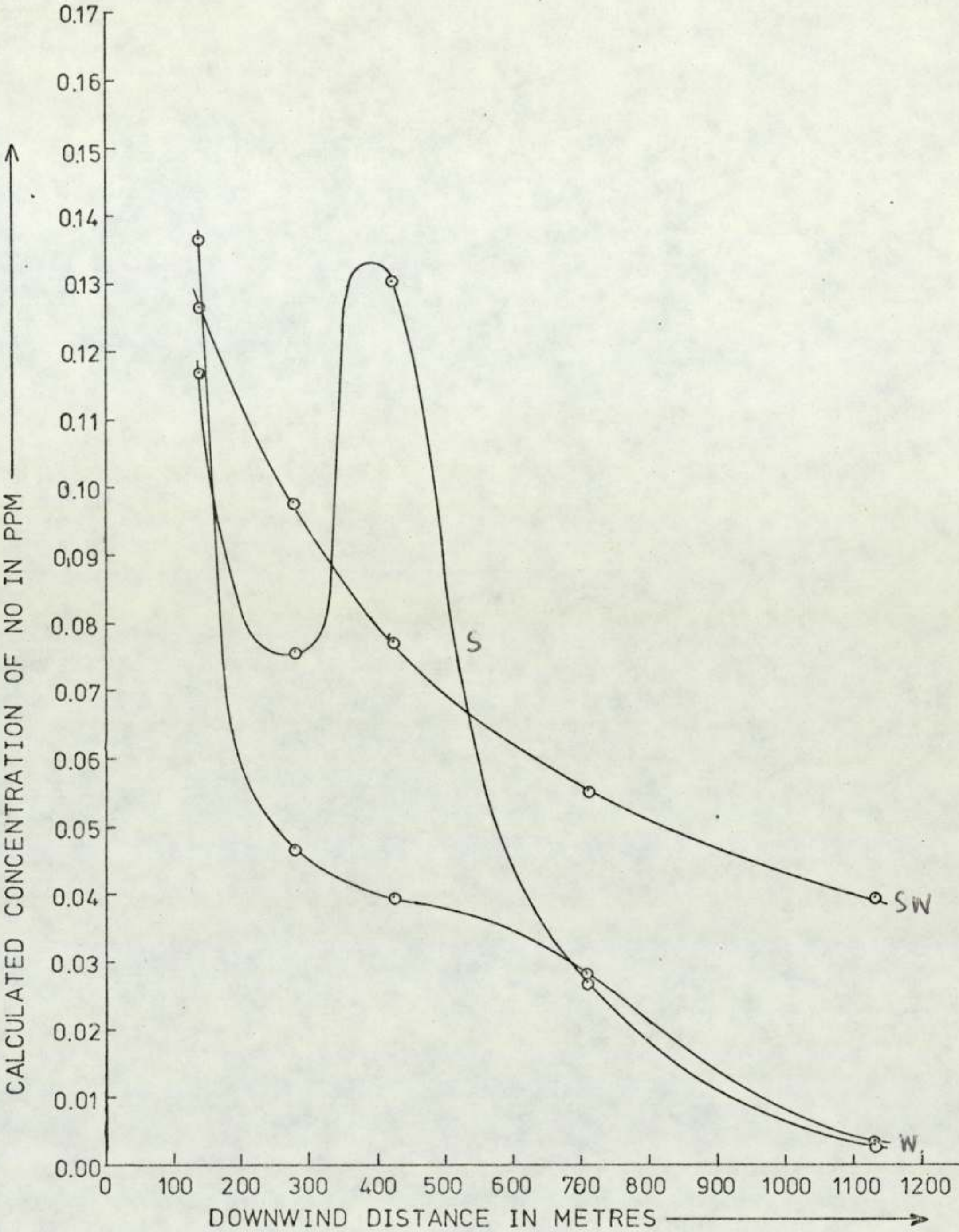

FIGURE 6.18 VARIATION WITH DISTANCE DOWNWIND FROM THE INTERSECTION OF NO CONCENTRATION, CALCULATED FOR THREE WINDDIRECTIONS WITH MST2 = 5 (CLASS C).

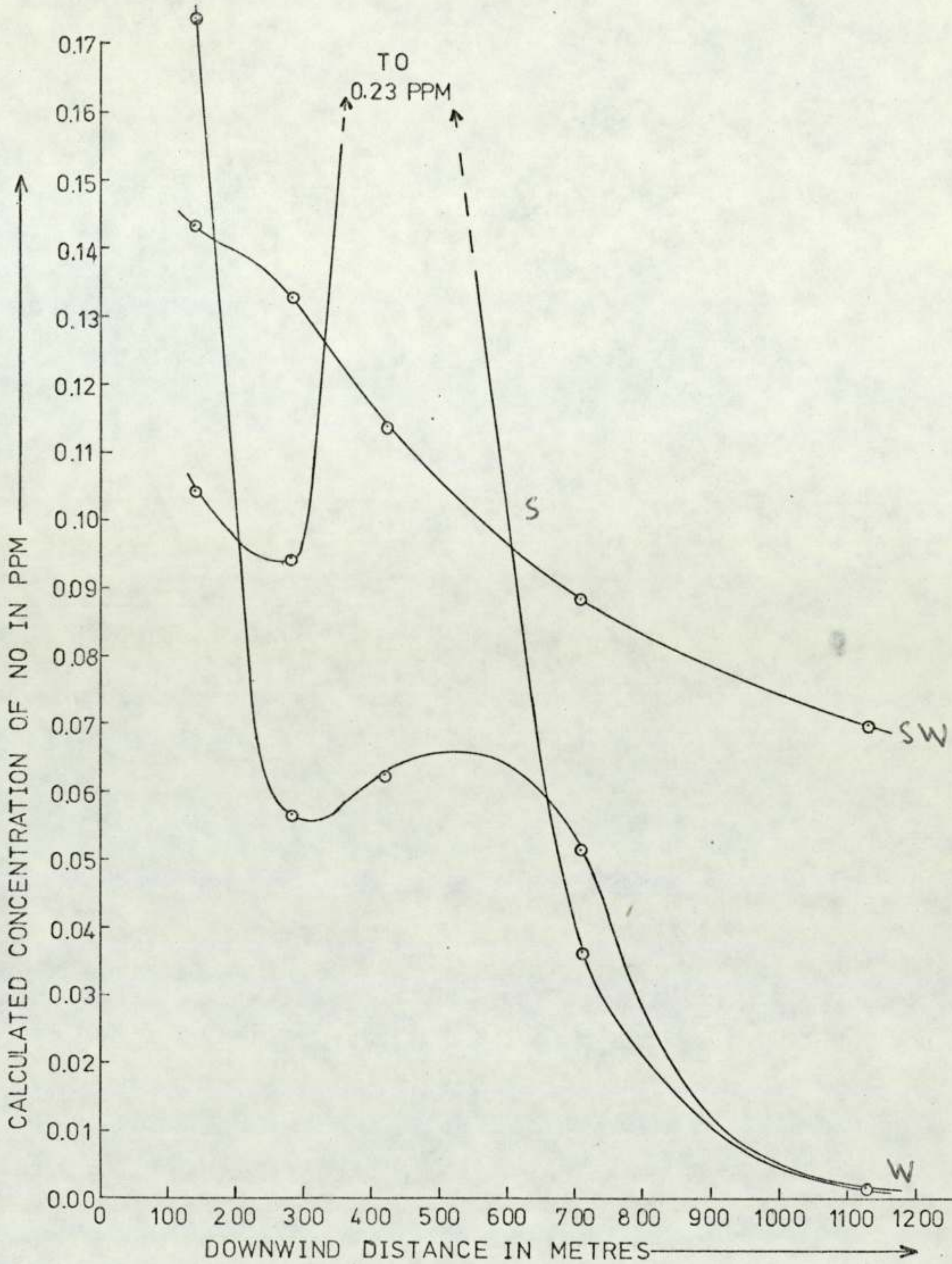

FIGURE 6.19 VARIATION WITH DISTANCE DOWNWIND FROM THE INTERSECTION OF NO CONCENTRATION, CALCULATED FOR THREE WINDDIRECTIONS WITH MST2=7(CLASS D)

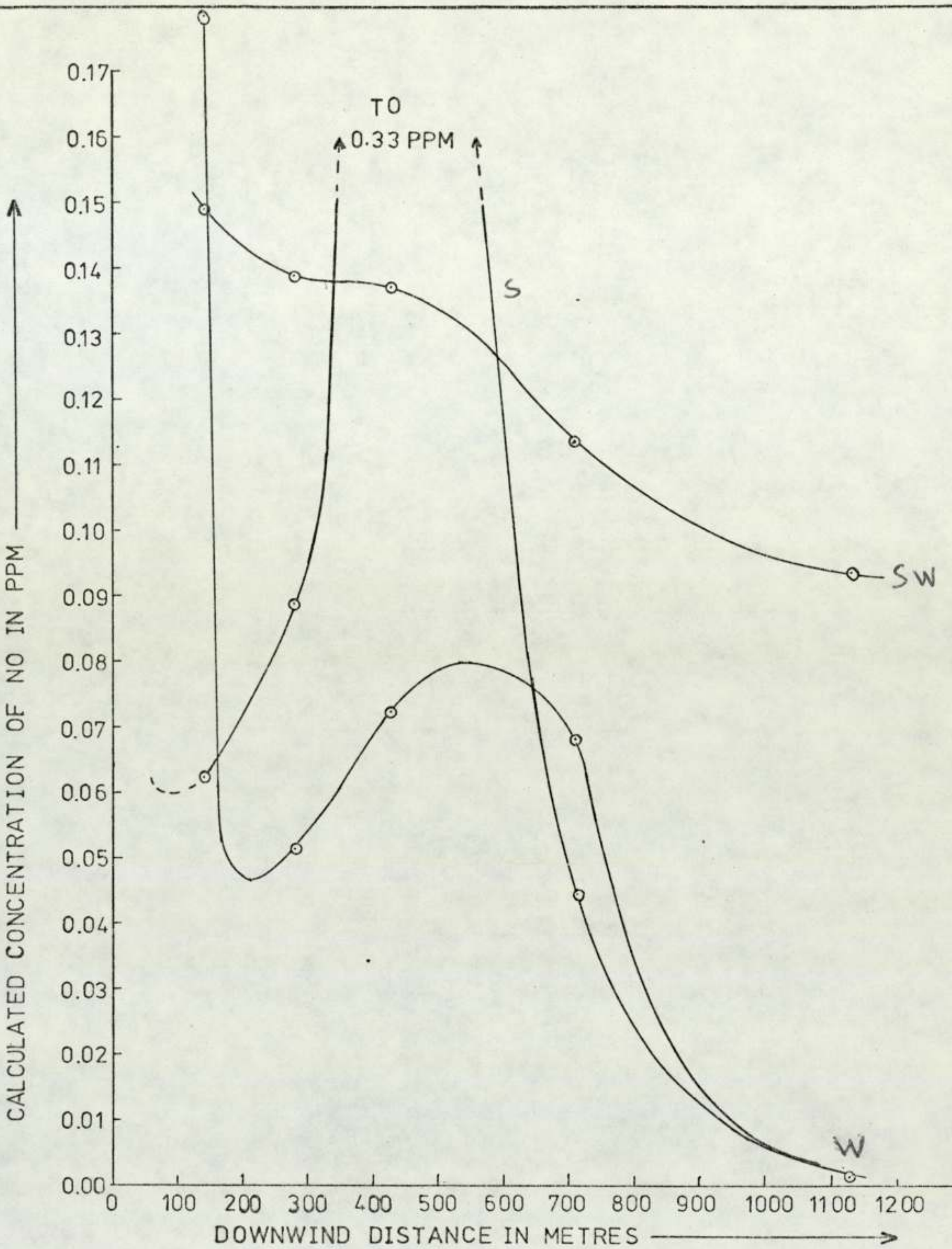

FIGURE 6.20 VARIATION WITH DISTANCE DOWNWIND FROM THE INTERSECTION OF NO CONCENTRATION, CALCULATED FOR THREE WINDDIRECTIONS WITH MST2 = 8 (CLASS E).

between concentration and wind-speed for any given downwind distance (assuming no change in MST2: a complete analysis of wind-dependence including changes in stability category would have required greater programme changes).

The Figures 6.16 to 6.20 are a series of plots which together may be explained by reference to the map (Figure 6.12). As the stability index MST2 increases so does the general level of pollutant concentration. In addition for a S wind the peak (Figures 6.16 to 6.20) at a place approximately due North of Salford Circus is due to the pattern of source-strengths implied by the map (Figure 6.12) and the traffic densities. The diagonal traverse through the roundabout plume superimposes a pollutant peak on the broad decay. In practice the peak would be less pronounced: our model of the intersection is a simplified one.

6.5 Programme Limitations and Possible Improvements

The following limitations and suggested modifications draw on Chapter 5 and Sections 6.1 - 6.4.

1. Source-strength parameter is difficult to arrive at satisfactorily: a variable emission parameter might be of value.

2. The effect of finite plumes as represented by the variable c (set to 27m here) has not been closely examined: Figure 6.8 summarises a study of its effect on $\sigma_y(0)$ and $\sigma_z(0)$. The format $\sigma(X + c)$ was used, but $\sigma(X) + \sigma_c$ should be studied (Section 6.2.4).

3. Extrapolation of open country plumes to the structurally complex

intersection ignored local eddy effects.

4. Zero winds cannot be modelled (cf. discussion in Chapter 5).

5. A version (SPAGSIMP) was developed with simplified data input for predictive work only: the input of field results was removed, observer positions were read to the nearest metre and traffic for all roads read from input channel 5. This will be used in Chapter 7.

6. The subroutine GEOMET was constructed from curves for five stability classes (Table 5.3), while there are ten possible values for stability index MST2. It does generate in-between categories (e.g., A-B) as suggested by Pasquill (1961), but does not fully exploit the range of MST2 (categories E,F,G treated as E). Modifications here might well be linked to the problem of urban diffusion (see above Paragraph 3).

7. The programme is limited in application to latitudes 48N and 60N: subroutine STABIL could be replaced by one applicable to all locations, e.g., using solar elevation (Johnson et al., 1971), or where measurements permit, turbulence statistics from bivanes (Section 5.3.1).

8. No consideration was given to downwind limits on vertical mixing (in this study downwind distances were < 1km) or to pollutants from outside the intersection. The latter defect is partly a matter of data entry (additional, more distant roads may be used) and partly of programme changes to include other, non-traffic, sources (cf. introduction, Chapter 1: Figure 1.3).

9. Sloping roads could be handled by a height-interpolation subroutine.

10. Application to particulates has not been discussed: the programme may be used directly if settling is to be ignored, or a modified plume equation with a term for the mean settling velocity could be integrated.

6.6 Programme Calculations and Routine Monitoring Results

So far in this Chapter we have described emissions estimates and a programme to calculate concentrations of NO, CO and HC from traffic: the accuracy of the programme for a simple test case was assessed by reference to the model of Calder (1973). The sensitivity of the calculations to several parameters was considered. Following these discussions of the programme's development and behaviour, which aimed at highlighting limitations due to its construction, we turn now to assess its performance in practice. This will require reference to a large body of monitoring results: to avoid repetition and awkward cross-referencing this section is in three parts - the first considers model performance, and the other two, general features of the measured levels. This section as a whole essentially completes discussion of the routine monitoring work.

6.6.1 Comparison of Measured Pollutant Levels with Programme Calculations

The measured and calculated levels for Salford Circus were analysed with the aid of the ICL 1900 series statistical Analysis Package (XDS3/22) on the 1904S computer.

Simple regressions of the straight line form Y = MX + c, with calculated level Y, measured level X, assessed programme performance.

Table 6.8 summarises the analyses, which used the concentrations displayed in Figures 6.21 to 6.25. For a perfect model the regression coefficient (M) and correlation coefficient would be unity. Figure 6.31 draws on earlier discussions to suggest possible discrepancies. If we assume the emissions parameter Q_i (representing Q_{NO}, Q_{CO}, or Q_{HC}) is causing the regression coefficient M to deviate from unity, a parameter (Q_i/M) would remove the deviation: rearranging the above we have

$$\text{measured level} \quad X = \frac{Y}{M} + \left(\frac{-C}{M}\right)$$

with a background level of (-C/M) to add to the new calculated level, i.e. after Y has been enlarged to (Y/M). For NO_X, CO and HC the regression gave c as negative, or the background, $\left(\frac{-C}{M}\right)$, as positive. For all the gases, except NO_2, there is a good correlation (Table 6.8) between the measured and calculated levels, suggesting that the model is adequately describing the hourly fluctuations of pollutant levels at Salford Circus. The regression coefficients are not unity: this suggests a discrepancy due to the uncertainties in emissions estimate on one hand and the uncertainties in absolute calibration on the other. Table 6.10 indicates the emissions parameters increased from those as used (Table 6.4) to make the model "fit", and associated ppm levels in the exhaust. The new exhaust levels for NO appear reasonable in the light of those for various driving modes given in Table 6.3.

For CO, they seem high and for HC very high. These results probably reflect the combined effect of the various errors (Figure 6.31): the CO analyser was running at the low end of its scale, while the HC levels showed a steady high background (Figures 6.25 and 6.30). Considering the general problems of calibration (Chapter 2) and of deciding which driving mode and hence which emissions estimate to use, it is likely that improvements in model fit require work on various fronts: techniques of monitoring (accurate zeroes, calibrations, use of additional sites to identify the incoming background level and the level at the intersection), emissions estimates (particularly driving mode effects and other sources as contributing to the incoming background level), and on site meteorological measurements.

6.6.2 Background Levels

Table 6.9 and Figures 6.26 to 6.30 summarise the levels at the Murdoch Point site (500m from the intersection on the city side), for a period when winds were generally from the city.

For NO and NO_x at Murdoch Point the mean levels were respectively one quarter and one tenth of those at the intersection. They were similar both to the minimum levels of NO and NO_x, and to the background level (estimated as $^{-C}/M$ from the regression) for NO_x. The background level estimated for NO was negative: this reflects the inaccuracies of both the data and the model.

For all the gases, except NO_2, mean levels at Murdoch Point tended to be lower than at Salford Circus. The ratios of mean level at Murdoch Point to that at Salford Circus were, For NO_x, 0.23; for NO, 0.10; for NO_2, 1.1; for CO, 0.36 and for HC, 0.74.

6.6.3 Oxides of Nitrogen

At Salford Circus, NO and NO_x were very similar (Figures 6.21, 6.22 and Table 6.8) with correlation coefficients of 0.76 with the calculated levels, and similar means (NO, 0.117 ppm; NO_x, 0.106 ppm), minima (NO, 0.015 ppm; NO_x, 0.011 ppm), maxima (NO, 0.381 ppm; NO_x, 0.410 ppm), and variances (NO, 0.00711 ppm^2; NO_x, 0.00813 ppm^2). This is because NO_x is NO plus NO_2, and the levels of NO_2 were low relative to those of NO: mean NO_2 was 0.0141 ppm and the maximum 0.086 ppm.

NO_2 (Figure 6.23) at Salford Circus shows frequent zero values: the NO_2 value was the difference between mean hourly values of NO_x and NO. Periods of least fluctuation (to zero and back) of the NO_2 appeared when the NO and NO_x levels were low, and, probably more important, showed less fluctuation in magnitude: the hourly averages were for finite samples from a non-stationary random process (cf. Chapter 3) so have greatest uncertainty at times of greatest fluctuation. The behaviour of NO_2 at Murdoch Point was consistent with this for the NO and NO_x levels were much less variable (Figures 6.26, 6.27) and the NO_2 (Figure 6.28) shows no such oscillation.

The measurement of NO_2 as (NO_x - NO) using finite sampling (15 points per hour) of NO_x and NO was unsatisfactory at Salford Circus, which was near traffic and where large rapid fluctuations occurred in NO levels. It was satisfactory where levels of NO fluctuated much less.

The ratio of mean NO to mean NO_2 at Salford Circus was 7.5:1, consistent with the suggestion (Derwent and Stewart, 1973) that exhaust gases enter the atmosphere with nine parts of NO to one part of NO_2 by volume. At Murdoch Point the ratio of mean NO to mean NO_2 was 0.68:1. This site is further from sources (for the period in question winds were from the city) and the general level of NO was lower than at Salford Circus. The ratio suggests there has been significant dilution and probably oxidation of the NO. According to Derwent and Stewart (1973), the ration NO/NO_2 may be expressed in the form

$$[\mathrm{NO},\ \mu gm^{-3}] / [\mathrm{NO_2},\ \mu gm^{-3}] = 0.130 + 0.009\,[\mathrm{NO},\ \mu gm^{-3}]$$

where square brackets represent concentrations in the units shown. Bibbero and Young (1974a) give conversions ($0^{o}C$, 1atm)

$$[\mathrm{NO},\ \mu gm^{-3}] = [\mathrm{NO, ppm}]\,.\,M_{NO}\,.44.64 = 1.3392.10^{3}\,[\mathrm{NO, ppm}]$$

$$[\mathrm{NO_2},\ \mu gm^{-3}] = [\mathrm{NO_2 ppm}]\,.\,M_{NO_2}\,.44.64 = 2.0534.10^{3}\,[\mathrm{NO_2, ppm}]$$

In Table 6.11 we give, using μgm^{-3} units, the ratios of NO and NO_2 as recorded and as derived from the recorded NO concentrations using the empirical rule (Derwent and Stewart, 1973) above. The ratios from the recorded concentrations are comparable with those given by the rule.

M = Mol. Wt.

6.7 Summary

Traffic counts and concentrations of pollutants in the exhaust were used to estimate the emission of pollutants from traffic on the intersection. We described trigonometry to define the geometry of any intersection using a minimum of map references. Drawing on the discussions in Chapter 5 of turbulent diffusion, the dilution of gas blown from any part of the intersection to the observer was estimated by integrating a point-source plume formula. Plume parameters were estimated indirectly, and rotation of axes solved the problem of wind direction. Programme improvements were suggested.

The programme was compared with numerical results of Calder (1973), and a sensitivity analysis studied the behaviour of the model. It was also compared with hourly measurements taken over a ten day period, giving a good correlation with all gases except NO_2, which had a measurement problem.

Results of the routine monitoring were recorded and processed with a view to checking such a programme as the one developed, and therefore the emphasis was on reliable measurement of all gases simultaneously. Realising that the data cover only three weeks, and could therefore be unrepresentative, we have given some discussion of the concentrations reported for the two sites.

In the next Chapter we describe an experiment to study dilution as a function of distance and height. The design of equipment precedes comparison of concentration gradients recorded in the field with those given by the programme.

TABLE 6.8

Comparison of Calculated and Measured Pollutant Concentrations:

Regression Results for (calculated) = m(measured) + c

Gas	Regression Analysis (5% significance level)						Measured levels, ppm			
	Regression Coefficient m	Intercept c	Correlation Coefficient R	Degrees of Freedom	$^1/_m$	Background ($^-c/m$)	Mean	Minimum	Maximum	Variance
NO_x	0.340	- 0.00322	0.76	236	2.940	+ 0.00947	0.117	0.015	0.381	0.00711
NO	0.319	0.00246	0.76	236	3.135	- 0.00771	0.106	0.011	0.410	0.00813
NO_2	rejected at 5% significance level			237	-	-	0.0141	0.000	0.086	0.000175
CO	0.0471	- 0.0521	0.67	236	21.2	+ 1.106	2.95	1.20	11.7	1.66
HC	0.00492	- 0.0236	0.72	236	203	+ 4.80	5.89	4.50	8.8	0.670

TABLE 6.9

Background Levels from Murdoch Point: prevailing wind from city and not from intersection

Gas	No regression: model gave zero results because of wind direction			Measured levels, ppm			
				Mean	Minimum	Maximum	Variance
NO_x		140 obsn^s		0.0264	0.0080	0.129	0.000297
NO		140 obsn^s		0.0107	0.0040	0.081	0.000123
NO_2		140 obsn^s		0.0157	0.0010	0.048	0.0000729
CO		140 obsn^s		1.07	0.40	3.10	0.148
HC		140 obsn^s		4.33	3.40	6.60	0.591

TABLE 6.10

Increased Emission Parameters, Qi/m,

Using Regression Coefficient of Calculated to Measured Levels. (See Table 6.4)

Gas	Emission parameter used Qi (Table 6.4)	Increased Emission			
		$^{1}/_{m}$	Qi/m	ppm Petrol	ppm Diesel
(NO_x)	$4.7843.10^{-4}$	2.940	$1.407.10^{-3}$	-	-
NO		3.135	$1.500.10^{-3}$	5330	1550
(NO_2)	-	-	-	-	-
CO	$1.1400.10^{-3}$	21.2	$2.417.10^{-2}$	127000	6360
HC	$7.116.10^{-5}$	203	$1.445.10^{-2}$	52800	14200

<u>TABLE 6.11</u>

<u>Ratios of NO and NO_2 Concentrations</u>

Site	Measured Concentrations					Empirical Rule[3]
	[NO_2 ppm]	[NO, ppm]	[NO_2, μgm^{-3}]	[NO, μgm^{-3}]	[NO, μgm^{-3}]/ [NO_2, μgm^{-3}]	
Salford[1] Circus	0.0141	0.106	28.952	141.95	4.9	1.4
Murdoch[2] Point	0.0157	0.0107	32.238	14.329	0.44	0.26

Note 1: See Table 6.8

Note 2: See Table 6.9

Note 3: [NO, μgm^{-3}] / [NO_2, μgm^{-3}] = 0.130 + 0.009 [NO, μgm^{-3}] after Derwent and Stewart (1973), with [NO, μgm^{-3}] as recorded

The following 25 pages
contain Figures 6.21 to 6.30
inclusive

Figures 6.21 to 6.25 each have three parts (1/3, 2/3, 3/3) and are for November 1974 at Salford Circus

Figures 6.26 to 6.30 each have two parts (1/2, 2/2) and are for March 1974 at Murdoch Point

Observations are labelled by time and date: some times are missing.

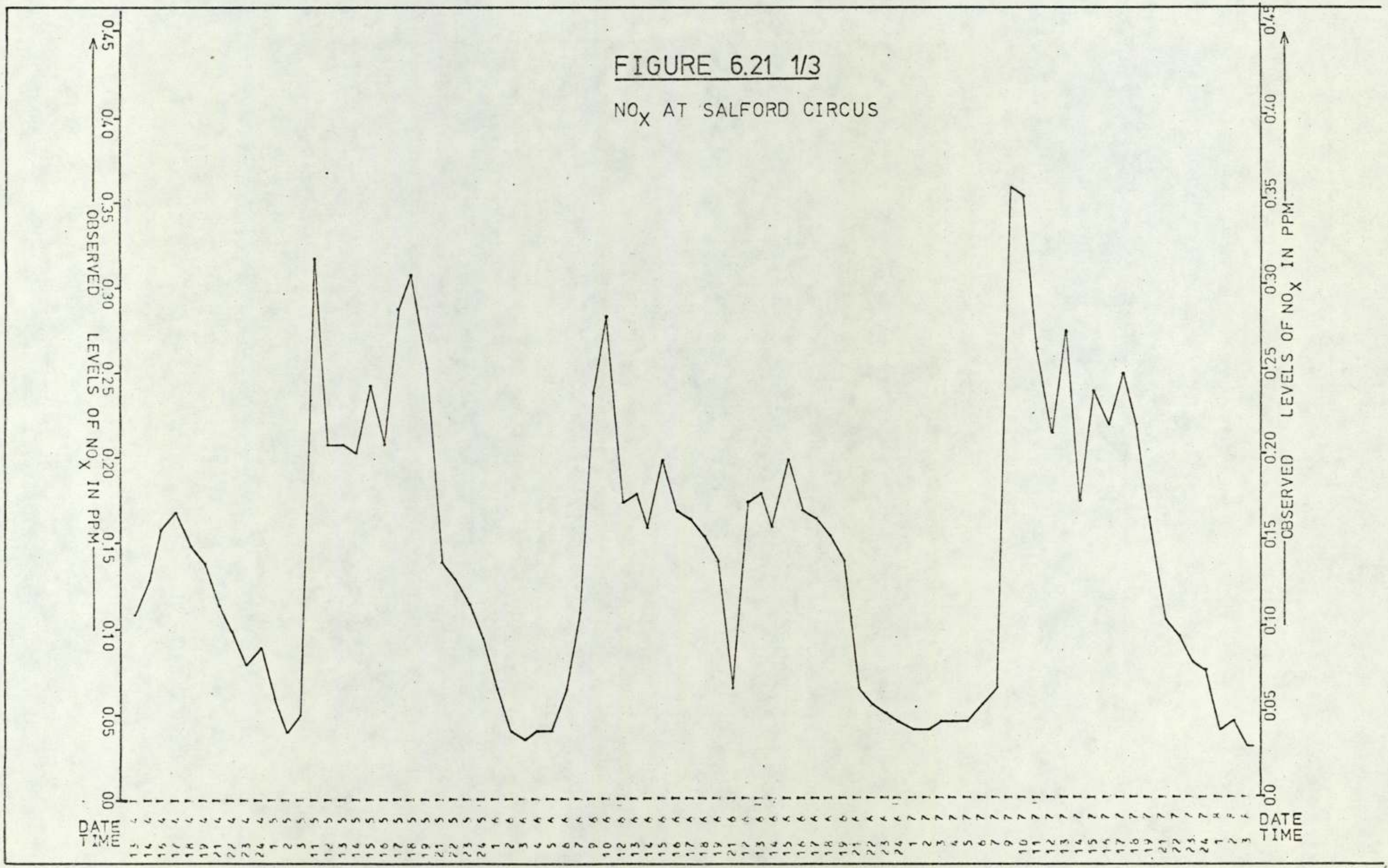

FIGURE 6.21 1/3

NO_X AT SALFORD CIRCUS

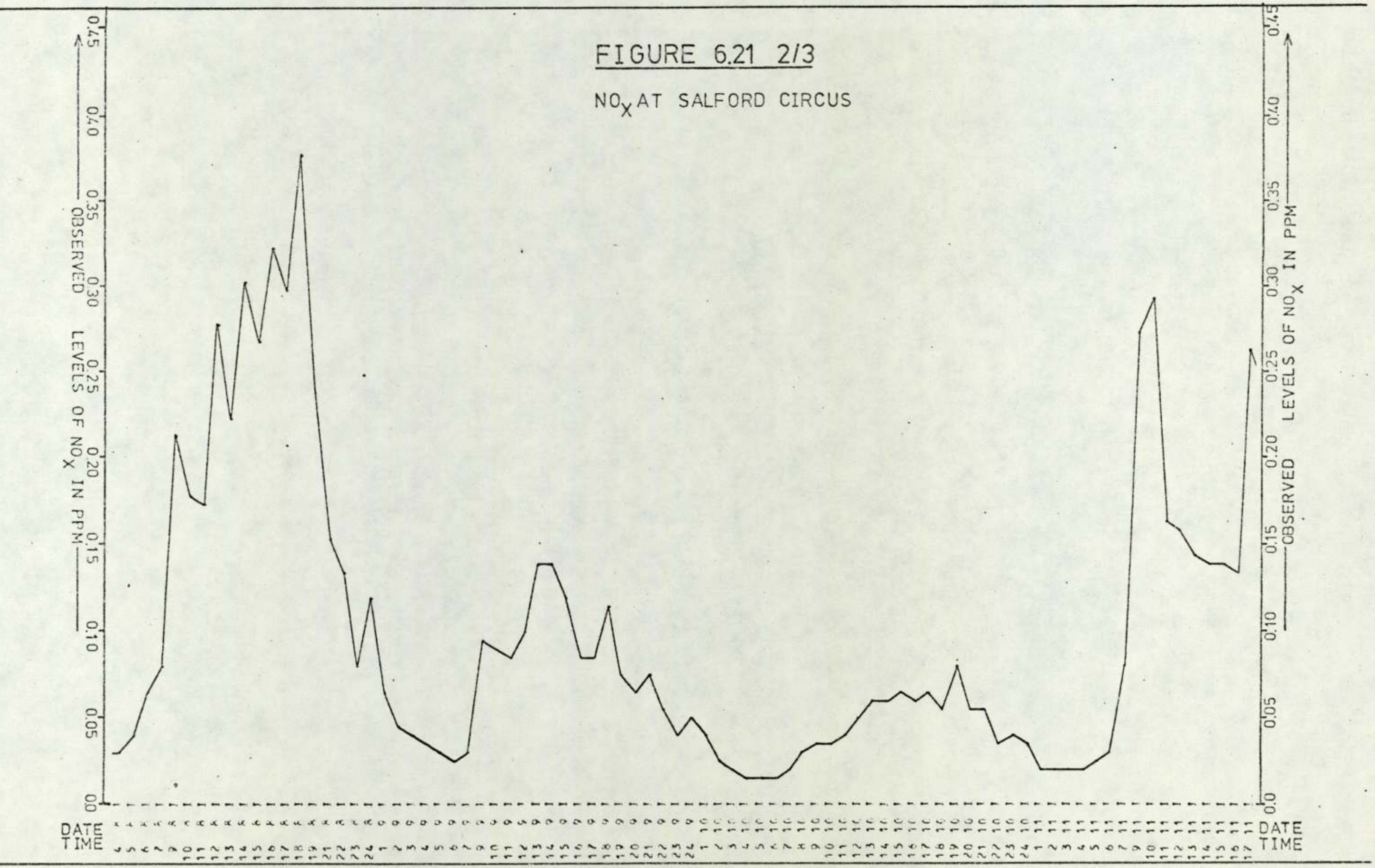

FIGURE 6.21 2/3

NO_X AT SALFORD CIRCUS

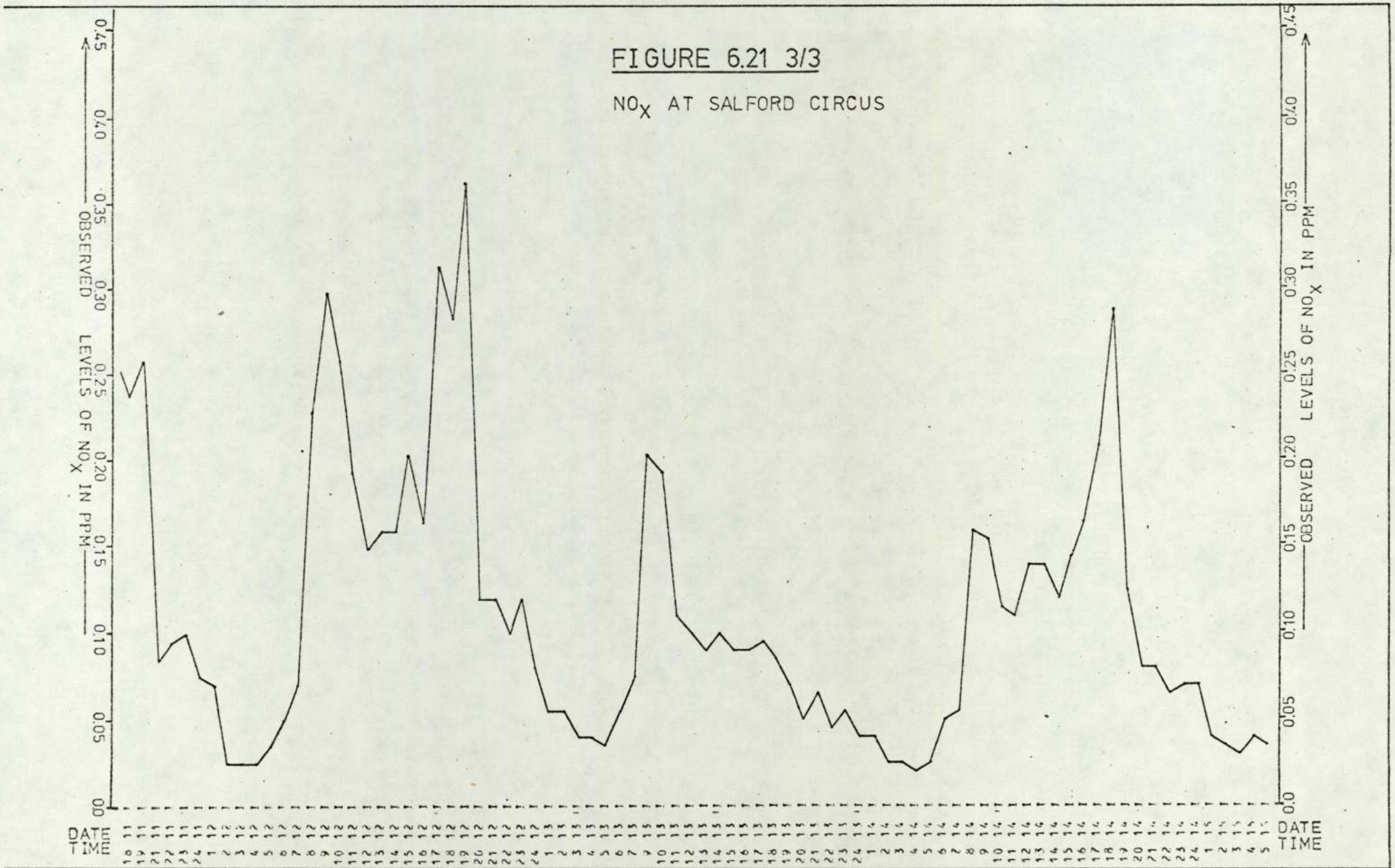

FIGURE 6.21 3/3

NO_X AT SALFORD CIRCUS

FIGURE 6.22 1/3

NO AT SALFORD CIRCUS

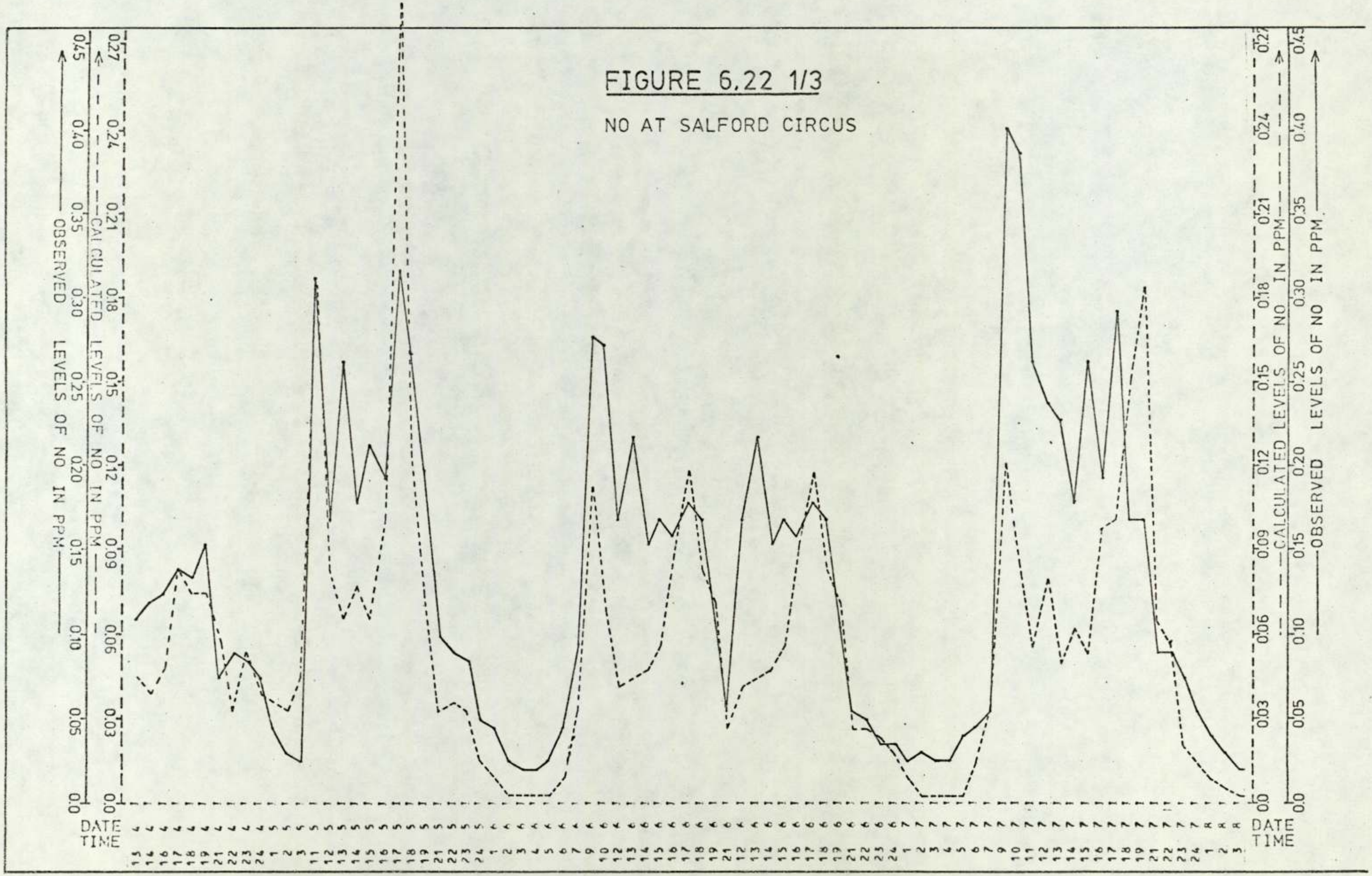

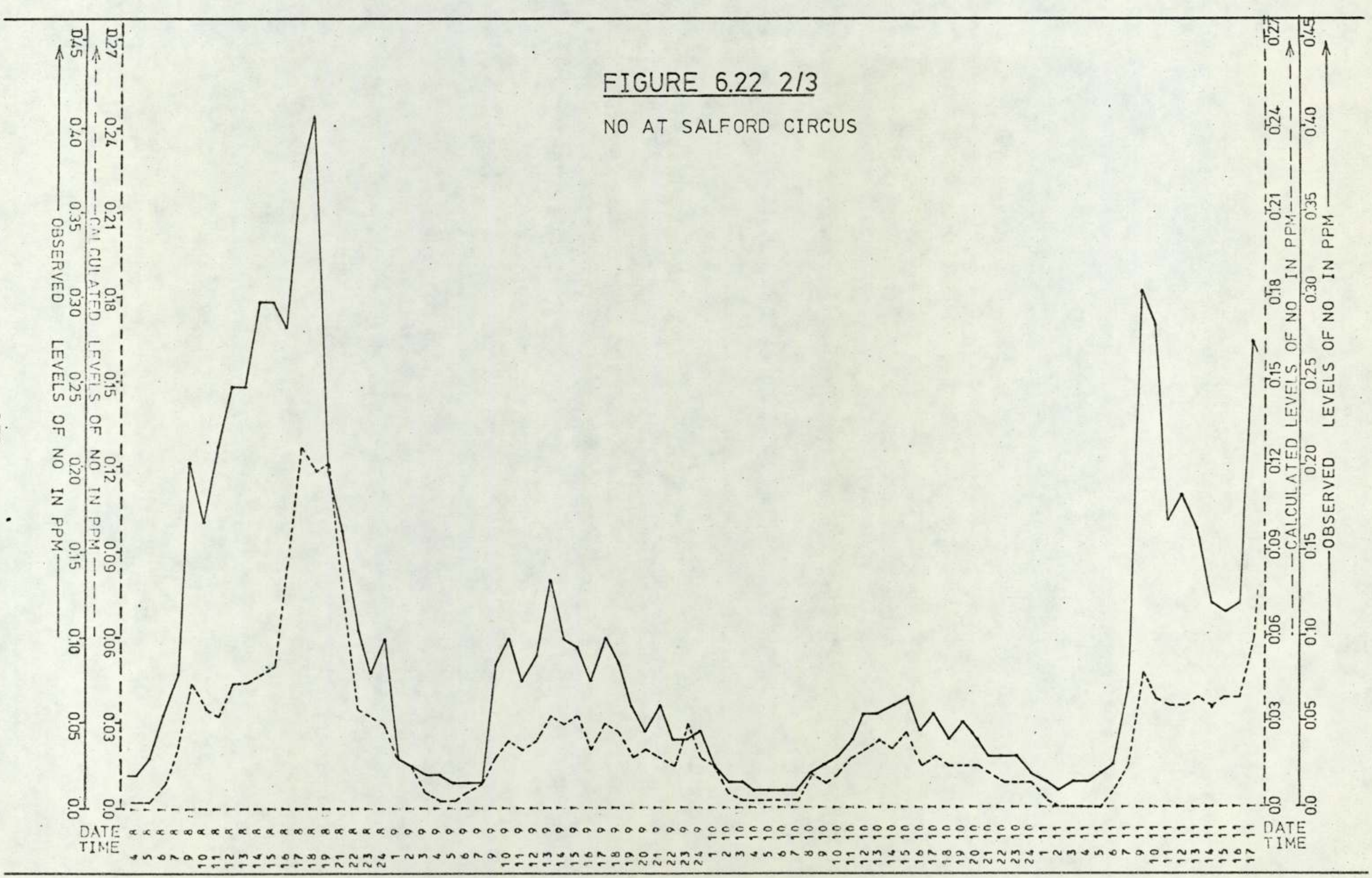

FIGURE 6.22 2/3

NO AT SALFORD CIRCUS

FIGURE 6.22 3/3

NO AT SALFORD CIRCUS

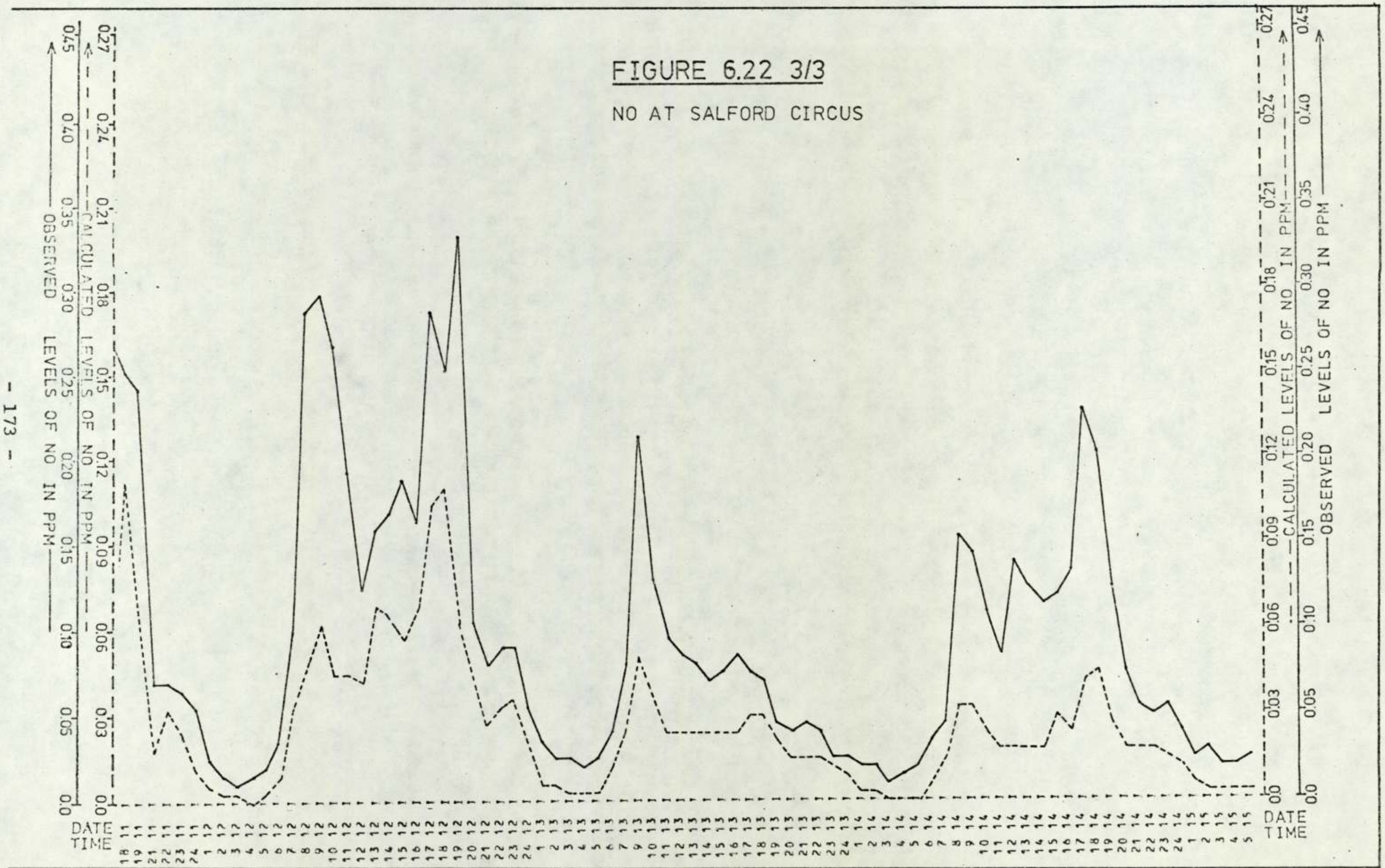

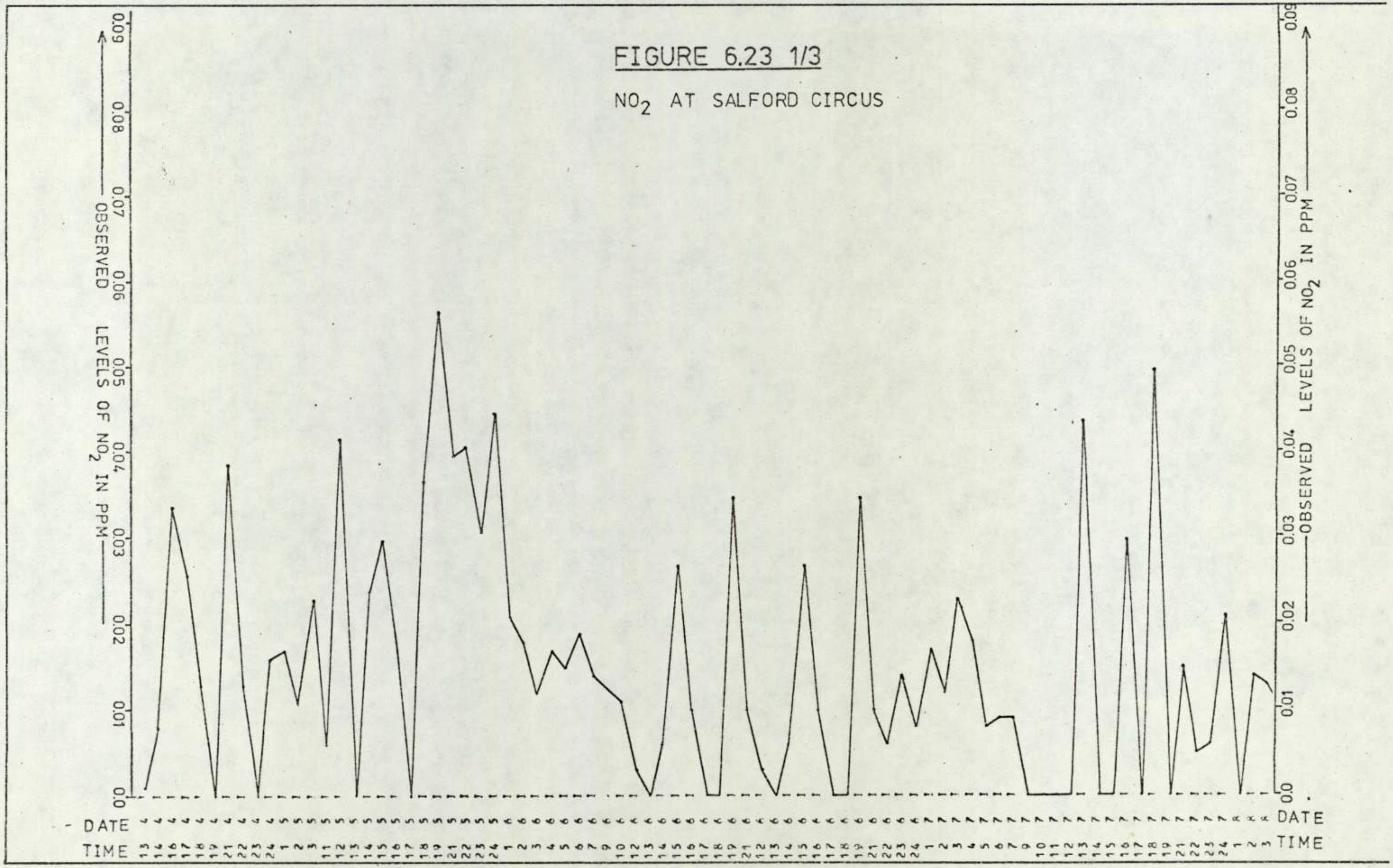

FIGURE 6.23 1/3

NO_2 AT SALFORD CIRCUS

FIGURE 6.23 2/3

NO_2 AT SALFORD CIRCUS

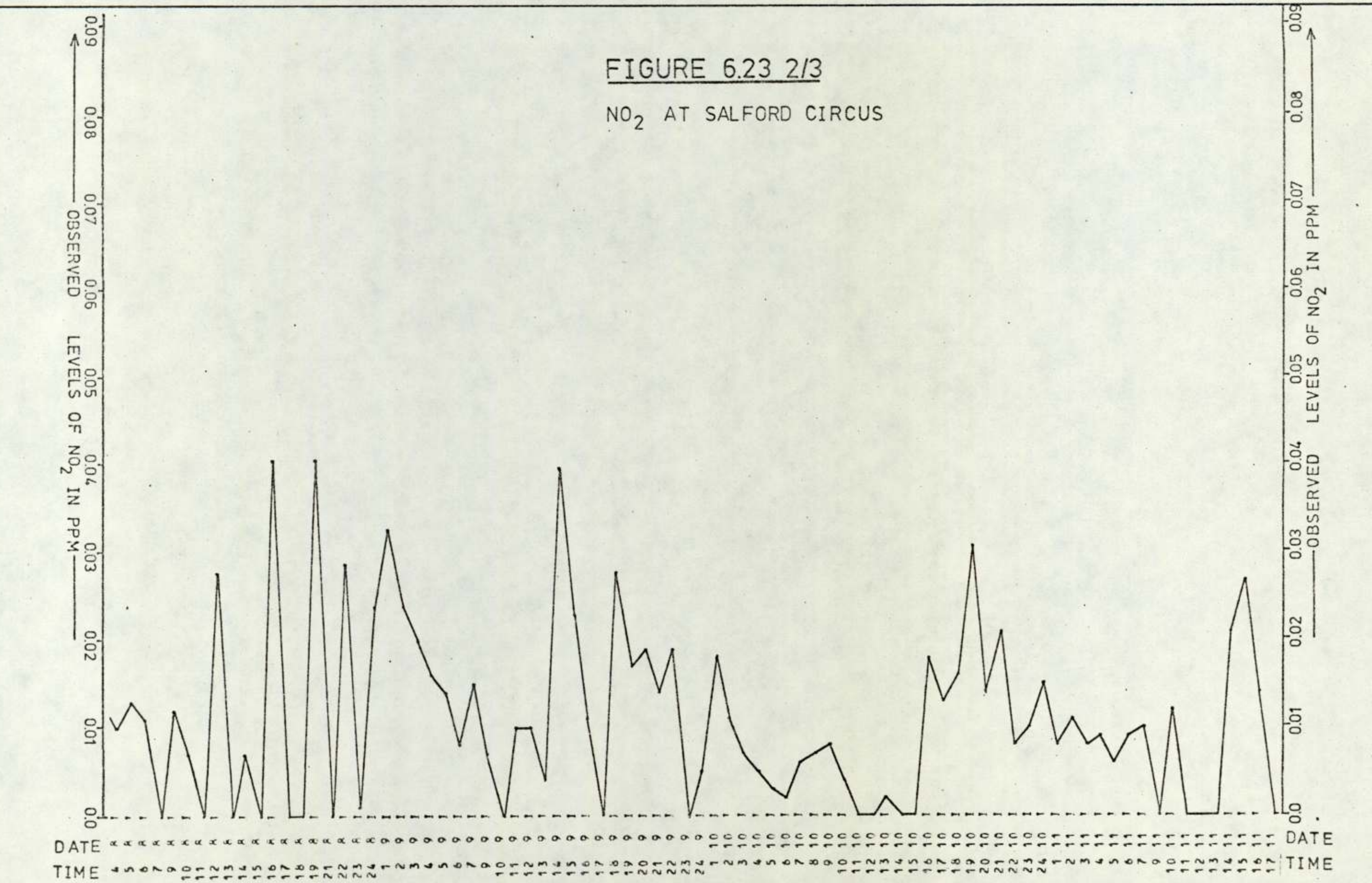

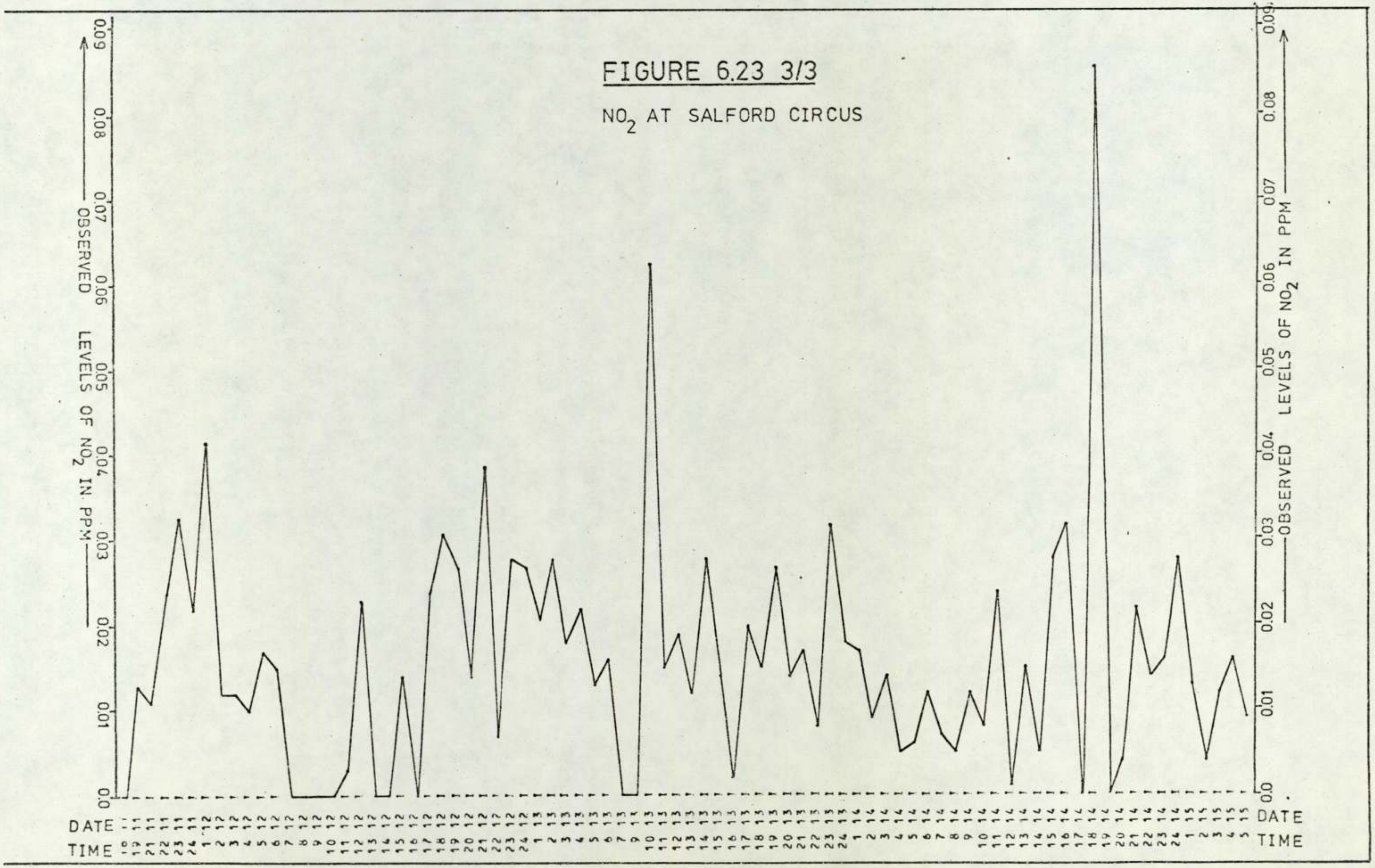

FIGURE 6.23 3/3

NO_2 AT SALFORD CIRCUS

FIGURE 6.24 1/3

CO AT SALFORD CIRCUS

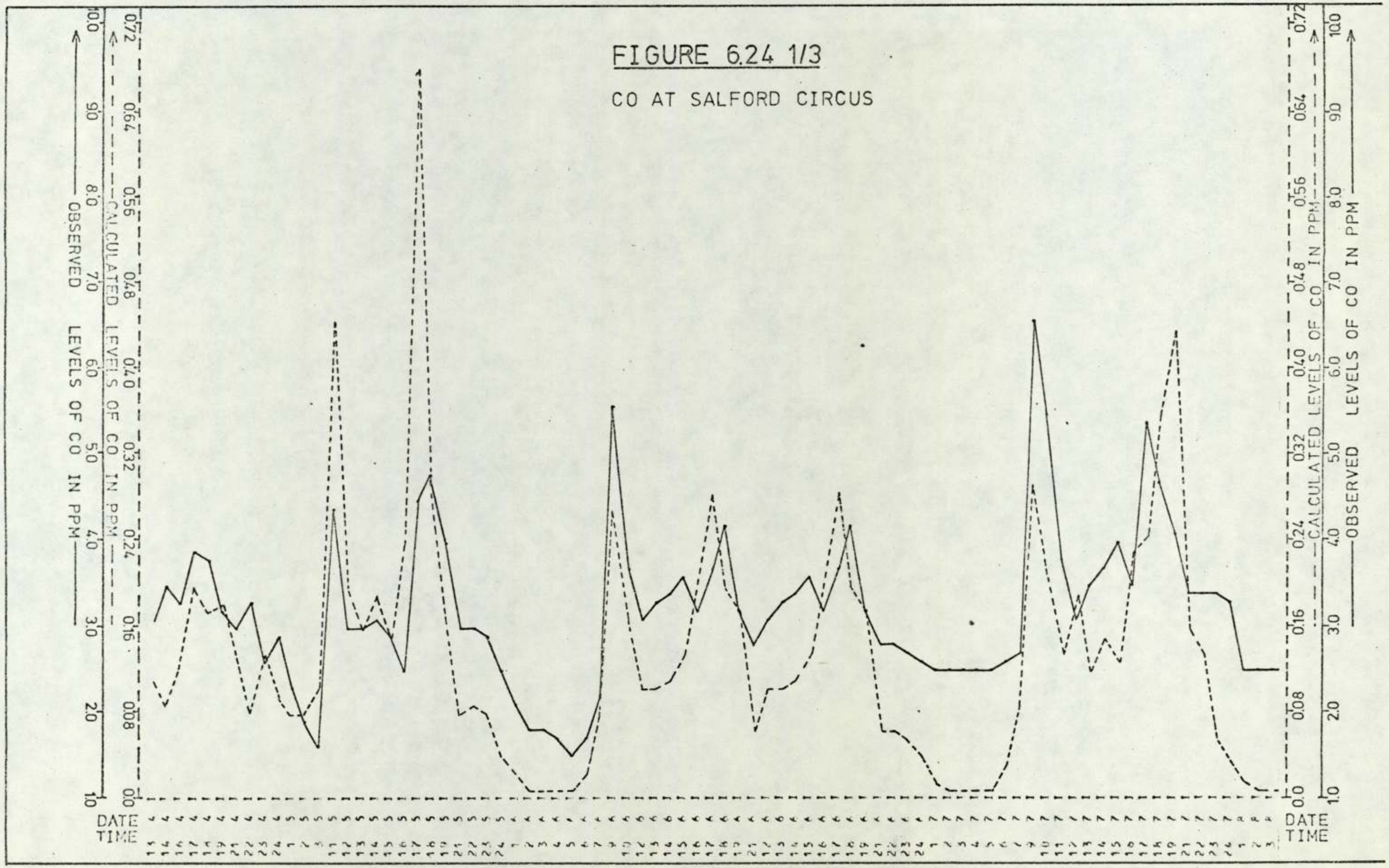

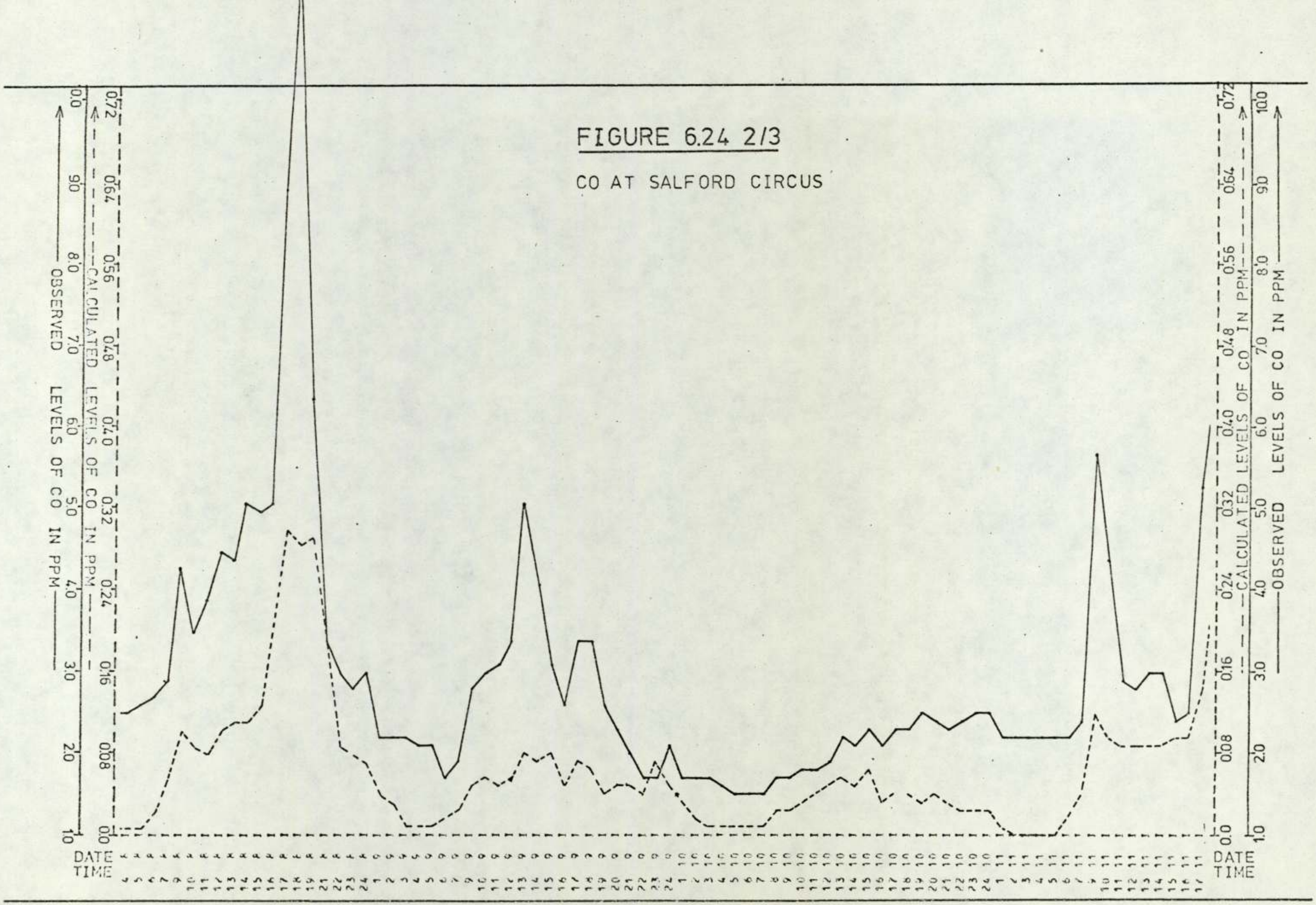

FIGURE 6.24 2/3

CO AT SALFORD CIRCUS

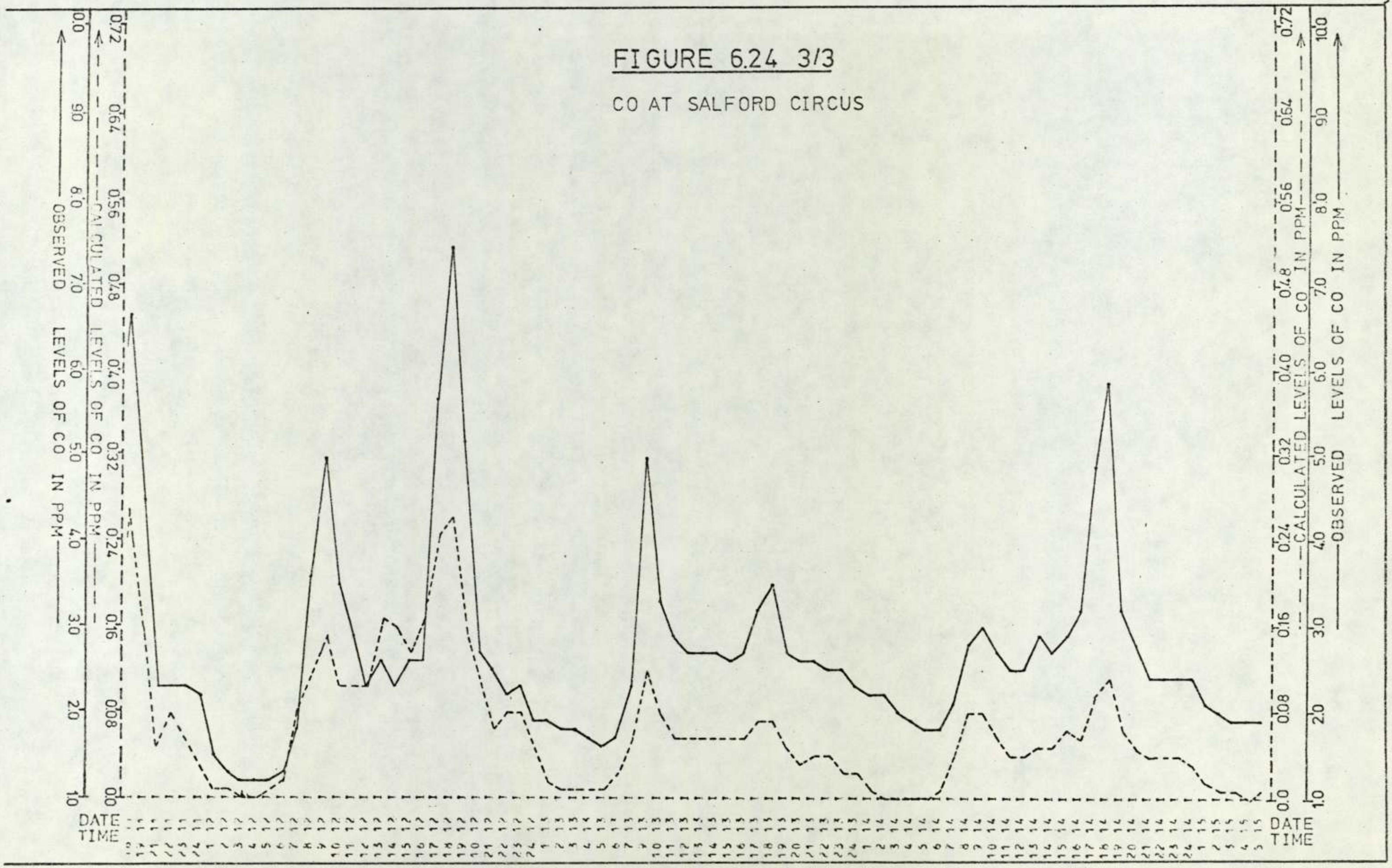

FIGURE 6.24 3/3

CO AT SALFORD CIRCUS

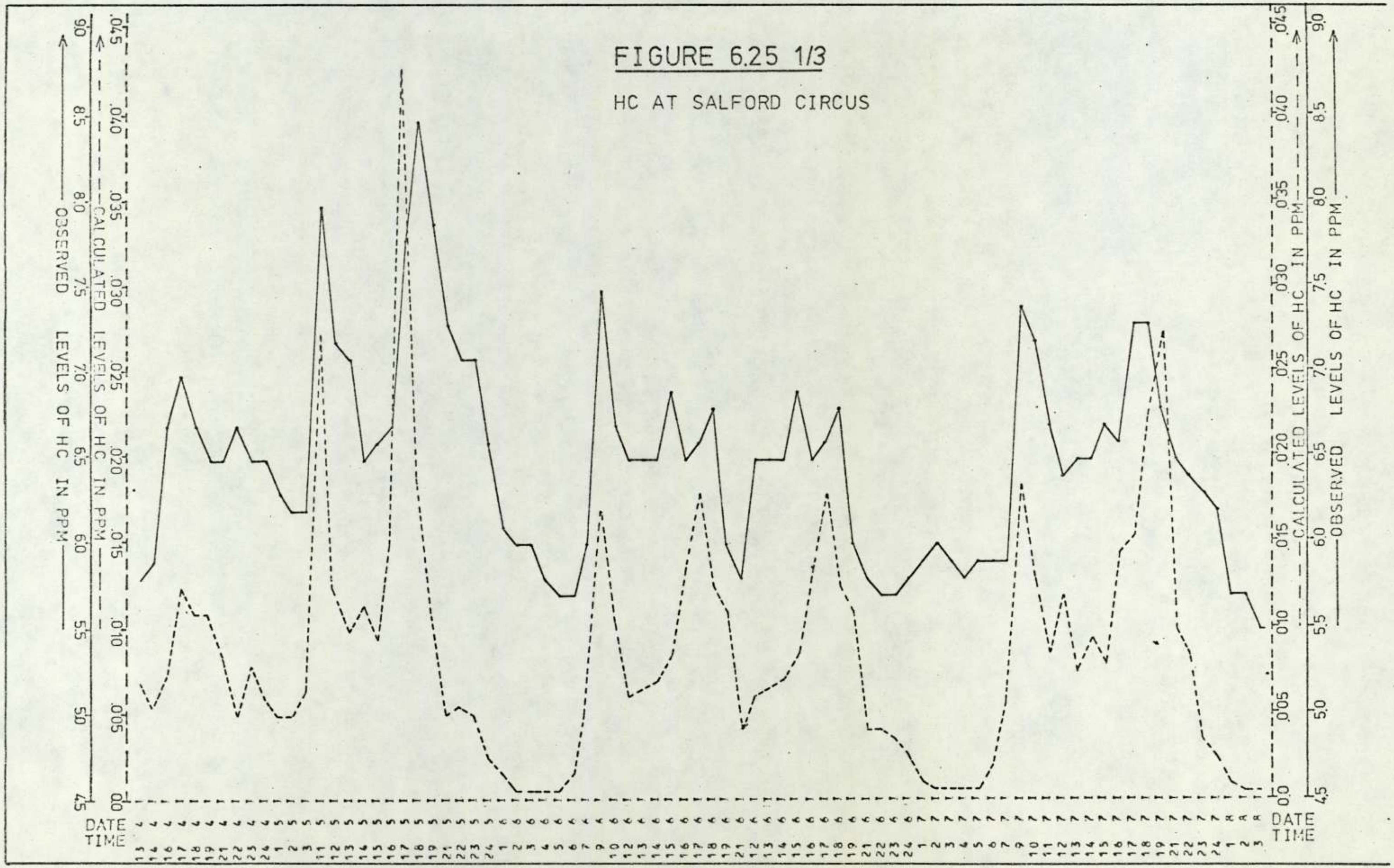

FIGURE 6.25 1/3

HC AT SALFORD CIRCUS

FIGURE 6.25 2/3

HC AT SALFORD CIRCUS

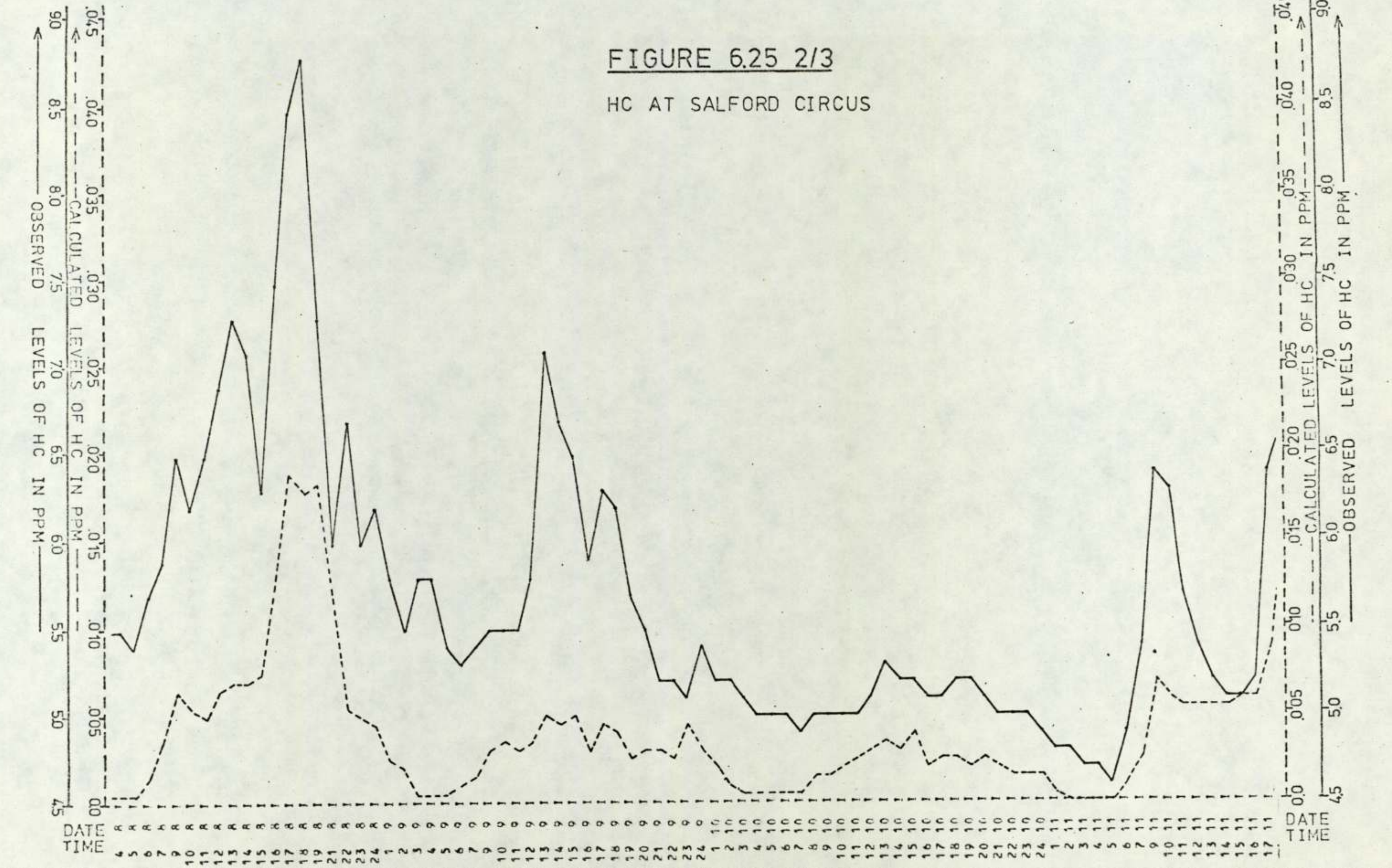

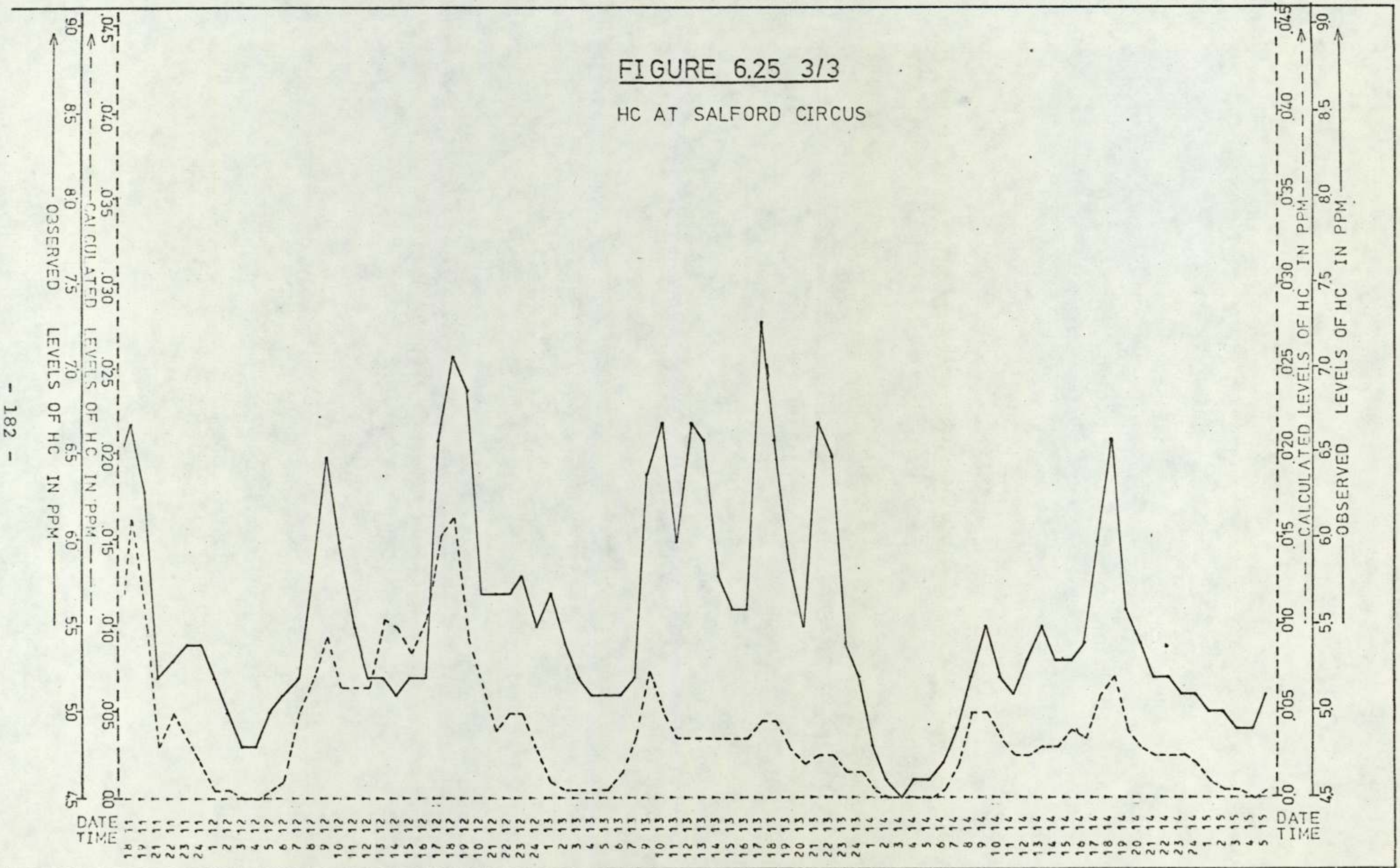

FIGURE 6.25 3/3

HC AT SALFORD CIRCUS

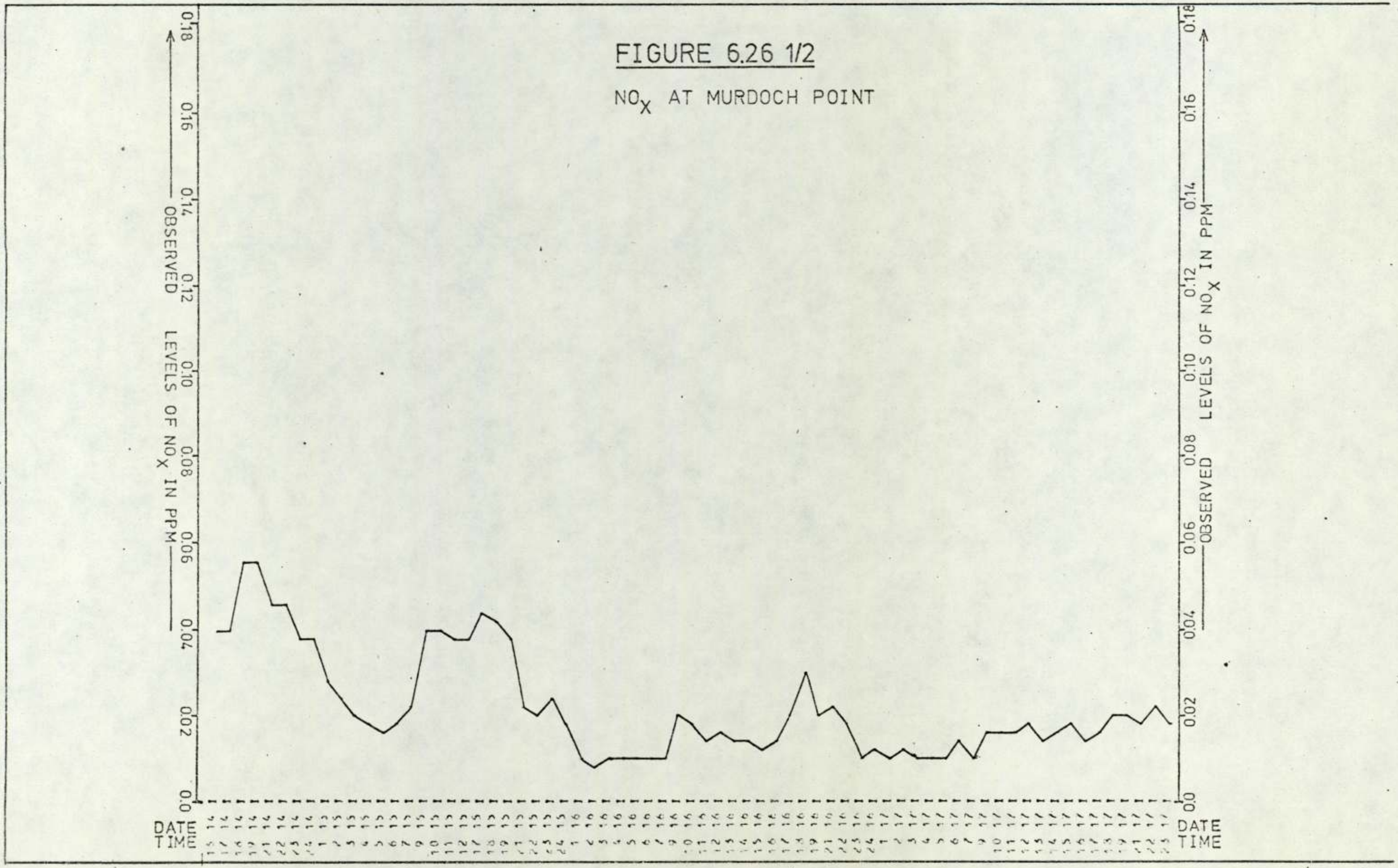

FIGURE 6.26 1/2

NO_X AT MURDOCH POINT

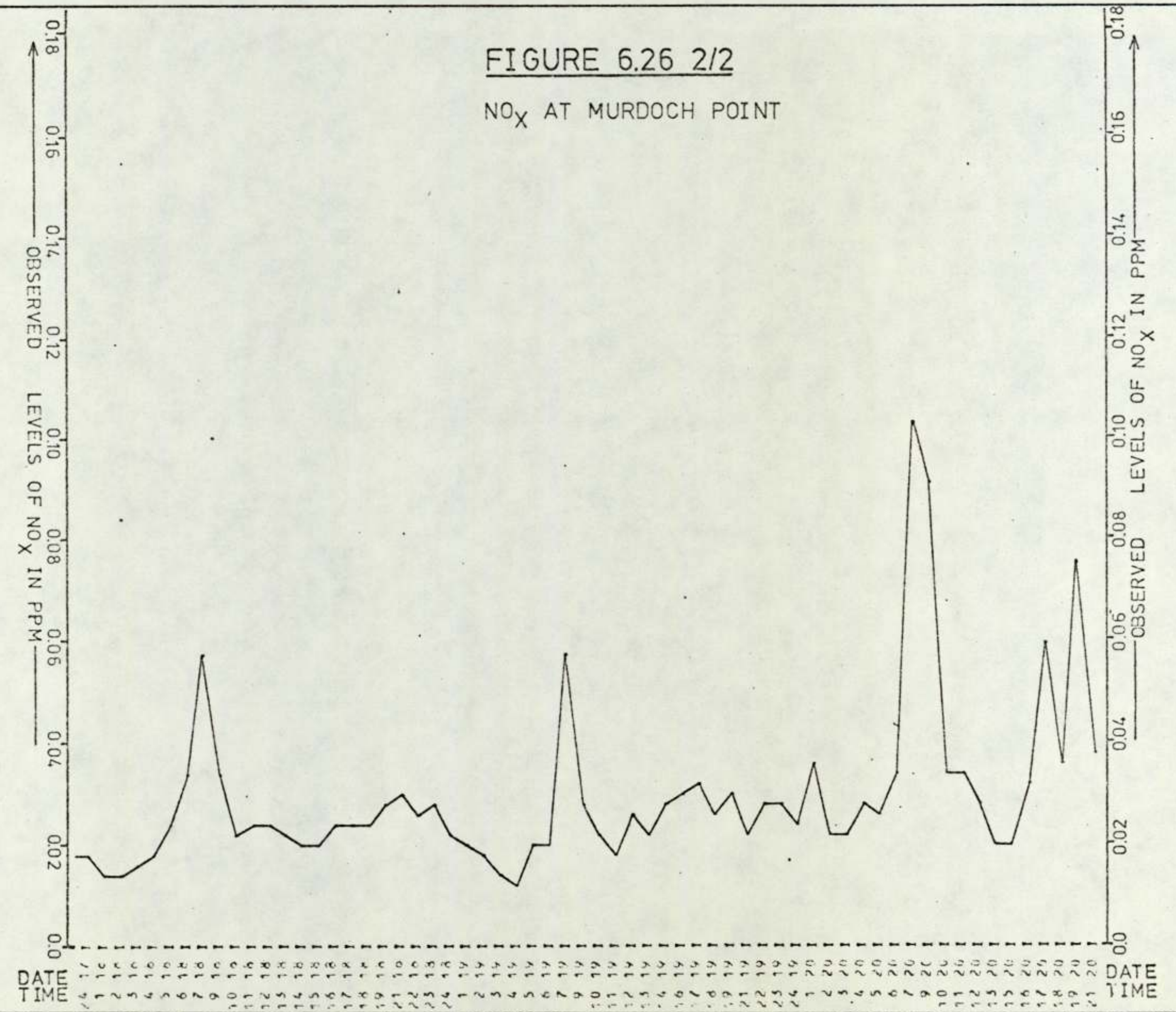

FIGURE 6.26 2/2

NO_X AT MURDOCH POINT

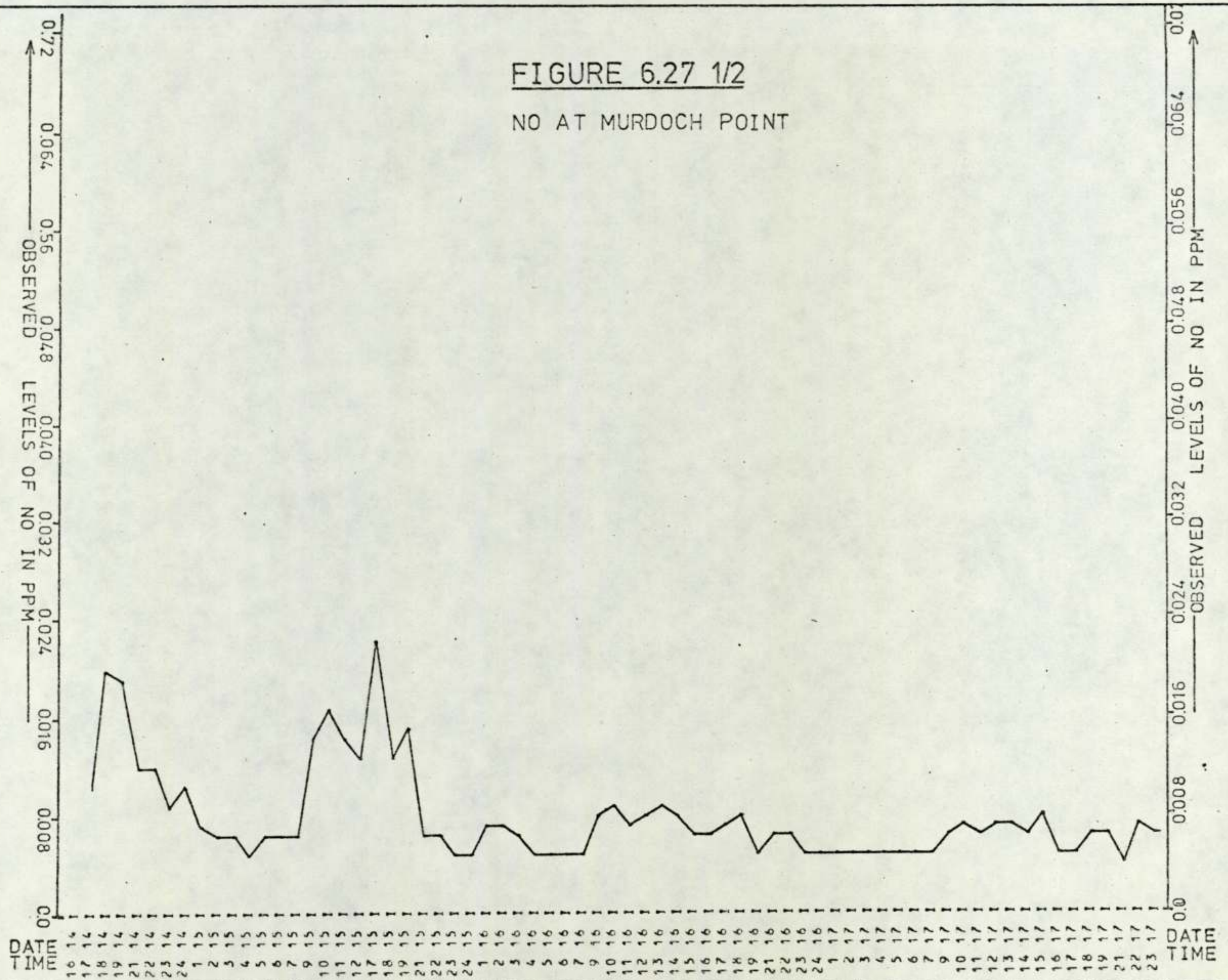

FIGURE 6.27 1/2

NO AT MURDOCH POINT

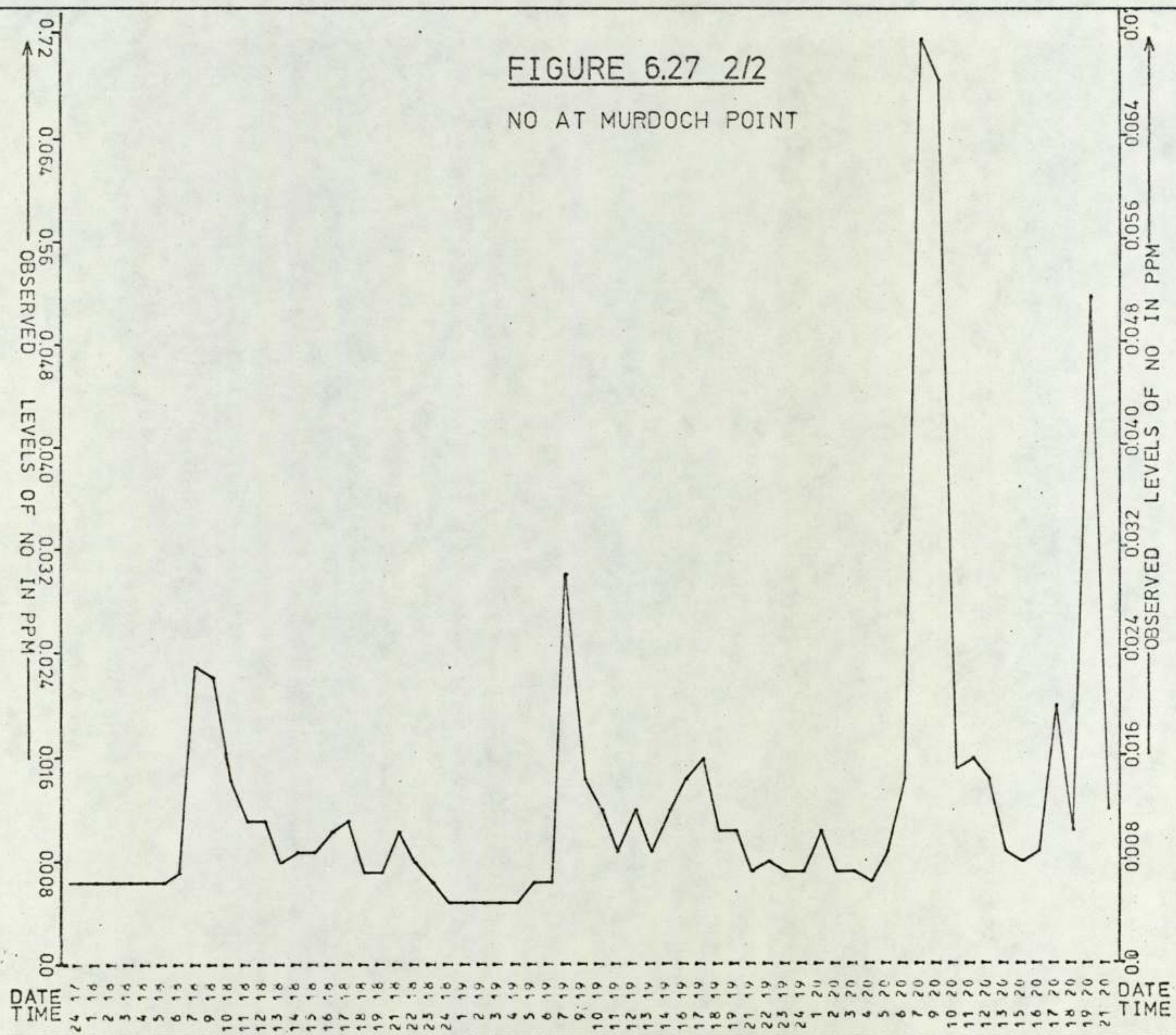

FIGURE 6.27 2/2

NO AT MURDOCH POINT

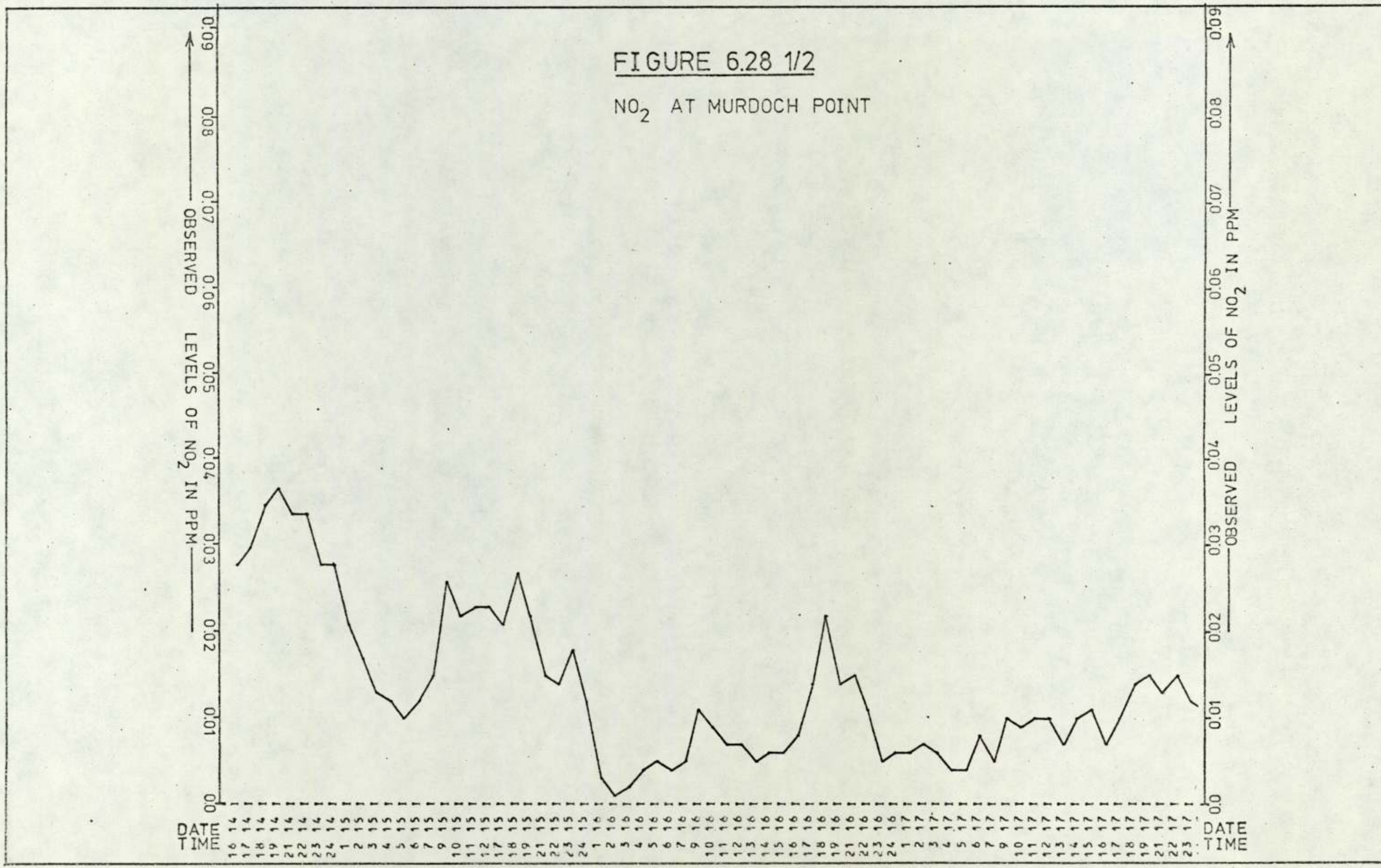

FIGURE 6.28 1/2

NO_2 AT MURDOCH POINT

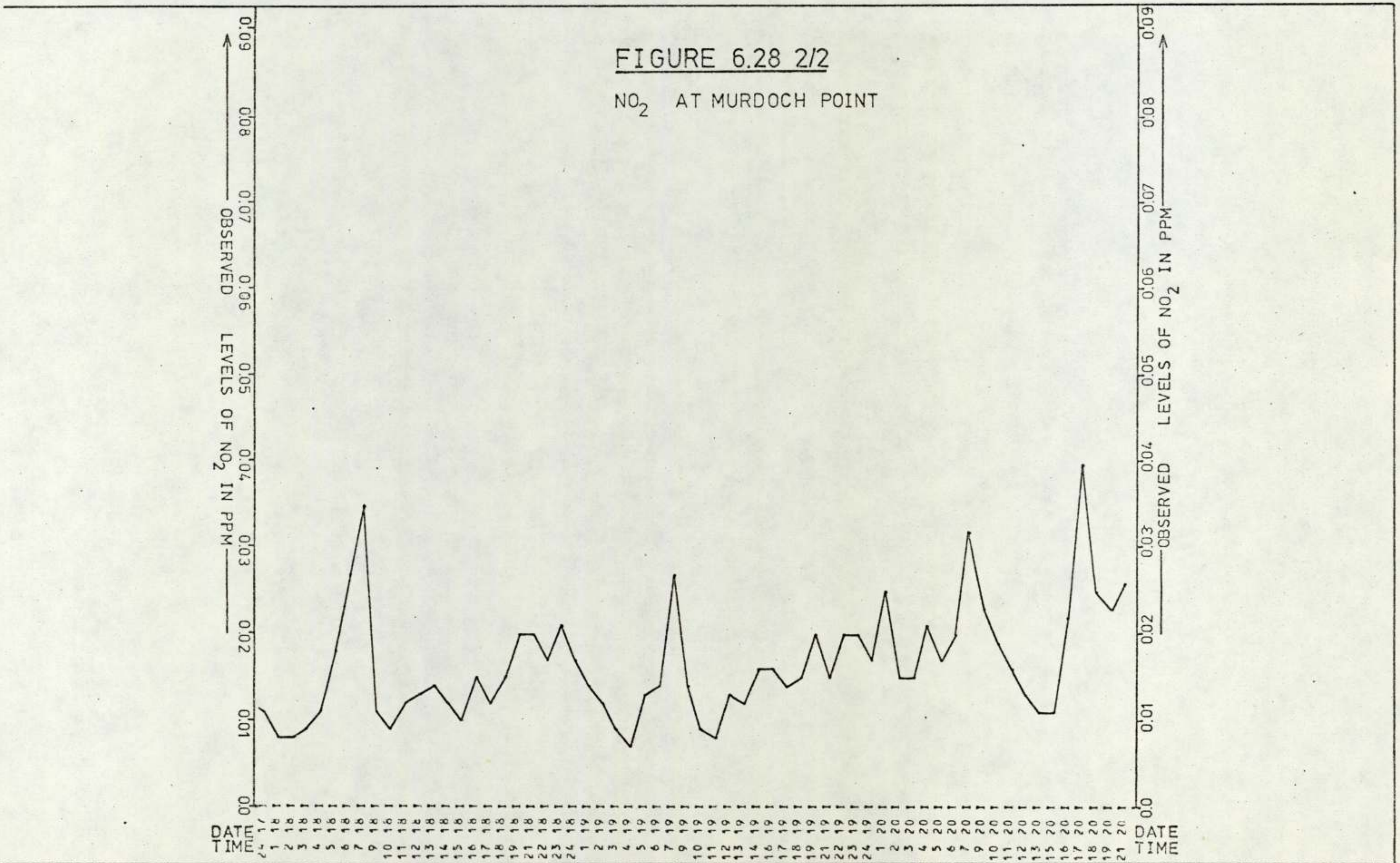

FIGURE 6.28 2/2

NO_2 AT MURDOCH POINT

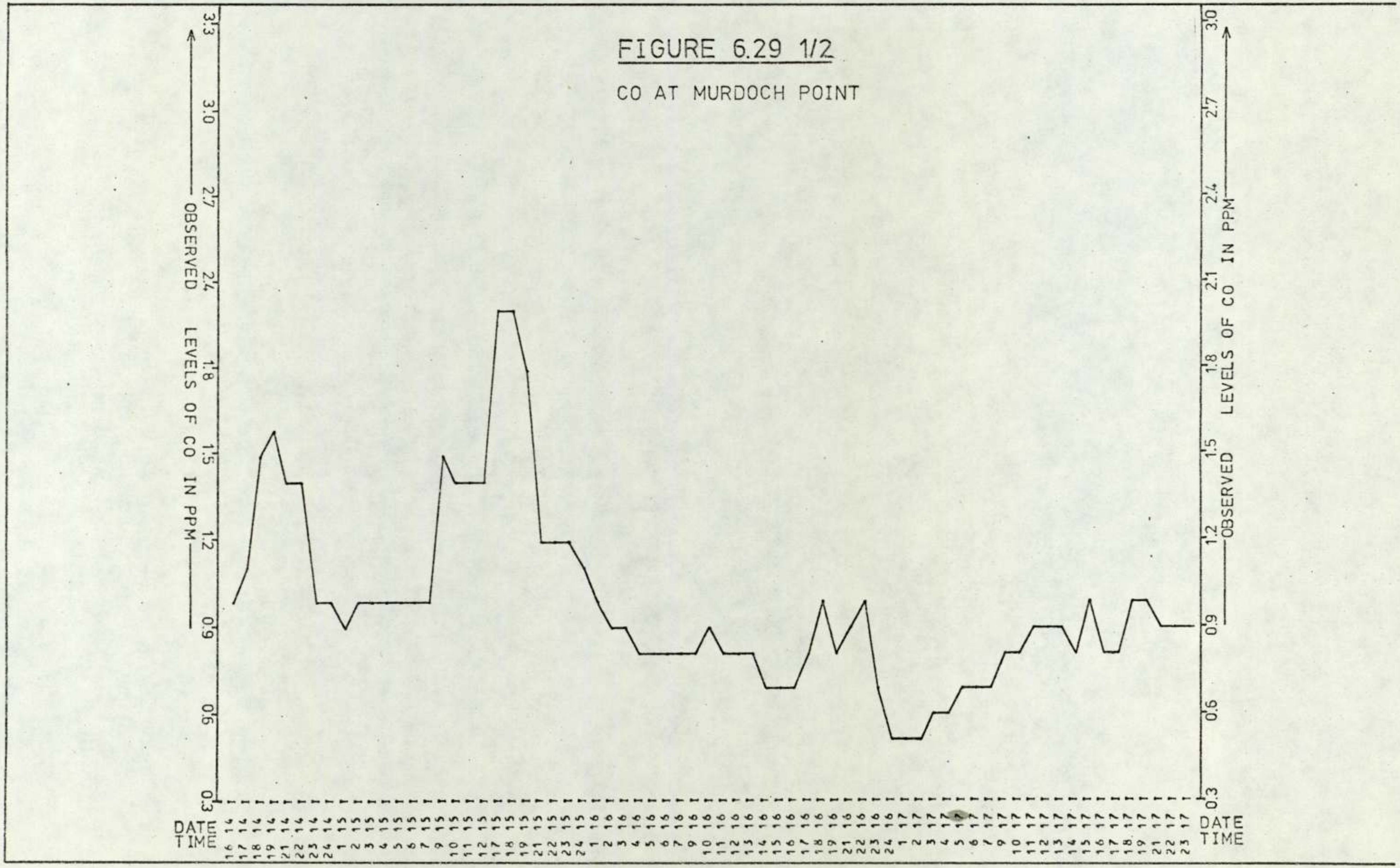

FIGURE 6.29 1/2

CO AT MURDOCH POINT

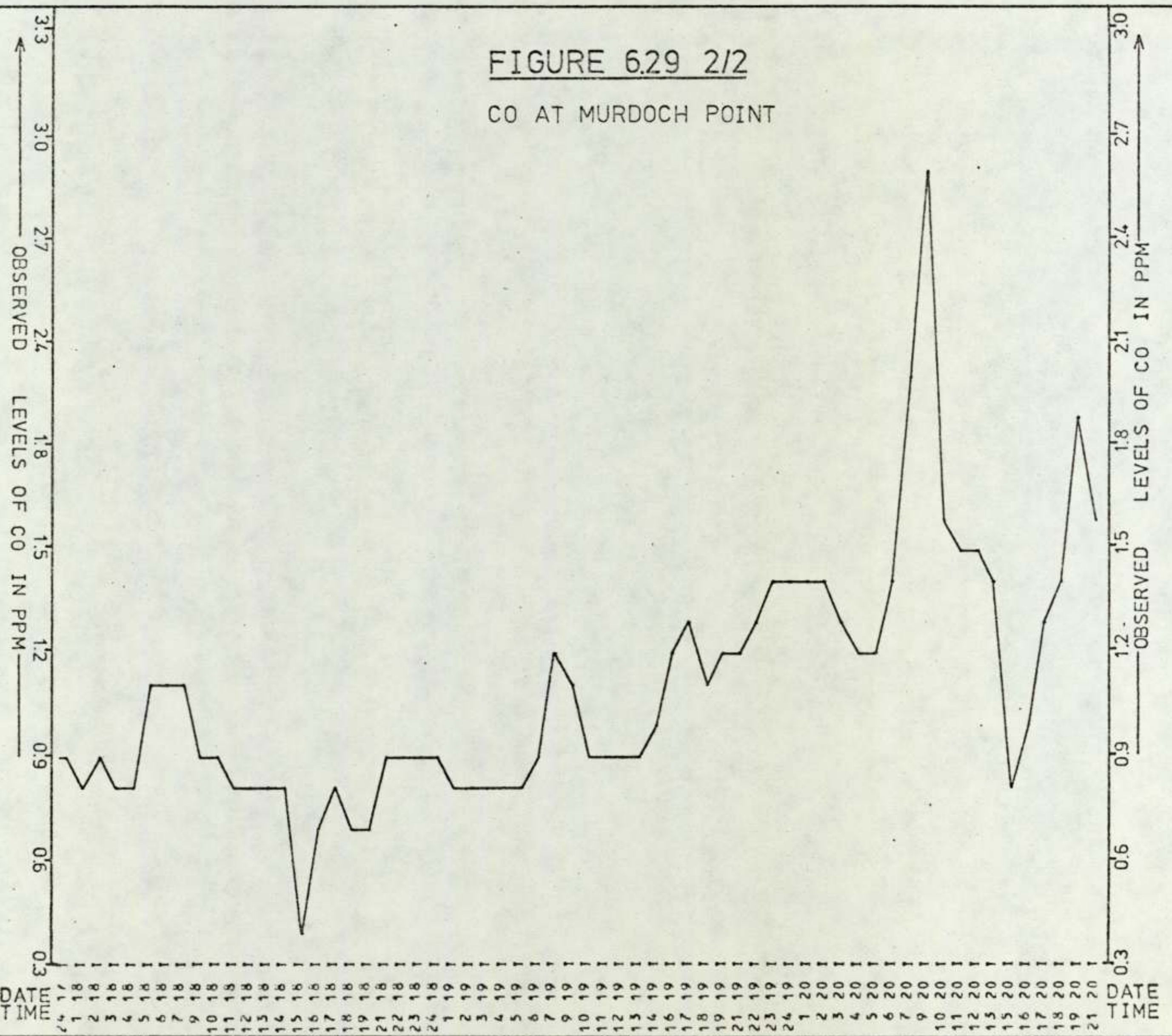

FIGURE 6.29 2/2

CO AT MURDOCH POINT

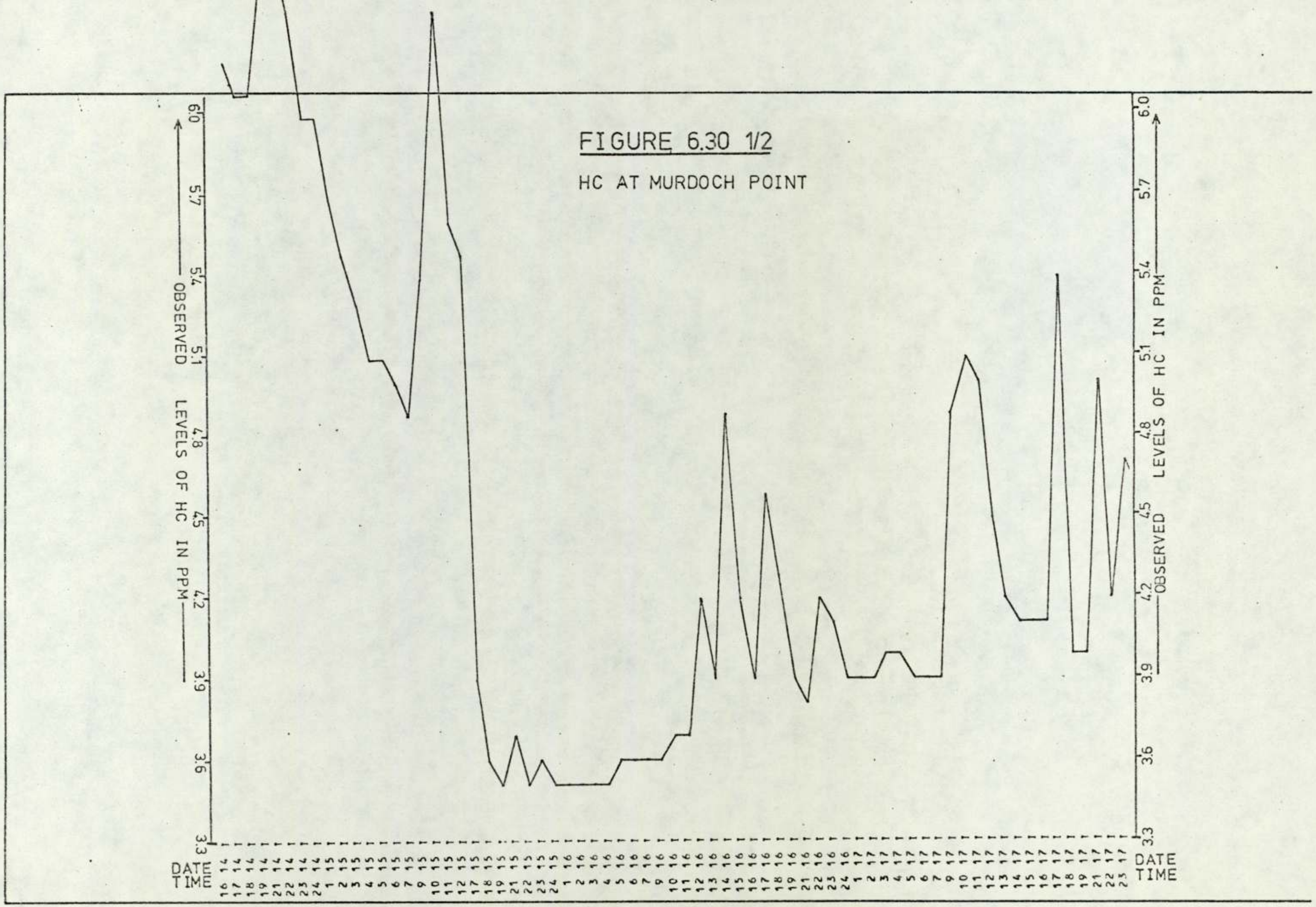

FIGURE 6.30 1/2

HC AT MURDOCH POINT

FIGURE 6.30 2/2

HC AT MURDOCH POINT

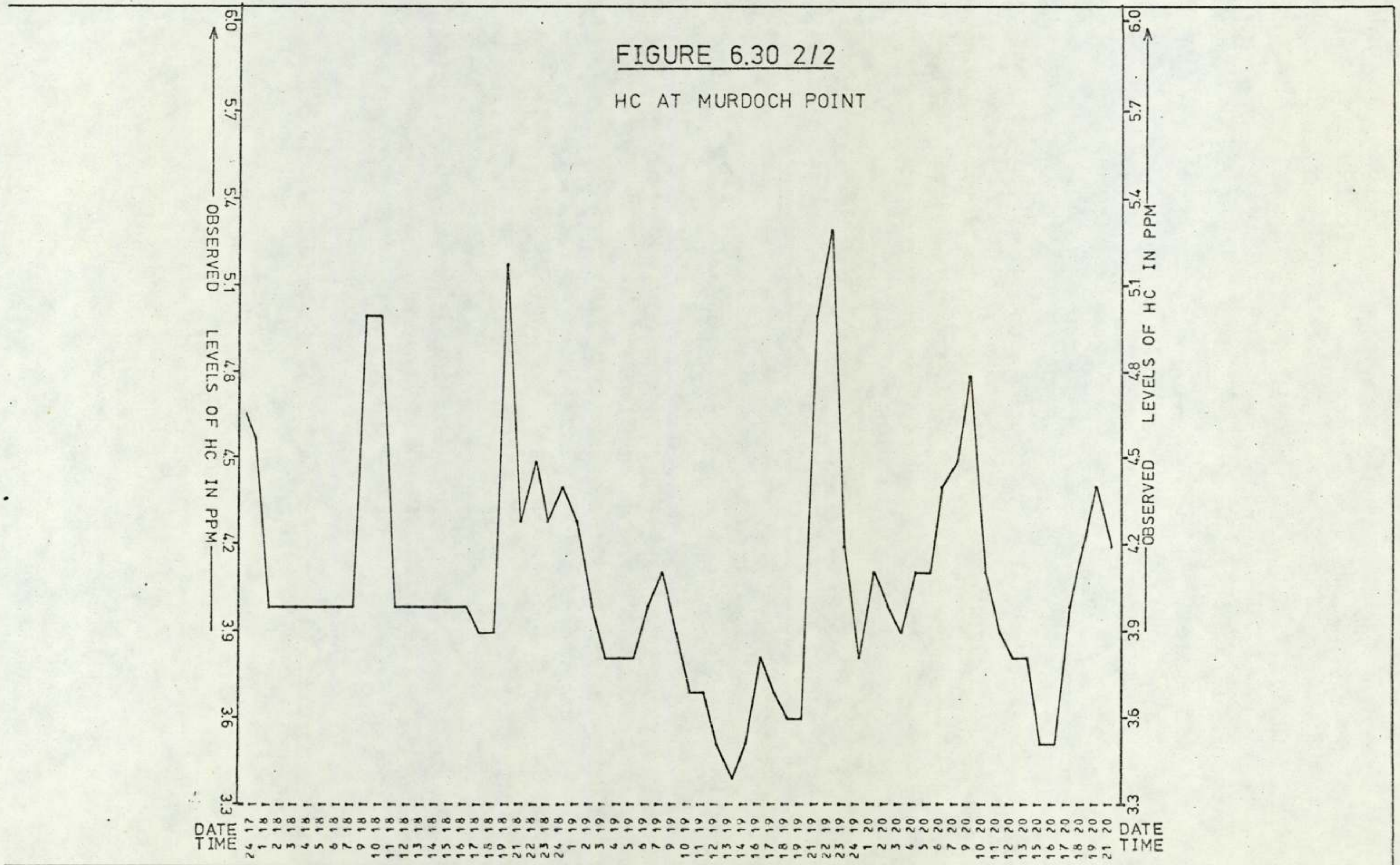

FIGURE 6.31 ERRORS IMPLICIT IN COMPARING THE CALCULATED WITH THE MEASURED CONCENTRATIONS OF POLLUTANTS.

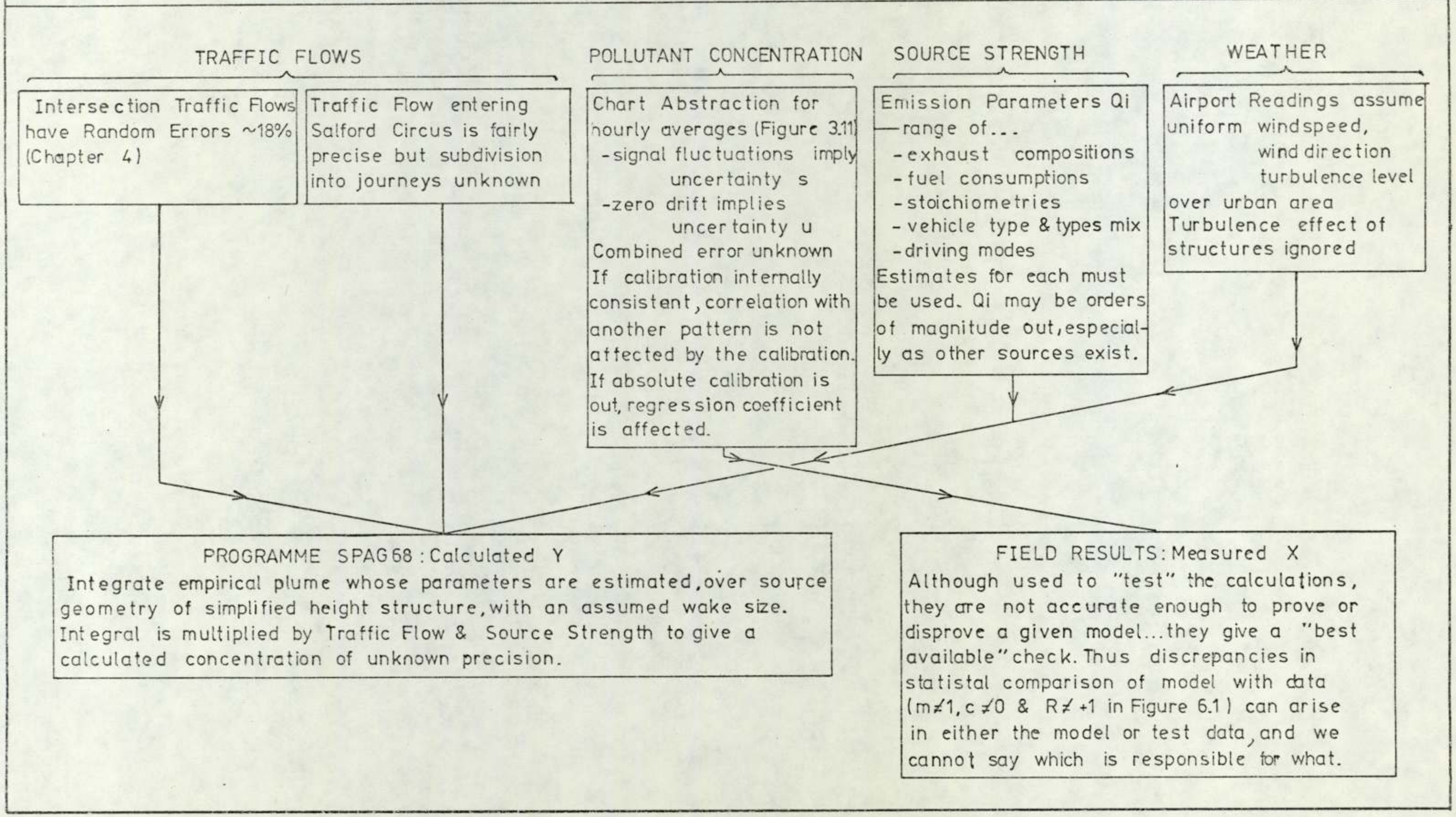

CHAPTER 7

INSTANTANEOUS CONCENTRATION GRADIENTS BY A TWO-TUBE SAMPLING TECHNIQUE

The present Chapter describes apparatus to measure gaseous pollutant concentrations at two locations simultaneously, using a single analyser. Instantaneous concentration gradients can be measured over a range of 56m and possibly more depending on equipment parameters. The design and system tests are followed by a collection of field results for NO reduced alongside a motorway and at the intersection. The field results are used to check dilution curves predicted by the programme (Chapter 6).

7.1 Principle of Technique

7.1.1 Main Features

The analyser operates in a two part cycle. First, an immediate air sample is analysed, while another separate sample is drawn into a long sample tube. This sample is delayed for the transit time of gas in the long tube before being analysed (Figure 7.1).

The long and short tubes are taken to opposite inlets of a rotary valve (Figure 7.2). The NO_x analyser and ballast pump are joined to the two outlets of the valve. Rotation of the valve generates two logic states:

In state 1 connections are 12A - ST and BP - LT

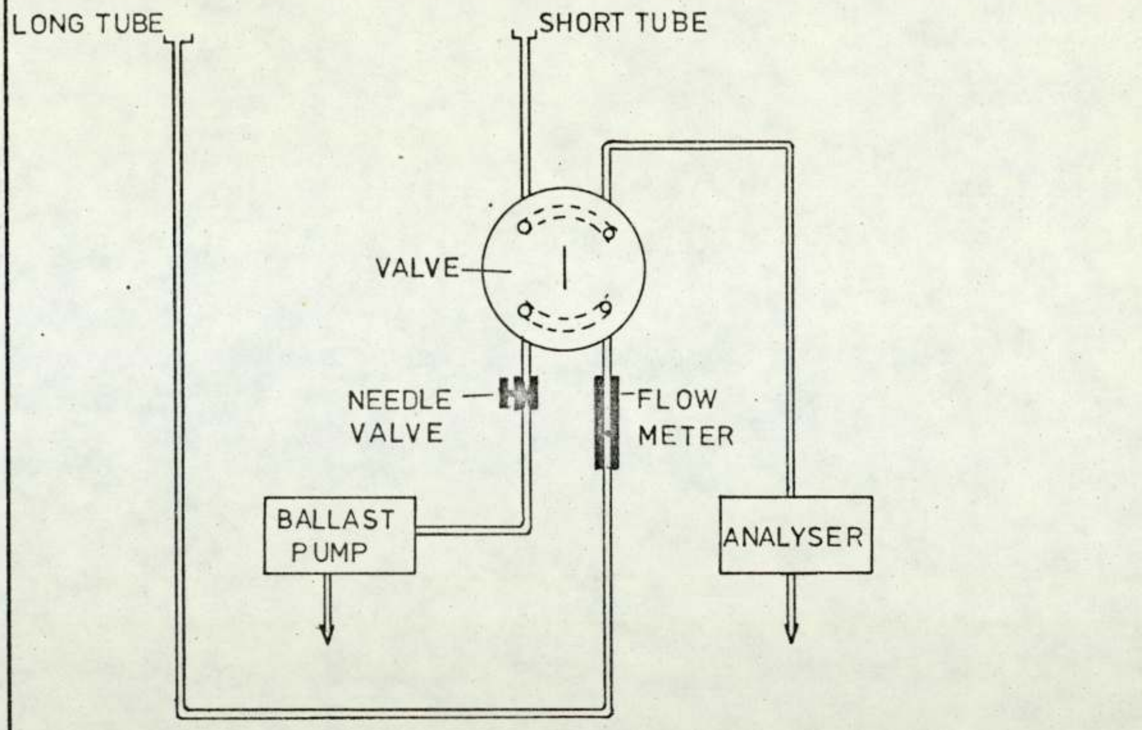

FIGURE 7.1 GENERAL SET UP OF VALVE AND TUBES

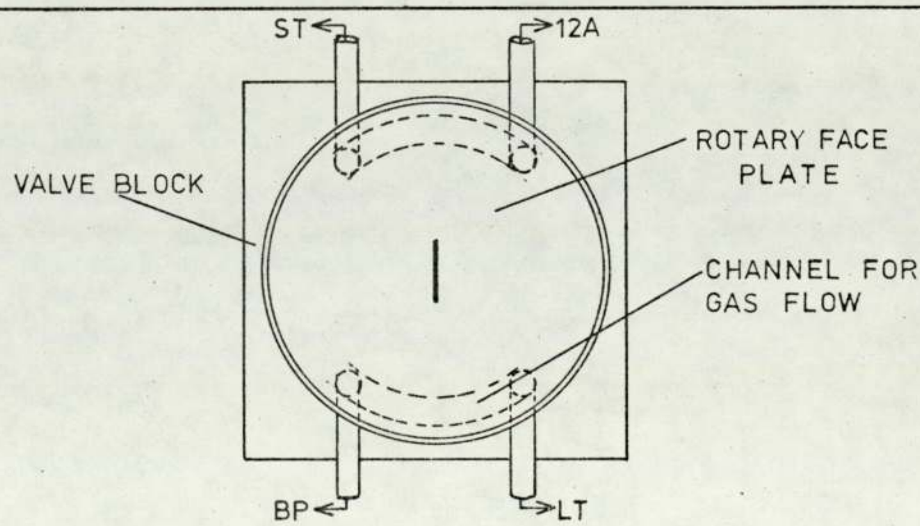

FIGURE 7.2 VALVE CONSTRUCTION.THE VALVE ROTATES THROUGH NINETY DEGREES AT EACH CHANGE.

In state 2 connections are 12A - LT and BP - ST where 12A, LT, ST and BP denote Thermo-Electron Model 12A NO_x Analyser, Long Tube, Short Tube and Ballast Pump respectively. The cycle begins in state 1. A direct air sample is analysed and recorded by the red pen of a two pen chart recorder. At the same time a sample is drawn into the long tube. Then the valve changes. In state 2 the sample in the long tube from state 1 is analysed (Figure 7.3) and recorded by the green pen. These traces from states 1 and 2 are simultaneous analyses. The cycle repeats. Figure 7.4 gives a sample of the traces.

Concentration events sampled by both short and long tubes will remain equally spaced in linear distance and in time provided the linear gas velocities in each tube are identical. The tubes have equal cross-sections; equal volume flow is sufficient condition to have equivalent time scales in each state. Failure to meet this condition results in time scale expansion.

7.1.2 Theory of Time Scale Expansion

We define flow rates

STATE	CONNECTION	VOLUME FLOW	LINEAR VELOCITY
1	12A - ST	V_1	v_1
2	12A - LT	V_2	v_2
1	BP - LT	V_3	v_3
2	BP - ST	V_4	v_4

All the tubes have the same cross-section, so we define the distance

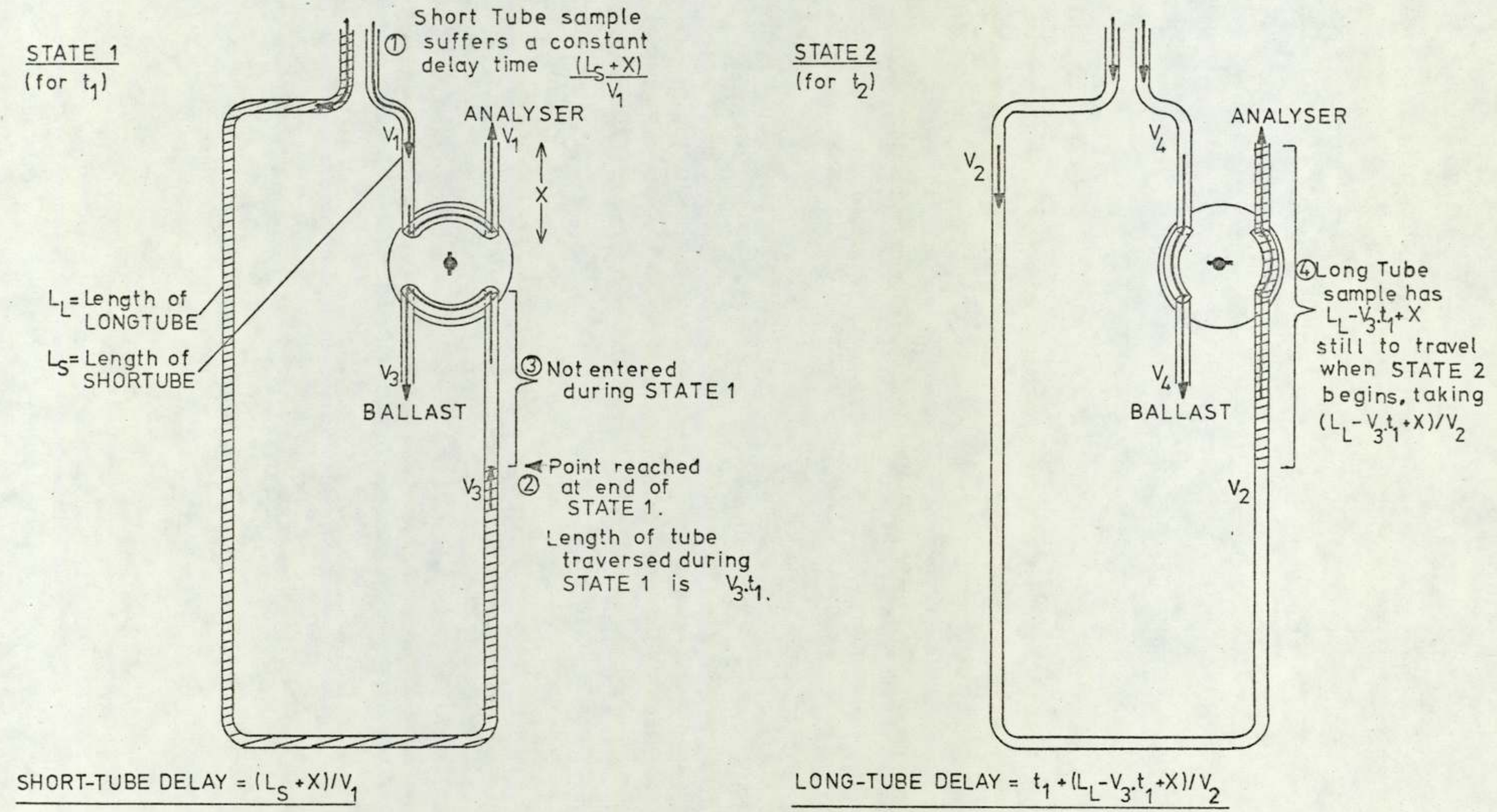

FIGURE 7.3 FLOW SEQUENCES AND TIME DELAYS FOR A SAMPLE TAKEN INTO BOTH INLETS AT THE START OF A CYCLE. FOR A SAMPLE TAKEN AT TIME T, AFTER THE START OF THE CYCLE, $(t_1 - T)$ REPLACES t_1.

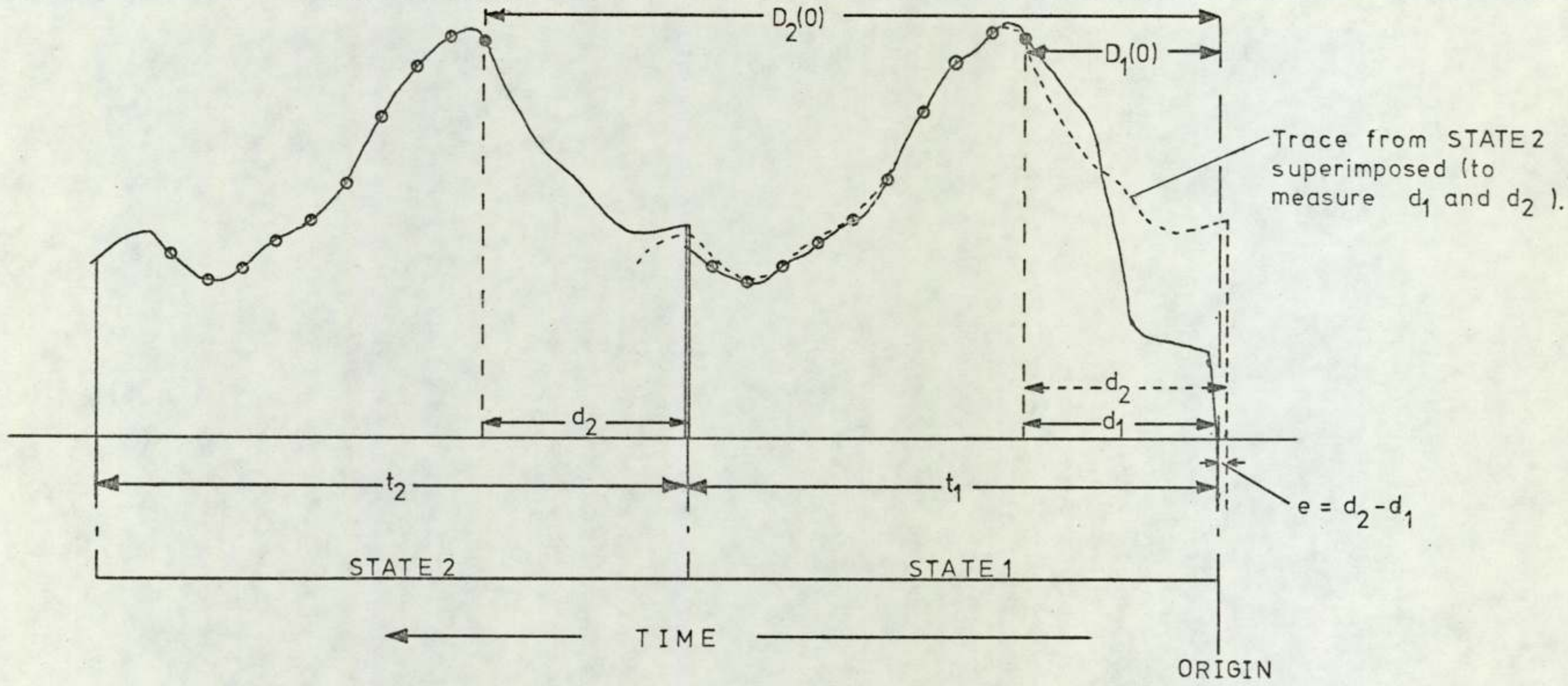

FIGURE 7.4 ILLUSTRATIVE CHART RECORD FOR A JOINED INLETS ANALYSIS TO SHOW THE VARIOUS TIME INTERVALS(t_1 , t_2 , $D_1(0)$, $D_2(0)$, d_1 , d_2 , e).

travelled vt using time t and linear velocity v.

We define

t_1	= time in state 1)	
	)	set by electronic timer
t_2	= time in state 2)	

L_S = length of short tube from inlet to valve

L_L = length of long tube from inlet to valve

x = length of tube from valve to analyser

$D_1(T)$ = time at which an event sampled at time T is recorded in state 1.

$D_2(T)$ = time at which an event sampled at time T is recorded in state 2 (times measured from start of cycle).

From Figure 7.3 we see that

$$D_1(O) = (L_S + x)/v_1 \quad \ldots \quad (7.1)$$

$$D_2(O) = t_1 + (L_L - v_3\, t_1 + x)/v_2 \quad \ldots \quad (7.2)$$

Consider two pollution events sampled by both inlets at time T after the cycle begins. The short tube analysis is recorded (Figure 7.3) at a time

$$D_1(T) = T + D_1(O) \quad \ldots \quad (7.3).$$

The time delay is constant, and equals $D_1(O)$.

For the long tube analysis, the event sampled at T has a time $(t_1 - T)$ to travel down the long tube at v_3 before the state changes. This leaves a distance $(L_L + x - v_3(t_1-T))$ to travel before analysis in state 2, taking a time $(L_L + x - v_3(t_1-T))/v_2$.

This event is recorded at the time $D_2(T)$. $D_2(T) = T + \text{Delay}$. $D_2(t) = T + (t_1-T) + (L_L + x - v_3(t_1-T))/v_2$. ... (7.4)

Events occurring at T = O and T = T are recorded in state 1 at times $D_1(O)$ and $D_1(T)$, with unchanged time separation $D_1(T) - D_1(O) = T$ (using Equations 7.1, 7.3).

The same events are recorded in state 2 at times $D_2(O)$ and $D_2(T)$ with a new time separation $D_2(T) - D_2(O) = (v_3/v_2)T$ (using Equations 7.2, 7.4).

The long tube contains a rotameter flow-meter. The ballast pump is connected through a needle valve which is adjusted until the flow-meter gives equal readings in each state. Then $V_2 = V_3$, so that $v_2 = v_3$ and no time scale expansion is present.

7.1.3 Condition for Coincident Sampling: Chart Abstraction

A concentration event occurs at time T after the cycle begins. It will be recorded during

state 1 if $O < D_1(T) < t_1$ ... (7.5)

and during

state 2 if $t1 < D_2(T) < t_1 + t_2$ ... (7.6).

If both conditions 7.5, 7.6 are met then the event is recorded in both states.

An observer wishing to abstract the chart must know where on the chart these conditions are met (Figure 7.4). Assuming that $v_2 = v_3$

we have from 7.5

$$0 < T + (L_s + x)/v_1 < t_1 \qquad \ldots \quad (7.7)$$

and from 7.6

$$0 < \frac{(L_L + x)}{v_2} - t_1 + T < t_2 \qquad \ldots \quad (7.8)$$

Now $D_1(0)$ and $D_2(0)$ are measured from the origin. Thus

$$D_2(0) = d_2 + t_1 = d_1 + e + t_1 \quad \therefore \quad e = D_2(0) - t_1 - d_1$$

also, $d_1 = D_1(0)$ from Figure 7.4,

$$e = D_2(0) - D_1(0) - t_1$$

$$e = t_1(\chi - \frac{v_3}{v_2} - \chi) + \frac{L_L + x}{v_2} - \frac{L_s + x}{v_1}$$

For the two traces to be exactly coincident, e = o so that $d_1 = d_2$: abstraction begins at the same point along each state trace if

$$\frac{+v_3 t_1}{v_2} = \frac{L_L + x}{v_2} - \frac{L_s + x}{v_1}$$

or $$t_1 = \frac{v_2}{v_3}\left(\frac{L_L + x}{v_2} - \frac{L_s + x}{v_1}\right)$$

A useful rule for setting-up follows from this: for $v_3 = v_2$ and $v_2 \sim v_1$, the electronic timer period t_1 (in state 1) should be

$t_1 \sim$ Long Tube flow time - Short Tube flow time.

The earliest sample occurs at T subject to the left hand conditions of inequalities 7.7, 7.8 and the latest sample is at T subject to the right hand sides. In the present work, full information was not available for 7.7 and 7.8 to be used to define initial and final values of T numerically.

7.1.4 Operation of the System

The needle valve was adjusted to set $v_2 = v_3$ (Section 7.1.2). The electronic timer was set so that e was as near zero as possible (Section 7.1.3), with

$t_1 \sim$ long tube delay - short tube delay.

Joined inlets traces were then recorded, and traced as in Figure 7.4 to derive empirical values of d_1, d_2 for the system as set. Inlets were then separated to measure concentration gradients. Using d_1, d_2, equally spaced intercepts were abstracted and averaged.

7.2 Construction

7.2.1 Circuit of Timer Unit

The circuit (Figures 7.5, 7.6 and Table 7.1) was designed to provide a square wave of continuously variable period with positive pulses at each change of logic state. The square wave half cycles (states 1 and 2) control a pen relay which selects the appropriate chart recorder pen. The pulses are needed to drive the servocoil which controls the valve. A novel circuit creates these pulses using a full wave rectifier and an operational amplifier. The operational amplifier IC1 is wired as a multivibrator, of period t_E

$$t_E = 2R_5C_1 \text{ loge } (1 + 2\ R_A/R_B)$$

where the time constant $R_5C_1 \sim 50$ secs, and $R_A = R_3 + VRI$, $R_B = R_4 + VR2$, $R3 = R4 = 22K\Omega$, and $VR1 = VR2 = 0 - 2M\Omega$.

The multivibrator output (24 volts peak to peak) drives

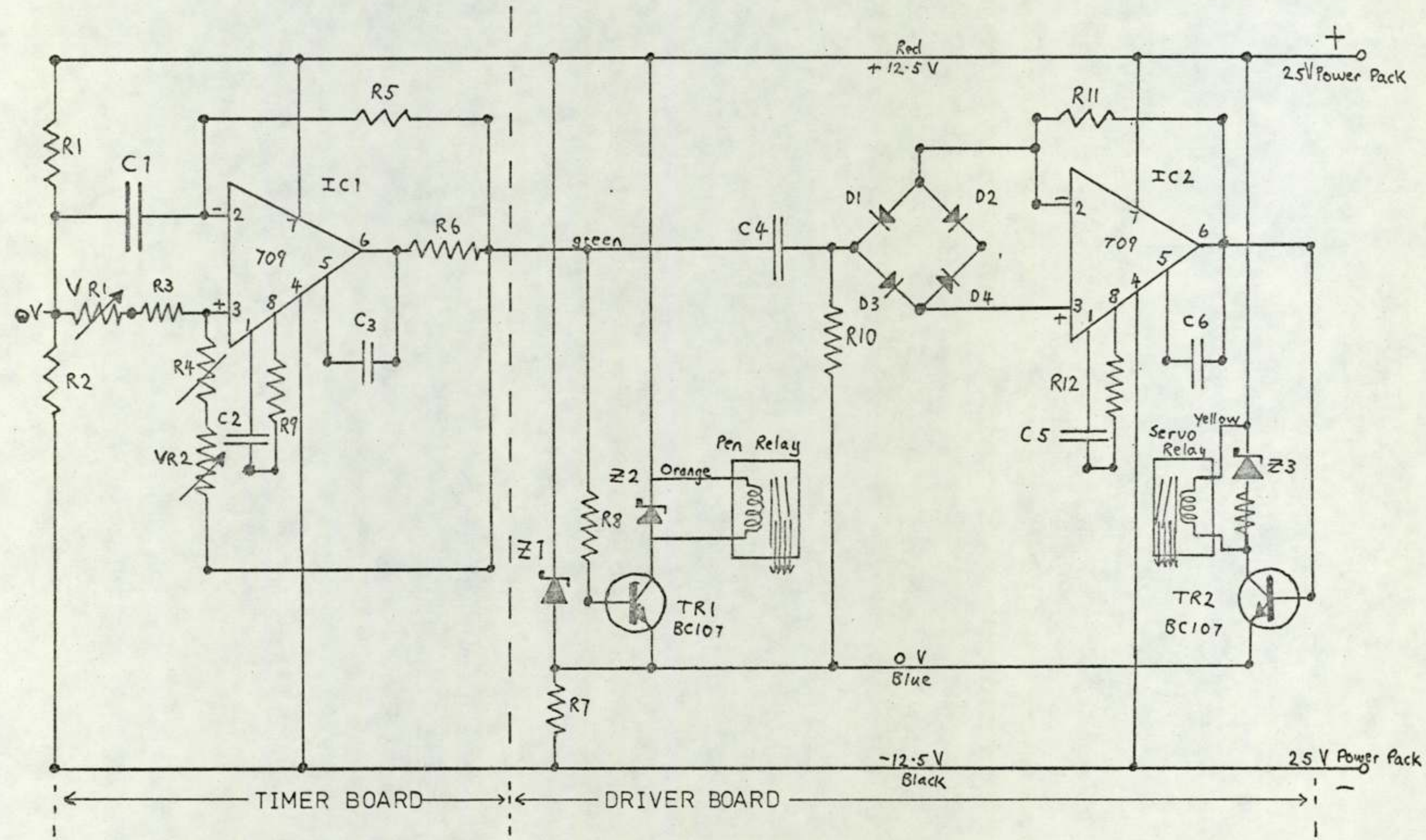

FIGURE 7.5 CIRCUIT FOR THE TIMER TO CONTROL VALVE AND PENS.

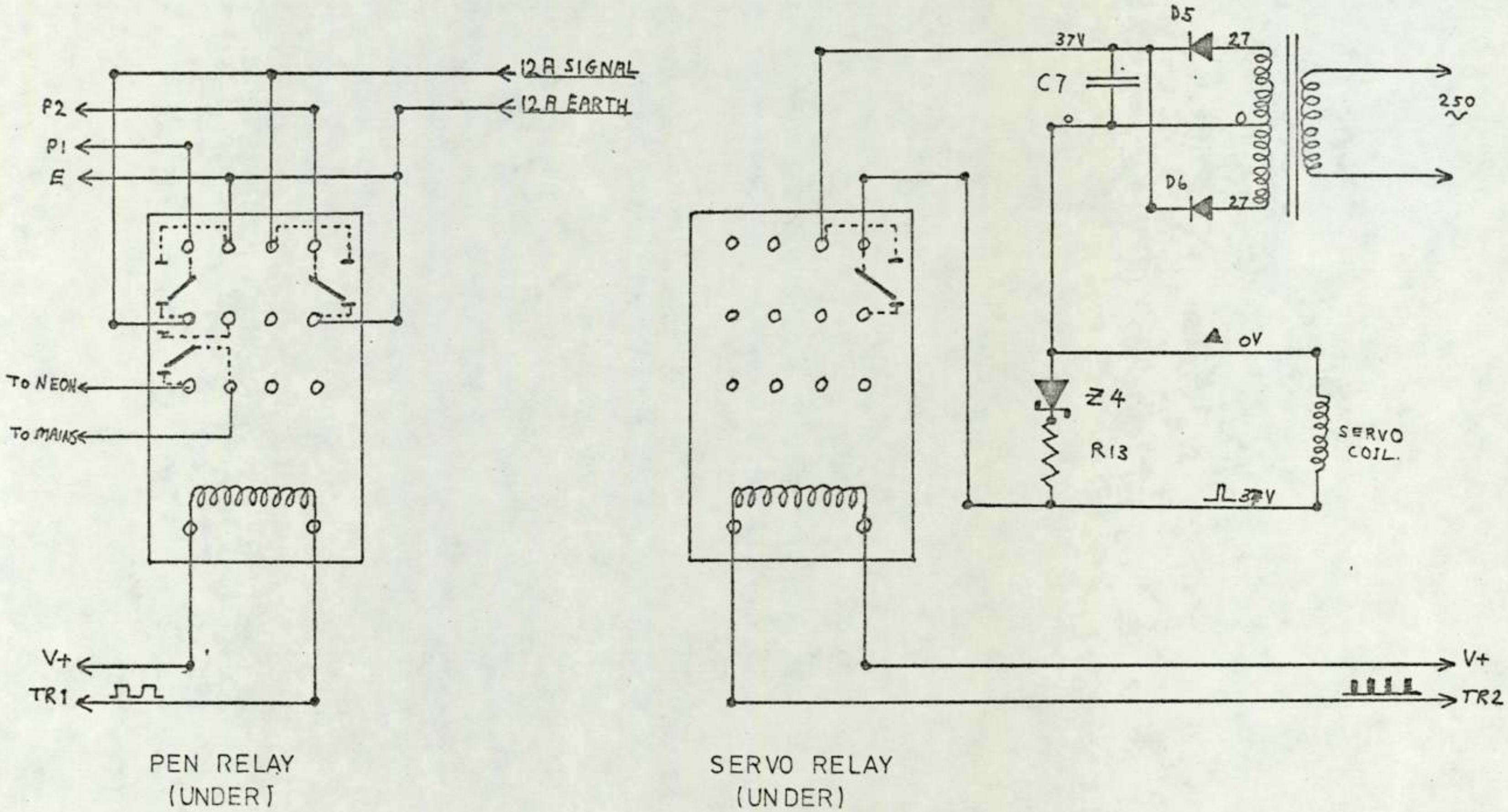

FIGURE 7.6 CONNECTIONS TO RELAYS IN TIMER.

TABLE 7.1

Components

IC1, IC2	SN72709		
TR1, TR2	BC107		
R1	3.3KΩ	C1	1000 μF, 25 UDC
R2	3.3KΩ	C2	100 pF polystyrene
R3	22KΩ	C3	3.3 pf
R4	22KΩ	C4	2 μF polystyrene
R5	330KΩ	C5	100 pF polystyrene
R6	51Ω	C6	1000 pF polystyrene
R7	1.2KΩ	C7	1000 μF electrolytic
R8	15KΩ		
R9	1.5KΩ		
R10	120KΩ	D1)	Signal diodes, 15 PIV
R11	1MΩ	D2)	
R12	1.5KΩ	D3)	
R13	750Ω	D4)	
VR1	2MΩ, log	D5	50 PIV, 1A
VR2	2MΩ, log	D6	50 PIV, 1A
		Z1	12V, 1 watt
Relays : GEC/MK		Z2	30V, 400 mw
M1492		Z3	30V, 400 mw
24V, 670		Z4	30V, 400 mw

transistor TR1 as a switch. TR1 controls the pen relay. Also, the multivibrator is differentiated by C4 and R10 (time constant C4.R10 $\sim$ 0.2 s) giving alternate positive and negative pulses at each state change. These pulses are relative to the OV rail. IC2 is used as a differential amplifier to amplify pulses occurring across the full wave rectifier (D1, D2, D3, D4). Positive pulses enter the non-inverting input, negative pulses the inverting input. The output is always a positive pulse and is used to drive transistor TR2 as switch. TR2 controls power through the relay from a 37V D.C. supply to the valve servocoil, (resistance 450 Ω) as in Figure 7.5. The combination of full wave rectifier and operational amplifier exploits the two inputs to prevent loss of pulses of one polarity to the negative rail as would occur with a single input amplifier. A feedback resistance (R11; 1MΩ) prevents IC2 acting as a Schmitt trigger. Inductive kicks on all coils are filtered by zenner diodes (Z2, Z3) thus avoiding transistor damage and preventing oscillatory feedback to IC2. A neon bulb wired to the mains through the pen relay is useful to check that the pens and valve keep in phase.

7.2.2 Valve and Servo

The valve face plate seats on the lapped surface of the brass valve body. The face plate is grooved to connect adjacent gas inlets in pairs (Figures 7.2, 7.7, 7.8). The flotation springs provide axial load to seat the face plate at all seating angles. The shaft peg carries the torque through to the face plate without disturbing the seating. This arrangement improves the gas seal over the valve surface. The photograph (Figure 7.8) shows how the weight on the string tends to

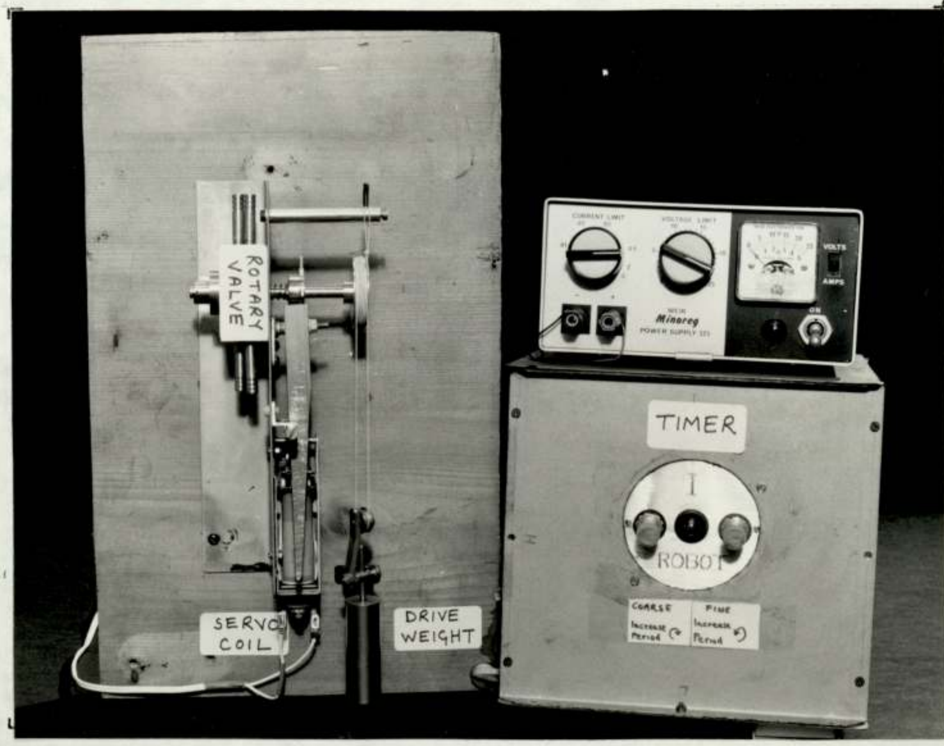

FIGURE 7.7 GENERAL VIEW OF THE TWO TUBES APPARATUS, WITH THE VALVE MECHANISM ON THE LEFT AND CONTROL ELECTRONICS ON THE RIGHT.

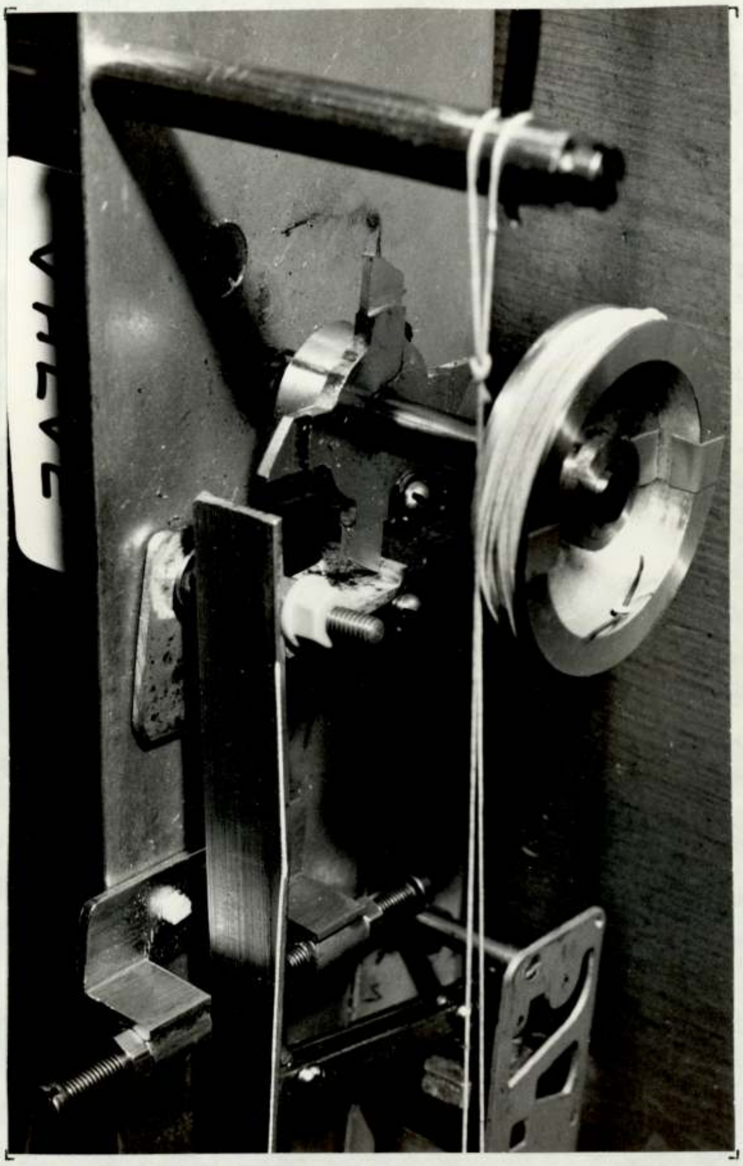

FIGURE 7.8 VALVE SERVO ASSEMBLY. THE WEIGHTED STRING GIVES TORQUE TO THE VALVE SHAFT, WHICH CAN ONLY ROTATE WHEN THE SOLENOID IS ENERGISED TO RELEAS THE SERVO. THE VALVE ROTATES NINETY DEGREES WITH EACH PULSE.

rotate the valve. When a voltage pulse is applied the solenoid moves the servo arm. The valve rotates through ninety degrees as the hook is released and caught again at the end of the pulse.

7.3 Laboratory Tests

7.3.1 The Valve

The flow system was set up to sample laboratory air, with the connections to the valve as in Figure 7.1. The electronic timer was not used, and the I2A was connected direct to the chart recorder. The I2A set to full scale deflection of 100ppm gave an insignificant reading on laboratory air. A source of 100ppm NO in N_2 was connected to the short tube. The valve was rotated into each position by hand. Any significant reading on the I2A when connected to the long tube would have been due to cross leaks but in fact no leak was observed.

The procedure was repeated with the air and NO inlets reversed, and no leak from the long tube to the short tube was seen. Leaks were obtained only when excessive NO/N_2 pressure was applied or an inlet was sealed. In the normal mode with both sides of the valve passing comparable flows of gas the leaks were insignificant.

7.3.2 Tube Flow Dynamics

The long tube finally used was a fifty six metre length of 0.48 cm i-d Teflon, sleeved in PVC. The down tube transit time as measured by pulse injection of NO was ninety seconds. The flow was $\sim$ 0.7 $1min^{-1}$. The Reynolds number is therefore $3.4 \cdot 10^4$ and the flow probably laminar (Monin and Yaglom, 1971j).

In the long tube, viscous effects cause a gradient of longitudinal velocity across the tube, with the fastest flow in the centre. The resulting longitudinal mixing mixes adjacent elements of gas as they pass down the tube.

With an infinitely long tube, a point injection of material is dispersed along the axial direction into a Gaussian concentration distribution (Monin and Yaglom, 1971k).

This dilution effect, or non ideal plug flow, smooths the changes in concentration.

Let the smoothing to have a time constant τ. Then τ is the time taken for pollutant concentration, with a step input, to rise to $1/e$ of its final value (Bair, 1962) With step height Sm, and signal S_t at time t,

for a rising signal $S_t/Sm = 1 - \exp(-t/\tau)$, and

for a falling signal $S_t/Sm = \exp(-t/\tau)$

Thus for the former $-\log_e (S_t/Sm - 1) = t/\tau$, and for the latter $-\log_e (S_t/Sm) = t/\tau$. The results from an injection of 100 ppm NO into the air stream of the long tube are plotted in Figure 7.9. For the rise, $\tau = 2.1s$, and for the fall $\tau = 1.4s$. The model I2A has a time constant of $\sim 1s$, on the 0.25ppm scale. The long tube therefore was causing only a slight smoothing effect. The close fit of the finer structure between the long and short tube traces when

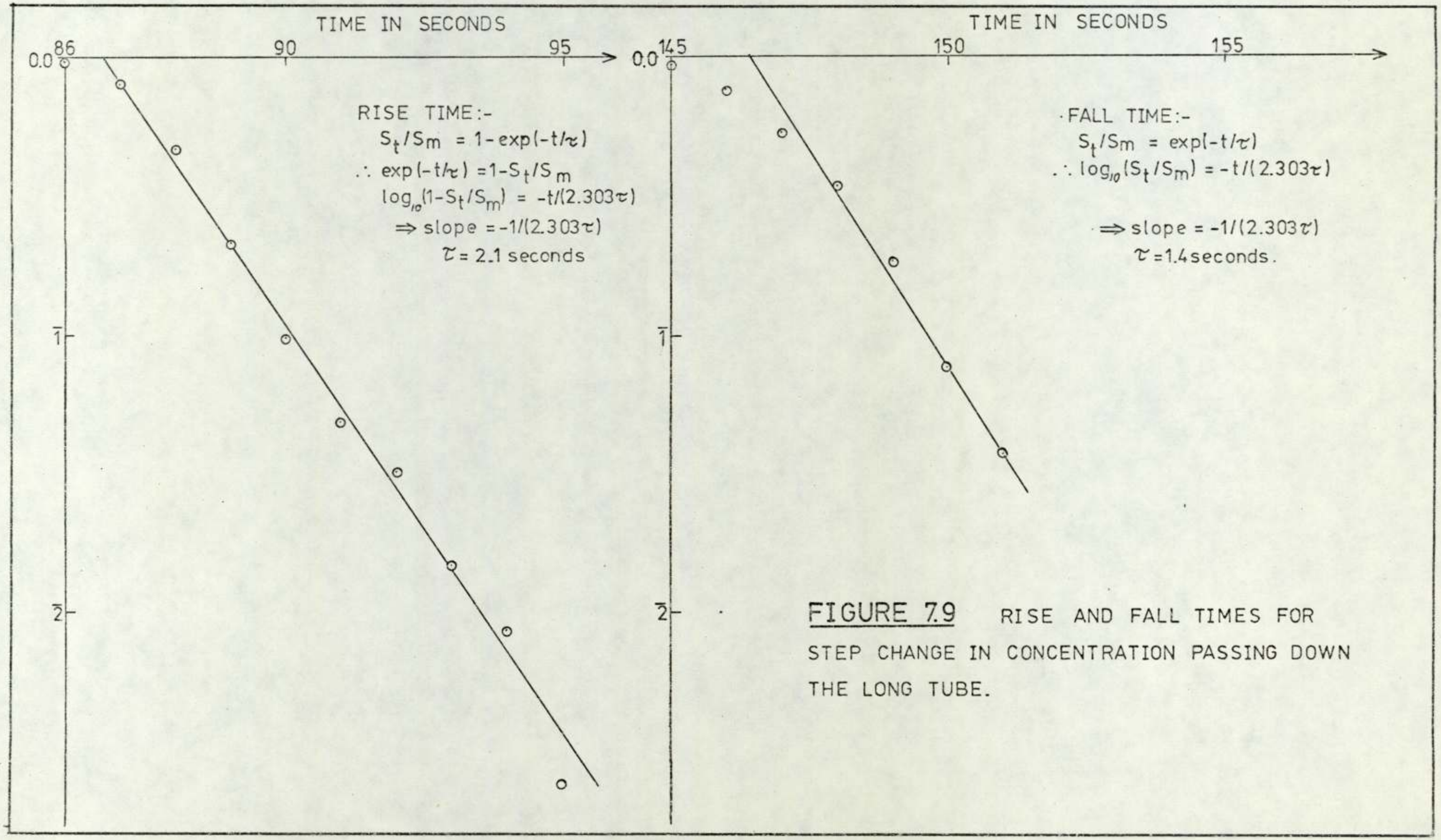

FIGURE 7.9 RISE AND FALL TIMES FOR STEP CHANGE IN CONCENTRATION PASSING DOWN THE LONG TUBE.

sampling the same inlet, as in Figure 7.12, is typical of the results obtained.

7.3.3 Accuracy of the Long Tube Record

The equipment was run with the long and short tube inlets joined (Figure 7.10) at Y-(1). At Y-(2), ambient air entered when the cylinder supply of standard gas was closed. Pulses of pollutant were generated by briefly opening the cylinder: Y(2) kept the flow constant by allowing either excess pressure to escape or air to enter. An example pulse injection is shown in Figure 7.11; a comparison of long and short tube analyses for a common inlet of atmospheric air is shown in Figure 7.12. Table 7.2 gives a numerical comparison of analyses for three cycles: the means of the long and short tube analyses agree within three per cent. The superimposed traces also showed (Table 7.3) that the time error $e = d_2 - d_1$ was reasonably constant.

7.3.4 Summary of Testing

The long tube caused slight smoothing of the trace (two seconds for a ninety second flow-time down a fifty six metre tube). From superimposed tracings with joined inlets the time error e could be measured with good consistency ($\pm$ 1 second). Time scale expansion could be set to unity. Intercepts could therefore be read from each state and averaged: the means agreed to within three per cent.

The similarity of joined inlets results showed that the equipment

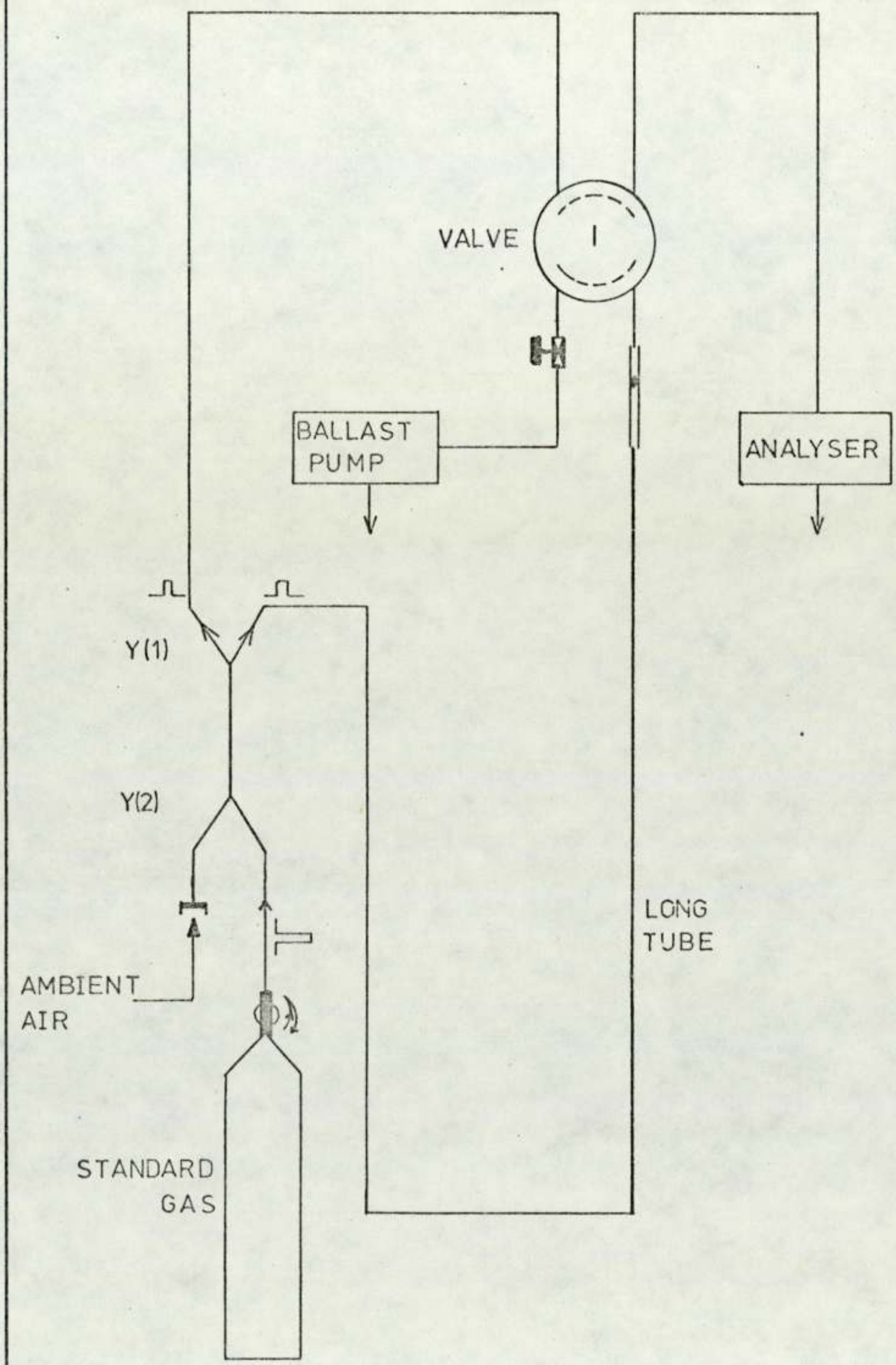

FIGURE 7.10 ARRANGEMENT OF INLETS FOR INJECTION OF IDENTICAL PULSES OF CONCENTRATION INTO BOTH TUBES AT THE SAME TIME. THE AMBIENT AIR INLET ACTS BOTH AS EXCESS PRESSURE RELEASE AND REFERENCE CONCENTRATION.

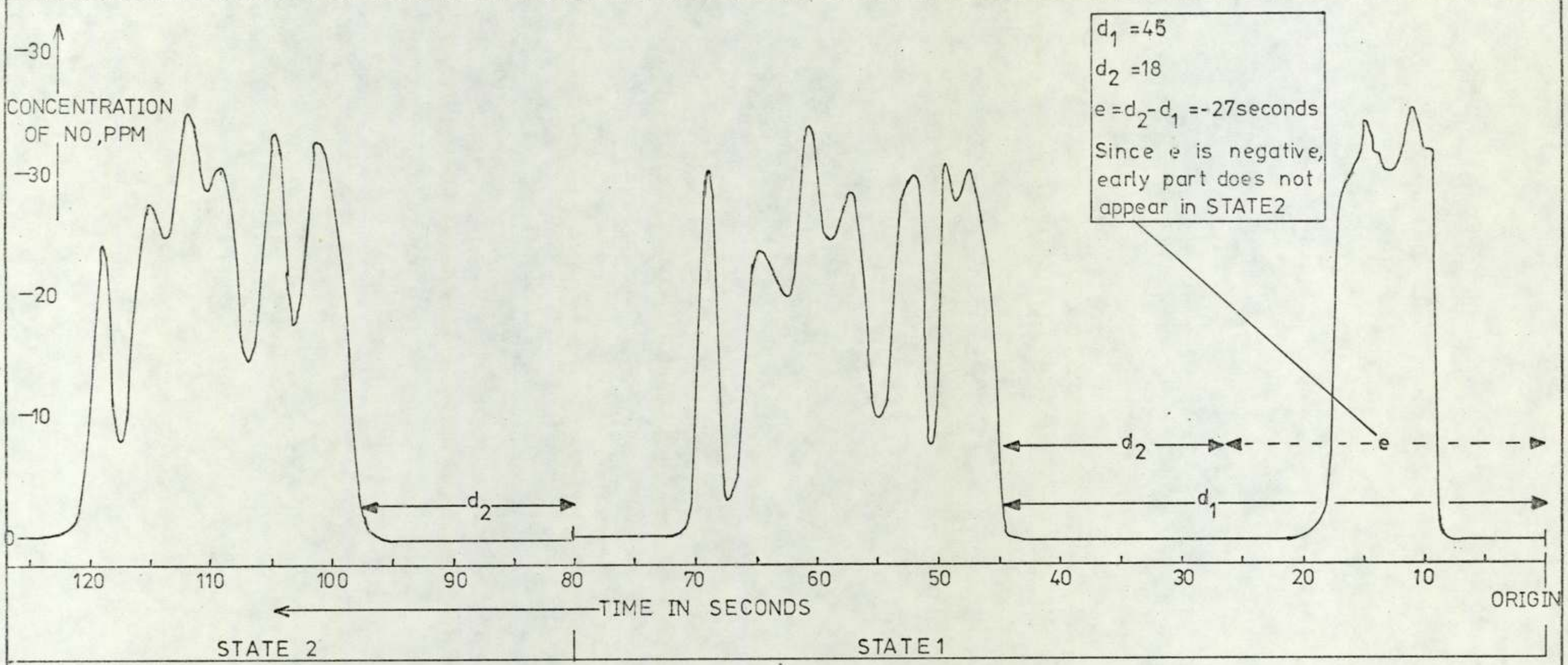

FIGURE 7.11 COMPARISON OF LONG AND SHORT TUBE ANALYSES OF CONCENTRATION PULSES GENERATED BY THE ARRANGEMENT SHOWN IN FIGURE 7.10.

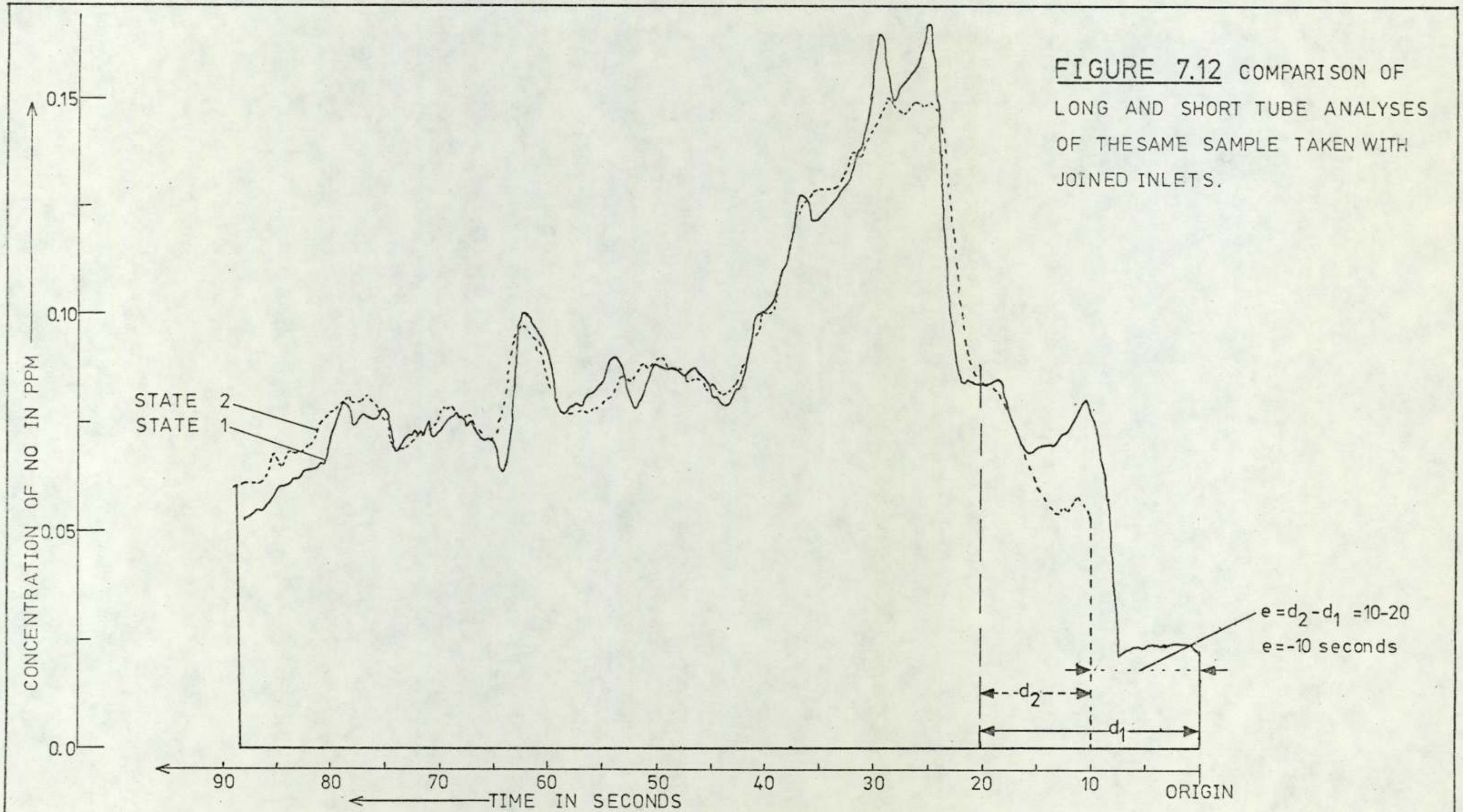

FIGURE 7.12 COMPARISON OF LONG AND SHORT TUBE ANALYSES OF THE SAME SAMPLE TAKEN WITH JOINED INLETS.

TABLE 7.2

Comparison of Long and Short Tube Traces

Cycle Number	Mean of 14 Intercepts, 5 seconds apart		Ratio
	Short Tube	Long Tube	
3	0.093212	0.090535	0.97
4	0.11750	0.11517	0.98
5	0.14125	0.14321	1.01

Source: 56m tube; 90 second flow time; ppm NO.

TABLE 7.3

Consistency of Time Error e (27-11-1974)

Cycle Number	Seconds		$e = d_2 - d_1$
	d_1	d_2	
5	17.5	12.5	5.0
6	15.0	10.0	5.0
7	14.0	9.0	5.0
8	14.0	9.0	4.5
9	14.5	10.0	4.5

as constructed could measure instantaneous analyses from two places using one pollutant analyser.

7.4 Application Beside M6 Motorway

7.4.1 Field Set-Up

The site was at the Perry Barr works entrance adjacent to the Police Motorway Control Centre. The Motorway runs through relatively open country at this point (Figure 7.13: Map). There are no other major roads nearby. The Bedford van containing the equipment was driven on to the grass by the sliproad; it was $\sim$ 25 metres from the Motorway. The site was not ideal: the sliproad passes under the Motorway here so an artificial valley and hill are present. The van was as far from the bridge as possible. When set up the Model J2A developed noise but since such experiments require special arrangement (e.g. with the police and for electricity) the run was made. The aim was to evaluate the application of the technique in the field.

The instrument noise (from a damp PM tube despite prior servicing) meant the joined inlets traces agreed to within $\pm$ fifteen percent; this is unusually large.

7.4.2 Results

Two positions of the long tube were used. For each cycle fifteen points were abstracted at five second intervals for both states. For each cycle, the averages of these are shown in Figure 7.14. The graph covers thirty cycles (each of 1.5 minutes) every three minutes: a total time of forty five minutes. The lower line is

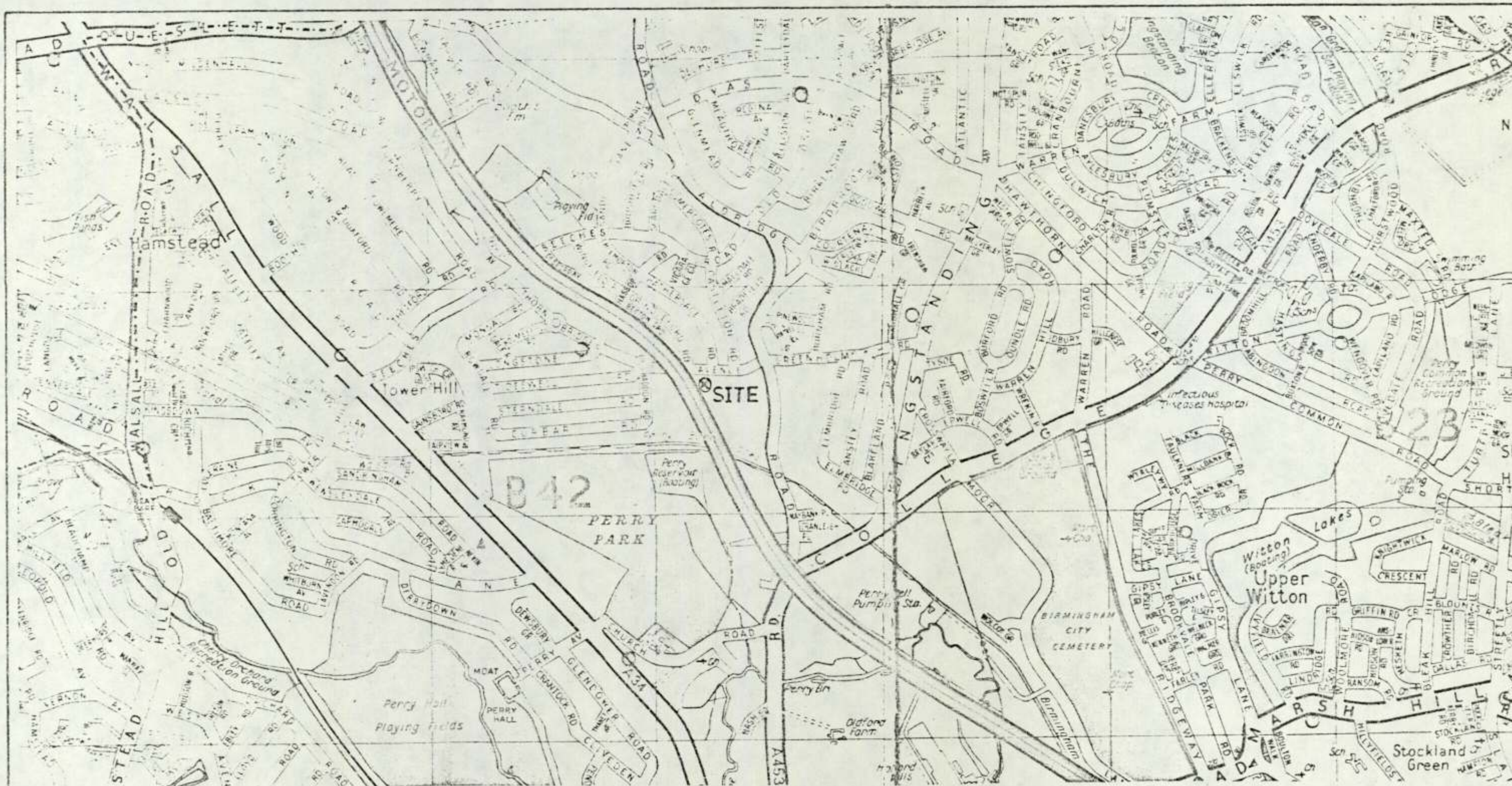

FIGURE 7.13 SITE OF THE TWO TUBES STUDY OF CONCENTRATION OF NO FROM M6 MOTORWAY.

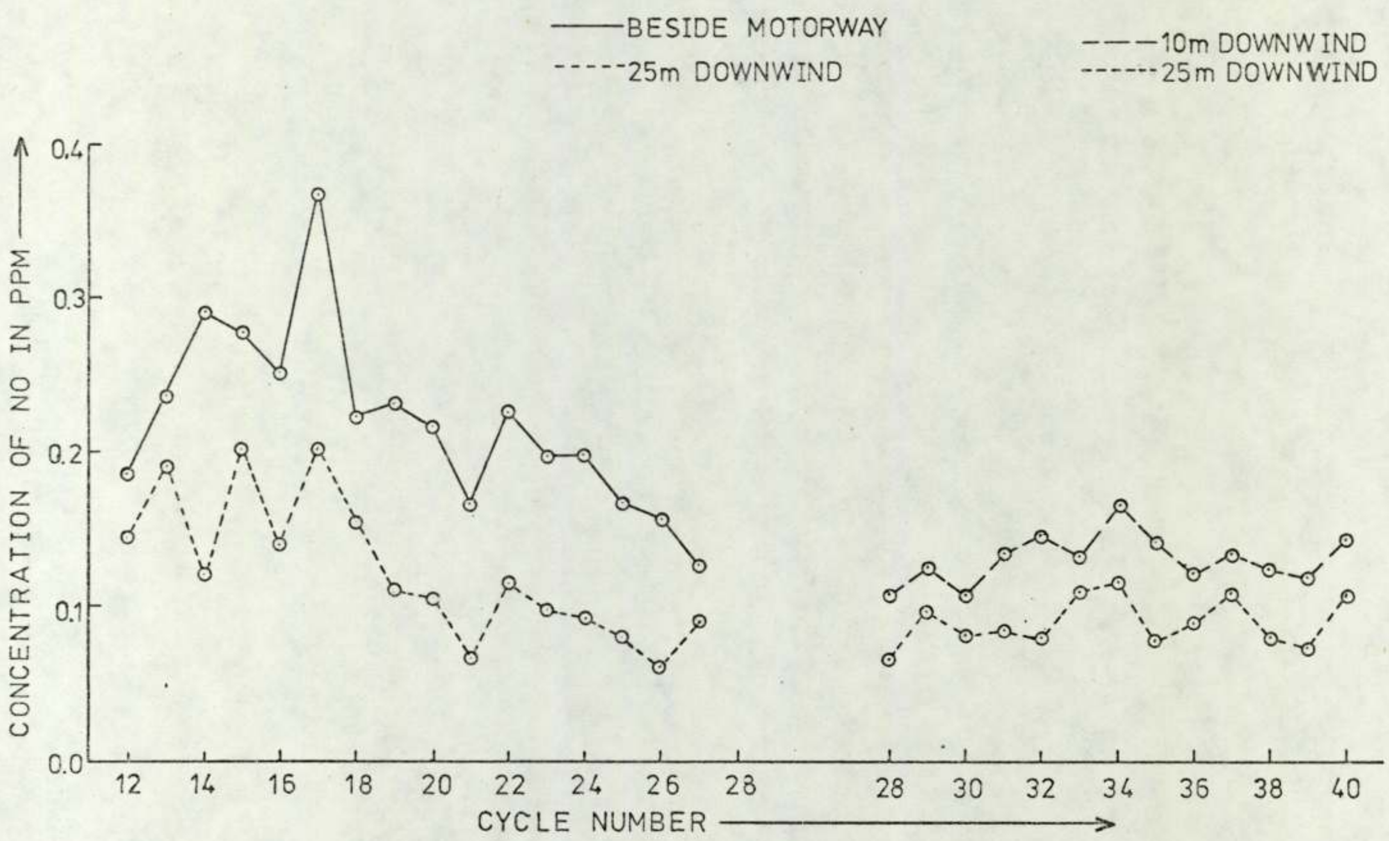

FIGURE 7.14 SIMULTANEOUS MEASUREMENTS OF NO CONCENTRATION AT TWO DISTANCES DOWNWIND FROM M6 MOTORWAY.

concentration for the short tube placed twenty five metres downwind; the upper, for the long tube at two positions.

The fluctuations in both the short-term concentration (averaging time $\sim$ 75 seconds) and the short-term concentration gradient (ratio of time coincident concentrations from two downwind positions) can be seen in Table 7.4, and Figures 7.15, 7.16. These changes are associated with fluctuations in traffic flow, wind-speed and atmospheric conditions.

7.4.3 Comparison With Theory

During the experiment the traffic-flow was 4,500 vehicles per hour, wind-speed was 13 knots and cloud 7 oktas so the stability was class D. The wind was perpendicular to the Motorway.

The programme described in Chapter 6 was used to predict the NO concentration from a straight ground-level road with these conditions and an NO source emission factor of $Q_{NO} = 4.7843.10^{-4}$ppm $m^2 s^{-1} (vh^{-1})^{-1}$ described in Chapter 6. The predictions made for a straight road 1,000 metres long with five metre steps extending equal distances to either side of the observer line (Figure 7.17) are shown in Table 7.5 and Figure 7.18.

The agreement is satisfactory considering the uncertainties in the readings (from instrument noise), emissions estimate and weather readings (from Elmdon Airport).

Concentrations were measured alongside a Motorway as sequential half-hour averages (Butler, MacMurdo, Middleton, 1974) on Thursday

TABLE 7.4

Concentrations recorded at Perry Barr alongside M6 Motorway.

Results have 0.08ppm background subtracted.

Cycle	Concentrations Short Tube	Concentrations Long Tube	Ratio Long ÷ Short Tube
	25m downwind	at M6	
12	0.148	0.187	1.266
13	0.192	0.238	1.240
14	0.123	0.293	2.386
15	0.204	0.279	1.369
16	0.141	0.252	1.783
17	0.203	0.369	1.813
18	0.156	0.225	1.440
19	0.112	0.233	2.077
20	0.106	0.219	2.063
21	0.069	0.169	2.442
22	0.116	0.227	1.954
23	0.099	0.198	1.993
24	0.094	0.198	2.106
25	0.081	0.168	2.083
26	0.064	0.158	2.469
27	0.092	0.177	1.920
	25m downwind	10m downwind	
28	0.067	0.107	1.594
29	0.097	0.125	1.297
30	0.081	0.107	1.320
31	0.087	0.135	1.562
32	0.080	0.147	1.833
33	0.110	0.134	1.218

Continued/......

TABLE 7.4 (continued)

	25m downwind	10m downwind	
34	0.117	0.167	1.429
35	0.078	0.142	1.821
36	0.089	0.121	1.358
37	0.108	0.134	1.241
38	0.080	0.124	1.550
39	0.072	0.119	1.648
40	0.109	0.144	1.325

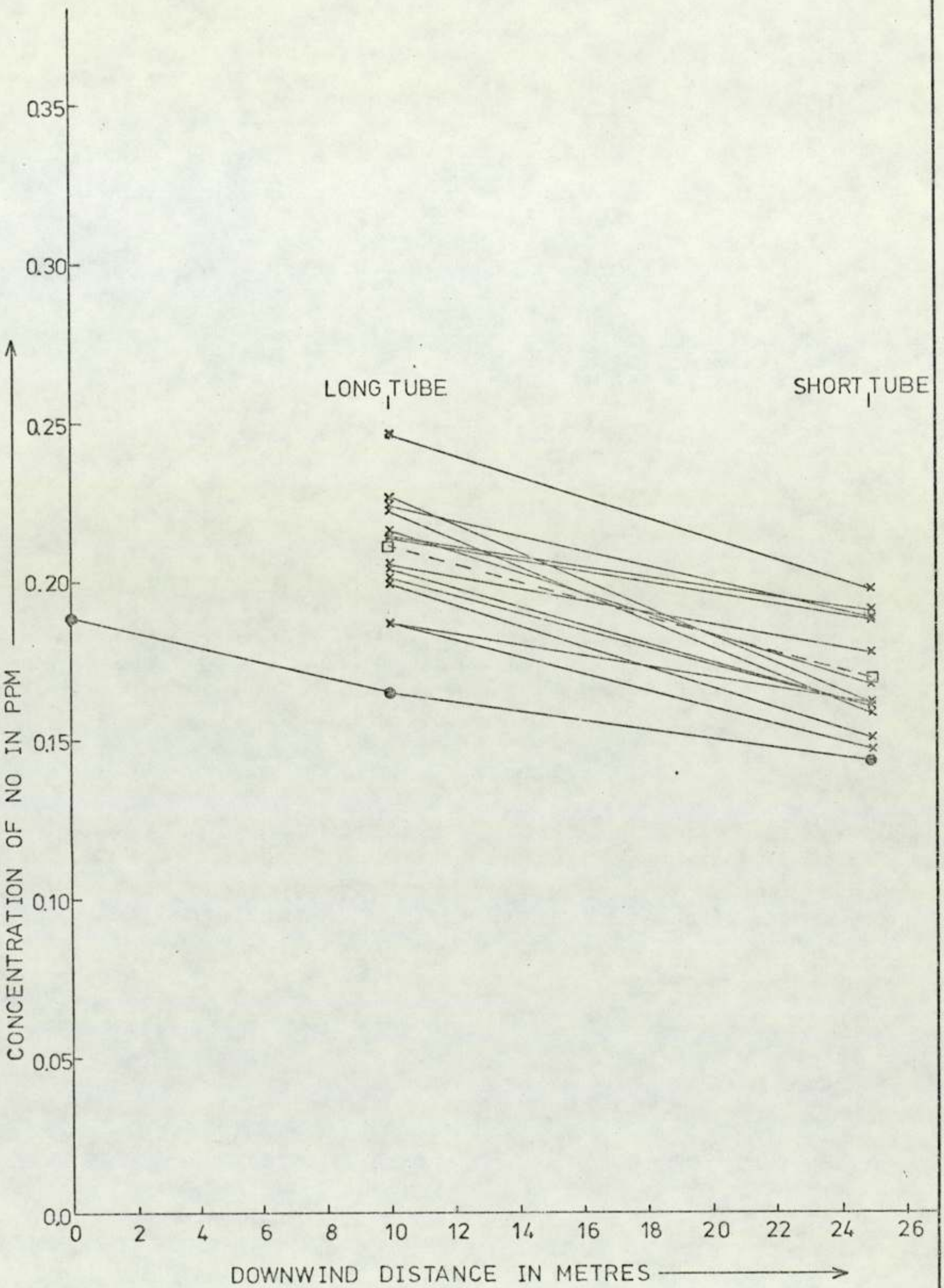

FIGURE 7.15 DECREASE IN CONCENTRATION OF NO WITH DISTANCE DOWNWIND FROM M6 MOTORWAY.

KEY :- ×——× EXPERIMENTAL (FOR A SINGLE CYCLE)

□- -□ MEAN OF ALL CYCLES

●——● CALCULATED USING PROGRAMME (SEE TEXT).

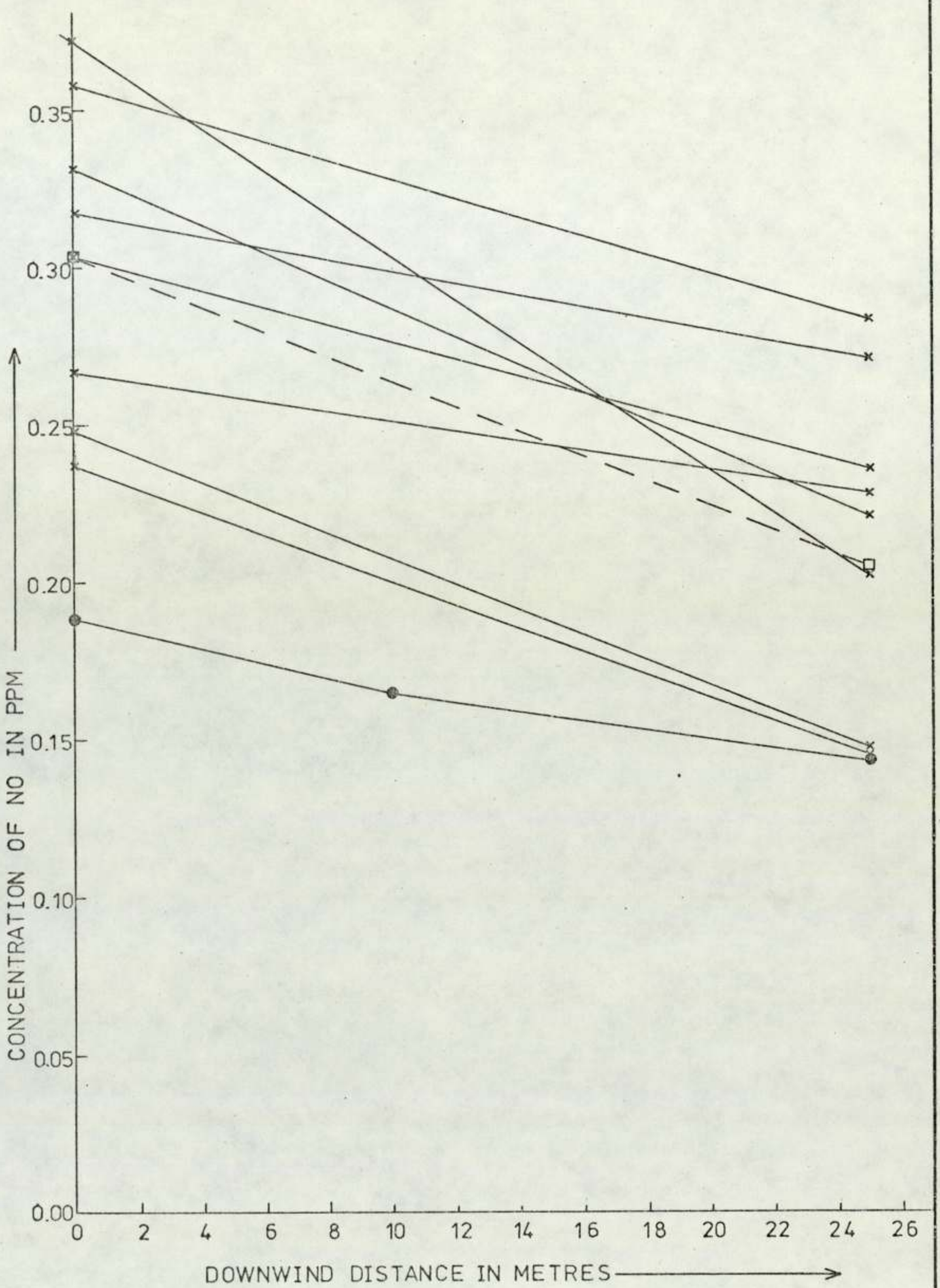

FIGURE 7.16 DECREASE IN CONCENTRATION OF NO WITH DISTANCE DOWNWIND FROM M6 MOTORWAY.

KEY:- ×—× EXPERIMENTAL (FOR A SINGLE CYCLE)

□- -□ MEAN OF ALL CYCLES

●—● CALCULATED USING PROGRAMME (SEE TEXT)

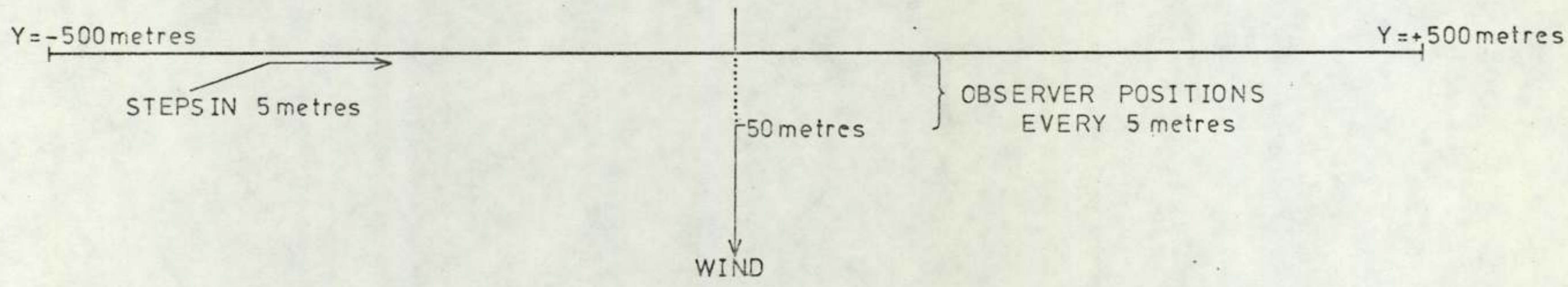

FIGURE 7.17 ROAD LAYOUT FOR THE CALCULATED RESULTS OF TABLE 7.5

TABLE 7.5

Average and Predicted Concentrations for Each Tube Position

Cycles	Mean concentrations[1], ppm NO, (measured)		
	Long Tube		Short Tube
	at road	10m downwind	
12 - 27	0.224	-	0.125
28 - 40	-	0.131	0.090
	Calculated concentrations		
Programme	0.164	0.125	0.094
Calder (1973)	0.173	0.133	0.099

Note 1: Zero level 0.08ppm measured in clean air blowing under the bridge was subtracted.

Note 2: Conditions:- 4500 vehicles h^{-1}, wind speed 13 knots, cloud 7 oktas.

Note 3: Discrepancy is due to slight differences in σ_z: Programme uses $\sigma_z(0)=1.6$, $\sigma_z(10)=2.1$, $\sigma_z(25)=2.76$ while Calder uses 1.5, 1.95, 2.6 respectively.

$Q_{NO} = 0.00047843\text{ppm } m^2s^{-1}(vh^{-1})^{-1}$, $T = 4500$ vehicles h^{-1},

$u = 6.63\ m^2s^{-1}(vh^{-1})^{-1}$, $Q_L = T.Q_{NO} = 2.1529\ m^2s^{-1}$

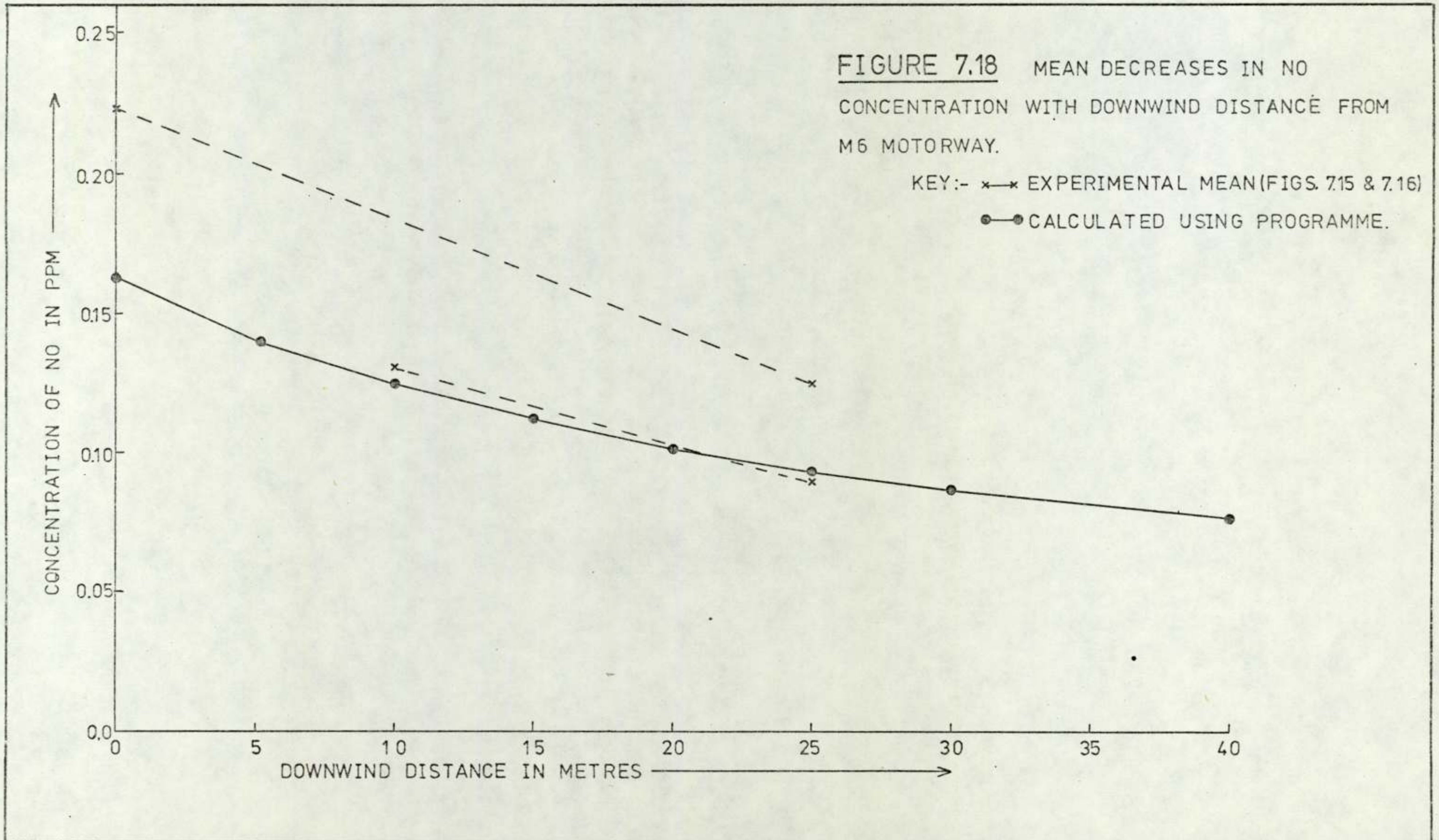

FIGURE 7.18 MEAN DECREASES IN NO CONCENTRATION WITH DOWNWIND DISTANCE FROM M6 MOTORWAY.

TABLE 7.6

Average and Predicted Concentrations -

for single inlet results

(Butler, MacMurdo, Middleton, 1974)

Source	Downwind Distance m	Concentration[1] NO, ppm
Butler et al.	0	0.257
	15	0.200
	27	0.155
Programme	0	0.164
	5	0.141
	10	0.125
	15	0.112
	20	0.102
	25	0.0940
	30	0.0871
	40	0.0762

Note 1: Zero of 0.037 subtracted

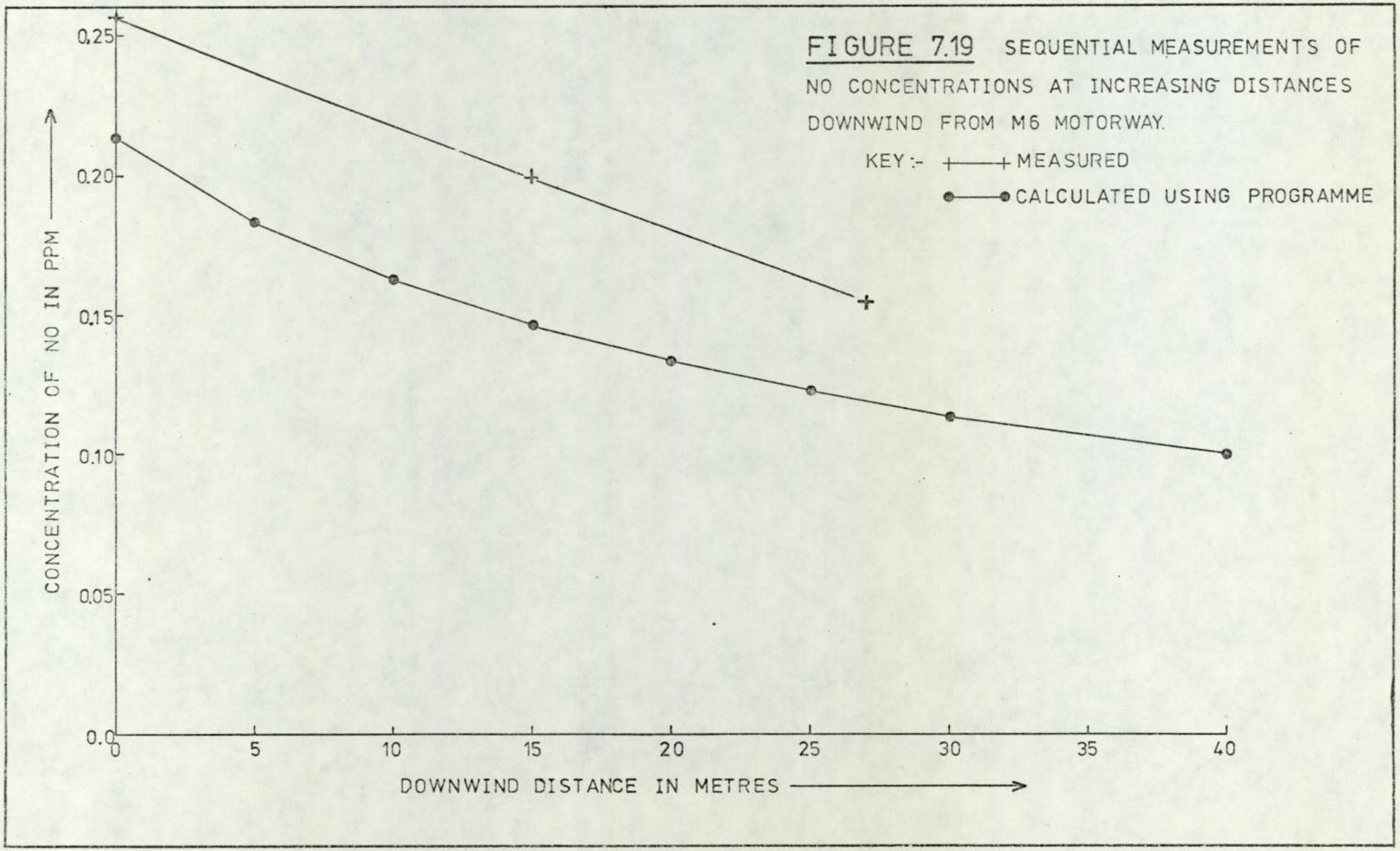

FIGURE 7.19 SEQUENTIAL MEASUREMENTS OF NO CONCENTRATIONS AT INCREASING DISTANCES DOWNWIND FROM M6 MOTORWAY.

03-05-1973. Conditions were 8 oktas cloud with wind-speed 4-5 ms^{-1}. The concentrations are compared in Table 7.6 and Figure 7.19 with similar predictions using a traffic-flow of 4,000 vehicles h^{-1}, a mean wind-speed of 4.5 ms^{-1} and class D stability. Figure 7.19 shows that the prediction is low.

7.5 Horizontal and Vertical Sampling at a Complex Site

The technique was used to measure concentrations across and vertically above the centre of the roundabout. The short tube inlet was placed on the roof of the toilets at the roundabout centre. For the vertical sampling a pulley was attached to the barrier at the side of the elevated section of road passing directly above the centre of the roundabout. A continuous loop of string over the pulley was attached to the long tube to raise and lower the inlet.

The concentrations fluctuated over a short time scale; average concentrations were calculated for each tube position (Table 7.7) and scaled to common units by dividing by the short tube result. The relative concentrations are plotted in Figures 7.20, 7.21 and 7.22, together with curves predicted using the programme SPAGSIMP, as described in Section 6.5. The concentration on 22-11-1974 and 25-11-1974 (Figures 7.21 and 7.22) decreased with downwind distance, across the roundabout: this is consistent with an effective increase in dilution distance. The concentration on 23-10-1974 (Figure 7.22) increased again at the far or downwind side: this unexpected increase at the far side is present in the calculated results also. This form of curve reflects the wind direction and source geometry. From Figures 7.20,

TABLE 7.7

Horizontal and Vertical Sampling at Salford Circus

Data and computer generated curves are shown in Figures 7.20, 7.21, 7.22 and 7.23 (Programme SPAGSIMP, using meteorological data and roundabout traffic count for the nearest hour on the day, and for simplicity, a 17.00 hours traffic (Friday) for the rest of the intersection). In the Table, numbers in brackets are ppm levels predicted by the programme (selected from the predictions used for the computer curves above).

SAMPLING	Set and Date	Number of Cycles	Short Tube Position	Long Tube Position	Mean Concentration for the set PPM		Ratio Long÷Short Normalised
					Short	Long	
HORIZONTAL	1 23.10.74	17	Centre: 40m	Upw 0	0.035 (.02866)	0.057 (.07195)	1.63
	2 23.10.74	10	Centre: 40m	Down 80	0.043 (.02866)	0.057 (.05680)	1.31
	3 22.11.74	14	Centre: 40m	Upw 0	0.350 (.08629)	0.502 (.1285)	1.43
	4 25.11.74	16	Centre: 40m	Upw 0	0.115 (.06342)	0.206 (.09203)	1.79

Continued/......

TABLE 7.7 (continued)

HORIZONTAL	5 25.11.74	12	Centre: 40m	Down 80	0.095 (.05035)	0.074 (.04291)	0.78
VERTICAL	6 27.11.74	9	Centre: 3m	H1: 13	0.117	0.105	0.90
	7 27.11.74	8	Centre: 3m	H2: 11	0.080	0.080	1.00
	8 27.11.74	8	Centre: 3m	H3: 8	0.086	0.078	0.90
	9 27.11.74	10	Centre: 3m	H4: 5	0.099	0.092	0.93

FIGURE 7.20 RELATIVE DECREASE IN NO CONCENTRATION ACROSS SALFORD CIRCUS ROUNDABOUT IN THE INTERSECTION.

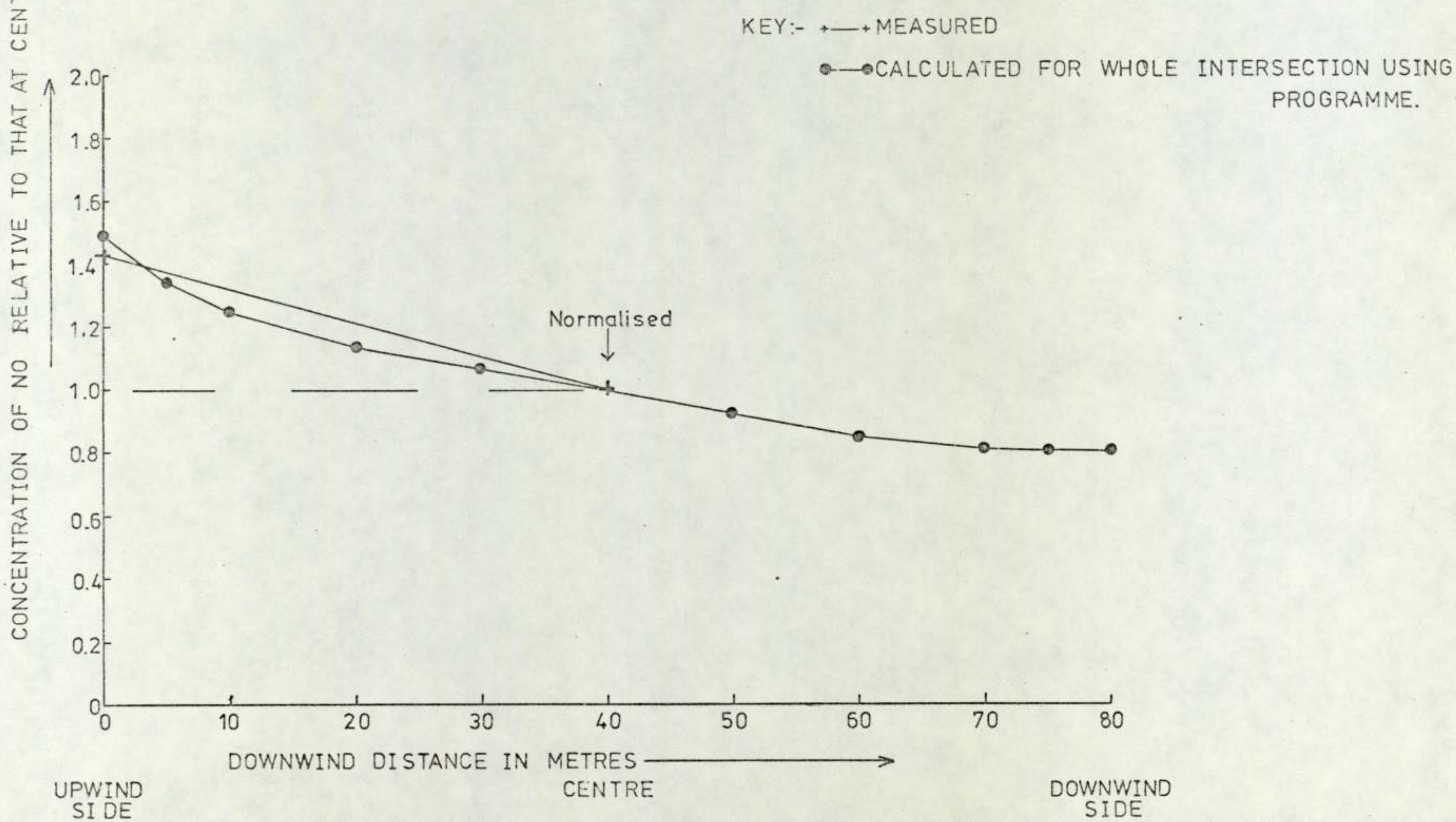

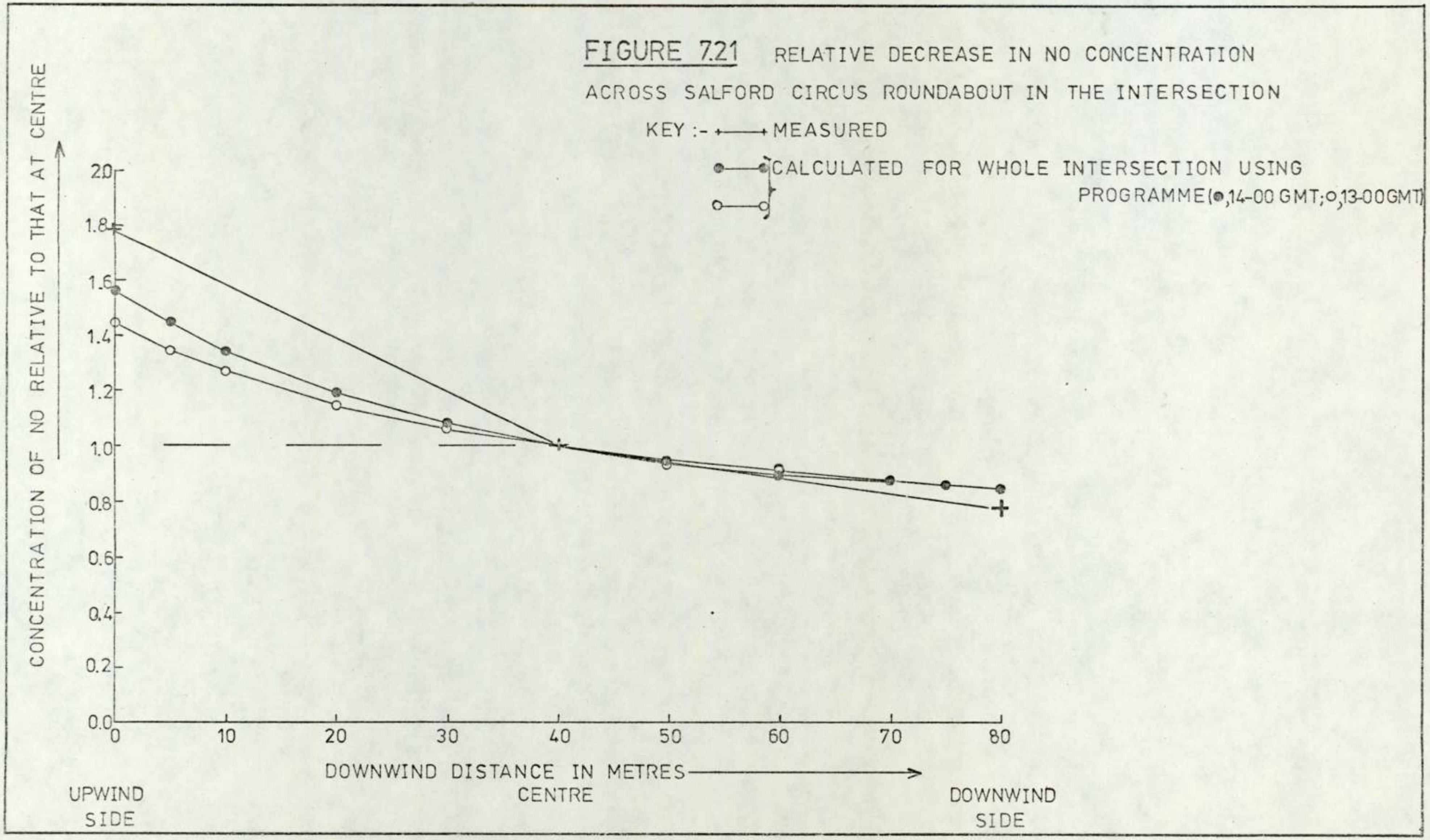
FIGURE 7.21 RELATIVE DECREASE IN NO CONCENTRATION
ACROSS SALFORD CIRCUS ROUNDABOUT IN THE INTERSECTION
KEY :- MEASURED
CALCULATED FOR WHOLE INTERSECTION USING PROGRAMME (●,14-00 GMT; ○,13-00GMT)
CONCENTRATION OF NO RELATIVE TO THAT AT CENTRE
2.0
1.8
1.6
1.4
1.2
1.0
0.8
0.6
0.4
0.2
0.0
0
10
20
30
40
50
60
70
80
DOWNWIND DISTANCE IN METRES
UPWIND SIDE
CENTRE
DOWNWIND SIDE

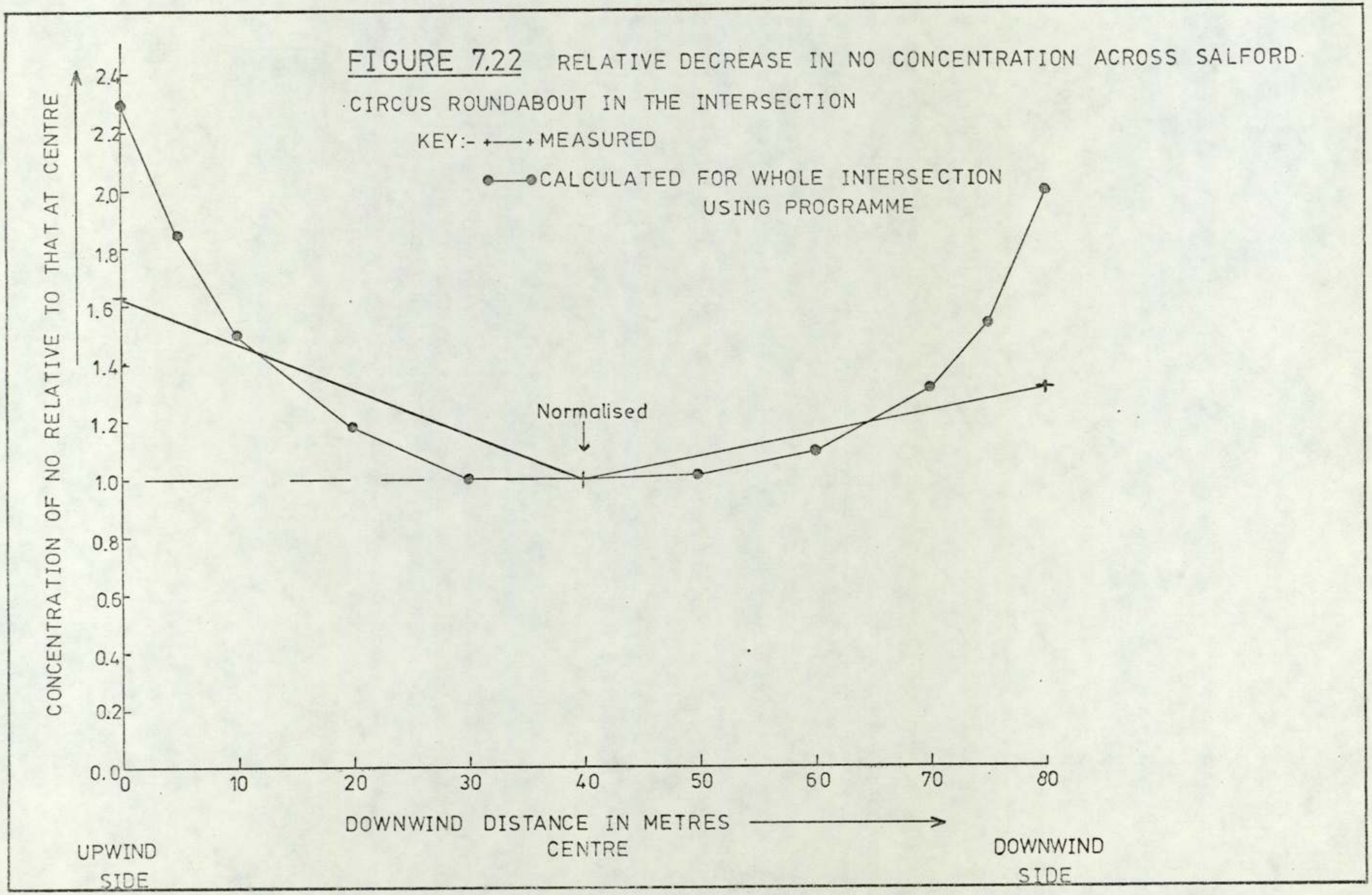
FIGURE 7.22 RELATIVE DECREASE IN NO CONCENTRATION ACROSS SALFORD
CIRCUS ROUNDABOUT IN THE INTERSECTION
KEY:- +—+ MEASURED
CALCULATED FOR WHOLE INTERSECTION USING PROGRAMME
CONCENTRATION OF NO RELATIVE TO THAT AT CENTRE
2.4
2.2
2.0
1.8
1.6
1.4
1.2
1.0
0.8
0.6
0.4
0.2
0.0
Normalised
0
10
20
30
40
50
60
70
80
DOWNWIND DISTANCE IN METRES
UPWIND SIDE
CENTRE
DOWNWIND SIDE

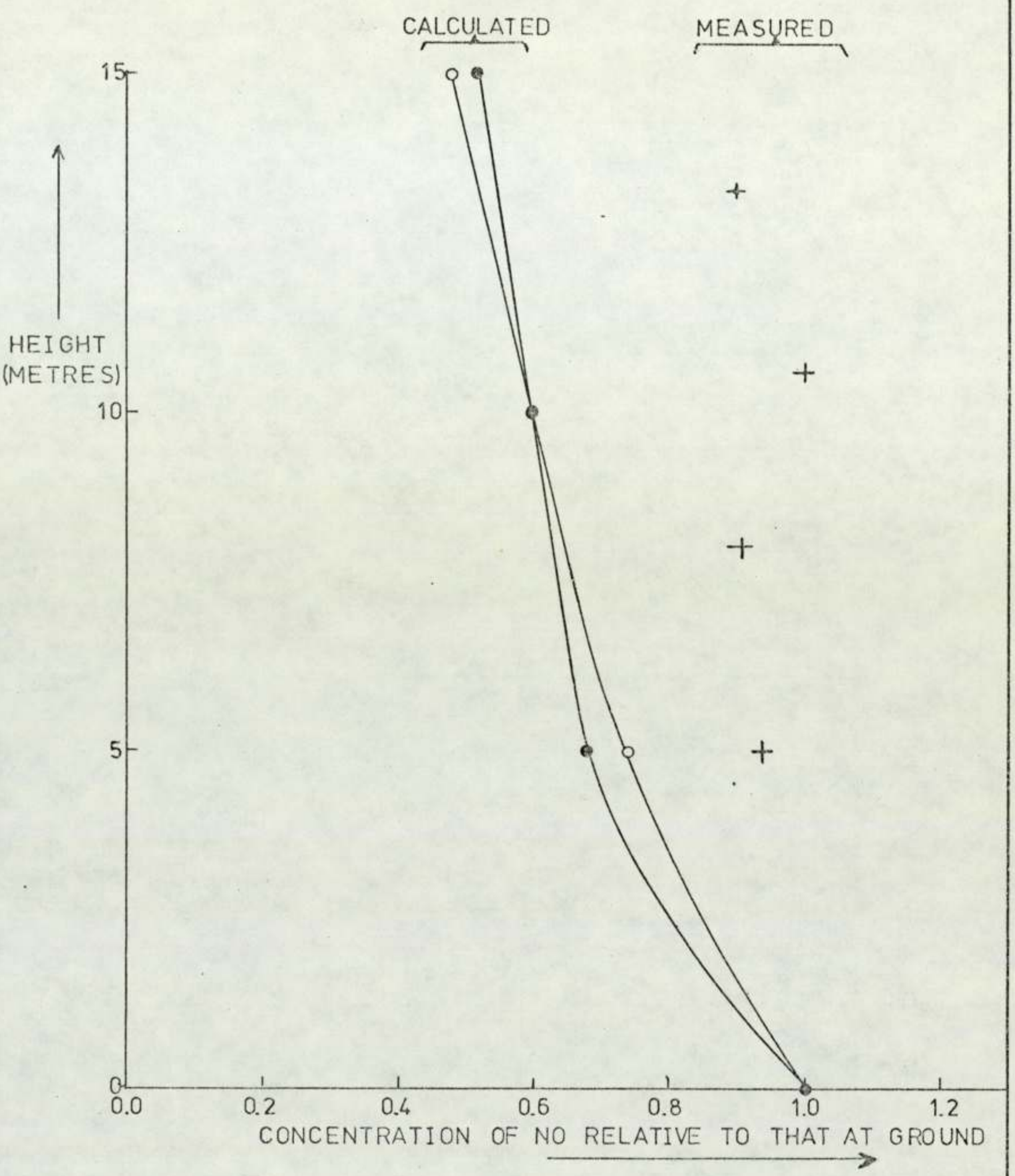

FIGURE 7.23 VERTICAL CHANGES IN NO CONCENTRATION AT SALFORD CIRCUS ROUNDABOUT IN THE INTERSECTION.

KEY:- +—+ MEASURED

●—● } CALCULATED USING PROGRAMME
○—○ }

7.21 and 7.22, the programme did give dilution curves of form consistent with the concentration gradients measured by the technique.

In Figure 7.23 a similar, though less satisfactory, comparison is made between the measured vertical gradient and programme curves. There was however much eddying, particularly when just below the elevated roads so the scatter present in the raw data and the poor agreement of Figure 7.23 was not surprising. The geometrical simplification present in the model, particularly the use of horizontal roads throughout, probably affects this comparison also: the roads above the sample tube do slope down, so there are pollutant contributions from all heights which would affect the programme curve.

7.6 Summary

A sampling technique to measure concentrations simultaneously at two different places, using only one analyser, has been described. The equipment was tested in part and then as an operating technique in the field: some measurements of pollutant plumes were presented.

The measurements were compared with predictions using the programme SPAGSIMP (Section 6.5, Paragraph 5); the same emissions estimate (per vehicle) was used for this work as for the analysis of the routine monitoring results (Chapter 6).

The results for horizontal sampling were consistent (both at the Motorway and in the roundabout) with the programme predictions: the vertical sampling was less conclusive and the weakness of the programme with regard to local eddying and road-slopes was suggested as responsible.

The general levels predicted by the programme for the roundabout were lower than as measured: this is consistent with the observations of Chapter 6. This lowness was less pronounced alongside the M6, where perhaps less acceleration occurs, and a more representative source description possible.

CHAPTER 8

CONCLUSIONS

As stated in the introduction (Chapter 1), the project studied the intersection as a source of pollution. We explained there that by the very nature of the problem, field monitoring would precede interpretation. Having described the work itself in previous Chapters, we now list the conclusions.

8.1 Calibrations

Dilution of NO and CO from 100% in two stages (Chapter 2) showed that calibrations using the commercial mixtures of standard gas would be accurate within an order of magnitude, but might be low. Concentrations reported for oxides of nitrogen could be $\sim$ 30% low, and for carbon monoxide, $\sim$ 40% low. Part of this uncertainty arises from experimental limitations and more sophisticated apparatus was referenced. Mixtures of standard gases can be unstable and should be treated with suspicion.

Single-stage dilution of standard mixtures showed that the analysers for oxides of nitrogen and carbon monoxide were linear to within 10% and 5% respectively.

A cross-check made by altering the hydrocarbon analyser to measure carbon monoxide as methane suggested that the standards for carbon monoxide and hydrocarbons were consistent.

Together, these results imply that, with regard to calibration, the concentrations recorded during the project were self-consistent. Some uncertainty remains as to their absolute magnitude.

8.2 Field Monitoring

This is an exercise in itself because instrument drift is more severe than in the laboratory. Ideally, automatic zero checks should be made, or failing that, daily visits. Chart recorders were very useful to watch both instrument performance and pollutant trends, but did make data abstraction lengthy.

The chemiluminescent analyser for oxides of nitrogen, NO and NO_x, was, with the automatic zero-checker added, quite adequate despite needing much maintenance. Measurement of nitrogen dioxide as $NO_2 = NO_x - NO$ was not satisfactory. The non-dispersive infra-red analyser for carbon monoxide was very reliable, but a 0-10ppm scale would have been useful. The flame ionisation detector for hydrocarbons was satisfactory, except that it was noisy at times. Ideally the zeroing of this instrument requires study as to whether an oxygen effect occurs.

Pollutant concentrations fluctuated widely and although several points were abstracted for each hour, there remains an uncertainty in the values quoted because of this fluctuation. This uncertainty and the selection of both instrument response-time and data-averaging time should be studied.

8.3 Data Processing

Monitoring generates large quantities of data (Chapters 3, 4). Errors and missing values occur. Thus data processing for this type of work must meet several requirements:-

1. Flexibility of data sequence and data set size.
2. Unique but efficient coding of information for time, date, year, site and identification of variables, followed by any number of observations. The use of pre-defined card-columns and a card character-search by the programme proved very helpful. The method could be made more efficient by greater use of header information (e.g. for year and site which may occur on every row in the set) to shorten each data row.
3. Ability to process incomplete data sets, either by deletion of incomplete rows, or by interpolation of occasional missing values if the data follow an understood pattern. This requirement is because simultaneous observations may be required for many variables, especially if modelling is to follow the observational study (in our case traffic on twenty four roads, five pollutant variables and three weather parameters).
4. Option to interpolate whole data sets from a smaller sample of real observations, where possible. E.g. we interpolated hourly traffic counts from twelve hourly photographs, thus drastically reducing the manhours in abstraction.
5. Correction for zero and calibration drifts, and averaging of pollutant levels, e.g. into hourly averages. This

requires complete flexibility in the numbers (from none upwards) and times of zeroes, calibrations and observations.

6. Ability to sort and manipulate the data easily, since errors are found in manually abstracted data.

8.4 Emissions - Dilution Model

A computer programme was developed (Chapter 6) to calculate the concentration of a gaseous pollutant at any site for any network of roads and traffic-flows. A simple map reference system based on the Ordnance Survey represents roads of any geometry (lines, curves or circles) and height. Any number of observer positions are similarly represented. Axes are rotated (X downwind) so that the distances of an observer downwind and crosswind from points along each road may be calculated. With these distances, if the element of road is upwind of the observer, the contribution of that element to pollution at the observer is calculated and added to that of previous elements. Pollutant concentrations for each element are represented by the continuous point-source or Gaussian plume formula, with plume widths and heights obtained by the Pasquill category method using windspeed, cloud cover and insolation (latter is estimated). The integral over the intersection is scaled by the constants, namely (windspeed)$^{-1}$ and the source strength, to give the calculated concentration. Source strength is, in effect, the product of road-length (m), traffic-flow (vehicle h^{-1}) and emission parameter (m^3 pollutant m^{-1} road (vehicle $h^{-1})^{-1} s^{-1}$. The programme thus calculates concentrations of pollutants with no reference to measured concentrations, relying on source geometry and literature values for plume dilution and emissions parameters.

8.5 Model Test: Dilution

For a simple line source, the concentration decay calculated by the programme was similar to that given in numerical form by Calder (1973).

A two-tubes sampling technique (Chapter 7) was tested to assess its use for the measurement of concentration gradients, and in so doing, obviate limitations arising from the restricted availability of monitoring sites and gas analysers. Concentrations recorded simultaneously at two separate places on the one analyser were converted to relative decreases in concentration. The latter were consistent in form with those calculated by the programme.

8.6 Model Test: Routine Monitoring

Routine monitoring results for the heart of the intersection were compared statistically with levels calculated by the programme from weather readings and traffic counts taken at the same time. With 236 hourly observations, the correlation coefficients between calculated and measured levels were, for NO_x and NO, 0.76; for CO, 0.67; for HC, 0.72; NO_2 was rejected. The model gave values lower than those observed.

New emissions estimates were calculated to see what was implied by the low nature of the calculated levels. For NO, the new emissions estimate was reasonable; for CO, rather high; for HC, extremely high. One should not use these without further thought for there are many deficiencies in the model - both in its representation of the intersection as a source (Chapter 6), and the possibility of sources not considered. For example, although the HC levels given by the model correlated well with the measured ones, they differed by two orders of magnitude. Nevertheless, with NO, and less so with CO, the behaviour of the model was encouraging. It appears that in the intersection, traffic was a significant source of nitric oxide and carbon monoxide.

The model was not used at the site outside the intersection because of an interfering chimney, but data were recorded for winds from the city. For all gases except HC, the concentrations in the city background at that site were noticeably lower than at the intersection.

A high background level of HC seen at both sites has not been explained.

8.7 Sensitivity Analysis

A simulation by the programme of the plume from the intersection revealed several points.

Pollutant concentration decreases rapidly with downwind distance at first (Figure 6.13), although this drop levels out at greater distances. With very unstable conditions (Class A, MST2 =1), the initial drop is very steep in comparison to that for neutral (Class D, MST2 =7) and stable (Class E, MST2 =8) conditions.

If the effect of wind speed on the choice of stability index is ignored, the concentration is proportional to the reciprocal of wind speed.

The concentration field from the intersection as modelled by the programme reflected the source density of the intersection (Figures 6.16 to 6.20), since a plume from the roundabout at Salford Circus was recognisable. Although exaggerated by the source representation employed, this does stress the need for as full a source representation as possible. It also implies that the downwind pollutant pattern depends on the layout of the intersection, consistent with "common sense".

Study of a line source showed that at small downwind distances, the concentration was very dependent on road height. Thus the elevated nature of the structure would tend to reduce ground-level concentrations in the immediate vicinity of the intersection; this would be less pronounced further away.

8.8 Summary

The use of continuously operating gas analysers in the field made it possible to obtain a set of hourly measurements of NO_x, NO, NO_2, CO and HC at a complex motorway intersection. Simultaneously, traffic counts and weather readings were obtained.

A programme was developed to use published models of turbulent diffusion to calculate pollution concentrations from the traffic and weather data for any layout of roads. The calculated concentrations had a high correlation with the measured concentrations, suggesting that the programme was adequately describing the fluctuations of pollutant concentrations even though it tended to give values that were low.

A further cross-check of the programme was provided by the measurements of concentration gradients. For this a sampling technique was designed to take simultaneous samples from two separate places for analysis on the one available analyser. These results, and those of the programme, were mutually consistent.

The previous sections in this Chapter describe main features of the work in order to outline further directions of study.

8.9 Perspective

It is not easy to draw a satisfying conclusion from this type of work, because of the many ways of looking at it. The project relates directly to the frequently asked question "Well, how bad is the pollution at the intersection?" This implies both questions of what pollutant concentrations occur, and how do they fluctuate, and questions of given these concentrations over a period of time, what was the exposure of people to them, and how might such an exposure affect their health in years to come. There is therefore a matter of defining the question to be answered.

This work aimed specifically at seeing if a contribution from traffic to the pollution could be recognised, which implied distinguishing the various contributions of surrounding sources. To facilitate the latter, we restricted work to a site near where the traffic-effect, if any, might be readily seen, and further away for comparison. This gave us a basic check on the calculations.

With many factors involved (Figure 1.3) and each either measured inaccurately (Figure 6.31) or not at all, we cannot expect too good a fit between calculations and experiment, particularly at greater distances where dilution has occurred. Thus the "ideal test-case" does not give an exact check on calculation, so extrapolation to practical problems of deciding transport policy (e.g. road versus rail, or both) will not give accurate figures for immediate debate.

Nevertheless public concern over pollution does demand some idea of the concentrations occurring, and what affects them, in the hope that then sensible decisions may be taken. In this study we have simply looked for an understanding of the dilution of gases emitted by road vehicles at the intersection, and do not attempt to define or answer these other important but difficult questions.

APPENDIX 1

CHART-DATA

PROCESSING PROGRAMME

This programme written in ICL Algol uses character handling procedures for the flexible data entry. The following numbered paragraphs outline the main features of the programme (Flow chart: Figure 3.8; example output: Figure 3.9).

1. Coding of Data

Numbers can be comma or space (2) separated. A slash, /, ends the data. Each card represents one hourly observation: the card end is recognised as a character marking the end of data for that particular hour. Each card is uniquely defined by the first eight columns as in Table A1.1. G ranges from 1 to 6 to represent the pollutant identity; Z, from 0 to 2 to represent a zero, observation or calibration card. For example input: see Figure A1.1.

2. Procedure Definitions

PMØNTH (YR, MTH, DINMTH) uses the year YR and month MTH to calculate the number of days in the month; the answer is returned as DINMTH. Due note is taken of leap years.

TIMELAPSE (DATA, G, Z, B1, B2, PMØNTH, DINMTH, PERIØD) is used to obtain the difference in hours between the times of two data-cards B1 and B2 for the observation of type G, Z. This procedure uses PMØNTH so that the cards B1 and B2 could be in different months (as might happen in data taken at the end of a month and beginning of the next). When the number of days between the two cards has been found as T1DAY,

```
2,2,4,15,04,11,74,100,100,80.5,
1,2,4,15,04,11,74,100,100,90.0,
5,2,4,15,04,11,74,50,50,35,
6,2,4,15,04,11,74,10,8,79.5,
```

CALIBRATIONS

```
1,0,4,12,04,11,74,1,1.0,
2,0,4,12,04,11,74,1,1.0,
1,0,4,14,04,11,74,1,0.2,
2,0,4,14,04,11,74,1,1.2,
```

ZEROES

```
1,1,4,13,04,11,74,1,07,06,05,10,12,10,11,14,14,09,20,10,11,12,10,
2,1,4,13,04,11,74,1,20,20,05,06,07,04,11,20,09,12,03,10,10,10,08,
1,1,4,14,04,11,74,1,17,05,23,07,11,11,09,11,11,11,
2,1,4,14,04,11,74,1,22,07,05,25,06,08,06,22,          07,12,11,
1,1,4,15,04,11,74,1,07,14,10,13,09,          13,25,13,13,07,
2,1,4,15,04,11,74,1,03,          08,08,13,10,14,14,10,10,13,
1,1,4,16,04,11,74,1,10,27,09,10,11,37,18,19,15,10,09,10,10,10,11,
2,1,4,16,04,11,74,1,10,23,08,06,15,10,15,13,06,14,10,13,10,09,10,
1,1,4,17,04,11,74,1,12,13,17,13,25,15,26,14,18,22,13,09,11,13,15,
2,1,4,17,04,11,74,1,14,10,20,16,14,17,10,08,12,20,09,12,06,12,15,
1,1,4,18,04,11,74,1,10,13,19,17,12,16,11,16,12,15,15,20,17,11,13,
2,1,4,18,04,11,74,1,10,11,11,10,12,14,17,17,11,11,13,10,12,10,13,
1,1,4,19,04,11,74,1,14,15,16,14,09,
2,1,4,19,04,11,74,1,10,16,20,10,14,
1,1,4,20,04,11,74,1,10,09,15,14,09,14,10,13,29,11,09,10,09,18,08,
2,1,4,20,04,11,74,1,06,10,07,05,09,09,09,10,13,17,07,10,10,07,06,
1,1,4,21,04,11,74,1,10,11,10,20,12,10,08,11,08,09,09,12,09,19,07,
2,1,4,21,04,11,74,1,06,16,09,09,10,04,05,06,07,04,07,06,06,07,06,
1,1,4,22,04,11,74,1,08,10,10,10,09,10,10,08,09,09,07,13,12,12,12,
2,1,4,22,04,11,74,1,10,09,10,10,10,07,06,08,10,10,08,05,10,08,05,
1,1,4,23,04,11,74,1,07,07,10,10,08,07,09,09,08,05,06,10,07,06,07,
2,1,4,23,04,11,74,1,07,10,08,06,06,11,09,06,10,05,05,07,05,11,15,
1,1,4,24,04,11,74,1,13,09,08,06,09,08,07,11,11,10,06,09,07,06,05,
2,1,4,24,04,11,74,1,08,10,13,11,08,06,05,05,05,09,04,10,05,05,05,
```

OBSERVATIONS FOR OXIDESOF NITROGEN

```
1,0,4,19,04,11,74,1,0.8,
2,0,4,19,04,11,74,1,0.8,
```

```
4,1,4,01,04,11,74,0389,
4,1,4,02,04,11,74,0161,
4,1,4,03,04,11,74,0066,
4,1,4,04,04,11,74,0054,
4,1,4,05,04,11,74,0050,
4,1,4,06,04,11,74,0347,
4,1,4,07,04,11,74,0941,
4,1,4,08,04,11,74,2698,
4,1,4,09,04,11,74,2698,
4,1,4,10,04,11,74,2447,
4,1,4,11,04,11,74,2118,
4,1,4,12,04,11,74,2171,
4,1,4,13,04,11,74,2321,
4,1,4,14,04,11,74,2355,
4,1,4,15,04,11,74,2471,
4,1,4,16,04,11,74,2261,
4,1,4,17,04,11,74,3370,
4,1,4,18,04,11,74,3411,
4,1,4,19,04,11,74,2073,
4,1,4,20,04,11,74,1413,
4,1,4,21,04,11,74,1163,
4,1,4,22,04,11,74,1044,
4,1,4,23,04,11,74,0866,
4,1,4,24,04,11,74,0634,
```

SALFORD CIRCUS TRAFFIC COUNTS

```
5,1,4,12,04,11,74,50,17,16,17,17,12,14,15,15,
5,1,4,13,04,11,74,50,15,15,16,16,16,16,18,17,17,17,17,17,
5,1,4,14,04,11,74,50,17,17,18,17,17,17,17,18,18,16,20,17,
5,1,4,15,04,11,74,50,16,17,
5,1,4,16,04,11,74,50,06,07,09,08,06,11,07,07,06,07,06,08,
5,1,4,17,04,11,74,50,08,06,07,09,08,08,10,09,08,08,08,11,
5,1,4,18,04,11,74,50,06,09,07,08,09,07,06,06,12,09,06,07,
5,1,4,19,04,11,74,50,06,06,07,08,08,06,06,07,07,07,06,07,
5,1,4,20,04,11,74,50,07,07,09,08,07,07,08,06,07,07,07,08,
5,1,4,21,04,11,74,50,07,06,06,07,08,06,05,06,06,09,08,06,
5,1,4,22,04,11,74,50,07,08,07,08,08,07,08,08,06,08,07,06,
5,1,4,23,04,11,74,50,07,06,06,06,06,06,06,05,06,08,05,05,
5,1,4,24,04,11,74,50,10,08,07,08,06,07,06,06,05,05,05,05,
```

OBSERVATIONS FOR CARBON MONOXIDE

```
5,0,4,12,04,11,74,50,10.2,
5,0,4,15,04,11,74,50,11.0,
5,0,4,15,04,11,74,50,1.0,
```

```
6,0,4,12,04,11,74,100,03.0,
```

```
6,1,4,13,04,11,74,100,08.7,
6,1,4,14,04,11,74,100,06.7,
6,1,4,16,04,11,74,100,09.5,
6,1,4,17,04,11,74,100,09.8,
6,1,4,18,04,11,74,100,09.5,
6,1,4,19,04,11,74,100,09.3,
6,1,4,20,04,11,74,100,09.5,
6,1,4,21,04,11,74,100,09.3,
6,1,4,22,04,11,74,100,09.5,
6,1,4,23,04,11,74,100,09.5,
6,1,4,24,04,11,74,100,09.5,
```

OBSERVATIONS FOR HYDROCARBONS

```
6,0,4,15,04,11,74,100,02.8,
```

FIGURE A1.1 ROUTINE MONITORING RESULTS CODED FOR CALIBRATION AND ZERO CORRECTION, AS INPUT TO CHART50.

it is multiplied by 24 and the hours added. The result is PERIØD.

TIMECROS (DATA, G1, G2, Z1, Z2, B1, B2, PMØNTH, DINMTH, TIMDIF) is similar to TIMELAPSE. They differ only in that TIMECROS is a more general procedure: it compares the time of a card B2 of type G2, Z2 with that of B1 of G1, Z1. TIMECRØS is used to get all times relative to a common origin, the first NO_x card, by setting G1 =1, Z1 = 1 when the procedure is called.

3. Data Entry

G, Z are read from the card and a counter, CRDNUM [G,Z] , incremented (maximum value: 50) as cards of type G, Z are read. This provides serial counting of each card within its type and forms the subscript for storage by card number. The six numbers defining site, time and instrument fsd (nominal) are read into the elements of DATA[G, Z, CRDNUM [G,Z]] for J = 1 to 6. If the card were a traffic card, G = 4, no more need be read. If it is for a calibration, Z = 2, and control passes to CALREAD. If it is an observation, Z = 1, or zero, Z = 0, card, it is handled as follows: the characters on the card are checked for spaces (skipped), end-of-card (see below) or end-of-data (begin calculations). Failing these the next number is read. A second counter, MØNITR [G, Z, CRDNUM [G,Z]] is stepped to record how many observations are read off the card. Thus any number of observations can be put on a card as room allows, provided the last two characters are spaces to ensure correct character handling following use of the Algol procedure READ. Any order of card types is allowed, but all cards of the same type must be in chronological order. At the end of the card the points read in from the chart are averaged and multiplied by the nominal instrument fsd over 100. The result, DATA [G, Z,[CRDNUM [G,Z]],6] , is the hourly average (obtained from the chart average as a percentage of the nominal fsd) in ppm. This is calibrated later.

If the card were for a calibration (Z = 2), then the concentration GASCNC of the standard gas in ppm and the chart reading DIVS the instrument at nominal fsd DATA [G, Z, P, 6] showed are read. Then for the Pth calibration card, the nominal fsd was DATA [G, Z, P, 6], and ONEDIV [G, P] := (GASCNC*100)/(DATA [G, Z, P, 6] *DIVS), i.e. the factor by which the instrument readings must be multiplied to read true, e.g. if the 100 ppm gas reads 95 divisions on the 100ppm nominal sensitivity, ONEDIV = $\frac{100.100}{100.\ 95}$.

4. Calibration

When all cards have been read the hourly averages for zeroes and observations are calibration-corrected. For the Pth card (observation or zero), the average is multiplied by ONEDIV [G, CP]; DATA [G, Z, P, 6] := DATA [G, Z, P, 6] *ONEDIV [G, CP] where CP is the card number for the calibration card either coincident with or immediately before the hourly-average being calibrated. The appropriate calibration card is identified as card-number CP by comparison of the time of the Pth observation ØBSTIM [G, Z, P] with the times CALTIM [G, CP] of all calibrations CP = 1 to CRDNUM [G,2] for the gas G. For that card CP the correction factor ONEDIV G,[CP] is used in the above equation.

Where no calibration cards for gas G are read a correct instrument calibration is assumed.

5. Zero Correction

The calibrated zeroes are now subtracted from the calibrated observations. The times OBSTIM [G, O, Z] of the zero cards (numbered here as Z) are compared with the times ØBSTIM[G, 1, P] of the Pth observation. If a zero is coincident with the observation it is subtracted. If the zero occurs before the observation the next zero is tested until either a coincident zero is found for subtraction, or the zero immediately preceding and that immediately following the observation have been identified (using two card-numbers Z1, Z2 for the preceding and following zeroes). In the latter case the equation of the line joining these two zeroes is used to interpolate the (drifted) zero at the time of the observation. The interpolated value is subtracted. If no zero cards for gas G are present a true zero is assumed.

6. Traffic Storage

Streeter-Amet counts are included for ease of processing as a whole: their presence enables the output table to include all measurements made in the project except intersection counts (Chapter 4) and weather readings. The values need no calculation: they are merely read into DATA [4, 1, P, 6] and later stored in ANSWR [4, P] for traffic card P.

7. Procedure Call for CHEKTIM G,P

CHEKTIM[G, P] is the time in hours of all observations G, P measured in hours from the first NO_x or G = 1 card. This is so that, unlike OBSTIM [G, P] we have in the matrix CHEKTIM values for the times from a common origin, and therefore can sort the cards for each gas G according to whether an observation of one gas is coincident in time with that of another.

8. Card Sequence Checks

The data entry may have cards within a type G, Z not in correct chronological order: this may be due to wrong card sequencing or a data error. All cards are checked so that one programme run finds all the sequence errors in the data; if an error is found the programme quits.

9. Coincidence Sorting

Given correctly sequenced data the cards are sorted into rows: there is one row per hourly observation. Each row contains the value for each gas G at the time of the row. The table is created by a coincidence search of the times CHEKTIM [G, P] of each card. For G2 = 2, 4, 5, 6 a variable LØGIC [G2, B1] is set equal to 1 only if the card B2 of gas G2 is coincident with card B1 of gas G2 = 1. When all cards G2, B2 have been tried against the card B1 of gas G1 = 1 the variables LØGIC [G2, B1] are multiplied together.

LØGAL [B1] = LØGIC [2,B1] *LØGIC [4,B1] *LØGIC [5,B1]
*LØGIC [6,B1]

The product, LØGAL [B1] is unity only if all gases have an observation taken at the time of G1, B1. When such a coincidence has been found, the card numbers of each G2 card that had the same time as G1, B1, are stored as the value of the element CØØRD [ØCC,G2], where ØCC is a counter incremented at each coincidence. Thus for G+1 to 6 the six elements CØØRD [ØCC,G] equal the card numbers for those cards that are mutually coincident.

Also, if LØGIC [2,B1] is unity then the coincident NO reading can be subtracted from the NO_x to estimate the NO_2.

10. Test Output

The results of the calibrations, zero abstractions and data sorting are output gas by gas for checking.

11. Results Output

The results are then output as a Table of hourly rows: each row contains the time and site, followed by the NO_x, NO, NO_2, traffic at Salford Circus, CO and HC levels for that time and site.

APPENDIX 2

DETAILS OF

THE TRAFFIC PROGRAMMES

The programmes perform tasks as outlined in Chapter 4 and Figure 4.1. The following paragraphs apply to the general flowchart (Figure A2.1). The roads are defined by Figure 4.1 and Tables A2.1, A2.2.

1. The numbered cards are read into DATA [I,J] . A counter M is increased whenever a value of -1 signifying a missing value is read. DATA [I,J] is split into TIME [I,J] which holds the six values defining the photograph's time, and CØUNT [I,J] which holds the counter-readings for all twenty eight counters in the Ith photograph.

2. The count of vehicles over the Jth counter during the period PERIØD [I] from TIME [I - 1, J] to TIME [I,J] is

   DIFF [I,J] = CØUNT [I,J] - CØUNT [I - 1, J]

   since the counts are cumulative. When a counter passes zero, DIFF [I,J] < 0 so 999999 is added.

3. If either CØUNT [I,J] or CØUNT [I - 1, J] is missing DIFF [I,J] is not obtainable directly. The subscripts I, J of the missing difference DIFF [I,J] are stored in MISSI [Q], MISSJ [Q], where Q is a counter incremented for each missing difference.

4. PERIØD [I] is calculated using the procedures PMØNTH, to obtain the number of days in the month, and TIMELAPSE to give the period in hours and decimal fraction of the hour.

5. LØGIC [I,J] is 1 if DIFF [I,J] exists, else zero.

6. Missing differences are interpolated as follows:-

Each row I is scanned, and for each the columns J are scanned. If LØGIC [I,J] = 1, then DIFF [I,J] exists and may be added to those other differences existing for the Ith row.

$$\text{RØWSUM}[I] = \sum \text{DIFF}[I,J]$$

summed over J for which DIFF [I,J] exists

Also

$$\text{SIGMAR}[I] = \sum \text{RJ}[J]$$

summed over J for which DIFF [I,J] exists

where RJ [J] is the fraction of a complete twenty eight counter count that each counter contributed to that complete count. RJ [J] represents the relative proportions of traffic-flow over the various counters. The twenty eight values RJ [J] , J = 1.. ....28, were calculated using the programme TRRLRATGEN, a modified form of the first programme, i.e. based on 1 - 4 above, as it was before the missing value interpolation was inserted. Table A2.3 shows the values for RJ [J] .

RØWSUM [I] is the total of the available differences and is a fraction SIGMAR [I] of a full twenty eight counter count T that would exist were all the differences present.

Then

RØWSUM [I] = SIGMAR [I] *T

We redefine the value of RØWSUM to save storage as T.

RØWSUM [I] = T = RØWSUM [I] /SIGMAR [I]

This full count may be subdivided according to RJ [J]to estimate the missing differences.

If LØGIC [I,J] = O, then we interpolate

DIFF [I,J] = RJ [J] *RØWSUM [I]

to substitute for the missing value.

7. The counters in general read high (because of lane discipline) thus FAC [ ] in the programme holds the factors for correction.

FACDIF [I,J] := FAC [J] *DIFF [I,J]

8. Several counters contribute to one road.

The combinations of counters are defined for any numbered road by the alphabetic-groups as on the map, Figure 4.1 and as in Tables A2.1, A2.2. Thus the number of vehicles passing along any one road between the photographs I - 1, I and during PERIØD [I] is the summation of FACDIF [I,J] for those J relevant to the road. Some terms may be subtracted, dependent on the counter combinations.

$$\text{E.g.}\quad \text{M6FLØW}\,[\,I\,] = \sum_{J = 1,\,2,\,3,\,6,\,7,\,8} \text{FACDIF}\,[\,I,J\,]$$

9. The programmes output the total flow elapsed as above during PERIØD [I] , and the flow per hour as total flow divided by PERIØD [I] . These flows are printed for M6, A38(M), M6-South & North, A38(M)-North and A38(M)-South.

10. In addition TRRLRØFLØ gives the flow PBF [RD,I] for every road RD of the junction. This requires a full labelling of the roads as on the map (Figure 4.1), and two procedures to set up the complex set of counter combinations. The function procedure BØX becomes the traffic-flow elapsed for the alphabetic-group as

defined by a parameter K of the procedure. A switch is used to select those counters appropriate to the group (Table A2.1). Thus

$$BØX = \sum FACDIF [I,J]$$

summed according to those counters contributing to the Kth alphabetic-group. BØX is calculated for the Kth group using the Ith row of the matrix FACDIF by a call

Function := BØX (K,I,FACDIF).

The procedure RØFLØW has a similar use of switch to select those alphabetic-groups contributing to the desired road RD. The combinations are defined in Table A2.2.

E.g. for the M6 we need group A plus group B, to sum

FACDIF [I,J] for J = 1, 2, 3, 6, 7, 8

The procedure call RØFLØW (1, BØX, I, FACDIF, PBF) will set up the element

PBF [1,I] := BØX (1,I,FACDIF) + BØX (2,I,FACDIF).

The two calls of BØX give us

PBF [1,I] := FACDIF [I,1] + FACDIF [I,2] + FACDIF [I,3]
+ FACDIF [I,6] + FACDIF [I,7] + FACDIF [I,8]

for the M6. The programme will print

PBF [1,I] /PERIØD [I], the flow along the road in vehicles per hour.

11. TRRLBØX will interpolate hourly flows if the periods between the photographs exceed one hour.

The procedures RØFLØW and BØX are called as above to obtain the flow along each road. PBF [RD,I] is the number of vehicles which passed during PERIØD [I] ; PERIØD [I] might have been twelve hours. To subdivide this into hourly flows, we need the hourly traffic-pattern; this reflects the rise and fall with peak periods. We suppose the hourly traffic-pattern is different for every road and for each type of day. In practice Mondays, Tuesdays, Wednesdays, Thursdays are similar (Errors: Appendix 3), and Fridays, Saturdays and Sundays are distinct. A sample set of hourly photographs were abstracted (12-09-74 to 16-09-74) and used in the programme TRRLRØFLØ. The results were stored in a "standard" matrix STD which holds the traffic-flows for all roads of the junction for four day-types, where a Monday is denoted 1 and so on to Sunday, 7. The programme TRRLBØX uses this standard to interpolate hourly flows. STD [RD,I,J] is read for every road RD, and all twenty four hours I of the day, for day-types J = 5, 6, 7, 1. Then STD [RD,I,J] for J = 2, 3, 4 is set equal to STD [RD,I,1] making Tuesday, Wednesday and Thursday equivalent in pattern to Monday. The reading of STD is complex: crosschecks are made to be sure the proper data are read.

STD now has the flow for every road for every hour of each day-type throughout the week. We assume the total flow of vehicles may change, but that from the elements of STD scaled according to the total flow we may estimate hourly flows. The value of each hour between the Ith and I-1th photographs is calculated. Fig. A2.2 shows overlapped hours numbered for illustration and the photograph times. The variables A1, A2, H1, H2 are also defined on the Figure.

Define A1, the fractional time after photograph I-1, and before the first full hour.

A1 = 1 -(TIME [I-1,6])/60   i.e. minutes/60

A2, the fractional time after that last full hour still within the overlap period

A2 =(TIME [I-1,6])/60   i.e. minutes/60

(H1 + 1), the first full hour overlapped

H1 = TIME[I-1,5] + 1   hours

H2, the last full hour overlapped

H2 = TIME[I,5]   hours

We use an hour-subscript, HSUB, to step over the overlapped hours. HSUB is initially set equal to H1. The day-type D is required when calling the elements of STD.

D = TIME [I-1,4]

HSUB will be incremented as HSUB = HSUB + 1; the number of full hours overlapped is INTERV, which is related to PERIØD[I] . It is possible that the fractional times A1, A2 together account for over an hour, and since INTERV will be used to control the number of interpolations required it must be integral. Rounding errors must be avoided. Hence INTERV = ENTIER (PERIØD [I]) - ENTIER (A1 + A2) where ENTIER, an ALGØL procedure, rounds to the nearest integer below the function.

We now have the number of full hours overlapped and the start and end points of overlap.

HSUB is incremented: if midnight is passed HSUB is set to unity and day-type D reset to unity at the end of a week.

As J increases from unity to INTERV we increment HSUB and D as each hour is passed, and store them as HR [J] , DY [J] . The relevant elements of STD are retrieved and summed:

$$TØTSTD = \sum_{J=1}^{INTERV} STD[RD,D,HSUB]$$

(at present D = DY [J] , HSUB = HR[J])

At the end of summation TØTSTD is the total count present in the standard matrix for those hours in the day-types which are overlapped. The fractional terms from either end of the overlap are added

TØTSTD = TØTSTD + A1*STD [RD, TIME [I-1,4] , H1]

+ A2*STD [RD, TIME [I, 4] , H2 + 1]

For each overlapped hour the flows are estimated assuming the same traffic-pattern existed during PERIØD [I] as that represented by those elements of STD that were overlapped.

$$FLØW = \frac{STD [RD,DY[J] , HR [J]] * PBF [RD,I]}{TØTSTD [RD]}$$

The interpolated FLØW is printed.

TABLE A2.1

Counter Numbers by Alphabetic Group

Alphabetic Group (Map: Figure 4.1)	Counters included[1] in the group (Values of J)	Calibration Factor (Measured: Section 4.2.4)
A	1, 2, 3	0.80
B	6, 7, 8	0.91
C	4, 5	0.97
D	9, 10	0.81
E	11, 16	0.96
F	21, 26	0.86
G	12	0.89
H	22, 27	0.76
I	13, 18	0.89
J	28	0.78
K	14, 15, 19, 20	0.90
L	24, 25	0.77

Note 1: Procedure BØX sums the matrix elements DIFF [I,J] for the Ith photograph over those counters or J values given by this Table.

TABLE A2.2

Alphabetic Counter-Groups contributing to Each Road

Road	Alphabetic group combination[1]
1	A + B
2	C + D + G + I + K + L - E - J
3	--- (Salford Circus)
4	I
5	C - E + F
6	H
7	C
8	F --- D - F
9	D
10	F
11	L
12	K
13	½(L)
14	½(L)
15	G
16	G - J
17	H - I
18	J
19	H - I + J
20	C - E + F --- E - F
21	½(K)
22	½(K)
23	G - J + I
24	E

TABLE A2.2 (continued)

Note 1: Procedure RØFLØW calls each combination of alphabetic groups: for each alphabetic group a call of the function BØX is made to select the counters as in Table A2.1.

TABLE A2.3

Values RJ[J] for interpolation of

Missing Values

J	RJ[J]	J	RJ[J]
1	0.006026	15	0.003828
2	0.003892	16	0.000001
3	0.006810	17	0.003150
4	0.005262	18	0.000608
5	0.003315	19	0.000104
6	0.004698	20	0.003531
7	0.008829	21	0.004241
8	0.003141	22	0.003716
9	0.001400	23	0.004094
10	0.003080	24	0.008776
11	0.000001	25	0.004102
12	0.001246	26	0.000692
13	0.003869	27	0.005944
14	0.005086	28	0.000560

FIGURE A2.1 OUTLINE FLOWCHART FOR THE COMPUTER PROGRAMMES TO CALCULATE TRAFFIC FLOWS FROM REGULAR PHOTOGRAPHS OF THE COUNTER READINGS.

PART 1: RELATIONSHIPS BETWEEN THE PROGRAMMES, AND PARTS THEY HAVE IN COMMON.

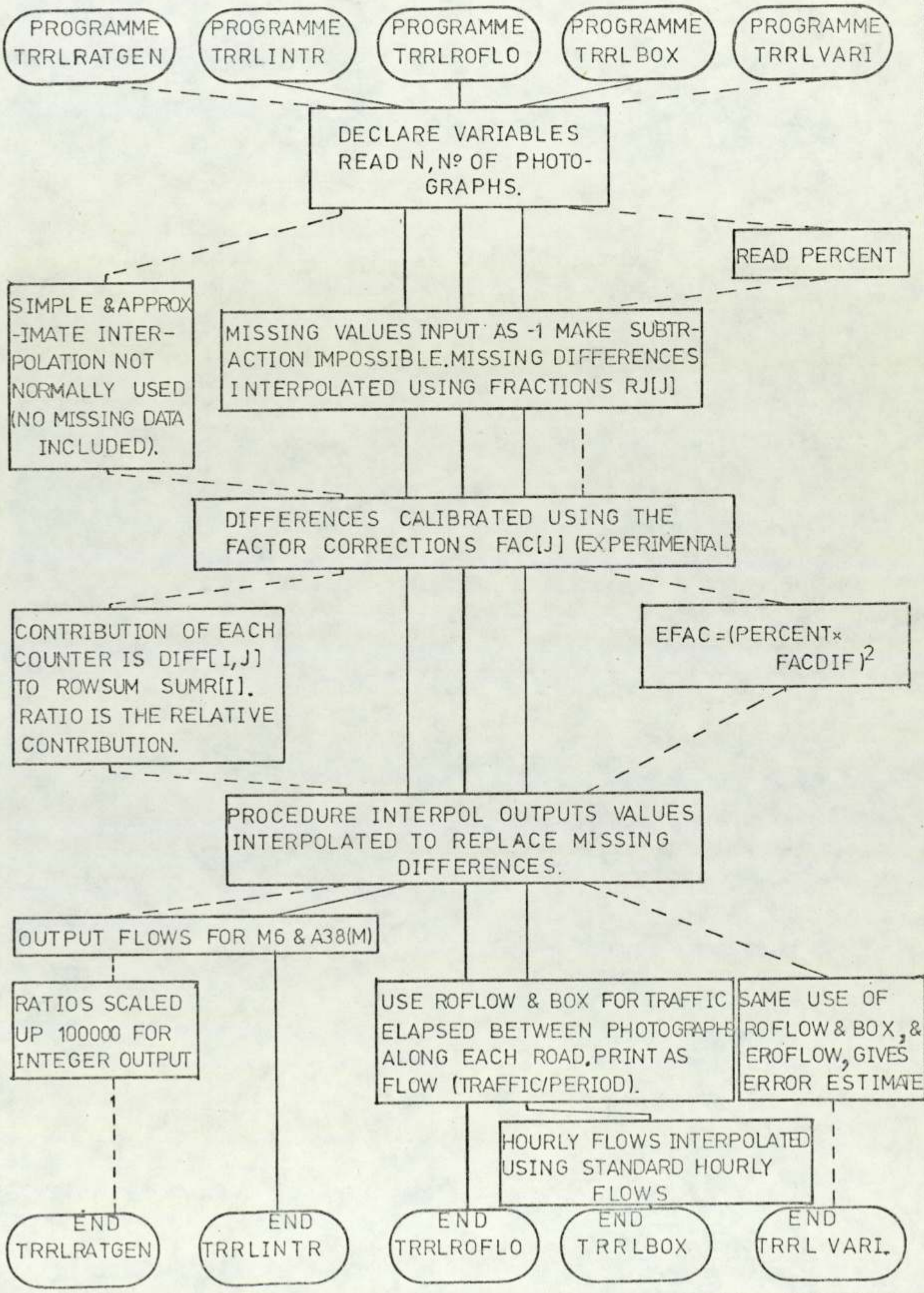

CONTINUED ON NEXT PAGES

FIGURE A2.1 (CONTINUED) 2

PART2: OUTLINE FLOWCHART

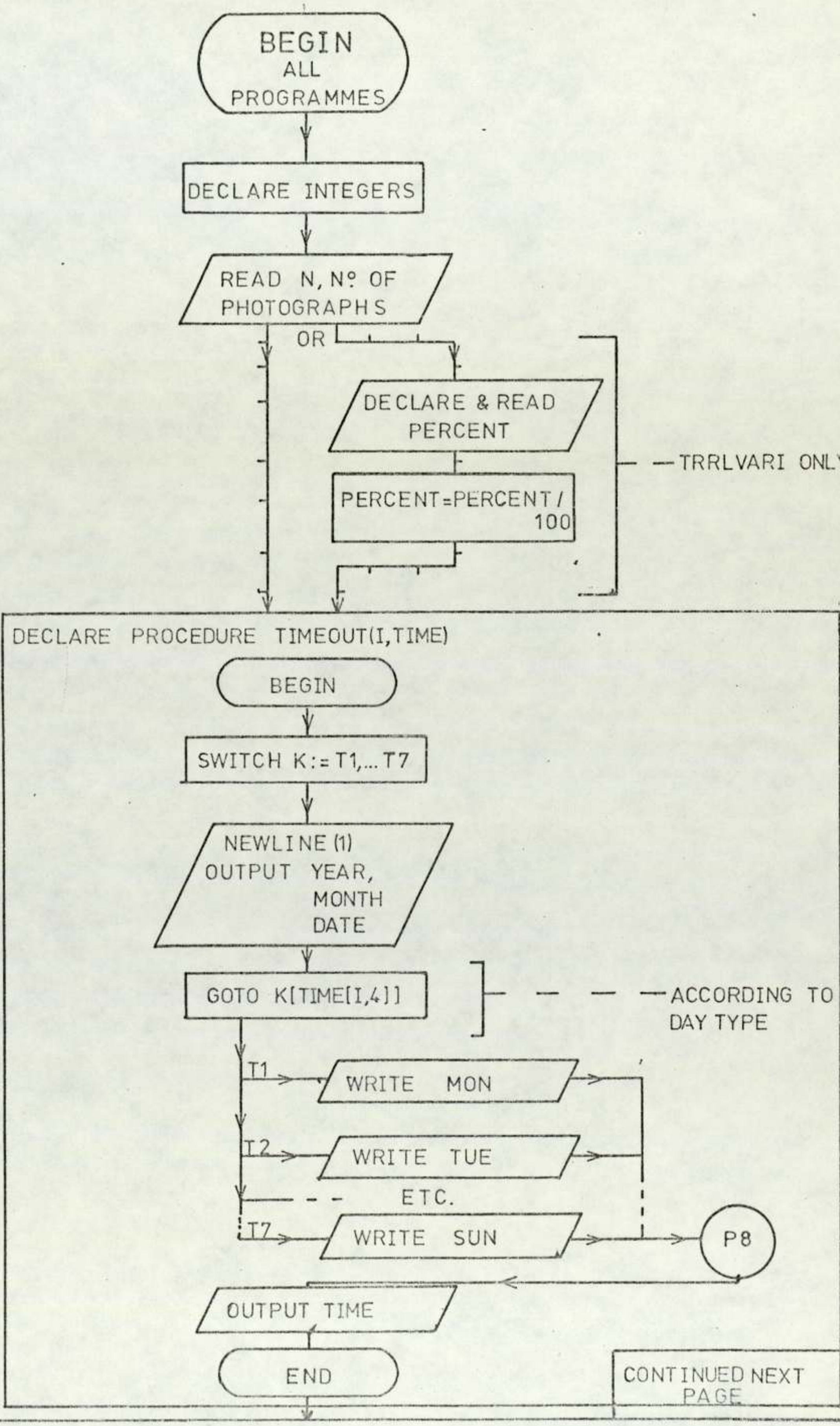

CONTINUED NEXT PAGE

FIGURE A2.1 (CONTINUED) 3

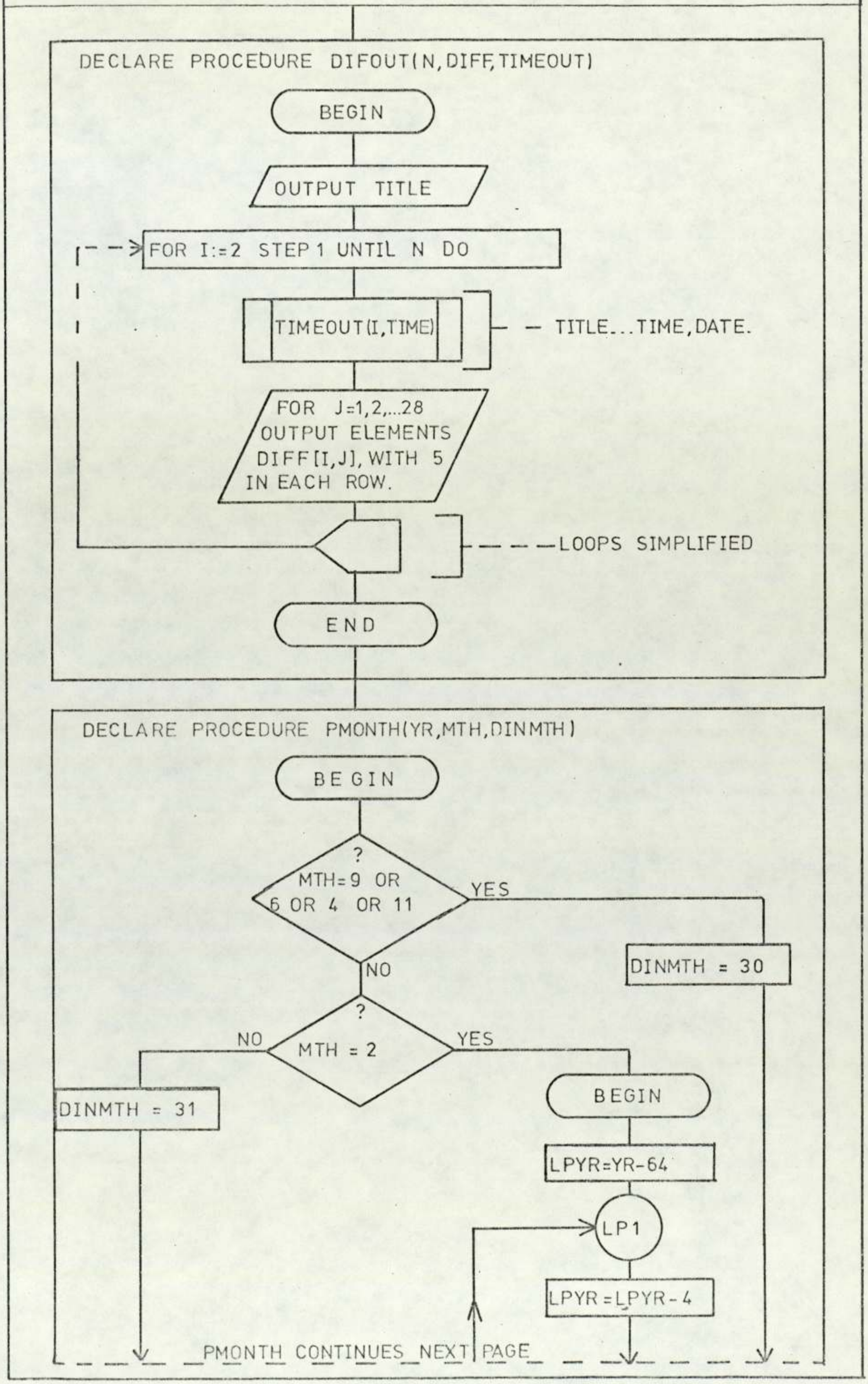

FIGURE A2.1 (CONTINUED) 4

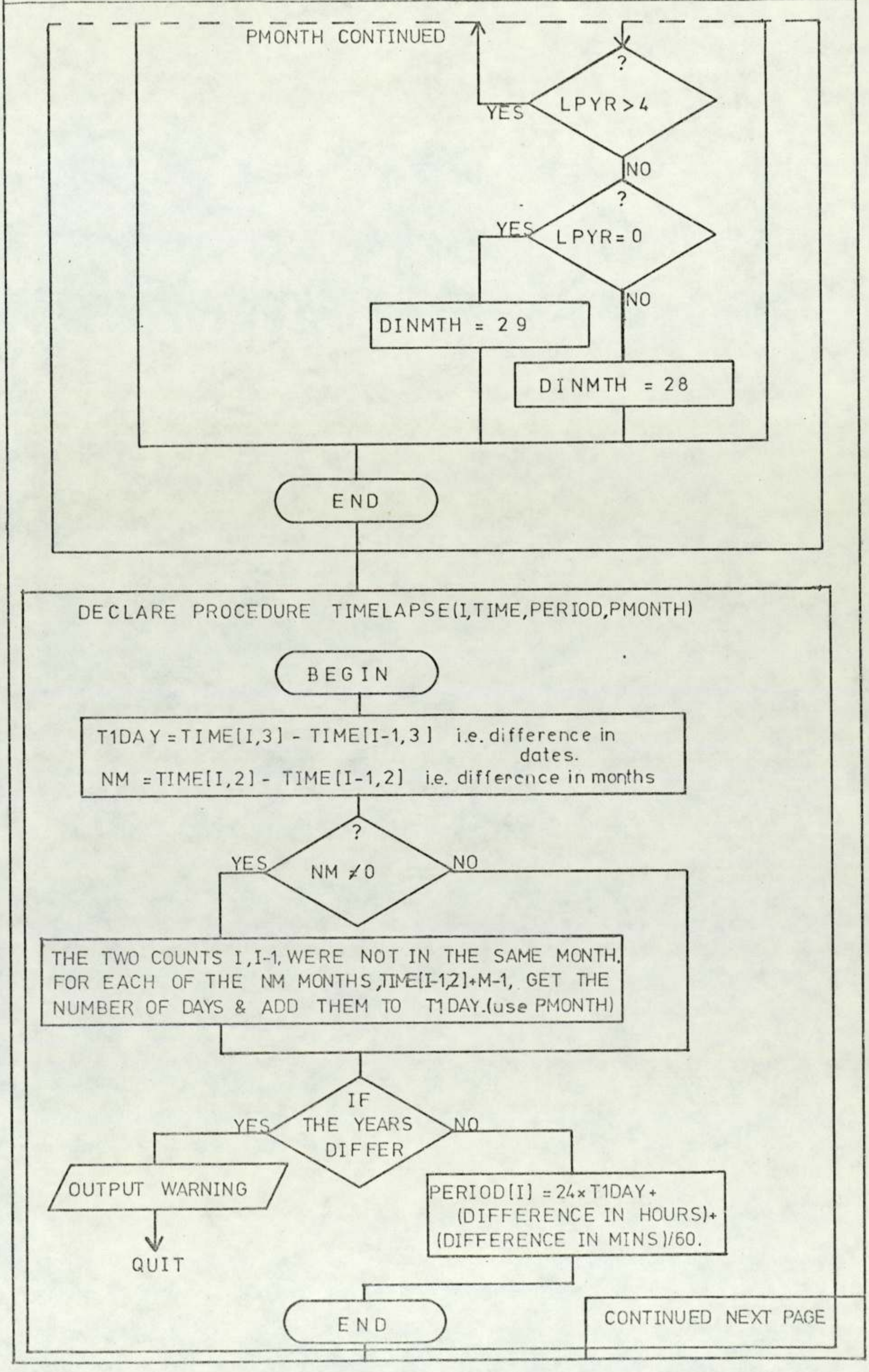

CONTINUED NEXT PAGE

FIGURE A2.1 (CONTINUED) 5

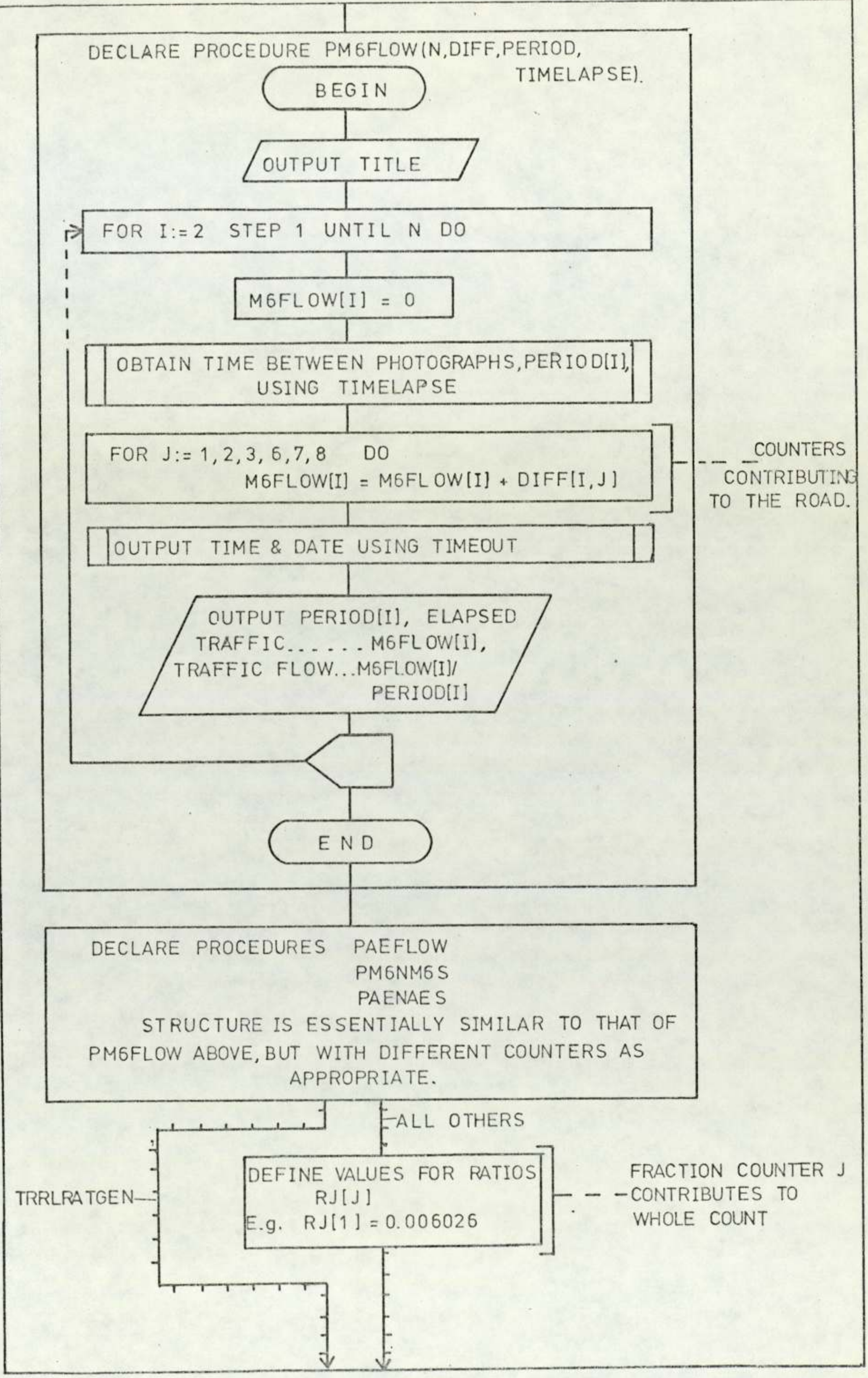

FIGURE A2.1 (CONTINUED) 6

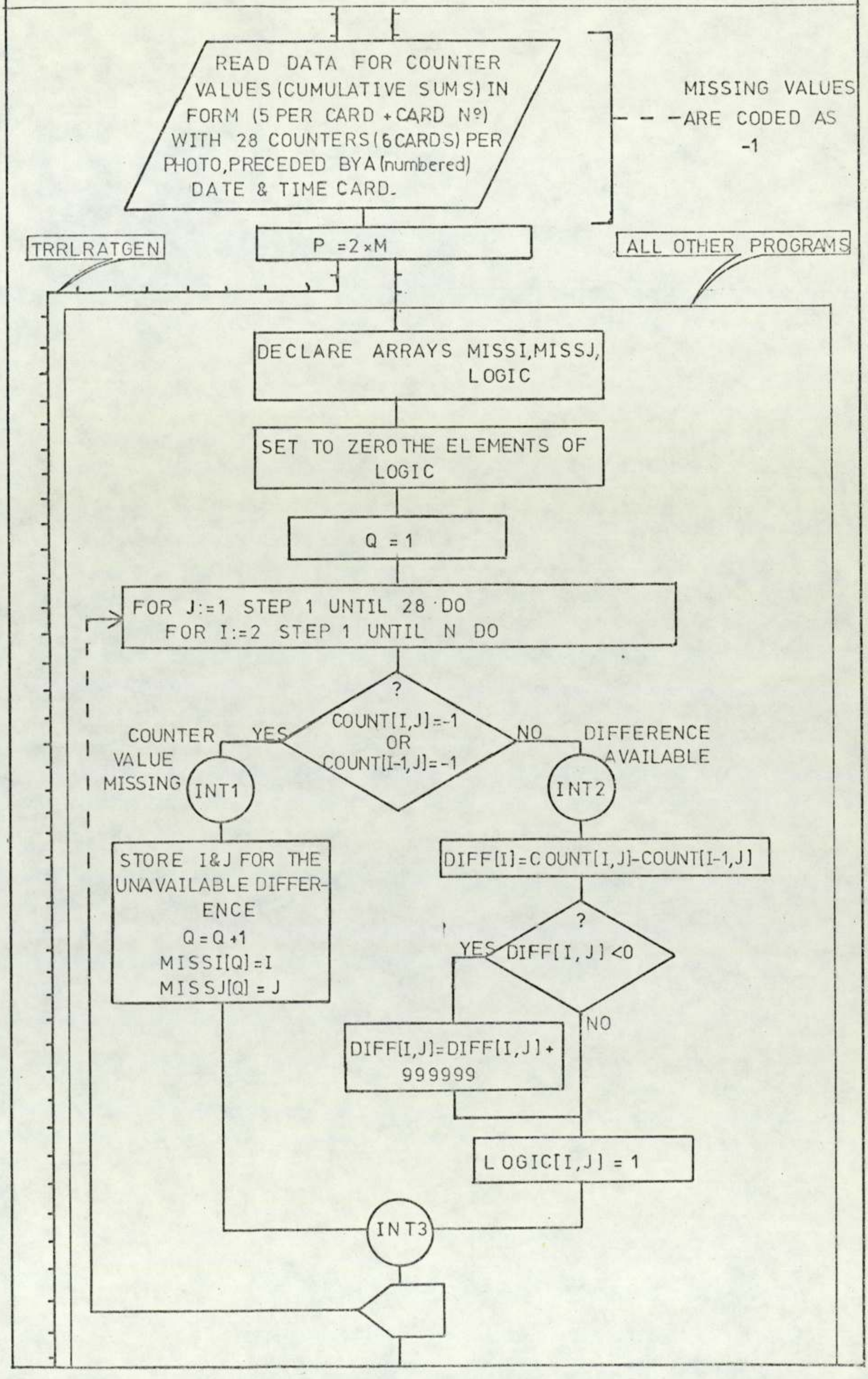

FIGURE A2.1 (CONTINUED) 7

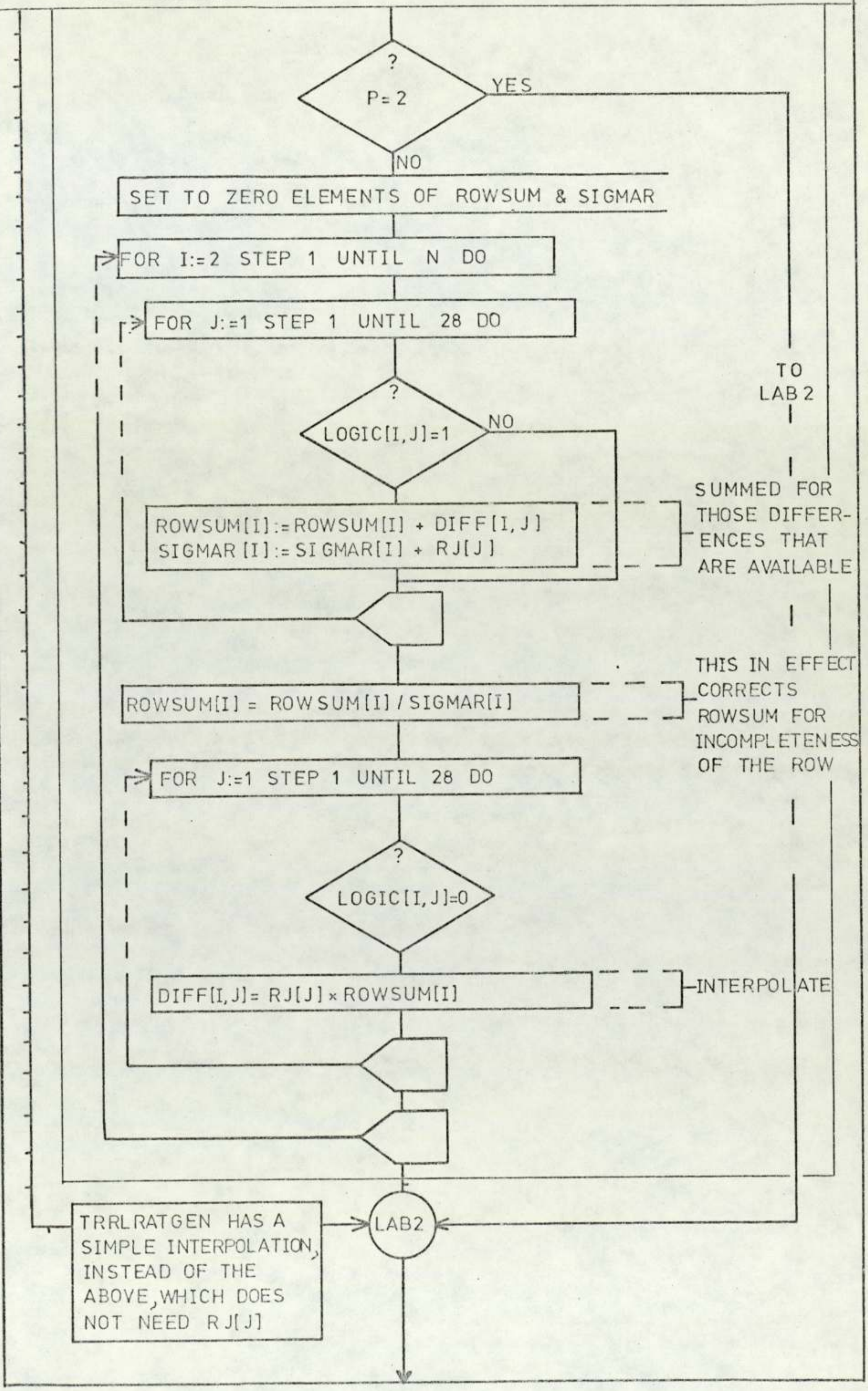

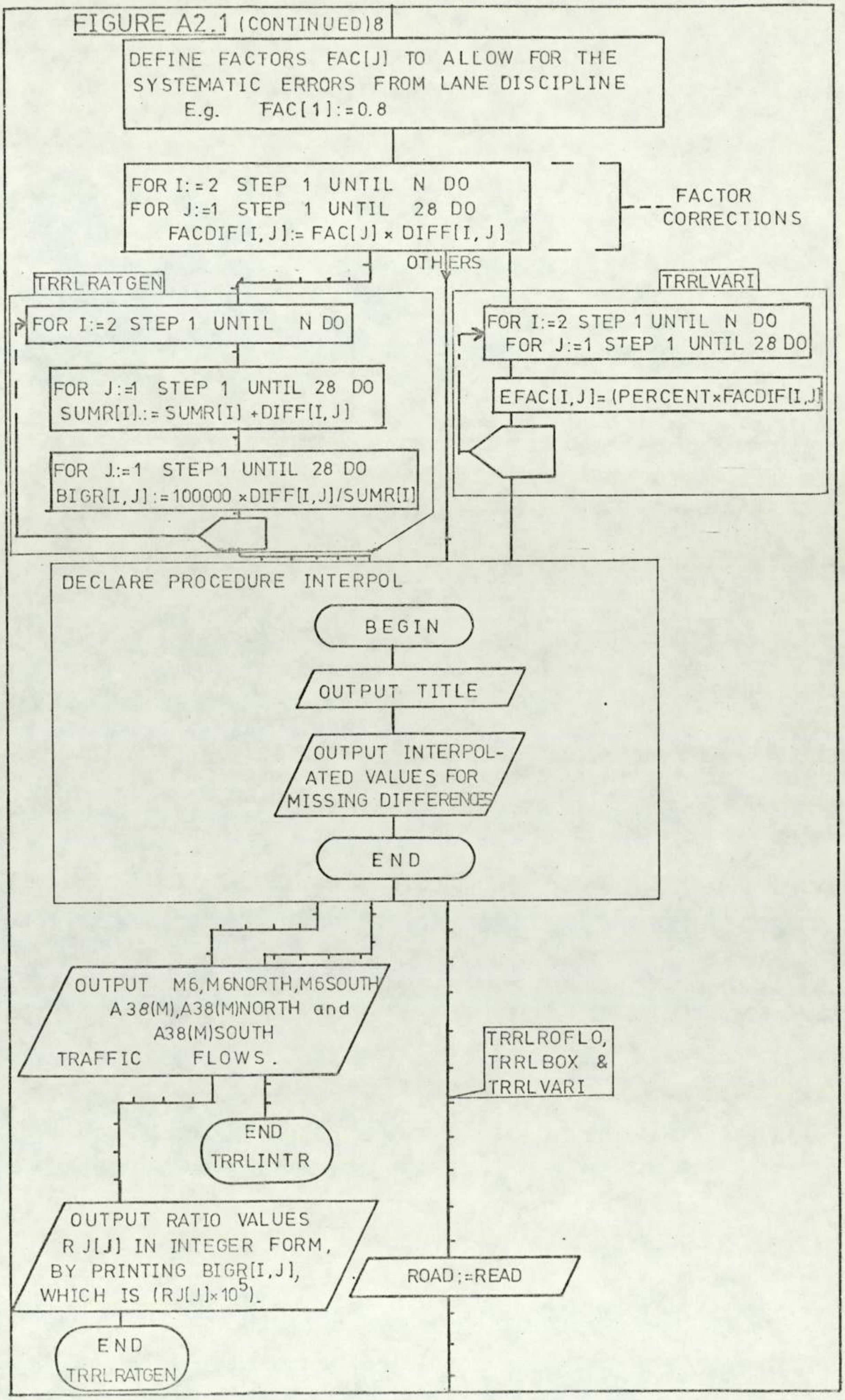
FIGURE A2.1 (CONTINUED) 8
DEFINE FACTORS FAC[J] TO ALLOW FOR THE SYSTEMATIC ERRORS FROM LANE DISCIPLINE
E.g. FAC[1]:=0.8
FOR I:=2 STEP 1 UNTIL N DO
FOR J:=1 STEP 1 UNTIL 28 DO
FACDIF[I,J]:= FAC[J] × DIFF[I,J]
FACTOR CORRECTIONS
OTHERS
TRRLRATGEN
FOR I:=2 STEP 1 UNTIL N DO
FOR J:=1 STEP 1 UNTIL 28 DO
SUMR[I]:= SUMR[I] +DIFF[I,J]
FOR J:=1 STEP 1 UNTIL 28 DO
BIGR[I,J]:=100000 ×DIFF[I,J]/SUMR[I]
TRRLVARI
FOR I:=2 STEP 1 UNTIL N DO
FOR J:=1 STEP 1 UNTIL 28 DO
EFAC[I,J]=(PERCENT×FACDIF[I,J]
DECLARE PROCEDURE INTERPOL
BEGIN
OUTPUT TITLE
OUTPUT INTERPOLATED VALUES FOR MISSING DIFFERENCES
END
OUTPUT M6, M6NORTH, M6SOUTH A38(M), A38(M)NORTH and A38(M)SOUTH TRAFFIC FLOWS.
TRRLROFLO, TRRLBOX & TRRLVARI
END TRRLINTR
OUTPUT RATIO VALUES RJ[J] IN INTEGER FORM, BY PRINTING BIGR[I,J], WHICH IS (RJ[J]×10^5).
ROAD:=READ
END TRRLRATGEN

FIGURE A2.1 (CONTINUED) 9

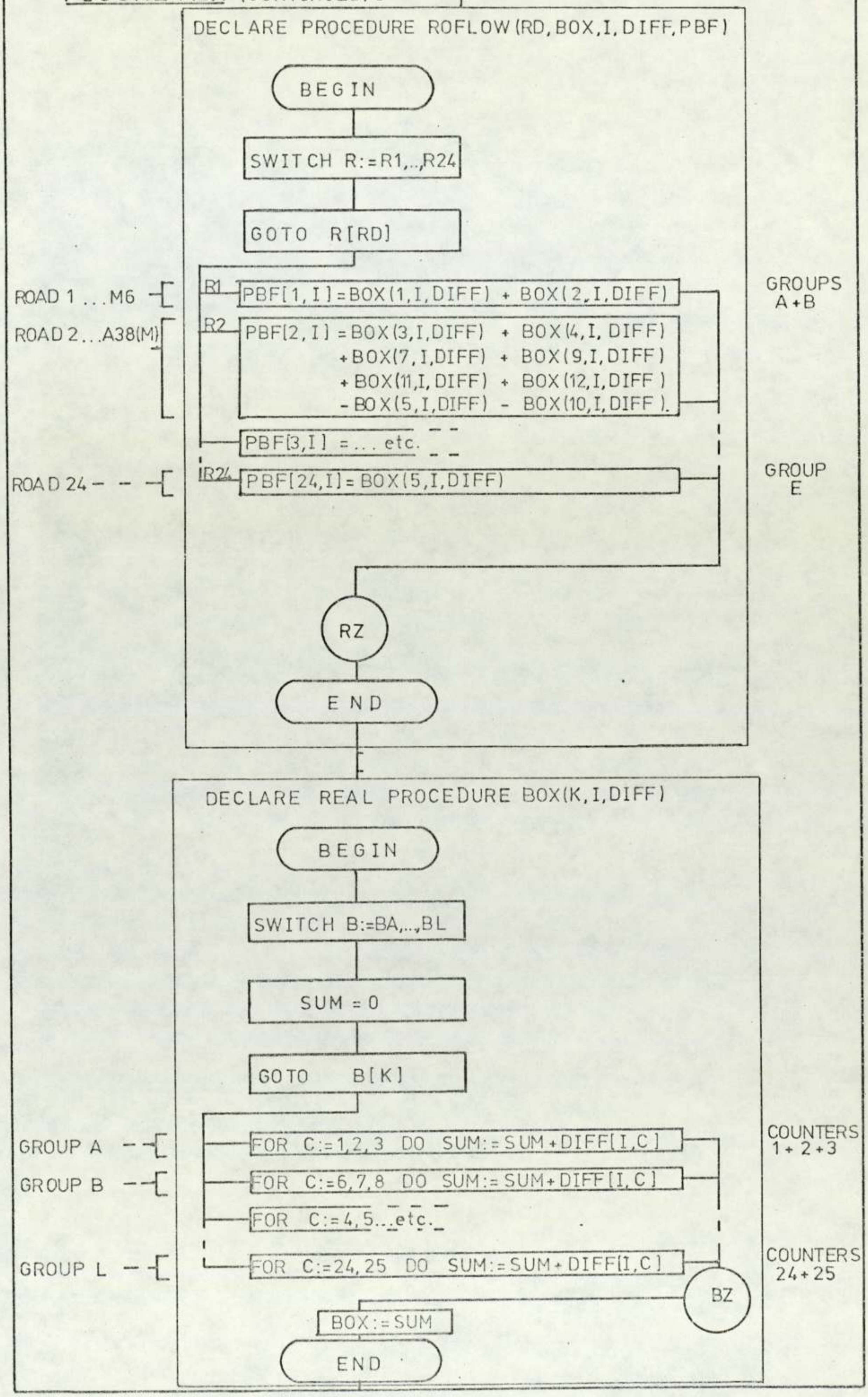

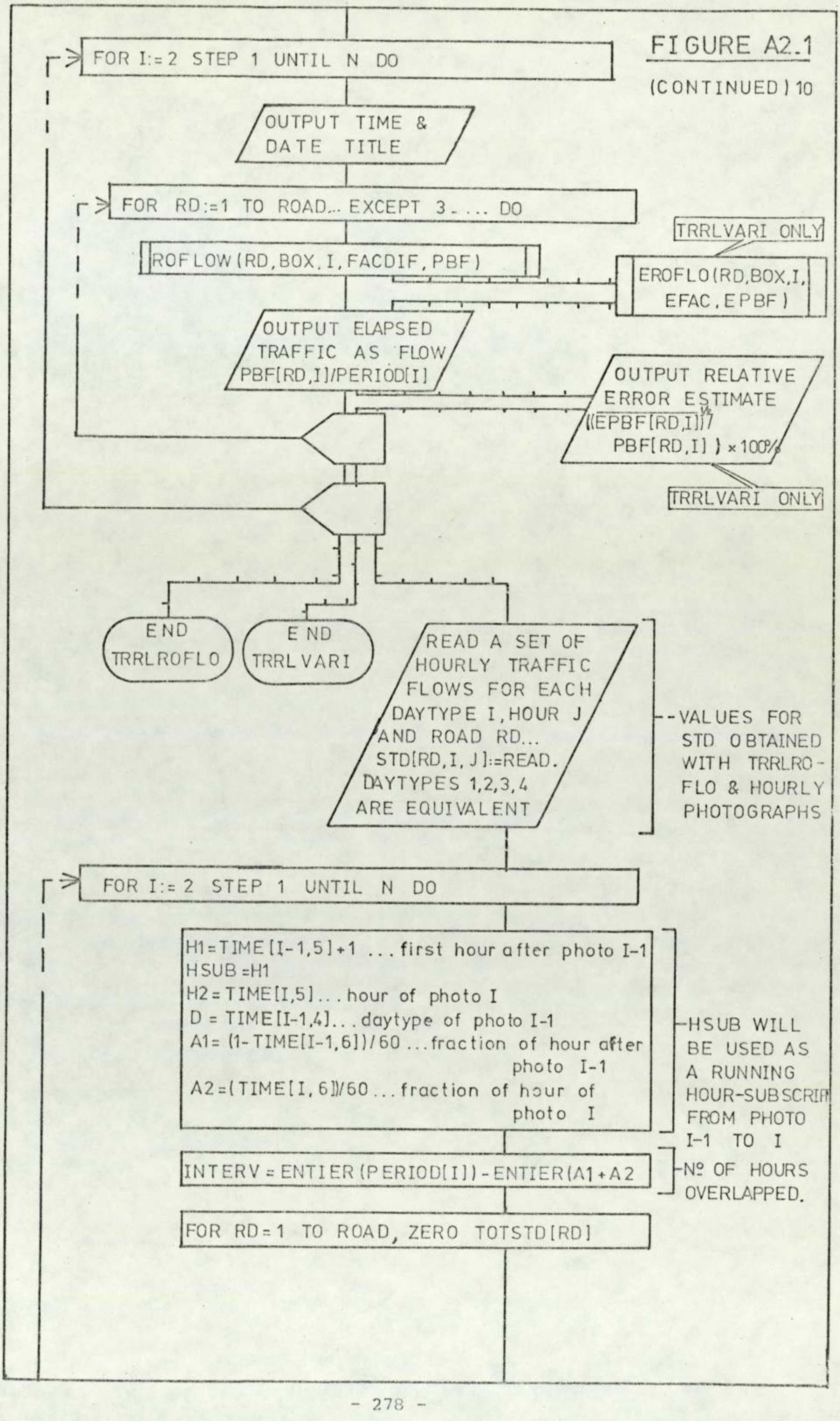

FIGURE A2.1

(CONTINUED) 10

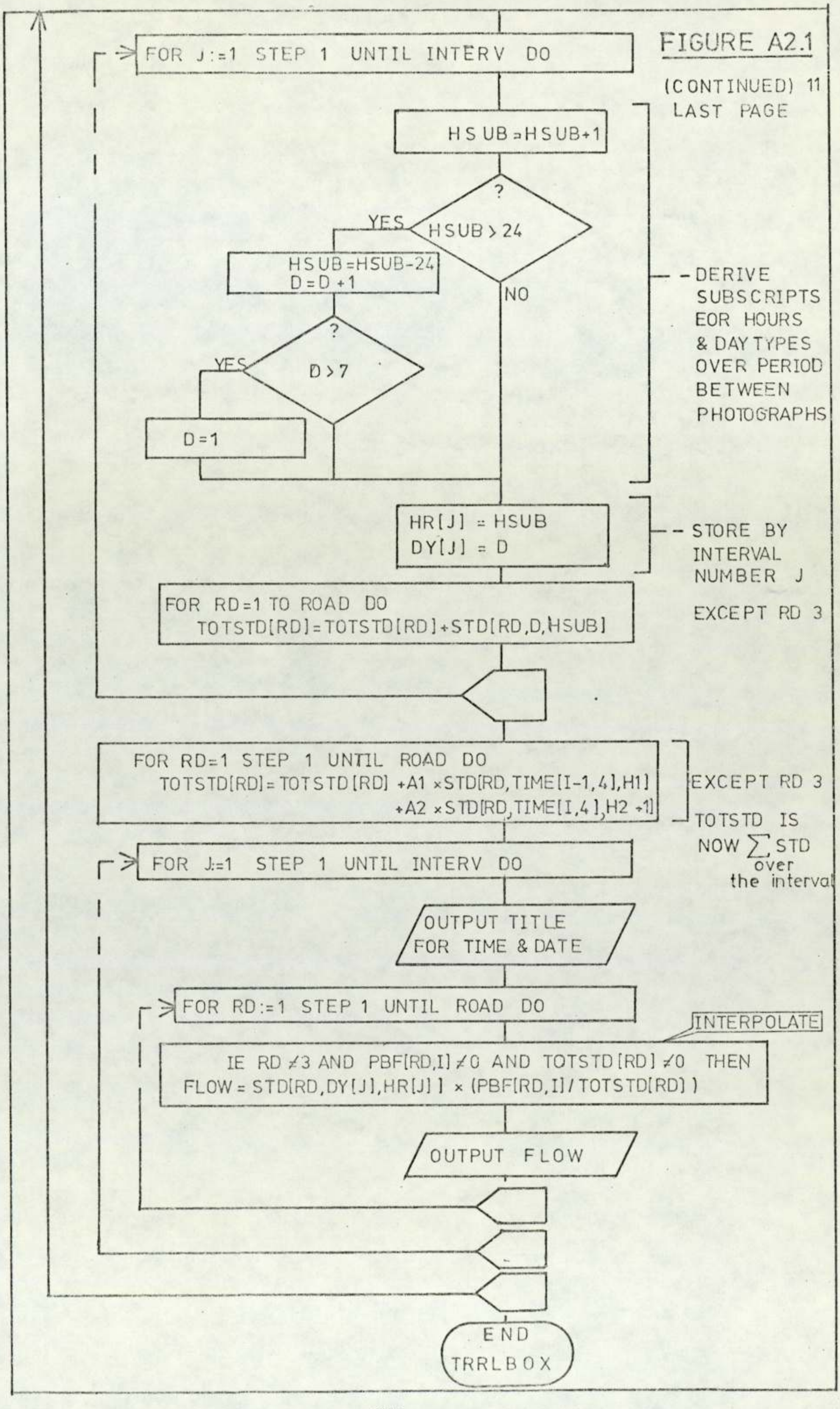
FIGURE A2.1
(CONTINUED) 11
LAST PAGE
FOR J:=1 STEP 1 UNTIL INTERV DO
HSUB=HSUB+1
?
HSUB > 24
YES
NO
HSUB=HSUB-24
D=D+1
?
D > 7
YES
D=1
- DERIVE SUBSCRIPTS EOR HOURS & DAY TYPES OVER PERIOD BETWEEN PHOTOGRAPHS
HR[J] = HSUB
DY[J] = D
- STORE BY INTERVAL NUMBER J
FOR RD=1 TO ROAD DO
TOTSTD[RD]=TOTSTD[RD]+STD[RD,D,HSUB]
EXCEPT RD 3
FOR RD=1 STEP 1 UNTIL ROAD DO
TOTSTD[RD]=TOTSTD[RD] +A1 ×STD[RD,TIME[I-1,4],H1]
+A2 ×STD[RD,TIME[I,4],H2 +1]
EXCEPT RD 3
TOTSTD IS NOW ∑ STD over the interval
FOR J:=1 STEP 1 UNTIL INTERV DO
OUTPUT TITLE FOR TIME & DATE
FOR RD:=1 STEP 1 UNTIL ROAD DO
INTERPOLATE
IE RD ≠3 AND PBF[RD,I] ≠0 AND TOTSTD[RD] ≠0 THEN
FLOW = STD[RD,DY[J],HR[J]] × (PBF[RD,I]/TOTSTD[RD])
OUTPUT FLOW
END
TRRLBOX

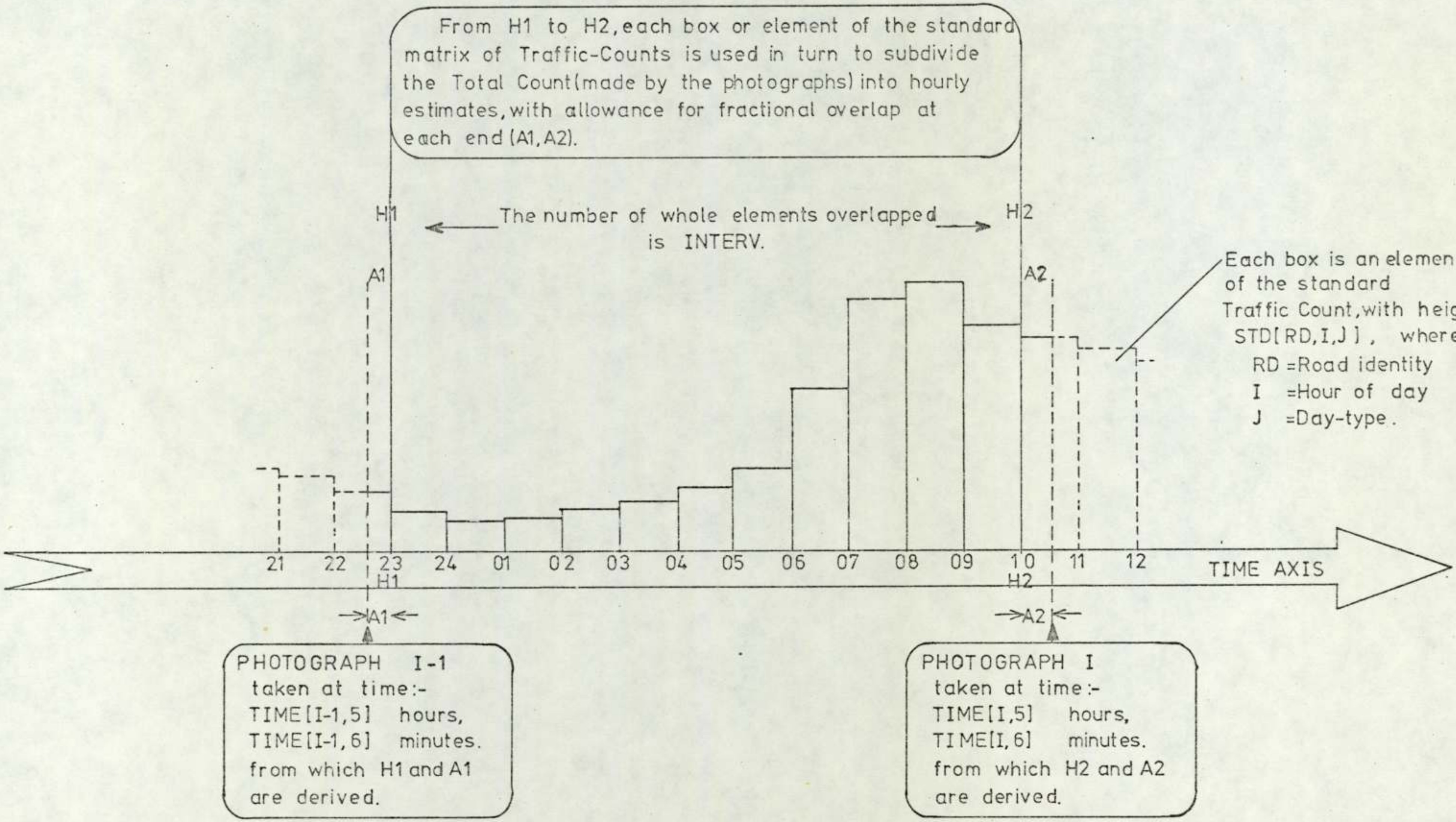

FIGURE A2.2 OVERLAP OF PHOTOGRAPHS WITH THE COINCIDENT PART OF THE STANDARD TRAFFIC PATTERN.

APPENDIX 3

ERRORS IN THE TRAFFIC-FLOW RESULTS

This appendix provides more detail than Section 4.3.3 could: it is the basis for the comments made in that Section. It is assumed that Appendix 2 has been read.

In the following numbered paragraphs we discuss sources of error and their separate effects. We then combine these errors to assess the accuracy of the calculated traffic-flows.

A3.1 Sources of Error

1. Record pulses:-

   Systematically high readings arise from poor lane discipline. The correction factors (from calibration: Section 4.2.4) were derived from a limited sample, so have probable error of say 5%, i.e. there is a loss in precision from the attempt to correct a systematic error (cf. Bevington, 1969

2. Abstract numbers; punch cards:-

   Observers may misread numbers: counts are in error occasionally. Gross errors seen from programme output are correctable while errors in less significant digits may escape detection. This type of error has been ignored: it is regarded as an occasionally wrong data-point, perhaps analagous to noise in the information.

3. Interpolate missing values:-

   The data for November 1974 had counter 13 missing, affecting block I and therefore roads 2, 4, 17, 19, 23 (Tables A2.1, A2.2). The error varies with the combination of counters that defines the flow of the road. Test runs on a count with counter 13 present and missing gave results as in Table A3.1.

4. Counter combinations:-

Propogation of errors through counter combinations:-

The traffic-flows for each road are sums and differences of (inaccurate) counter differences. Subtraction tends to increase the relative error of the calculated traffic-flow. The exact size of the error varies with the number of additions and subtractions, the sizes of the terms and the uncertainty in each term.

For addition of n equal functions f, each having relative error e, we have a result nf with absolute error $\sqrt{n}fe$. If these operations included s subtractions, the result is (n - s)f with absolute error $\sqrt{n}fe$. In this case the relative error is increased from e to $\sqrt{n}fe/((n - s)f)$, or $\sqrt{n}/(n - s)$ times. This simple argument indicates the effect expected. In practice there are varying numbers of terms with varying errors. An estimate was made as follows using a modified form of the programme TRRLRØFLØ.

We assume each counter error is a random error uncorrelated with any other errors. If, for example, $Z = X \pm Y$ we have $\sigma_Z^2 = \sigma_X^2 + \sigma_Y^2$ (Bevington, 1969 a) where σ_Z, σ_X, σ_Y are the standard deviations in the estimates of Z, X and Y respectively. In the programme TRRLVARI, derived from TRRLRØFLØ, a modified form of the procedure RØFLØW was used to call the counter combinations (through the use of function procedure BØX) in addition (subtractions in RØFLØW were changed to addition); the terms summed were elements of EFAC, where the element

EFAC [I,J] = (PERCENT*FACDIF [I,J] /100)^2 is equivalent to σ_J^2 for the variable FACDIF [I,J] . PERCENT was read in as 5. The procedure call ERØFLØ (RD,BØX,I,EFAC,EPBF) stores in the element EPBF [RD,I] the sum $\sum_J \sigma_J^2$ for those counters J contributing to the road RD. The square root E = (EPBF RD,I)$^{\frac{1}{2}}$ is printed as a percentage of the flow PBF [RD,I] existing in the road (E is shown in Table A3.2).

Comparison between roads of the error propagation due to the particular counter combination for each road can be seen in Table A3.2. The data used PERCENT = 5 and a twenty four hour count. The graph (Figure A3.1) shows a positive correlation between $\sqrt{n}/(n - s)$ and the relative increase in error E ÷ PERCENT, due to the combining of counters. Thus the function $\sqrt{n}/(n - s)$ is a useful guide to the relative increase in error for n counters, of which s are subtracted. Typical effect is that the standard deviation of a road flow measured as a percentage of the road flow is ($\sqrt{n}/(n - s)$)(E_J), where E_J is the percentage error of the single counter J (measured as a percentage of the counter flow: E_J = PERCENT/100 here; in general a counter J has σ_J, so $E_J = \sigma_J$/FACDIF [J] .

In summary, the present traffic counts for each road have an error equal to $\sqrt{n}/(n - s)$ times the typical percentage error of the counters.

5. Timer Drift: Error in STD:-

The photograph time although not at the hour desired is known exactly. No error is incurred through use of PERIØD [I] to divide elapsed counts since PERIØD [I] is accurate to one minute. The resultant traffic-flow will be used to represent that existing on the hour H as the count in H - 1 to H. There is a phase-error between the times of photographs I, I - 1 which are not exactly on the hours H, H - 1.

This phase-error between the time at which the flow is measured, and the time H used to represent that time, is serious where the traffic-flow changes rapidly with time about the hour H. Figure A3.2 shows a histogram of actual counts; the circled points show how each box in the histogram is rounded to H as if it represented a period H - 1 to H. This particular plot is taken from the counts used to set up the matrix STD and by chance the effect of the phase-error is not severe for most of the time where the traffic-flow changes gradually. The phase-error can be half an hour: when the traffic rises from 700 h^{-1} at 07.00 to 1600 h^{-1} at 08.00 to 2900 h^{-1} at 09.00, $dT/dH \sim 1000$ h^{-2}.

Assuming $dT/dH \sim \Delta T/\Delta H$, for $H = \frac{1}{2}h$, $\Delta T = 500$ h^{-1}. At 08.00 the count is 1600 $\pm$ 500 h^{-1}; an error of $\sim$ 30%. Those elements of STD for this time (09.00 on a FRIDAY, day-type 5) have the worst error since in the rest of the elements of STD the error in timing is less than $\pm$ 10 minutes.

The morning rush-hour flows interpolated for Fridays have systematic error at 07.00 and 08.00 hours when the values are probably 30% low; otherwise the probable error due to timer drift (of $\sim \pm$ 10 minutes in the hour) is $\sim \pm$ 10%. These errors are additional to those discussed earlier.

6. Hourly Interpolation

The interpolation of hourly flows relies on the reproducibility of traffic patterns for each day-type, as stored in the matrix STD. These values in STD have error as in paragraphs 1 to 5 immediately above because of the method of measurement. We then assume the traffic pattern is constant. A series of hourly traffic-flows for Salford Circus and twelve hourly traffic-flows for the M6 were abstracted in groups according to time of day and day-type. Table A3.3 shows the variation derived from groups of Mondays; Table A3.4 that for day and night values.

This suggests the traffic pattern is constant to within 4%. The values in STD are thus an inaccurate (from measurement) single sample from a distribution of traffic patterns which themselves are scattered. To represent the traffic pattern by STD implies both a random measurement-error and a random sampling-error. We combine these to estimate the error in any element of STD as typically $\pm$ 14%. The fractions A1, A2 at the start and end of the overlapped period take into account the exact times of the two photographs which together form the twelve hourly count; the timer drift in twelve hourly photographs causes no additional error. For the overlapped period the appropriate elements of STD are summed into TØTSTD. Only summation is involved: the element TØTSTD [RD] has the same relative error as the elements for the road RD of STD [RD,D,H] from which it was derived; these errors have been discussed already at the beginning of this paragraph 6. The interpolation itself uses

$$\frac{\text{STD [RD, DY [J] , HR [J]] *PBF [RD,I]}}{\text{TØTSTD [RD]}}$$

to interpolate hourly subdivisions of PBF [RD,I] . Each element of PBF has errors as in paragraphs 1, 3, 4, but not 5 since the drift in twelve hourly photographs is slight. The elements of STD and TØTSTD have errors as discussed above in this paragraph 6. The interpolated answer has a combined error of $\sim \pm 18\%$.

For roads 2, 4, 17, 19, 23 the error (from missing values) is larger (Table A3.1). On a Friday morning rush-hour the value is low by $\sim 30\%$.

TABLE A3.1

Effect of Missing Counters:

Case Study for Counter 13 (missing during

November 1974 when monitoring at Salford Circus)

Road	Flow with true counter readings	Flow with reading for Counter 13 (missing) interpolated	Error
2	1460	1511	+ 4%
4	84	135	+ 60%
17	124	73	- 40%
19	145	93	- 35%
23	121	172	+ 42%

TABLE A3.2

Error Propagation due to the Combination of Inaccurate Counter Readings;

Results from a 5 per cent Fraction of the Flow recorded by Each Counter over Twenty

Four Hours (07.49 on 27-09-74 to 07.51 on 28-09-74)

Road	Counter Combinations			Mean Flow in Period	Error[1] $E=(EPBF[RD,I])^{\frac{1}{2}}$	E/5	$\sqrt{n}/(n - s)$
	n	s	n - s				
1	6	0	6	2218	2.2	0.44	0.408
2	16	3	13	2776	1.7	0.34	0.308
3	-	-	-	-	-	-	-
4	2	0	2	299	4.4	0.88	0.707
5	16	2	14	875	2.8	0.56	0.286
6	2	0	2	558	3.6	0.72	0.707
7	2	0	2	586	3.6	0.72	0.707
8	2	0	2	289	4.4	0.88	0.707
9	2	0	2	272	3.8	0.76	0.707
10	2	0	2	289	4.4	0.88	0.707
11	2	0	2	860	3.8	0.76	0.707

TABLE A3.2 (continued)

Road	Counter Combinations			Mean Flow in Period	Error[1] $E=(EPBF[RD,I])^{\frac{1}{2}}$	E/5	$\sqrt{n}/(n - s)$
	n	s	n - s				
12	4	0	4	716	2.9	0.58	0.500
13	2	0	2	430	5.3	1.06	0.707
14	2	0	2	430	5.3	1.06	0.707
15	1	0	1	80	5.0	1.00	1.00
16	2	1	1	43	10.4	2.08	1.414
17	4	2	2	259	9.3	1.86	1.00
18	1	0	1	38	5.0	1.00	1.00
19	5	2	3	297	8.1	1.62	0.745
20	6	2	4	875	2.8	0.56	0.612
21	4	0	4	358	4.1	0.82	0.500
22	4	0	4	358	4.1	0.82	0.500
23	4	1	3	342	4.0	0.80	0.667
24	2	0	2	0	-	-	0.707

Note 1: See text: paragraph 4 of Appendix 3.

TABLE A3.3

Variation of Traffic Pattern at Salford Circus.

Hourly Traffic-Flows at Time H for Each of Eight Mondays

(28.10.74 to 16.12.74) were averaged and

Standard Deviation Calculated

H	Mean Flow	Standard Deviation	Coefficient of Variation, %
08-00	2755	49	1.9
09-00	2783	60	2.4
12-00	2204	39	1.9
15-00	2379	46	2.0
17-00	3426	53	1.6
20-00	1423	75	5.6
		Mean	2.6%

TABLE A3.4

Variation of Twelve Hour Total of Traffic on M6 Motorway.

Traffic elapsed over Twelve Hours averaged in Groups of Three

Day (or Night) Time Values for Three Days of the Same Type

Day-type	Mean	Standard Deviation	Coefficient of Variation, %
THUR-DAY*	55671	861	1.9
THUR-NIGHT*	11518	248	2.6
FRI-DAY	59686	549	1.1
FRI-NIGHT	12040	912	9.3
SAT-DAY	29104	973	4.1
SAT-NIGHT	08009	1015	15.6
SUN-DAY	25216	287	1.4
SUN-NIGHT	15219	374	3.0
MON-DAY*	53949	441	1.0
MON-NIGHT*	10478	221	2.6
TUE-DAY*	53945	251	0.6
TUE-NIGHT*	11014	251	2.8
WED-DAY*	54247	296	0.7
WED-NIGHT*	11371	445	4.8
		Mean	3.7%

* These four days were grouped as one type, the Friday flow being somewhat higher.

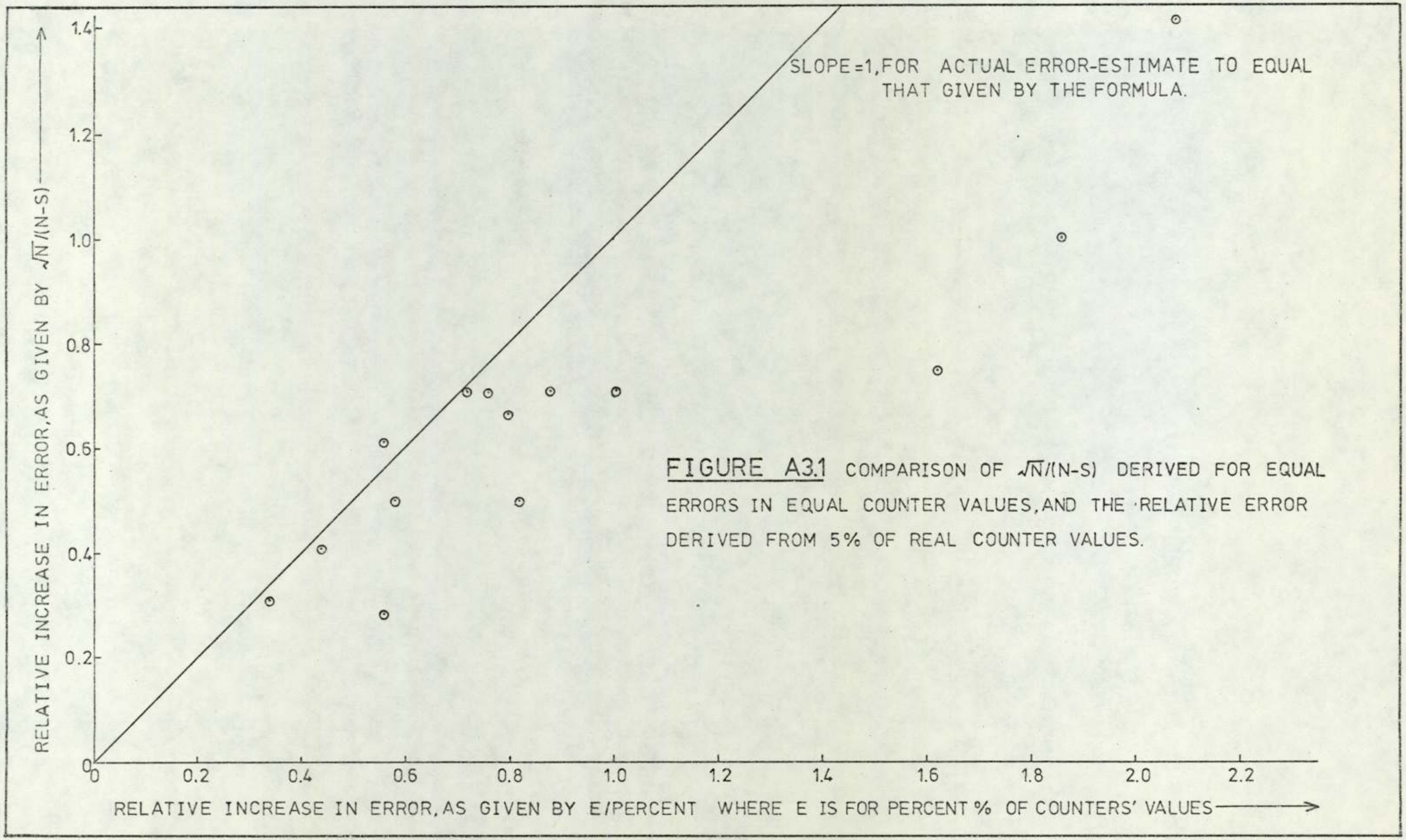

FIGURE A3.1 COMPARISON OF √N/(N-S) DERIVED FOR EQUAL ERRORS IN EQUAL COUNTER VALUES, AND THE RELATIVE ERROR DERIVED FROM 5% OF REAL COUNTER VALUES.

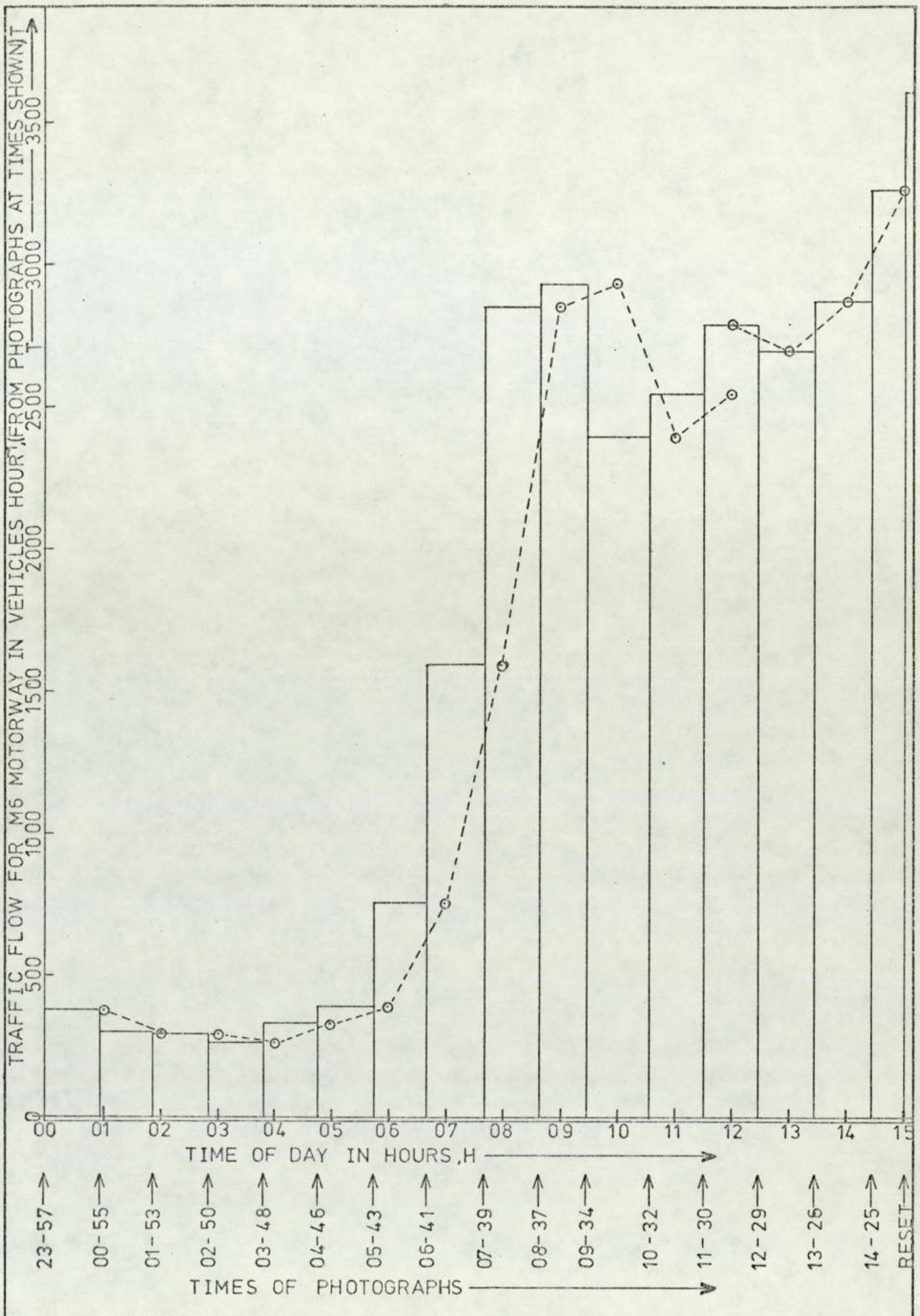

FIGURE A3.2 HISTOGRAM OF TRAFFIC-FLOWS AS RECORDED AND AS ROUNDED TO THE NEAREST WHOLE HOUR H.

KEY:- ⎍ AS RECORDED

-⊙- TIME ROUNDED TO H

APPENDIX 4

SEMI-EMPIRICAL DIFFUSION EQUATION

In this Appendix we give an outline understanding to the equation rather than a rigorous derivation.

For an element volume dV at location $\underline{P}$ downwind of a pollutant release. Concentration $C(\underline{P})$ is uniform over dV, and the mass of pollutant is either:

$C(\underline{P})dV$ if $C(\underline{P})$ is in mass volume^{-1} units

$\rho C(\underline{P})dV$ if $C(\underline{P})$ is in volume volume^{-1} units.

We use the former.

The transport wind is $U(\underline{P})$ along the X axis, and particles settle with a velocity S(P). (Figure A4.1). The concentration within the element changes with time:

$$\text{ACCUMULATION} = dV\left(\frac{\partial C(P)}{\partial t}\right) = \text{INPUT} - \text{OUTPUT}$$

Now transport, diffusion, settling and chemical reaction may all contribute to the right hand side.

1. Transport

Into face X by wind $U(P).C(P).dy.dz$

Out of face (X + dX) by wind $U(P).C(P).dy.dz +$

$$U(P).\left(\frac{\partial C(P)}{\partial x}.dx\right)dy.dz$$

$\therefore$ Nett transport into face = $- U(P)\dfrac{\partial C(P)}{\partial x}.dV$

2. Diffusion: occurs by turbulent and molecular diffusion, conveniently defined by assuming a form similar to Fick's Law.

Diffusivity K is such that the flux F is proportional to concentration gradient.

$$F_x = -K_{xx} \frac{\partial C(P)}{\partial x} \quad , \quad F_y = -K_{yy} \frac{\partial C(P)}{\partial x} \quad , \quad F_z = -K_{zz} \frac{\partial C(P)}{\partial z}$$

where F_x, F_y, F_z are components of flux $F(\underline{P})$ of particles or molecules at $\underline{P}$.

We assume K_{xx} is constant in X, K_{yy} in Y, but K_{zz} varies with height.

$$\therefore \quad \frac{\partial F_x}{\partial x} = -K_{xx} \frac{\partial^2 C(\underline{P})}{\partial x^2} \quad , \quad \frac{\partial F_y}{\partial y} = -K_{yy} \frac{\partial^2 C(\underline{P})}{\partial y^2} \quad ,$$

$$\frac{\partial F_z}{\partial z} = \frac{-\partial}{\partial z} \left(K_{zz} \frac{\partial C(P)}{\partial z}\right)$$

Rate of flow of particles or molecules

Into the element = F.dy.dz across X face

Out of the element = $F.dy.dz + \frac{\partial F}{\partial x}(P).dx.dy.dz$ across X face.

Similar equations apply to the other faces.

Differencing,

Nett flow into element = $-\left(\frac{\partial F}{\partial x} + \frac{\partial F}{\partial y} + \frac{\partial F}{\partial z}\right) dxdydz$

$\therefore$ Nett diffusion into element =

$$\left[K_{xx} \frac{\partial^2 C(P)}{\partial x^2} + K_{yy} \frac{\partial^2 C(P)}{\partial y^2} + \frac{\partial}{\partial z} \left(K_{zz} \frac{\partial C(P)}{\partial z}\right) \right] dV$$

3. Sedimentation: this is defined to have the same sence as $\underline{Z}$, as in Figure A4.2.

Particles settling across lower face in unit time =

$C(P).(-S).dxdy$

Partides settling across upper face in unit time =

$$C(P).(-S).dxdy + \left(\frac{\partial C(P)}{\partial z}.dz\right)(-S).dxdy$$

$$\text{Nett sedimentation} = \frac{-\partial C(P)}{\partial z}.S.dV$$

4. Chemical reaction: for simplicity, suppose a series of species R_i are reacting with rate constants K_i and orders of reaction m_i to produce C.

$$\text{Nett Accumulation} = -KC^N \prod_i (R_i^{m^i})dV$$

Thus combining,

$$\frac{\partial C(P)}{\partial t}dV = -U(P).\frac{\partial C(P)}{\partial x}dV + \left[K_{xx}\frac{\partial^2 C(P)}{\partial x^2} + K_{yy}\frac{\partial^2 C(P)}{\partial y^2} + \frac{\partial}{\partial z}\left(K_{zz}\frac{\partial C(P)}{\partial z}\right) \right] dV$$

$$- \frac{\partial C(P)}{\partial z}.S.dV - KC^N \prod_i (R_i^{m^i})dV.$$

Whence if no reaction or settling occur one has Equation 5.2, and otherwise

$$\frac{\partial C(P)}{\partial t} + U(P)\frac{\partial C(P)}{\partial x} + S\frac{\partial C(P)}{\partial z} + KC^N \prod_i R_i^{m^i}$$

$$= \left(K_{xx}\frac{\partial^2 C(P)}{\partial x^2} + K_{yy}\frac{\partial^2 C(P)}{\partial y^2} + \frac{\partial}{\partial z}\left(K_z\frac{\partial C(P)}{\partial z}\right)\right)$$

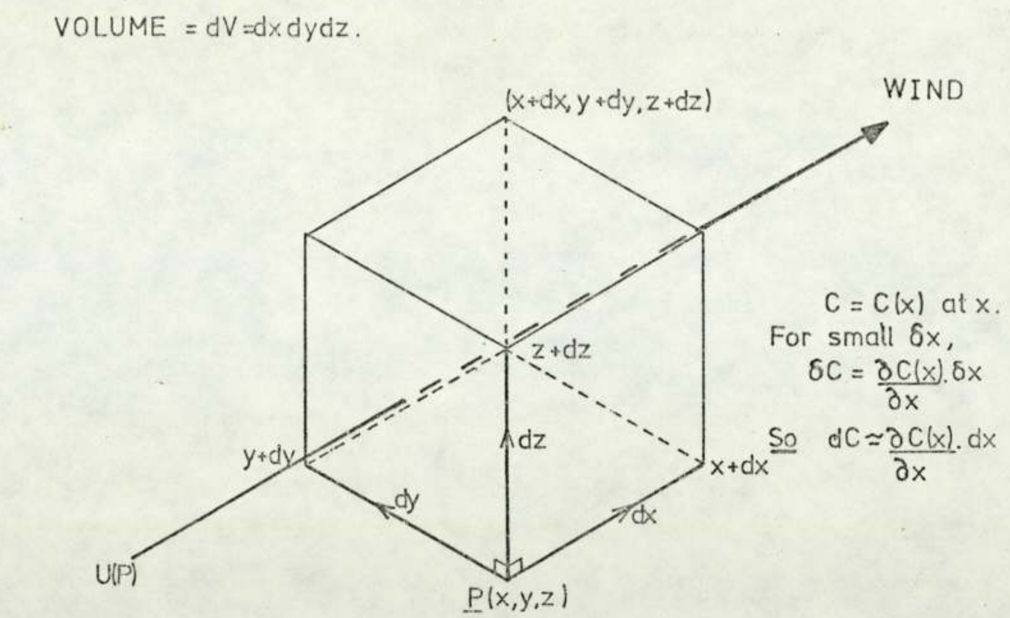

FIGURE A4.1 CO-ORDINATES FOR THE ELEMENT dV AT P.

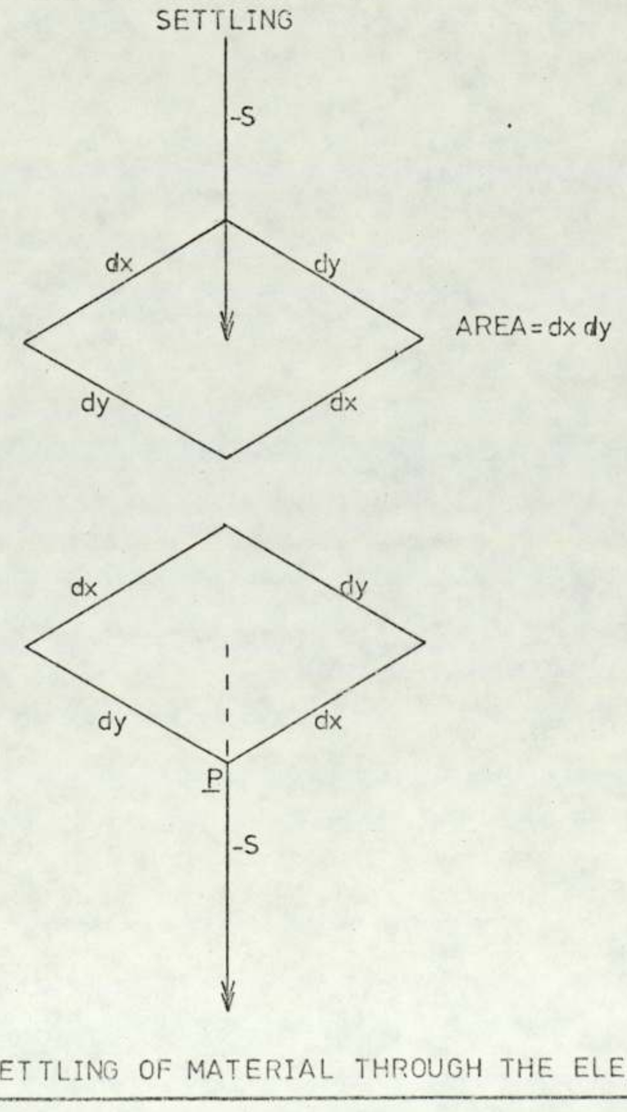

FIGURE A4.2 SETTLING OF MATERIAL THROUGH THE ELEMENT.

REFERENCES

REFERENCES

"Am. Conf. Govt. Hygienists" 4th Edition. 1972. Air Sampling instruments for evaluation of atmospheric contaminants. American Conference of Governmental Industrial Hygienists, P O Box 1937, Cincinnati, Ohio 45201.

Bair, E.J. 1962. Introduction to chemical instrumentation. 349 p. New York: McGraw-Hill Book Co.

Bendat, J.S. and A.G. Piersol. 1966. Measurement and analysis of random data. New York: John Wiley and Sons.

Bevington, P.R. 1969. Data reductions and error analysis for the physical sciences. 320 p. New York: McGraw-Hill Book Co.

Bevington, P.R. 1969a. Data reductions and error analysis for the physical sciences. New York: McGraw-Hill Book Co. P 7.

Bevington, P.R. 1969b. Data reductions and error analysis for the physical sciences. New York: McGraw-Hill Book Co. P 64.

Bibbero, R.J. and I.G. Young. 1974. Systems approach to air pollution control. 531 p. New York: John Wiley and Sons.

Bibbero, R.J. and I.G. Young. 1974a. Systems approach to air pollution control. New York: John Wiley and Sons. 20 - 21.

Butler, J.D., S.D. MacMurdo and D.R. Middleton. 1974. Motor vehicle generated pollution in urban areas. Assoc. Public Health Inspectors Environmental Health Congress and Exhibition, Torbay, U.K. 69 - 77.

Calder, K.L. 1970. Some miscellaneous aspects of current urban pollution models. Chapter 4 in Proc. Symposium on multiple-source urban diffusion models. Environmental Protection Agency, Research Triangle Park, N.C. AP 86. 416 P. Ed: A.C. Stern.

Calder, K.L. 1973. On estimating air pollution concentrations from a highway in an oblique wind. Atmospheric Environment 7: 863 - 868.

Chamberlain, A.C. 1974. Travel and deposition of lead aerosols. Atomic Energy Research Estab., Harwell, U.K. R7676.

Drivas, P.J. and F.H. Shair. 1974. Dispersion of an instantaneous cross-wind line source of tracer released from an urban highway. Atmospheric Environment 8: 475 - 485.

Derwent, R.G. and H.N.M. Stewart. 1973. Air pollution from the oxides of nitrogen in the United Kingdom. Atmospheric Environment 7: 385 - 401

Fontijn, A., A.J. Sabadell and R.J. Ronco. 1970. Homogeneous chemiluminescent measurement of nitric oxide with ozone-implications for continuous selective monitoring of gaseous air pollutants. Analytical Chemistry 42: 575 - 579

Fussel, D.R. 1970. Atmospheric pollution from petrol and diesel engined vehicles. Petrol. Rev. 24: 192 - 202.

Geomet Inc. 1971. Validation and Sensitivity Analysis of the Gaussian plume multiple-source urban diffusion model. R.C. Koch et al. Geomet EF-60. APTD 0935. CA 7094. 351 P. Nov 1971. FLD/GP 13B

Gifford, F.A. 1961. Use of routine meteorological observations for estimating atmospheric dispersion. Nuclear Safety 2 4: 47 - 51

Hay, J.S. and F. Pasquill. 1959. Diffusion from a continuous source in relation to the spectrum and scale of turbulence. Adv. in Geophysics 6: 345 - 365.

Hewson, E.W. and G.C. Gill. 1944. Air pollution survey trail, British Columbia, Canada. U.S. Bureau of Mines, Bulletin 453: 23, 138 - 149, 154, 167 - 172, 189, 289.

Hoffert, M.I. 1972. Atmospheric transport, dispersion, and chemical reactions in air pollution: a review. Amer. Inst. Aeronautic and Astronautics Journal. 10: 377 - 387.

Islitzer, N.F. 1961. Short range atmospheric-dispersion measurements from an elevated source. Jnl. Meteorology 18: 443 - 450

Johnson, W.B., W.F. Dabberdt, F.L. Ludwig and R.J. Allen. 1971. Field study for initial evaluation of an urban diffusion model for carbon monoxide. Stanford Research Instit., California, U.S. CRC APRAC - CAPA 3 68 2. 254 P
FLD/GP 4A 13B

Lamb, A.B., W.C. Bray and J.C.W. Frazer. 1920. The removal of carbon monoxide from air. Indus. Engineer. Chem. 12: 213 - 221.

Leahey, D.M. and J. Halitsky. 1973. Low wind turbulence statistics and related diffusion estimates from a site located in the Hudson River Valley. Atmospheric Environment 7: 49 - 61.

Linford, A. 1961. Flow measurement and meters. Pp. 143, 255 - 6. E. & F.N. Spon Ltd.

McElroy, J.L. 1969. A comparative study of urban and rural dispersion. Jour. Applied Meteorology 8: 19 - 31.

Monin, A.S. and A.M. Yaglom. 1971. Statistical Fluid Mechanics: mechanics of turbulence. Volume 1, 769 p. English translation (edited by J.L. Lumley) of Statisicheskaya gidromekhanika - Mekhanika Turbulentnosti, published in 1965 by Nauka Press, Moscow. Cambridge, Massachusetts: MIT Press.

Monin, A.S. and A.M. Yaglom. 1971a: above text, 579 - 580.

Monin, A.S. and A.M. Yaglom. 1971b: above text, 591 - 606.

Monin, A.S. and A.M. Yaglom. 1971c: above text, 604

Monin, A.S. and A.M. Yaglom. 1971d: above text, 606 - 614.

Monin, A.S. and A.M. Yaglom. 1971e: above text, 576, 607 - 9ff.

Monin, A.S. and A.M. Yaglom. 1971f: above text, 643 - 657.

Monin, A.S. and A.M. Yaglom. 1971g: above text, 644, 647.

Monin, A.S. and A.M. Yaglom. 1971h: above text, 650 - 651.

Monin, A.S. and A.M. Yaglom. 1971i: above text, 577.

Monin, A.S. and A.M. Yaglom. 1971j: above text, 618.

Monin, A.S. and A.M. Yaglom. 1971k: above text, 617 - 632.

Pasquill, F. 1961. The estimation of the dispersion of windborne material. The Meteorological Magazine, Meteorological Office, U.K. 90: 33 - 49

Pasquill, F. 1970. Prediction of diffusion over an urban area - current practice and future prospects. Chapter 3 in Proc. Symposium on multiple-source urban diffusion models. Environmental Protection Agency, Research Triangle Park, N.C. Ap 86. 416 P. Ed. A.C. Stern.

Pasquill, F. 1971. Atmospheric dispersion of pollution. Quart. Jour. Roy. Met. Soc. 97: 369 - 395

Pasquill, F. 1974. Atmospheric diffusion: the dispersion of windborne material from industrial and other sources. 2nd ed. Chichester: Horwood; New York; London: Distributed by Wiley. P. 373.

Pooler, F., JR. 1966. A tracer study of dispersion over a city. Jour. Air Pollution Control Assoc. 11: 677 - 681.

Porter, K. and D.H. Volman. 1962. Flame ionisation detection of carbon monoxide for gas chromatographic analysis. Analyt. Chem., 34: 748 - 749

Smith, F.B. 1972. A scheme for estimating the vertical dispersion of a plume from a source near ground-level (a first draft). Extended summary communicated personally by F.B. Smith, Department Met.O.14., Meteorological Office, Bracknell, Berkshire, England; closely related to Smith (1972a) and Pasquill (1974).

Smith, F.B. 1972a. A scheme for estimating the vertical dispersion of a plume from a source near ground level. Chapter 18 in Proc. Third Meeting Expert Panel on Air Pollution Modelling. NATO Committee on Challenges to Modern Society.

Stern, A.C. 1970. Proc. symposium on multiple-source urban diffusion models. Environmental Protection Agency, Research Triangle Park, N.C. AP 86. 416 P.

Turner, D.B. 1970. Workbook of atmospheric diffusion estimates. Public Health Service, Cincinnati, Ohio. Div. of air pollution. PHS PUB 999 AP 26. 88P.

Williams, O.T. 1974. Some considerations in the design and operation of multi-level interchanges. The Highway Engineer - Jour. Instit. Highway Engineers. 21 5: 12 - 20.

SUPPORTING DOCUMENTS

Listings for the following programmes will be found under separate cover.

CHART50	Chart data zero corrected, calibrated and averaged ... Chapter 3, Appendix 1.
TRRLINTR	Traffic flows for M6 and A38(M) ... Chapter 4, Appendices 2, 3.
TRRLRATGEN	Calculate RJ[J]for missing value interpolation by other traffic programmes ... Chapter 4, Appendices 2, 3.
TRRLROFLO	Calculate traffic flow for all roads - uses hourly photographs ... Chapter 4, Appendices 2, 3.
TRRLBOX	Calculate mean traffic flows between photographs, and interpolate hourly flows for all roads for each hour between photographs ... Chapter 4, Appendices 2, 3.
TRRLVARI	Error analysis for traffic programmes ... Chapter 4, Appendix 3.
SPAG68	Calculation of pollutant concentrations by integration over road geometry ... Chapter 6.
SPAGSIMP	As for SPAG68, using either same input format as SPAG68, or a simplified one with observer position to nearest metre. No field observations need be read ... Chapter 6.
SPAGSENS	Sensitivity analysis for SPAG68 ... Chapter 6.

STUDIES OF ATMOSPHERIC POLLUTANTS IN URBAN DISTRICTS

by

DOUGLAS RAYMOND MIDDLETON, M. A. CANTAB.

A Thesis presented for the Degree of

Doctor of Philosophy

in

The University of Aston in Birmingham

August 1976

STUDIES OF ATMOSPHERIC POLLUTANTS IN

URBAN DISTRICTS

by

DOUGLAS RAYMOND MIDDLETON, M. A. CANTAB.

A Thesis presented for the Degree of

Doctor of Philosophy

in

The University of Aston in Birmingham

August 1976

SUMMARY

To study pollution near a motorway intersection, concentrations of oxides of nitrogen, carbon monoxide and total hydrocarbons were monitored, and calculated by a generally applicable programme. Road-side dilution was measured.

After calibration by flow and exponential dilution, unattended instruments recorded pollutant concentrations in analogue form. Zeroes and calibrations were measured during visits and automatically. Intersection traffic-flows, and simultaneous weather readings from a nearby airport, were obtained.

The data were stored and manipulated by computer - principles for processing environmental data are suggested. Data, identified by gas, observation type, site, time and date, were calibrated, zero corrected and averaged by an appropriate programme. Similarly, programmes calculated hourly traffic-flows from instantaneous readings of cumulative counters; hourly flows were interpolated from non-hourly counts, to minimise abstraction. For simple usage, input was flexible and accepted missing values; default options included an assumed zero or calibration.

Another programme calculated gaseous pollutant concentrations for any elevated, curved or straight roads from dilution of traffic-emissions. Ordnance Survey map references defined road geometries and axes were rotated downwind. Point-source plumes, from elements stepped along each road, were integrated.

Statistical comparison of calculated with measured concentrations showed a high correlation; the regression coefficients were not unity because of uncertain emissions estimates, errors of measurement and approximations of calculation.

Concentrations at a more distant site were noticeably lower than at the intersection.

A sampling technique was developed to measure concentrations at two separate locations simultaneously using a single analyser: dilution curves calculated by the programme for the motorway and the intersection were compatible with concentration gradients measured in the field.

Concentrations of pollutants at the intersection were related to the traffic-based model, but exact agreement between calculation and field measurement is still hard to achieve, because many variables are involved.

ACKNOWLEDGEMENTS

The work required many arrangements with organisations outside the University so that we could have monitoring sites and traffic-counts around the Motorway Intersection. I am particularly grateful to my Supervisor, Dr J D Butler, who in making these arrangements made all the rest possible.

The project was sponsored by the Transport and Road Research Laboratory of the Department of the Environment, and I would like to thank Mr D M Colwill from the Transport and Road Research Laboratory for his efforts to assist us: he made many visits to discuss the work.

I thank also the many officials representing the City of Birmingham, the Motorway Control Police, the Department of the Environment, and other Public Bodies, who contributed to the provision of facilities needed in the field.

Within the Chemistry Department, I was assisted by the technical staff, of whom Tony, Squadron Leader A S Aldridge, D.F.C., is especially thanked for much moral and physical support in the field. He would say, "Remember you're British!" when trouble struck.

To my friends, my thanks for their patience - Suru Patel, who whilst also working for the Degree always made time to listen or offer advice, and Phyllis and Christopher Gilford who in leading the folk dance group gave me many friends, including Penny, my fiancee.

Finally I am grateful for the opportunity to work on a problem related to the common good, for, as the Poet suggests ...

"We dance
    to a whispered voice
        overheard by the soul
            undertook by heart
                and you may know it
                    if you may know it ..."

.... from .... " Be ",

by Neil Diamond (Stonebridge Music, 1973)

for the Sound Track (CBS 69047) of the film

" Jonathan Livingstone Seagull ",

a parable on perfection and life by

Richard Bach.

Published by Turnstone Press, 1972 and Pan Books, 1973.

To Mother,

thanks, and with love.

STUDIES OF ATMOSPHERIC POLLUTANTS IN URBAN DISTRICTS

CONTENTS

Page No

LIST OF FIGURES

LIST OF TABLES

ABBREVIATIONS

M6) A38(M))	Major roads (see Figure 1.1)
NO	Nitric Oxide
NO_2	Nitrogen Dioxide
NO_x	($NO + NO_2$ in unknown proportions)
CO	Carbon Monoxide
HC	Total Hydrocarbons, measured as methane
12A	Analyser for Oxides of Nitrogen
MGA2	Analyser for Carbon Monoxide
AA521	Analyser for Total Hydrocarbons
ppm	parts per million by volume

CHAPTER 1

INTRODUCTION

1.1 The Problem

The object was to monitor gaseous pollutants around the Midland Links Motorway-Intersection and with this information assess the contribution such an intersection makes to the overall air pollution of the area. The emphasis was on measurement and interpretation of these pollutant levels: the work did not include medical aspects.

The intersection lies four kilometres from the city centre but well within the urban area (Map: Figure 1.1). An elevated and interlocking set of roads join a ground-level roundabout to the local roads, the M6 Motorway and the A38(M) or Aston Expressway (Map: Figure 1.2). The interconnections are flyover or underpass roads so that all turning movements are made without crossings. Elevated roads are largely mounted on pillars; the rest, on mounds. The intersection occupies thirteen hectares of land, and the highest viaduct is twenty four metres above the ground (Williams, 1974).

The observed levels of pollutants depend on many variables. The surrounding area contains sources: other roads at greater distances, chimneys of houses and factories, and Nechells Power Station. There

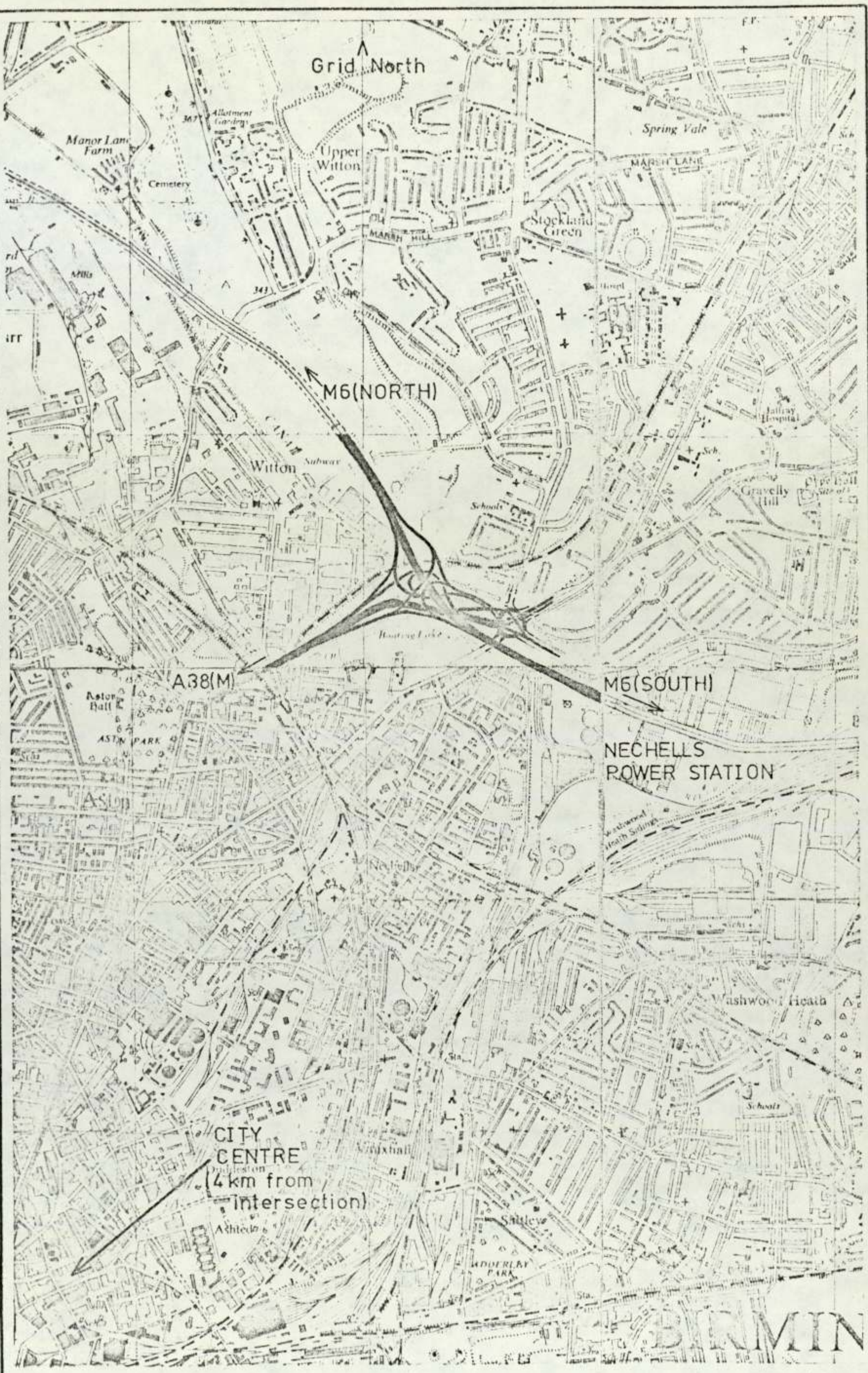

FIGURE 1.1 POSITION AND SURROUNDINGS OF THE MIDLAND LINKS MOTORWAY INTERSECTION (Based on Ordnance Survey)

0 1km

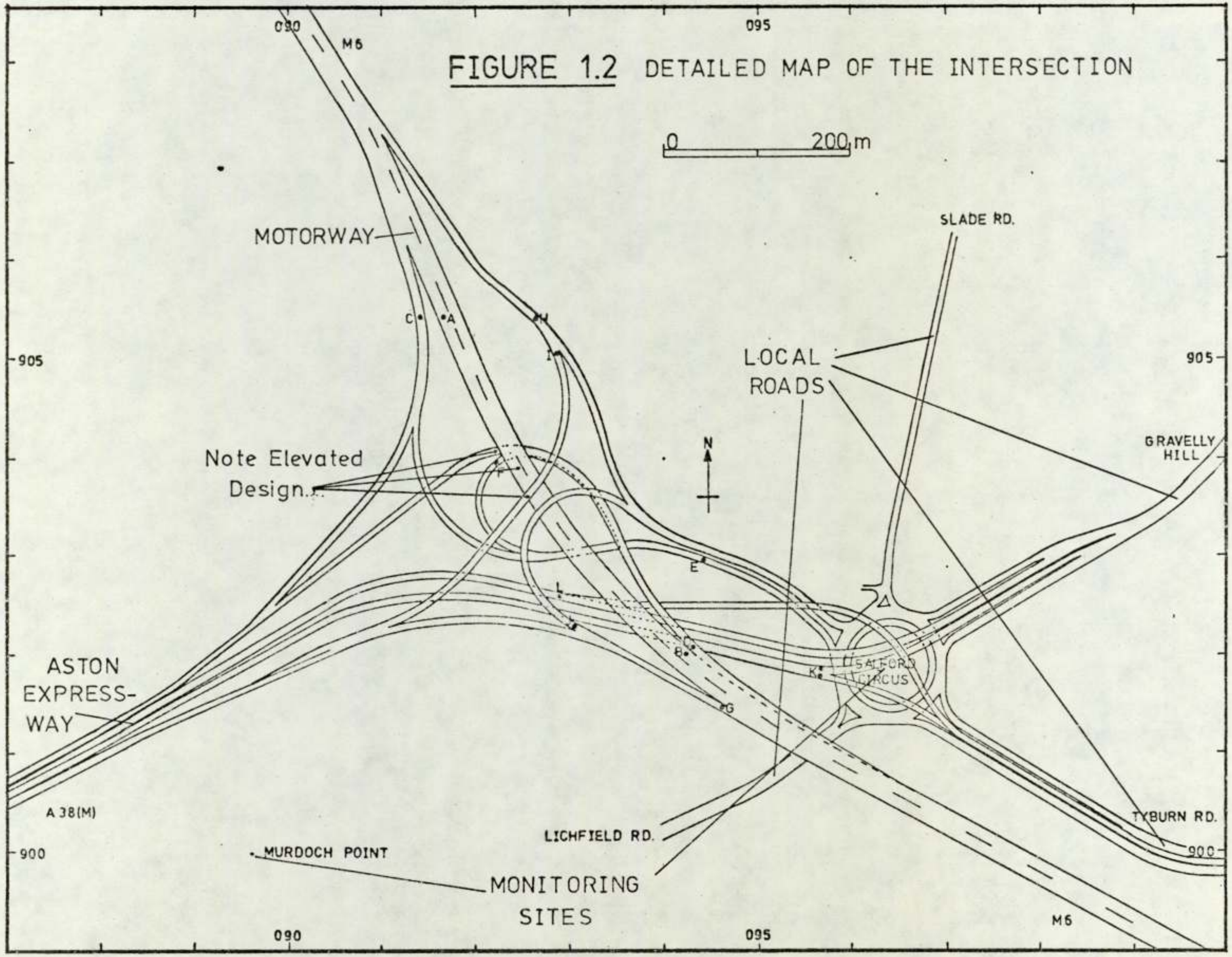

FIGURE 1.2 DETAILED MAP OF THE INTERSECTION

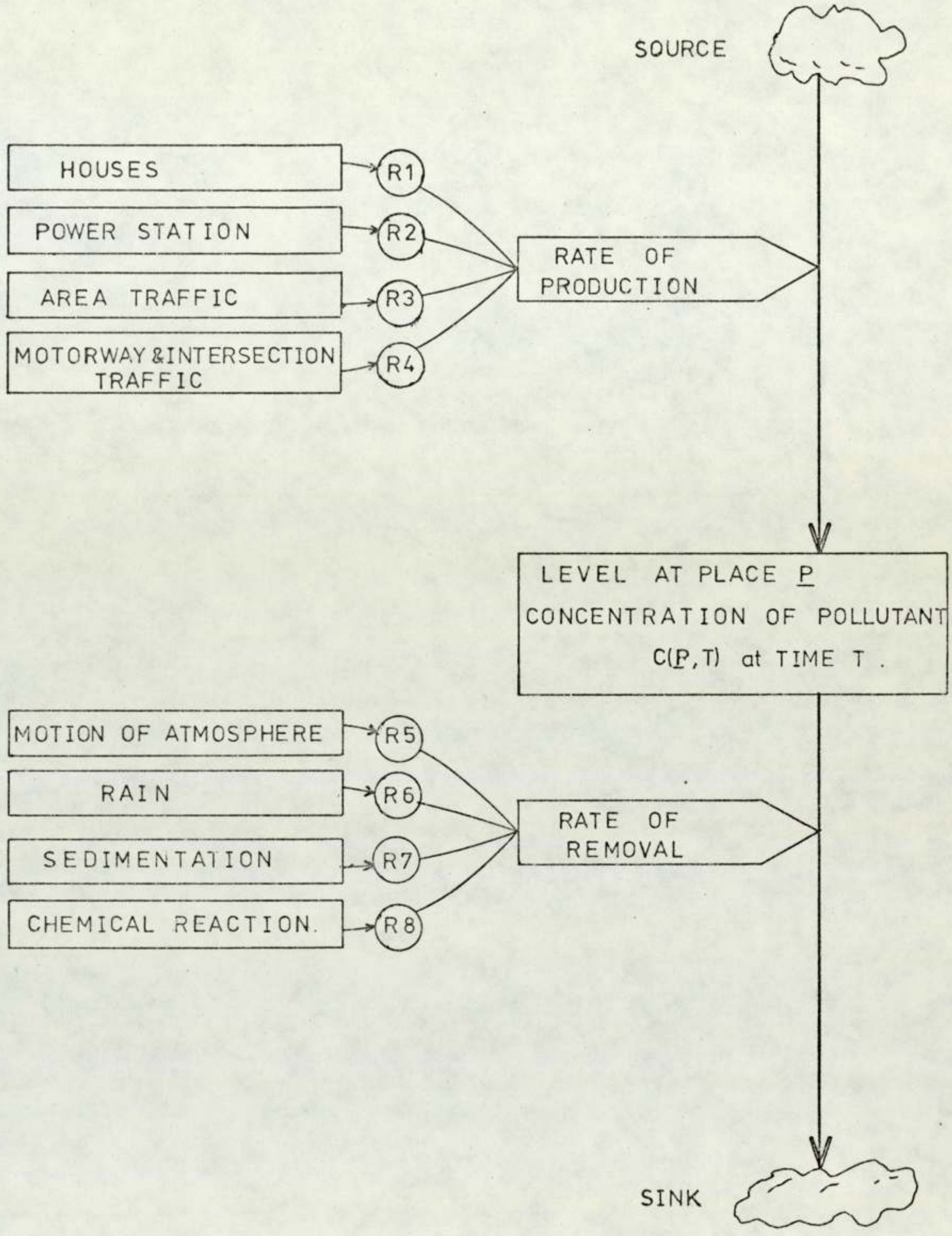

FIGURE 1.3 PROCESSES DETERMINING THE CONCENTRATION OF POLLUTANTS. R1 TO R4 INCREASE C, WHILE R5 TO R8 MAY REDUCE IT. THE PRESENT PROJECT ONLY STUDIED R4 AND R5, AND EACH OF THESE COULD NOT BE CONTROLLED.

is therefore a varying baseline of city pollution to which exhaust gases from the intersection are added. In general terms the wind speed and atmospheric mixing are expected to affect both the size of the background levels and the dilution characteristics of the source whose contribution we are trying to recognise and measure. This makes for a complicated study best described by a diagram (Figure 1.3). As compared to a laboratory experiment the problem is not closed. Traditionally one might vary one variable at a time to see the effects, but here we cannot. The spirit behind the research must be a feeling that each factor is an independent variable affecting the observed pollution levels: the individual effects of each variable have to be acknowledged by the use of their measured values to predict the pollution levels as observed. The rates of emissions and their dilution were the prime variables selected.

Source patterns were partly described using traffic counts while area sources such as houses were ignored. Dilution factors were estimated from weather observations taken at an adjacent airport; this assumed that the meteorological conditions were similar at the airport and in the city.

1.2 Outline of the Work

Following calibration of the instruments much of the work was monitoring in the field. Problems of calibrations and field-work are discussed. Routine monitoring involves large data sets for pollutants, traffic and weather, so computerised data processing as relevant to this type of project is considered. A new experimental technique to help the study of the dilution of plumes is presented. The results from the routine monitoring and this technique are discussed in terms of a Gaussian-plume dilution model. A programme to predict the pollutant levels is described and the predictions compared with field observations.

1.3 Information Available

Routine monitoring for a period at a fixed site needs time and effort. The periods of monitoring time were a compromise between the number of variables measured and the manpower requirements of the instruments used for the analyses. Since the study was designed to investigate pollution from vehicles, carbon monoxide and oxides of nitrogen were the gases of primary interest, but hydrocarbons were added later. A limiting resource was manpower, although the author had help from a technician.

With the three gas analysers and associated equipment the monitoring system had reached a level of complexity at which maintenance problems took up much of the author's time. The data were hourly measurements of NO_x, NO, CO, HC; NO_2 was available as NO_x less NO. Weather readings from Elmdon Airport (10 kilometres from the city centre) were at first hand-copied from the log- book at the airport and later from a line-printer output purchased from the Meteorological Office, Bracknell, Berkshire. There were two counters of traffic: one at Perry Barr covered the whole junction; the other, Salford Circus roundabout (Map: Figure 1.2). Reliable field measurements were made at Salford Circus and at Murdock Point (Map: Figure 1.2). The concentration decay was measured alongside the M6 Motorway away from the junction, and in the heart of the junction.

To calculate the pollution, traffic counts were scaled by literature values of emissions estimates for exhaust gases. The source geometry was represented as lines, curves and circles set in horizontal planes; Gaussian point-source plumes were integrated over this source representation by the trapezium rule. The plumes were defined by empirical curves (Geomet, 1971) according to a modified form of the Pasquill stability categories (Smith, 1972).

1.4 Summary

The following chapters describe the measurement and estimation of parameters believed to influence the levels of pollutants as observed. The problem is not closed since the variables are not under our control: this determines the approach to the problem and the discussion of the results.

CHAPTER 2

INSTRUMENTS USED FOR ROUTINE MONITORING

In the present chapter we describe the principles of operation of the instruments, and the calibration and zero checks as carried out. The following chapter will describe the monitoring sites and how the machines were used; together these chapters will indicate the limitations on the measurements made in the field. We begin with the machines themselves.

2.1 Description of the Instruments[1]

2.1.1 Analyser for Oxides of Nitrogen:-

Thermo Electron Chemiluminescent Model 12A NO-NO_x Analyser (Waltham, Massachusetts, United States of America)

This machine measures both NO and NO_x at eight sensitivities from 1000ppm down to 0.01ppm full scale. It has a negligible interference from water vapour, carbon and sulphur compounds. It is designed for continuous monitoring; the response time is 5 - 7 seconds at 0.25ppm full scale. Accuracy is quoted as ± 1% on standard gas and ± 3% on the 0.01ppm scale. Linearity is ± 1% of full scale.

The NO is measured by the light ($\lambda \sim 600$ - 875nm) emitted from the chemiluminescent reaction (Fontijn et al., 1970).

$$NO + O_3 \longrightarrow NO_2 + O_2 + h\nu$$

Note 1: Notes based upon Manufacturer's Manuals.

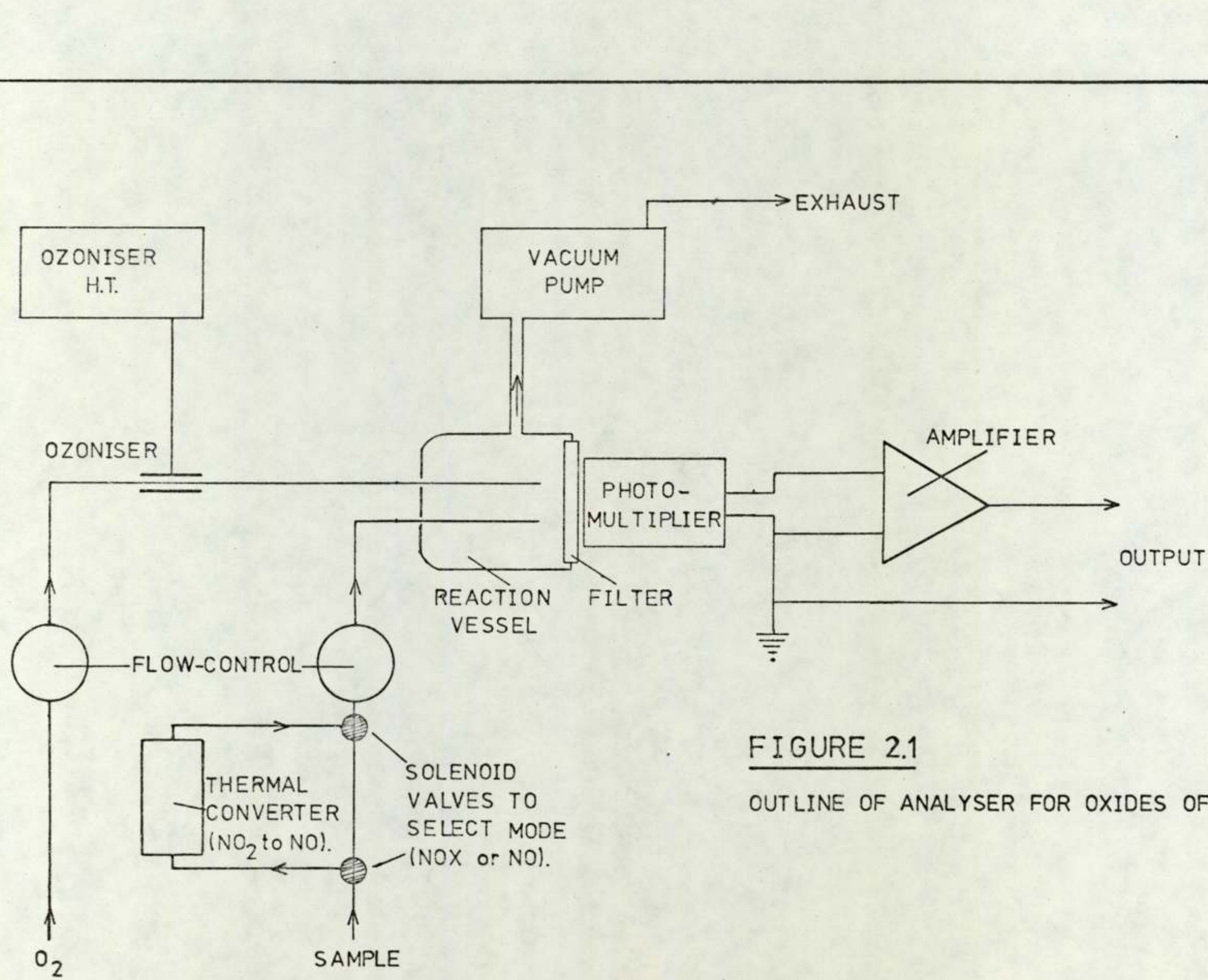

FIGURE 2.1

OUTLINE OF ANALYSER FOR OXIDES OF NITROGEN

An optical filter in front of the photomultiplier makes the response specific to this reaction and therefore to NO. The flow parameters are set up to give a light emission proportional to the NO concentration. NO_x (NO plus NO_2) is measured as the NO produced by thermal pyrolysis of the NO_2 as it passes down a heated (stainless steel) converter. The diagram (Figure 2.1) shows the instrument schematic.

2.1.2 Analyser for Carbon Monoxide:-
Grubb Parsons MGA2 (Newcastle, United Kingdom)

The instrument is analagous to that described in "Am. Conf. Govt. Hygienists", 4th Edition. It has one range 0 - 100ppm. It has no response to water vapour. Atmospheric fluctuations have a negligible effect. The high selectivity to carbon monoxide derives from the use of the characteristic absorption-spectra in the infra-red. The zero point is stabilised by double compensation, and sensitivity is electronically adjusted for temperature drift.

The arrangement is shown in Figure 2.2. Infra-red radiation from the lamp passes alternately through the chopper disc into either the sample vessel(4) or reference vessel(5). The reference does not absorb the IR; it contains N_2. Either beam enters the diffuser(7), and thence the first section(9) of the receiver block(8). The CO in the first section absorbs radiation of wavelengths at the band centres of the CO spectrum. The longer second section(10) absorbs the remainder, which is chiefly from the band flanks. The energy absorbed by the CO in each section produces heating and expansion; the sections

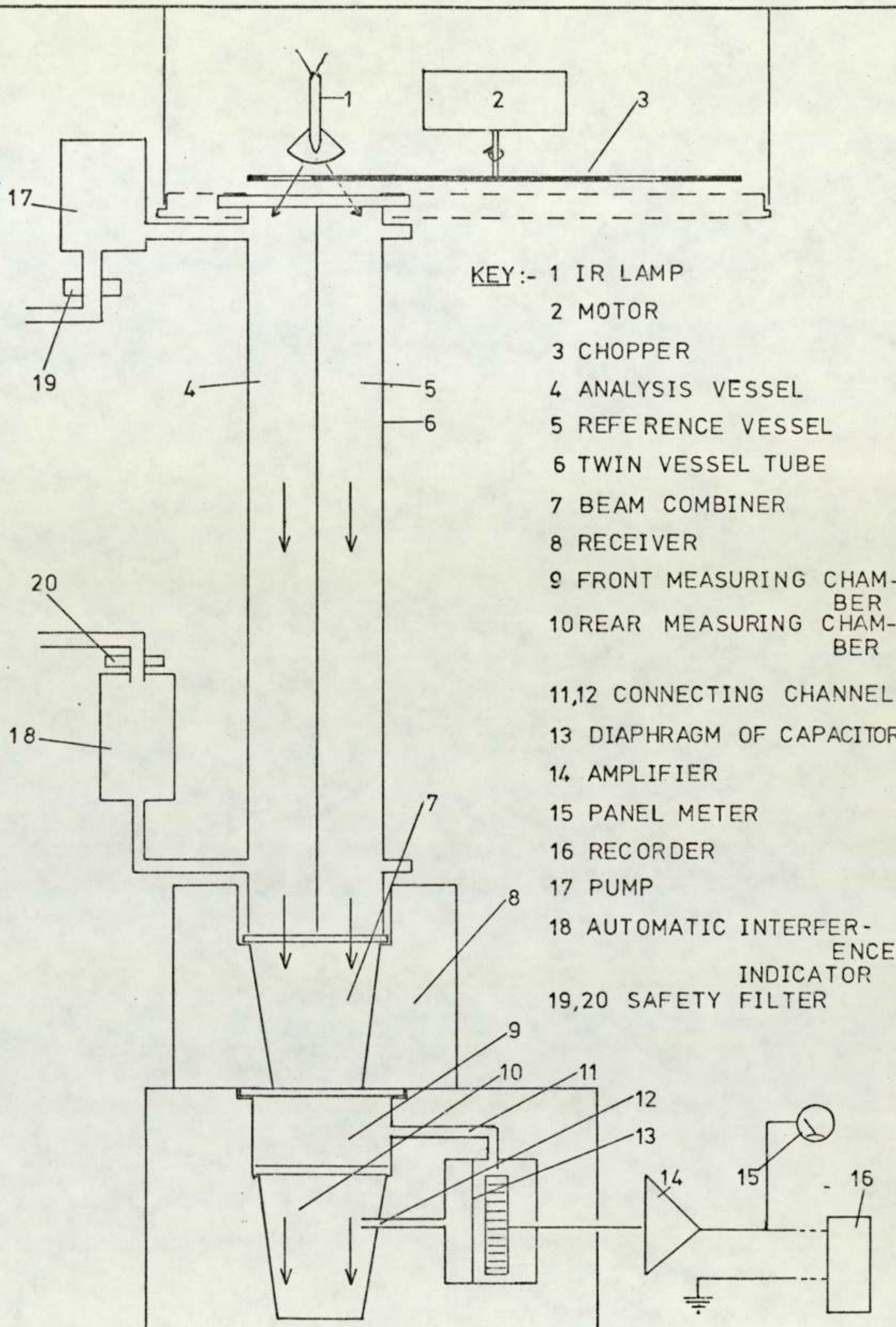

FIGURE 2.2 OUTLINE OF ANALYSER FOR CARBON MONOXIDE

are separated by windows but connected by tubes to the opposite sides of a diaphragm. This moves according to the pressure difference. The geometry and concentration of the CO in each section are arranged to give equilibrium when the sample vessel(4) contains no CO. When there is CO present in the sample, it absorbs band-centre radiation; the first section(9) is affected and the diaphragm moves. In practice the radiation is modulated and the oscillations of the diaphragm measured as capacitance, amplified and displayed as a DC signal.

2.1.3 Analyser for Total Hydrocarbons:-
Analysis Automation Model 521 Total Hydrocarbon Analyser (Oxford, United Kingdom)

This uses a hydrogen-air flame in a flame ionisation detector to measure total organics. It does not respond to other gases such as CO, CO_2, NO, SO_2 and water vapour. The detector response to molecules of the same carbon number is roughly the same; oxygenated compounds give a smaller response. The instrument has four ranges from 1ppm to 1000ppm methane, and is linear over the range 0 - 1ppm to 0.1% full scale.

The sample is passed into the hydrogen flame; a potential difference is applied between the jet and a collector electrode. The ions normally present give a standing current. When organic compounds (with a CH bond) are present, the ion current increases in proportion to the number of carbon atoms in the flame. The flow rates and cabinet temperature are held constant to maintain steady conditions.

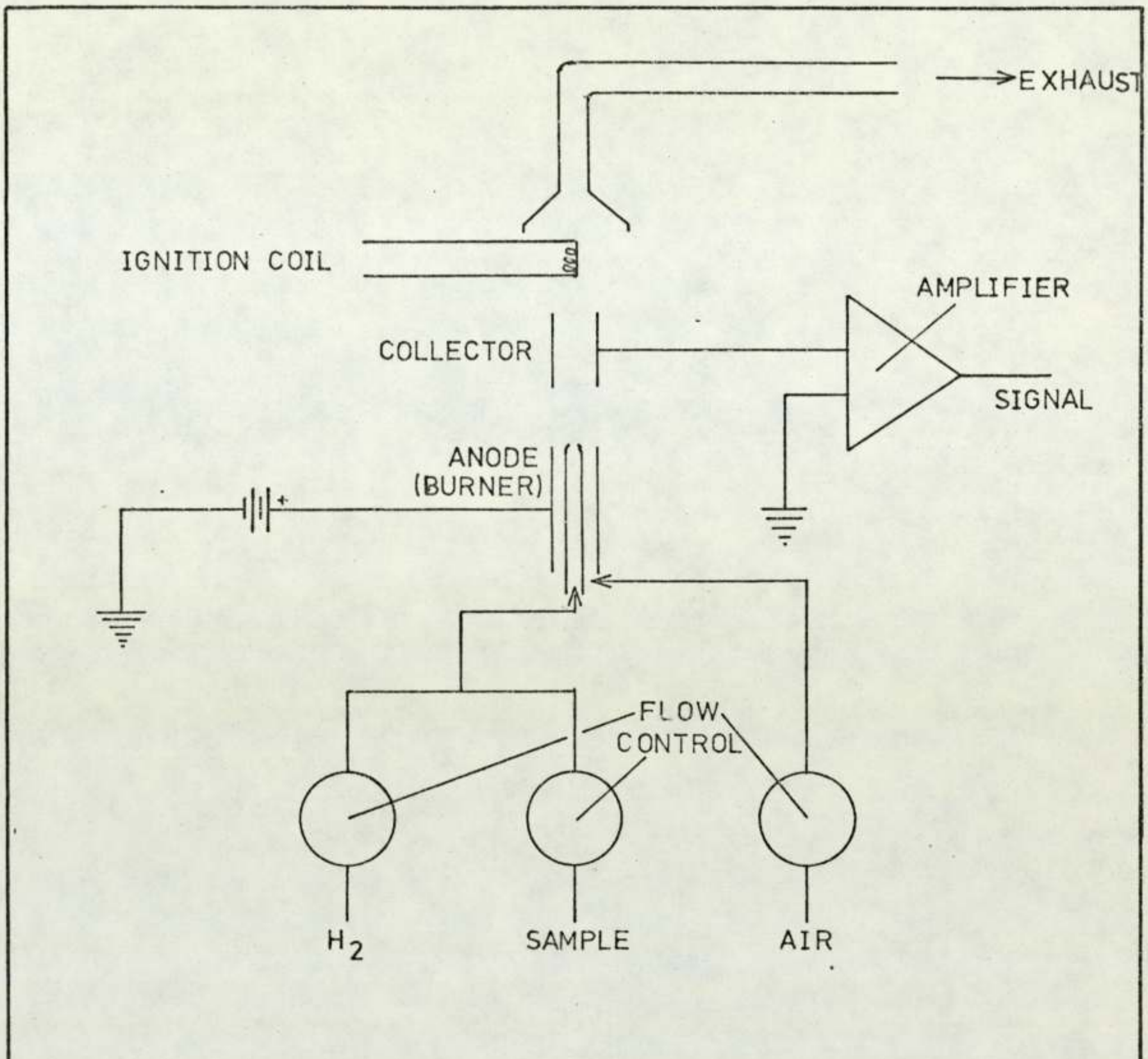

<u>FIGURE 2.3</u> OUTLINE OF ANALYSER FOR HYDROCARBONS

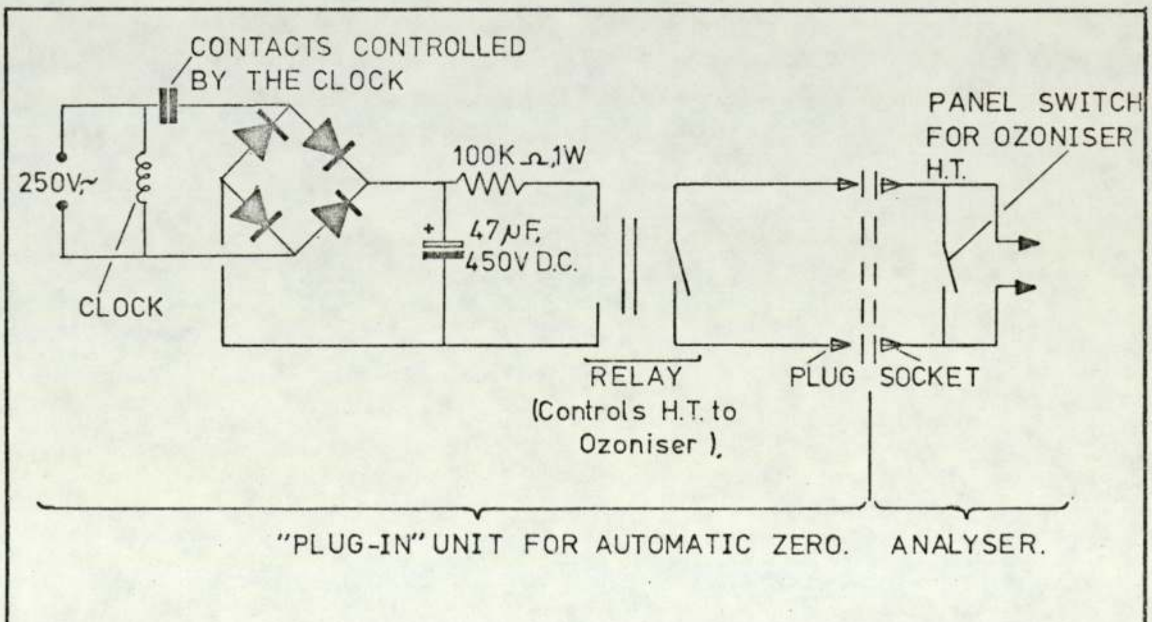

<u>FIGURE 2.4</u> AUTOMATIC ZERO CHECKER FOR NO/NO_X ANALYSER

Figure 2.3 shows an outline.

2.2 Zero Measurement

2.2.1 NO - NO_x Analyser

The NO - NO_x Analyser was zeroed by switching off the power supply to the ozonator. Production of ozone ceased and the response fell to zero. The zero was that current remaining after subtraction of a standing current from the photomultiplier dark current.

The noise and drift depended on the ambient temperature of the machine and the degree of moisture present in the photomultiplier housing. The latter continually collected water by condensation and caused most of the trouble experienced with this machine. A time clock was wired to switch off the power supply to the ozonator every six hours to give an automatic zero check, (Figure 2.4).

2.2.2 CO Analyser

The CO Analyser was zeroed originally with cylinder N_2. Later a tube of silica gel followed by Hopcalite (Lamb et al., 1920) was used to dry the sample air, and oxidise any CO to CO_2. The CO free air thus gave the zero. A tube of 2.5cm diameter holding 10cm silica gel followed by 8cm Hopcalite gave the same readings on laboratory air as cylinder N_2. It gave consistent results with easy portability in the field.

2.2.3 HC Analyser

The HC Analyser uses a hydrogen/air flame and the sample is injected directly into the fuel line. Zeroes were measured as the ion-current existing in the flame without the passage of sample gas: the sample-pump was simply turned off. The zero had to be taken on the same sensitivity range as that used for monitoring.

2.2.4 Frequency of Zeroes

The NO/NOx machine was zeroed automatically every six hours. The CO and HC Analysers were zeroed daily as part of the routine checks.

2.3 Calibration Checks

2.3.1 Introduction to the Calibrations

It was decided for convenience that the instruments when on site would be calibrated with mixtures of gas made up in the ppm range. This assumed that such mixtures delivered from cylinders were stable and that the instrument responses were linear. Cylinders of standard gases, as listed in Table 2.1, were purchased from Rank-Precision Industries. They do not necessarily deliver a mixture of composition as prepared since absorption losses and decomposition may occur. Indeed a mixture of 100ppm NO and 100ppm NO_2 in N_2 was unstable: the NO_2 disappeared in a few weeks.

To cross-check the concentrations delivered from the cylinders,

TABLE 2.1

Commercial Gas Mixtures Purchased and

Concentration Levels at which Calibrations were Needed

Pollutant	Concentration[1]	Field Sensitivity
NO, NO_2	100ppm $\pm$ 5% NO, in N_2 100ppm $\pm$ 5% NO_2, in N_2	<1ppm, often <.25ppm
NO	100ppm $\pm$ 5% NO, in N_2	<1ppm, often <.25ppm
CO	50ppm $\pm$ 5% CO, in N_2	<10ppm
HC	8ppm $\pm$ 5% CH_4, in N_2	<10ppm

Note 1: Generally above field level as harder to prepare and store at lower concentrations.

carbon monoxide and nitric oxide were diluted in N_2 to the ppm level; this required a two-stage process. The commercial mixture was diluted in one step to measure the instrument linearities at sensitivities near to that required in the field. Exponential dilution was used to check the NO/NO_x analyser below 1ppm. The HC Analyser was used as a carbon monoxide analyser to compare the CO and CH_4 standards.

2.3.2 Two-Stage Dilution: CO and NO

Precise dilution by 10^5 times requires careful pressure regulation and flow control (Am. Conf. Govt. Hyg., 4th Edition). A small part of the mixture produced by the first stage (Figure 2.5) was diluted in the second (Figure 2.6), with the surplus led to waste down a capillary. The latter kept the pressure above atmospheric to aid flow control. Micrometer gas-valves (Hoker) were used for fine flow control. The diluent, N_2, was held at a standing pressure in the line from the cylinder regulator to the input control valve. Soap bubbles (Figure 2.6) were injected from the teat and timed; their pressure was measured on the water manometer. The appendix kept the feed line free of surplus soap solution. Wherever possible materials were glass, teflon or stainless steel. Either of the two mixing ranges could be selected using the tap on the first board to change the rotameter in use. The second stage gave a total flow equal to the sample flow of the instrument under test. The flow-meter capacities are listed in Table 2.2. Scatter arising from the use of several rotameters was increased for the oxides of nitrogen work by the lack of a non-corrosive pressure-regulator.

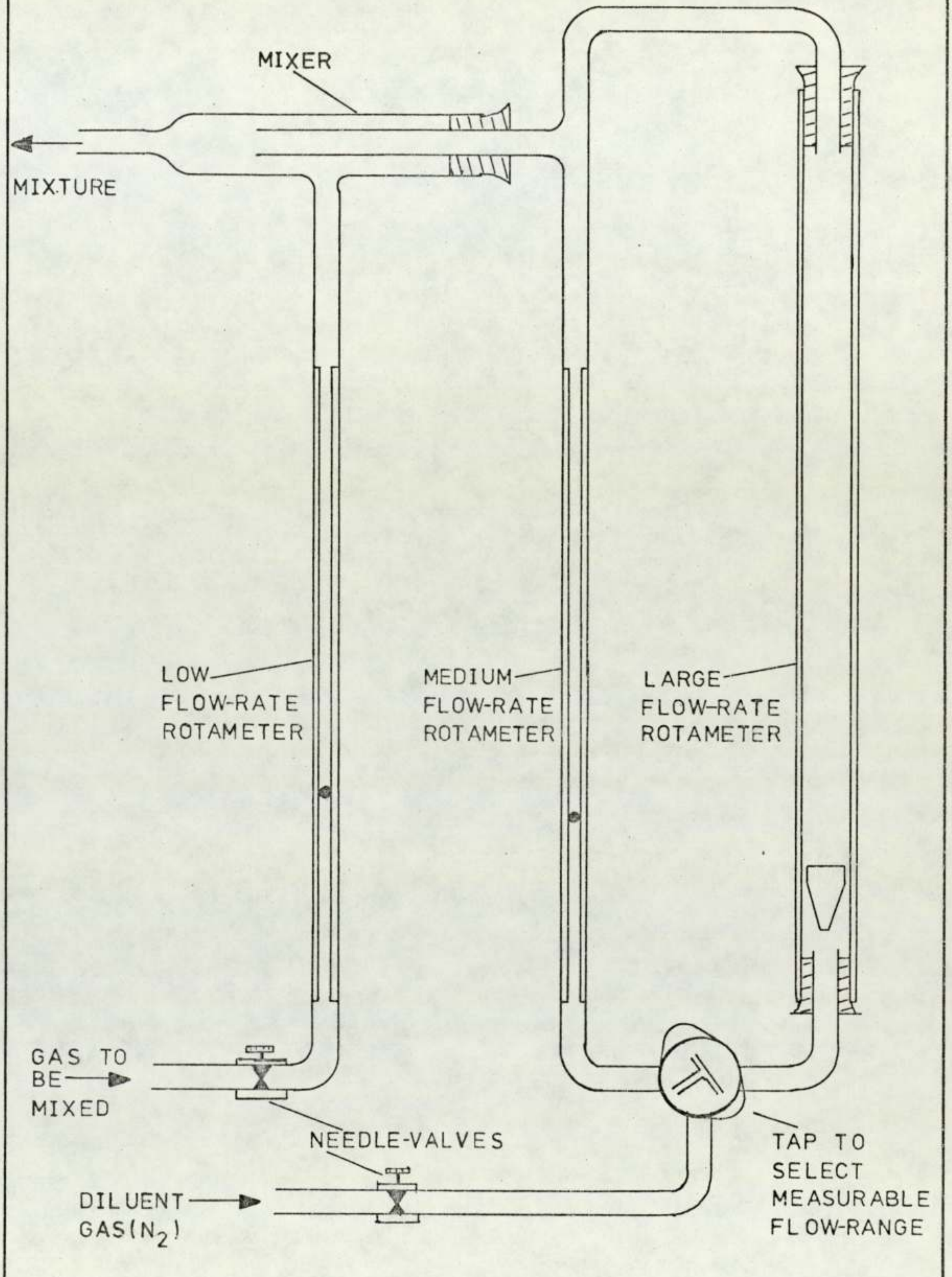

FIGURE 2.5 FIRST-STAGE DILUTION APPARATUS

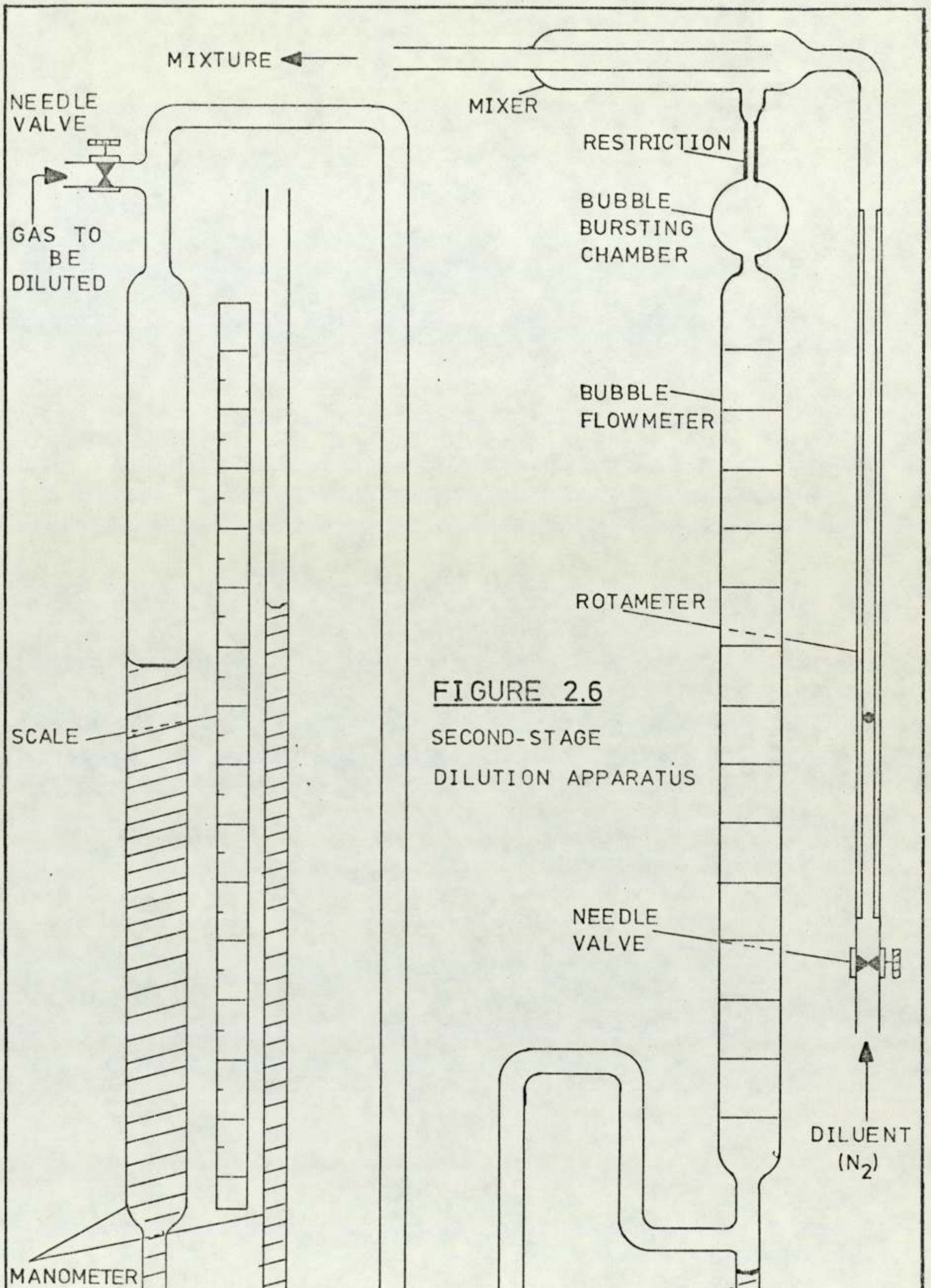

FIGURE 2.6

SECOND-STAGE DILUTION APPARATUS

TABLE 2.2

Flow Meter Capacities

Flowmeter	Flow Range AIR, $ml\,min^{-1}$, STP	Comments
Rotameter[1] (A Glass)	5 - 45	Poor float stability
Rotameter[1] (B St-St)	50 - 450	Good float stability
Rotameter[1] (C St-St)	150 - 1300	Good float stability, covers I2A, MGA2 input
Rotameter[2] (Metric 7P)	1000 - 9000	Good float stability
Bubble meter[3]/Stop-watch	2.4 - 180	Assume absorption into soap solution reaches negligible steady state

Notes 1: Glass Precision Engineering Limited, Hemel Hempstead, Hertfordshire, United Kingdom.

2: Rotameter Manufacturing Company Limited, United Kingdom

3: Constructed from 25ml burette, ~1cm i - d;
Minimum flow depends on bubble life time;
Maximum flow on shortest stop-watch period.

The instruments were calibrated on standard gases (Table 2.1). On analysis by these instruments, the concentration measured in the flow-mixture was lower than expected on the basis of the flows and extent of dilution.

For agreement between instrument analysis of the flow-mixture and the calculated flow-concentration it is necessary that:-

1. Standard gas is correct, so that instrument reads true;
2. Correct calibration of flow-meters so that the calculated concentration derived from the dilution is correct;
3. Absence of leaks and absorption on the walls or in the bubble meter.

The instrument responses were low, with about 10% scatter:-

1. 12A/NO_x was 70% of expected flow-dilution concentration;
2. 12A/NO was 73% of expected flow-dilution concentration;
3. MGA2/CO was 60% of expected flow-dilution concentration.

The low readings imply that:-

1. Instrument reads low: cylinder mixtures were of a higher concentration than as labelled.
2. Incorrect calibration, or error accumulation: reading large and small flows near ends of rotameters.
3. Leaks: not considered significant. Absorption losses should

appear also in the single stage dilution which follows, but the deviations are much smaller, so unlikely.

It is not known which is responsible for the discrepancy, but the important point is that standard gas mixtures as commonly used in air-pollution research are not completely reliable (e.g. disappearance of NO_2 as above), and that to cross-check instruments by dilution of the neat gas requires more sophisticated apparatus than that used here. The work does suggest that the concentrations as reported could be 30 to 40% low. For the field work the instruments were always calibrated on the standard gases because the two-stage dilution was felt to be only a little better than an order-of-magnitude check.

2.3.3 Single-Stage Dilution of ppm level mixtures of CO and NO

Standard gases (Table 2.1) were diluted in the bubble-meter board (Figure 2.6) to check the linearity of the instruments. Within the concentration range covered (1 - 15ppm CO; 0.5 - 10ppm NO), the instruments gave a linear response. Table 2.3 summarises the results (Figures 2.7, 2.8, 2.9).

Rotameters (Linford, 1961) give a volume-flow reading which varies with temperature as $T^{1/2}$, pressure as $P^{-1/2}$ and density of the gas as $\rho^{-1/2}$. The apparatus was used at pressures within 3% of atmospheric pressure. Temperature effects are negligible since the flow-meters were calibrated in the laboratory. Unsteadiness of the float relative to the float height can be 1% at large flows, and exceed 5% at low flows. Allowing for the pressure effect the error is $\sim$3-5 %

TABLE 2.3

One-Stage Dilutions: Discrepancy between the Instruments' Response and the Calculated Concentration (Calculated from the Flow Rates and Standard Gas Composition)

Instrument	Observation Range, ppm	Least Squares Line[1] of Instrument Response to Calculated Concentration m	c	s	Source Gas, ppm in N_2
MODEL I2A/NO	0.07 - 9	0.900	0.0513	0.0513	100ppm,NO + 100ppm,NO_2
MGA2/CO[2]	3 - 15	0.988	-0.058	0.257	50ppm.CO

Note 1: Instrument reading = m.calc-conc + c, with standard deviation s.

Note 2: CO Analyser 0 - 50ppm, as modified for field use (Chapter 3)

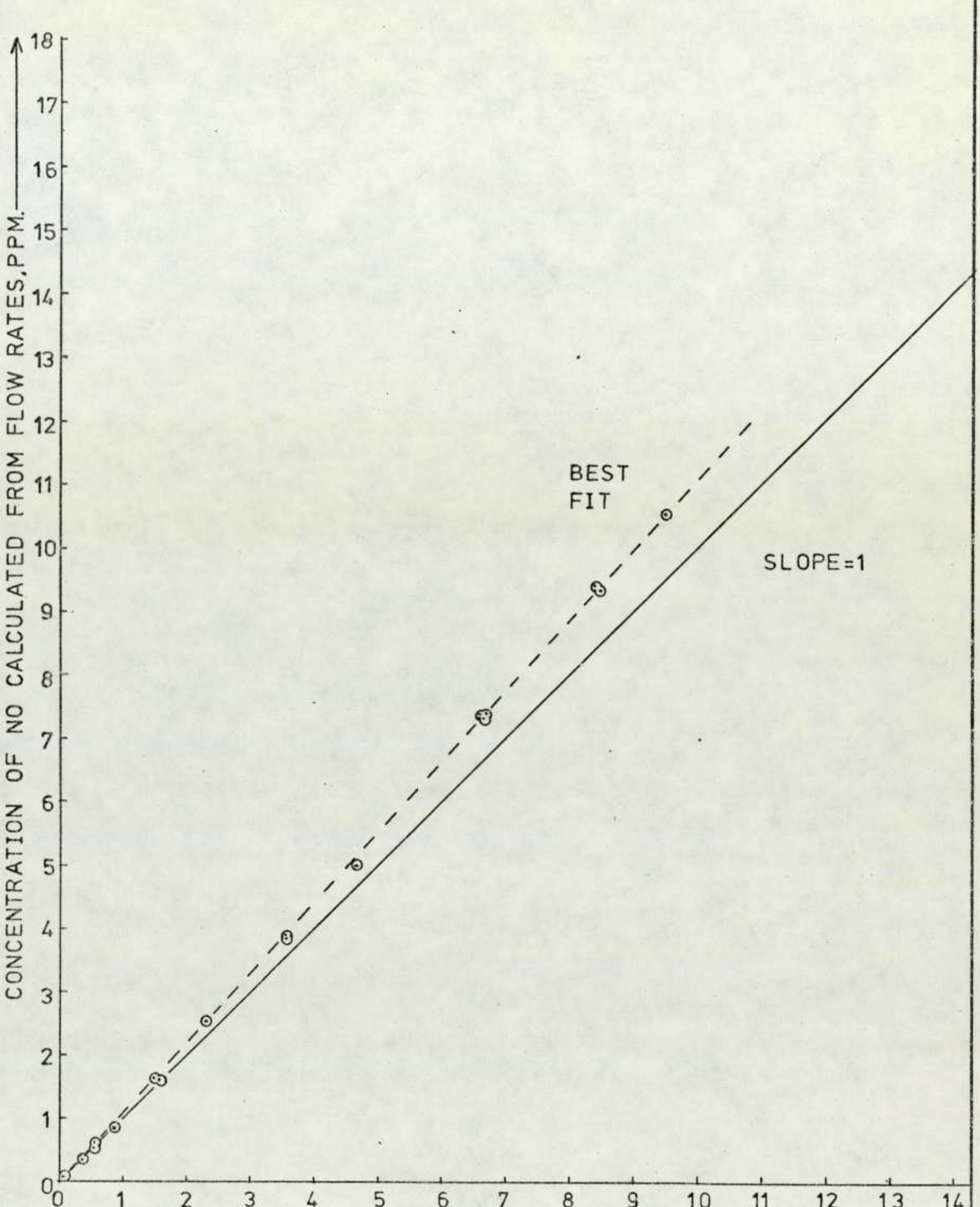

FIGURE 2.7 CHECK OF LINEARITY OF THE OXIDES OF NITROGEN ANALYSER (NO mode) BY SINGLE STAGE DILUTION OF STANDARD GAS (100 ppm NO in N_2)

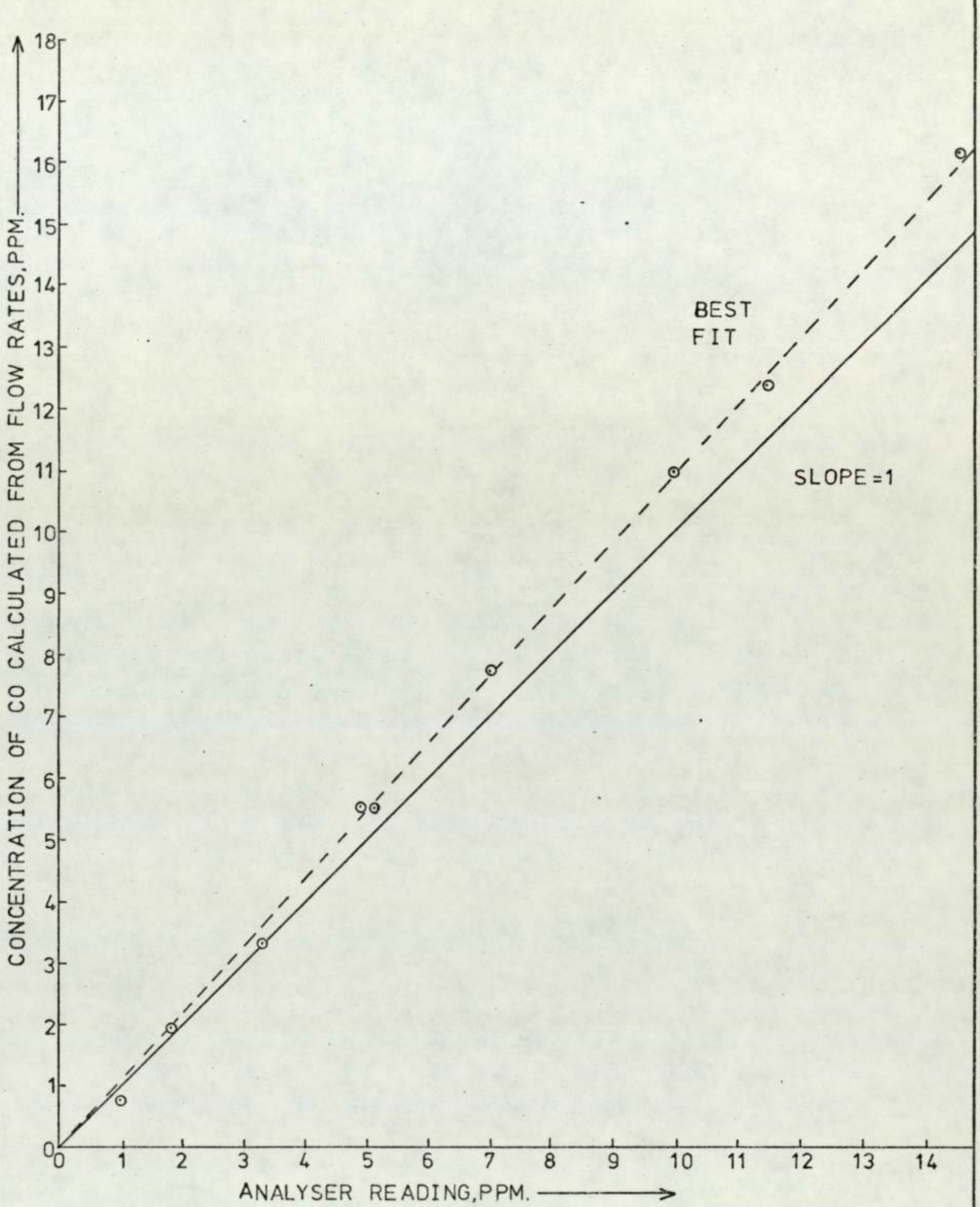

FIGURE 2.8 CHECK OF LINEARITY OF THE CARBON MONOXIDE ANALYSER (0-100 ppm fsd) BY SINGLE STAGE DILUTION OF STANDARD GAS (50 ppm CO in N_2)

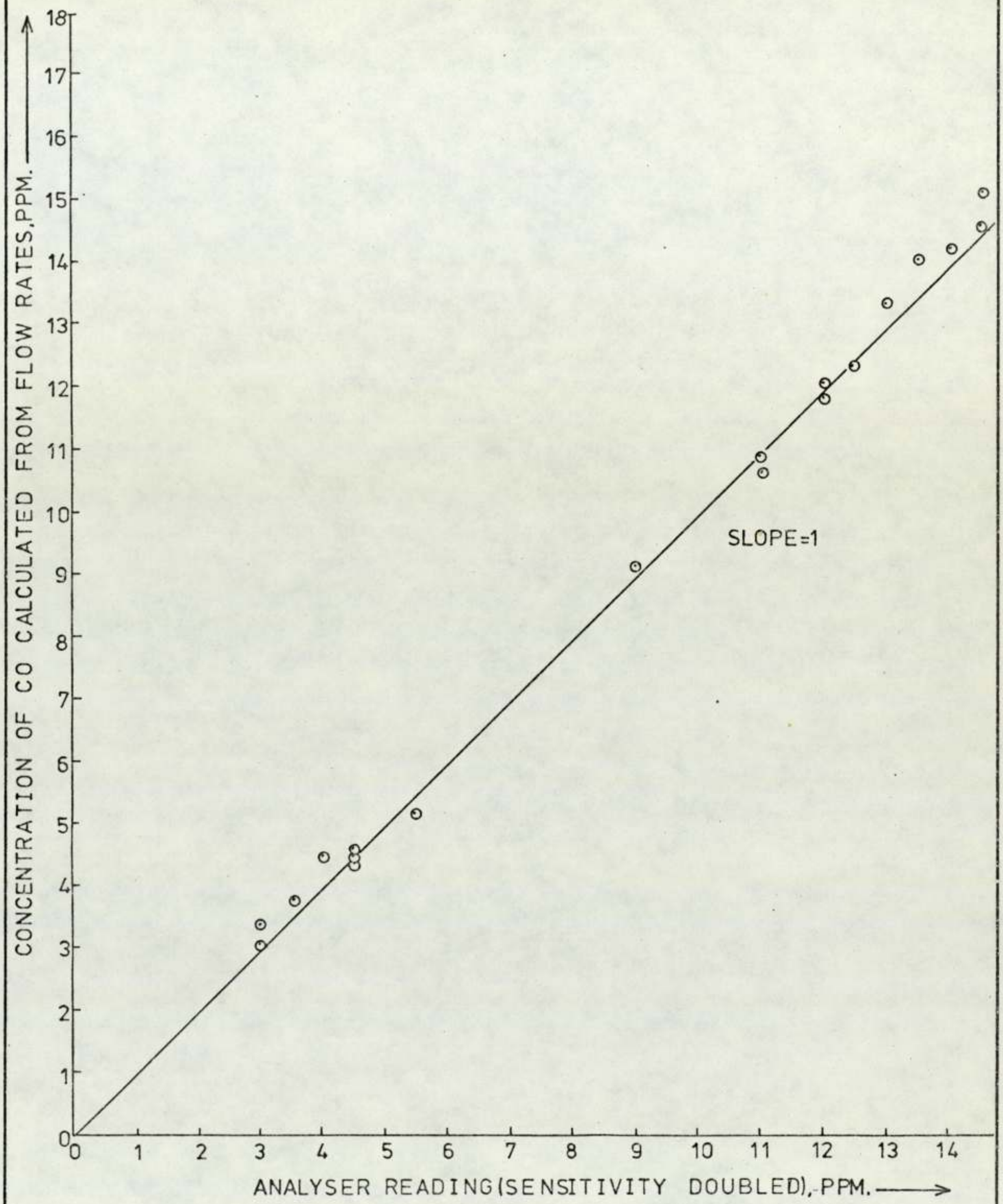

FIGURE 2.9 CHECK OF LINEARITY OF THE CARBON MONOXIDE ANALYSER (0-50ppm fsd), AS USED IN THE FIELD WITH SENSITIVITY DOUBLED, BY SINGLE STAGE DILUTION OF STANDARD GAS (50 ppm CO in N_2)

Thus single-stage dilution has an error of $\sim$5%, and two-stage, $\sim$ 7%.

The single-stage dilution showed, for the CO Analyser, good linearity within this scatter: for the NO/NO_x analyser there was a systematic deviation of around 10%; this may be partly due to absorption losses.

2.3.4 Exponential Dilution

When a gas of concentration C_o is passed into a well mixed vessel of volume V and the supply is then suddenly changed to diluent, the concentration C at time t after the start of dilution is:-

$$C = C_o \exp(-Qt/V),$$

(Fontijn et al., 1970), where Q is the volume flow rate. Fontijn et al., found the NO monitor they made was linear from 4.10^{-3}ppm to 100ppm. Figure 2.10 shows a plot of $\log_{10}(C)$ against t, obtained by the dilution of standard gas (Table 2.1) with nitrogen. With perfect mixing and no absorption-desorption effects the graph should be linear. In fact the curvature increases at lower concentrations where the time since dilution began is ten times the time constant V/Q (200 sec as against 180 sec). During one run the mixer was heated: the concentration rose rapidly, consistent with desorption.

The NO/NO_x analyser appears to be linear down to 0.25ppm on the NO mode, and 1ppm on the NO_x mode. The curvature below these levels is thought to arise from the effects (e.g. inadequate mixing and

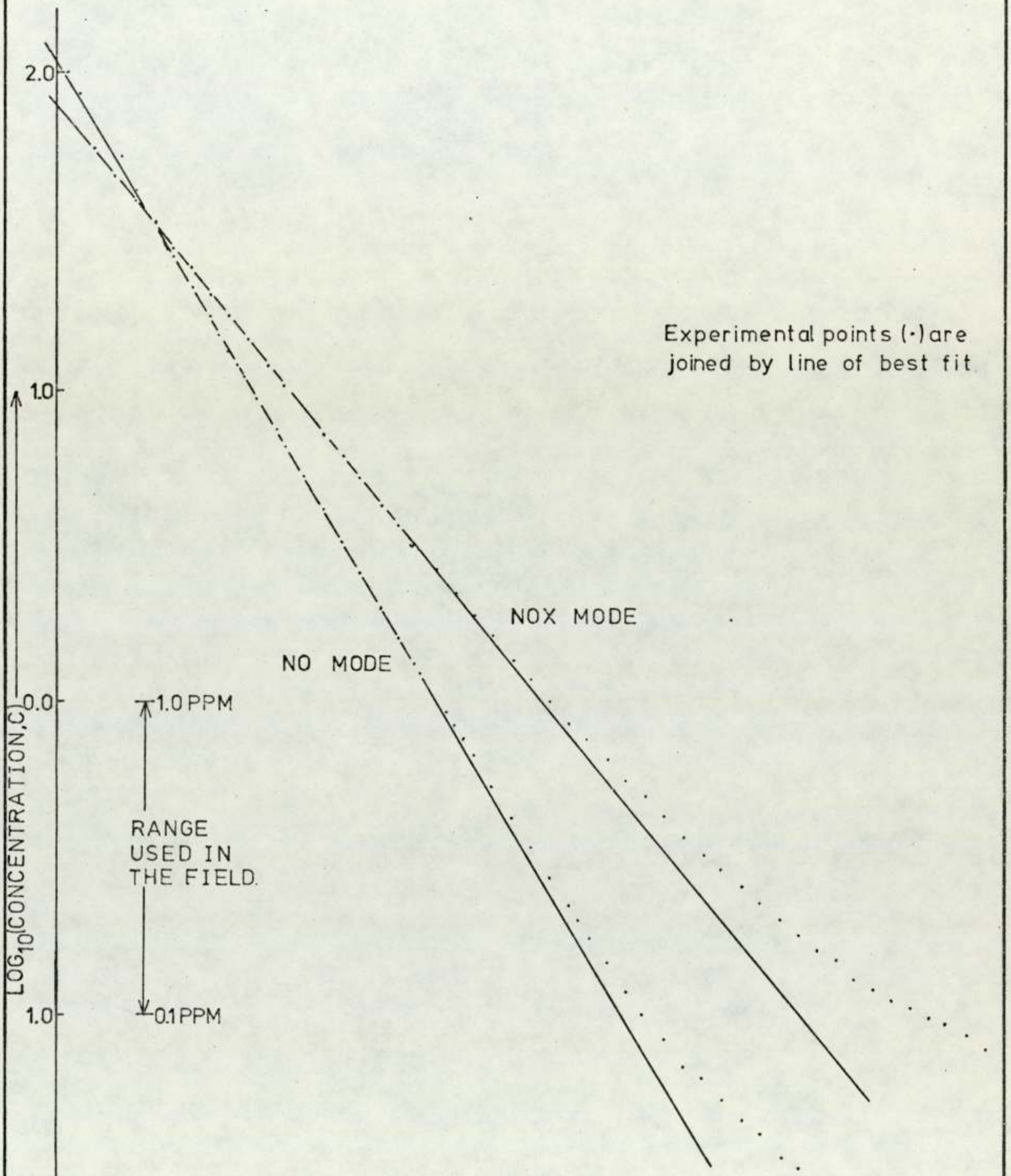

FIGURE 2.10 CHECK OF LINEARITY OF THE OXIDES OF NITROGEN ANALYSER BY EXPONENTIAL DILUTION

absorption-desorption) of the long mixing-time needed to reach that level rather than any non-linearity of the instrument.

2.3.5 Cross-Check of CO and HC Calibrations

The total HC Analyser, purchased later in the project, was calibrated on our own standard (8ppm CH_4 in N_2). Cross-checks with mixtures from Transport and Road Research Laboratory were consistent with a linear response and that our standard was valid.

The HC Analyser was adapted to estimate the carbon monoxide content of the standard (50ppm CO in N_2). A nickel catalyst was inserted in the hydrogen-fuel/sample line before it entered the burner. Hydrogen from the fuel reduced the carbon monoxide present as the mixture passed over the heated catalyst (Porter and Volman, 1962). The results were:-

CO standard over cold catalyst	1ppm
CO standard over hot catalyst	46ppm
CH_4 standard over cold catalyst	7ppm
CH_4 standard over hot catalyst	20ppm

The latter discrepancy is thought to be impurities in the methane standard, since with fuel alone no change with catalyst temperature occurs. The methane standard did not contain carbon monoxide however, for it gave no response on the carbon monoxide analyser.

It was concluded that the methane and carbon monoxide standards were mutually consistent, although the methane standard appeared to have an impurity not normally detected by the FID, unless reduced by the hydrogen over the hot catalyst. This reinforces the earlier comments on the problems experienced with cylinder supplies of standards.

2.4 Summary

Absolute calibration requires careful design with regard to absorption of constituents, flow stability and the measurement of large and small flows before mixing. More sophisticated equipment is now available: the reader is referred to "Am. Conf. Govt. Hygienists", 4th Edition.

Absolute concentrations were checked by dilution of CO and NO down to 5ppm; the standard gases were checked to better than an order of magnitude.

Linearity was within 10% for the NO/NO_x analyser and 5% for the CO Analyser in the ranges 100 - 1 and 50 - 3 ppm, respectively. The commonly used cylinders of standard gases, although used in the field, are felt to be not completely reliable.

CHAPTER 3

FIELD OPERATION OF INSTRUMENTS AND ABSTRACTION OF THE RESULTS

The instruments were left unattended at various sites to record data. We shall discuss the nature of the sites and their effect on both the performance of the instruments and the attention they required. The chart records were abstracted manually and processed by computer. We shall outline the programme to show how this method of unattended field monitoring with manual data abstraction determined the calculations required, and how the results were output to storage ready for later use. These results, together with those calculated from emissions and dilution, will be discussed in Chapter 6.

3.1 Sites Used for Routine Monitoring

The project began with little knowledge of the levels of gaseous pollutants expected. The site at Salford Circus (Map: Figure 3.1) provided a junction monitor while that at Murdoch Point was further away to give a distance effect and a city "background" level. A further site at Slade Road Schools was used but the results were not accurate for technical reasons.

An unattended monitoring site must have:-

1. Security against vandalism;

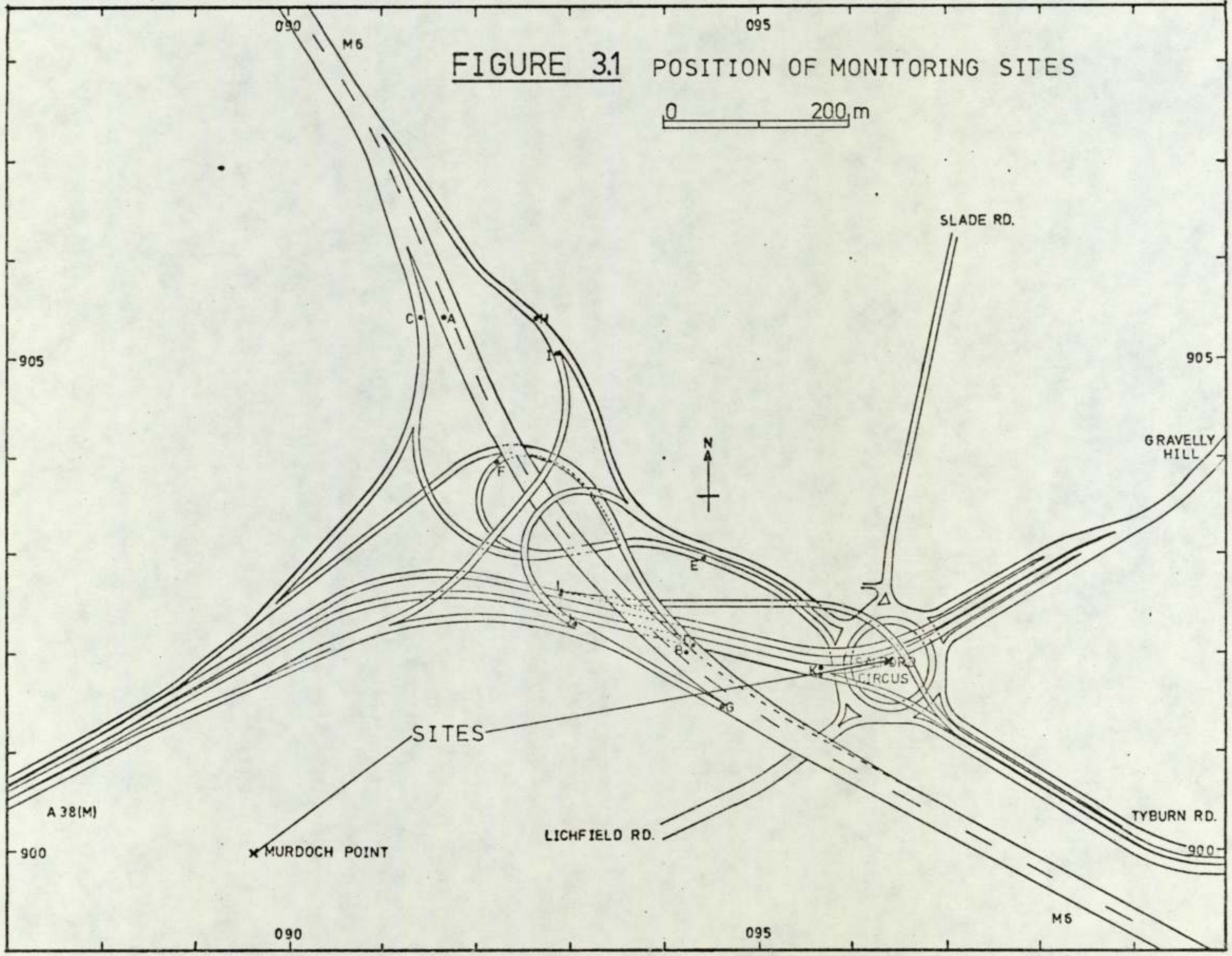

FIGURE 3.1 POSITION OF MONITORING SITES

2. Mains supply;

3. No severe temperature drift to upset instruments.

If the project has a specific source to monitor there should not be interfering sources nearby or the results will be hard to interpret. Buildings of potential use may be privately or publicly owned: in either case special facilities such as lockable doors and mains supplies may be needed; this requires much negotiation with public bodies. The positions available for monitoring are therefore restricted. The choice of sites for monitoring programmes larger than the present project has been analysed theoretically (Bibbero and Young, 1974).

The site at Salford Circus (Map: Figure 3.1) was used as the intersection monitor. It consisted of a triangular room ($\sim$ 9 square feet available) in the public conveniences at the centre of the roundabout. The equipment was installed with the chart recorders on the walls, the cylinders at the back of the room, the NO-NO_x Analyser on the floor, the CO machine on the wall and the HC Analyser on a shelf aloft (Photograph: Figure 3.2). Inlets were mounted on the roof.

The site at Murdoch Point (Map: Figure 3.1) was further from the intersection. It was less satisfactory as a site to study pollution from the Motorway, for there was an interfering chimney in a building between it and the intersection. It was useful as a guide to the pollution levels in air approaching the intersection from the city. The equipment was placed at the top of the building in the winch room ($\sim$ 50 square feet available).

FIGURE 3.2 EQUIPMENT IN THE FIELD

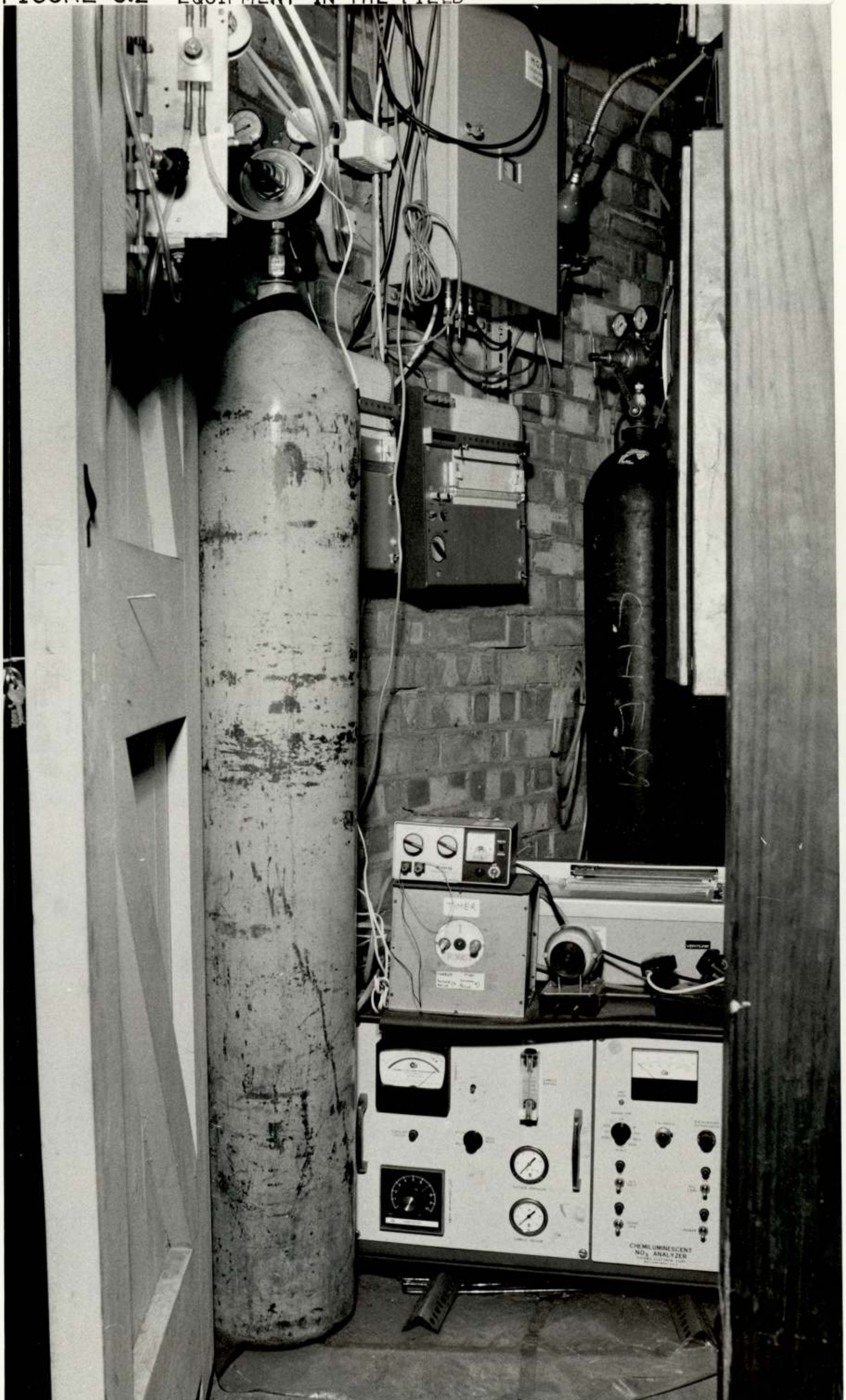

3.2 Method of Operation

Chart recorders were linked to each instrument. A clock was fitted to the NO-NO_x Analyser to switch it alternately from the NO to the NO_x mode and back; the results for each mode were distinguished by colour on a dual pen recorder. During daily visits the charts were labelled and collected, and zero and calibration readings taken. Filters (Whatman 3.7 GF/A) in the gas inlets were changed regularly: sample lines were Teflon for HC and NO_x, and PVC for CO. Experience showed many items might be left undone so a checklist (Table 3.1) was used. The site determined ease of checking: that at Salford Circus was rather cramped while at Murdoch Point space was ample, although a hand winch was needed to lift equipment into the room.

3.3 Field Performance of Instruments

The CO and HC Analysers gave little trouble. The No-NO_x Analyser required constant servicing because there was an unknown source of condensation so that water slowly collected on the photomultiplier tube. This showed itself as noise and spikes in the signal. Intermittant faults such as noise or drift were especially hard to find as they were often only apparent from the charts when the daily visit was made, yet the machine could appear to be satisfactory. Unattended operation increased the fraction of monitoring time during which faults or incomplete data were produced, but it did give periods of continuous data with limited manpower.

The CO Analyser was run on a 0 - 50ppm scale using the chart recorder on a more sensitive scale with load resistors wired as in

TABLE 3.1

Checklist for Routine Monitoring

<table>
<tr><th>Chart Recorders</th><th>Oxides of Nitrogen Analyser</th></tr>
<tr><td>Paper, ink, pens
Electric connections
Drive - Speed
Sensitivity
Recorder zero = instrument zero
Chart labelled - date, time, FSD, speed, site, mode, gas</td>
<td rowspan="3">Chart recorder
Mode:- AUTO or NO/NO_x
Pens agree with mode
NO_x = Red
Connections: 10V+ to X1,
10V- to X2,
10mV- to Earth
Sample flow
NO_x converter on, temperature set
Reaction chamber vacuum
O_2 cylinder tap on
O_2 pressure
Gas leaks?
O_3 generator: on only if O_2 flowing. If automatic dark current, O_3 generator switch off, and clock plugged in to instrument.
Dark current - steady and low
Sensitivity
Gas filters clean
Exhausts connected
Calibration: standard gas</td></tr>
<tr><td><u>Hydrocarbon Analyser</u>

Chart recorder
H_2, Air, sample pressures
Cylinder taps on
Sample pump on
Sample tube connected
Gas leaks?
Cabinet warm
Flame alight
Zero: sample off
Calibration: standard gas</td></tr>
<tr><td><u>Carbon Monoxide Analyser</u>

Recorder
Sample tube connected
Filter clean
Cabinet on inside
Zero: silica gel/Hopcalite
Calibration: standard gas</td></tr>
</table>

Figure 3.3. The sensitivity was not ideal but a further increase was unwarranted because of zero drift. The arrangement gave linear results (Figure 2.9).

Table 3.2 shows the drift experienced with the machines in the field.

3.4 General Requirements for a Programme to Process the Charts

Although the signal varied rapidly (Figures 3.4, 3.5, 3.6, 3.7), analogue smoothing was not used as it would have obscured instrument noise and intermittant faults. To cope with this variance of signal (Table 3.3) a fast chart speed was used (typically 30cm h^{-1} for NO-NO_x; 12cm h^{-1} for CO, HC) and up to 30 points abstracted per hour. The chief task of the programme was to average these, taking due note of zero and calibration readings.

Any given instrument may be run on any sensitivity range even within a week's monitoring. Zeroes and calibrations may be recorded at any, usually irregular, times as demanded by the quality of instrument performance and the available manpower for checking. Various instruments may be out of action at differing times. It follows that the monitoring data must be sorted by time to eliminate incomplete data rows and to identify the appropriate zero and calibration readings from those taken.

Various chart speeds are used for resolution of the finer parts of the trace so any number of observations per hour may be read in and averaged.

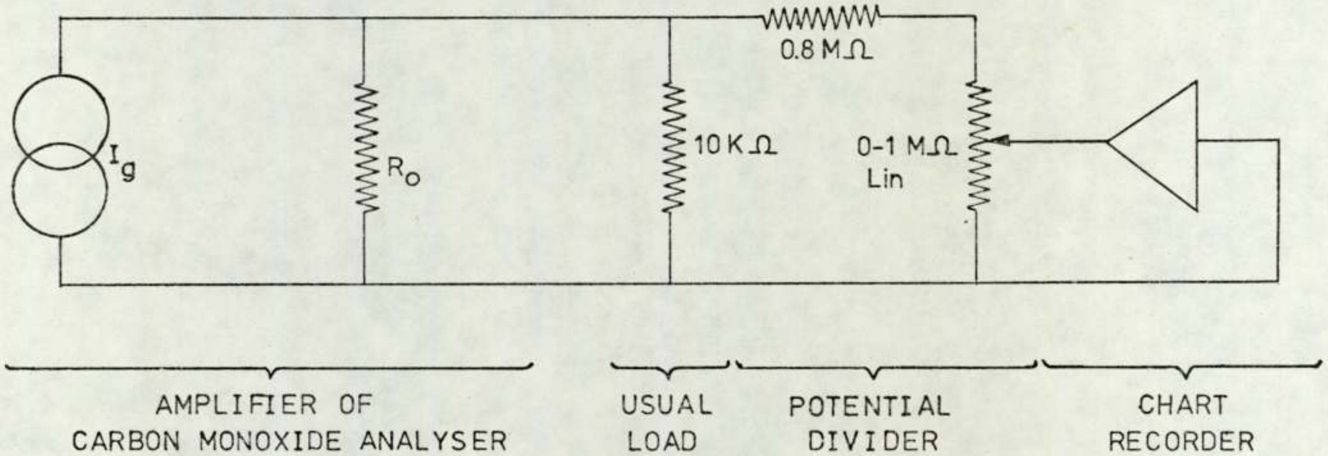

FIGURE 3.3 CIRCUIT TO DOUBLE THE SENSITIVITY OF THE CARBON MONOXIDE ANALYSER

TABLE 3.2

Zero Drift relative to Observed Levels

Gas	Instrument	Zero Drift		Zero Drift ÷ Mean Level		Zero Drift ÷ Maximum Level	
		SC ppm	MP ppm	SC %	MP %	SC %	MP %
NO_x	MODEL I2A	± 0.005	± 0.004	4	15	1	3
NO	MODEL I2A	± 0.005	± 0.004	5	37	1	5
NO_2[2]	MODEL I2A	± 0.010	± 0.008	71	51	12	17
CO	MGA2	± 0.3	± 0.13	10	12	3	4
HC	AA.521	± 0.2	± 0.1	3	2	2	2

Note 1: Salford Circus (SC)
Murdoch Point (MP)

Note 2: NO_2, recorded as (NO_x - NO), shows a larger drift effect because of subtraction.

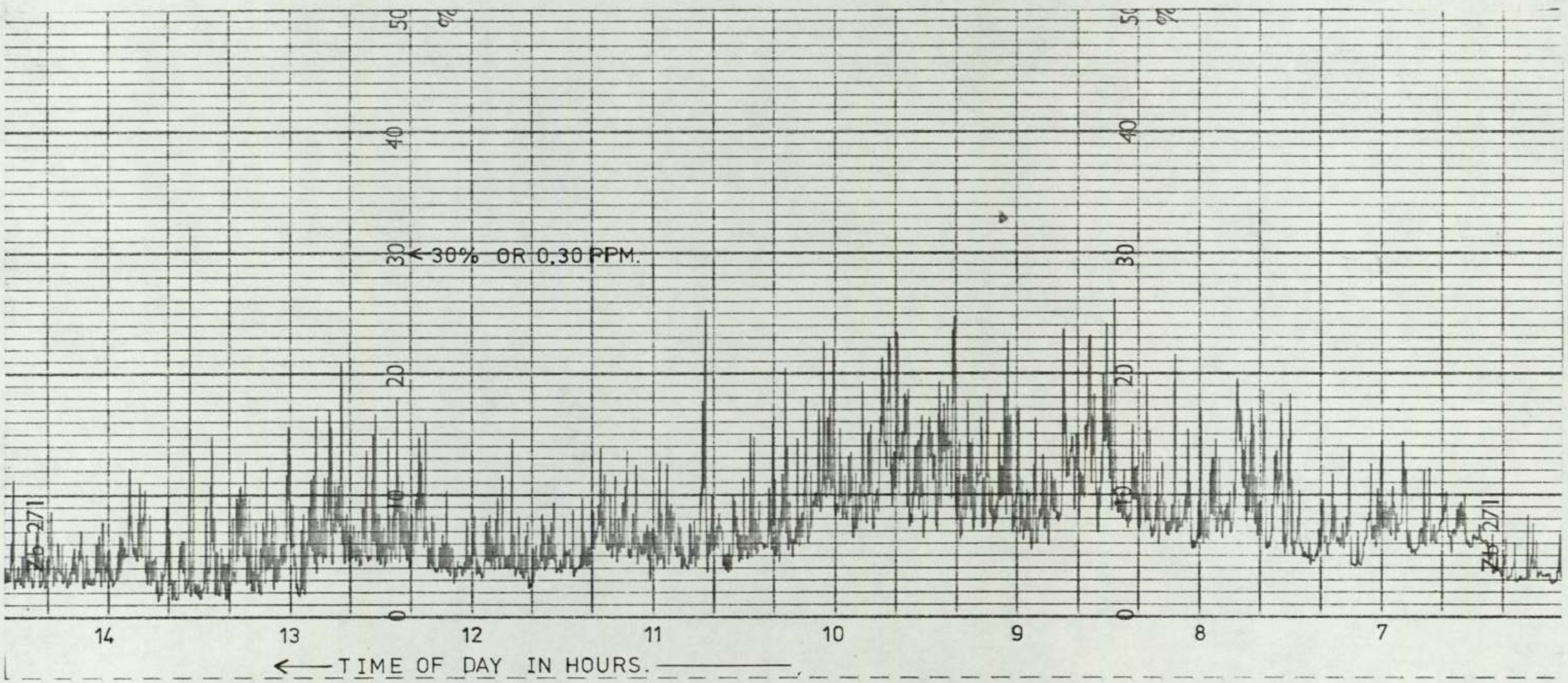

FIGURE 3.4 CHART OF NO_X AS RECORDED ON 17-03-1973 AT SALFORD CIRCUS.

CONDITIONS:- 0-1PPM FSD IS 100% ON CHART; CHART SPEED 3 cm h^{-1}, WHICH IS TOO FAST FOR ACCURATE ABSTRACTION.

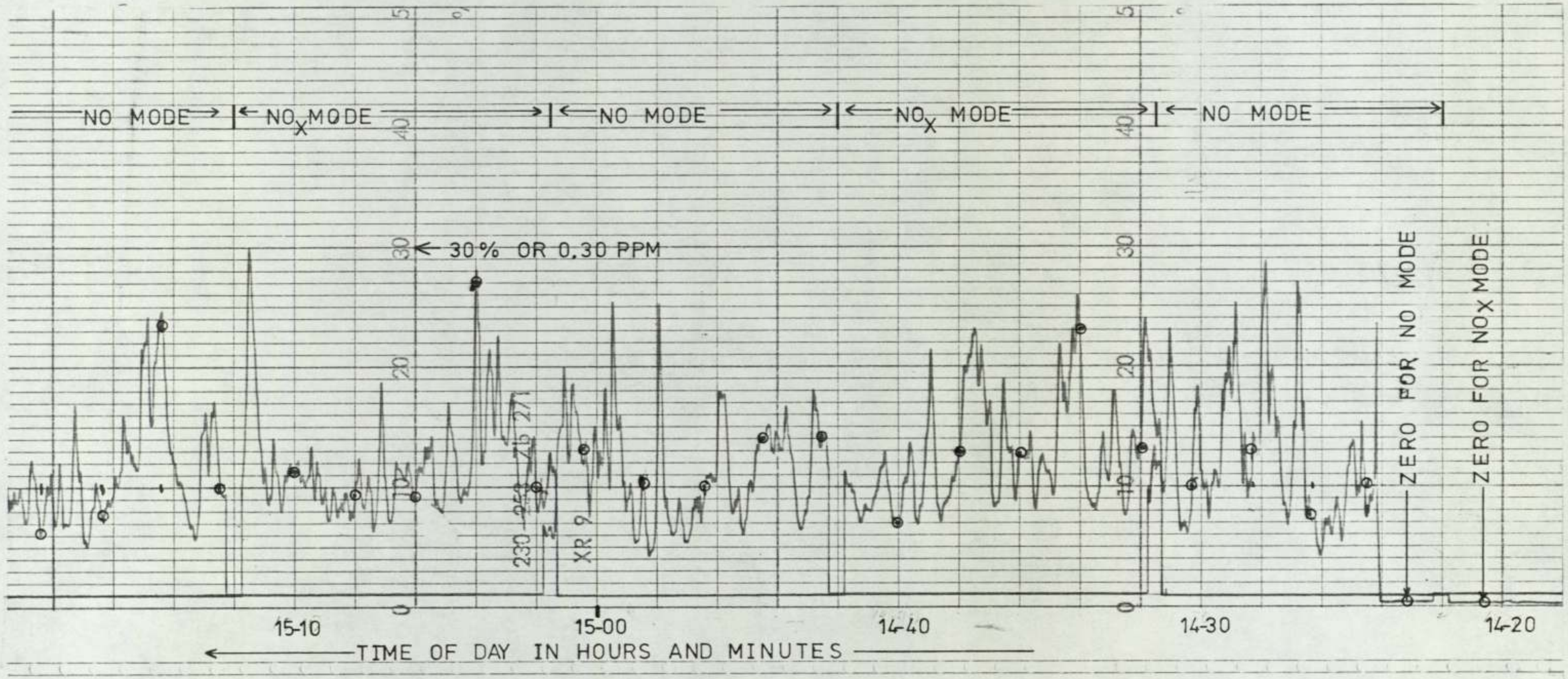

FIGURE 3.5 CHART OF NO AND NO AS RECORDED ON 04 11 1974 AT SALFORD CIRCUS.

CONDITIONS:- 0-1 PPM FSD IS 100% ON CHART; CHART SPEED 30cm h^{-1} AS USED FOR ABSTRACTION.

o SIGNIFIES ABSTRACTED POINT.

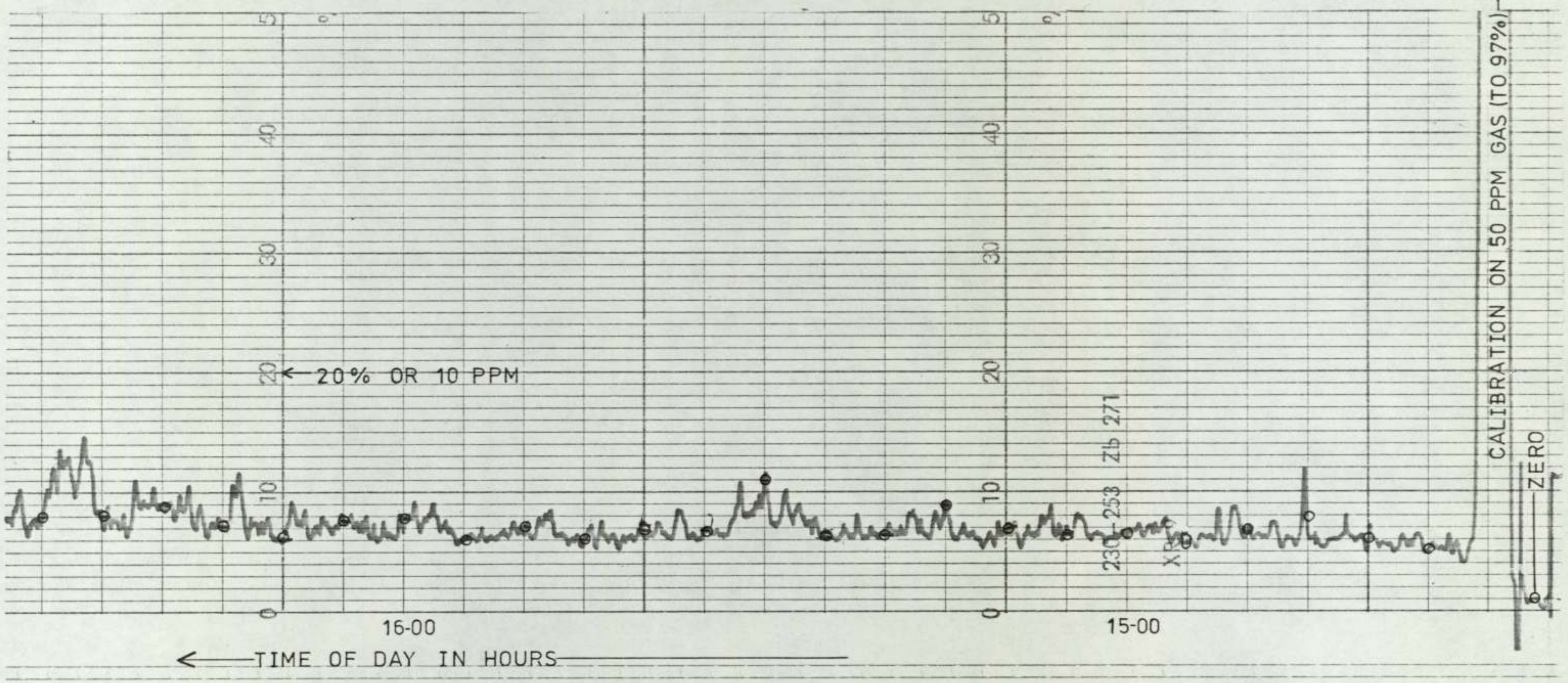

FIGURE 3.6 CHART OF CO AS RECORDED ON 04-11-1974 AT SALFORD CIRCUS.

CONDITIONS:- 0-50 PPM FSD IS 100% ON CHART; CHART SPEED 12 cm h^{-1} AS USED FOR ABSTRACTION.

o SIGNIFIES ABSTRACTED POINT.

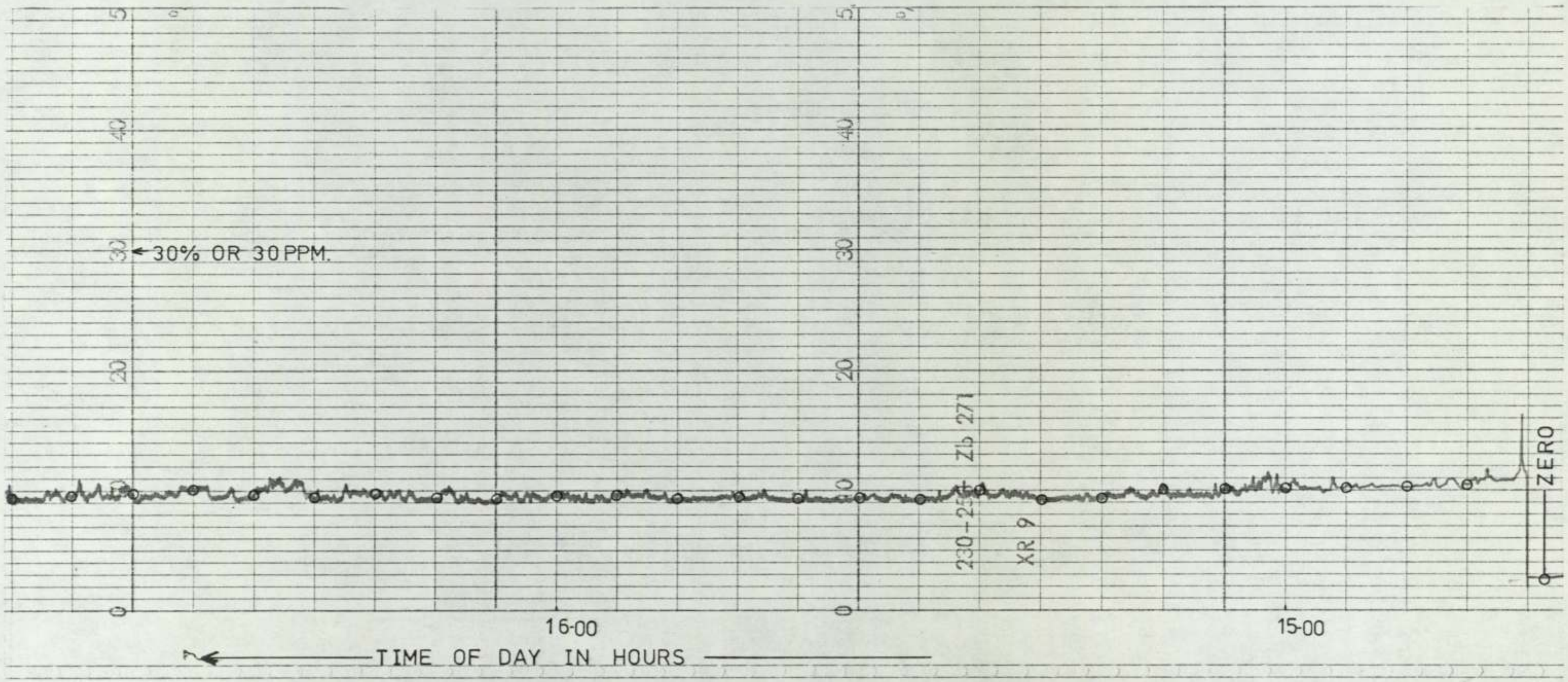

FIGURE 3.7 CHART OF HC AS RECORDED ON 04-11-1974 AT SALFORD CIRCUS.

CONDITIONS:-0-100 PPM FSD IS 100% ON CHART; CHART SPEED IS 12 cm h^{-1} AS USED FOR ABSTRACTION.

o SIGNIFIES ABSTRACTED POINT.

TABLE 3.3

Fluctuations of recorded signal:

Coefficient of variation (standard-deviation ÷ mean)

of points abstracted and averaged to give hourly averages

Gas and sensitivity	NO_x 0 - 1ppm	NO 0 - 1ppm	CO 0 - 50ppm	HC 0 - 100ppm
Coefficient of Variation, %	20 - 60	20 - 60	15 - 25	<5

Data errors are bound to be present: the programme run must not be abortive due to one number being in error. The most serious error would be faulty assignment of whole arrays of data following one invalid entry. This is avoided to some extent by the somewhat lengthy card description of which the first eight columns define the observation uniquely by pollutant, zero/observation/calibration, site, hour, date, month, year, full-scale, observation points. The first two are used to define the subscripts of the arrays, and the time information is used for card sorting and sequence checking. This reduces the number of errors from a faulty data point since array-subscript overflow or a time sequence error will be spotted.

The zero-corrected and calibrated hourly-averages are required for comparisons with prediction results so are sorted into rows and output. In each hourly row is listed the site and time information followed by the levels of each pollutant as hourly averages. For convenience in data processing the traffic counts from Salford Circus are input, sorted and printed along with the pollutant levels.

A fuller description is given in Appendix 1, and example output in Figure 3.9 (details of the input are less important: Figure A1.1 in Appendix 1).

3.5 Use of the Instruments and Programme

We have shown how the instruments were operated and explained the programme used to process the results (Flow Chart: Figure 3.8). Charts were brought back from site and labelled in Greenwich Mean Time. It was necessary to check zeroes for excessive noise or drift, and the charts for timing errors due to power failures. Abstraction was then made. The data were run in sets of forty eight hours (programme maximum was fifty) and the output stored in the ICL 1904S filestore. The results tables were then edited into one file and stored as hourly means of pollutant concentrations. For one week (168 observations) about 16000 numbers would be input and the final table would have about 2000 numbers. Figure 3.9 shows example results and indicates the levels found at Salford Circus and Murdoch Point. The present work will discuss the most reliable results obtained: covering seventeen days or an output of 5000 numbers. Much data of poorer quality was recorded but rejected. In fact the very size of the data base presents a problem of time and the flexible nature of the programme was a great help when abstracting charts. The early work used very slow chart speeds (3cm h^{-1}, cf Figure 3.4): a ruler was drawn through the trace to get an eye-average for the reading. The results were of low accuracy but did indicate a dependence on traffic: Figure 3.10 shows some early results obtained this way. The results (Figure 3.9) from fast chart/programme processing are plotted in Chapter 6. The fast chart speed demanded a programme to ease the work of abstraction but made it feasible to discuss the results in a more sophisticated manner (Chapter 6). There is a problem in this type of project of balancing time for monitoring with that for interpretation. The observed hourly mean concentrations (Figure 3.9) were compared with calculated values so are discussed later (Chapter 6).

FIGURE 3.8 OUTLINE FLOWCHART OF PROGRAMME CHART50 TO AVERAGE, CALIBRATE, ZERO-CORRECT AND SORT ROUTINE-MONITORING CHART-DATA

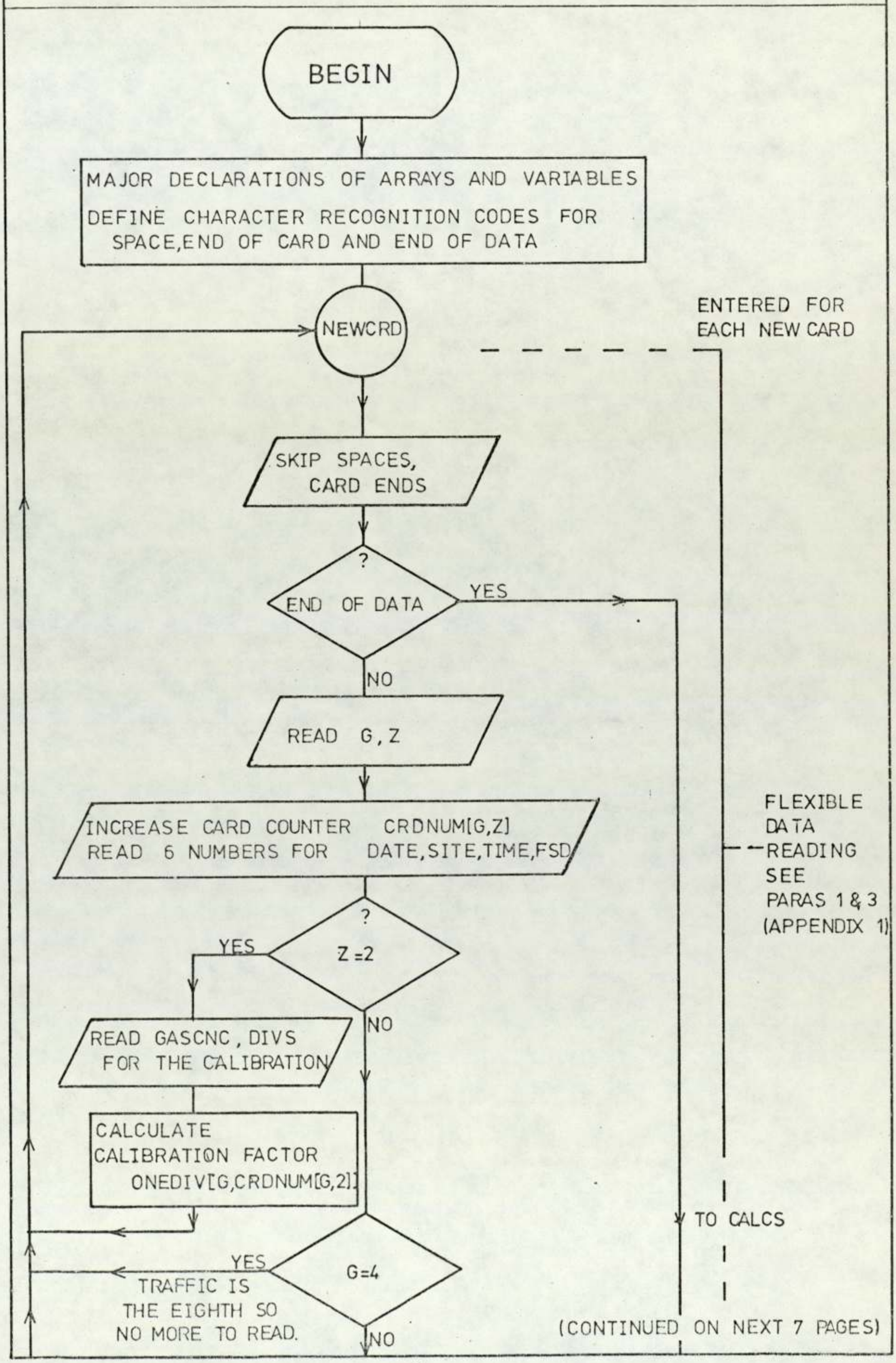

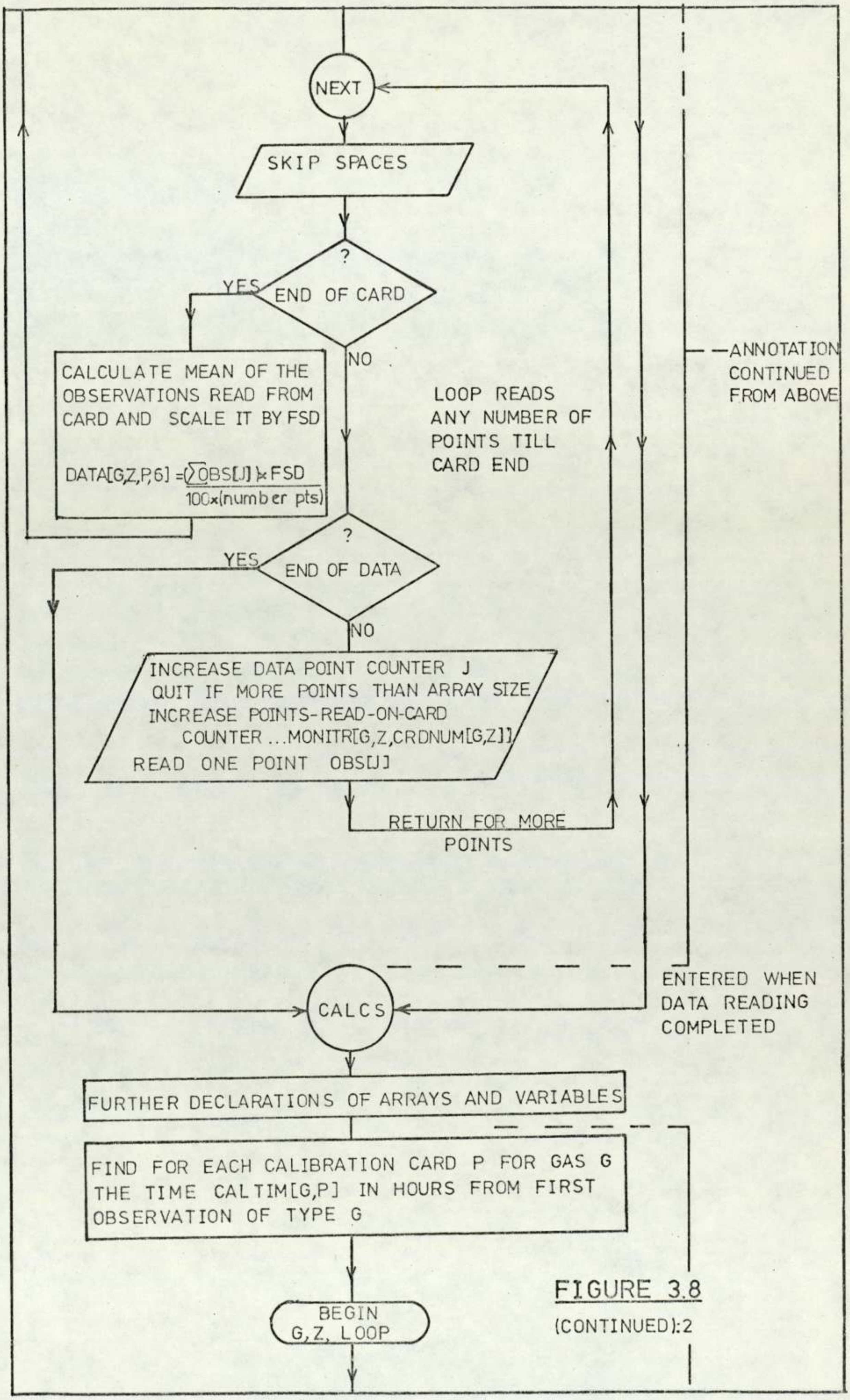

FIGURE 3.8

(CONTINUED):2

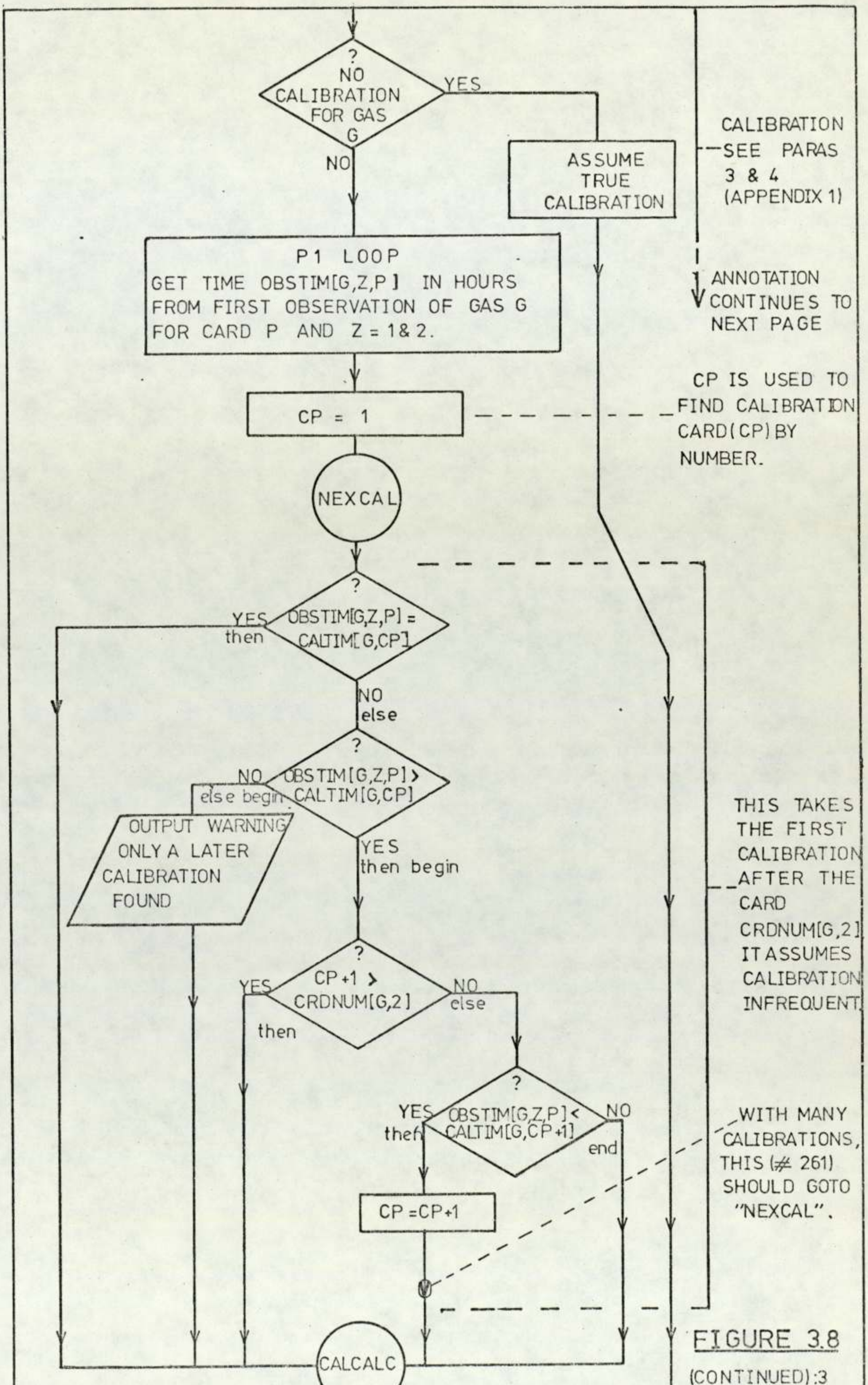

FIGURE 3.8

(CONTINUED):3

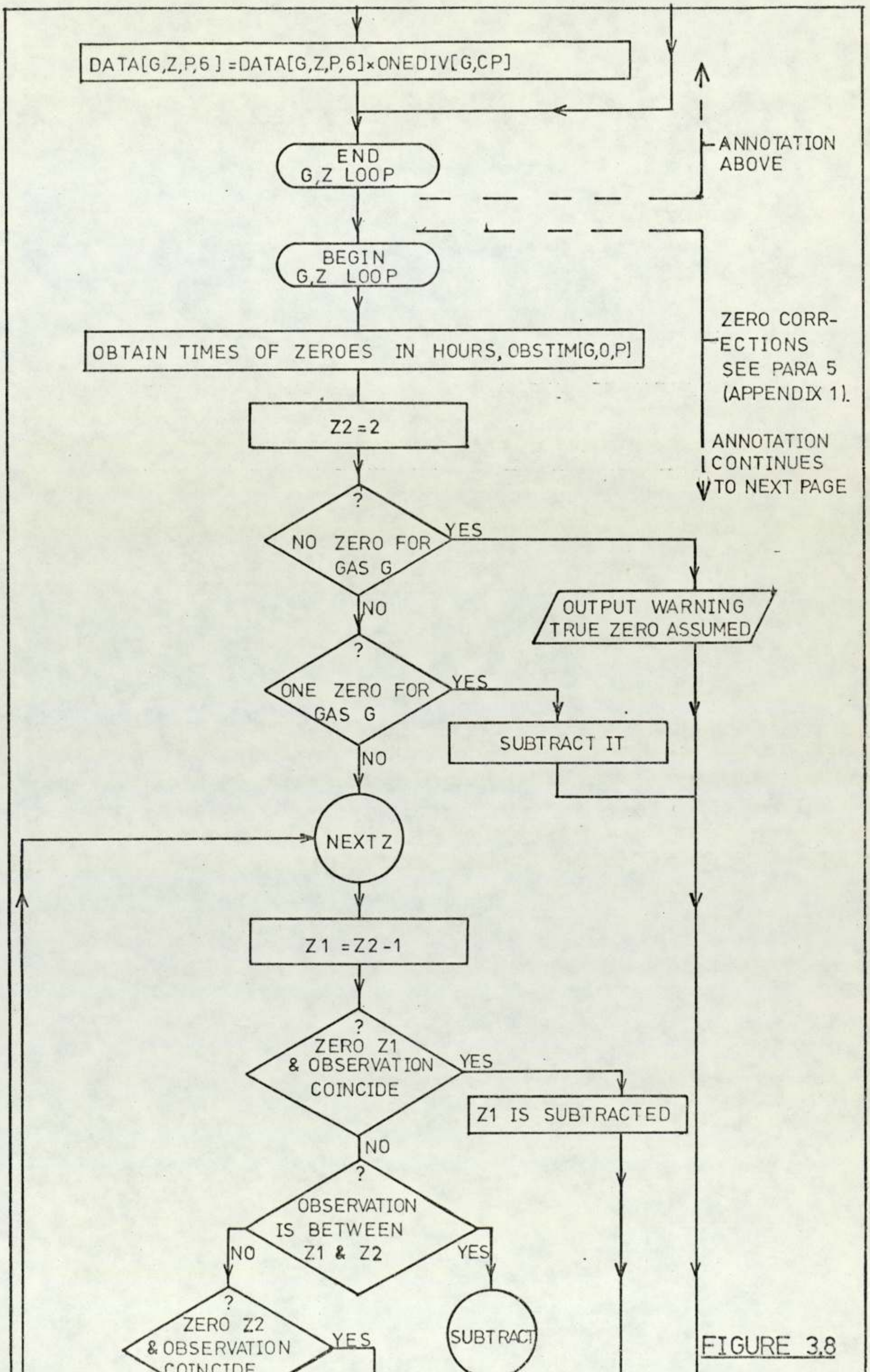

FIGURE 3.8

(CONTINUED): 4

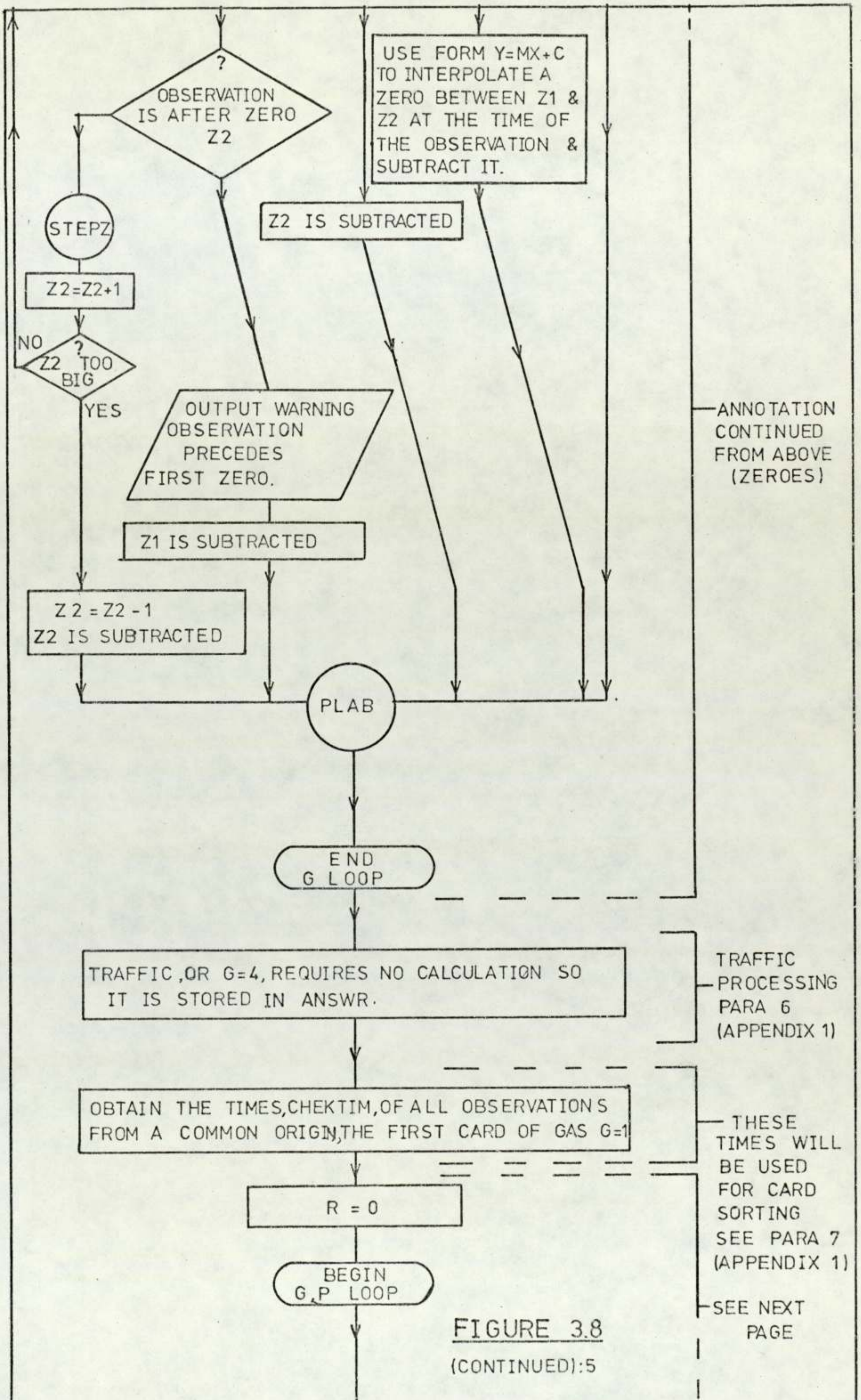

FIGURE 3.8

(CONTINUED):5

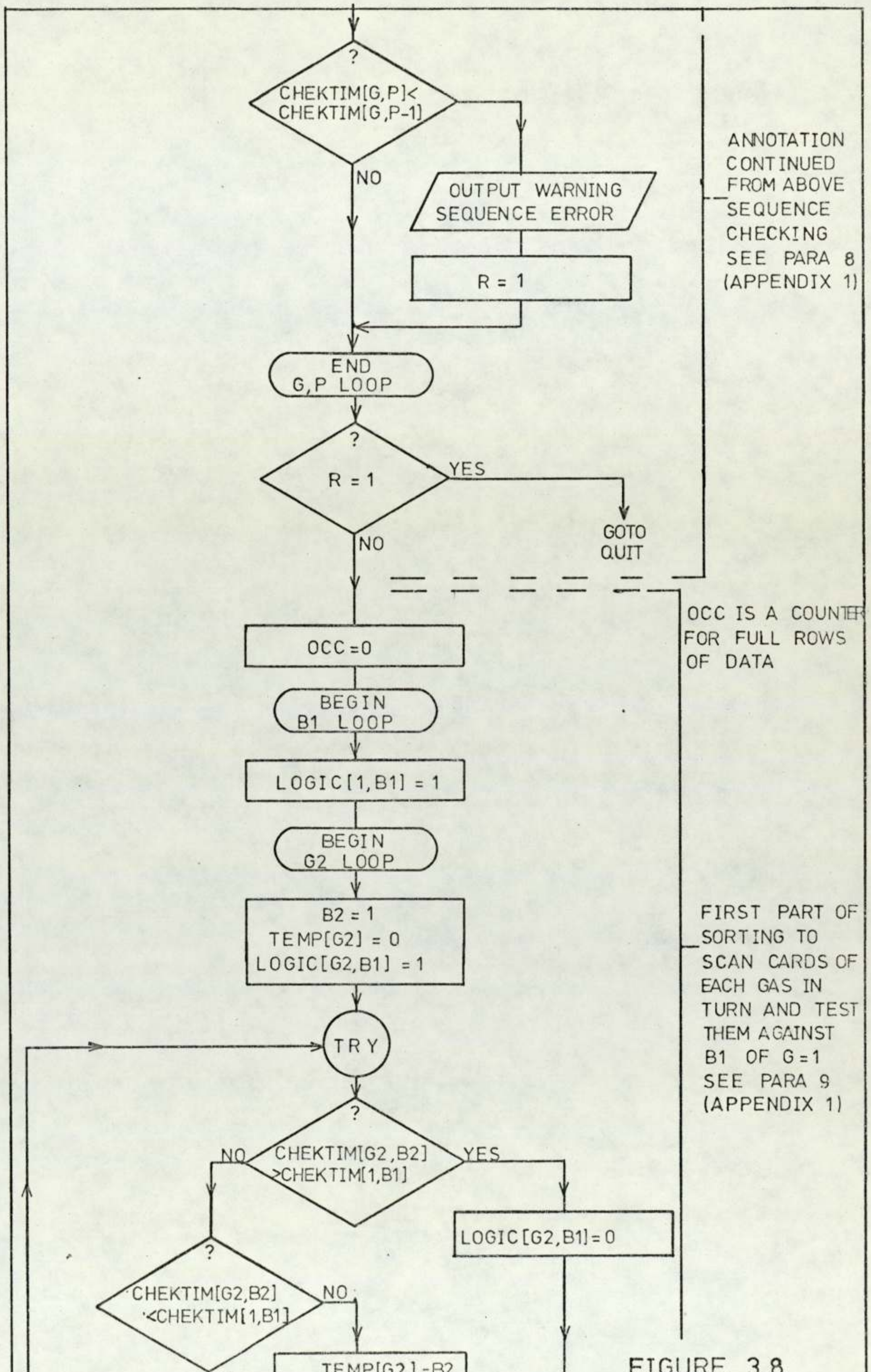

FIGURE 3.8

(CONTINUED): 6

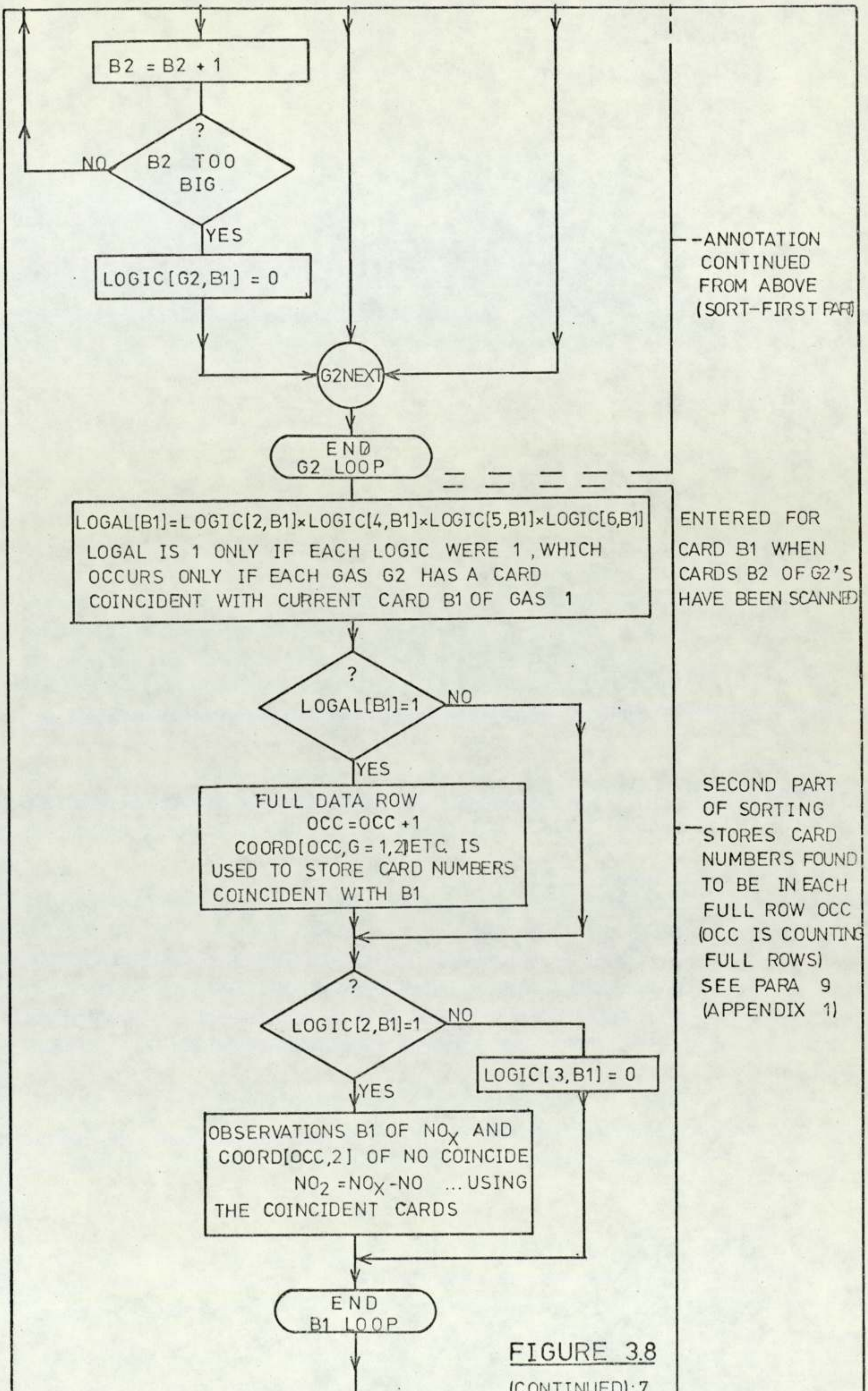

FIGURE 3.8

(CONTINUED): 7

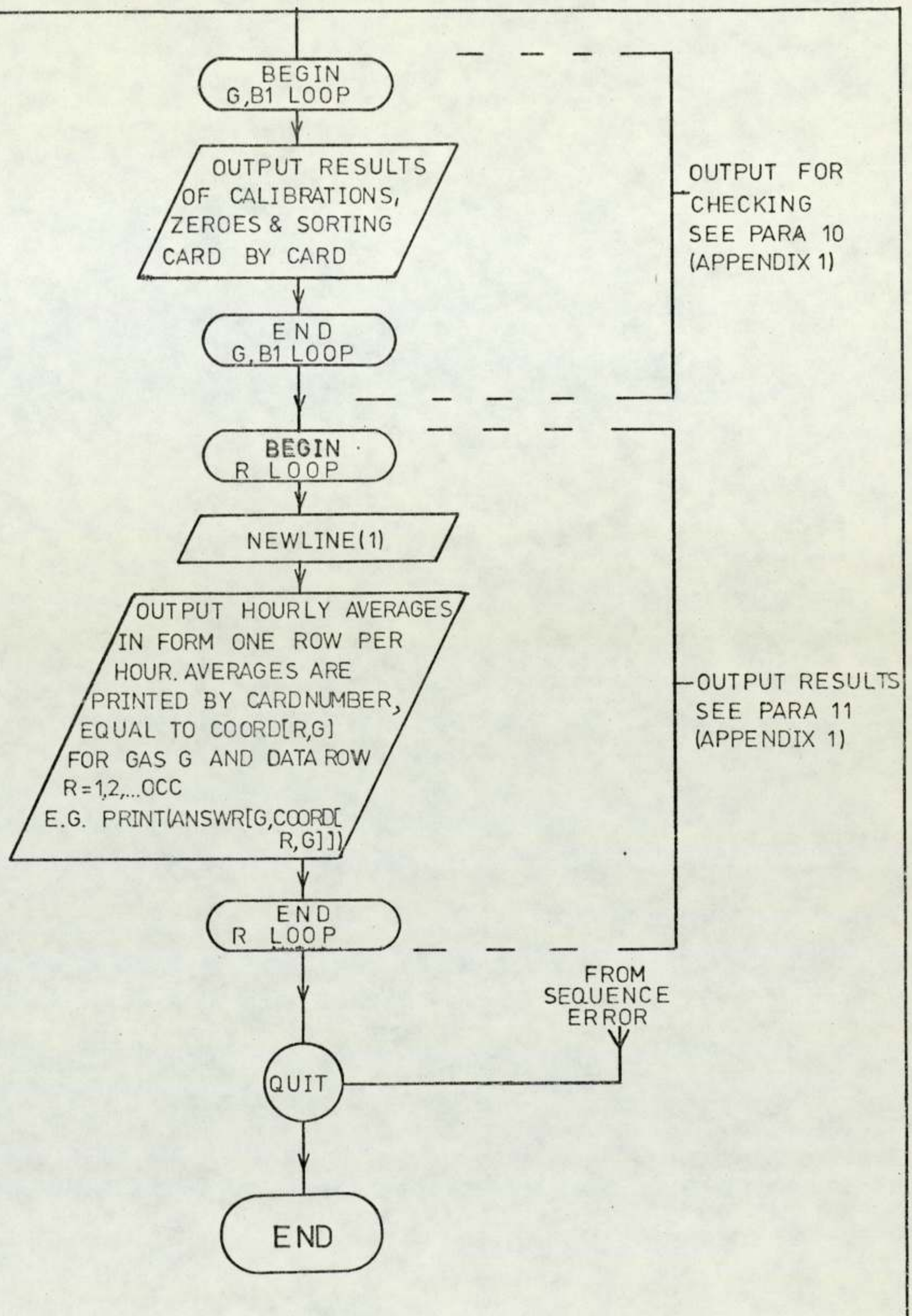

FIGURE 3.8

(CONTINUED-LAST PAGE):8

DOCUMENT AFS03/401

ONLY A LATER CALIB FOUND FOR GAS 1 OF OBSN TYPE 0 CALIB CARD NO WAS 1 OBSN CARD NO WAS 1
THE NEXT CALIBN WAS USED
ONLY A LATER CALIB FOUND FOR GAS 2 OF OBSN TYPE 0 CALIB CARD NO WAS 1 OBSN CARD NO WAS 1
THE NEXT CALIBN WAS USED

DATA MEANS AND CHEKTIM

G	Z	SITE	HR	DY	MT	YR	DATAJ6	ANSWR	CHEKTIM
1	1	8	16	14	3	74	0.044	0.039	0
1	1	8	17	14	3	74	0.044	0.040	1

COINCIDENCE RESULTS

G	Z	CARDNO 29	SITE	HOUR	DAY	MONTH	YEAR	ANSWR	CHEKTIM	COINC NOX CRDNO	NOX TIME
1	1	1	8	16	14	3	74	0.039	0	1	0
1	1	2	8	17	14	3	74	0.040	1	2	1
1	1	3.	8	18	14	3	74	0.055	2	3	2
1	1	4	8	19	14	3	74	0.056	3	4	3

PROGRAM RUNNING COMMENTS

RESULTS OF CHART ABSTRACTION

YEAR	SITE	HOUR	DAY	MONTH	NITROX	NITICO	NITDIO	TRAFIC	CMONOX	HYDROC
74	8	16	14	3	0.039	0.011	0.028	2301	1.0	6.2
74	8	17	14	3	0.040	0.010	0.030	3358	1.1	6.1
74	8	18	14	3	0.055	0.020	0.035	3338	1.5	6.1
74	8	19	14	3	0.056	0.019	0.037	2225	1.6	6.5
74	8	20	14	3	0.049	0.015	0.034	1546	1.5	6.4
74	8	21	14	3	0.046	0.012	0.034	1268	1.4	6.6
74	8	22	14	3	0.046	0.012	0.034	1167	1.4	6.4
74	8	23	14	3	0.037	0.009	0.028	912	1.0	6.0
74	8	24	14	3	0.036	0.010	0.026	684	1.0	6.0
74	8	1	15	3	0.028	0.007	0.021	373	0.9	5.7
74	8	2	15	3	0.023	0.006	0.017	154	1.0	5.5
74	8	3	15	3	0.019	0.006	0.013	120	1.0	5.3
74	8	4	15	3	0.017	0.005	0.012	75	1.0	5.1
74	8	5	15	3	0.016	0.006	0.010	82	1.0	5.1
74	8	6	15	3	0.018	0.005	0.012	379	1.0	5.0
74	8	7	15	3	0.021	0.006	0.015	1041	1.0	4.9
74	8	8	15	3	0.035	0.012	0.023	2603	1.2	6.2
74	8	9	15	3	0.040	0.014	0.026	2749	1.5	5.4
74	8	10	15	3	0.039	0.017	0.022	2364	1.4	6.4
74	8	11	15	3	0.037	0.014	0.023	2072	1.4	5.6
74	8	12	15	3	0.037	0.013	0.023	2130	1.4	5.5
74	8	17	15	3	0.043	0.022	0.021	3363	2.0	5.9
74	8	18	15	3	0.041	0.013	0.027	3423	2.0	5.6
74	8	19	15	3	0.037	0.015	0.022	2111	1.5	5.5
74	8	20	15	3	0.022	0.007	0.015	1531	1.4	5.3
74	8	21	15	3	0.021	0.006	0.015	1472	1.2	5.7
74	8	22	15	3	0.019	0.006	0.014	1269	1.2	5.5
74	8	23	15	3	0.023	0.005	0.018	1058	1.2	5.6
74	8	24	15	3	0.017	0.005	0.012	878	1.1	5.5

SITE 8:-MURDOCH POINT.

DOCUMENT MEAS1174

74	4	13	4	11	0.105	0.108	0.001	2321	3.1	5.8
74	4	14	4	11	0.130	0.122	0.008	2555	3.3	5.9
74	4	16	4	11	0.160	0.126	0.034	2251	3.3	5.7
74	4	17	4	11	0.169	0.142	0.026	3370	3.9	7.0
74	4	18	4	11	0.149	0.135	0.013	3411	3.8	5.7
74	4	19	4	11	0.142	0.153	-0.010	2073	3.2	5.5
74	4	20	4	11	0.131	0.098	0.032	1413	3.4	5.5
74	4	21	4	11	0.114	0.075	0.039	1103	3.0	5.5
74	4	22	4	11	0.102	0.090	0.013	1044	3.3	5.7
74	4	23	4	11	0.080	0.087	-0.007	658	2.5	5.5
74	4	24	4	11	0.089	0.073	0.016	534	2.9	6.5
74	4	1	5	11	0.060	0.043	0.017	274	2.3	6.3
74	4	2	5	11	0.042	0.031	0.011	135	1.9	4.2
74	4	3	5	11	0.050	0.027	0.023	106	1.6	4.2
74	4	4	5	11	0.080	0.053	0.012	53	1.8	5.5
74	4	5	5	11	0.083	0.083	-0.005	78	2.1	5.9
74	4	6	5	11	0.125	0.097	0.026	550	2.2	5.9
74	4	7	5	11	0.193	0.208	-0.015	1036	3.3	7.7
74	4	8	5	11	0.556	0.653	-0.096	2821	10.5	12.1
74	4	9	5	11	0.571	0.573	-0.005	2791	12.1	11.9
74	4	10	5	11	0.340	0.427	-0.087	2524	5.1	9.3
74	4	11	5	11	0.321	0.314	0.005	2101	4.4	8.0
74	4	12	5	11	0.210	0.168	0.042	2144	3.0	7.2
74	4	13	5	11	0.210	0.263	-0.053	2252	3.0	7.1
74	4	14	5	11	0.203	0.179	0.024	2343	3.1	5.5
74	4	15	5	11	0.246	0.216	0.030	2274	2.9	6.6
74	4	16	5	11	0.212	0.195	0.017	2324	2.5	5.7
74	4	17	5	11	0.291	0.322	-0.031	3339	4.3	7.8
74	4	18	5	11	0.306	0.270	0.037	3304	4.8	8.5
74	4	19	5	11	0.257	0.200	0.057	2031	4.0	7.9
74	4	20	5	11	0.185	0.131	0.053	1353	3.0	7.4
74	4	21	5	11	0.133	0.098	0.040	1127	3.0	7.3
74	4	22	5	11	0.129	0.088	0.041	1075	3.0	7.1
74	4	23	5	11	0.114	0.083	0.031	855	2.9	7.1
74	4	24	5	11	0.082	0.051	0.035	[illegible]	2.5	[illegible]

SITE 4:-SALFORD CIRCUS

FIGURE 3.9

HOURLY AVERAGES OF ROUTINE MONITORING AS OUTPUT BY CHART50.

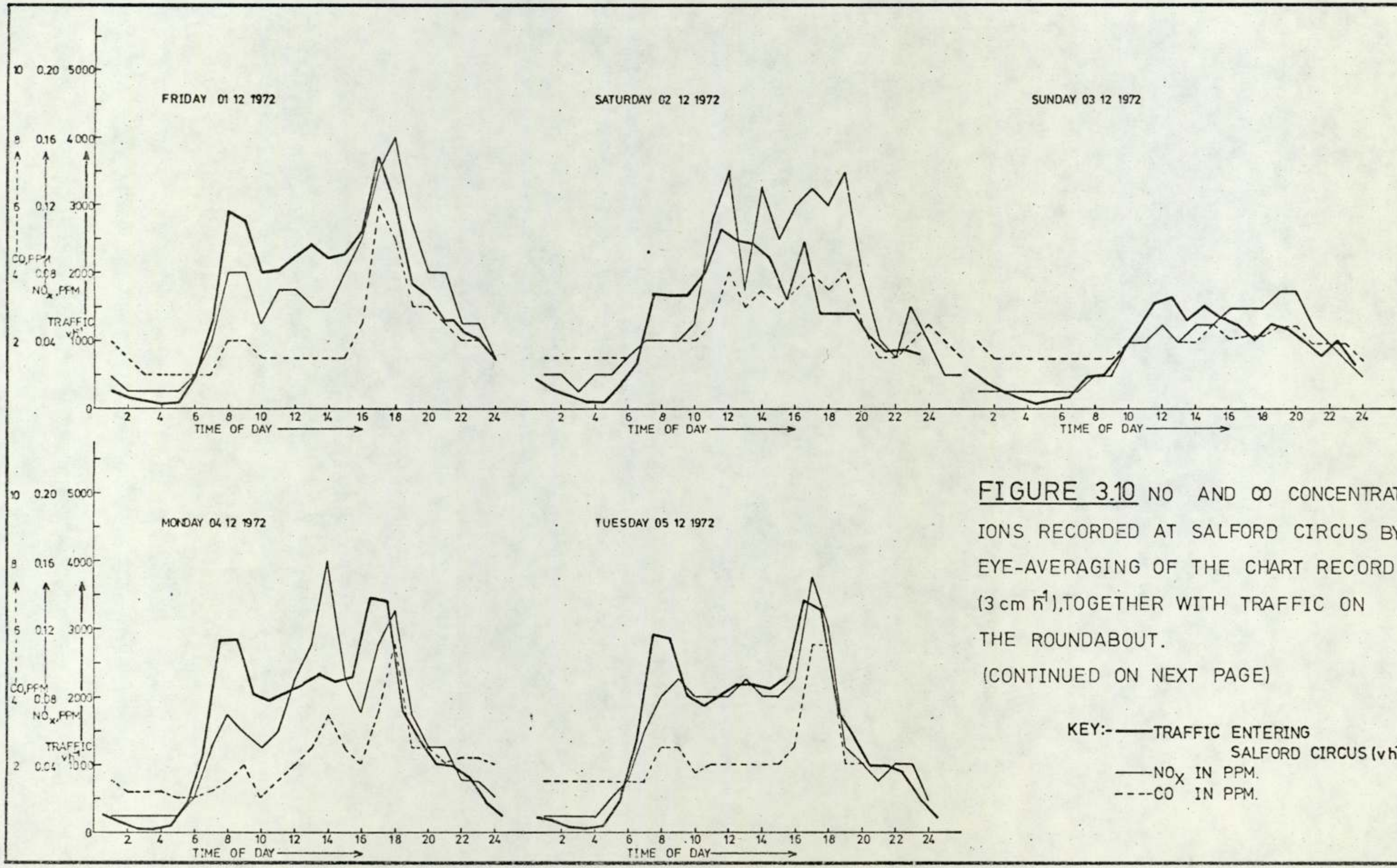

FIGURE 3.10 NO AND CO CONCENTRATIONS RECORDED AT SALFORD CIRCUS BY EYE-AVERAGING OF THE CHART RECORD (3 cm h^{-1}), TOGETHER WITH TRAFFIC ON THE ROUNDABOUT.

(CONTINUED ON NEXT PAGE)

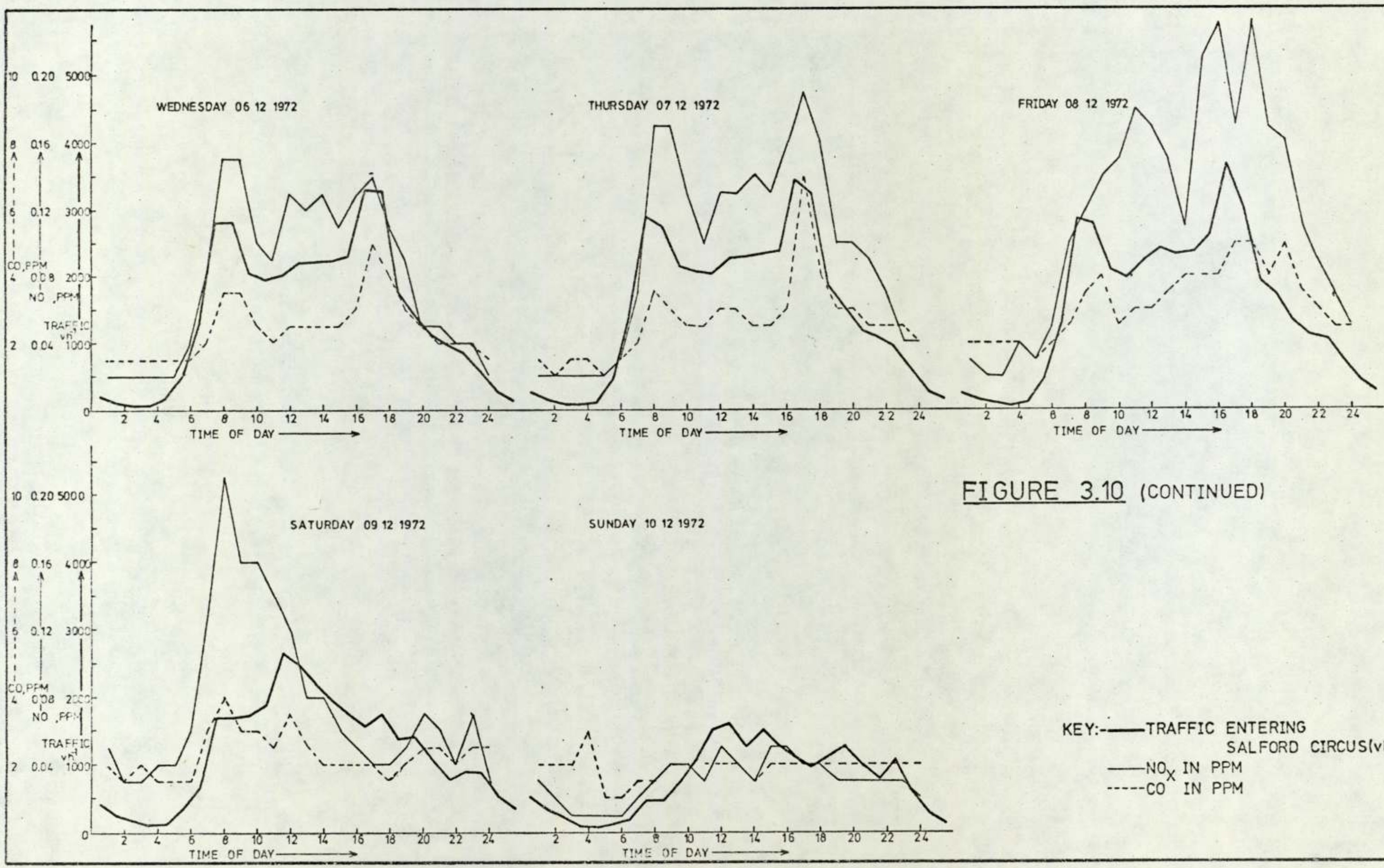

FIGURE 3.10 (CONTINUED)

3.6 Precision and Accuracy of Monitored Results

The hourly mean concentrations are averages of between twelve and fifteen points read from a fluctuating record. The average therefore lacks precision. The effect of the averaging of a finite sample from the hour may be described statistically - the readings are samples from a non-stationary random process (cf Bendat and Piersol, 1966) and have an uncertainty due to the finite number of points. Theoretical aspects of this uncertainty were not considered: in Table 3.3 we summarise the coefficients of variation for some hourly averages. They indicate a large range of signal values. Between twelve and fifteen points were used in a compromise between precision and the amount of chart and work required. This implies in Figures 3.5, 3.6, 3.7 that one point was read at each centimetre of chart.

There was in addition to signal fluctuation an uncertainty due to zero drift (Table 3.2): the effects of this were minimised by the method of operation and by interpolation of zeroes by the programme when subtracting the zero from the recorded average.

Finally each data set is consistent within itself as regards calibration, since the instruments were checked on commercial mixtures, but the data set as a whole may have error in absolute calibration (Chapter 2). We summarise these points in Figure 3.11. With automated data abstraction (e.g. data logger), the limitations on sample size are probably less severe and the effect of signal fluctuation may be considered more fully.

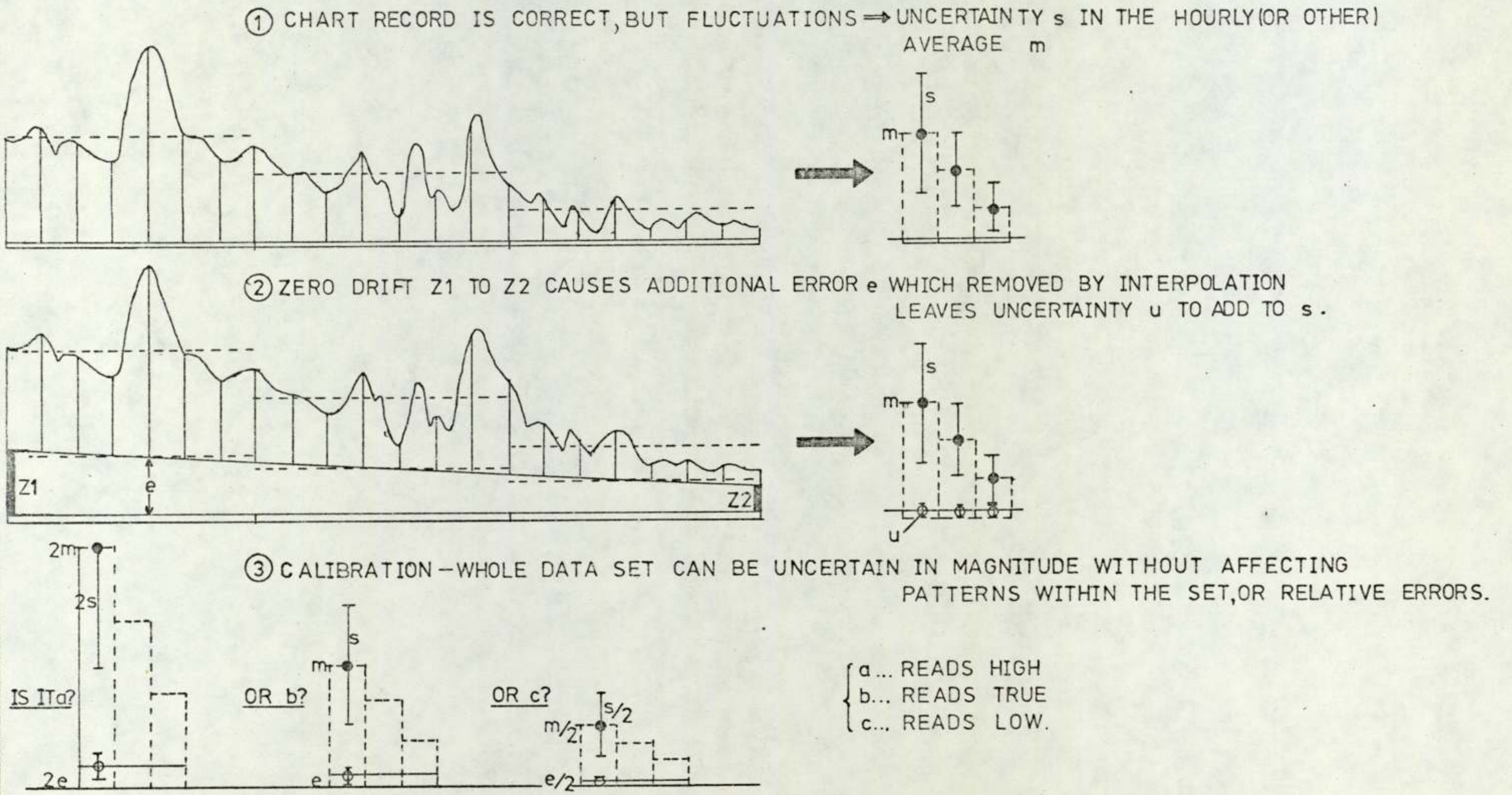

FIGURE 3.11 ERRORS OF ROUTINE MONITORING.

3.7 Summary

The instruments were left operating at permanent sites, enabling other tasks to be performed at the same time. This did mean the choice of distance as a parameter for study was restricted. The levels fluctuated rapidly: as many points as practicable were abstracted to be averaged into hourly means, corrected for calibration and zero drift and stored for later comparison with emissions-based calculations. Typical levels are shown in Figure 3.9, but more detailed discussion follows in Chapter 6.

CHAPTER 4

TRAFFIC COUNTS

The project aimed particularly at assessing the influence of traffic on air quality near the intersection and therefore fairly extensive traffic counts were required. In the present chapter we describe the traffic counting and the principles of the computer programmes used to calculate traffic flows. We estimate the errors associated with the traffic flows. In later chapters we use the traffic flows to help understand the pollutant levels as recorded.

4.1 Traffic Count for the Roundabout (Salford Circus)

The Streeter-Amet equipment has detectors on each entrance to the roundabout (Map: Figure 4.1). The count, summed for an hour, and the time are printed on paper tape. The numbers were abstracted by hand on to coding sheets for card-punching. The counts were hourly traffic flows (without further calculation) for vehicles entering the roundabout; subdivision into journeys around the roundabout was not possible so the flows on each feeder road were not separately available.

4.2 Traffic Count for the Intersection and Motorway

4.2.1 Principle

Sub-surface loops set in the various lanes of the intersection have electrical pulses induced as vehicles pass over them. The loops are

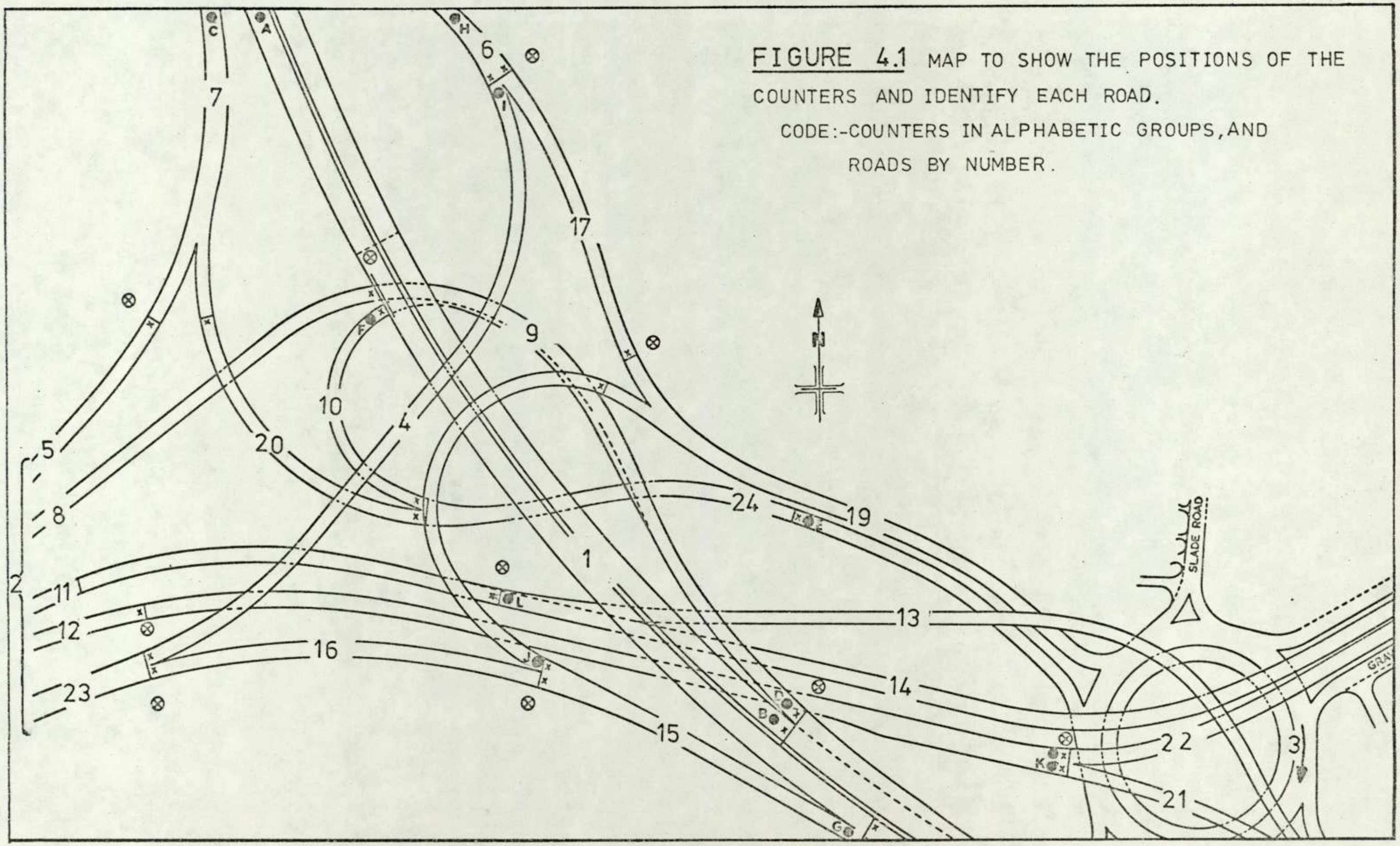

FIGURE 4.1 MAP TO SHOW THE POSITIONS OF THE COUNTERS AND IDENTIFY EACH ROAD.
CODE:-COUNTERS IN ALPHABETIC GROUPS, AND ROADS BY NUMBER.

used by the Motorway Control Police as a flow indicator. For the present project equipment was installed at the Motorway Control Centre (Perry Barr) to monitor twenty eight loops. The loops are in groups identified alphabetically on the map (Figure 4.1). Pulses are summed continuously on electromechanical counters. A camera photographs the array of counters and the face of a continuously running clock at regular intervals: an interval timer creates the period between photographs. Possible periods range from minutes to hours. The traffic-flow is the elapsed count divided by the period.

4.2.2 Drift of Photograph Times

The camera-timer operates by resetting itself at the end of each period. Unfortunately the small, variable errors in the reset accumulate so that the timing drifts away from that desired: hourly-counts photographs can be on the half hours. The clock-face included in the photograph has the exact time at which the photograph was taken, so the traffic counts are recorded over a known period of approximately one hour.

The traffic-flow has a drifting time which bears no simple relationship with on-the-hour measurements made in the rest of the work. This point will reappear in the discussion of errors.

4.2.3 Maintenance: Missing Values

Pulses from the loops are frequency-coded and sent by land-line to the counter at Perry Barr. It was difficult to keep all counters operating simultaneously: the system was sometimes disturbed by engineers working on other equipment. Often at least one counter was not working so missing values exist as a potential data loss, or as an error source if a substitute value is interpolated.

4.2.4 Calibration

The sub-surface loops were installed before the white road-markings; the two do not always coincide exactly. This, together with the variable lane discipline of drivers, means that the counters tend to read high. The closed-circuit television used for surveillance of the intersection by the police was pointed at each lane in turn and a visual count of vehicles was recorded for comparison with the counter value. This gave a set of factors to correct the results from each alphabetic group of counters (Appendices 2, 3).

4.3 Computer Programmes to Calculate Intersection Traffic-Flows

4.3.1 General Requirements

The photograph times are available as year, month, day, day-type (Monday = 1, Tuesday = 2, ... Sunday = 7), hours and minutes. The counts, possibly including missing values, are six-digit cumulative sums. The flow over any loop is the difference between the sums, or counter readings, on the first and second of any pair of photographs, divided by the period. The counter may pass zero during this period.

We require traffic-flows on the various roads of the intersection. A separate listing for the major roads M6 and A38(M) is useful. The flows should run from the hour to the next hour; the time is denoted by the hour ending the period.

Hourly counts are expensive in film and time, and suffer noticeably from timer drift, so twelve-hourly photographs were taken for much of the work. The programme should estimate hourly flows from twelve-hourly ones, using the hourly pattern of traffic-flow.

Four programmes (Table 4.1) were developed in response to these requirements.

4.3.2 Principles of the Traffic Programmes

The programmes perform differing calculations on a common theme so are described together. Fuller details are given in Appendix 2.

Data are read and missing values recognised. The counts are cumulative so the number of vehicles that passed during the time between two adjacent photographs is the difference between the two counts (with allowance for a counter passing zero). If either of the two counter readings is missing this subtraction is not possible: the traffic that passed is interpolated. We suppose that the distribution of traffic over the intersection is constant. Then the relative contributions of each counter to the total of the counters in each row are constant. These relative contributions are RJ [J] for the Jth counter.

From counts C [J] of traffic passing between photographs, $RJ[J] = (C[J]) / (\sum_{J=1}^{28} C[J])$. These RJ [J] were stored in the

TABLE 4.1

Programmes to Process Traffic-Counts

for the Intersection

PROGRAMME	INPUT	OUTPUT
TRRLINTR	Abstracted photographs Including missing values	Counter differences Calibrated counter differences Estimates of missing values M6, A38(M) flows as total and per hour
TRRLRATGEN	Abstracted photographs No missing values	Counter differences Calibrated counter differences M6, A38(M) flows as total and per hour Ratios RJ J of each counter contribution to total count: used in other programmes
TRRLRØFLØ	Abstracted photographs Including missing values Number of roads	Counter differences Calibrated counter differences Estimates of missing values Flows per hour
TRRLBØX	Abstracted photographs Including missing values Number of roads Standard matrix	Counter differences Calibrated counter differences Estimates of missing values Mean flows per hour Interpolated flows per hour

programme as parameters of the counters. In any row where a counter is missing, RJ [J] is summed for those counters which are available. This sum is SIGMAR [I] and it represents what fraction the available counters make to the total twenty eight counter count that would exist were all the counters present. If the full count (i.e. from all twenty eight counters) is T then the total of those counts which are available is

RØWSUM [I] = SIGMAR [I] .T

Thus T is calculated. The missing value would have contributed a fraction RJ [J] to T: the missing elapsed traffic-flow is therefore RJ [J] *T .

The counters tend to read high because of driver lane discipline, so the elapsed traffic is scaled by the calibration factors (Section 4.2.4).

The traffic passing along a given road is counted by several counters: in some cases the flow is only available as the difference between say that entering a road common to two roads and that leaving by a side road. The traffic-flows are therefore printed as the appropriate combination of (calibrated) counter differences (or elapsed traffic) divided by the time period between the two photographs. The programmes produce as output the total traffic and the hourly traffic-flow for A38(M) and M6. In addition, the programme TRRLROFLO gives the hourly elapsed traffic for all roads in the intersection. This used the road labelling of Figure 4.1 and two procedures to set up the complex set of counter combinations required. Figure 4.2

gives an example input. Figure 4.3 gives an example output. The programme TRRLBØX will interpolate hourly flows if the periods between the photographs exceed one hour. It uses the same two procedures as in TRRLROFLO to derive the number of vehicles which passed along each road between the photographs. The latter may have been taken say twelve hours apart: the number of vehicles which passed is subdivided into hourly flows according to the hourly traffic pattern (which reflects the rise and fall with peak periods). The pattern was obtained (using hourly photographs and TRRLROFLO) for all roads for four day-types, (Monday, Friday, Saturday, Sunday with Tuesday, Wednesday, Thursday equivalent to Monday: cf footnote to Table A3.3). Figure 4.3 shows an example for day-type 5.

From the times of the photographs, the times and day-type of each hour occurring between the two photographs are obtained: for each hour the traffic-flow is estimated as the standard count for that hour (and day-type), scaled by the ratio of how much the elapsed count exceeded the sum of those standard counts occurring at the same time (and day-type). This ratio is to allow for differences in the general level of traffic-flow between the date of the standard counts, and the date of the twelve-hour (or other) photographs.

$$\text{FLOW} = (\text{STANDARD COUNT(HOURLY)}) \times \frac{(\text{ACTUAL TWELVE-HOUR COUNT})}{(\text{SUM OF TWELVE STANDARD COUNTS OF SAME TIME, DAY-TYPE AS OCCUR BETWEEN THE TWO PHOTOGRAPHS})}$$

The interpolated flows are printed. Fuller details are given in Appendix 2.

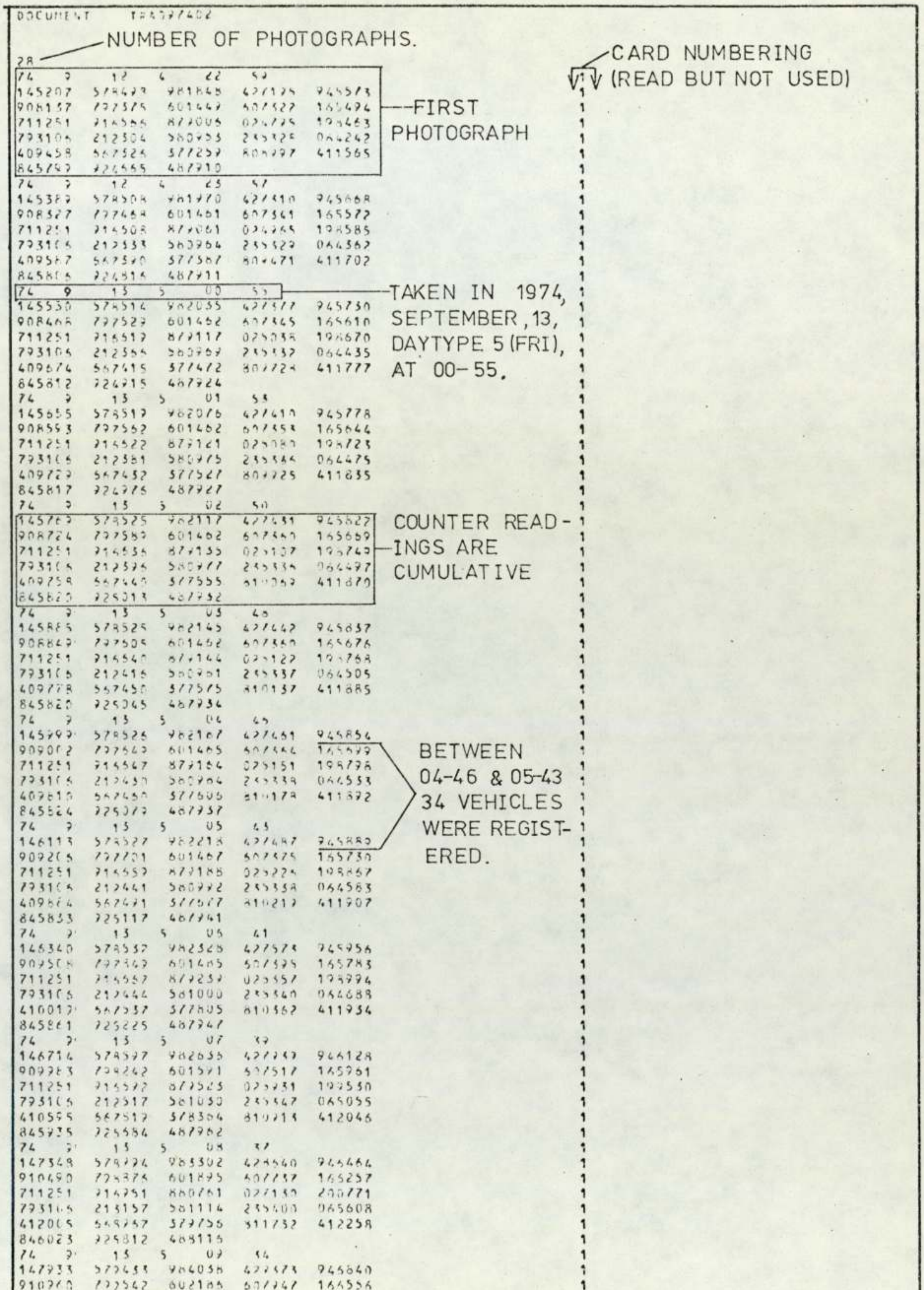

FIGURE 4.2 FORMAT OF TRAFFIC-COUNTS FOR INPUT TO THE TRAFFIC PROGRAMMES.

1974	9	15	FRI 0	55	3	5	1		
379	700		56	196	99	121	75	35	75
305	184	155	155	10	-2	43	12	55	196
92	92	54	0						
1974	9	15	FRI 1	53	4	5	2		
300	455		9	125	62	76	48	35	48
235	109	117	117	3	-0	33	3	56	125
55	55	9	0						
1974	9	15	FRI 2	50	5	5	3		
297	340		15	89	36	62	26	27	26
168	80	84	84	13	8	21	5	26	89
30	30	25	0						
1974	9	15	FRI 3	48	6	5	4		
261	134		12	41	33	24	16	6	16
75	34	38	38	4	2	21	2	23	41
17	17	14	0						
1974	9	15	FRI 4	46	7	5	5		
331	195		21	63	35	34	29	23	29
44	69	22	22	6	3	14	3	17	63
35	35	25	0						
1974	9	15	FRI 5	43	8	5	6		
385	339		30	127	56	38	68	36	68
52	135	26	26	11	7	26	4	30	127
78	.78	37	0						
1974	9	15	FRI 6	41	9	5	7		
753	705		54	276	123	144	132	61	132
157	287	78	78	7	2	68	6	74	276
143	143	55	0						
1974	9	15	FRI 7	39	10	5	8		
1595	2832		289	1031	590	306	524	251	524
610	1157	305	305	22	8	301	14	313	1031
383	383	297	0						
1974	9	15	FRI 8	37	11	5	9		
2854	6037		1217	2185	1016	976	1209	432	1209
949	2395	475	475	230	87	-201	143	-57	2185
1197	1197	1304	0						
1974	9	15	FRI 9	34	12	5	10		
2939	5403		999	1956	2308	1062	894	434	894
952	1890	476	476	248	126	1310	122	1432	1956
945	945	1125	0						
1974	9	15	FRI 10	32	13	5	11		
2398	3390		323	1272	917	667	405	354	405
773	1010	387	387	133	62	394	72	466	1272
305	305	383	0						
1974	9	15	FRI 12	29	15	5	12		
2793	3737		535	1256	942	921	336	390	336
1019	925	510	510	106	47	407	59	466	1256
413	413	382	0						
1974	9	15	FRI 13	26	16	5	13		
2700	3379		408	1209	618	918	291	376	291
1095	839	548	548	100	43	210	57	267	1209
420	420	450	0						
1974	9	15	FRI 14	25	17	5	14		
2874	3776		460	1235	1014	863	372	359	372
1081	951	540	540	104	52	354	52	606	1235
481	481	512	0						
1974	9	15	FRI 15	0	18	5	15		
3265	4100		473	1370	892	1028	342	451	342
1211	881	808	505	124	56	419	68	487	1370
440	440	529	0						
1974	9	15	FRI 16	7	19	5	16		
3600	4534		419	1525	886	1193	338	318	338
1425	926	713	713	122	60	467	62	529	1525
463	463	479	5						
1974	9	15	FRI 17	7	20	5	17		
4151	6805		478	2268	909	1848	420	947	420
2305	1038	1255	1253	138	49	431	88	319	2268
329	329	327	0						
1974	9	15	FRI 18	6	21	5	18		
4151	5405		368	2165	926	1760	386	916	386
2325	837	1265	1253	103	39	337	64	621	2165
429	429	406	0						
1974	9	15	FRI 19	6	22	5	19		
3318	3835		310	1115	680	816	299	385	299
1387	888	693	493	111	70	370	41	412	1115
444	444	379	0						
1974	9	15	FRI 20	6	23	5	20		
2779	2809		236	821	541	316	305	223	305
952	874	476	476	110	68	305	42	347	821
437	437	304	0						
1974	9	15	FRI 21	6	24	5	21		
1944	2325		178	633	391	304	269	143	269
859	735	429	429	72	45	213	27	240	633
368	358	225	0						
1974	9	15	FRI 22	5	25	5	22		
1429	1881		124	408	262	262	146	89	146
659	475	429	429	71	32	138	19	158	408
238	238	175	0						
1974	9	15	FRI 23	5	26	5	23		
879	1282		86	342	208	221	121	87	121
489	355	244	244	58	37	124	21	145	342
162	162	121	0						

TIME,DATE

ROADS 1-24 (EXCEPT 3)

FIGURE 4.3 HOURLY TRAFFIC FLOWS AS OUTPUT BY TRRLROFLO AND AS USED TO INTERLATE HOURLY FLOWS (ONLY DAYTYPE 5 SHOWN).

4.3.3 Errors in the Traffic-Flows

We now discuss the errors and attempt to combine them to assess the accuracy of the calculated traffic-flow: fuller details are given in Appendix 3.

1. The sample used to calibrate the counters is not statistically representative but allows some correction to be made. The calibration factors have probable error of say 5% (this estimate is not available directly).

2. Occasional misread or mispunched numbers may escape detection: their effect on the data-set as a whole is probably random, analagous to noise in the information.

3. Missing values as interpolated have errors whose effects vary with the counter-combination, for each road has an error if it uses the missing counter: the error is specific to the road.

4. The traffic-flows of each road are obtained from sums and differences of (inaccurate) counter differences so the errors tend to propagate. The size of the error varies with the number of operations and the sizes of terms: with n functions combined by additions and subtractions (s of them), the error appears to be $\sqrt{n}/(n - s)$ times the typical percentage error in the counter differences (Appendix 3).

5. The time drift of the photographs causes a phase error between the time of the photographs and the integer value of the time

TABLE 4.2

Summary of Errors in the Traffic-Flows

Text Reference to Paragraph in Para. 4.3.3	Process	Error	% Error
1	Correction of systematic lane discipline error	Probable error $\pm 5\%$	5
2	Abstraction of numbers	Noise -	-
3	Missing values Roads 2, 4, 17, 19, 23	Depends on road 2 + 4% 4 + 60% 17 - 40% 19 - 35% 23 + 42%	
4	Propagation by counter combinations. With addition error tends to diminish since random errors sometimes counteract.	Varies as $\sqrt{n}/(n-s)$ n counters; s subtracted. Error typically $\sim \pm 4\%$ from 5% in each counter. Roads in (3) above larger error.	4
5	Timer drift.	Mostly probable error $\sim \pm 10\%$ Friday mornings (0700, 0800) systematic $\sim 30\%$ low	10
6	Traffic pattern constant?	Error $\sim \pm 4\%$	4

TABLE 4.2

(Continued)

Summary:-	
Combining 4, 5, 6	Overall error typically ± 18%
Noting 4	Roads 2, 4, 17, 19, 23 systematic
Noting 5	Friday 07.00, 08.00 systematic

used to represent the photograph time. The effect on the traffic-flows is most serious when the traffic-flow changes rapidly with time. For the data used, the error in traffic-flow is usually $\sim \pm$ 10%, since the time drift was usually less than ten minutes from the hour. An exception occurs for the Friday morning rush-hour values of the standard counts, when the values are probably $\sim$ 30% low.

6. The hourly interpolation relies on the reproducibility of the hourly traffic-pattern. Test data (Appendix 3) suggested that the traffic-pattern was constant to within 4%. The standard counts are therefore an inaccurate sample from a distribution of traffic patterns, so to represent the traffic pattern by these standards counts implies both a random measurement-error (Paragraphs 1 - 5) and a random error from limited sampling (the standard photographs were a limited set). The standard counts probably have error $\sim$ 14% (Appendix 3). An interpolated count is made using perhaps a twelve-hour count and the standard counts: together the error in the interpolated flow will be $\sim$18%. In addition, for roads 2, 4, 17, 19, 23 the error is larger because of the missing counter 13, and on a Friday morning rush-hour the count is probably low by 30%. These points are discussed more fully in Appendix 3, and Table 4.2 summarises these discussions.

4.4 Summary

Traffic entering Salford Circus was counted precisely; the results are available without calculation. They do not give a resolution as to how the traffic is destributed over the roads to and from the roundabout.

Traffic-flows for all roads on the junction were derived as hourly and twelve-hourly counts from the combination of counter differences. Errors arose from poor lane-discipline, drift of the photograph times and missing values. The need to reduce the amount of abstraction and the problem of timer drift ruled out hourly junction-counts on a routine basis: the method of interpolation based on a sample hourly junction count has been discussed.

Estimates of traffic flow were made for all sections of the intersection (except Slade Road, Gravelly Hill, Tyburn Road and Lichfield Road). The propagation of errors has been discussed: it is suggested that the typical error in interpolated hourly counts is 18%, and extreme situations have been described where the error may be much larger. Table 4.2 presents a convenient review. Despite these errors the two counters and the programmes described here gave counts of the traffic over all roads in the intersection and in the roundabout: these in turn made feasible the pollution calculations (Chapter 6) based on emission estimates.

CHAPTER 5

DIFFUSION IN THE ATMOSPHERE

In the introduction we remarked that a major part of the work would be the measurement of pollutants around the junction. This has been described above. We now draw on the literature to show how the dilution of gases emitted into the atmosphere may be estimated numerically: we can then discuss an experiment (Chapter 7) to measure this dilution and a model (Chapter 6) to compare estimates based on emissions and dilution of the levels of pollutants with those recorded. The bulk of this Chapter reviews literature on atmospheric diffusion; the summary discusses those results actually used in the present work.

5.1 Turbulent and Molecular Diffusion

The effects of wind in transporting airborne material and of turbulence in spreading it have long been recognised (e.g. Hewson and Gill, 1944). If the material is not to alter the flow it should behave as part of the fluid: it should have a velocity coincident with the instantaneous flow-velocity at any point. Ideally it should have the same density as the fluid so that buoyancy and settling do not occur (Monin and Yaglom, 1971a).

It is hard to estimate the relative importance of turbulent and molecular diffusion in spreading material: the problem is discussed at greater length in Monin and Yaglom (1971b). They suggest eddy diffusivity is $\sim 10^5 - 10^6$ times greater than the molecular diffusivity and that for practical purposes both molecular diffusion and the interaction between turbulent and molecular diffusion may be neglected relative to turbulent diffusion (Monin and Yaglom, 1971c). This is implicit in many models of air-pollution.

5.2 Semi-empirical equation for turbulent diffusion

By analogy with diffusion from a region of high to low concentration, one can define an eddy diffusivity K so that the flux S is proportional to the gradient of mean concentration C of material in the direction X_i say.

$$\text{i.e.} \quad S = -K \frac{\partial C}{\partial X_i} \qquad \dots (5.1)$$

Thus a general equation may be derived for the nett transport of material in and out of a small element by turbulent diffusion and advection by a wind of speed U(Z) (in the X direction). Terms can be included for transport by settling and removal or formation by chemical reaction (Appendix 4). For advection and diffusion,

$$\frac{\partial C}{\partial t} + U(Z)\frac{\partial C}{\partial X} = K_{XX}(Z)\frac{\partial^2 C}{\partial X^2} + K_{YY}(Z)\frac{\partial^2 C}{\partial Y^2} + \frac{\partial}{\partial Z}\left(K_{ZZ}(Z)\frac{\partial C}{\partial Z}\right)$$

This equation (Semi-empirical diffusion equation, Monin and Yaglom, 1971d; K Theory or Gradient-Transfer Theory, Pasquill, 1971) assumes that the flux is proportional to the gradient of concentration. Pasquill (1970) questioned this for it implies that the diffusive spread should be over dimensions larger than all effective eddies and that diffusivity is a function only of position in the flow. Monin and Yaglom (1971e) consider that provided the diffusion time significantly exceeds the Lagrangian integral time scale (which in the atmosphere $\sim$ 1 second) the equation may be used to describe turbulent diffusion.

The semi-empirical theory is useful because it can be applied to inhomogeneous or non-stationary turbulence and because it offers a framework for formulae which frequently occur in discussions of air-pollutant plumes. It can be used for both continuous and instantaneous releases of material.

Two other theories in particular (Statistical Theory and Similarity Theory) have been developed to describe turbulent diffusion but we will not discuss them: we are primarily interested in plume formulae and their limitations. The reader will find a review of all three theories in Pasquill (1971) and in Bibbero and Young (1974).

5.3 Solutions of the Semi-empirical Equation

The semi-empirical diffusion equation (Monin and Yaglom, 1971d) describing advection and turbulent diffusion without losses of material is equation 5.2.

$$\frac{\partial C}{\partial t} + U(Z)\frac{\partial C}{\partial X} = K_{XX}(Z)\frac{\partial^2 C}{\partial X^2} + K_{YY}(Z)\frac{\partial^2 C}{\partial Y^2} + \frac{\partial}{\partial Z}\left(K_{ZZ}(Z)\frac{\partial C}{\partial Z} \right) \qquad \text{... (5.2)}$$

Additional terms for losses by settling, reaction or decay can be added (Appendix 4).

To completely define the problem the coefficients U(Z), K(Z) and the boundary conditions must be specified. The boundary conditions are

TABLE 5.1

Analytic Solutions: U,K constant; no settling, no reaction; reflection at $z = o$; $z > o$

Point Source Instantaneous release (Monin & Yaglom, 1971, Eq. 10.89). EQUATION 5.3

$$C(X,Y,Z,t) = \frac{Q}{[4\pi.\Delta t]^{3/2}(K_{xx}K_{yy}K_{zz})^{\frac{1}{2}}} \exp\left(-\frac{[X - u.\Delta t]^2}{4K_{xx}.\Delta t}\right) \exp\left(-\frac{y^2}{4K_{yy}.\Delta t}\right) \left[\exp\left(-\frac{(Z - H)^2}{4K_{zz}.\Delta t}\right) + \exp\left(-\frac{(Z + H)^2}{4K_{zz}.\Delta t}\right) \right] \quad \ldots (5.3)$$

Point Source Continuous release (Monin & Yaglom, 1971, Eq. 10.90). EQUATION 5.4

$$C(X,Y,Z) = \frac{Q}{4\pi X(K_{yy}K_{zz})^{\frac{1}{2}}} \exp\left(-\frac{y^2\ U}{4K_{yy}.X}\right) \left[\exp\left(-\frac{(Z - H)^2.U}{4K_{zz}.X}\right) + \exp\left(-\frac{(Z + H)^2\ u}{4K_{zz}.X}\right) \right] \quad \ldots (5.4)$$

TABLE 5.1 (continued)

Line Source   Instantaneous release (Drivas & Shair, 1974, Eq. 3) using $K_z = K_x = K$;   EQUATION 5.5

$$C(X,Z,t) = \frac{Q}{2\pi K.\Delta t} \exp\left(-\frac{[X - u.\Delta t]^2}{4K.\Delta t}\right)\left[\exp\left(-\frac{(Z - H)^2}{4K.\Delta t}\right) + \exp\left(-\frac{(Z + H)^2}{4K.\Delta t}\right)\right] \qquad \ldots (5.5)$$

Line Source   Continuous release (Monin & Yaglom, 1971, Eq. 10.91)   EQUATION 5.6

$$C(X,Z) = \frac{Q}{2(\pi K_{zz} uX)^{\frac{1}{2}}}\left[\exp\left(-\frac{(Z - H)^2 u}{4K_{zz}.X}\right) + \exp\left(-\frac{(Z + H)^2 u}{4K_{zz}.X}\right)\right] \qquad \ldots (5.6)$$

Notes: Travel time Δt; Downwind distance X, Crosswind Y, Vertical Z; Source Q; Eddy diffusivities K; Source at (O,O,H); u = U = windspeed.

usually linear in concentration, having form

$$\chi \frac{\partial C}{\partial n} + \beta C = f(t)$$

for the flow bounded at n with β representing absorption. With $\beta = \infty$, absorption is complete, while $\beta = 0$ corresponds to total reflection. For a flow bounded by solid walls the boundary conditions are homogeneous: $f(t) = 0$. For a flow unbounded in any direction, $f(t) = 0$ and $\beta = \infty$, so that $C \longrightarrow 0$ as $n \longrightarrow \infty$ With instantaneous sources initial conditions on $C(\underline{X},t)$ are used ($\underline{X}$ = position): for continuously active sources the boundary conditions are inhomogeneous with $f(t) \neq 0$.

The ease of solution varies with the problem: we require some perspective on the validity of formulae common in models of air pollution (e.g. the collection of results in Turner, 1970; Bibbero and Young, 1974).

Analytical solutions are available for the case of constant wind speed U and constant diffusivities K_X and K_Y: Table 5.1 presents four results under this condition (constant U, K). The equation 5.4 will be recognised as the Gaussian continuous point source formula (Pasquill, 1961: Section 5.4 below) used to define the functions $\sigma_Z(X)$, $\sigma_Y(Z)$ in the Pasquill category scheme, provided the relationships

$$\sigma_Z = \sqrt{2K_Z t} \quad \text{and} \quad \sigma_Y = \sqrt{2K_Y t} \qquad \ldots(5.7)$$

apply. Then equation 5.4 becomes

$$C(X,Y,Z) = \frac{Q}{2\pi\sigma_Y\sigma_Z U} \exp\left(\frac{-Y^2}{2\sigma_Y^2}\right)\left[\exp\left(\frac{-(Z-H)^2}{2\sigma_Z^2}\right) + \exp\left(\frac{-(Z+H)^2}{2\sigma_Z^2}\right)\right] \quad ..(5.8)$$

Experimentally however all four equations (constant U, K: Table 5.1) are unsatisfactory (Monin and Yaglom, 1971f): they do not give at large X the correct dependence of concentration on X. Presumably they are satisfactory at small X though. Monin and Yaglom (1971f) ascribe the discrepancy to the constant U and K: they suggest inclusion of wind shear.

When variable functions U(Z), K(Z) are used in the equation, analytic solution becomes difficult: numerical integration is required although integral moments give some information (Monin and Yaglom, 1971g).

Returning to the equations 5.4, 5.7, 5.8, we note that Hoffert (1972) plots σ_Y and σ_Z in the form $\sigma = \sqrt{X}$ (remember $t \simeq X/U$), showing that the latter is not as in the empirical curves for $\sigma_Z(X)$ and $\sigma_Y(X)$. This discrepancy between $\sigma_Z(X)$, $\sigma_Y(X)$ and $X^{\frac{1}{2}}$ is explained by the discussion in Monin and Yaglom (1971h) suggesting that the simple form $\sigma = \sqrt{2Kt}$ is inadequate when wind shear is included and that the functional relationship between σ, K and t depends on the type of functions U(Z), K(Z) that are assumed. (See also Section 5.6.2: Drivas and Shairs' work). Therefore it seems that the equations in Table 5.1 (constant U, K) are useful formulae provided empirical functions (Section 5.4) of $\sigma(X)$ are used.

When considering long range diffusion, one must also consider the possibility of restricted vertical diffusion. Pasquill (1961) suggested the use of a constant σ_Z when the plume reaches the ceiling. We are dealing with pollutants close to the source and so do not consider this further although it is important in city models (e.g. Johnson et al., 1971).

5.4 Estimation of Plume Standard Deviation to Downwind Distance

Two schemes have been suggested. The first relates plume widths to measured fluctuations of the wind direction (Hay and Pasquill, 1959; Pasquill, 1961) and the second, for when measured fluctuations are unavailable, defines a stability category by wind-speed and solar radiation (Pasquill, 1961); the plume geometry is then defined for each category.

5.4.1 Plume Standard Deviation from Fluctuations of Wind Direction

Hay and Pasquill (1959) assumed that the Lagrangian and Eulerian autocorrelograms were similar in shape but that their integrals decayed to the same value in times whose ratio was β . Knowing β (specified originally by short-range crosswind diffusion and later by the intensity of turbulence (Pasquill, 1971)) one could smooth the wind-fluctuation trace over a time s, such that the spread of material by turbulence could be uniquely related to the measured statistics of the turbulence. Empirical values for β are scattered but 4 is typical (Pasquill, 1961; Monin and Yaglom, 1971i).

Bivanes record vertical and horizontal wind-direction fluctuations with a good time resolution during a sampling time τ . The mean wind speed U and travel distance X are measured to obtain $s = X/\beta U$ for that sample. The traces are smoothed over a moving interval s. The standard deviations for horizontal and vertical wind-direction fluctuations, σ_θ and σ_ϕ (radians) respectively, are then calculated. The plume widths are estimated as $\sigma_Y(X) = X.\sigma_\theta$ and $\sigma_Z(X) = X.\sigma_\phi$, ... (5.9) (Hay and Pasquill, 1959; Pasquill, 1961; Pasquill 1971) for use in the continuous point-source formula (equation 5.8).

Islitzer (1961) used an elevated point-source in a tracer experiment to derive $\sigma_Y(X)$ from the plume concentrations at ground level and σ_θ from a bivane recording. He suggested $\sigma_Y(X) = 0.81.\sigma_\theta.X$, when σ_θ was smoothed over five seconds, with good correlation. With $\sigma_Y(X)$ thus determined he applied the continuity condition to the continuous point-source formula (equation 5.8) to derive $\sigma_Z(X)$. Using the downwind positions of concentration maxima as additional evidence he obtained for the plume

$$\sigma_Y(X) = \frac{1}{1.23} \sigma_\theta.X \quad \text{and} \quad \sigma_Z(X) = \frac{1}{1.23} \sigma_\phi.X$$

Leahey and Halitsky (1973) measured with bivanes the turbulence of the air in the Hudson River valley so as to study possible diffusion without using tracers: they were able to recognise the possible role of inversions in initiating katabatic winds or surges of dense air which may cause large changes in wind direction. They also studied the diurnal changes in turbulence with the break up of inversions at sunrise causing a maximum in horizontal fluctuation then, and the increase in vertical fluctuation during the day, as insolation increased. This is an interesting application of the bivane method to study turbulence as relating to diffusion in a complex site.

5.4.2 Plume Standard Deviation from Stability Categories

Mechanical turbulence arising from wind shear may be increased or decreased by the effects of buoyancy. The former depends on wind speed and surface roughness and the latter on heat transfer to the air from incoming radiation. Hoffert (1972) gives a fuller review of these aspects of stability than we have room for here. Thus the method of Pasquill (1961) as reworked by Gifford (1961) gave curves of plume standard deviation to downwind distance for a continuous point-source release (equation 5.8) in terms of six categories (Table 5.2); the categories were defined by wind speed and insolation (using time of day and cloud cover). These curves have been expressed as power law functions by Geomet (1971) as in Table 5.3 and were used in the present project.

A modified form of the Pasquill stability categories has been described by Smith (1972) and Pasquill (1974) ; a closely related scheme was obtained from M J O Dutton in Department Met O9 of the Meteorological Office as two FØRTRAN subprogrammes.

1. FUNCTIØN MST2 (Z, NCLØUD, NWIND) to derive a value of the stability index MST2 ranging from 1 to 10 for categories A,A-B, B, B-C, C, C-D, D, E, F, or G according to the incoming solar-radiation Z, mwatt cm^{-2} (assuming clear skies), cloud cover NCLOUD, oktas, and wind speed NWIND in knots. The subprogramme is based on Table 5.4. In the present project when the intermediate categories (e.g. A-B) occurred, the average of two curves (A and B) from Table 5.3 were used.

TABLE 5.2

Pasquill Stability Categories (Pasquill, 1961)

Surface wind speed (at 10m) ms^{-1}	Insolation			Night	
	Strong	Moderate	Slight	Thinly overcast or ≥ 4/8 low cloud	≤3/8 cloud
< 2	A	A - B	B	-	-
2 - 3	A - B	B	C	E	F
3 - 5	B	B - C	C	D	E
5 - 6	C	C - D	D	D	D
> 6	C	D	D	D	D

Note: Bibbero and Young (1974) relate categories to σ_θ for a bivane trace as, approximately, (cf. Section 5.3.1)

A, 25^{o} or 0.436 rad; B, 20^{o} or 0.349 rad;

C, 15^{o} or 0.262 rad; D, 10^{o} or 0.175 rad;

E, 5^{o} or 0.0873 rad; F, 2.5^{o} or 0.0436 rad.

TABLE 5.3

Power Law Functions for Plume Parameters σ_z and σ_y (Geomet, 1971)

Class		σ_y [1]	σ_z [2]							
Geomet	MST2 [3]	a_y	a_x	b_x	$X < X_1$ X_1	a_x	b_x	$X_1 < X < X_2$ X_2	a_x	b_x
A	(1)	0.40	0.125	1.03	250	0.00883	1.51	500	0.000226	2.10
B	(3)	0.295	0.119	0.986	1000	0.0579	1.09	10000	0.0579	1.09
C	(5)	0.200	0.111	0.911	1000	0.111	0.911	10000	0.111	0.911
D	(7)	0.130	0.105	0.827	1000	0.392	0.636	10000	0.948	0.540
E	(8)	0.098	0.100	0.778	1000	0.373	0.587	10000	2.85	0.366

Note 1: $\sigma_y(X) = a_y(X^{0.903})$

Note 2: $\sigma_z(X) = a_x(X^{b_x})$

Note 3: Index MST2 as used in present work

TABLE 5.4

Modified Pasquill Categories: Stability Index MST2 used in present work (Chapter 6)

Wind Speed, kt	Daytime (excluding 1h after sunrise, 1h before sunset) Incoming solar radiation (mW cm^{-2})				Within 1h of sunset or sunrise	Night time[1] Cloud amount (oktas)		
	Strong ≥ 60	Moderate 30-60	Slight ≤ 30	Overcast		0 - 3	4 - 7	8
<4	A	A - B	B	C	D	F or G	F	D
4-6	A - B	B	C	C	D	F	E	D
6-10	B	B - C	C	C	D	E	D	D
10-12	C	C - D	D	D	D	D	D	D
>12	C	D	D	D	D	D	D	D

Note 1: Night was originally defined to include periods of one hour before sunset and after sunrise. These two hours are always categorised here as D.

Note 2: See over.

TABLE 5.4 (continued)

Note 2: Pasquill (1961) said that in light winds on clear nights the vertical spread may be less than for category F, but excluded such cases because the surface plume is unlikely to have any definable travel. They are important from the point of view of the build up of pollution and category G (night time, 0 or 1 okta of cloud, windspeed 0 or 1 kt) was added when coding to derive MST2 was written at the Meteorological Office. Present project used the coding supplied, but (Chapter 6) when MST2 was returned with a value of 8, 9 or 10, for E, F or G respectively, category E (Table 5.3) was used. No calculation was made for zero windspeed.

2. FUNCTIØN SØLR2(NNTIME, NNDAY, NMØNTH, NLAT) to estimate incoming solar radiation Z for clear skies from ten years of data gathered at Cambridge; the subprogramme incorporates a correction for latitude so that it can be applied over latitudes 48N to 60N. SØLR2 is a function of time of day, NNTIME (Greenwich Mean Time; hours and tenths), day of month NNDAY, month NMØNTH and latitude NLAT (degrees and tenths). Figure 5.1 shows the radiation contours from which Z is interpolated; Table 5.5 shows the allowance made in SØLR2 for cloud cover.

Other modified category schemes have been published but these are tied up with studies of urban influences on diffusion as discussed in the next Section.

5.5 Diffusion over Urban Areas

The above descriptions of plume behaviour stem from the open-country predictions for continuous emissions (Pasquill, 1961). Extrapolation to urban areas has been made for convenience in predictions of urban pollution although the surface roughness and thermal properties are different for city and country.

Pasquill (1970) discussed heat-island effects in some detail; he suggested that when predicting air pollution over any terrain two meteorological conditions can be considered:

1. When geostrophic winds exceed 5 ms^{-1}, the airflow is well defined

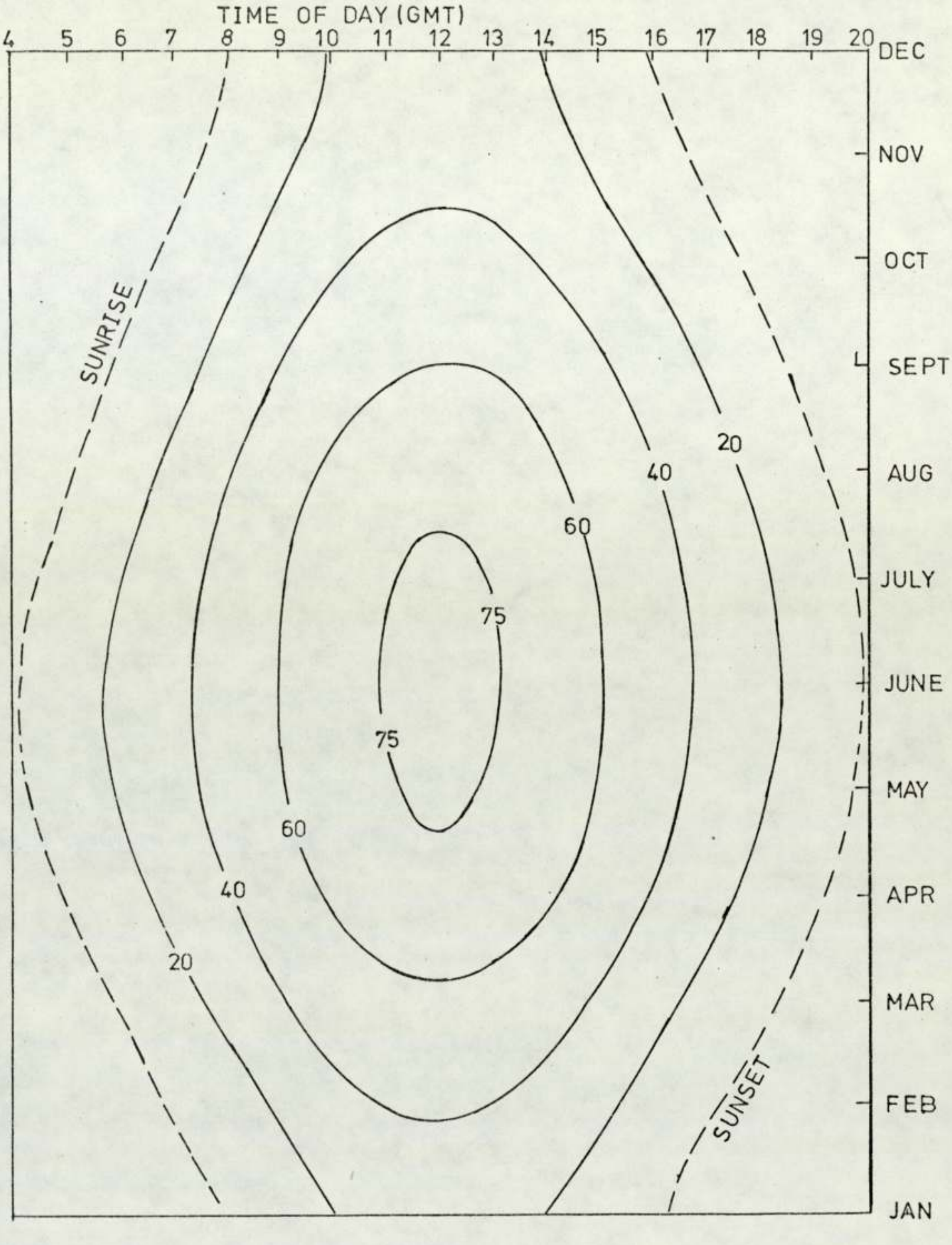

FIGURE 5.1 INCOMING SOLAR RADIATION IN MILLIWATTS PER CM^2 REACHING THE GROUND ON A CLOUDLESS DAY, AS A FUNCTION OF TIME OF DAY AND MONTH. TABLE 5.5 SHOWS CORRECTION FACTORS FOR CLOUDY CONDITIONS. (Information supplied with the punched cards for Functions SOLR2 & MST2 – see Section 5.3.2).
THIS FIGURE IS BASED ON CAMBRIDGE DATA:- FUNCTION SOLR2 HAS A CORRECTION FOR LATITUDE, EXTENDING IT OVER 48N TO 60N.

TABLE 5.5

Reduction of Incoming Solar Radiation by Cloud

Cloud Amount (oktas)	Fraction to Multiply I.S.R.[1]
0	1.07
1	0.89
2	0.81
3	0.76
4	0.72
5	0.67
6	0.59
7	0.45
8	0.23

Note 1: I.S.R. is Incoming Solar Radiation:

See Figure 5.1

and the open-country method can be extended to the city.

2. When light winds occur the flow is not subject to large-scale control.

Comparisons of urban and country diffusion were made by Pooler (1966), McElroy (1969) using tracers in St Louis, United States of America. They measured wind movements with anenometers, bivanes and a radar-tracked tetroon; the tracer plume was sampled at ground-level to give $\sigma_Y(X)$. The continuity equation applied to the continuous point-source formula gave $\sigma_Z(X)$. Indirect (Pasquill type) and direct (gustiness; wind-direction fluctuations from bivanes with conditions of vertical stability by temperature) indices of turbulence were compared with $\sigma_Y(X)$ and $\sigma_Z(X)$ for the tracer plume. These city $\sigma_Y(X)$ and $\sigma_Z(X)$ were similar to the Pasquill curves for open-country provided an initial plume-size similar to that of buildings was used: Pooler (1966) suggested an extra 80 m to $\sigma_Y(0)$ and 30 m to $\sigma_Z(0)$. Dispersion could be described by the common indices (cf. Pasquill type) although the most detailed one using directional-fluctuations (cf. bivane method of Section 5.4.1) σ_θ and vertical stability (Ri or Richardson number) were the best. Either travel distance, X, or travel time, t, can be used to define the plume: $\sigma_Y(X)$ was better than $\sigma_Y(t)$ while $\sigma_Z(X)$ was comparable to $\sigma_Z(t)$ (this depended on whether it was day or night).

The urban area increased the initial crosswind dispersion though this converged to open-country results at greater distances. Vertical dispersion was significantly enhanced, particularly in stable conditions. Restrictive layers aloft sometimes significantly affected the vertical dispersion and concentrations near the ground.

Following this urban tracer-work, Johnson et al. (1971) found a surface-based inversion often occurred in mornings with low wind-speeds, yet the Pasquill type scheme predicted moderately unstable weather conditions: they suggested an additional time classification (Table 5.6) for early morning and late afternoon cases. They allowed for the enhanced vertical diffusion in the city by an initially finite plume size of σ_Z = 10m at X = 50m for all stabilities. A comparison of initial plume sizes to allow for local roughness is given in Table 5.7.

In view of Pasquill's remarks as to the predictability of air-flow (weather condition 1), we note that Johnson et al. (1971) proposed a helical circulation in street canyons as a function of wind-speed above roof-level. It has been suggested (Calder, 1970) that puff models which follow the trajectories of individual puffs of gas may be useful in calm conditions (where a continuous Gaussian "plume" is undefined) or where local flow effects are important. Such models are more complex (see, for example, Chapters Six and Ten in Stern, 1970); no further discussion will be presented here.

5.6 Line-Source Result for Idealised Road

We have seen above that the continuous point-source (Gaussian) formula, with constant U and K, (equations 5.4, 5.7 and 5.8). conveniently defines plume behaviour when empirical curves for $\sigma_Z(X)$

TABLE 5.6

Alternative Scheme for Stability Index[3] allowing for early morning and late afternoon cases (Given as Table 12 by Johnson et al., 1971)

Surface winds (Knots)	Daytime (SR[1] + 4 hours to SS[1] 3 hours)			Early morning and late afternoon (SR + 1 to SR + 3 and SS - 2 to SS - 1)	Night time SS to SR	
	Strong Insolation	Moderate Insolation	Slight Insolation		$\geq$5/10 cloud[2]	$\leq$4/10 cloud[2]
$\leq$3	1	2	2	4	5	5
3 - 6	1	2	3	4	4	5
6 - 10	2	3	3	4	4	4
10 - 12	3	3	4	4	4	4
$\geq$13	3	4	4	4	4	4

Note 1: SR = sunrise, SS = sunset

Note 2: Cloud in tenths ...... American publication

Note 3: Johnson et al., (1971) use five stability classes 1 to 5

TABLE 5.7

Estimates of Initial Plume Size

		Initial Size	Reference
Urban Diffusion	Add 80m to σ_y Add 30m to σ_z	σ_y = 80m, σ_z = 30m (all stabilities)	Pooler (1966)
Urban Diffusion	(1) Add 50-60m to σ_y Add 20-30m to σ_z (2) $\sigma_z(0)$ = BH/2.15 $\sigma_y(0)$ = BL/4.3	σ_y = 50-60m, σ_z = 20-30m (all stabilities) Varies with topography BH = Building Height BL = Building Length	McElroy (1969)
Urban Diffusion[1]	Curves for $\sigma_z = ax^b$ Cross at X = 50m	All stabilities σ_z = 10m for $0 \leqslant X \leqslant 50$m	Johnson et al. (1971)
Vehicle Wake[2] (used in present work)	$\sigma_y = 0.13X^{0.903}$ $\sigma_z = a(X+c)^b$ with c = 27m	Neutral stability σ_z = 1.5m at X = 0	Calder (1973)

Note 1: Model extended to include a streets submodel - a more detailed approach to topography than use of an initial plume size (Johnson et al., 1971).

Note 2: Has disadvantage: varies with stability class - see Section 6.2.4, Paragraph 1.

and $\sigma_Y(X)$ are used. We draw on this background to consider the concentration from a road: an integral of the continuous-source Gaussian-plume for a long straight road (Calder, 1973), and a tracer study of SF_6 released from a vehicle travelling crosswind (Drivas and Shair, 1974).

5.6.1 Integral of Continuous-Source Gaussian-Plume Formula Along a Road

Calder (1973) draws on the classic result for an infinite line source to predict the concentration distribution at various wind angles for small enough distances that the road may be regarded as infinitely long. He defines axes as in Figure 5.2, and a general function

$$Cp = Qp.\varnothing\ (x,y) \qquad \ldots (5.10)$$

to define the concentration Cp at the point x, y for a point-source of constant strength Qp at the origin, with a dilution function in general form $\varnothing(x,y)$. With x, x_o, y, t, θ defined in Figure 5.2, we have $x = x_o + t\sin\theta$ and $y = t\cos\theta$. The integral of the point-source concentration along the infinite line parallel to the road (i.e. along BB^1) is

$$D\ (\theta,x_o) = \int_{-\infty}^{+\infty} Qp.\varnothing\ (x_o + t\sin\theta,\ t\cos\theta)\ dt \qquad \ldots(5.11)$$

If the plume is not too wide, the crosswind gradient of concentration is greater than the downwind gradient: over the traverse BB^1 through

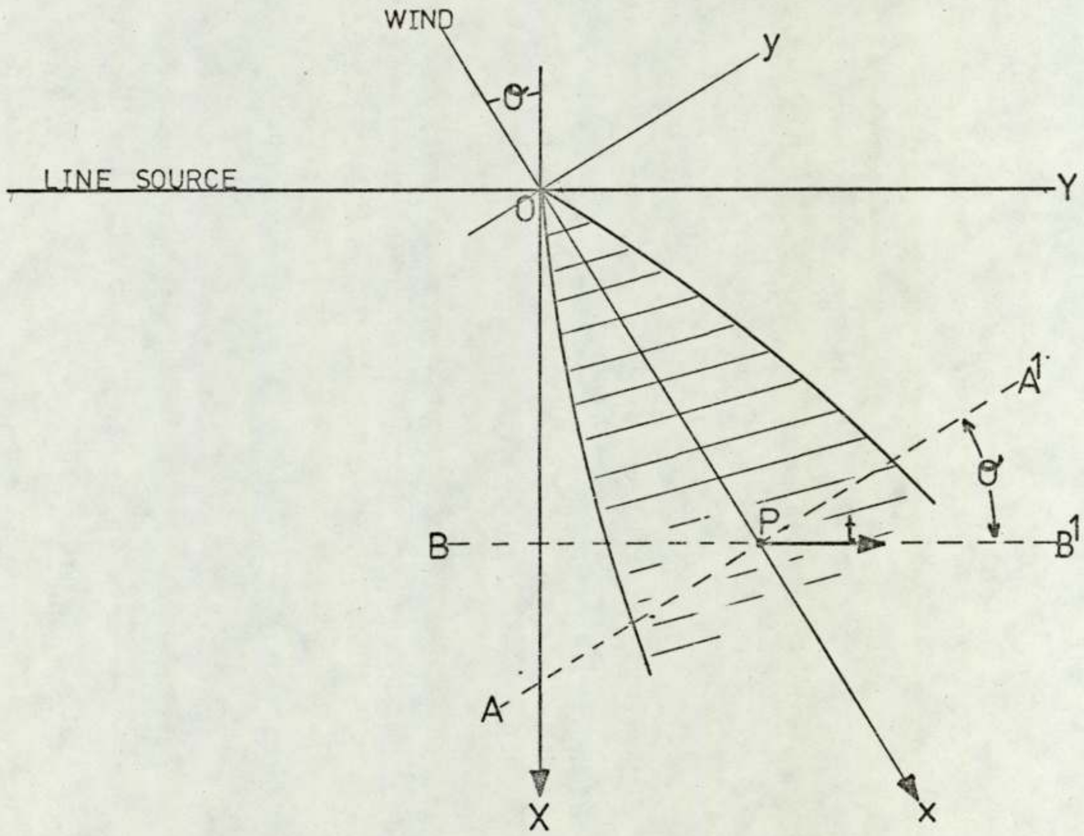

FIGURE 5.2 AXES FOR CALCULATION OF CONCENTRATION DOWNWIND FROM A HIGHWAY, AFTER CALDER, 1973.

the plume, the concentration will vary primarily with perpendicular distance from the plume-axis rather than with distance parallel to the plume-axis. Then $t\sin\theta < x_o$ so

$$D(\theta, x_o) = \int_{-\infty}^{+\infty} Q_p \quad \phi(x_o, t\cos\theta)\, dt \qquad \ldots (5.12)$$

which may be written as $Qp \cdot \frac{\psi(x_o)}{\cos\theta}$, where

$$\psi(x_o) = \int_{-\infty}^{+\infty} \phi(x_o, y) \frac{dy}{\cos\theta} \qquad \ldots (5.13)$$

Consider the line-source distribution as the superposition of infinitesmal point-sources distributed along the line-source, so that Q_p is replaced by the line-source strength Q_L per unit length. Then at the perpendicular distance $X_o = x_o\cos\theta$ from the source, the concentration is

$$C_L(\theta, X_o) = Q_L \frac{\psi(X_o/\cos\theta)}{\cos\theta} \qquad \ldots (5.14)$$

This general result shows the dependence of downwind concentration on wind obliquity θ at perpendicular distance X_o from the source, where $\psi(x_o)$ is as defined above (5.13) for any dilution law $\phi(x, y)$.

Calder (1973) uses the point-source formula (Equation 5.8)

$$\phi\ (x,\ y) = \frac{1}{\pi U \sigma_y(x), \sigma_z(x)} \quad \exp\left(- \frac{y^2}{2\sigma_y^2(x)} \right) \exp\left(\frac{-\ H^2}{2\sigma_z^2(x)} \right)$$

for concentration at ground level from a continuous point-source of unit strength at (O, O, H) to derive the exact result

$$C\ (\theta, X_o) = \frac{Q_L}{\pi U} \int_{-\infty}^{\infty} \frac{\exp\left(- \frac{t^2 \cos^2 O}{2\sigma_y^2(\lambda)} \right) \exp\left(- \frac{H^2}{2\sigma_z^2(\lambda)} \right)}{\sigma_y(\lambda)\sigma_z(\lambda)}\ dt$$

... (5.15)

where $\lambda = \left(\frac{X_o}{\cos\theta} + t\sin\theta \right)$.

For a perpendicular wind, $\theta = O$,

$$C\ (O, X_o) = \frac{Q_L}{\pi U} \int_{0}^{\infty} \frac{\exp\left(- \frac{X_o^2}{2\sigma_y^2(\xi)} \right) \exp\left(- \frac{H^2}{2\sigma_z^2(\xi)} \right)}{\sigma_y(\xi)\sigma_z(\xi)}\ d\xi$$

... (5.16)

These two results must be obtained numerically: an approximate result is

$$C\ (\theta, X_o) = \frac{\sqrt{\left(\frac{2}{\pi}\right)}\ Q_L\ \exp\left(- \frac{H^2}{2\sigma_z^2(X_o/\cos\theta)} \right)}{U\ \cos\theta . \sigma_z(X_o/\cos\theta)}$$

... (5.17)

The functions $\sigma_z(x)$ and $\sigma_y(x)$ may be determined as in Section 5.4.

The turbulence from vehicle motion may be considered as causing an initially finite plume so that from the form (after Calder, 1973)

$$\sigma_z(x) = a(x + c)^b,$$

$$\sigma_z(o) = ac^b \qquad \ldots \quad (5.18)$$

where a, b may be determined as usual for the Pasquill-Gifford curves (cf Table 5.3) with c = o; c = 27m is used when defining the plume for the road (so that σ_z is 1.5m at x = o). In Table 5.8 we show his predictions for C (θ, X_o) derived from Equations 5.17 and 5.15, together with the functions $\sigma_z(x)$ and $\sigma_y(x)$ as used by him (we return to this in Section 6.3).

The present project used this form with c = 27m and a, b defined from Geomet (1971): Table 5.3.

5.6.2 Tracer Study of Instantaneous Cross-wind Line-source

Drivas and Shair (1974) released SF_6 from a quasi-instantaneous line-source, i.e. in the exhaust of an automobile travelling along a road perpendicular to the downwind sampling direction. Concentrations of the SF_6 cloud were determined as a function of time using a squeeze bottle and electron-capture gas chromatograph. For each concentration-to-time curve they calculated the along-wind standard deviation σ_x, the area under the curve, the average travel time and corresponding average wind velocity using average travel time and downwind distance.

TABLE 5.8

Concentration Estimates of Calder (1973) for Infinite Line Source

(Windspeed 1 ms^{-1}; Q_L = 1; wind angle θ;

downwind distance X_o).

Calder's Equation 9 (5.17) and Calder's Equation 12 (5.15)

gave the same results (below)

X_o m	$\theta = 0^o$	$\theta = 15^o$	$\theta = 30^o$	$\theta = 45^o$	$\theta = 60^o$	$\theta = 75^o$
50	0.218	0.221	0.231	0.250	0.282	0.338
100	0.141	0.143	0.148	0.156	0.171	0.197
200	0.085	0.086	0.088	0.092	0.099	0.121
400	0.049	0.050	0.051	0.054	0.061	0.076
800	0.031	0.031	0.032	0.034	0.038	0.048

The Gaussian model equation (Equation 5.7 into Equation 5.5 from Table 5.1) for an instantaneous cross-wind line source,

$$C(X, z = o, t) = \frac{Q_L}{\pi \sigma_x(X,I)\sigma_z(X,I)} \exp\left(\frac{-(x - Ut)^2}{2\sigma_x^2(X,I)} \right)$$

(for stability parameters defined for the stability index I as well as downwind distance X), was not a good description of their results when $\sigma_x(X,I)$ and $\sigma_z(X,I)$ were defined from empirical curves.

A transient solution (Equation 5.5, Table 5.1) using eddy co-efficient K for the diffusivity was also tested, but it too gave Gaussian curves.

Their experimental curves were, in contrast to these two models, decidedly non-Gaussian in shape. The constant U, K solution with a restrictive inversion-layer aloft and a large initial well-mixed zone (20m x 20m) was considered (as a numerical solution), but this also proved inadequate.

To explain the non-Gaussian concentration profiles and an apparent velocity which increases with height, the effect of wind shear was included (cf. Section 5.2: analytical solution is less easy).

They (Drivas and Shair, 1974) considered two possibilities by the method of integral moments:

1. $U = k_1 \ln z$; $k_z = k_2 z$ which predicts tracer spreading $\sigma_z \sim t$.

2. $U = k_1 z^a$; $k_z = k_2 z^c$ which predicts apparent velocity of tracer $U \sim t^{a/(2-c)}$ and tracer spreading $\sigma_z \sim t^{1 + a/(2-c)}$.

A plot of $\ln\sigma_x$ to $\ln t_{ave}$ for the tracer profiles showed slopes ranging from 1.11 to 1.47, which exceeds the prediction of case 1. A plot of ln U to $\ln t_{ave}$ gave slopes a/(2 - c) of 0.13 to 0.55.

These results are consistent with the observation in Section 5.2 that when U (Z), K (Z) are not constant, the simple relation $\sigma = \sqrt{2Kt}$ (Equation 5.7) no longer applies.

Thus the power-law model ($U = k_1 z^a$; $k_z = k_2 z^c$) accurately predicted the increase with time of both the spread and the apparent plume velocity.

They (Drivas and Shair, 1974) concluded that the Gaussian model arising from a constant U and constant K is less satisfactory: the model based upon the semi-empirical diffusion equation with power-law velocity profile and a power-law vertical eddy diffusivity profile was the most consistent interpretation of their data for an instantaneous cross-wind line source.

5.7 Summary: Application to the Present Work

Although there is some debate as to its generality, the semi-empirical diffusion equation usefully describes practical problems of pollutant dispersal. Terms may be included to allow for losses by settling, absorption at boundaries, chemical reaction or decay. Some common formulae have been listed and the present need for empirical definition of the plume parameters has been described. Given the availability of such functions we have discussed the problem of urban diffusion where vertical mixing is enhanced and the problem of low wind-speed particularly difficult. We have considered the use of the results to describe the ideal case of a long straight road analytically and experimentally.

In subsequent chapters we discuss both the routine monitoring results taken near the intersection and an experiment to measure the concentration distribution from the Motorway. In our analyses we shall use empirical functions for the plume parameters (Table 5.3) with stability categories defined by the parameter MST2 (Table 5.4) and a continuous point source plume (Equation 5.8) with initial size defined by Equation 5.18 where C = 27m. Integration will be made over curved and elevated roads by a computer programme (Chapter 6); no mixing ceiling limit is considered as travel distances were limited. Also, no adjustment of the curves was made for urban effects since there were other uncertainties, particularly in the emissions estimates.

CHAPTER 6

CALCULATION OF POLLUTION CONCENTRATIONS

In this Chapter we describe a computer programme which integrates the point source continuous-plume formula (Equation 5.8) over a simplified three dimensional model of the Motorway intersection. The integral is scaled by the emissions estimate and wind-speed to print an estimated concentration alongside that recorded in the field: the latter are then compared. This comparison is made to assess the combination of road layout, emissions estimate, airport weather readings, stability estimates and plume formula as a pollution level predictor. It therefore brings together (Figure 6.1) various parts of the work already described. The Chapter ends by discussing both the calculated pollution levels and those measured in the field.

6.1 Emissions Estimate

The Equation (5.17) given as Calder's (1973) Equation 9, for the concentration of pollution downwind of a line source will be used to estimate the source strength Q_L. The integral over the Y direction for a perpendicular wind

$$C(0,x_o) = \frac{\sqrt{\frac{2}{\pi}}\; Q_L \exp\left(-\frac{H^2}{2\sigma_z^2(X)}\right)}{U.\sigma_z(X)}$$

(Equation 5.17 with $\theta = o$)

Then C is dimensionally equivalent to $Q_L/(U.\sigma_z)$. Various concentration units may be used in the field when measuring C: related units for Q_L are given in Table 6.1.

FIGURE 6.1 DATA PROCESSING TO COMPARE OBSERVED AND CALCULATED CONCENTRATIONS OF POLLUTANTS

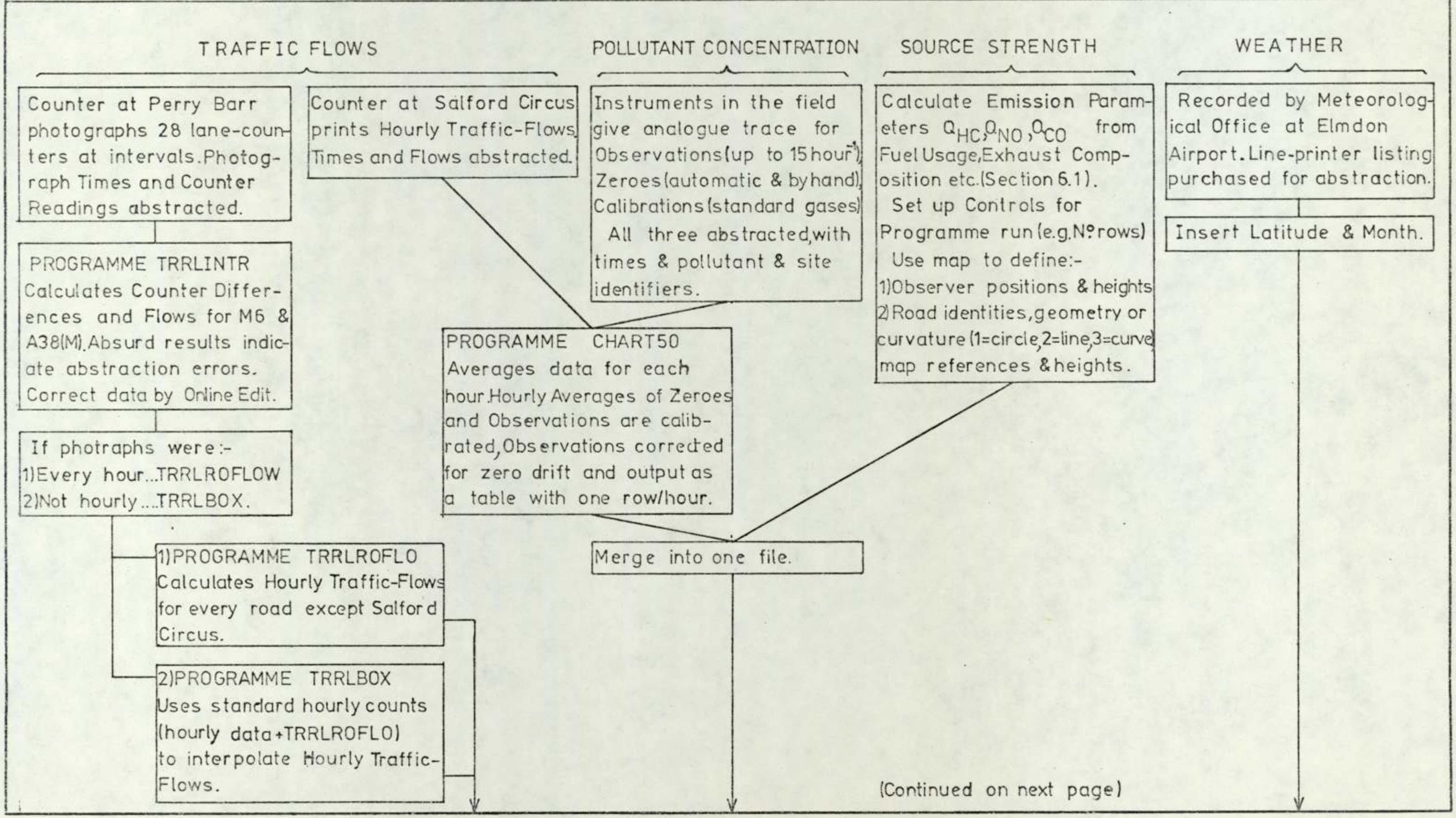

FIGURE 6.1 (CONTINUED)

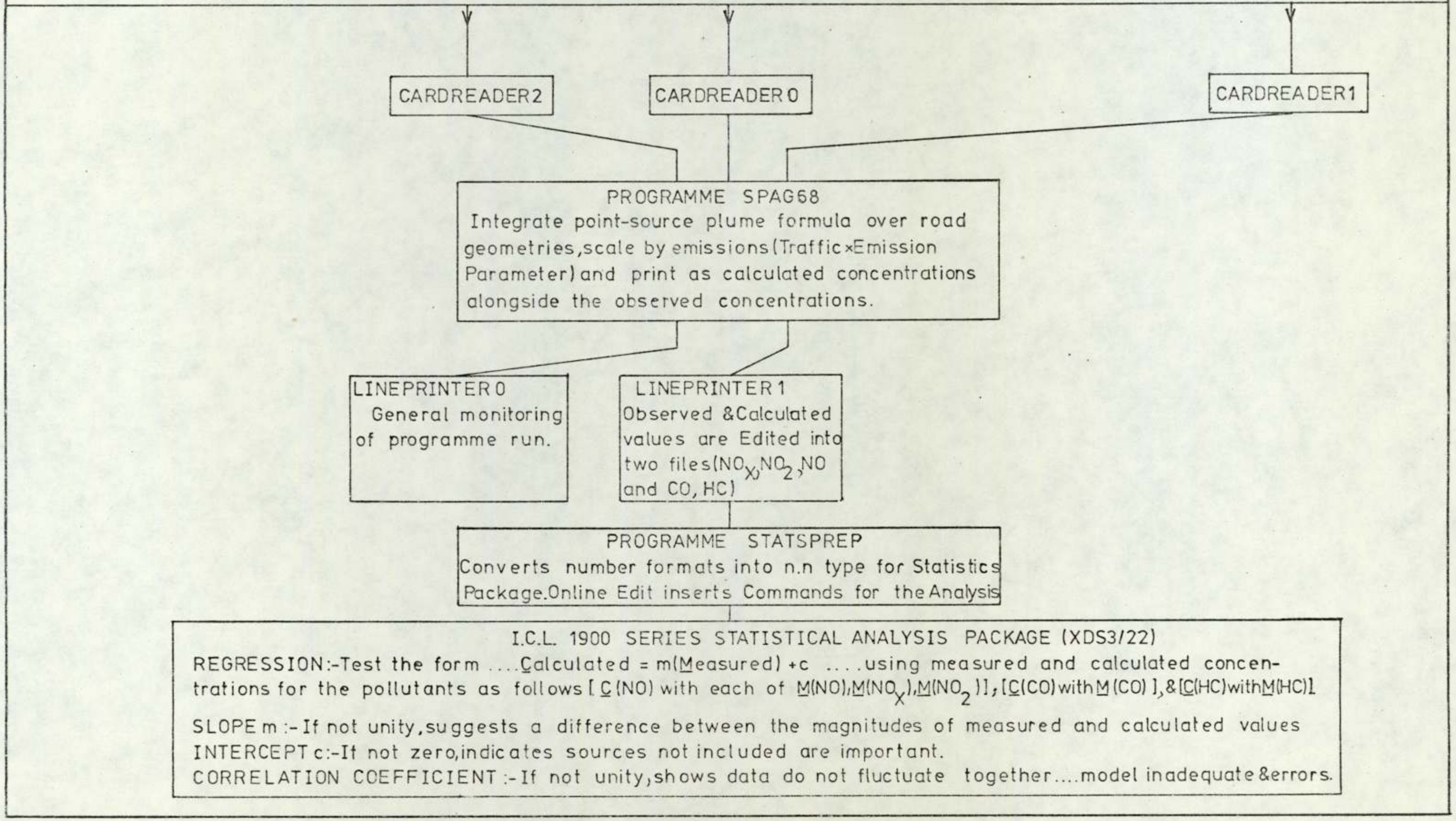

We consider a motorway to be a single line source (unlike Chamberlain, 1974).

Define Q_L = volume emitted per unit length of road per second for whatever traffic is passing. The emissions parameter Qi is the value of Q_L for the gas i emitted by unit traffic flow.

$$Qi = Q_L/T$$

Consider one vehicle:

Fuel consumption = F l per km road

∴ Fuel burnt per metre of road = $10^{-6}F^{-1}$ m^3 per m road

Density of fuel = ρ kg m^{-3}

Mass of fuel burnt per metre road = $10^{-6}F^{-1}.\rho$ kg per m road

Stoichiometry of combustion = s air:fuel ratio by mass

∴ Mass of exhaust gas per metre of road = $10^{-6}F^{-1}.\rho.s$ kg per m road

Density of air = ρA kg m^{-3}

Volume of exhaust gas per metre of road $V_E = 10^{-6}F^{-1}.\rho.s.(\rho A)^{-1}$

m^3 per m road

V_E (m^3 per m road) is the volume of exhaust gas emitted per metre of road when one vehicle travels down the road. If T vehicles travel the road in say one hour (corresponding to a flow T vehicles h^{-1}), the emission per metre of road is V_ET (m^3 per m road) and it occurs for one hour: converting to seconds the emission Q_L(EXH) of exhaust gas in m^3 per metre of road per second for a flow T vehicles h^{-1} is

$$Q_L(\text{EXH}) = \frac{V_ET}{3600} = \left(\frac{10^{-6}\rho s}{3600(\rho A)F}\right) T \quad m^3s^{-1} \text{ per m road}$$

The exhaust gas contains c ppm by volume of pollutant so

$$Q_L = \left(\frac{c\,\rho s\; 10^{-12}}{3600\,(\rho_A)F}\right) T \quad m^3 s^{-1} \text{ per m road},$$

which in Equation 5.17 will give the concentration in volume-volume ratio. For convenience, we define λ such that

$$Q_L = \lambda . c . T . 10^{-6} \qquad \text{"ppm" } m^3 s^{-1} \text{ per m road},$$

where

$$\lambda = \frac{\rho s\; 10^{-9}}{3{\cdot}6\;.\rho_A F} \qquad \text{to give concentration in ppm by volume.}$$

Where necessary, subscripts P and D will denote petrol and diesel respectively. In Table 6.2 we give some literature values for the parameters, and in Table 6.3 derive values for Q_L under several engine conditions. Under different conditions very different exhaust gas compositions are produced (cf. Fussel, 1970). In the present work we used the values for half power (Table 6.3) and a traffic mixture of 60% petrol, 40% diesel (manual count at site by J D Butler) to derive emission parameters Qi as in Table 6.4.

There is some difficulty in arriving at a satisfactory emissions estimate: there may be considerable errors in the values used. The uncertainty for NO could be 100% (for NO, half-load), or in the extreme, 1000%(for CO, half-load). Nevertheless the values in Table 6.4 are used throughout the project - at no time are calculated values "calibrated" using field measurements. Comparisons will be made between pollutant levels calculated from these uncertain emissions estimates and measured in the field: the range of values in Table 6.3 should be remembered.

TABLE 6.1

Dimensions and Units of Concentration C and Source

Strength Q_L for a Line Source (using $Q_L = u\sigma_z C$)

Emission	Dimensions		Example Units	
	C	Q_L	C	Q_L
Mass	$[M][L]^{-3}$	$[M][L]^{-1}[T]^{-1}$	$kg\ m^{-3}$	$kg\ m^{-1}s^{-1}$
Volume	$[L]^3[L]^{-3} = 1$	$[L]^3[L]^{-1}[T]^{-1} = [L]^2[T]^{-1}$	Volume-volume ratio	m^2s^{-1}

TABLE 6.2

Parameters for Fuels and Engines (λ defined so that $Q_L = \lambda\ CT$ gives calculated concentration in ppm by volume)

Variable		Value	Units	Foot-note	Comments
ρ_A		1.225	kg m^{-3}	1	Air at N.T.P.
ρ	ρ_P	$0.78.10^3$	kg m^{-3}	2	Petrol density
	ρ_D	$0.84.10^3$	kg m^{-3}	3	Diesel density
S	SP	14.5:1	mass ratio	4	Stoichiometry for petrol engine
	SD	25:1	mass ratio	4	Stoichiometry for diesel engine
F	F_P	9	km l^{-1}	5	Petrol vehicle fuel usage
	F_D	5	km l^{-1}	5	Diesel vehicle fuel usage
λ	λ_P	$2.8494.10^{-7}$			Petrol
	λ_D	$9.5238.10^{-7}$			Diesel

Note 1: Handbook of Chemistry and Physics (1970 - 1971) Edition 51 Table F147. The Chemical Rubber Co.

Continued/......

TABLE 6.2 (continued)

Note 2: Air Pollution Control in Transport Engines (1971) Table 132.3 Institute of Mechanical Engineers, London.

Note 3: Air Pollution Control in Transport Engines (1971) Table 137.1, Institute of Mechanical Engineers, London.

Note 4: Fussel D R (1970) Atmospheric Pollution From Petrol and Diesel Engined Vehicles Petrol Rev 24, 192 - 202.

Note 5: Derwent R G and Stewart H N M (1973) Air Pollution from the Oxides of Nitrogen in the United Kingdom Atmos. Environ. 7, 385 - 401.

TABLE 6.3

Exhaust Concentrations and Line-Source Strengths for Gaseous Pollutants. Concentration c ppm and Traffic Flow T = 1 vehicle h^{-1} are used in Equations $Q_L = (2.8494.10^{-7}Tc)$ for petrol and $Q_L = (9.5238.10^{-7}Tc)$ for Diesel so that Q_L will give calculated downwind concentrations in ppm: see Section 6.1

Gas Engine		FULL LOAD		HALF LOAD		NO LOAD		IDLE	
NO		C	$Qi = Q_L/T$	C	$Qi = Q_L/T$	C	$Qi = Q_L/T$	C	$Qi = Q_L/T$
Petrol	2	6000	$1.7096.10^{-3}$	2000	$5.6988.10^{-4}$	60	$1.7096.10^{-5}$	30	$8.5482.10^{-6}$
	3			1700	$4.8439.10^{-4}$				
	4	1050	$2.9918.10^{-4}$	650	$1.8521.10^{-4}$	20	$5.6988.10^{-6}$	30	$8.5482.10^{-6}$
Diesel	1	921	$8.7714.10^{-4}$	493	$4.6952.10^{-4}$	109	$1.0380.10^{-4}$	119	$1.1333.10^{-4}$
	4	850	$8.0952.10^{-4}$	250	$2.3809.10^{-4}$	30	$2.8571.10^{-5}$	60	$5.7142.10^{-5}$
CO		C	Q_L/T	C	Q_L/T	C	Q_L/T	C	Q_L/T
Petrol	3			6000	$1.7096.10^{-3}$				
	4	30000	$8.5482.10^{-3}$	40000	$1.1397.10^{-2}$	30000	$8.5482.10^{-3}$	70000	$1.9945.10^{-2}$
Diesel	1	2000	$1.9047.10^{-3}$	300	$2.8571.10^{-4}$	300	$2.8571.10^{-4}$	300	$2.8571.10^{-4}$
	4	1000	$9.5238.10^{-4}$						

Continued/......

TABLE 6.3 (continued)

HC		C	Q_L/T	C	Q_L/T	C	Q_L/T	C	Q_L/T
Petrol	3			260	$7.4084.10^{-5}$				
	4	700	$1.9945.10^{-4}$	500	$1.4247.10^{-4}$	4400	$1.2537.10^{-3}$	820	$2.3365.10^{-4}$
Diesel	1	29	$2.7619.10^{-5}$	70	$6.6666.10^{-5}$	90	$8.5714.10^{-5}$	106	$1.0095.10^{-4}$
	4	110	$1.0476.10^{-4}$	55	$5.238.10^{-5}$	160	$1.5238.10^{-4}$	220	$2.0952.10^{-4}$

Note 1: Fussel D R (1970) Atmospheric Pollution from Petrol and Diesel Engined Vehicles Petrol Rev. 24, 192 - 202.

Note 2: Derwent R G and Stewart H N M (1973) Air Pollution from the Oxides of Nitrogen in the United Kingdom, Atmos. Environ., 7, 385 - 401.

Note 3: Fussel D R (1970) Atmospheric Pollution from Petrol and Diesel Engined Vehicles Figure 3 Petrol Rev 24, 192 - 202.

Note 4: Economic and Technical Appraisal of Air Pollution in the United Kingdom PAUM20 (1972) HMSO London

TABLE 6.4

Line-Source-Strength Parameters used in the Present Work (60/40 petrol:diesel; half-power of Table 6.2; values are for unit traffic flow, 1 vehicle hour^{-1}; predicted pollutant concentration will be in ppm by volume)

Gas i	Vehicle Type	ppm in exhaust	Emission Parameters Qi		
			For engine type $Qi = Q_L/T$ in ppm $m^2s^{-1}(vh^{-1})^{-1}$	As used $Qi = Q_L/T$ for 0.6P + 0.4D	Units ppm in v/v ratio
NO	Petrol	1700	$4.8439.10^{-4}$	$4.7843.10^{-4}$	ppm $m^2s^{-1}(vh^{-1})^{-1}$
	Diesel	493	$4.6952.10^{-4}$		
CO	Petrol	6000	$1.7096.10^{-3}$	$1.1400.10^{-3}$	ppm $m^2s^{-1}(vh^{-1})^{-1}$
	Diesel	300	$2.8571.10^{-4}$		
HC	Petrol	260	$7.4084.10^{-5}$	$7.116.10^{-5}$	ppm $m^2s^{-1}(vh^{-1})^{-1}$
	Diesel	70	$6.6666.10^{-5}$		

6.2 Programme to Calculate Pollution from Roads

6.2.1 Outline

The programme (Flowchart: Figure 6.2) integrates numerically the point source continuous-plume formula (Equation 5.8) by the trapezium rule over a set of elevated, curved roads. Pollution was to be calculated at any observer position; for general application Ordnance Survey eight digit (four East, four North) reference positions were used to define all positions (to the nearest ten metres). The programme distinguishes straight, curved and circular sections of the roads. Roads are represented as horizontal, but can be elevated.

Emissions are read in two parts: the emissions parameter Qi (calculated for the unit traffic-flow in the petrol:diesel ratio normally present: Section 6.1) and the hourly traffic-flow of the road being integrated over. Thus Qi is read once and individual traffic-flows on each contributing road are recognised: no allowance for vehicle speed or road slope is made in the emissions estimate.

The integration step-length is read rather than defined as it can affect integral results. Data for measured field-levels of pollution, weather readings and traffic-flows are read hour by hour from three separate input channels: one integration is performed for each row and the prediction printed alongside the measured result. Additional information is printed on a second output channel separate from the table of calculated results.

FIGURE 6.2 FLOWCHART FOR PROGRAMME TO INTEGRATE A POINT-SOURCE PLUME OVER ELEVATED CURVED ROADS

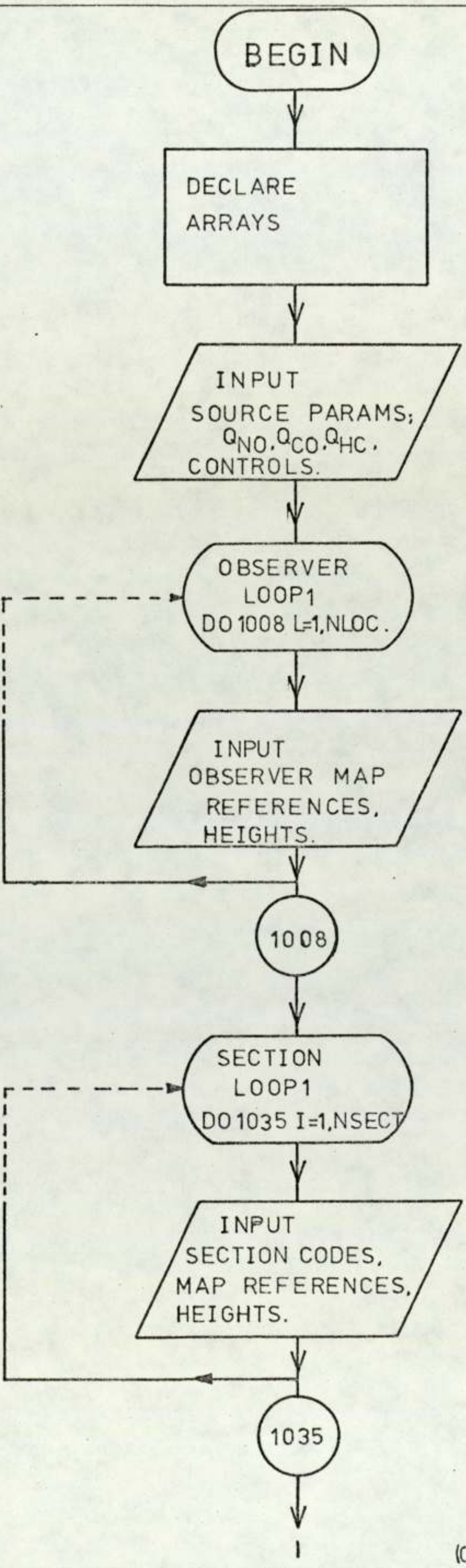

(Continued on next 4 pages):1

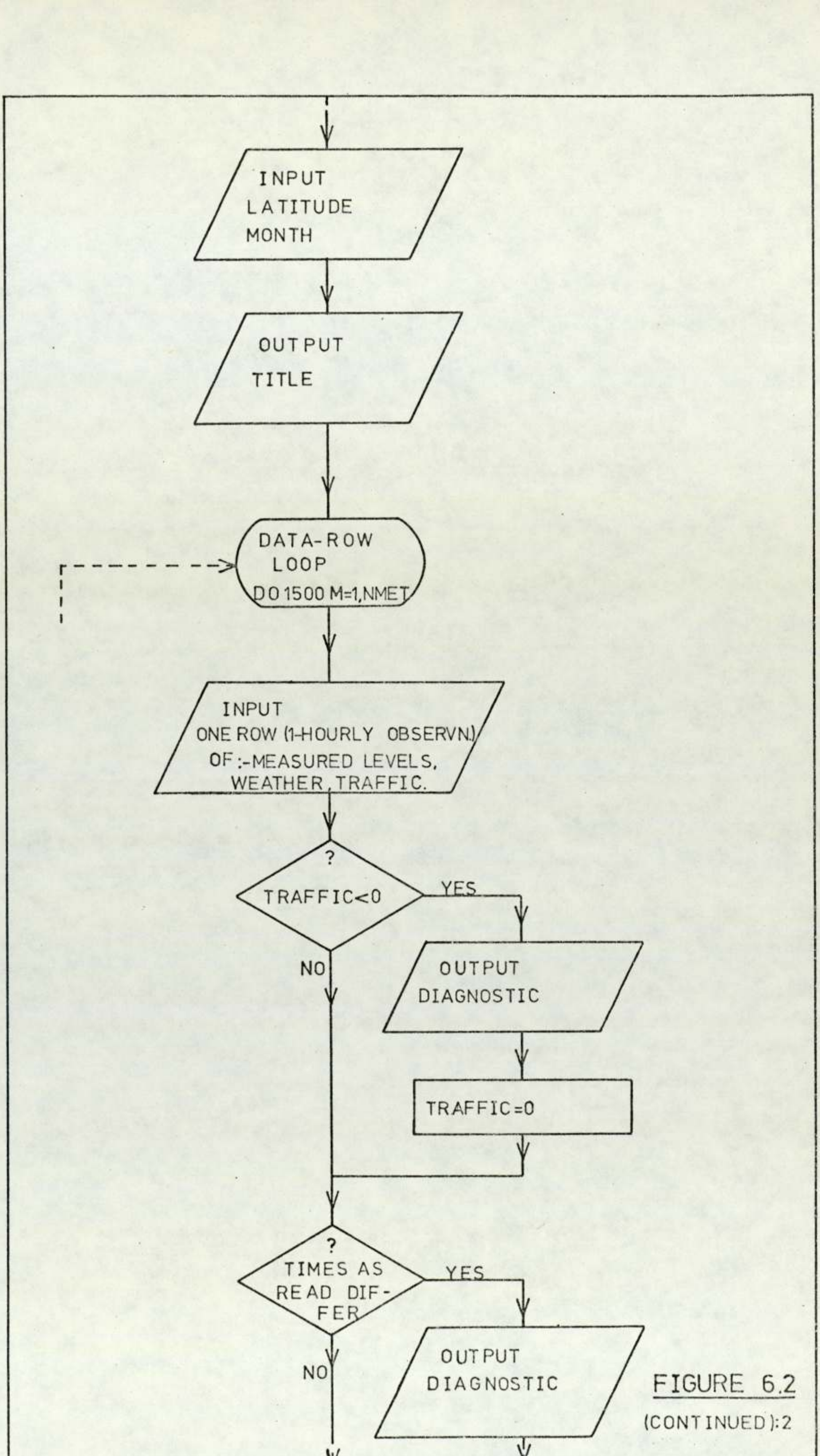

FIGURE 6.2
(CONTINUED):2

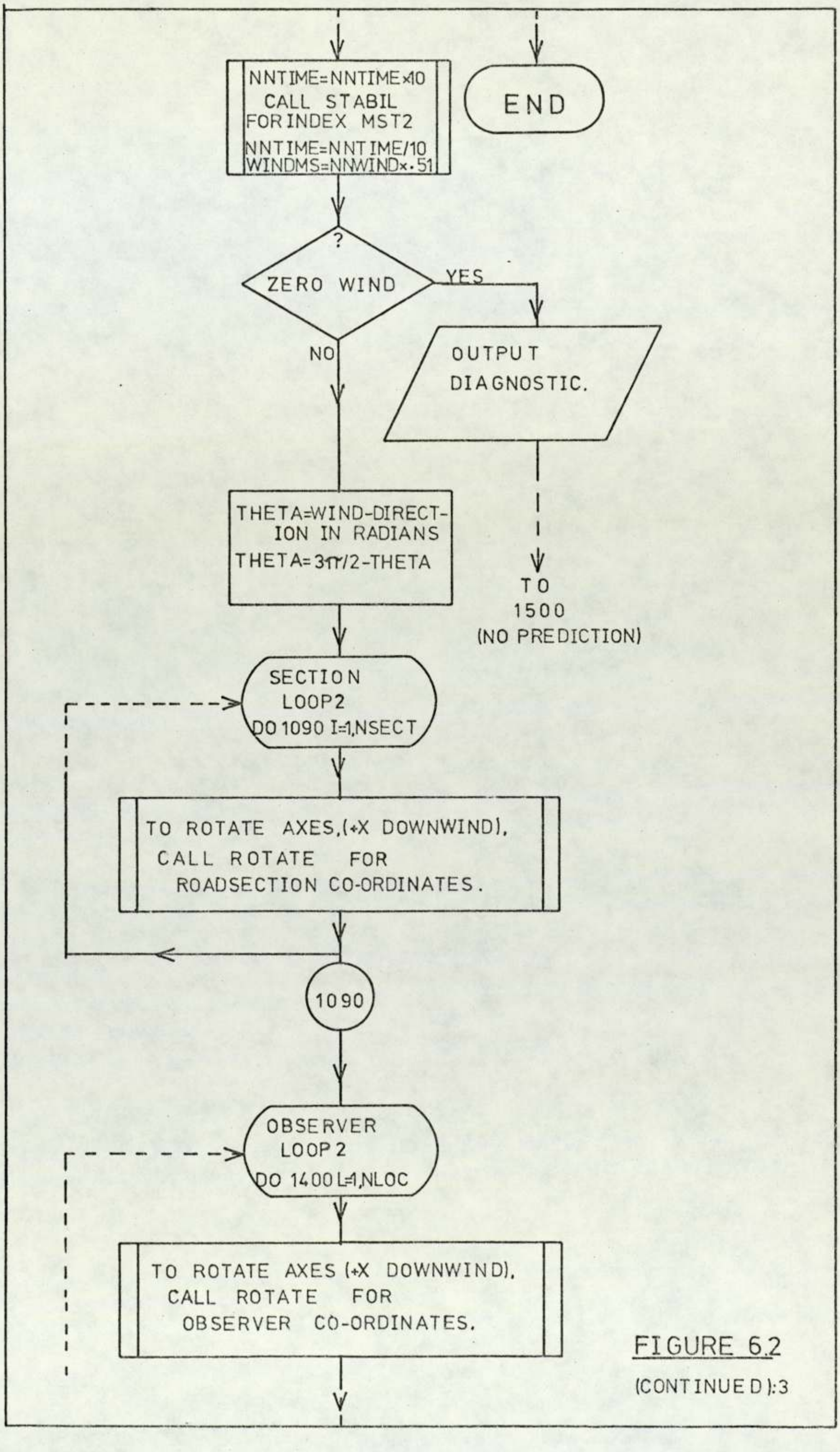

FIGURE 6.2

(CONTINUED):3

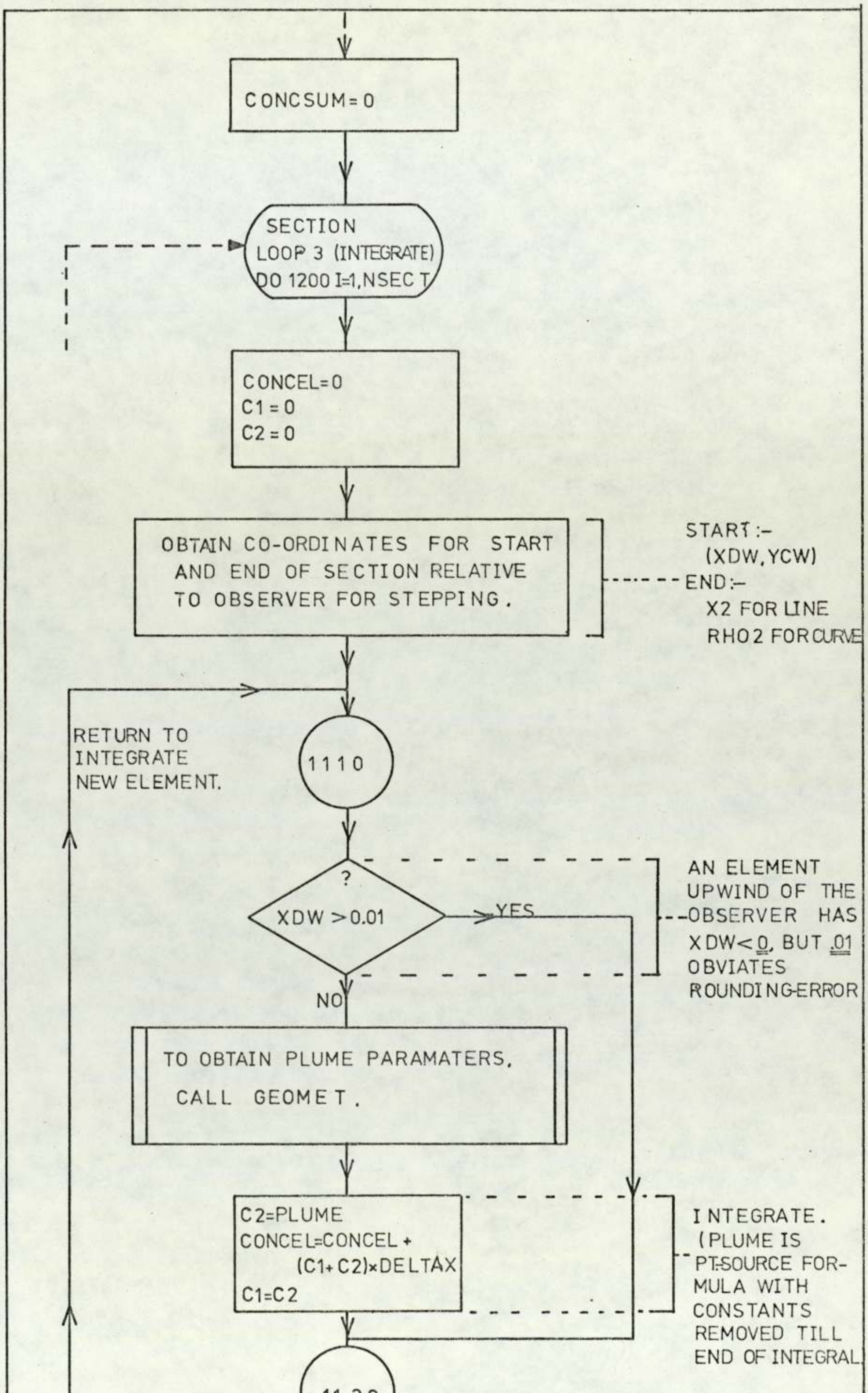

FIGURE 6.2 (CONTINUED):4

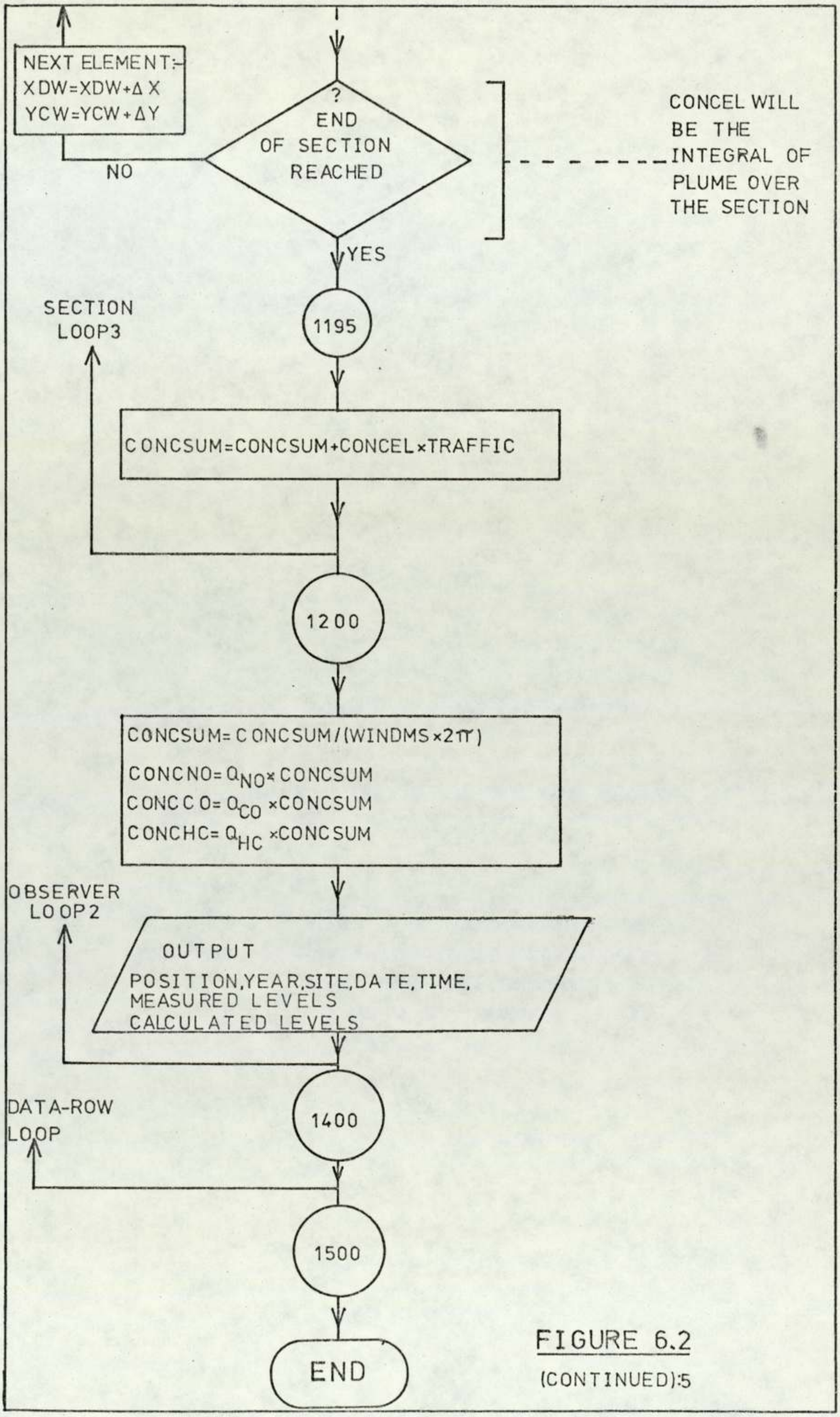

FIGURE 6.2

(CONTINUED):5

```
DOCUMENT     PRED117404                 INPUT TO CARDREADER0

  0.00047843   0.00114  0.000071116                                EMMISION PARAMETERS Q_NO Q_CO Q_HC
 50   1   43   5   24                                              OBSERVER POSITION (HEIGHT=0)
09649018
01   1 3   09099071   12   09289033   000   09609008   000__CURVE   ] MAP REFERENCES
02   1 2   10008988   12   09609608   000                  ]        | FOR ROAD POSITIONS
03   1 2   09099071   12   08909100   000                  }LINES   | (SECTIONS 6-42
04   2 2   08819012   12   08609000   000                  ]        |   DELETED)
05   3 1   09649018   00      50___________________________ CIRCLE  ]
45 23 2    09109022   12   08819011   000
 |  | \_CURVATURE            \_POSITION  \_HEIGHT
 |  \_ROAD IDENTITY
 \_SECTION NUMBER
 74    4   13    4   11   0.108   0.108   0.001   2321   3.1   5.8  FIELD OBSERVATIONS.
 74    4   14    4   11   0.130   0.122   0.008   2355   3.5   5.9
```

```
DOCUMENT     MET117402                  INPUT TO CARDREADER1

525  11______LATITUDE & MONTH
 4   13   350   10   8   900    86    74    60    93    84          0   0 ] WEATHER READINGS
 4   14   350    8   7   700    87    75    60    94    84          0   0 ]
```

```
DOCUMENT     TRARES117403               INPUT TO CARDREADER2

  1974      11        4    MON   19     34    13_ _ _TIME & DATE
  2492    2548              203        854        0      921      39      351       39 ] FLOW ON
  1073       1      537     537         99       44     -227      53     -152      854 ] EACH ROAD
     1       1      249       0_______________________________________________________]
  1974      11        4    MON   19     34    14
  2222    2344              183        874        0      816      64      322       64
   916       1      459     459        117       56     -216      60     -147      874
     1       1      235       0
```

```
DOCUMENT     BAC680400                  OUTPUT TO LINEPRINTER0

   943.6     367.3     751.2 ]
                             | SOME OF THE CENTRES & RADII CALCULATED FOR
   139.0    -478.8     272.2 | CURVED SECTIONS
                             |
   226.4     -65.0     225.0 ]

FIELD   DAY AND HOUR AS READ          4    13                     ]
METDATA DAY AND HOUR AS READ          4    13    350    10    8   | COMMENTS ON
TRAFFIC DAY AND HOUR AS READ          4    13                     | DATA READING
                                                                  |
NEGATIVE TRAFIC FOR I=     17 WAS SET ZERO                        |
NEGATIVE TRAFIC FOR I=     19 WAS SET ZERO                        ]
NEXTELEMENT=    1    1    3XDW   -617.5YCW   -449.6 ]
NEXTELEMENT=    1    1    3XDW   -612.5YCW   -449.5 | STEPPING OVER ELEMENTS
NEXTELEMENT=    1    1    3XDW   -607.5YCW   -448.9 v
```

```
DOCUMENT     BAC680401                  OUTPUT TO LINEPRINTER1

                          FIELDWORK AND THEORY
                                 ---MEASURED------------------------------------------------CALCULATED-
L=  OBSERVPOSN   YR ST HR DY MT  FIELDNOX    FIELDNO     FIELDNO2    FIELD CO    FIELD HC    PRED NO

 1  964. 9018. 74  4 13  4 11 .1080E 00  .1080E 00  .1000E-02  .3100E 01  .5600E 01  .4570E-01
 1  964. 9018. 74  4 14  4 11 .1300E 00  .1220E 00  .8000E-02  .3500E 01  .5900E 01  .3826E-01
                                                                 PRED CO     PREDHC

                                                               .1089E 00  .6793E-02
                                                               .9118E-01  .5688E-02
```

FIGURE 6.3 STRUCTURE OF INPUT AND OUTPUT FOR PROGRAMME SPAG68 TO CALCULATE CONCENTRATIONS OF GASEOUS POLLUTANTS.

Axes are rotated to point positive x in the downwind direction: co-ordinates for the start and end of each section are set up. The programme steps along each section in elements of length as read, and calculates the co-ordinates of the element thus stepped out. If the element is upwind of the observer it contributes to the pollution sum: the downwind distance of the element relative to the observer is negative so that element is included in the summation. Summation proceeds by the trapezium rule. Having summed for that element, the programme finds the next element and repeats until the section of road has been covered. The sum for that section is scaled by the traffic of that section. When all sections have been covered the constants for every section (π , wind-speed, Qi) are included in the sum which becomes the predicted level for print-out.

The plume is defined from empirical curves (Table 5.3) of plume standard deviation $\sigma_y(X)$, $\sigma_z(X)$ as a function of downwind-distance and stability index (Table 5.4). An initially finite plume is used (after Calder, 1973: Section 5.5.1): the distance 27 metres is added to X when calculating $\sigma_y(X)$ and $\sigma_z(X)$, and then subtracted to leave the location of co-ordinates for following elements unchanged. The stability index sub-routine was obtained from the Meteorological Office: Section 5.3.2. It uses cloud cover, wind-speed, time and date to estimate solar radiation and thence stability. Figure 6.3 summarises input and output.

6.2.2 Trigonometry for Road Positions

The curved and elevated structure of the intersection was simplified to lines, curves and circles, each at a particular horizontal level.

This layer structure avoided the need to interpolate heights along sloping sections, although the model could be extended to include this.

In Chapter 4 we described the measurement of traffic counts for each road in the intersection. For the present calculation, each of those roads is broken into sections according to their geometry. Each section has a section number, a road identity number (the same as in Chapter 4) and a curvature parameter. The latter is

1 for a circle (Figure 6.4), when the map-reference for the centre, the radius, and the height are read.

2 for a line (Figure 6.5) when map-references for the two end points, and the height, are read.

3 for a curve (Figure 6.6) when map-references for three points on the curve, and the height, are read:

the sequence is important as a circle is fitted through the three points. The section is defined as an arc of that circle, running from the first to the third point by increasing an angular co-ordinate ρ in the anti-clockwise direction. To define the correct part of the circle the points must be in sequence around the curve, with the most clockwise point first. Figures 6.4, 6.5 and 6.6 describe the trigonometry required to define the layout of the roads and the co-ordinates of small elements stepped out along the roads in steps of variable length Δs.

The prgramme reads the section data for storage by section number according to the curvature parameter (dummy variables are used in the read). Map references are split by the read format into East and North values, and converted to distances in metres from the point 09649018 (a convenient origin on the map in question) to reduce the magnitude of

Map References NS1E,NS1N define the centre at (RCX,RCY)

RCX=(NS1E-0964)×10 metres

RCY=(NS1N-9018)×10 metres

The radius is read as NS2E

RAD=NS2E metres

Axes are then rotated anticlockwise through θ to point the X-axis downwind,using the subroutine ROTATE

CALL ROTATE(θ,RCX,RCY,NCX,NCY) gives new co-ordinates (NCX,NCY) for the centre.

CALL ROTATE(θ,ROBSX,ROBSY,NOBSX,NOBSY) gives new coordinates (NOBSX,NOBSY) for the Observer.

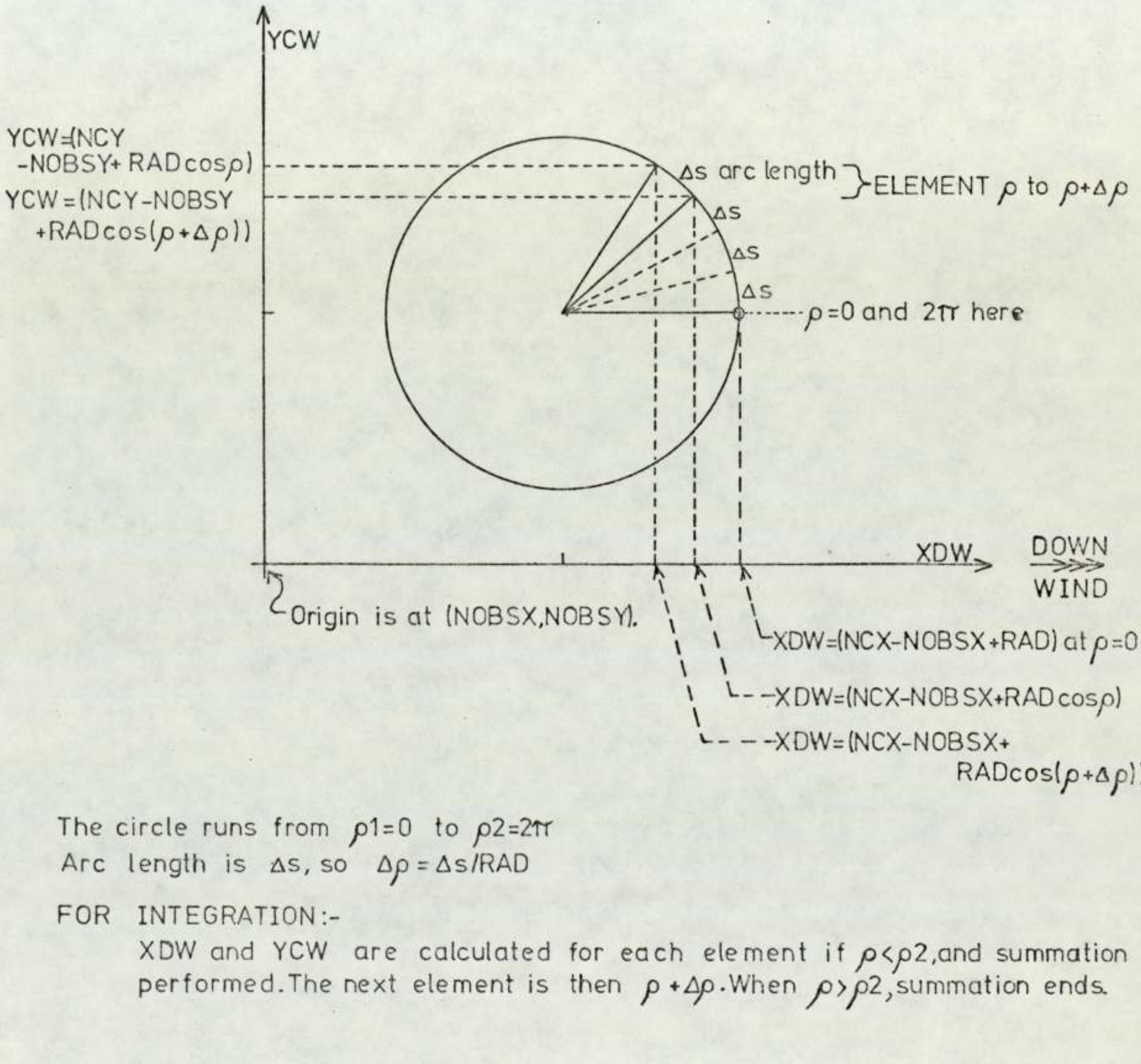

The circle runs from $\rho 1=0$ to $\rho 2=2\pi$

Arc length is Δs, so $\Delta\rho = \Delta s/RAD$

FOR INTEGRATION:-

XDW and YCW are calculated for each element if $\rho<\rho 2$, and summation performed. The next element is then $\rho+\Delta\rho$. When $\rho>\rho 2$, summation ends.

FIGURE 6.4 DEFINITION OF TRIGONOMETRY FOR A CIRCULAR ROAD.

Map References NS1E,NS1N and NS2E,NS2N define the start and end of the line

$RX1=(NS1E-0964)\times 10$ metres

$RY1=(NS1N-9018)\times 10$ metres

$RX2=(NS2E-0964)\times 10$ metres

$RY2=(NS2N-9018)\times 10$ metres

Axes are then rotated anticlockwise through θ to point the X-axis downwind, using the subroutine ROTATE

CALL ROTATE(θ,RX1,RY1,NX1,NY1) gives new co-ordinates (NX1,NY1) for the... start of the line.

CALL ROTATE(θ,RX2,RY2,NX2,NY2) gives new... co-ordinates (NX2,NY2) for the end of the line.

CALL ROTATE(θ,ROBSX,ROBSY,NOBSX,NOBSY) for the Observer, as in Figure 6.4

Axis rotation may change the size and sign of X-co-ordinates, which in turn would make difficult the recognition of line-start and line-end by a simple magnitude test. Hence the subroutine call...

CALL SHUFEL(NX1,NY1,NX2,NY2) swops NX1 for NX2 and NY1 for NY2 if NX1>NX2

Thus the line runs from (NX1,NY1) to (NX2,NY2), with NX1<NX2.

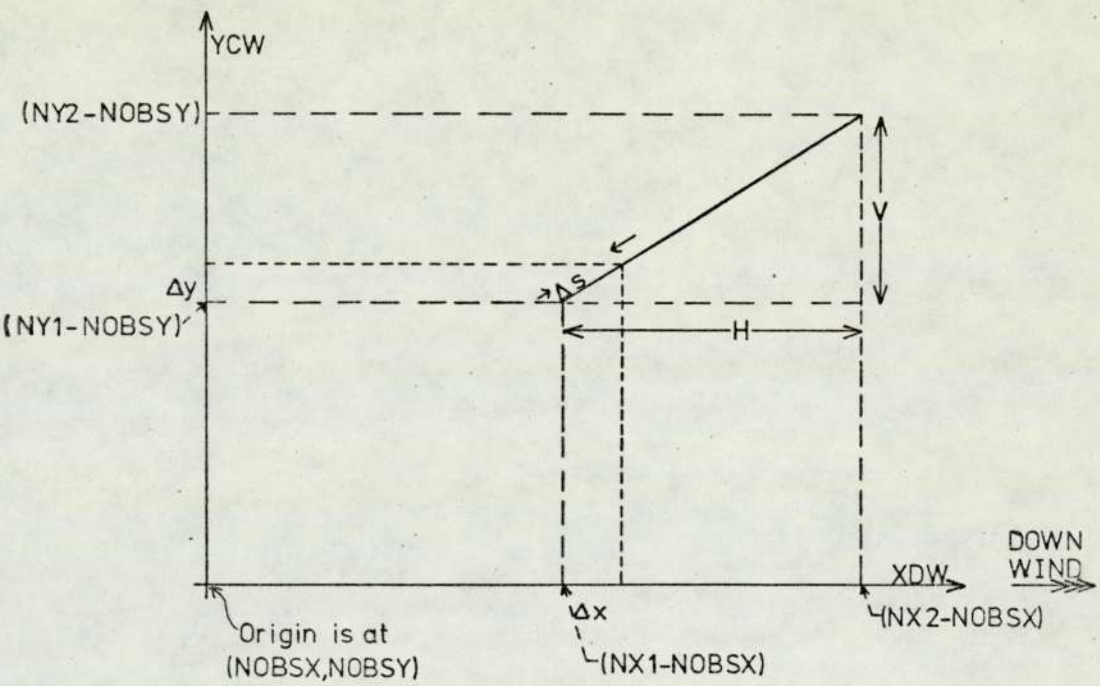

$V=NY1-NY2$

$H=NX1-NX2$

$G=V/H$

Using $Y=GX+C$, $\frac{dY}{dX}=G$, so $\Delta Y=G\Delta X$.

$\Delta s^2=\Delta X^2+\Delta Y^2=\Delta X^2(1+G^2)$

$\Delta X=\Delta s/\sqrt{1+G^2}$

$\Delta Y=G.\Delta X$

FOR INTEGRATION:-

XDW is set to NX1-NOBSX, YCW to NY1-NOBSY and summation occurs if XDW<0 and the end of the road has not been reached.

Next element is $XDW+\Delta X, YCW+\Delta Y$.

<u>FIGURE 6.5</u> DEFINITION OF TRIGONOMETRY FOR A STRAIGHT ROAD.

Map References NS1E,NS1N; NS2E,NS2N; NS3E,NS3N define three points taken in anticlockwise sequence along the curve with the most clockwise first

RX1=(NS1E-0964)×10	RX2=(NS2E-0964)×10	RX3=NS3E-0964)×10
RY1=(NS1N-9018)×10	RY2=(NS2N-0964)×10	RY3=(NS3N-0964)×10

. . . all in metres.

Centre C and Radius RAD are calculated by subroutine CURVE

CALL CURVE(RX1,RY1,RX2,RY2,RX3,RY3,RAD,RCX,RCY) fits a circle through the three points, having centre (RCX,RCY).

Axes are then rotated anticlocwise through θ to point the X-axis downwind, using the subroutine ROTATE

CALL ROTATE(θ,RX1,RY1,NX1,NY1) gives new co-ordinates (NX1,NY1) for first point.

CALL ROTATE(θ,RCX,RCY,NCX,NCY) gives new co-ordinates (NCX,NCY) for centre.

CALL ROTATE(θ,RX3,RY3,NX3,NY3) gives new co-ordinates (NX3,NY3) for 3rd point.

CALL ROTATE (θ,ROBSX,ROBSY,NOBSX,NOBSY) for the Observer, as in Figure 6.4

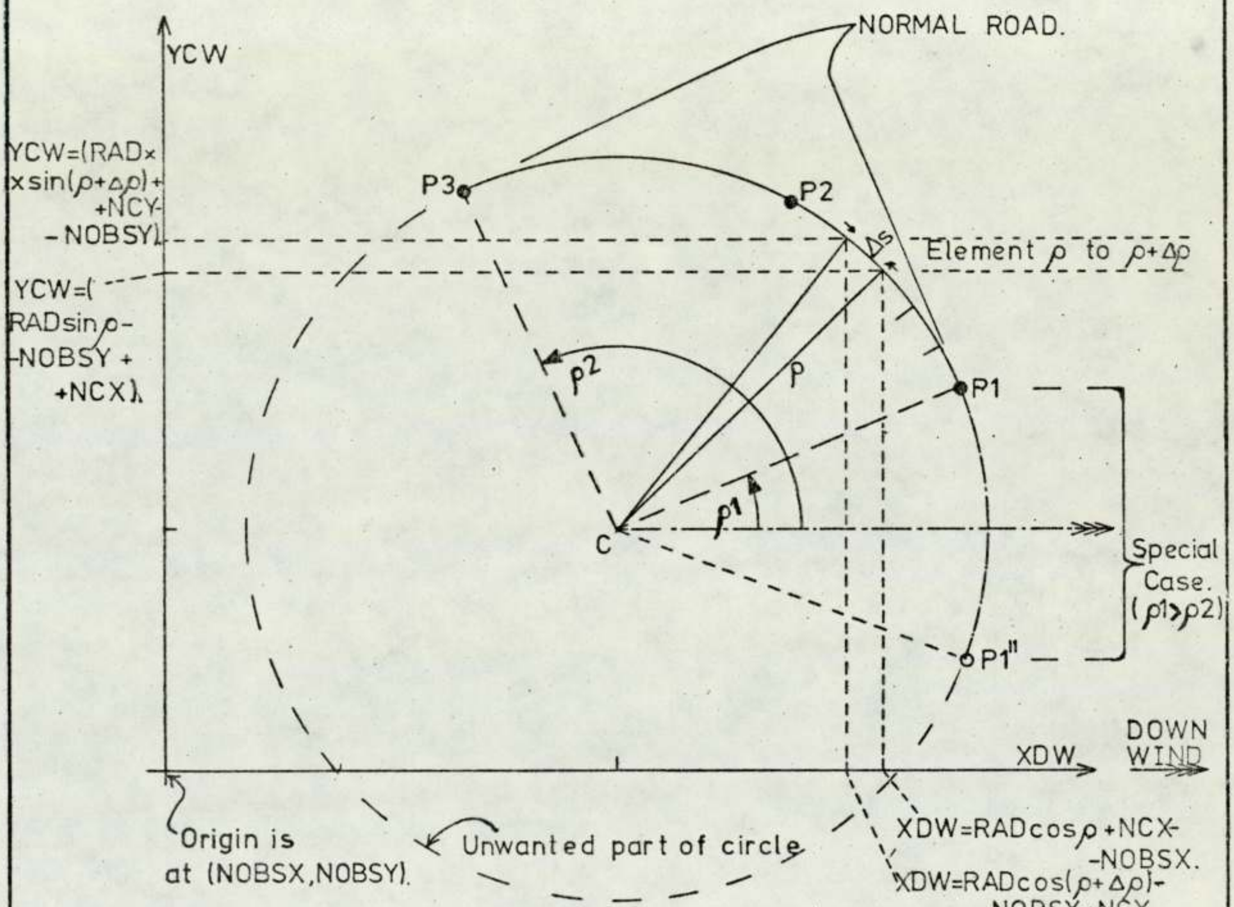

POINTS ARE :- C=(NCX,NCY), P1=(NX1,NY1), P2=(NX2,NY2), P3=(NX3,NY3).

Angular Co-ordinates for P1 and P3 measured about C are ρ1 and ρ2.
SubFunction ARCTAN uses arctangent of the slope of a line to give ρ1 and ...ρ2 in range 0-2π.
ρ1=ARCTAN(NX1,NY1,NCX,NCY), and ρ2 similarly.

FOR INTEGRATION:-

XDW and YCW are calculated for P1, and the limits of summation are ρ1 & ρ2. A Special Case occurs if the curve is intersected by the Downwind direction, which makes ρ1>ρ2 and positive stepping of elements Δρ from ρ1 to ρ2 impossible. Hence if ρ1>ρ2, we set ρ1=(ρ1-2π), which is <ρ2. Then ρ=ρ1. The summation is made for elements ρ=ρ+Δρ, until ρ>ρ2.

FIGURE 6.6 DEFINITION OF TRIGONOMETRY FOR A CURVED ROAD.

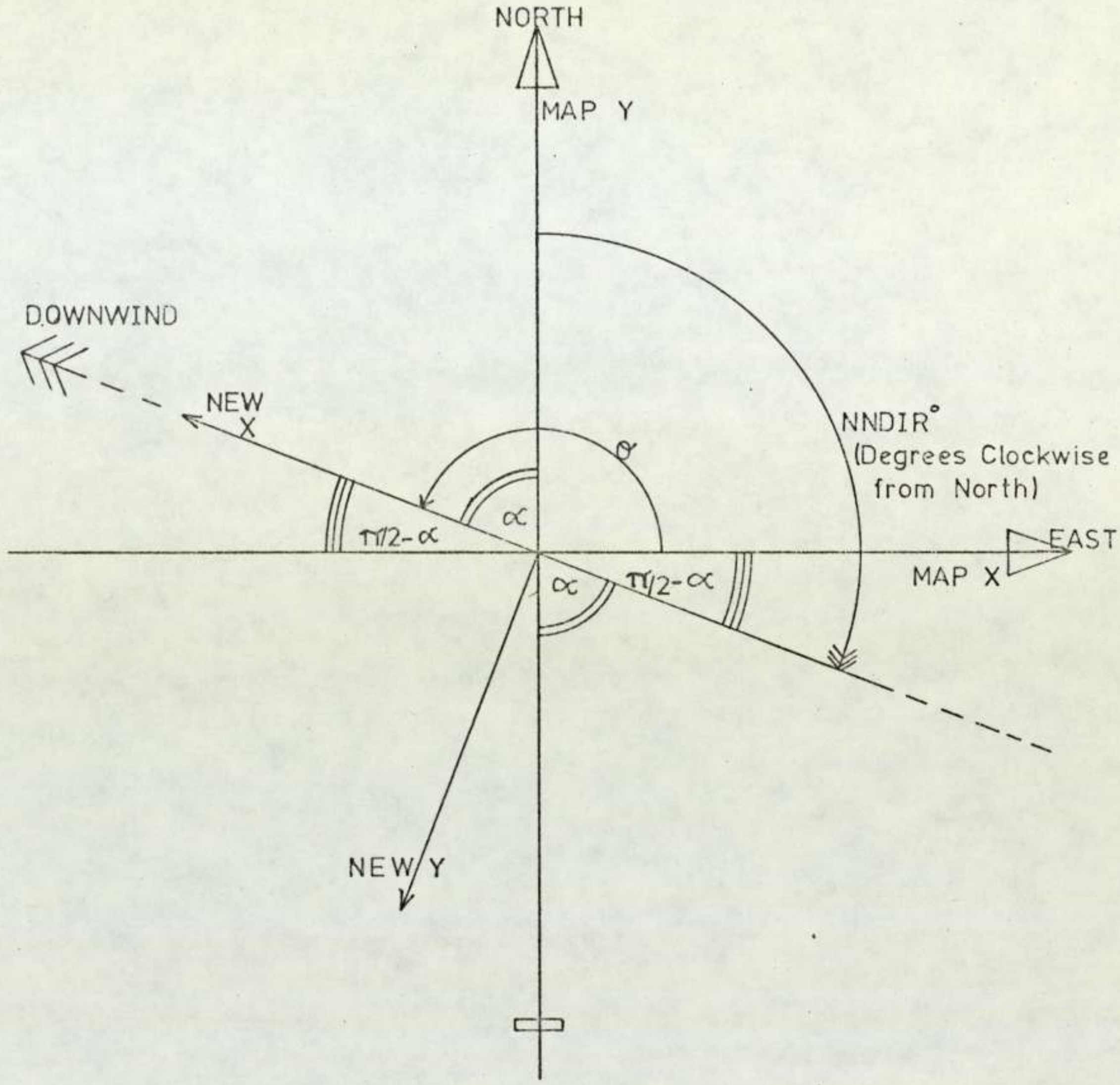

Define $\alpha = \pi - NNDIR \times \pi/180$ radians

Then $\theta = \pi/2 + \alpha$ radians

Whence $\theta = 3\pi/2 - NNDIR \times \pi/180$ radians

Thus the original axes (X=East) are rotated anticlockwise through θ to point X downwind.

FIGURE 6.7 DERIVATION OF THE ANGLE θ FOR AXIS ROTATION.

of numbers. The angle θ (Figure 6.7) is calculated from the wind-direction: the axes are rotated anti-clockwise through θ so that use of the above trigonometry defines the co-ordinates of elements along each road in the downwind and crosswind directions.

6.2.3 Integration of Plume Formula

For each hourly observation, the wind-speed, cloud cover, time and date are used by sub-routine STABIL (Section 5.3.2) to obtain the stability index MST2. If the wind-speed is zero, no integration is performed. One integral is returned for each observer position and each hourly observation.

Integration by the trapezium rule is carried out element by element along each road-section: C1, C2 and CONCEL are zeroed, and initial co-ordinates for the start of the road-section defined as XDW, YCW (downwind and crosswind distances from the observer respectively). If the element is upwind of the observer, XDW < 0 and the element contributes to the summation: sub-routine GEOMET is called to obtain parameters σ_y, σ_z for the point source plume of the element at the observer. The concentration C2 of that plume at the observer is, from Equation 5.8 with $(Qi/2\pi U)$ to be multiplied in later,

$$C2 = \frac{1}{\sigma_y \sigma_z} \exp\left(-\frac{YCW^2}{2\sigma_y^2}\right) \left[\exp\left(\frac{-(Z-H)^2}{2\sigma_z^2}\right) + \exp\left(\frac{-(Z+H)^2}{2\sigma_z^2}\right) \right]$$

where Z, H are the observer and element heights respectively. For the first element, C1 = 0; for later elements, C1 is the value of CZ from the previous element. C1 and C2 are combined by the trapezium rule as

$$\text{CONCEL} = \text{CONCEL} + \Delta s\frac{(C1 + C2)}{2} = \text{CONCEL} + (C1 + C2)\text{DELTAX}$$

for a steplength ΔS (read as DELTAS to give DELTAX = $\Delta S/2$). C1 is then set equal to the present C2 ready for the next element, if found. If not found, the end of the road section has been reached: summation of CONCEL ceases and it is scaled by the traffic-flow of that section and added to CONCSM, the sum from previously completed sections. When all sections have been covered, CONCSM is scaled by the constants: (windspeed $.2\pi)^{-1}$ and the appropriate emissions parameter Q_{NO}, Q_{CO} or Q_{HC} for unit traffic-flow per metre of road.

$$\text{CONCNO} = Q_{NO} \cdot \frac{\text{CONCSM}}{(2\pi.\text{WINDMS})}$$

where WINDMS is the windspeed, ms^{-1}.

CONCCO, CONCHC are derived similarly.

The calculated concentrations CONCNO, CONCCO, CONCHC (ppm) for NO, CO, HC respectively, together with the observer position, time and date are printed alongside the measured levels. This table forms the basis for comparison studies (Section 6.6).

6.2.4 Sub-routines

1. GEOMET (X,MST2,SY,SZ) gives SY = $\sigma_y(X)$ and SZ = $\sigma_z(X)$ for a positive downwind distance X and stability index MST2, by the curves in Table 5.3: these curves (Geomet, 1971) were used since both σ_y and σ_z were needed to integrate the point-source formula (Equation 5.8) over the complex source geometry. For an upwind road, XDW is negative, so the sub-routine is called with arguments (-XDW,MST2,SY,SZ).

Geomet (1971) gave but five classes, while the coding (supplied by Dutton of the Meteorological Office: Section 5.3.2) in subroutine STABIL returns MST2 in the range 1 to 10. We thus defined classes (cf. Pasquill, 1971)

Class	A	AB	B	BC	C	CD	D	E	F	G
MST2	1	2	3	4	5	6	7	8	9	10

This is one area for model development.

No attempt is made to allow for restricted vertical mixing as no mixing heights were available (e.g. see Johnson et al., 1971). After Calder (1973), initial plume sizes were obtained by adding 27m to X before and after using the above formulae for SY, SZ. This parameter requires study: Figure 6.8 gives a resumé for the value of 27m as used. Figure 6.8 shows that $\sigma_X(0)$ and $\sigma_Z(0)$ vary with MST2. This format, i.e. X = X + C, was used following Calder (1973): since the aim was to represent an initially finite wake, a format $\sigma(X) = \sigma(X) + \sigma_C$ might be better, for then σ_C would define wake size independent of stability. This would be of similar format to the suggestions of Pooler (1966): see Section 5.4 and Table 5.7. Urban effects are complex and we go no further save to comment that a thorough study of both formats is needed.

2. SHUFEL (AX,AY,BX,BY) interchanges the co-ordinates of the points A and B if AX exceeds BX. Thus AX is less than BX. For straight-line sections (Figure 6.5) SHUFEL is called to ensure NX1 < NX2, so that addition of ΔX (which is always positive) to XDW always implies positive stepping from P1 to P2: otherwise one might lose

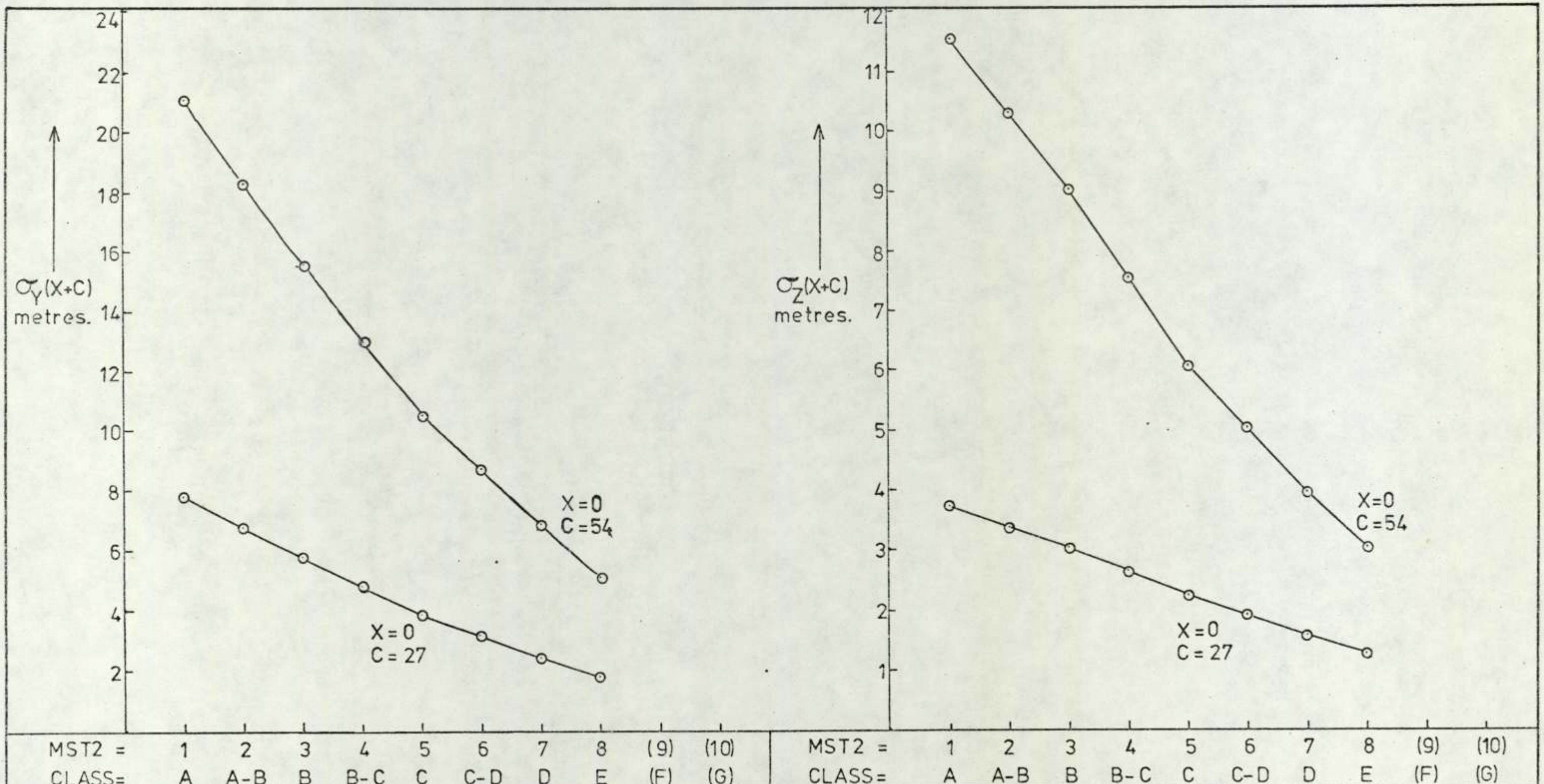

FIGURE 6.8 VARIATION OF INITIAL PLUME SIZE, AS GIVEN BY THE FORM $\sigma(X+C) = a(X+C)^b$ WITH X=0, DUE TO CHANGES IN STABILITY INDEX MST2. THE VALUES SHOWN WERE CALCULATED USING SUBROUTINE GEOMET.

the whole line when testing XDW against the end-point of the line (X2 for P2).

3. ROTATE (θ,X,Y,TX,TY) rotates the X, Y axes by +θ radians in the anticlockwise direction.

$$TX = X\cos\theta + Y\sin\theta$$

$$TY = -X\sin\theta + Y\cos\theta$$

4. CURVE(X1, Y1,X2,Y2,X3,Y3,R,CX,CY) fits a circle to three points (X1,Y1), (X2,Y2), (X3,Y3) and returns the radius R and centre (CX,CY). To avoid overflow when the Y axis happens to pass through (X1,Y1) and (X2,Y2), if Y1 equals Y2, the points are swopped around. This presupposes that no two points are co-incident, when an error occurs. The swop does not affect co-ordinates outside the sub-routine since X1,Y1, etc., are dummy variables local to the sub-routine.

5. STABIL (NNTIME, NNDAY, NMONTH, NLAT, NCLOUD, NWIND, MST2) returns the stability index MST2 according to the other variables (time, date, month, latitude, cloud cover, windspeed respectively). To match the coding (supplied by Dutton of the Meteorological Office: Section 5.3.2), the time NNTIME must be (hours x 10 + tenths), and the latitude NLAT (degrees x 10 + tenths). NLAT is input in this form; NNTIME is read as the hour, but multiplied by 10 before calling STABIL and divided by 10 afterwards. NWIND is in knots and NCLOUD is in oktas.

6. ARCTAN (X1,Y1,XC,YC) is a real function whose value is the arctangent (0 to 2π) of the gradient of the line (XC,YC) (X1,Y1). The ICL FORTRAN (1900 series) function ATAN(E) gives the arctangent of an expression E in the range $-\pi/2$ to $+\pi/2$. ARCTAN is called to calculate initial and final angular co-ordinates of curved sections (Figure 6.6) for element stepping: the angle is returned increasing in the anticlockwise sense from 0 at the X axis to 2π. Tests on the co-ordinates locate the relevant quadrant and appropriate multiples of $\pi/2$ are added to ATAN(E). Special cases arise at $3\pi/2$ and $\pi/2$, when X1 = XC. If Y1 $<$ YC the angle is $3\pi/2$, otherwise Y1 $>$ YC and the angle is $\pi/2$. By default if X1 = Y1 and Y1 = YC, the result is $3\pi/2$.

6.2.5 Input and Output

During data entry (Figure 6.3) extensive use is made of the ICL FORTRAN (1900 series) free formats (I0 and F0.0) with which spaces and ends of cards are skipped until the number is read. Since fixed formats are also used, care is needed in data preparation.

Input is arranged as follows:

1. Three emission parameters Q_{NO}, Q_{CO}, Q_{HC} (format F0.0). We used values of Q_L/T for 60/40 petrol:diesel mix as in Table 6.4.

2. Integer controls (format I0) to define programme operation. They are a number of hourly observations NMET, number of observer positions NLOC, total number of road sections (several may constitute one road) NSECT, step distance DELTAS in metres, and

number of distinct roads (and of traffic-counts to be read per hourly observation) NROAD.

3. Map references for observer positions entered as eight-digit (format I8: East and North each four-digit) Ordnance Survey references, accurate to nearest ten metres, followed by height to nearest metre.

4. Map references for road sections, in eight-digit Ordnance Survey, preceded by three identifying integers (format I2,I3, I2) for section number, road identity and curvature (equal to 1, 2 or 3: see Section 6.2.2). The road section map references, again in format I8, are each followed by the height in format I5. By default, spaces will be read as zero. At present only the height of the first map reference is used, but the input is general in case height interpolation is to be inserted (e.g. along a curve between the heights of the end-points).

5. NLAT as (degrees x 10 + tenths: 510 = $51^{\circ}\ 0'$) and NMONTH (format I0, I0).

6. Three channel input of field observations, weather readings and traffic counts, in the form of one data row (possibly several cards per row) per hourly observation. Field observations, for comparison purposes, had the time, date and site, followed by levels recorded for NO_x, NO, NO_2 (as NO_x - NO), Streeter Amet traffic flow at Salford Circus, CO and HC. Weather readings had time and date followed by wind-direction (degrees clockwise from North), windspeed (knots) and cloud cover (oktas). The traffic for each road (except road 3, Salford Circus) followed

the time and date. The three inputs used free format as far as possible.

Output is to two channels:

1. General run diagnostics and warnings such as error messages and various calculation results, including the co-ordinates of each element stepped out in the first integration only (Figure 6.9). This information is used for run checking.

2. A table of the levels of pollutant as measured and calculated.

6.3 Programme Accuracy

Calder (1973) gave approximate and exact formulae (Equations 5.15, 5.17) for the integral of the continuous point-source formula (Equation 5.8) over a linear source. The programme (section 6.2) should give the same results.

A special set of data files were set up to give the integral from the programme over finite-length line-sources (unit source-strength) for several distances and wind angles. Roads and observer positions were set up (Figure 6.10) using the usual Ordnance Survey type entry: downwind distance X ranged from 50 to 800m, so the line-source was 10X in length and the elements were in steps of X/10. Similar wind angles and unit wind speed (here 2 knots which is 1.02ms^{-1}) as Calder were used. Stability index MST2 was 7, which should give the same plume parameters as used by Calder, but in fact there was a slight difference: sub-routine GEOMET gave slightly different $\sigma_y(X)$ and $\sigma_z(X)$. The

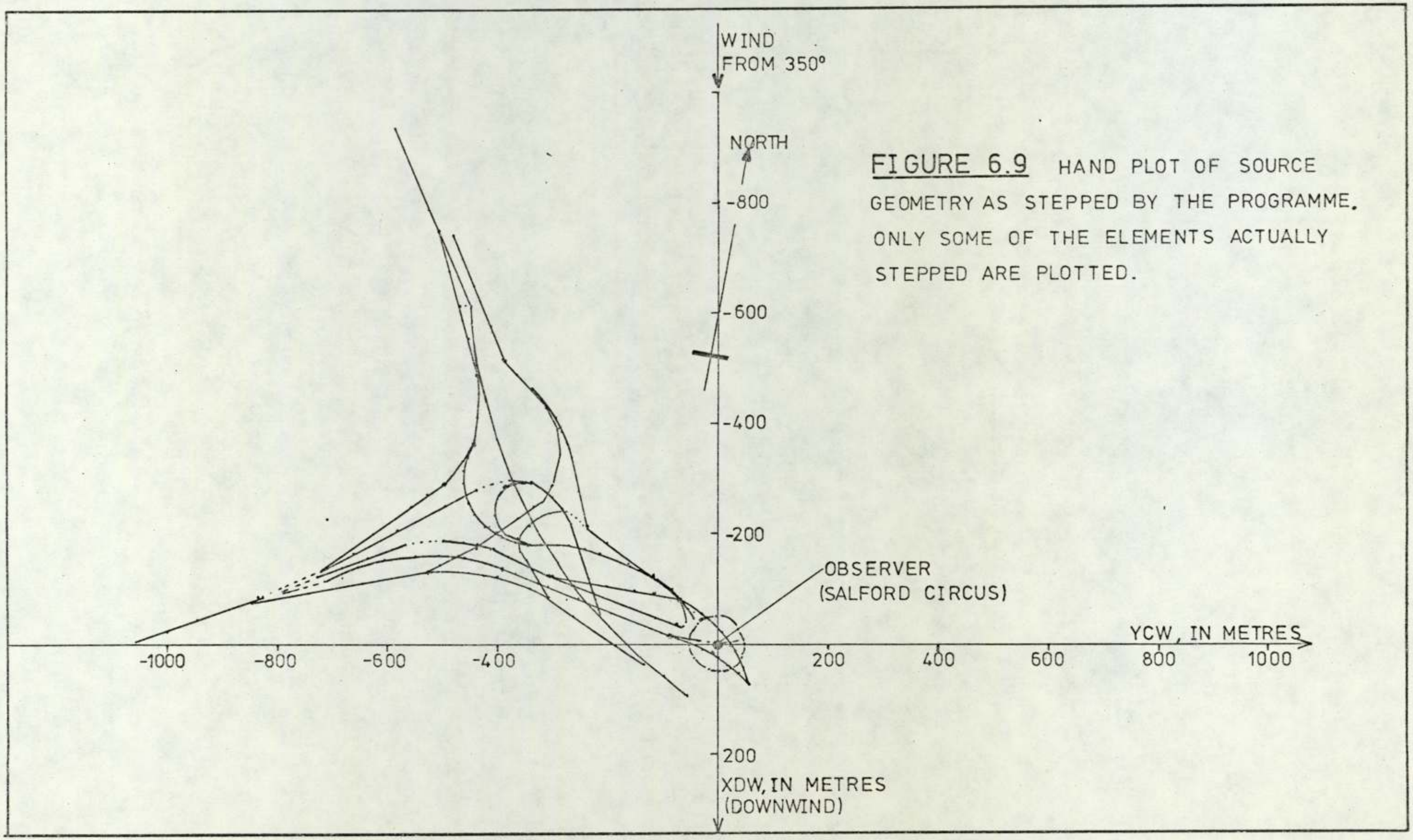

FIGURE 6.9 HAND PLOT OF SOURCE GEOMETRY AS STEPPED BY THE PROGRAMME. ONLY SOME OF THE ELEMENTS ACTUALLY STEPPED ARE PLOTTED.

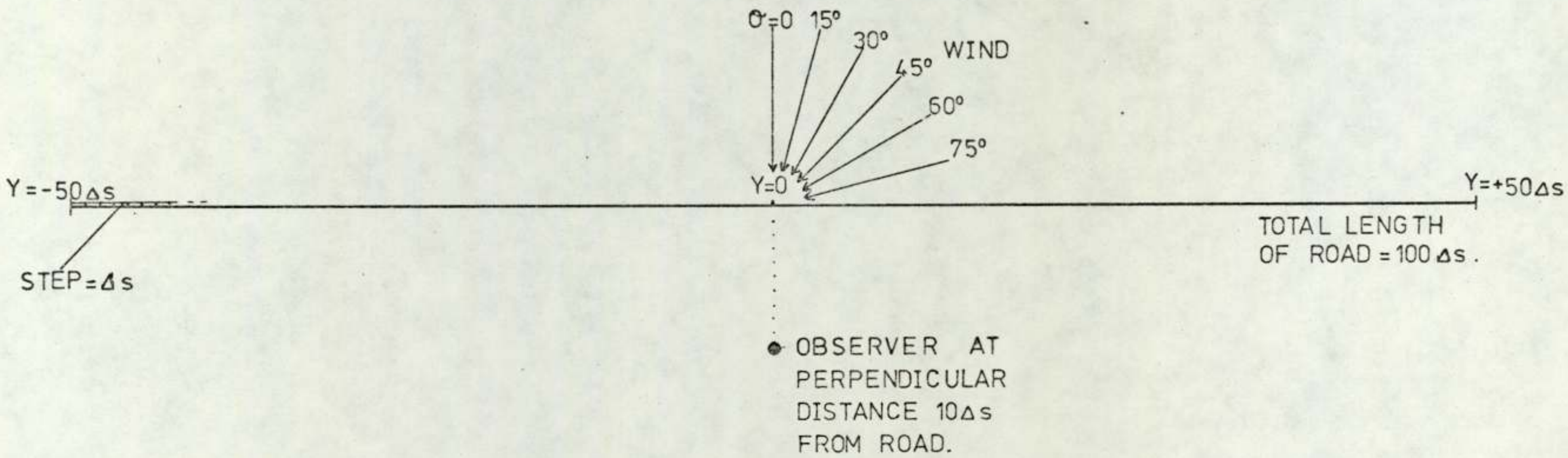

FIGURE 6.10 ROAD LAYOUT, OBSERVER POSITION AND WIND DIRECTIONS FOR COMPARING THE VALUES GIVEN BY THE PROGRAMME WITH THOSE OF CALDER(1973).

TABLE 6.5

Comparison of Programme Results with those of Calder (1973)

(Unit Q_L, Observer Height = o, Road Height = o, Class D, 1.02 ms^{-1})

	X_o in m	Wind Direction							s in m	RD in m	σ_z in m
		0°	15°	30°	45°	60°	75°	90°			
C[1]	50	0.218	0.221	0.231	0.250	0.282	0.338	–	–	–	3.666
P[1]		0.205	0.208	0.219	0.238	0.271	0.260	10^{-2}	5	500	3.813
C	100	0.141	0.143	0.148	0.156	0.171	0.197	–	–	–	5.652
P		0.136	0.137	0.142	0.152	0.168	0.160	10^{-3}	10	1000	5.767
C	200	0.085	0.086	0.088	0.092	0.099	0.121	–	–	–	9.342
P		0.084	0.085	0.087	0.092	0.099	0.095	10^{-3}	20	2000	9.326
C	400	0.049	0.050	0.051	0.054	0.061	0.076	–	–	–	16.13
P		0.050	0.050	0.051	0.054	0.058	0.060	10^{-4}	40	4000	15.73
C	800	0.031	0.031	0.032	0.034	0.038	0.048	–	–	–	26.15
P		0.029	0.029	0.030	0.032	0.036	0.040	10^{-4}	80	8000	27.16

Note 1: C = Calder, P = programme

discrepancy between Calder's integration values and those from the programme are believed to be due to this: Table 6.5 compares the two models. Some discrepancies (e.g. 200m and 75^{o}) may be due to the finite road-length and large wind-angle; the low values at 90^{o} probably reflect this.

6.4 Sensitivity of Calculated Levels

6.4.1 Effect of Step Length

The data file for comparing the programme with Calder (1973) for a downwind distance of 50m was used to study step lengths of 1m, 5m, and 50m. The first two gave practically the same results as Calder (1973) while a 50m step gave values that were higher (Table 6.6). In all work with the programme the step length was set to 5m (to balance accuracy with economy of iteration).

6.4.2 Effect of Heights

Observer and road heights were varied for a downwind distance of 50m (from the same line-source as in Section 6.3), with step length 5m.

In Table 6.7 we summarise these results: they show a very sensitive behaviour with height. The variation is rapid so the logarithm of the ground level concentration is plotted against road height in Figure 6.11. This shows an increasing dependence of the level on height: this is of particular importance at Salford Circus where the monitor is amongst elevated roads. The integral of pollution over the intersection may be very dependent on the heights of the roads that are used. The effect should be less at greater distances though.

TABLE 6.6

Effect of Step Length for 50m Downwind Distance:

Integral Values for Linear Source using Various Steps

and Wind Directions. (1.02 ms^{-1}, Class D, Unit Q_L)

Step, m	θ						
	0°	15°	30°	45°	60°	75°	90°
1	0.2051	0.2084	0.2188	0.2382	0.2712	0.2579	0.00357
5	0.2051	0.2084	0.2188	0.2382	0.2712	0.2598	0.00373
50	0.623	0.0858	0.0309	0.4137	0.231	0.2787	0.00566

TABLE 6.7

Effect of Road and Observer Heights on Pollutant Levels for Linear Source

(1.02 ms^{-1}, Class D, Observer X_o = 50m, perpendicular wind, unit QL)

Observer height m	Road height, m					
	0	2	5	10	15	25
0	0.2051	0.1788	0.08684	0.006589	$0.8960.10^{-4}$	10^{-10}
5	0.08684	0.09429	0.1059	0.04346	0.003295	10^{-6}
10	0.006589	0.01208	0.04346	0.1026	0.04342	$0.4480.10^{-4}$
15	$0.8960.10^{-4}$	0.0003122	0.003295	0.04342	0.1026	0.003294
20	10^{-6}	$0.1495.10^{-5}$	$0.4480.10^{-4}$	0.003294	0.04342	0.04342
25	10^{-10}	10^{-8}	10^{-6}	$0.4480.10^{-4}$	0.003294	0.1026
30	10^{-14}	10^{-12}	10^{-10}	10^{-6}	$0.4480.10^{-4}$	0.04342
50	10^{-38}	10^{-35}	10^{-31}	10^{-24}	10^{-19}	0.04769
100	0	0	0	0	0	0
200	0	0	0	0	0	0

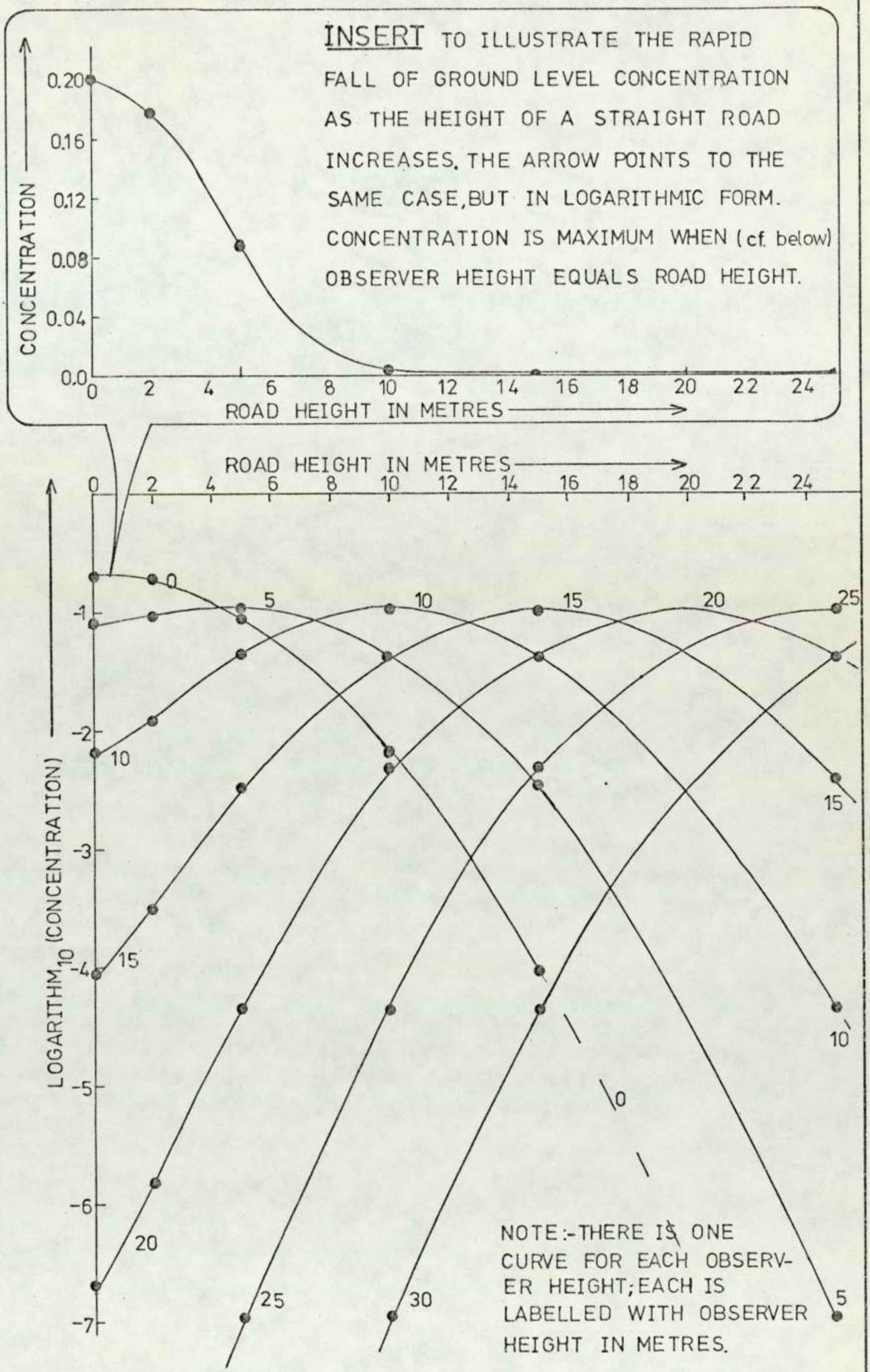

FIGURE 6.11 EFFECT OF ROAD HEIGHT ON DOWNWIND CONCENTRATION FOR SEVERAL OBSERVER HEIGHTS. CONCENTRATION WAS CALCULATED AS VOLUME-VOLUME RATIO USING PROGRAMME SPAG68, DOWNWIND DISTANCE 50m (cf. FIGURE 6.10, $\theta = 0°$), MST2 = 7, Q = 1, U = 2 kt or 1·02 ms^{-1}.

6.4.3 Wind Direction

In the case of a line source, the effect is slight: see Calder (1973) and Table 6.5. The integral runs into problems at large angles because a finite length of road is used.

6.4.4 Windspeed

Predictions vary as U^{-1} (an over-simplification since the choice of MST2 depends on U also).

6.4.5 Sensitivity of Integral over the Intersection

When studying real-life situations there is a problem as to how many combinations of variables should be considered (cf. Geomet, 1971). This study was restricted to predictions at locations outside of and downwind from the intersection (Map: Figure 6.12). A typical set of evening rush-hour traffic was used for all roads: the programme was modified with a special series of DO loops to generate combinations of wind-direction, stability category and wind-speed. Some of the more interesting results are shown in Figure 6.13 to 6.20. These predictions used the emission parameter given in Table 6.4 for NO.

In Figure 6.12 we show the observer positions and the wind directions used in the sensitivity study. Figures 6.13, 6.14 show the downwind concentration curves for a range of stabilities. Roughly speaking, the pollutant concentration varies by about 10 - 20% (Figure 6.14) with unit change in MST2 (although more exactly this depends on which part of the figure is used).

The wind-speed curves (Figure 6.15) reflect the inverse relation

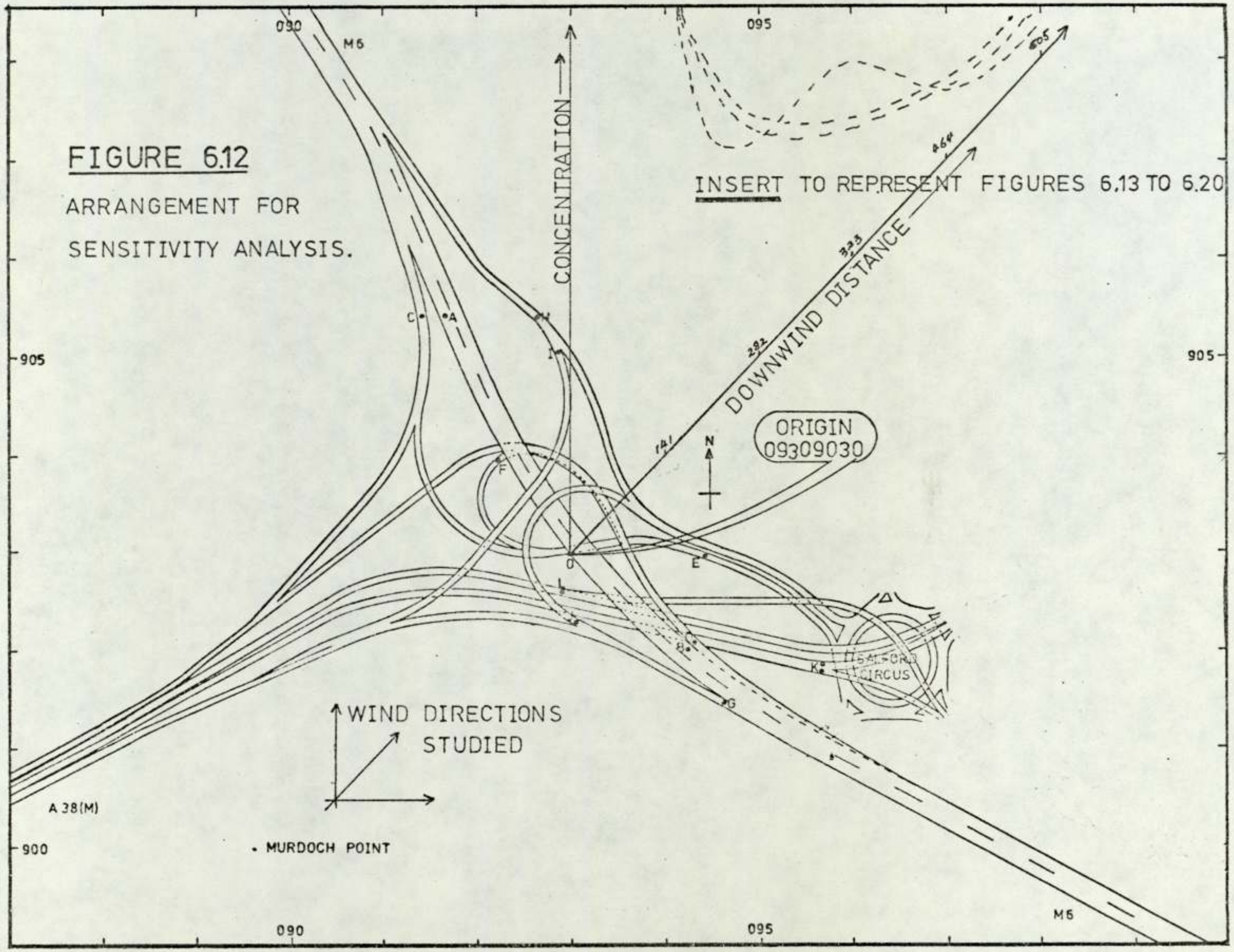

FIGURE 6.12

ARRANGEMENT FOR SENSITIVITY ANALYSIS.

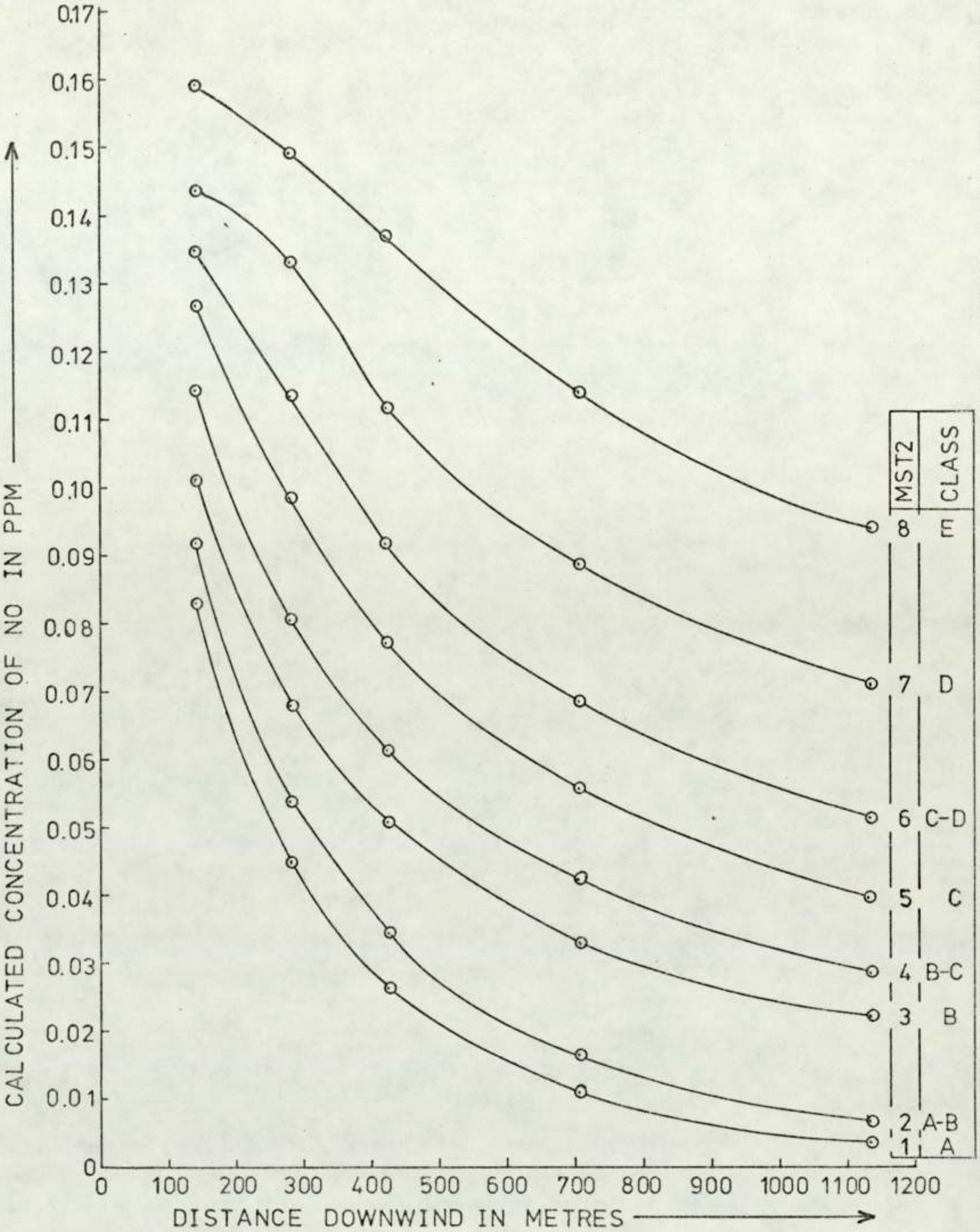

FIGURE 6.13 VARIATION WITH DISTANCE DOWNWIND FROM THE INTERSECTION OF NO CONCENTRATION, CALCULATED FOR STABILITY CLASSES A TO E USING MST2 = 1 TO 8.

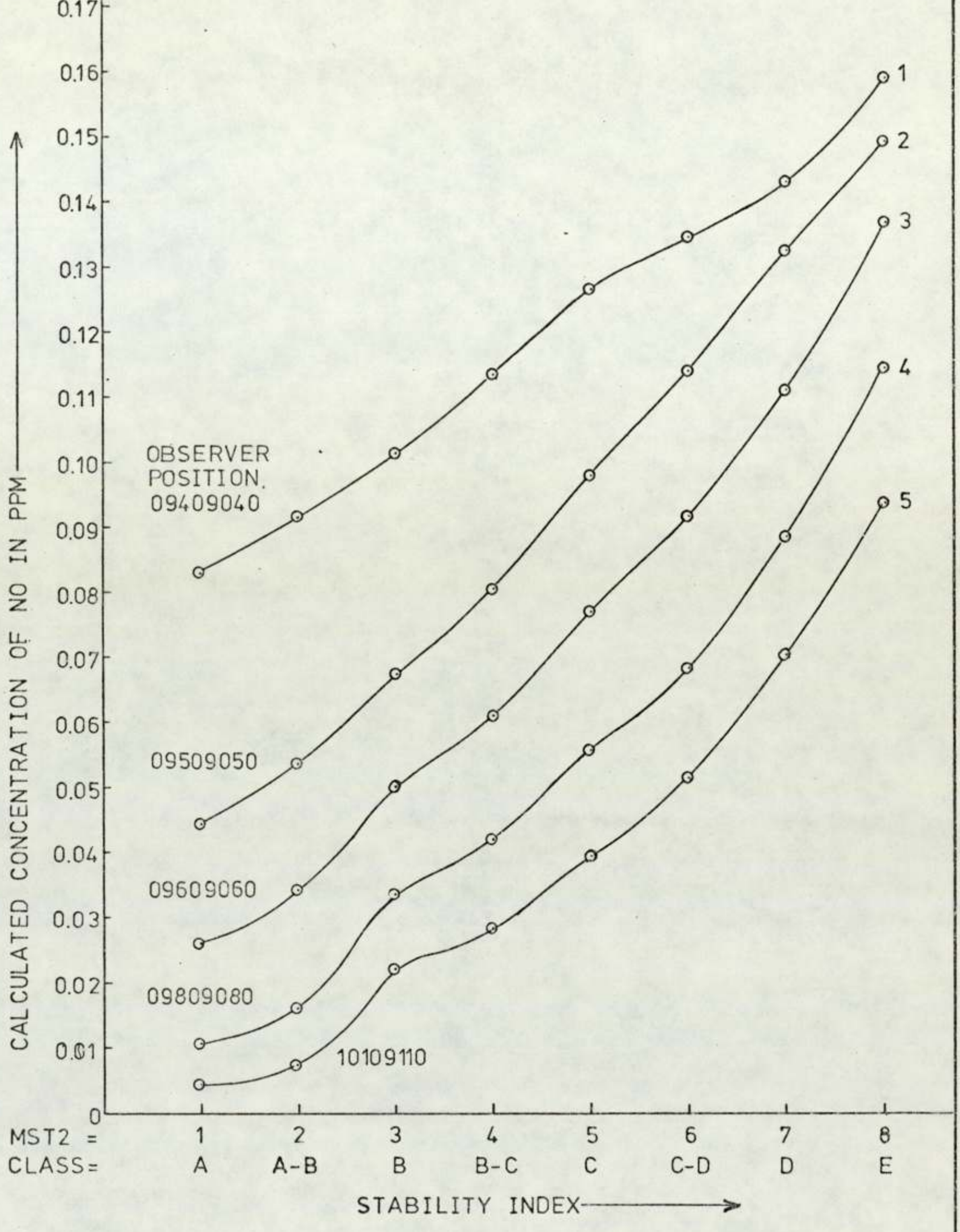

FIGURE 6.14 VARIATION WITH STABILITY INDEX MST2 OF NO CONCENTRATION, CALCULATED FOR SEVERAL DISTANCES DOWNWIND FROM THE INTERSECTION. TIME 17-00

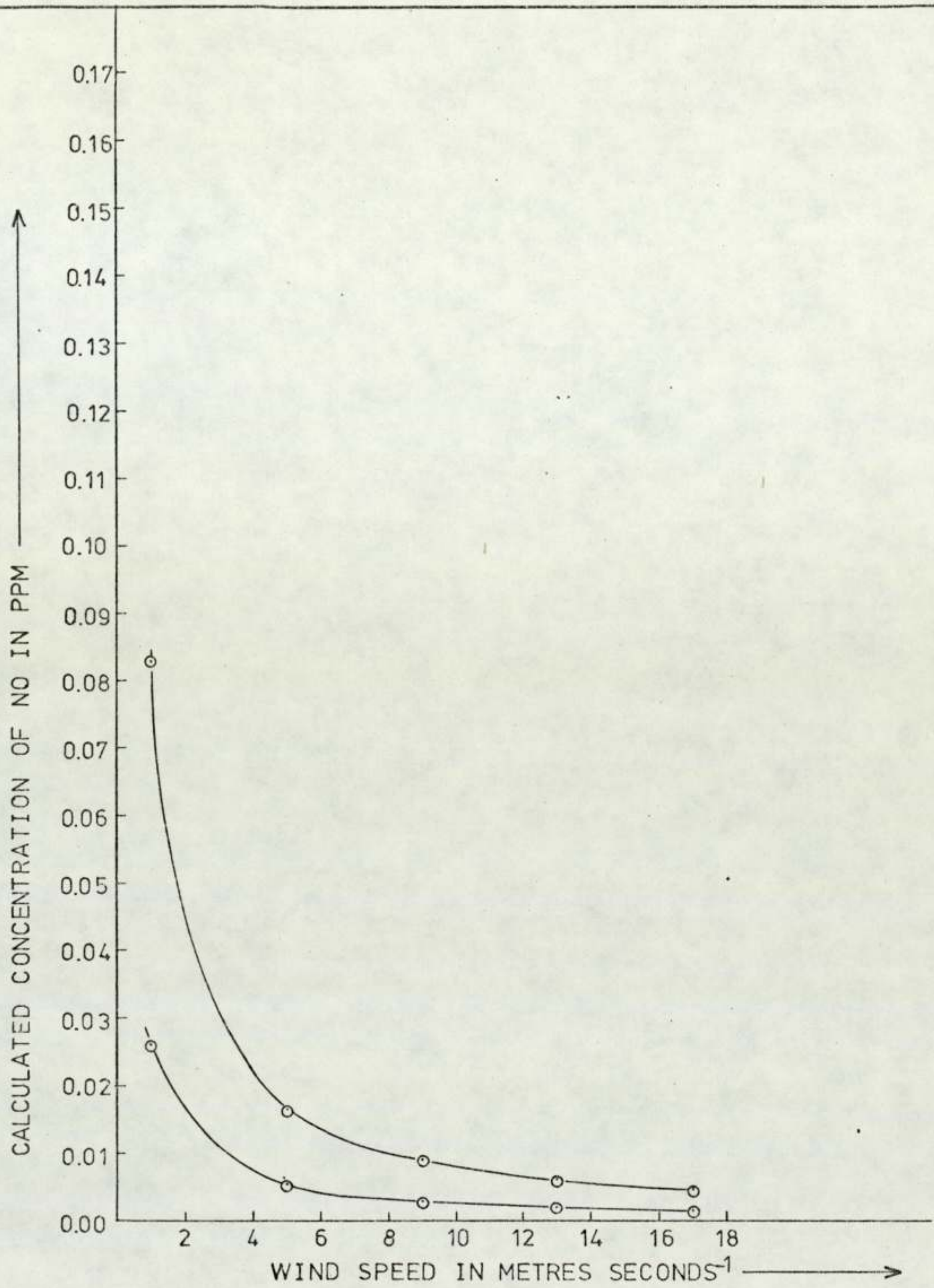

FIGURE 6.15 VARIATION WITH WINDSPEED OF NO CONCENTRATION, CALCULATED FOR TWO DOWNWIND DISTANCES.

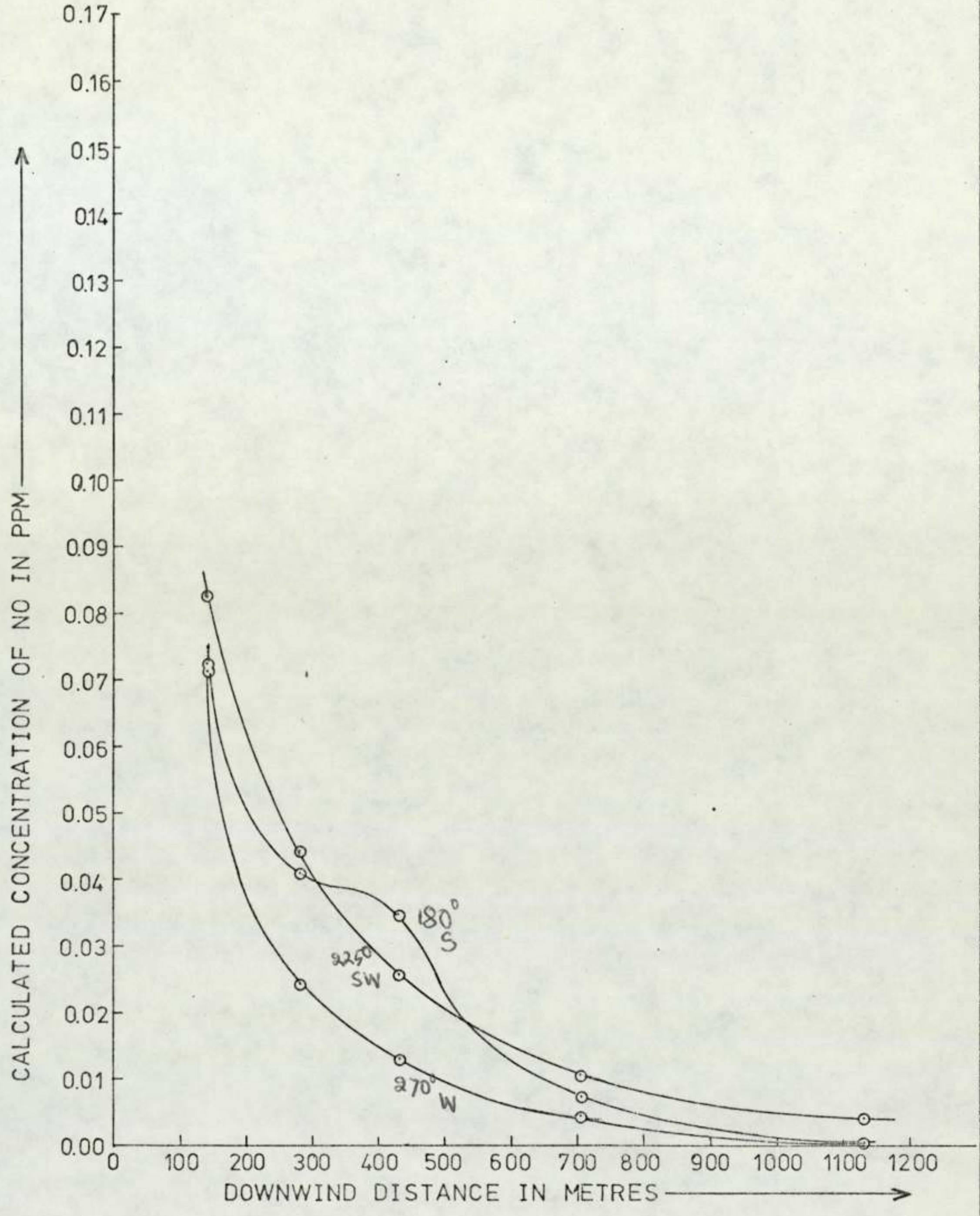

FIGURE 6.16 VARIATION WITH DISTANCE DOWNWIND FROM THE INTERSECTION OF NO CONCENTRATION, CALCULATED FOR THREE WINDDIRECTIONS WITH MST2=1 (CLASS A).

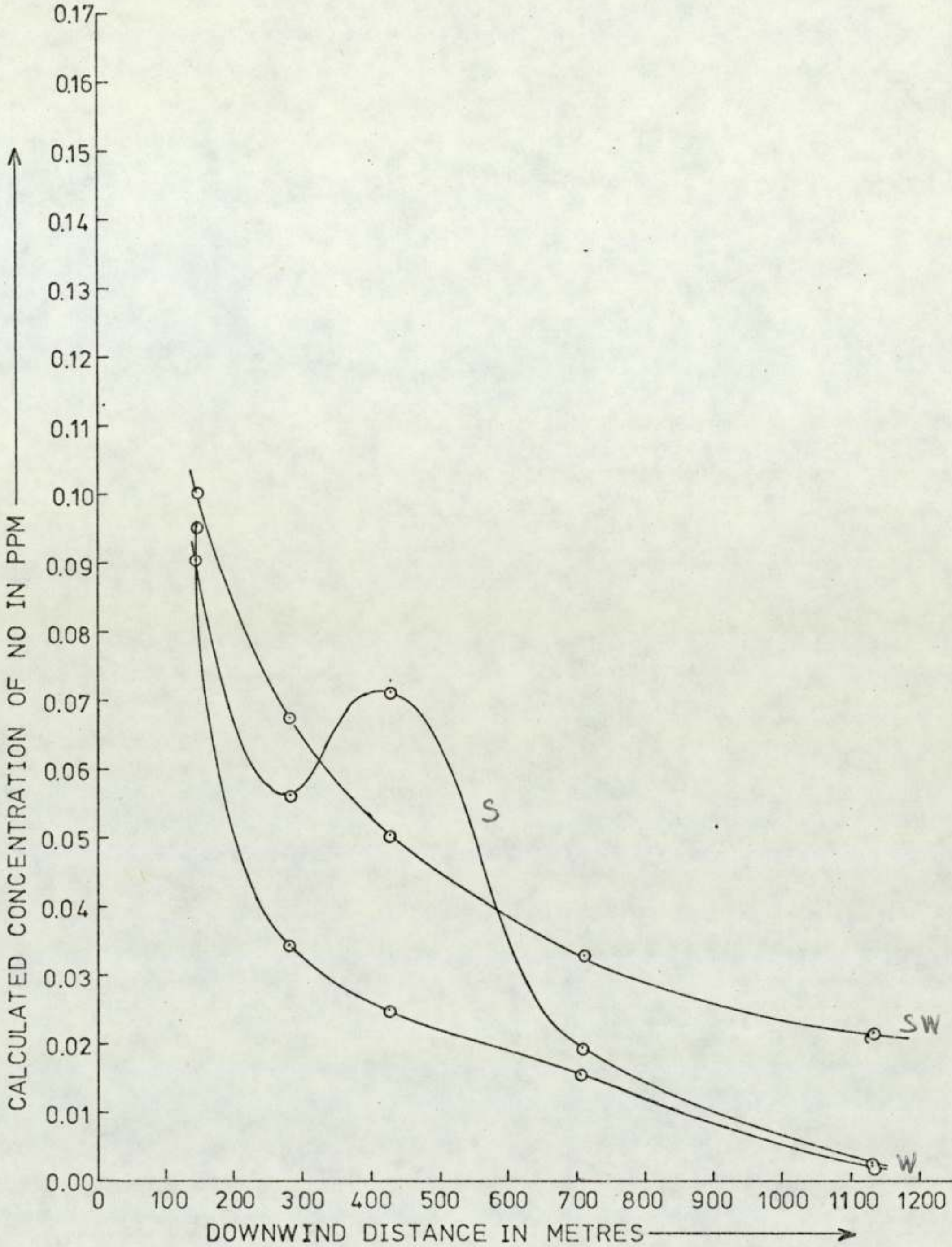

FIGURE 6.17 VARIATION WITH DISTANCE DOWNWIND FROM THE INTERSECTION OF NO CONCENTRATION, CALCULATED FOR THREE WINDDIRECTIONS WITH MST2 = 3 (CLASS B).

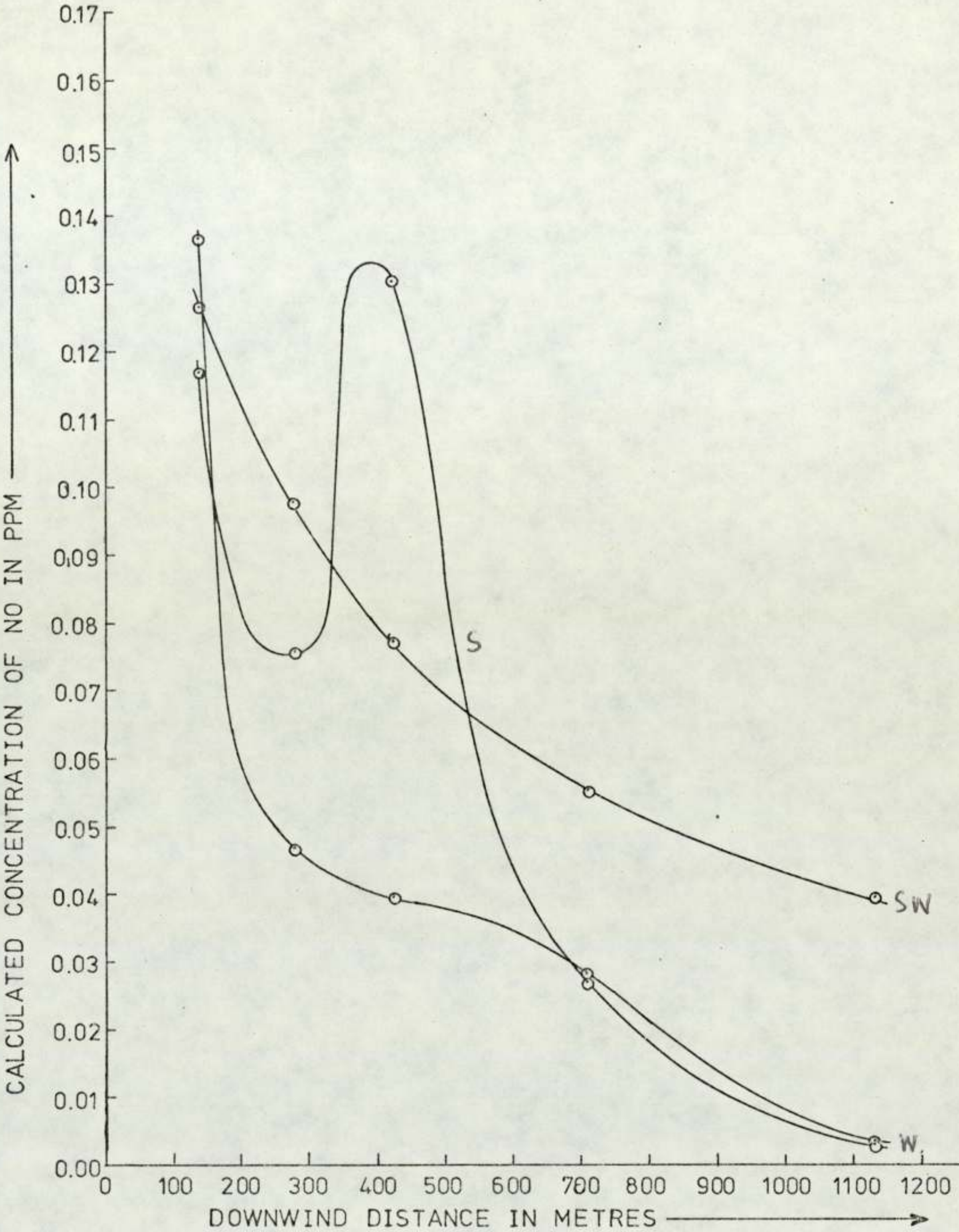

FIGURE 6.18 VARIATION WITH DISTANCE DOWNWIND FROM THE INTERSECTION OF NO CONCENTRATION, CALCULATED FOR THREE WINDDIRECTIONS WITH MST2 = 5 (CLASS C).

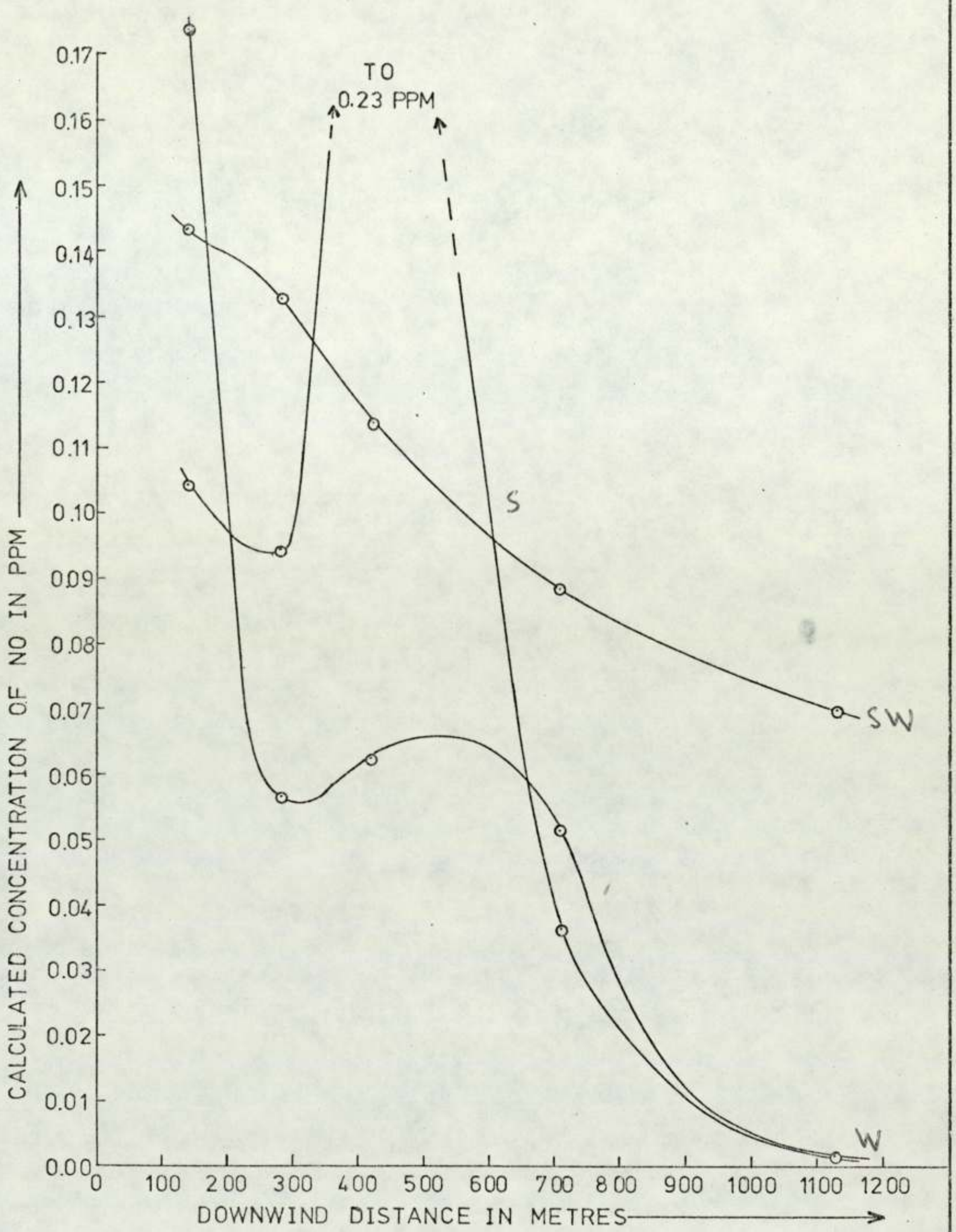

FIGURE 6.19 VARIATION WITH DISTANCE DOWNWIND FROM THE INTERSECTION OF NO CONCENTRATION, CALCULATED FOR THREE WINDDIRECTIONS WITH MST2=7(CLASS D)

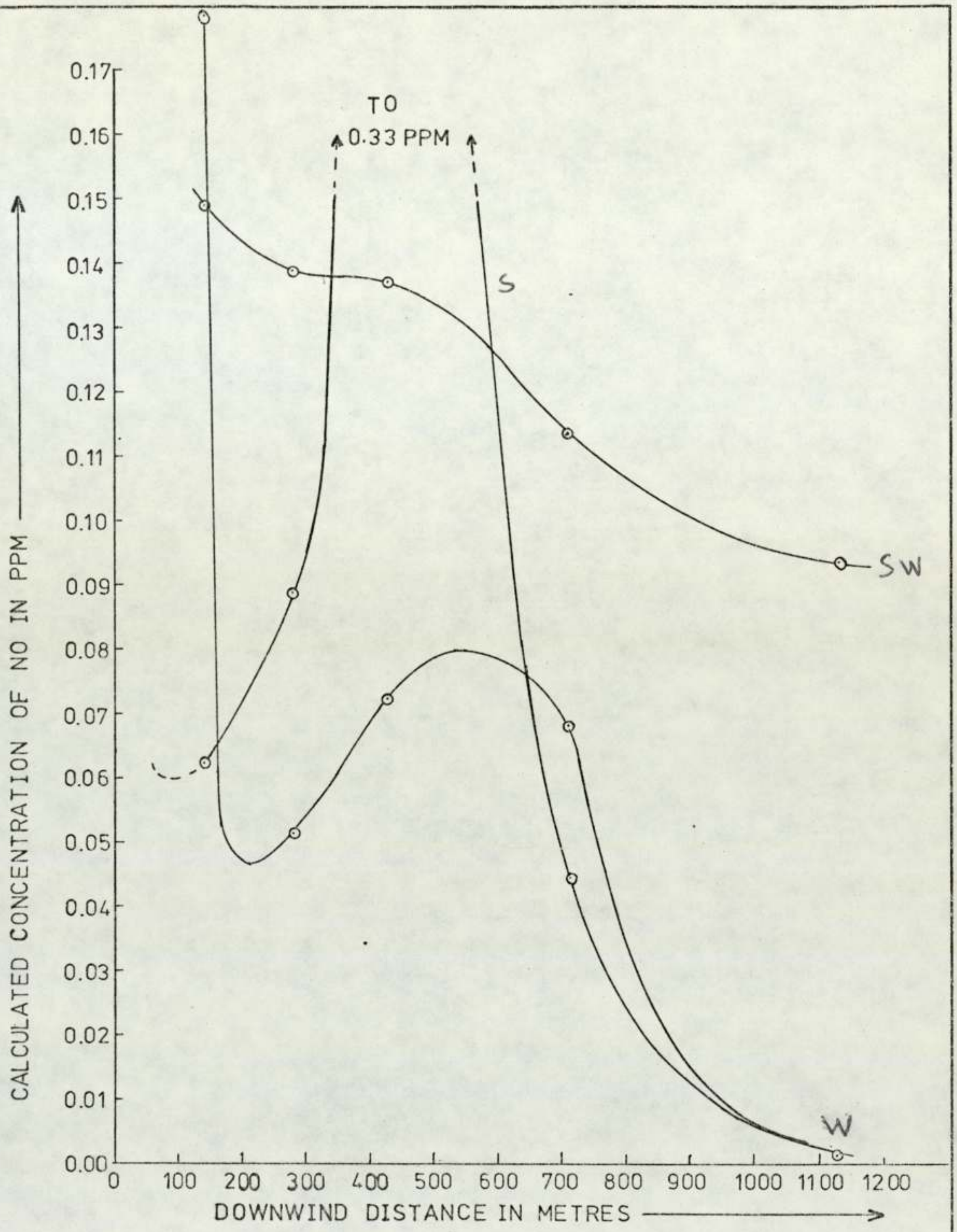

FIGURE 6.20 VARIATION WITH DISTANCE DOWNWIND FROM THE INTERSECTION OF NO CONCENTRATION, CALCULATED FOR THREE WINDDIRECTIONS WITH MST2 = 8 (CLASS E).

between concentration and wind-speed for any given downwind distance (assuming no change in MST2: a complete analysis of wind-dependence including changes in stability category would have required greater programme changes).

The Figures 6.16 to 6.20 are a series of plots which together may be explained by reference to the map (Figure 6.12). As the stability index MST2 increases so does the general level of pollutant concentration. In addition for a S wind the peak (Figures 6.16 to 6.20) at a place approximately due North of Salford Circus is due to the pattern of source-strengths implied by the map (Figure 6.12) and the traffic densities. The diagonal traverse through the roundabout plume superimposes a pollutant peak on the broad decay. In practice the peak would be less pronounced: our model of the intersection is a simplified one.

6.5 Programme Limitations and Possible Improvements

The following limitations and suggested modifications draw on Chapter 5 and Sections 6.1 - 6.4.

1. Source-strength parameter is difficult to arrive at satisfactorily: a variable emission parameter might be of value.

2. The effect of finite plumes as represented by the variable c (set to 27m here) has not been closely examined: Figure 6.8 summarises a study of its effect on $\sigma_y(0)$ and $\sigma_z(0)$. The format $\sigma(X + c)$ was used, but $\sigma(X) + \sigma_c$ should be studied (Section 6.2.4).

3. Extrapolation of open country plumes to the structurally complex

intersection ignored local eddy effects.

4. Zero winds cannot be modelled (cf. discussion in Chapter 5).

5. A version (SPAGSIMP) was developed with simplified data input for predictive work only: the input of field results was removed, observer positions were read to the nearest metre and traffic for all roads read from input channel 5. This will be used in Chapter 7.

6. The subroutine GEOMET was constructed from curves for five stability classes (Table 5.3), while there are ten possible values for stability index MST2. It does generate in-between categories (e.g., A-B) as suggested by Pasquill (1961), but does not fully exploit the range of MST2 (categories E,F,G treated as E). Modifications here might well be linked to the problem of urban diffusion (see above Paragraph 3).

7. The programme is limited in application to latitudes 48N and 60N: subroutine STABIL could be replaced by one applicable to all locations, e.g., using solar elevation (Johnson et al., 1971), or where measurements permit, turbulence statistics from bivanes (Section 5.3.1).

8. No consideration was given to downwind limits on vertical mixing (in this study downwind distances were < 1km) or to pollutants from outside the intersection. The latter defect is partly a matter of data entry (additional, more distant roads may be used) and partly of programme changes to include other, non-traffic, sources (cf. introduction, Chapter 1: Figure 1.3).

9. Sloping roads could be handled by a height-interpolation sub-routine.

10. Application to particulates has not been discussed: the programme may be used directly if settling is to be ignored, or a modified plume equation with a term for the mean settling velocity could be integrated.

6.6 Programme Calculations and Routine Monitoring Results

So far in this Chapter we have described emissions estimates and a programme to calculate concentrations of NO, CO and HC from traffic: the accuracy of the programme for a simple test case was assessed by reference to the model of Calder (1973). The sensitivity of the calculations to several parameters was considered. Following these discussions of the programme's development and behaviour, which aimed at highlighting limitations due to its construction, we turn now to assess its performance in practice. This will require reference to a large body of monitoring results: to avoid repetition and awkward cross-referencing this section is in three parts - the first considers model performance, and the other two, general features of the measured levels. This section as a whole essentially completes discussion of the routine monitoring work.

6.6.1 Comparison of Measured Pollutant Levels with Programme Calculations

The measured and calculated levels for Salford Circus were analysed with the aid of the ICL 1900 series statistical Analysis Package (XDS3/22) on the 1904S computer.

Simple regressions of the straight line form Y = MX + c, with calculated level Y, measured level X, assessed programme performance.

Table 6.8 summarises the analyses, which used the concentrations displayed in Figures 6.21 to 6.25. For a perfect model the regression coefficient (M) and correlation coefficient would be unity. Figure 6.31 draws on earlier discussions to suggest possible discrepancies. If we assume the emissions parameter Q_i (representing Q_{NO}, Q_{CO}, or Q_{HC}) is causing the regression coefficient M to deviate from unity, a parameter (Q_i/M) would remove the deviation: rearranging the above we have

$$\text{measured level} \quad X = \frac{Y}{M} + \left(\frac{-C}{M}\right)$$

with a background level of (-C/M) to add to the new calculated level, i.e. after Y has been enlarged to (Y/M). For NO_x, CO and HC the regression gave c as negative, or the background, $\left(\frac{-C}{M}\right)$, as positive. For all the gases, except NO_2, there is a good correlation (Table 6.8) between the measured and calculated levels, suggesting that the model is adequately describing the hourly fluctuations of pollutant levels at Salford Circus. The regression coefficients are not unity: this suggests a discrepancy due to the uncertainties in emissions estimate on one hand and the uncertainties in absolute calibration on the other. Table 6.10 indicates the emissions parameters increased from those as used (Table 6.4) to make the model "fit", and associated ppm levels in the exhaust. The new exhaust levels for NO appear reasonable in the light of those for various driving modes given in Table 6.3.

For CO, they seem high and for HC very high. These results probably reflect the combined effect of the various errors (Figure 6.31): the CO analyser was running at the low end of its scale, while the HC levels showed a steady high background (Figures 6.25 and 6.30). Considering the general problems of calibration (Chapter 2) and of deciding which driving mode and hence which emissions estimate to use, it is likely that improvements in model fit require work on various fronts: techniques of monitoring (accurate zeroes, calibrations, use of additional sites to identify the incoming background level and the level at the intersection), emissions estimates (particularly driving mode effects and other sources as contributing to the incoming background level), and on site meteorological measurements.

6.6.2 Background Levels

Table 6.9 and Figures 6.26 to 6.30 summarise the levels at the Murdoch Point site (500m from the intersection on the city side), for a period when winds were generally from the city.

For NO and NO_x at Murdoch Point the mean levels were respectively one quarter and one tenth of those at the intersection. They were similar both to the minimum levels of NO and NO_x, and to the background level (estimated as $^{-C}/M$ from the regression) for NO_x. The background level estimated for NO was negative: this reflects the inaccuracies of both the data and the model.

For all the gases, except NO_2, mean levels at Murdoch Point tended to be lower than at Salford Circus. The ratios of mean level at Murdoch Point to that at Salford Circus were, For NO_x, 0.23; for NO, 0.10; for NO_2, 1.1; for CO, 0.36 and for HC, 0.74.

6.6.3 Oxides of Nitrogen

At Salford Circus, NO and NO_x were very similar (Figures 6.21, 6.22 and Table 6.8) with correlation coefficients of 0.76 with the calculated levels, and similar means (NO, 0.117 ppm; NO_x, 0.106 ppm), minima (NO, 0.015 ppm; NO_x, 0.011 ppm), maxima (NO, 0.381 ppm; NO_x, 0.410 ppm), and variances (NO, 0.00711 ppm^2; NO_x, 0.00813 ppm^2). This is because NO_x is NO plus NO_2, and the levels of NO_2 were low relative to those of NO: mean NO_2 was 0.0141 ppm and the maximum 0.086 ppm.

NO_2 (Figure 6.23) at Salford Circus shows frequent zero values: the NO_2 value was the difference between mean hourly values of NO_x and NO. Periods of least fluctuation (to zero and back) of the NO_2 appeared when the NO and NO_x levels were low, and, probably more important, showed less fluctuation in magnitude: the hourly averages were for finite samples from a non-stationary random process (cf. Chapter 3) so have greatest uncertainty at times of greatest fluctuation. The behaviour of NO_2 at Murdoch Point was consistent with this for the NO and NO_x levels were much less variable (Figures 6.26, 6.27) and the NO_2 (Figure 6.28) shows no such oscillation.

The measurement of NO_2 as (NO_x - NO) using finite sampling (15 points per hour) of NO_x and NO was unsatisfactory at Salford Circus, which was near traffic and where large rapid fluctuations occurred in NO levels. It was satisfactory where levels of NO fluctuated much less.

The ratio of mean NO to mean NO_2 at Salford Circus was 7.5:1, consistent with the suggestion (Derwent and Stewart, 1973) that exhaust gases enter the atmosphere with nine parts of NO to one part of NO_2 by volume. At Murdoch Point the ratio of mean NO to mean NO_2 was 0.68:1. This site is further from sources (for the period in question winds were from the city) and the general level of NO was lower than at Salford Circus. The ratio suggests there has been significant dilution and probably oxidation of the NO. According to Derwent and Stewart (1973), the ration NO/NO_2 may be expressed in the form

$$[NO, \mu gm^{-3}] / [NO_2, \mu gm^{-3}] = 0.130 + 0.009\,[NO, \mu gm^{-3}]$$

where square brackets represent concentrations in the units shown. Bibbero and Young (1974a) give conversions ($0^{o}C$, latm)

$$[NO, \mu gm^{-3}] = [NO, ppm] \,.\, M_{NO} \,.44.64 = 1.3392.10^{3}\,[NO, ppm]$$

$$[NO_2, \mu gm^{-3}] = [NO_2 ppm] \,.\, M_{NO_2} \,.44.64 = 2.0534.10^{3}\,[NO_2, ppm]$$

In Table 6.11 we give, using μgm^{-3} units, the ratios of NO and NO_2 as recorded and as derived from the recorded NO concentrations using the empirical rule (Derwent and Stewart, 1973) above. The ratios from the recorded concentrations are comparable with those given by the rule.

M = Mol. Wt.

6.7 Summary

Traffic counts and concentrations of pollutants in the exhaust were used to estimate the emission of pollutants from traffic on the intersection. We described trigonometry to define the geometry of any intersection using a minimum of map references. Drawing on the discussions in Chapter 5 of turbulent diffusion, the dilution of gas blown from any part of the intersection to the observer was estimated by integrating a point-source plume formula. Plume parameters were estimated indirectly, and rotation of axes solved the problem of wind direction. Programme improvements were suggested.

The programme was compared with numerical results of Calder (1973), and a sensitivity analysis studied the behaviour of the model. It was also compared with hourly measurements taken over a ten day period, giving a good correlation with all gases except NO_2, which had a measurement problem.

Results of the routine monitoring were recorded and processed with a view to checking such a programme as the one developed, and therefore the emphasis was on reliable measurement of all gases simultaneously. Realising that the data cover only three weeks, and could therefore be unrepresentative, we have given some discussion of the concentrations reported for the two sites.

In the next Chapter we describe an experiment to study dilution as a function of distance and height. The design of equipment precedes comparison of concentration gradients recorded in the field with those given by the programme.

TABLE 6.8

Comparison of Calculated and Measured Pollutant Concentrations:

Regression Results for (calculated) = m(measured) + c

Gas	Regression Analysis (5% significance level)						Measured levels, ppm			
	Regression Coefficient m	Intercept c	Correlation Coefficient R	Degrees of Freedom	$^1/_m$	Background ($^-c/m$)	Mean	Minimum	Maximum	Variance
NO_x	0.340	- 0.00322	0.76	236	2.940	+ 0.00947	0.117	0.015	0.381	0.00711
NO	0.319	0.00246	0.76	236	3.135	- 0.00771	0.106	0.011	0.410	0.00813
NO_2	rejected at 5% significance level			237	-	-	0.0141	0.000	0.086	0.000175
CO	0.0471	- 0.0521	0.67	236	21.2	+ 1.106	2.95	1.20	11.7	1.66
HC	0.00492	- 0.0236	0.72	236	203	+ 4.80	5.89	4.50	8.8	0.670

TABLE 6.9

Background Levels from Murdoch Point: prevailing wind from city and not from intersection

Gas	No regression: model gave zero results because of wind direction			Measured levels, ppm			
				Mean	Minimum	Maximum	Variance
NO_x		140 $obsn^s$		0.0264	0.0080	0.129	0.000297
NO		140 $obsn^s$		0.0107	0.0040	0.081	0.000123
NO_2		140 $obsn^s$		0.0157	0.0010	0.048	0.0000729
CO		140 $obsn^s$		1.07	0.40	3.10	0.148
HC		140 $obsn^s$		4.33	3.40	6.60	0.591

TABLE 6.10

Increased Emission Parameters, Qi/m,

Using Regression Coefficient of Calculated to Measured Levels. (See Table 6.4)

Gas	Emission parameter used Qi (Table 6.4)	Increased Emission			
		$^1/_m$	Qi/m	ppm Petrol	ppm Diesel
(NO_x)	$4.7843.10^{-4}$ (NOx, NO)	2.940	$1.407.10^{-3}$	-	-
NO		3.135	$1.500.10^{-3}$	5330	1550
(NO_2)	-	-	-	-	-
CO	$1.1400.10^{-3}$	21.2	$2.417.10^{-2}$	127000	6360
HC	$7.116.10^{-5}$	203	$1.445.10^{-2}$	52800	14200

TABLE 6.11

Ratios of NO and NO_2 Concentrations

Site	Measured Concentrations					Empirical Rule[3]
	[NO_2 ppm]	[NO, ppm]	[NO_2, μgm^{-3}]	[NO, μgm^{-3}]	[NO, μgm^{-3}]/[NO_2, μgm^{-3}]	
Salford[1] Circus	0.0141	0.106	28.952	141.95	4.9	1.4
Murdoch[2] Point	0.0157	0.0107	32.238	14.329	0.44	0.26

Note 1: See Table 6.8

Note 2: See Table 6.9

Note 3: [NO, μgm^{-3}] / [NO_2, μgm^{-3}] = 0.130 + 0.009 [NO, μgm^{-3}] after Derwent and Stewart (1973), with [NO, μgm^{-3}] as recorded

The following 25 pages
contain Figures 6.21 to 6.30
inclusive

Figures 6.21 to 6.25 each have three parts (1/3, 2/3, 3/3) and are for November 1974 at Salford Circus

Figures 6.26 to 6.30 each have two parts (1/2, 2/2) and are for March 1974 at Murdoch Point

Observations are labelled by time and date: some times are missing.

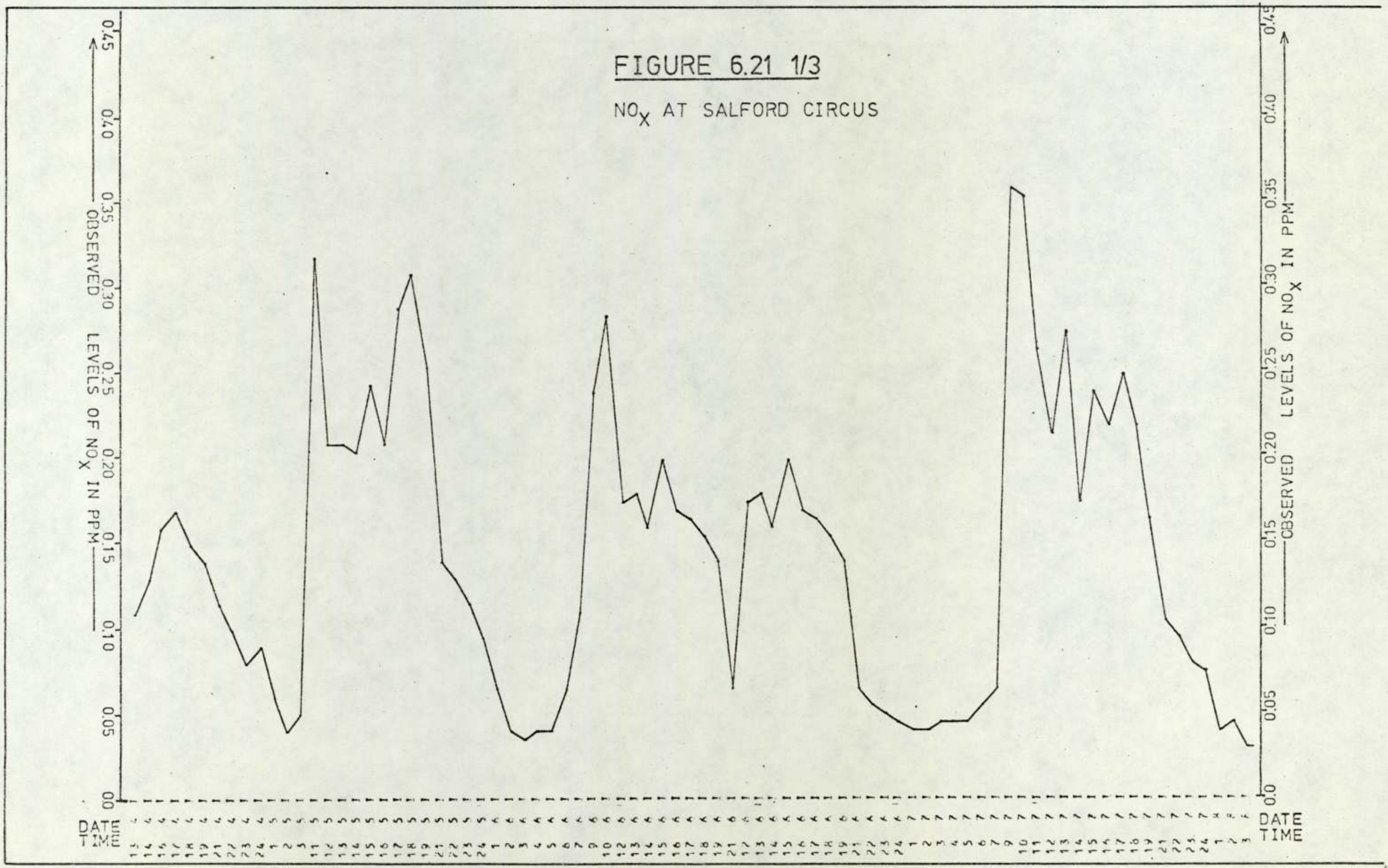

FIGURE 6.21 1/3

NO$_X$ AT SALFORD CIRCUS

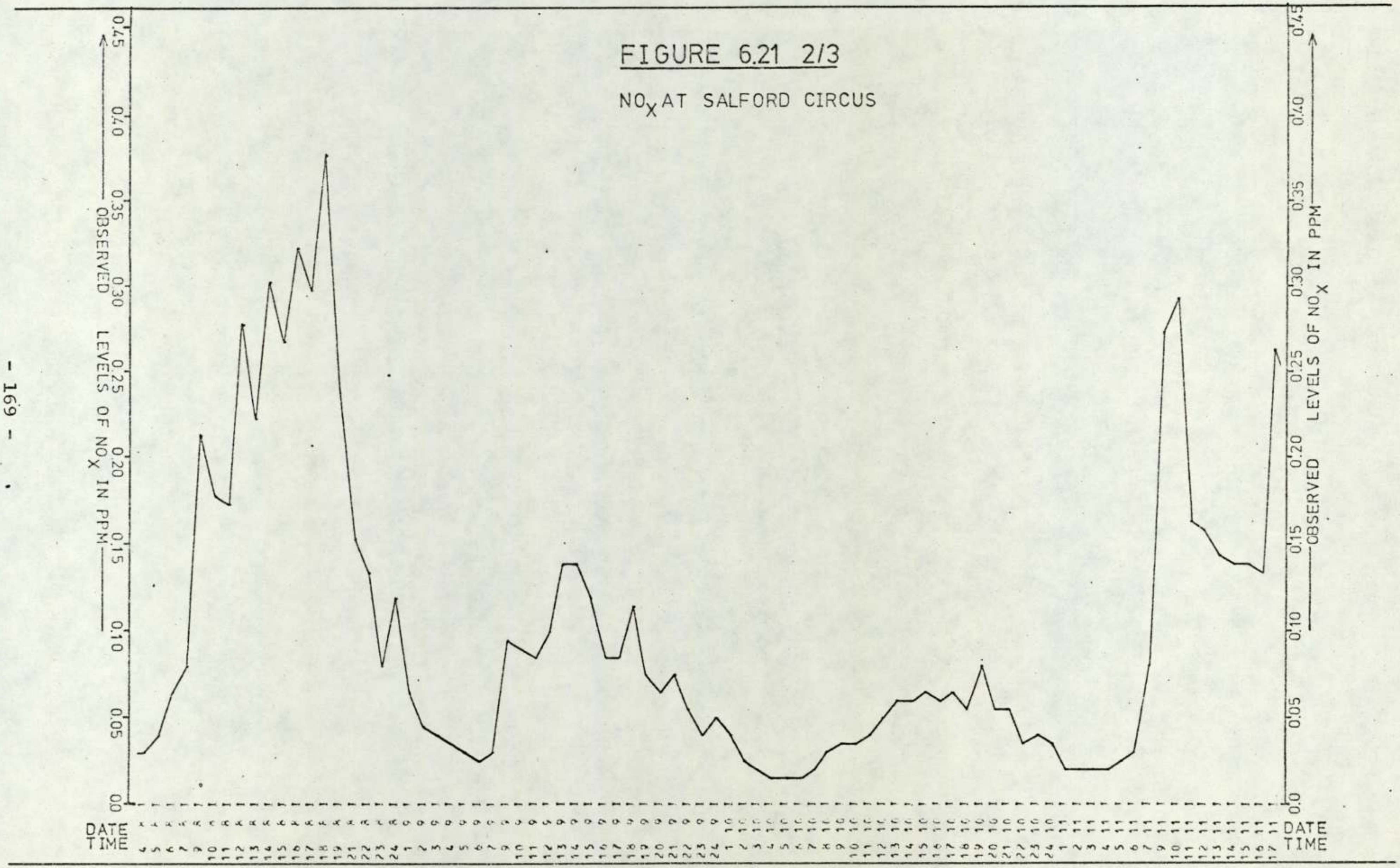

FIGURE 6.21 2/3

NO_X AT SALFORD CIRCUS

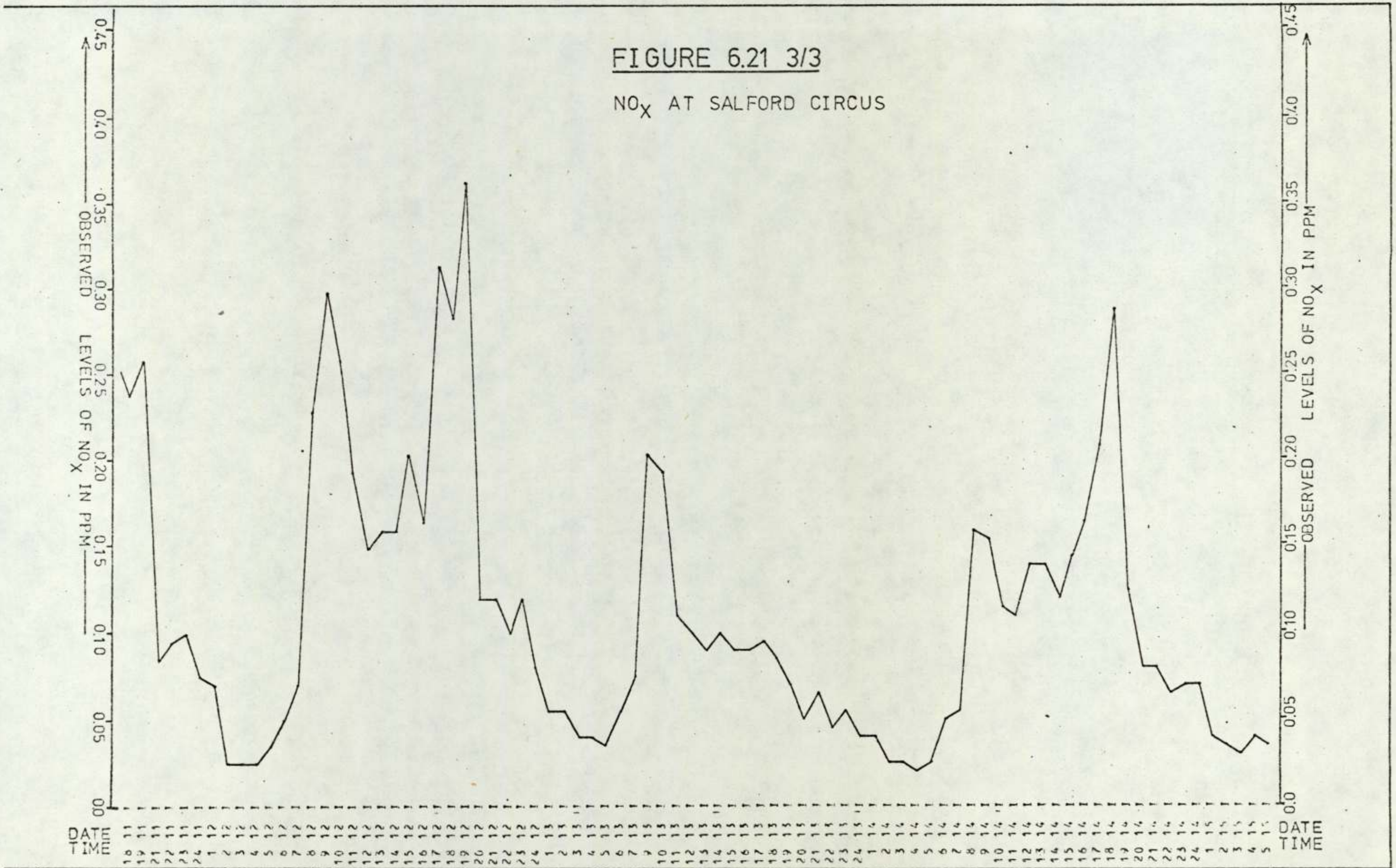

FIGURE 6.21 3/3

NO_X AT SALFORD CIRCUS

FIGURE 6.22 1/3

NO AT SALFORD CIRCUS

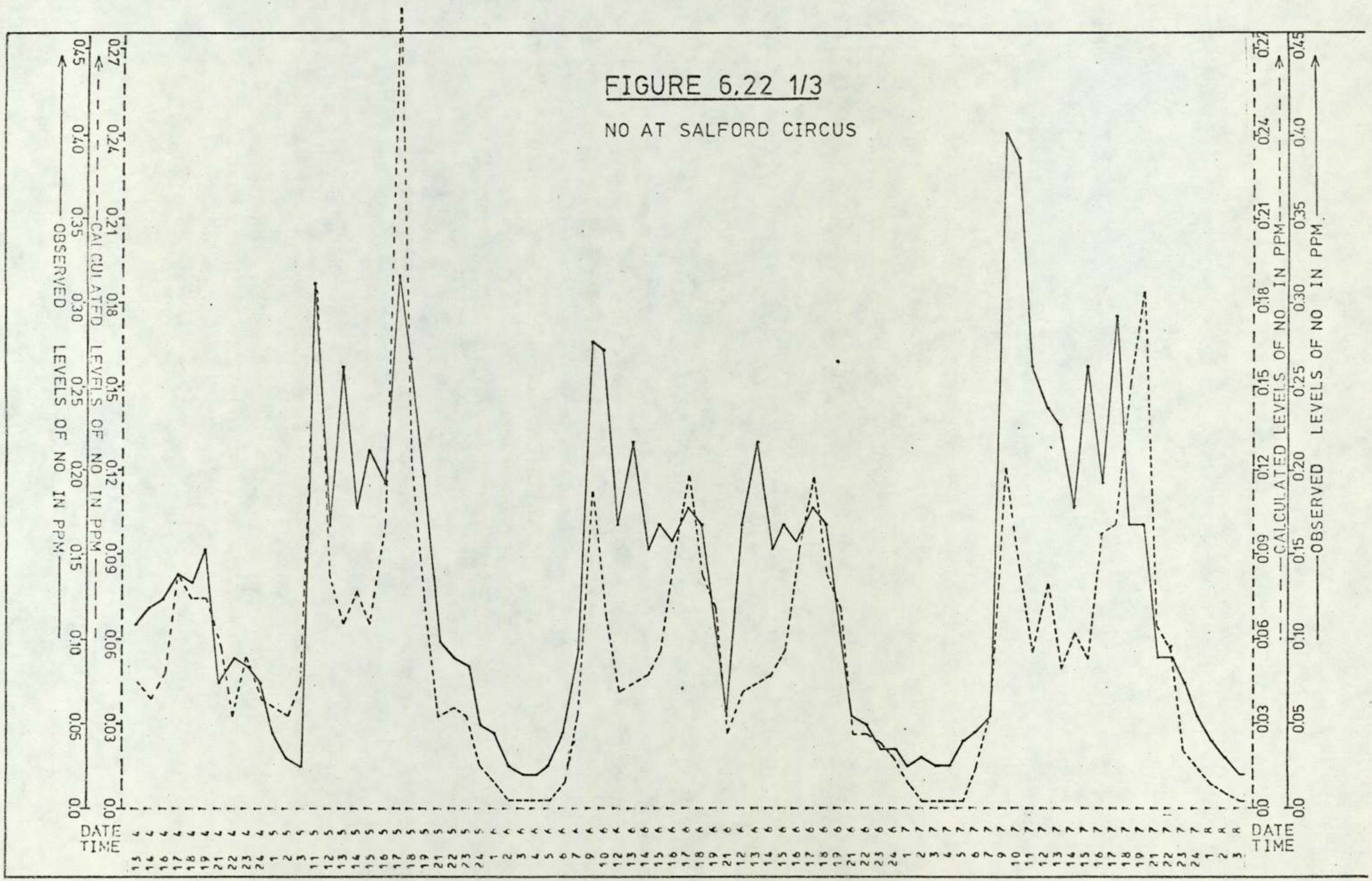

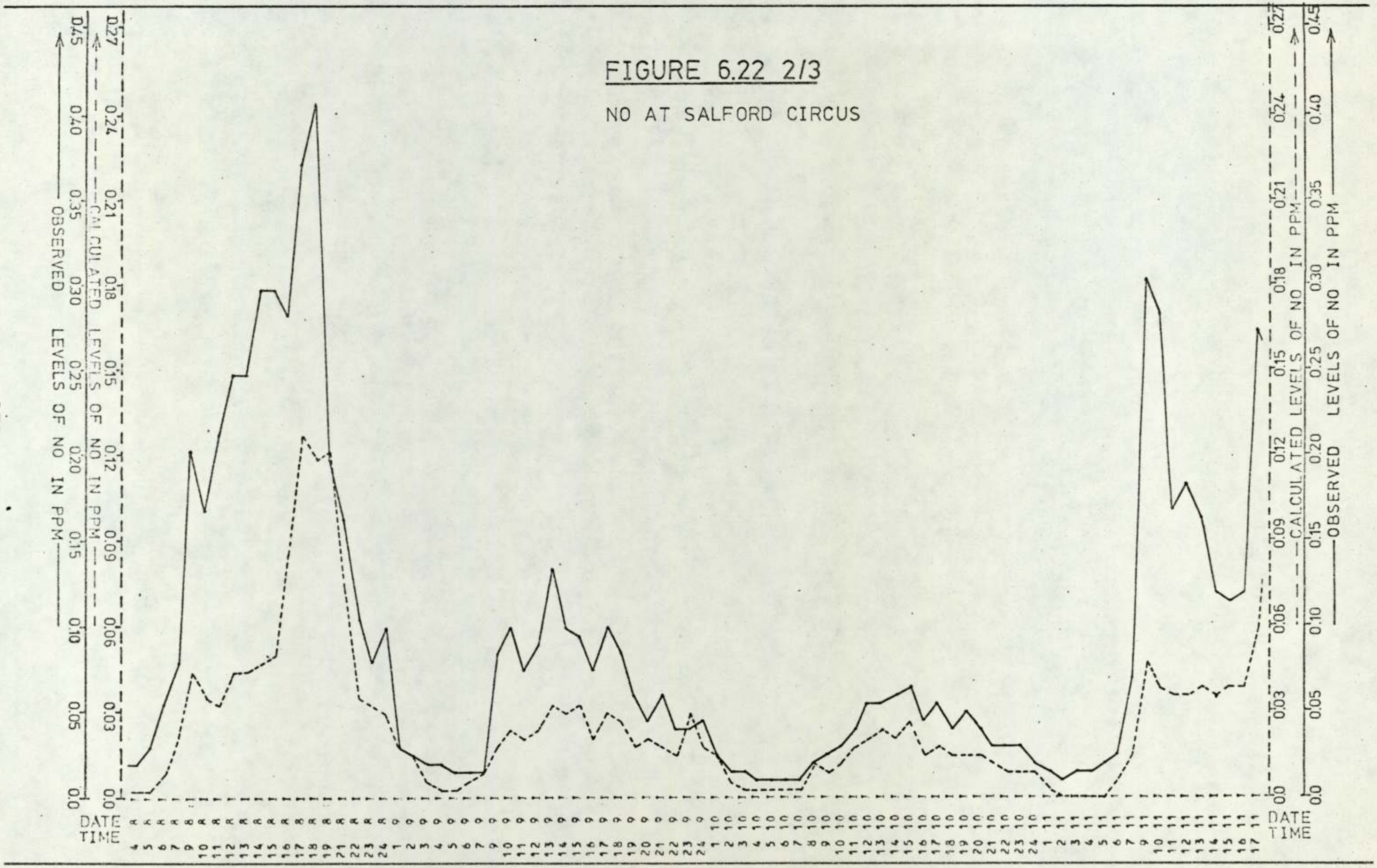

FIGURE 6.22 2/3

NO AT SALFORD CIRCUS

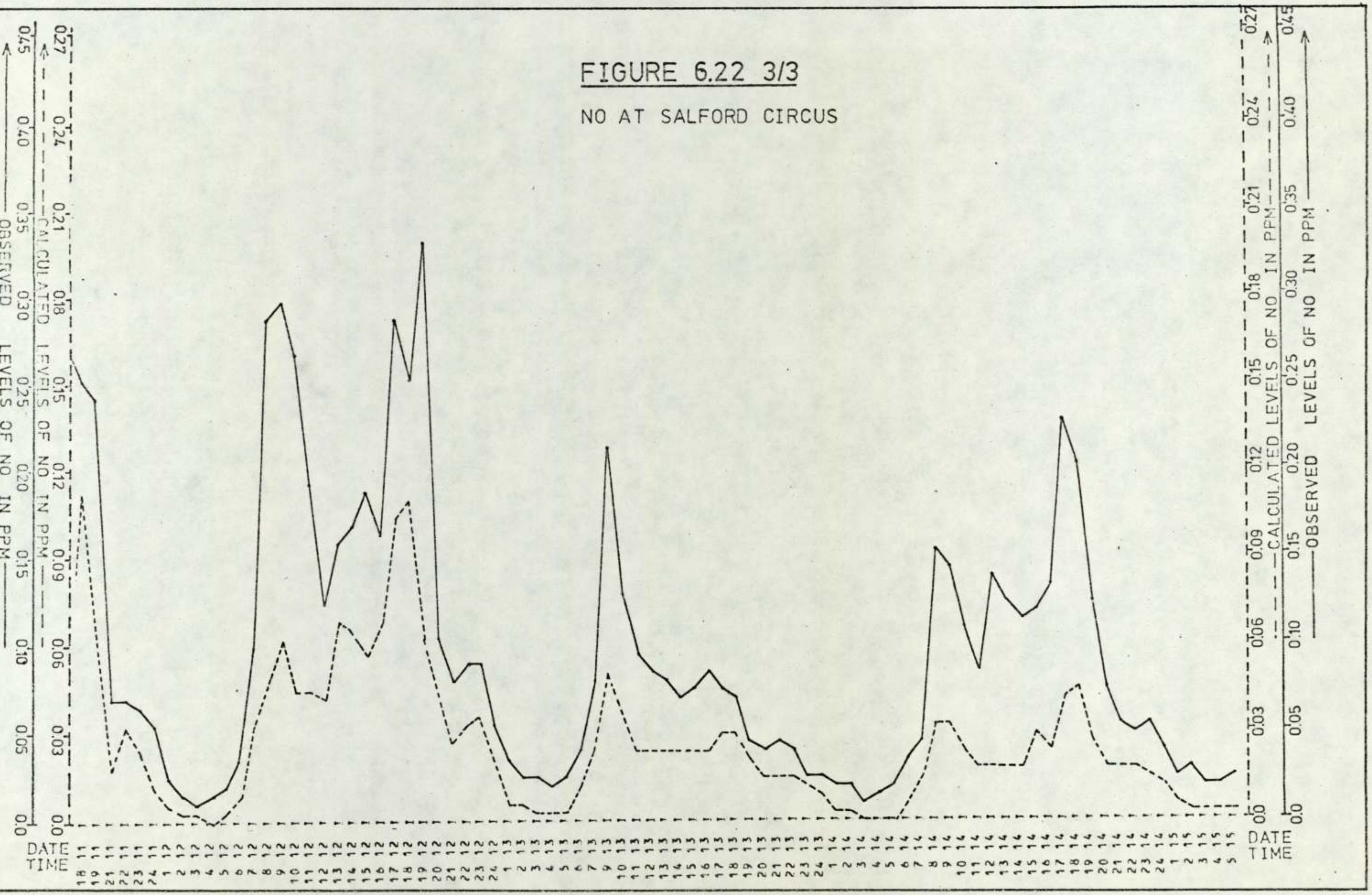

FIGURE 6.22 3/3

NO AT SALFORD CIRCUS

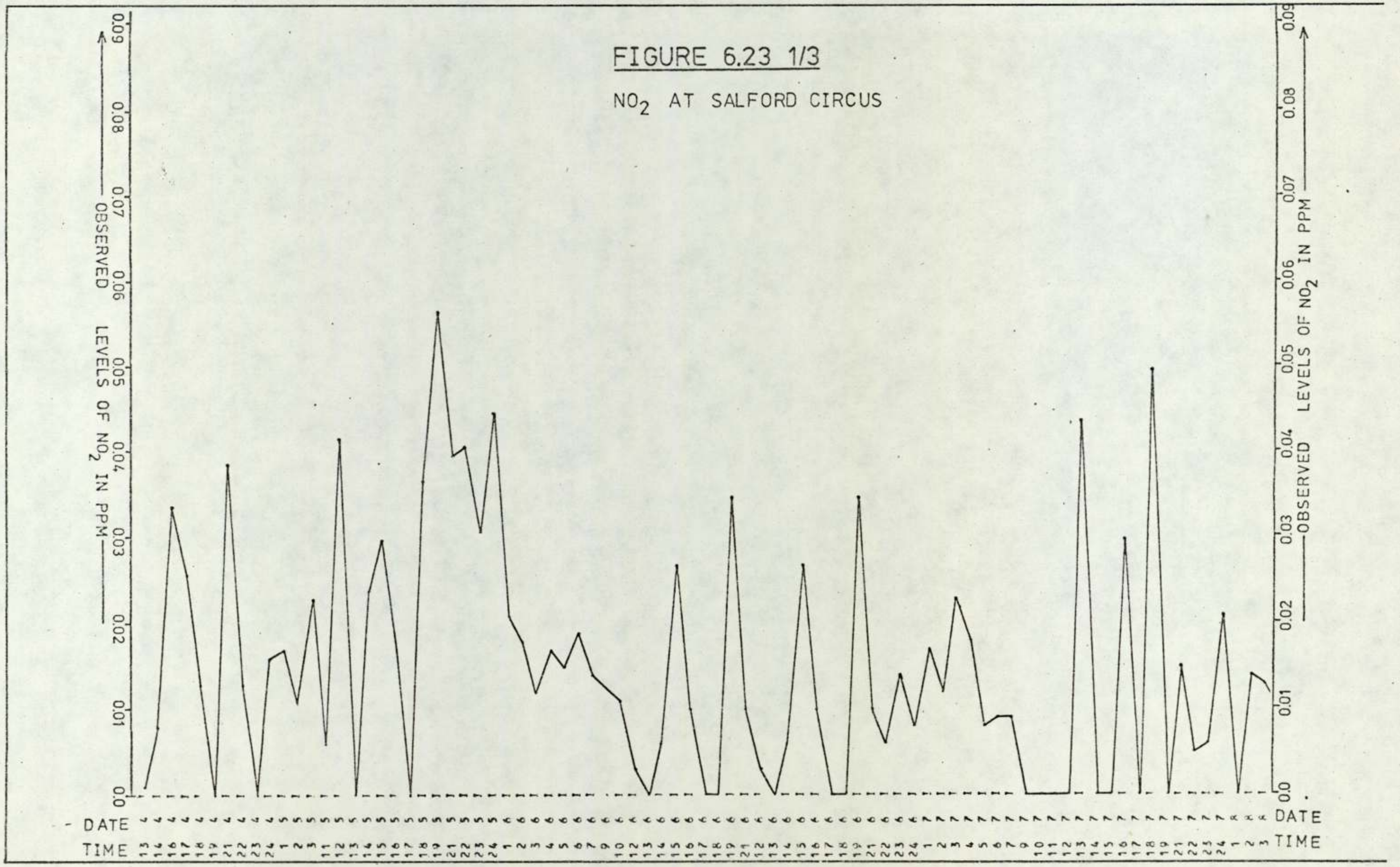

FIGURE 6.23 1/3

NO_2 AT SALFORD CIRCUS

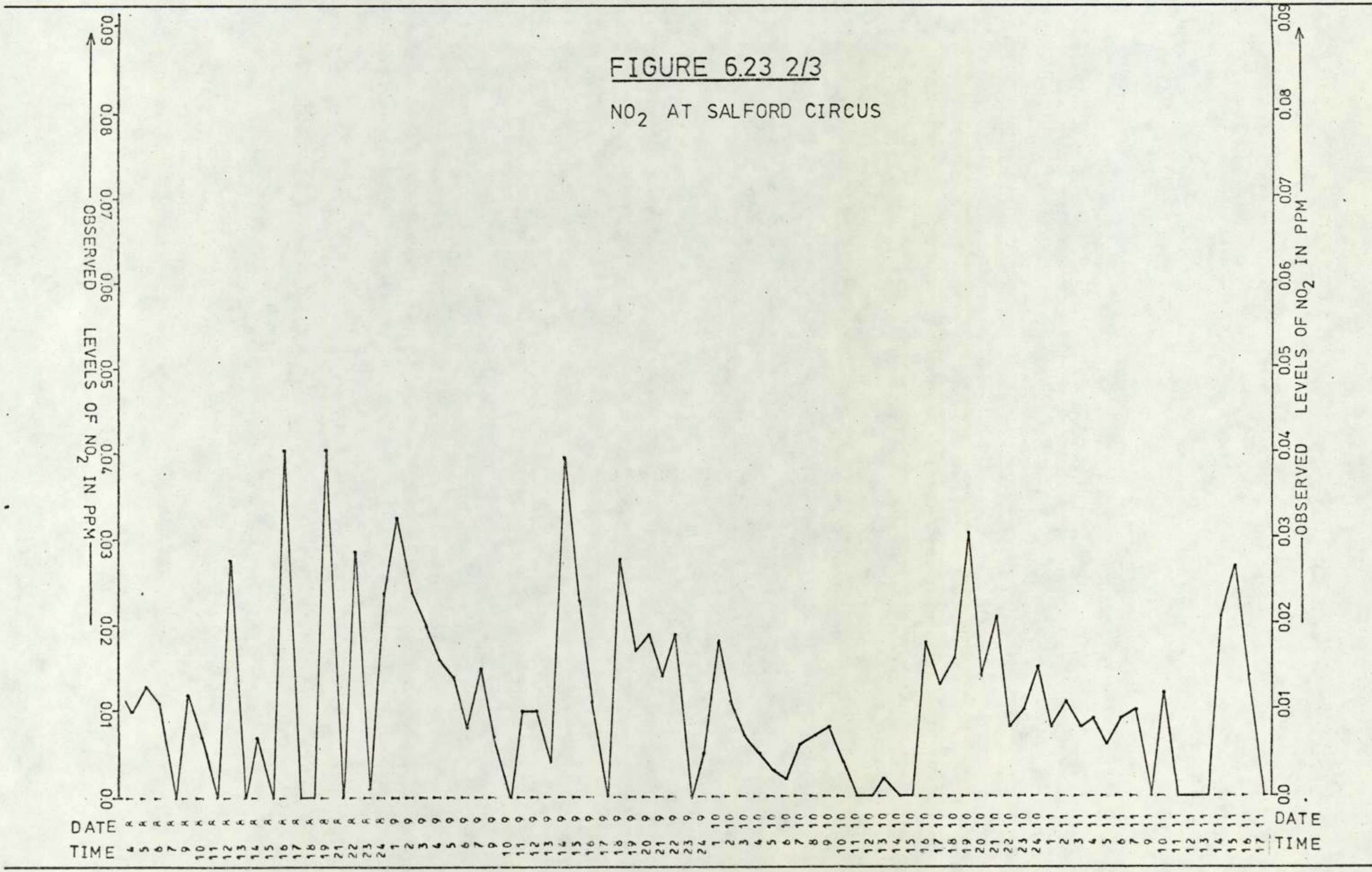

FIGURE 6.23 2/3

NO_2 AT SALFORD CIRCUS

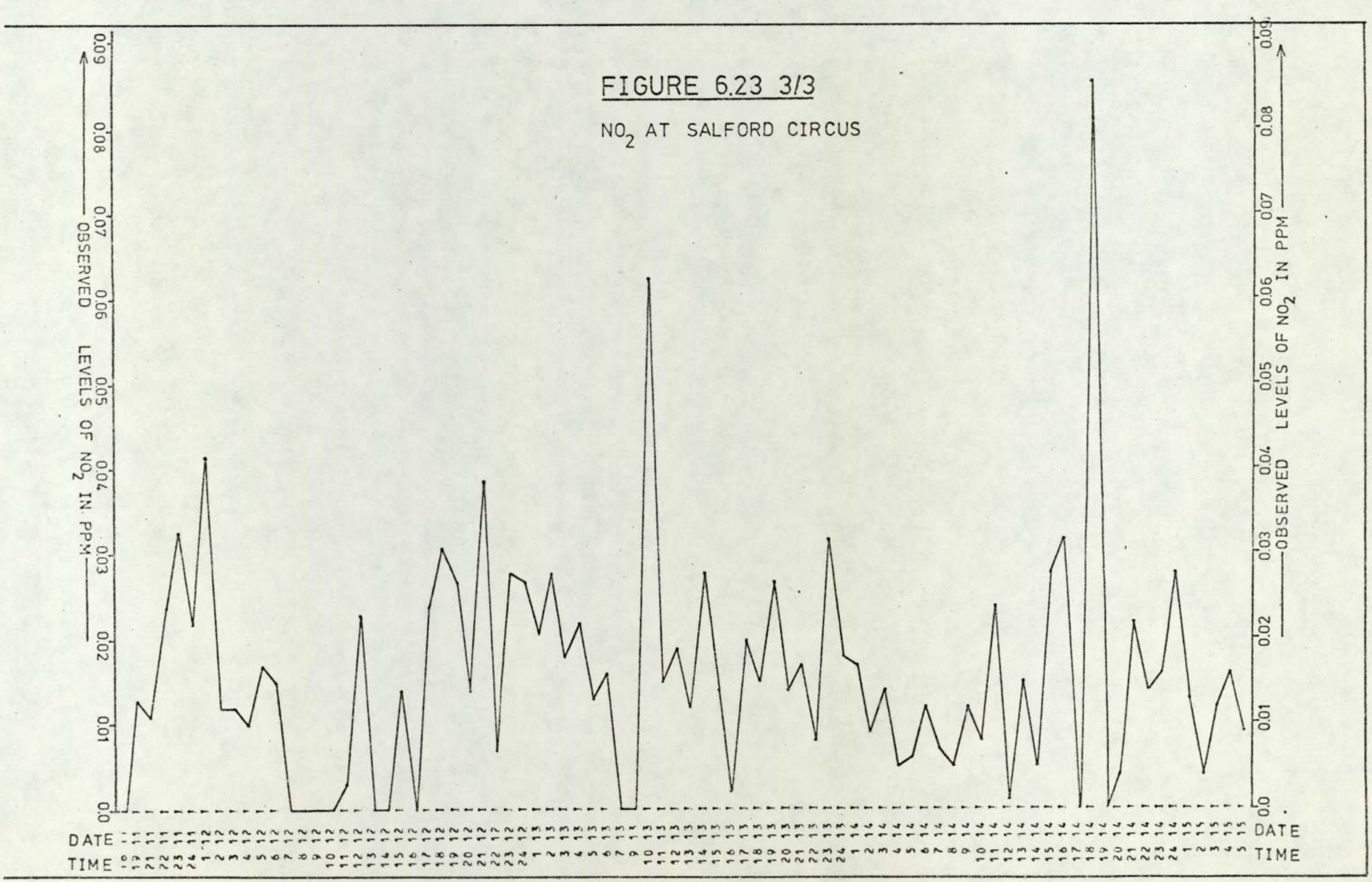

FIGURE 6.23 3/3

NO_2 AT SALFORD CIRCUS

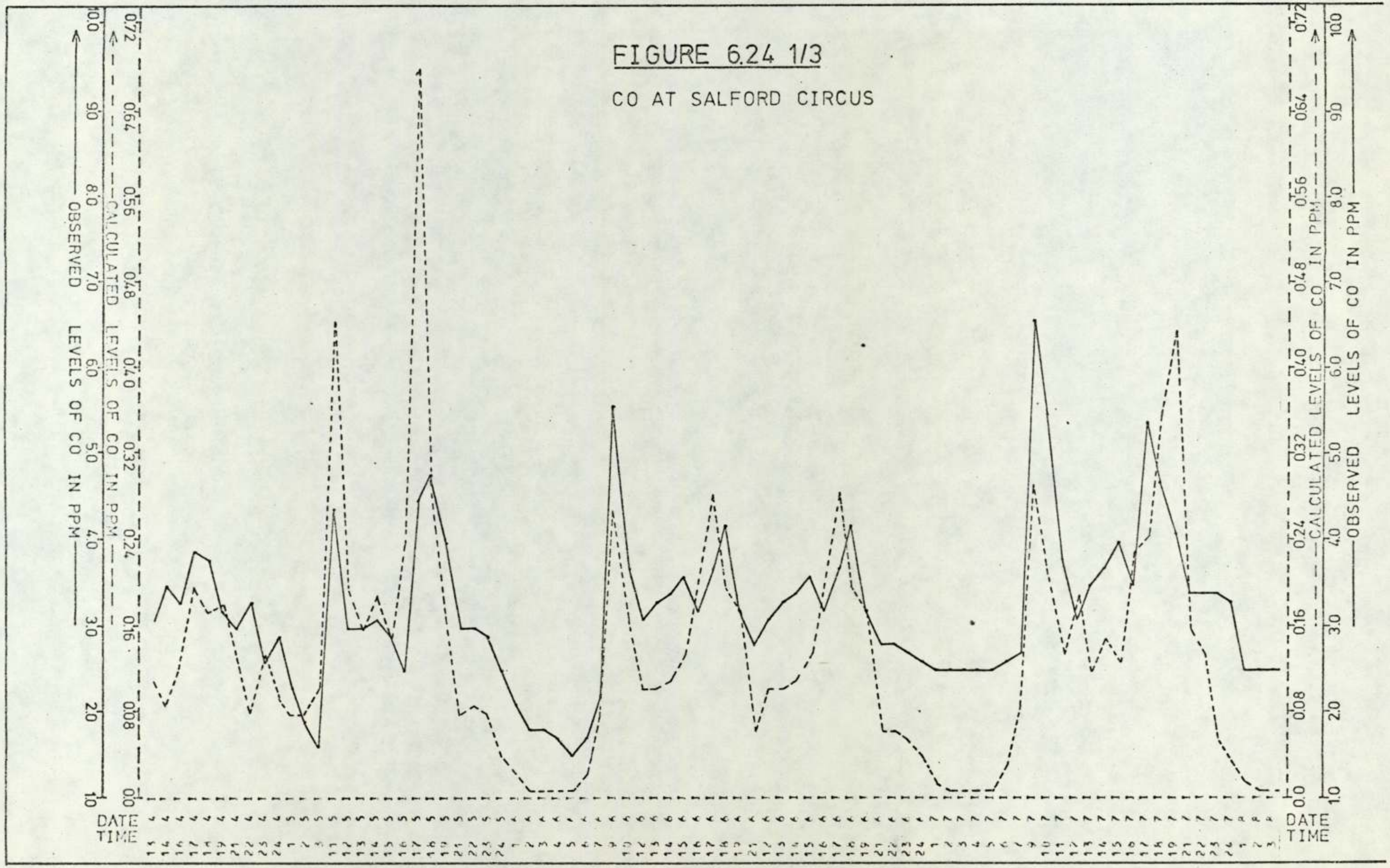

FIGURE 6.24 1/3

CO AT SALFORD CIRCUS

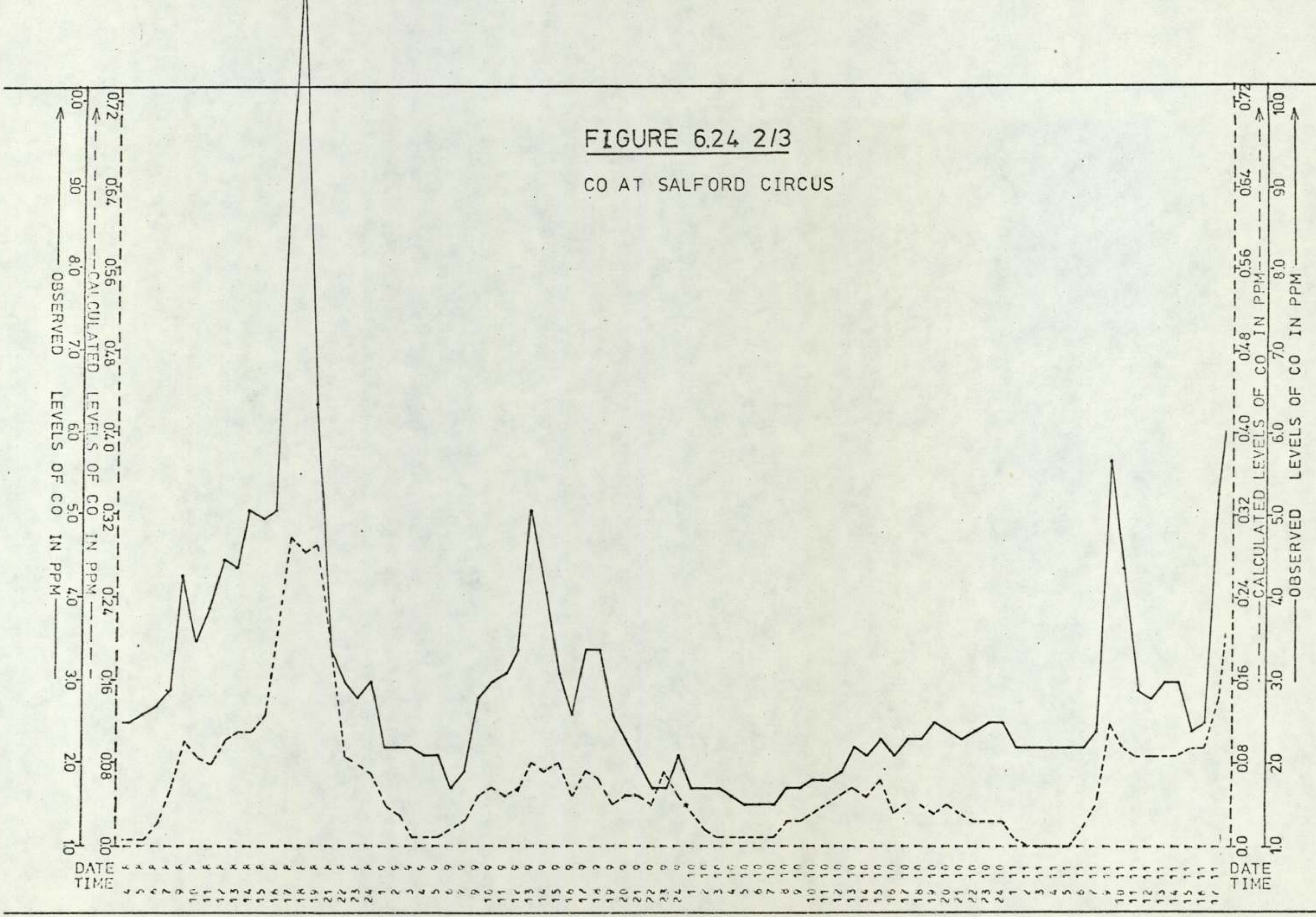

FIGURE 6.24 2/3

CO AT SALFORD CIRCUS

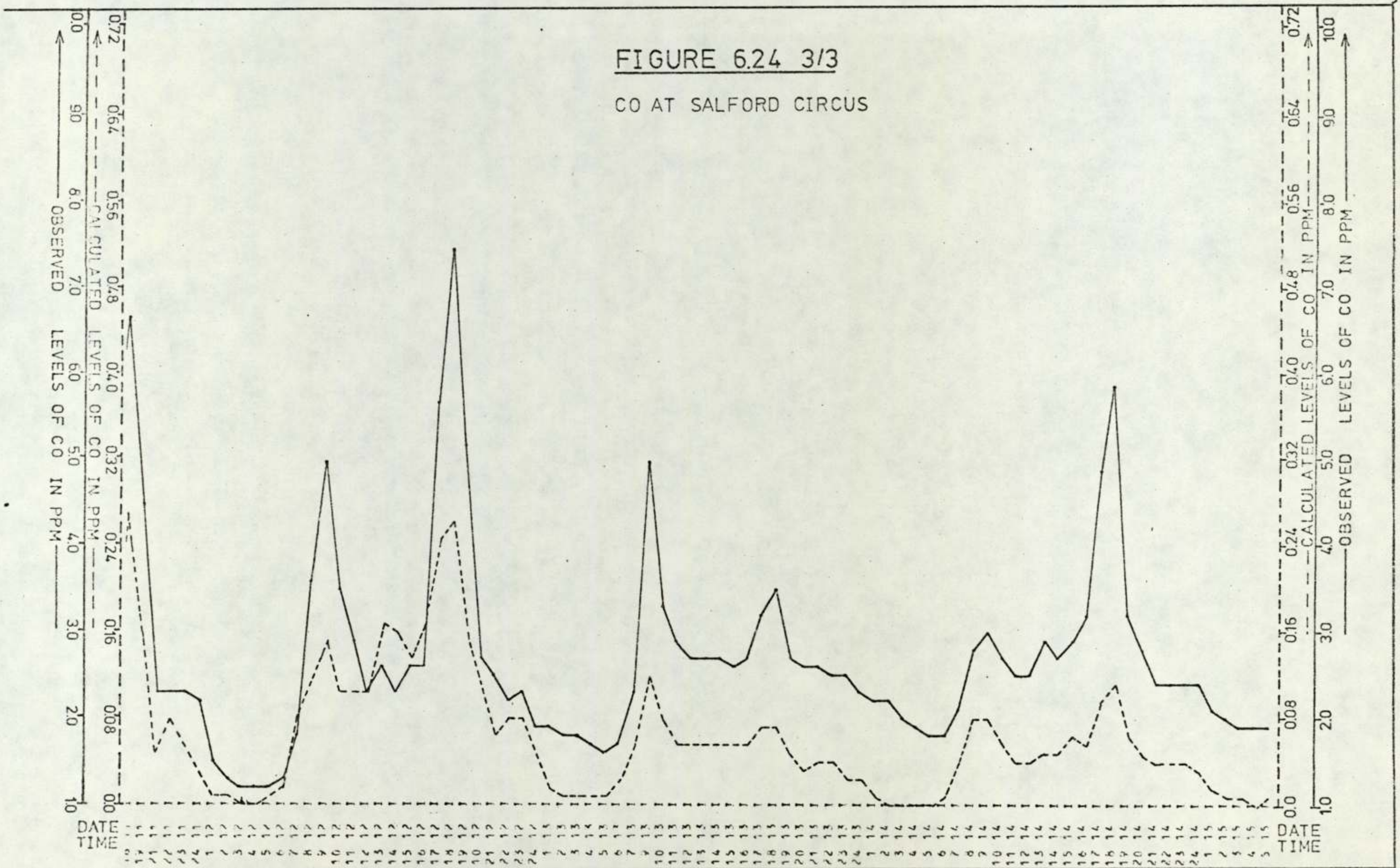

FIGURE 6.24 3/3

CO AT SALFORD CIRCUS

FIGURE 6.25 1/3

HC AT SALFORD CIRCUS

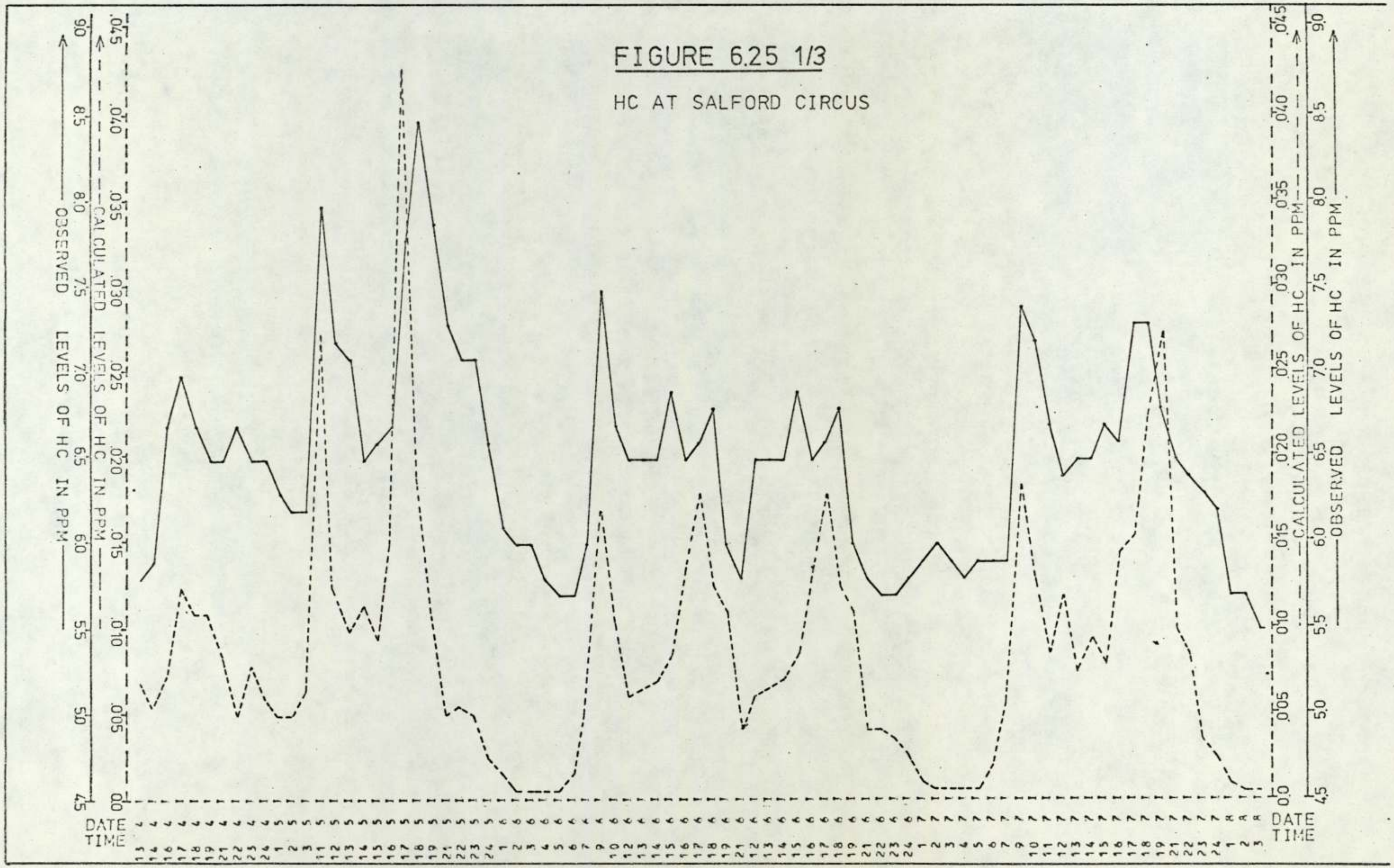

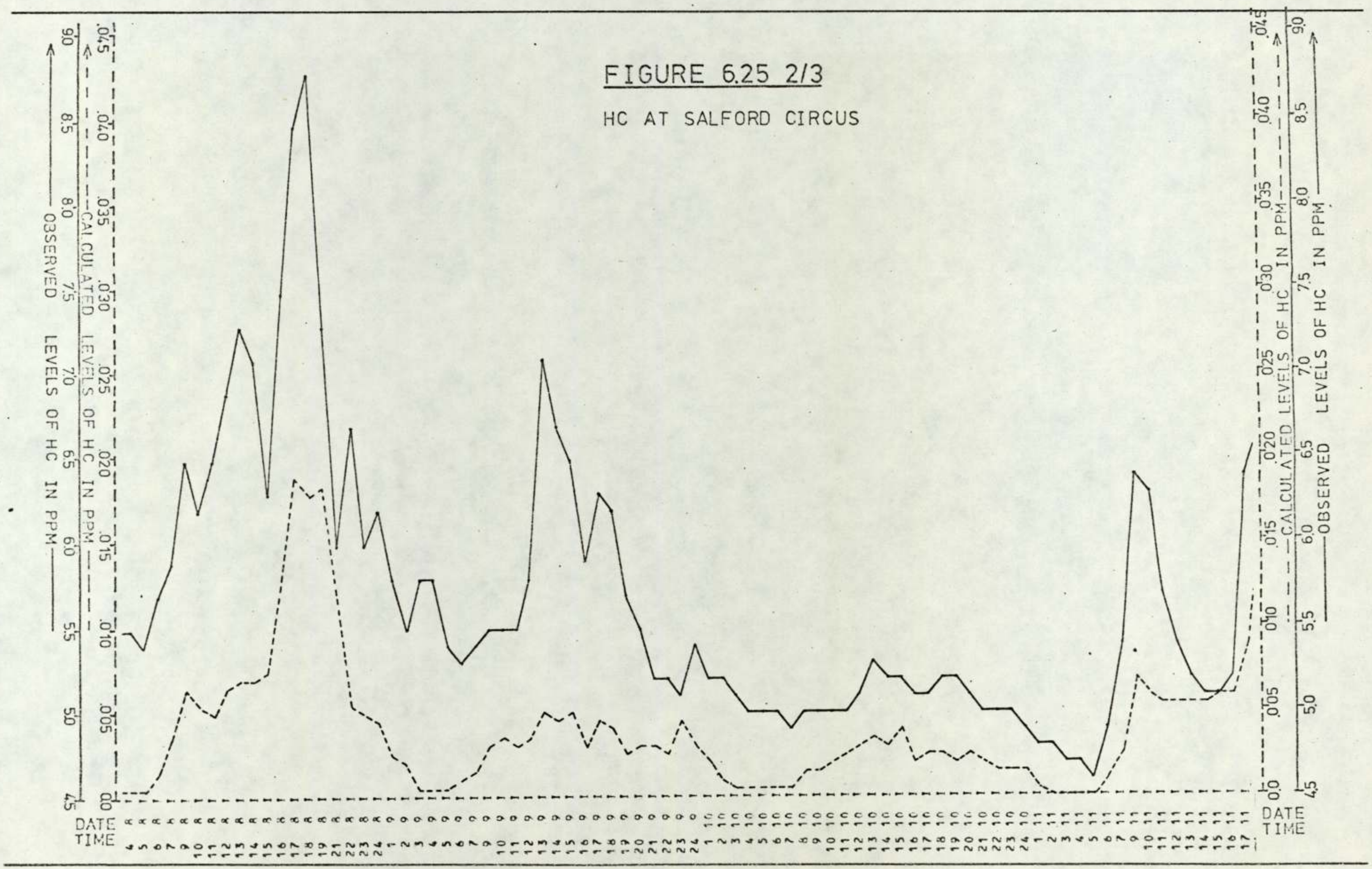

FIGURE 6.25 2/3

HC AT SALFORD CIRCUS

FIGURE 6.25 3/3

HC AT SALFORD CIRCUS

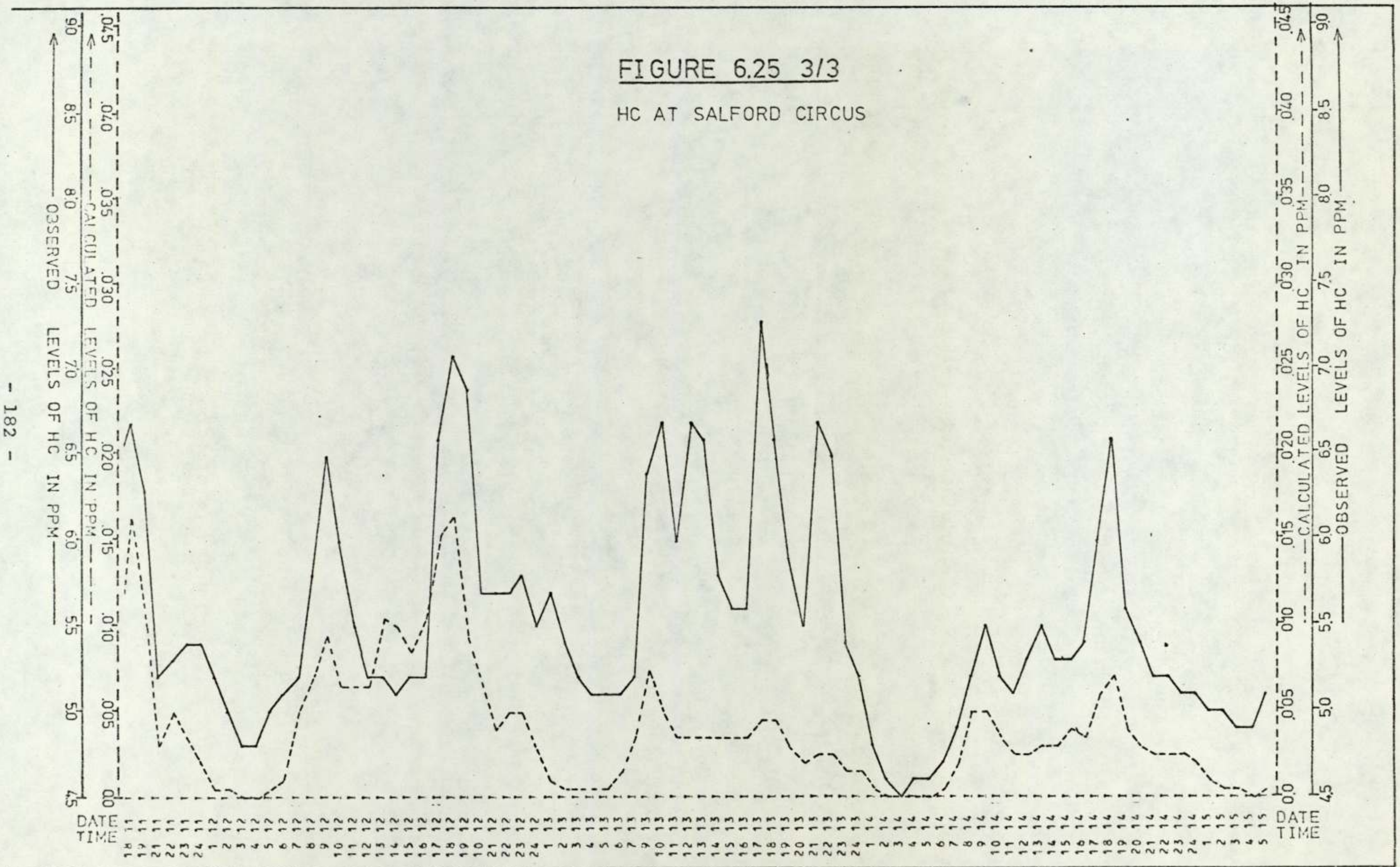

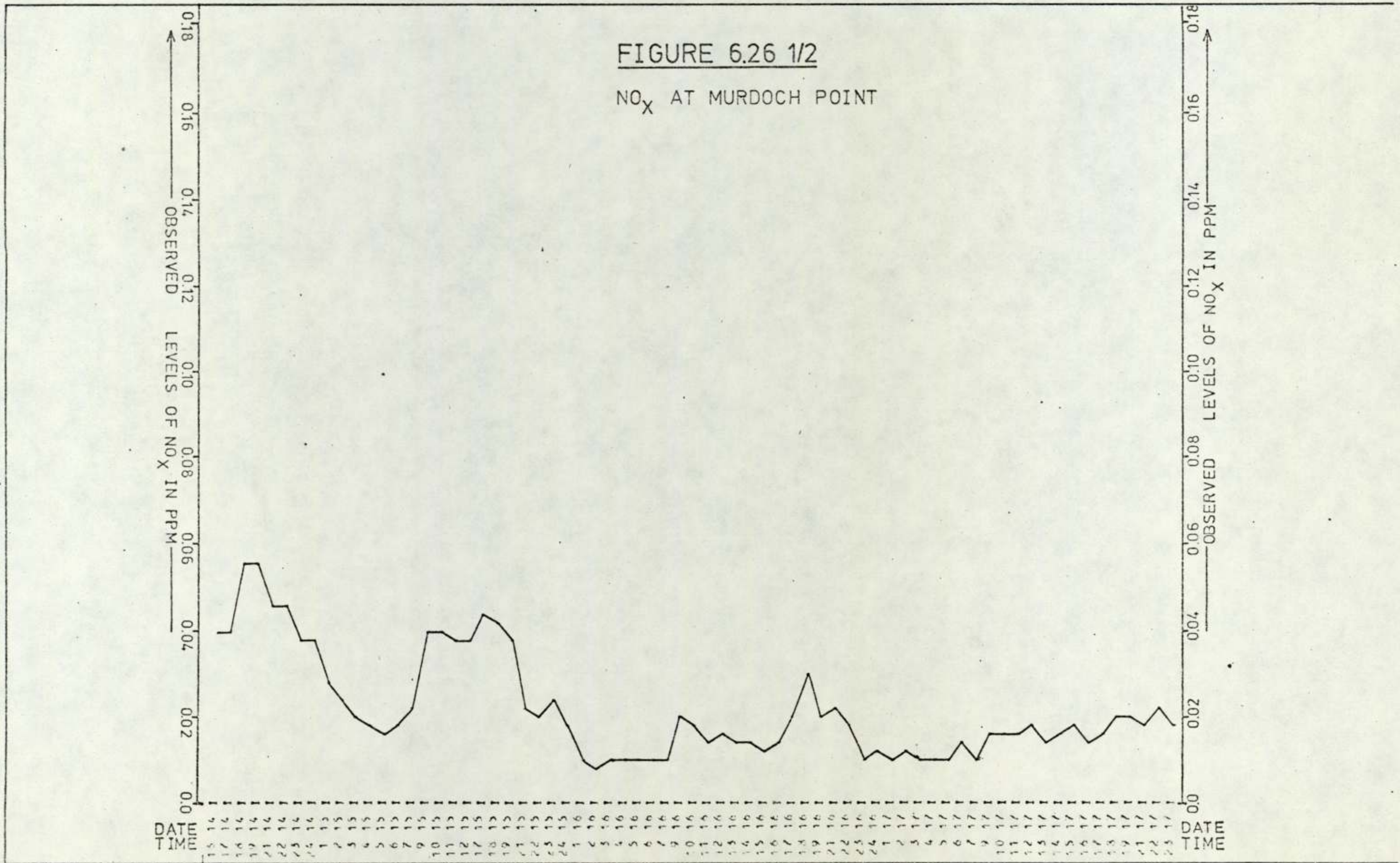

FIGURE 6.26 1/2

NO_X AT MURDOCH POINT

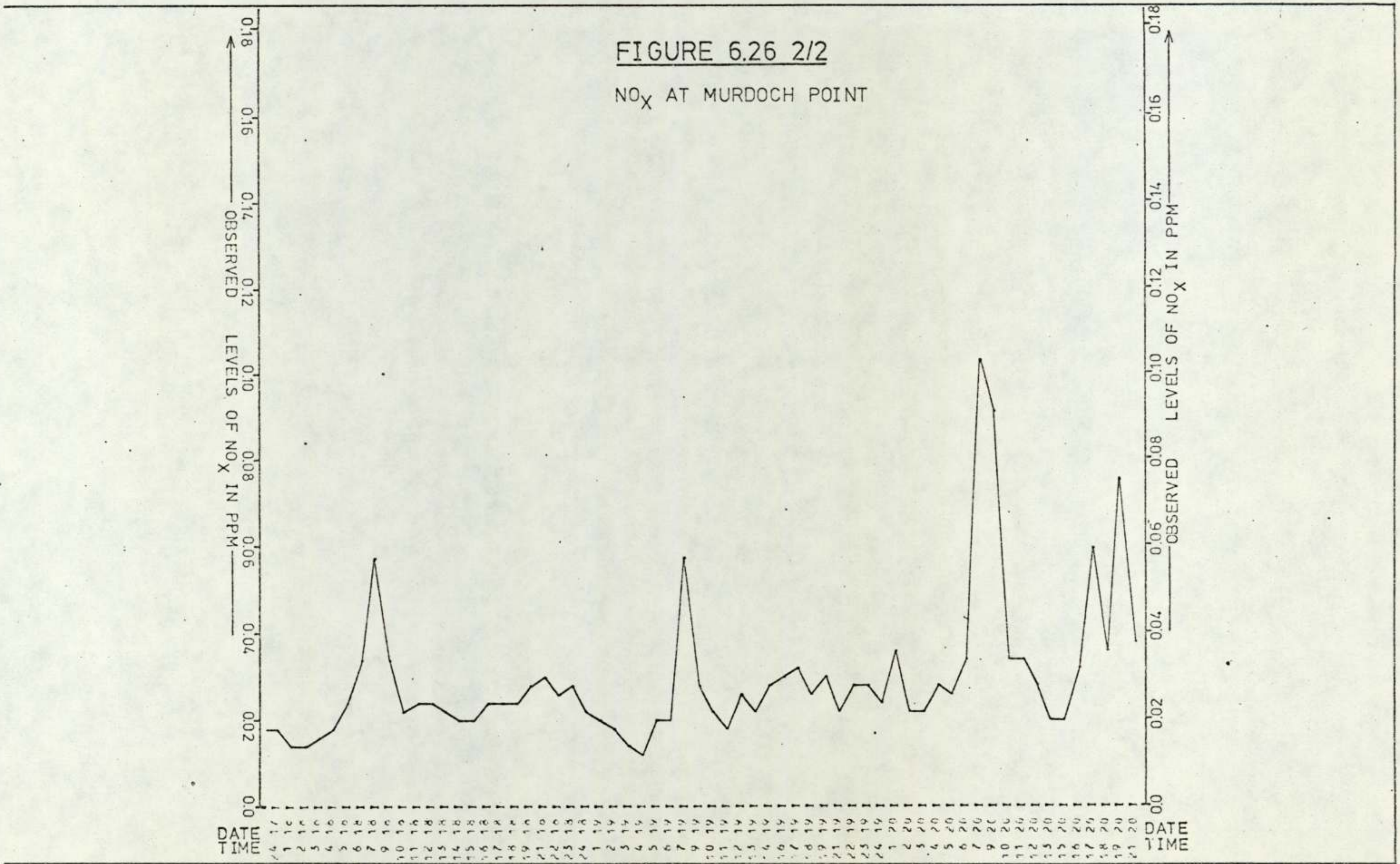

FIGURE 6.26 2/2

NO_X AT MURDOCH POINT

FIGURE 6.27 1/2

NO AT MURDOCH POINT

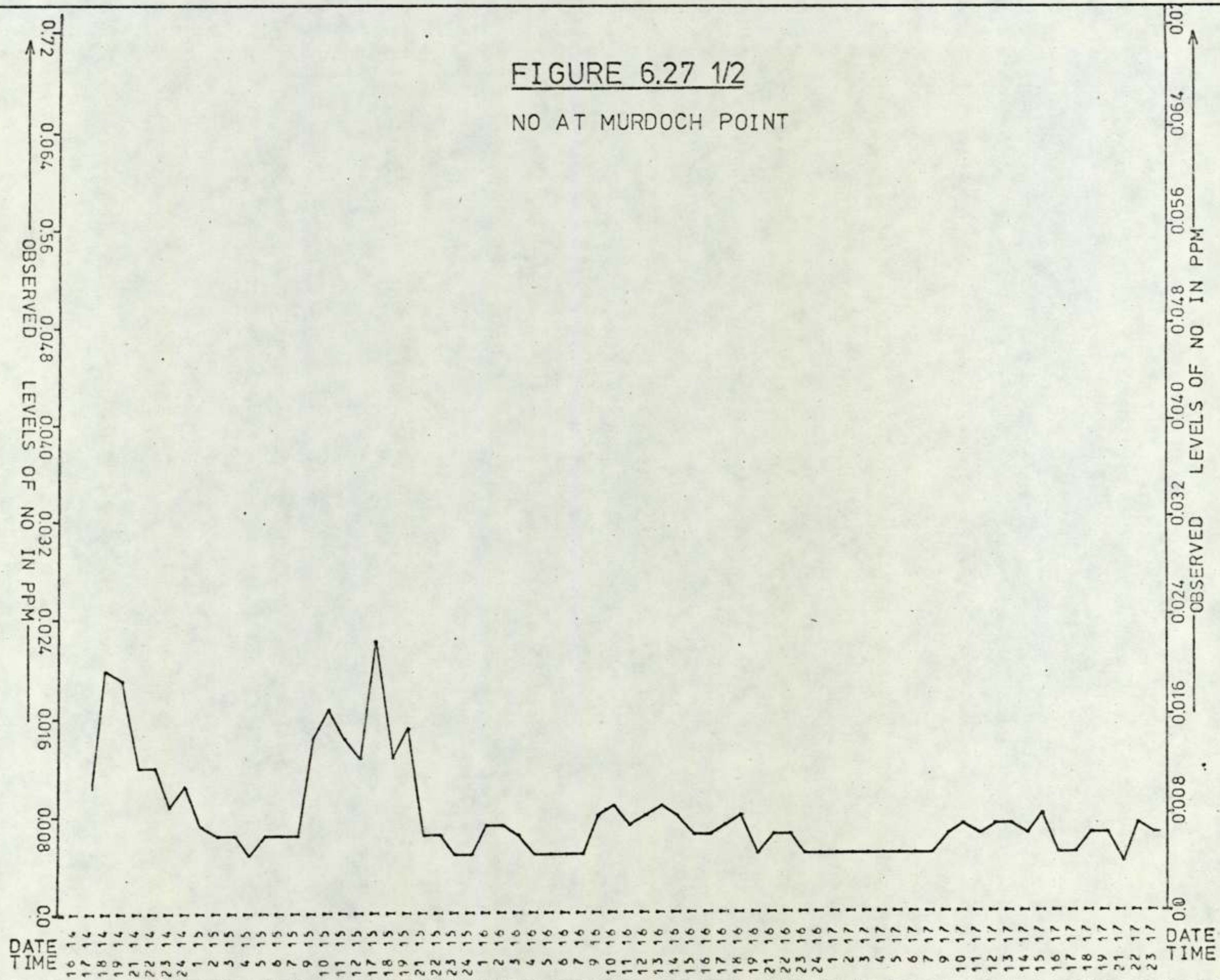

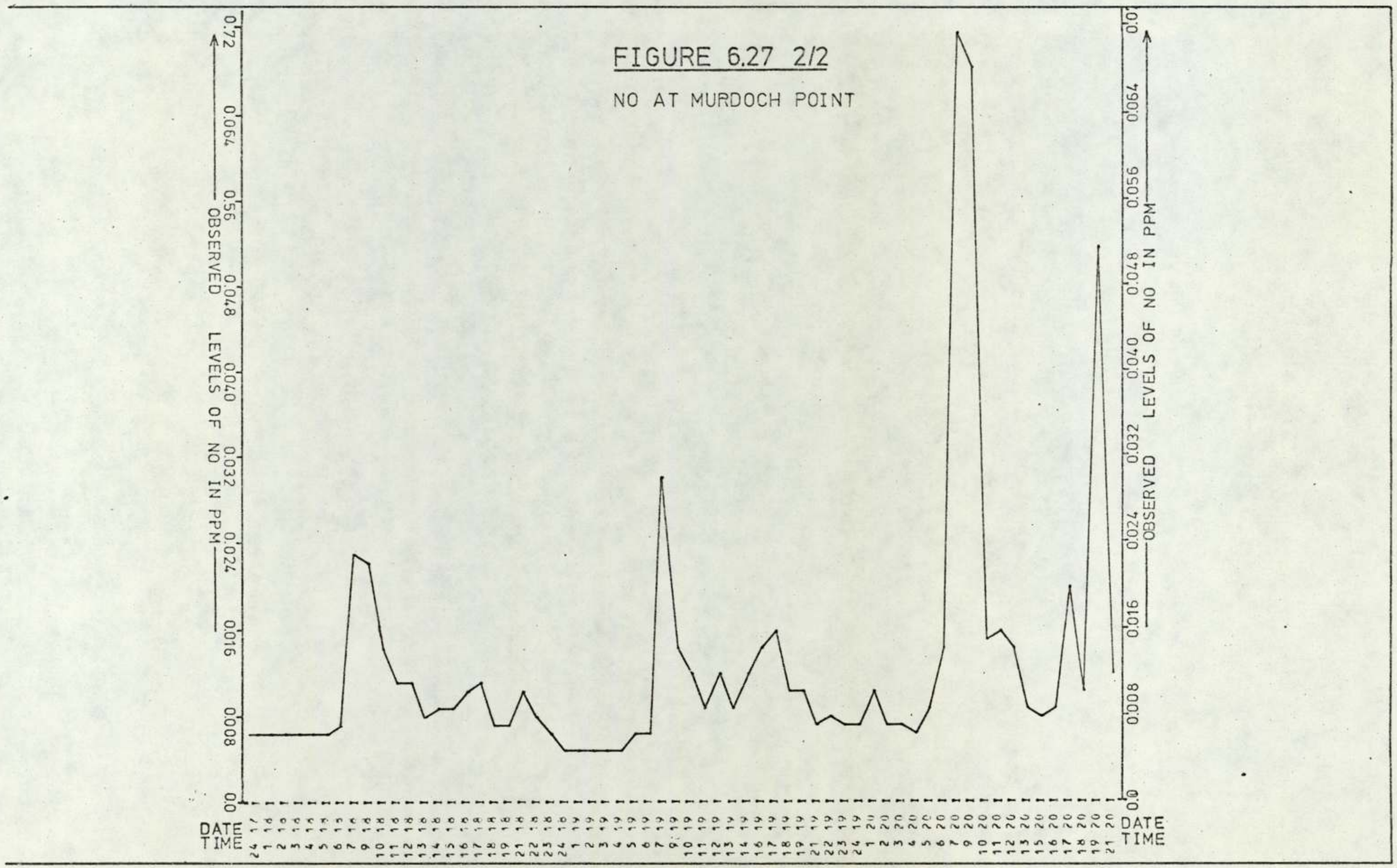
FIGURE 6.27 2/2
NO AT MURDOCH POINT
OBSERVED LEVELS OF NO IN PPM
DATE
TIME

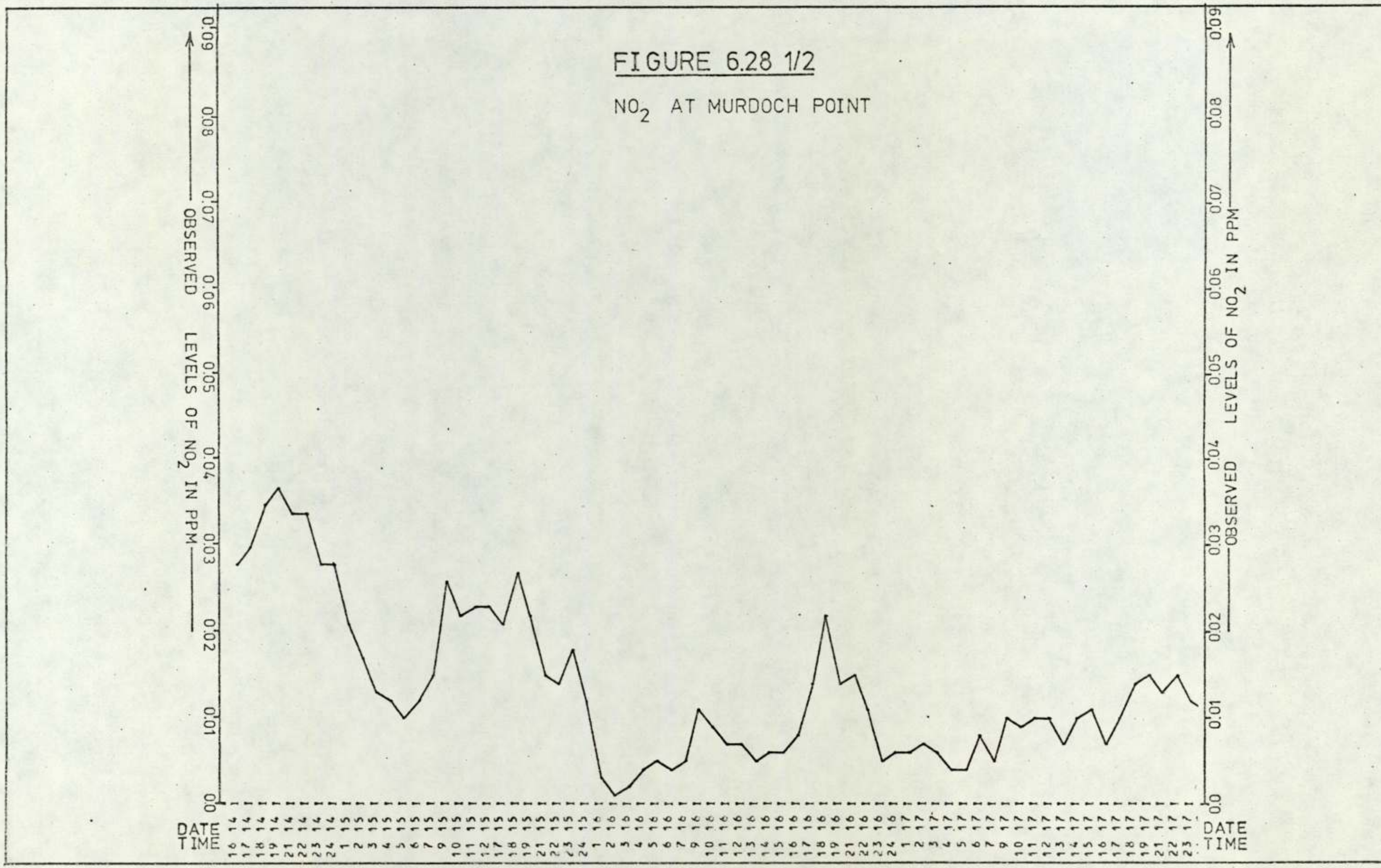

FIGURE 6.28 1/2

NO_2 AT MURDOCH POINT

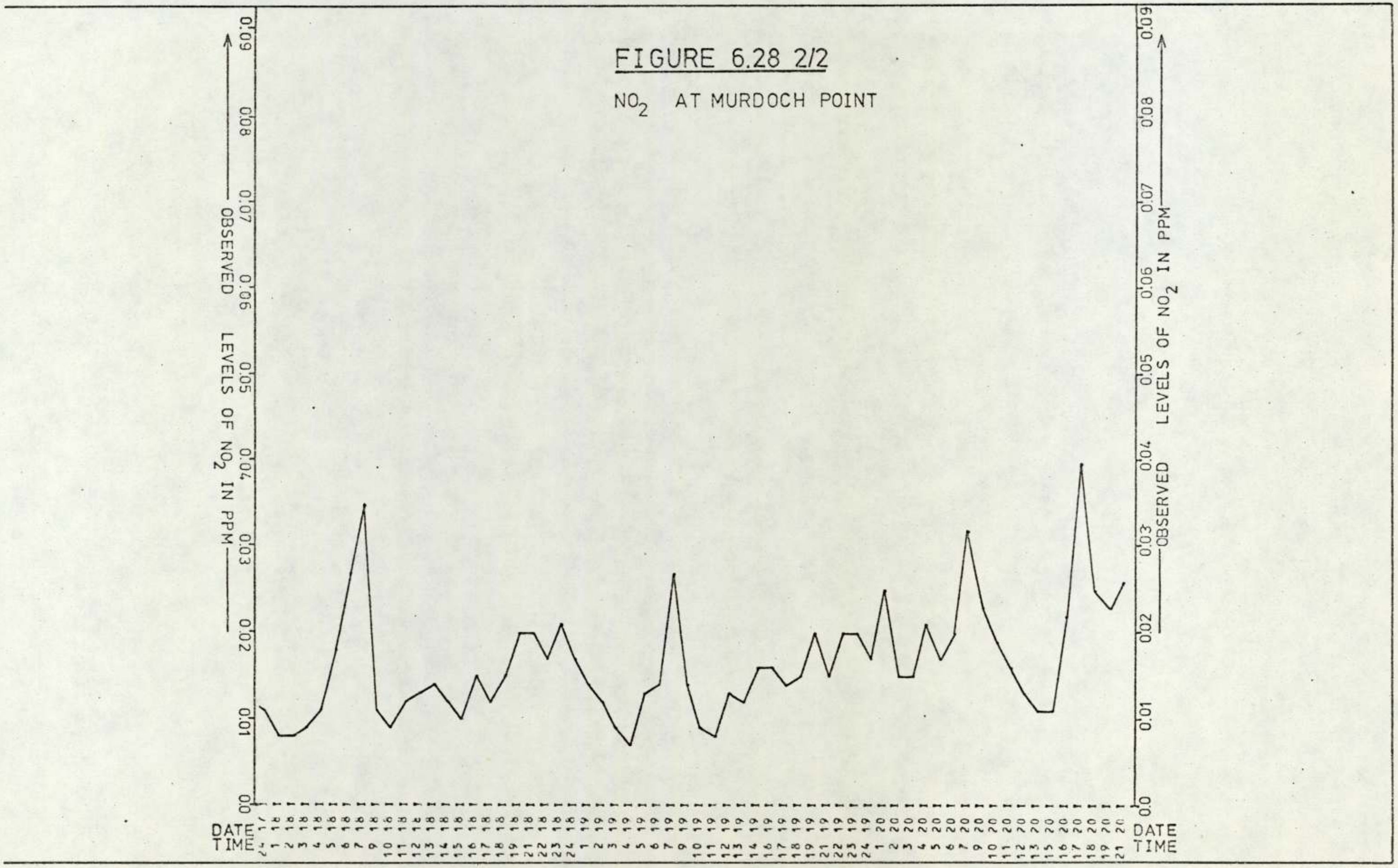

FIGURE 6.28 2/2

NO_2 AT MURDOCH POINT

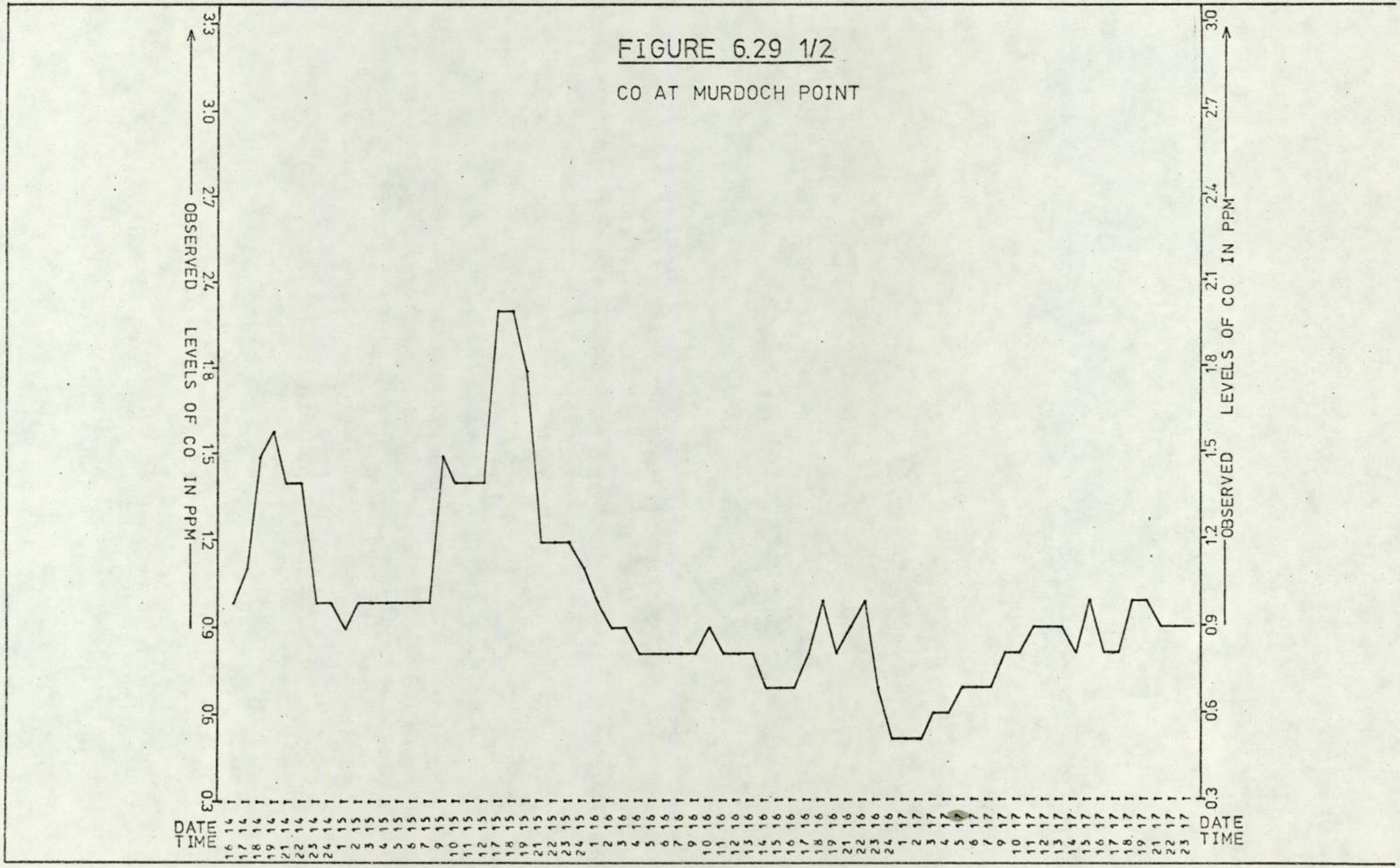

FIGURE 6.29 1/2

CO AT MURDOCH POINT

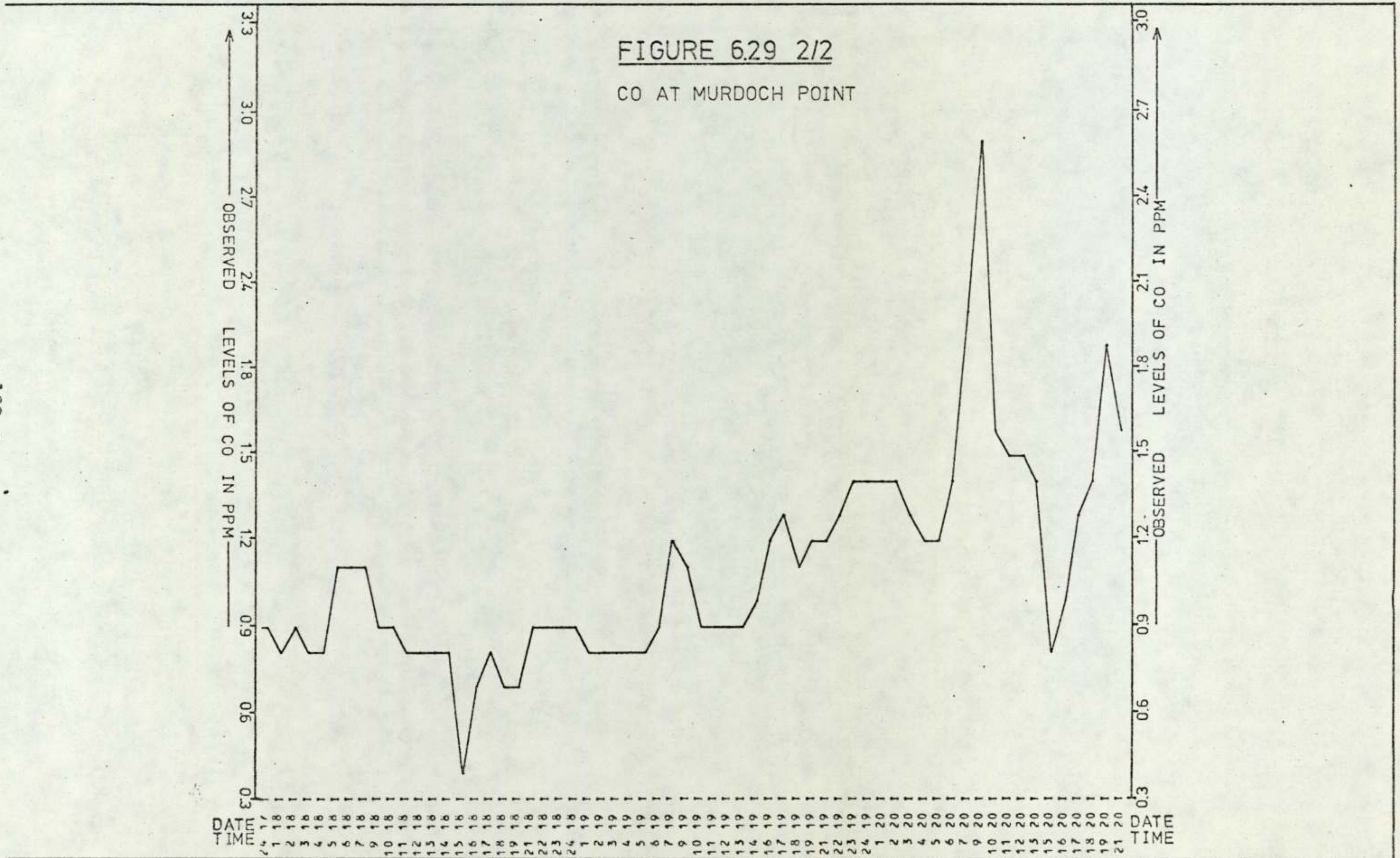

FIGURE 6.29 2/2

CO AT MURDOCH POINT

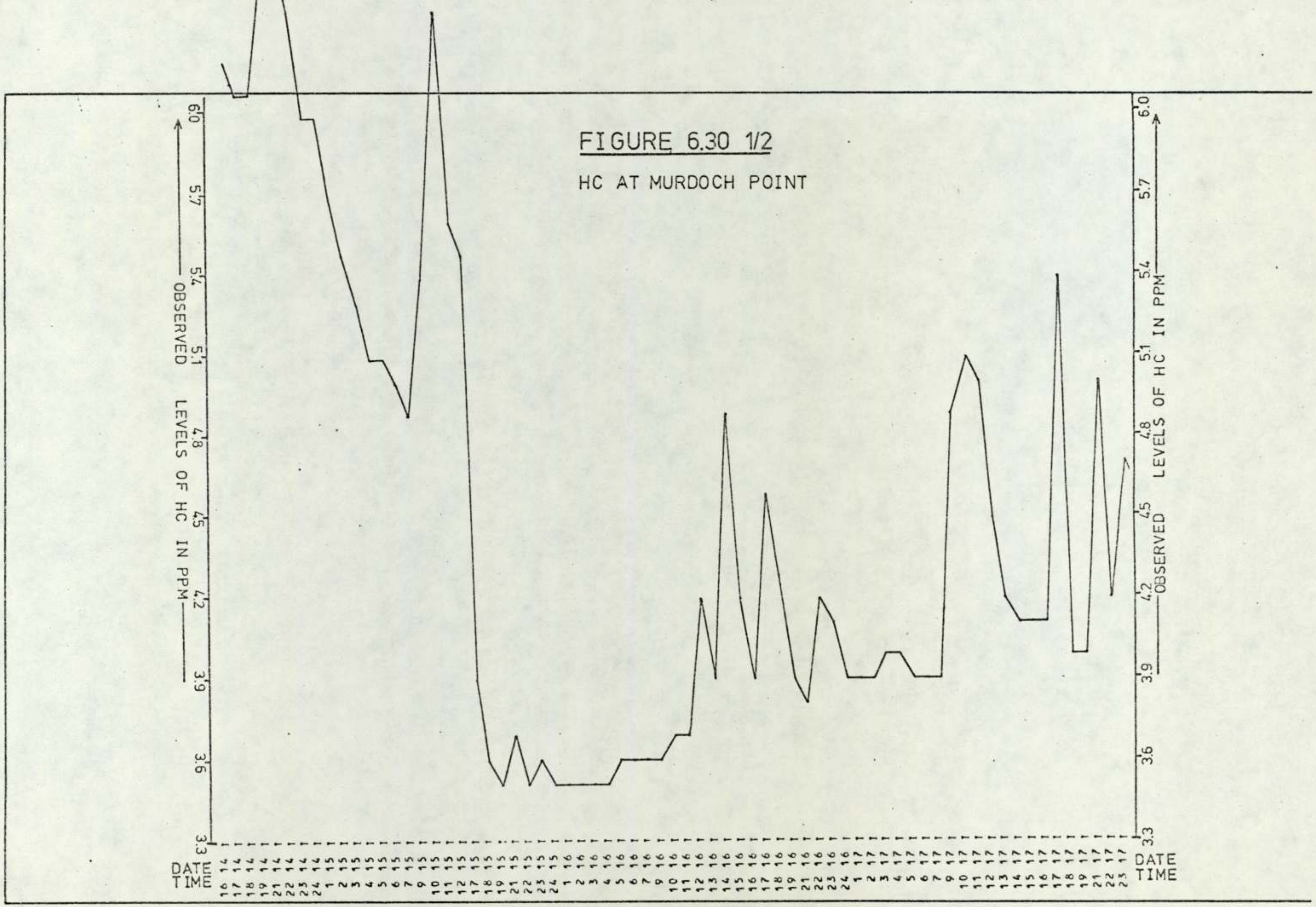

FIGURE 6.30 1/2

HC AT MURDOCH POINT

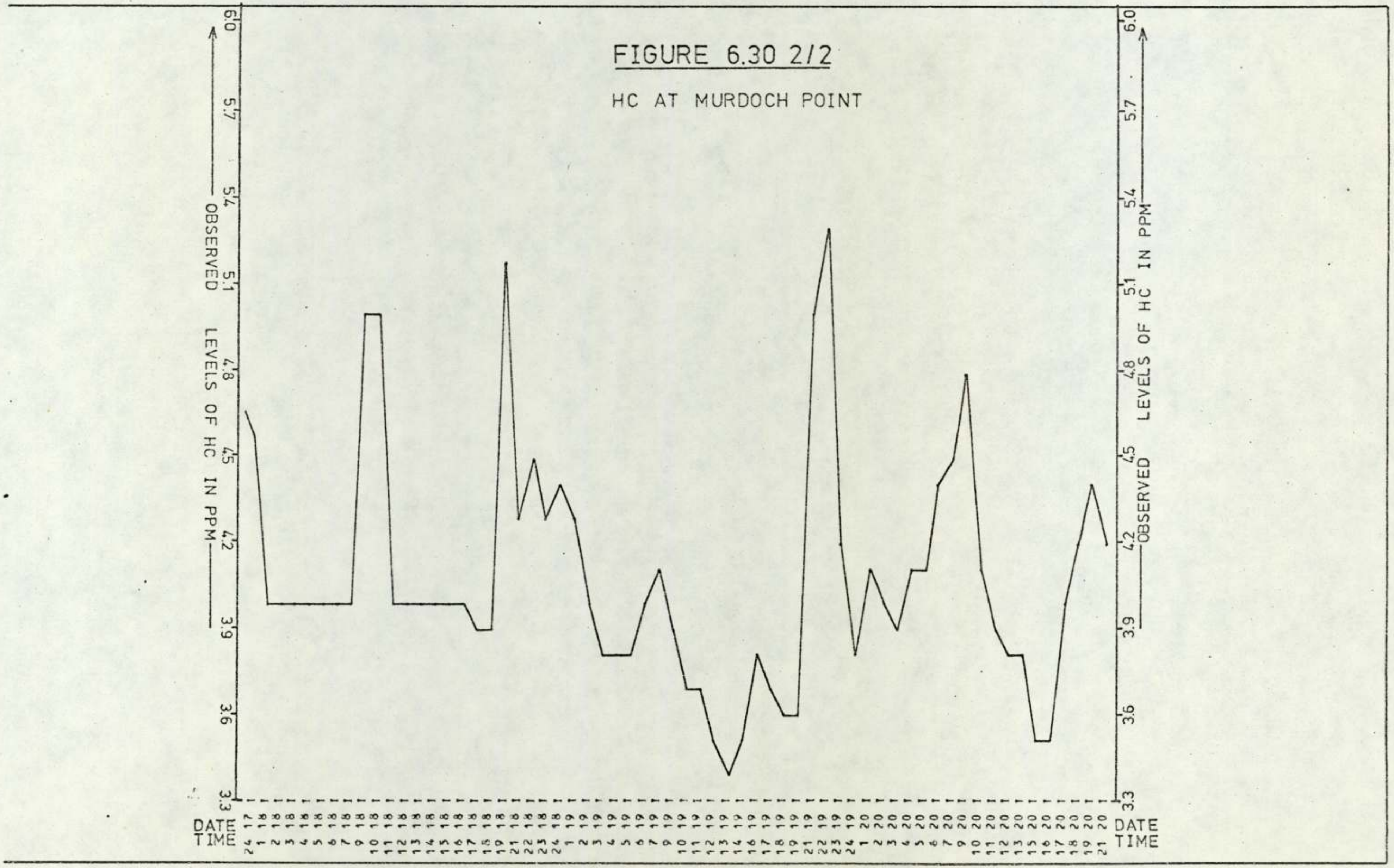

FIGURE 6.30 2/2

HC AT MURDOCH POINT

FIGURE 6.31 ERRORS IMPLICIT IN COMPARING THE CALCULATED WITH THE MEASURED CONCENTRATIONS OF POLLUTANTS.

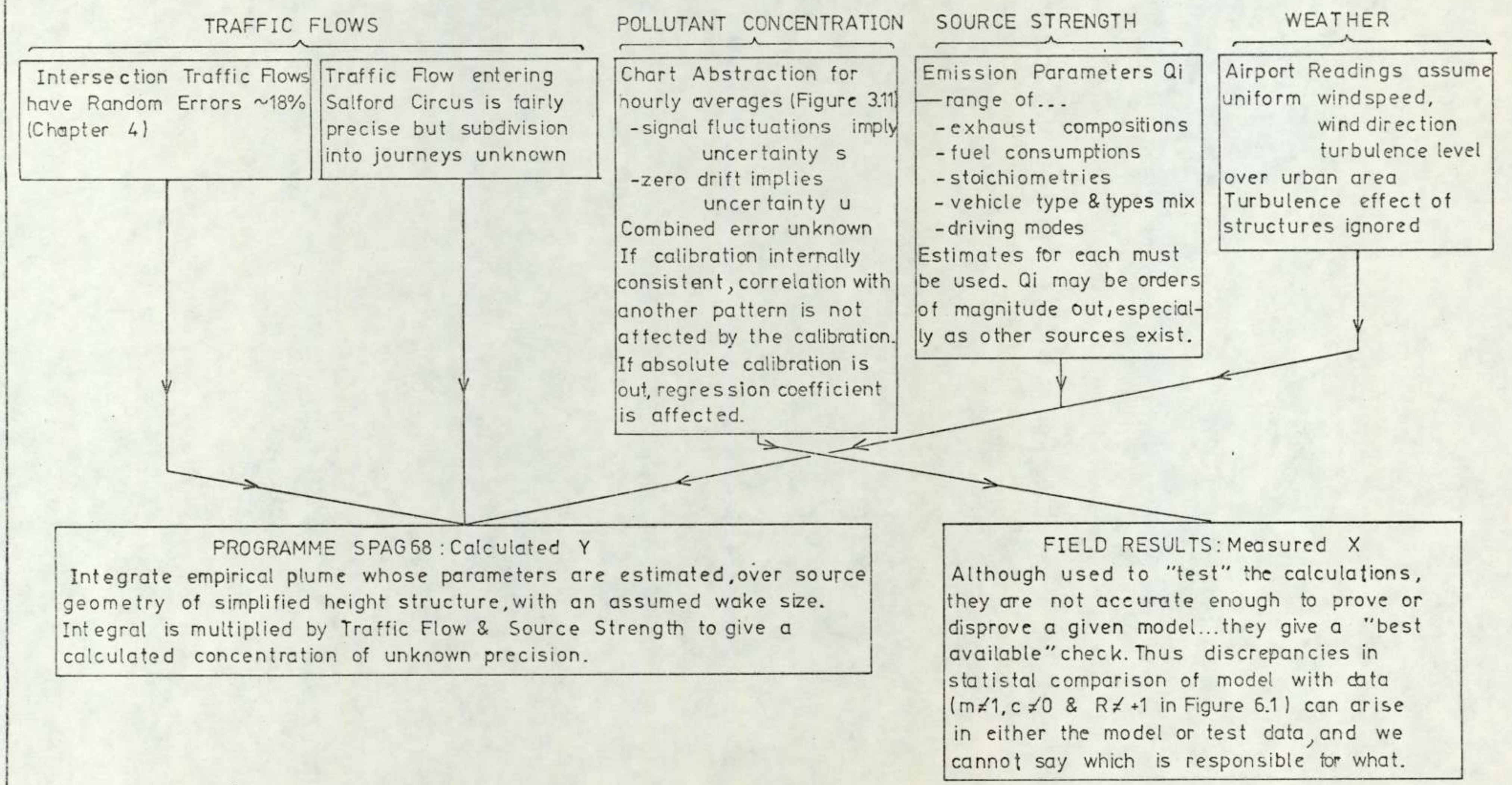

CHAPTER 7

INSTANTANEOUS CONCENTRATION GRADIENTS BY A TWO-TUBE SAMPLING TECHNIQUE

The present Chapter describes apparatus to measure gaseous pollutant concentrations at two locations simultaneously, using a single analyser. Instantaneous concentration gradients can be measured over a range of 56m and possibly more depending on equipment parameters. The design and system tests are followed by a collection of field results for NO reduced alongside a motorway and at the intersection. The field results are used to check dilution curves predicted by the programme (Chapter 6).

7.1 Principle of Technique

7.1.1 Main Features

The analyser operates in a two part cycle. First, an immediate air sample is analysed, while another separate sample is drawn into a long sample tube. This sample is delayed for the transit time of gas in the long tube before being analysed (Figure 7.1).

The long and short tubes are taken to opposite inlets of a rotary valve (Figure 7.2). The NO_x analyser and ballast pump are joined to the two outlets of the valve. Rotation of the valve generates two logic states:

In state 1 connections are 12A - ST and BP - LT

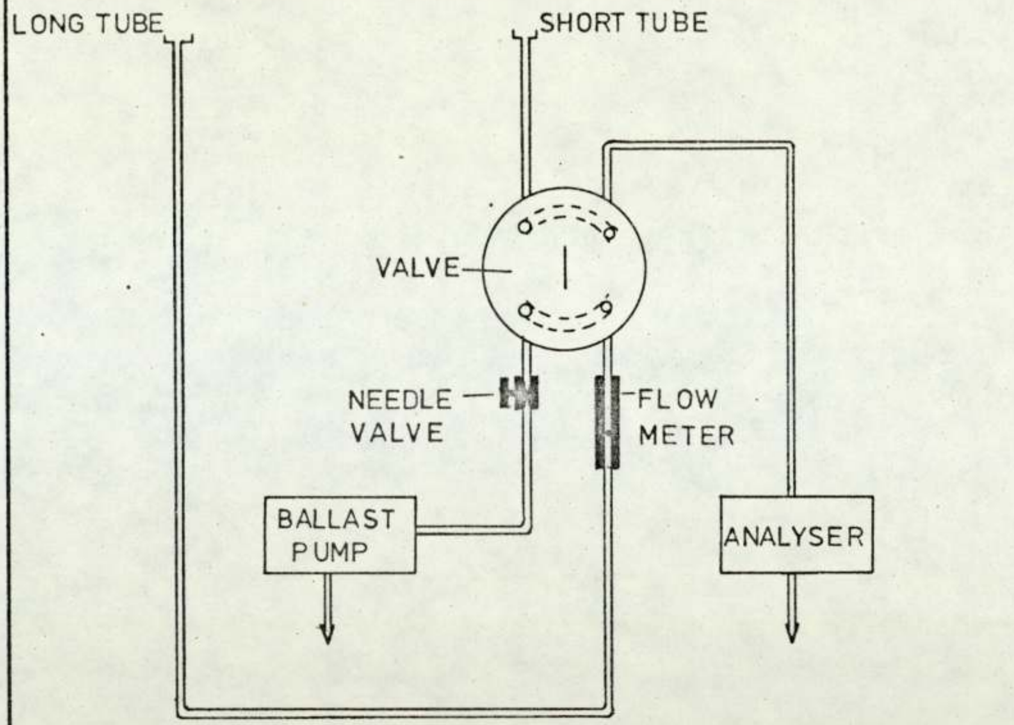

FIGURE 7.1 GENERAL SET UP OF VALVE AND TUBES

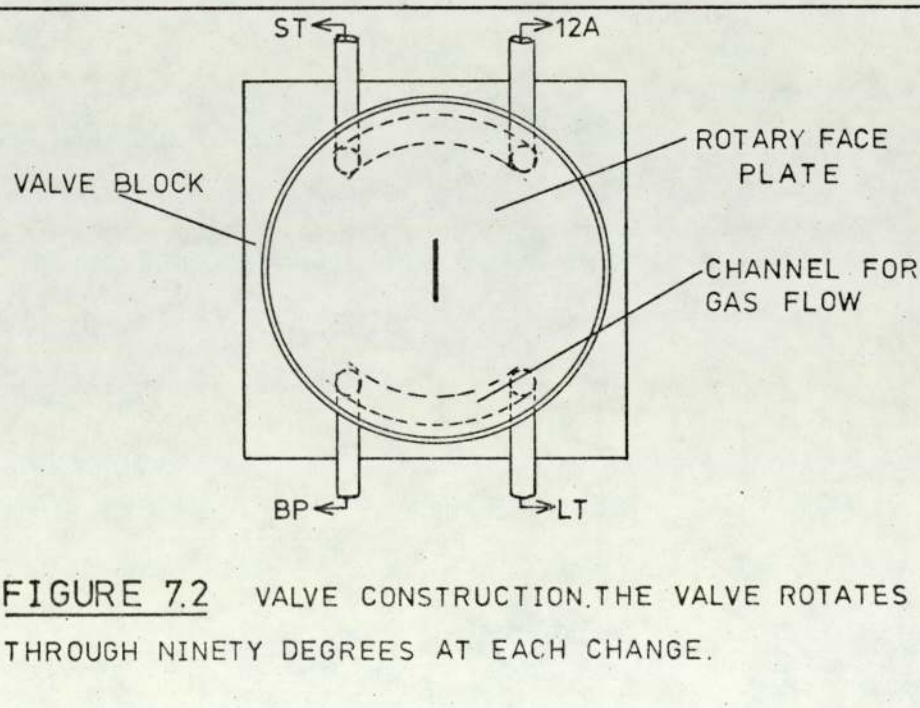

FIGURE 7.2 VALVE CONSTRUCTION.THE VALVE ROTATES THROUGH NINETY DEGREES AT EACH CHANGE.

In state 2 connections are 12A - LT and BP - ST where 12A, LT, ST and BP denote Thermo-Electron Model 12A NO_x Analyser, Long Tube, Short Tube and Ballast Pump respectively. The cycle begins in state 1. A direct air sample is analysed and recorded by the red pen of a two pen chart recorder. At the same time a sample is drawn into the long tube. Then the valve changes. In state 2 the sample in the long tube from state 1 is analysed (Figure 7.3) and recorded by the green pen. These traces from states 1 and 2 are simultaneous analyses. The cycle repeats. Figure 7.4 gives a sample of the traces.

Concentration events sampled by both short and long tubes will remain equally spaced in linear distance and in time provided the linear gas velocities in each tube are identical. The tubes have equal cross-sections; equal volume flow is sufficient condition to have equivalent time scales in each state. Failure to meet this condition results in time scale expansion.

7.1.2 Theory of Time Scale Expansion

We define flow rates

STATE	CONNECTION	VOLUME FLOW	LINEAR VELOCITY
1	12A - ST	V_1	v_1
2	12A - LT	V_2	v_2
1	BP - LT	V_3	v_3
2	BP - ST	V_4	v_4

All the tubes have the same cross-section, so we define the distance

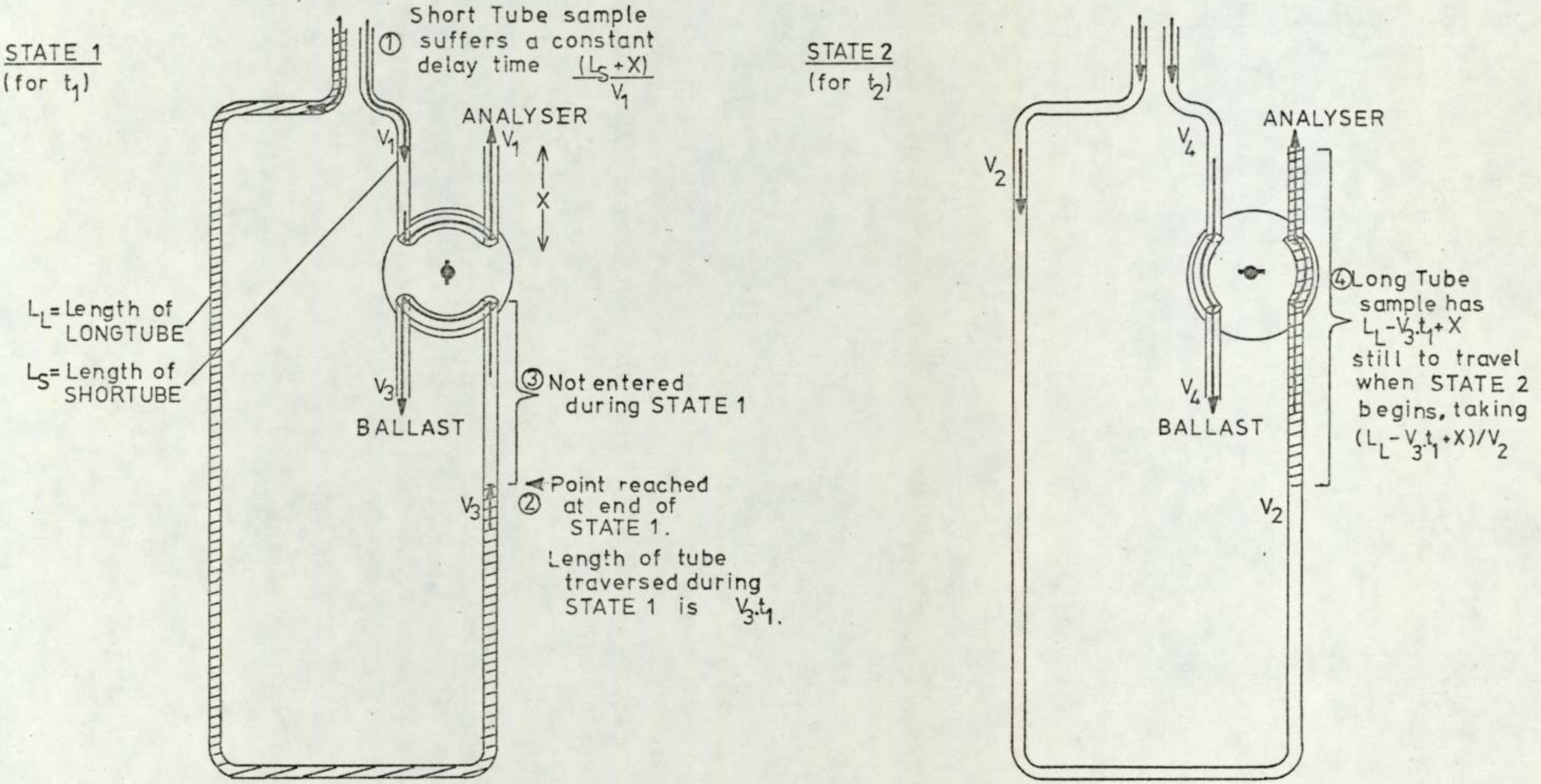

SHORT-TUBE DELAY = $(L_S + X)/V_1$

LONG-TUBE DELAY = $t_1 + (L_L - V_3.t_1 + X)/V_2$

FIGURE 7.3 FLOW SEQUENCES AND TIME DELAYS FOR A SAMPLE TAKEN INTO BOTH INLETS AT THE START OF A CYCLE. FOR A SAMPLE TAKEN AT TIME T, AFTER THE START OF THE CYCLE, $(t_1 - T)$ REPLACES t_1.

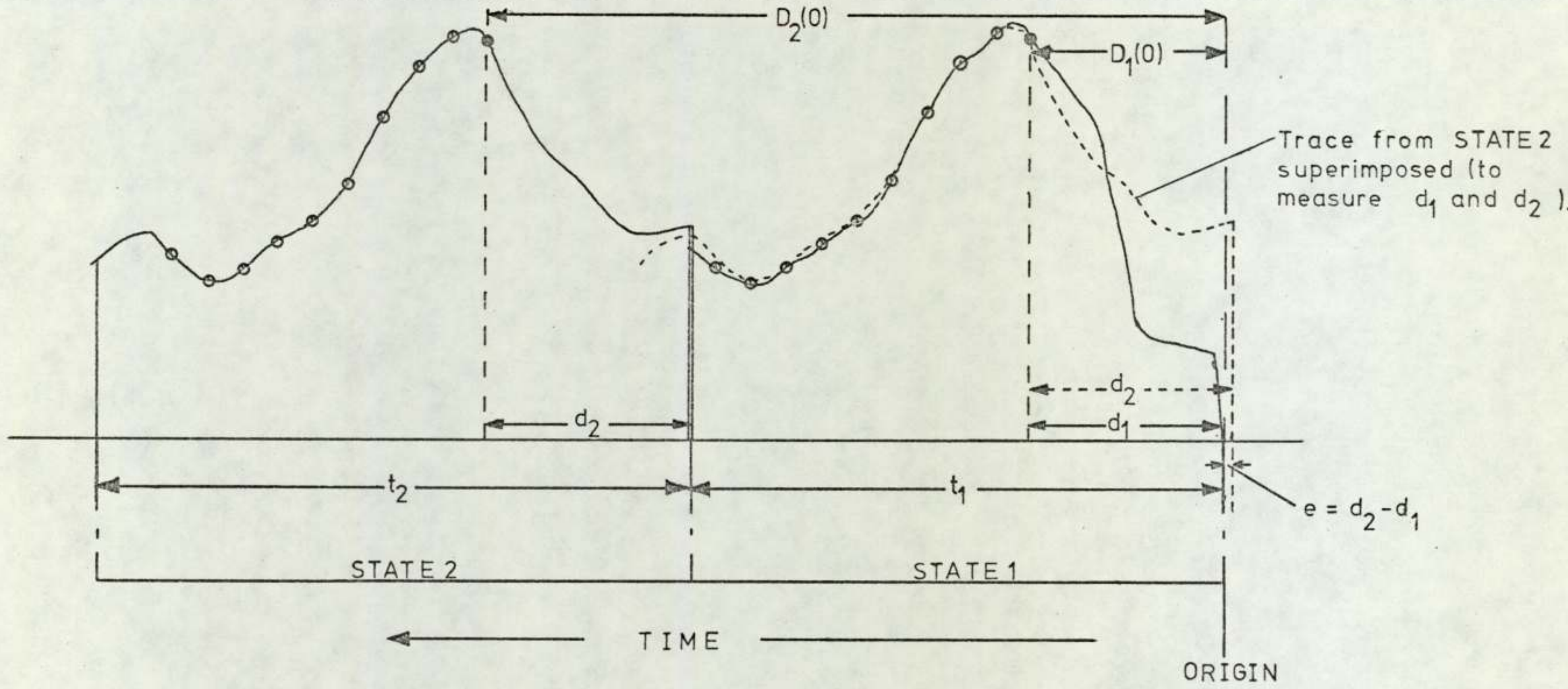

FIGURE 7.4 ILLUSTRATIVE CHART RECORD FOR A JOINED INLETS ANALYSIS TO SHOW THE VARIOUS TIME INTERVALS(t_1 , t_2 , $D_1(0)$, $D_2(0)$, d_1 , d_2 , e).

travelled vt using time t and linear velocity v.

We define

t_1 = time in state 1)
) set by electronic timer
t_2 = time in state 2)

L_S = length of short tube from inlet to valve

L_L = length of long tube from inlet to valve

x = length of tube from valve to analyser

$D_1(T)$ = time at which an event sampled at time T is recorded in state 1.

$D_2(T)$ = time at which an event sampled at time T is recorded in state 2 (times measured from start of cycle).

From Figure 7.3 we see that

$$D_1(0) = (L_S + x)/v_1 \qquad \dots \quad (7.1)$$

$$D_2(0) = t_1 + (L_L - v_3 t_1 + x)/v_2 \qquad \dots \quad (7.2)$$

Consider two pollution events sampled by both inlets at time T after the cycle begins. The short tube analysis is recorded (Figure 7.3) at a time

$$D_1(T) = T + D_1(0) \qquad \dots \quad (7.3).$$

The time delay is constant, and equals $D_1(0)$.

For the long tube analysis, the event sampled at T has a time $(t_1 - T)$ to travel down the long tube at v_3 before the state changes. This leaves a distance $(L_L + x - v_3(t_1-T))$ to travel before analysis in state 2, taking a time $(L_L + x - v_3(t_1-T))/v_2$.

This event is recorded at the time $D_2(T)$. $D_2(T) = T + \text{Delay}$. $D_2(t) = T + (t_1-T) + (L_L + x - v_3(t_1-T))/v_2$. ... (7.4)

Events occurring at T = O and T = T are recorded in state 1 at times $D_1(O)$ and $D_1(T)$, with unchanged time separation $D_1(T) - D_1(O) = T$ (using Equations 7.1, 7.3).

The same events are recorded in state 2 at times $D_2(O)$ and $D_2(T)$ with a new time separation $D_2(T) - D_2(O) = (v_3/v_2)T$ (using Equations 7.2, 7.4).

The long tube contains a rotameter flow-meter. The ballast pump is connected through a needle valve which is adjusted until the flow-meter gives equal readings in each state. Then $V_2 = V_3$, so that $v_2 = v_3$ and no time scale expansion is present.

7.1.3 Condition for Coincident Sampling: Chart Abstraction

A concentration event occurs at time T after the cycle begins. It will be recorded during

state 1 if $0 < D_1(T) < t_1$ ... (7.5)

and during

state 2 if $t1 < D_2(T) < t_1 + t_2$ ... (7.6).

If both conditions 7.5, 7.6 are met then the event is recorded in both states.

An observer wishing to abstract the chart must know where on the chart these conditions are met (Figure 7.4). Assuming that $v_2 = v_3$

we have from 7.5

$$0 < T + (L_s + x)/v_1 < t_1 \qquad \dots \quad (7.7)$$

and from 7.6

$$0 < \frac{(L_L + x)}{v_2} - t_1 + T < t_2 \qquad \dots \quad (7.8)$$

Now $D_1(0)$ and $D_2(0)$ are measured from the origin. Thus

$$D_2(0) = d_2 + t_1 = d_1 + e + t_1 \quad \therefore \quad e = D_2(0) - t_1 - d_1$$

also, $d_1 = D_1(0)$ from Figure 7.4,

$$e = D_2(0) - D_1(0) - t_1$$

$$e = t_1(\chi - \frac{v_3}{v_2} - \chi) + \frac{L_L + x}{v_2} - \frac{L_s + x}{v_1}$$

For the two traces to be exactly coincident, e = o so that $d_1 = d_2$: abstraction begins at the same point along each state trace if

$$\frac{+v_3 t_1}{v_2} = \frac{L_L + x}{v_2} - \frac{L_s + x}{v_1}$$

or $\quad t_1 = \frac{v_2}{v_3} (\frac{L_L + x}{v_2} - \frac{L_s + x}{v_1})$

A useful rule for setting-up follows from this: for $v_3 = v_2$ and $v_2 \sim v_1$, the electronic timer period t_1 (in state 1) should be

$t_1 \sim$ Long Tube flow time - Short Tube flow time.

The earliest sample occurs at T subject to the left hand conditions of inequalities 7.7, 7.8 and the latest sample is at T subject to the right hand sides. In the present work, full information was not available for 7.7 and 7.8 to be used to define initial and final values of T numerically.

7.1.4 Operation of the System

The needle valve was adjusted to set $v_2 = v_3$ (Section 7.1.2). The electronic timer was set so that e was as near zero as possible (Section 7.1.3), with

$t_1 \sim$ long tube delay - short tube delay.

Joined inlets traces were then recorded, and traced as in Figure 7.4 to derive empirical values of d_1, d_2 for the system as set. Inlets were then separated to measure concentration gradients. Using d_1, d_2, equally spaced intercepts were abstracted and averaged.

7.2 Construction

7.2.1 Circuit of Timer Unit

The circuit (Figures 7.5, 7.6 and Table 7.1) was designed to provide a square wave of continuously variable period with positive pulses at each change of logic state. The square wave half cycles (states 1 and 2) control a pen relay which selects the appropriate chart recorder pen. The pulses are needed to drive the servocoil which controls the valve. A novel circuit creates these pulses using a full wave rectifier and an operational amplifier. The operational amplifier IC1 is wired as a multivibrator, of period t_E

$$t_E = 2R_5C_1 \text{ loge } (1 + 2\, R_A/R_B)$$

where the time constant $R_5C_1 \sim 50$ secs, and $R_A = R_3 + VR1$, $R_B = R_4 + VR2$, $R3 = R4 = 22K\Omega$, and $VR1 = VR2 = 0 - 2M\Omega$.

The multivibrator output (24 volts peak to peak) drives

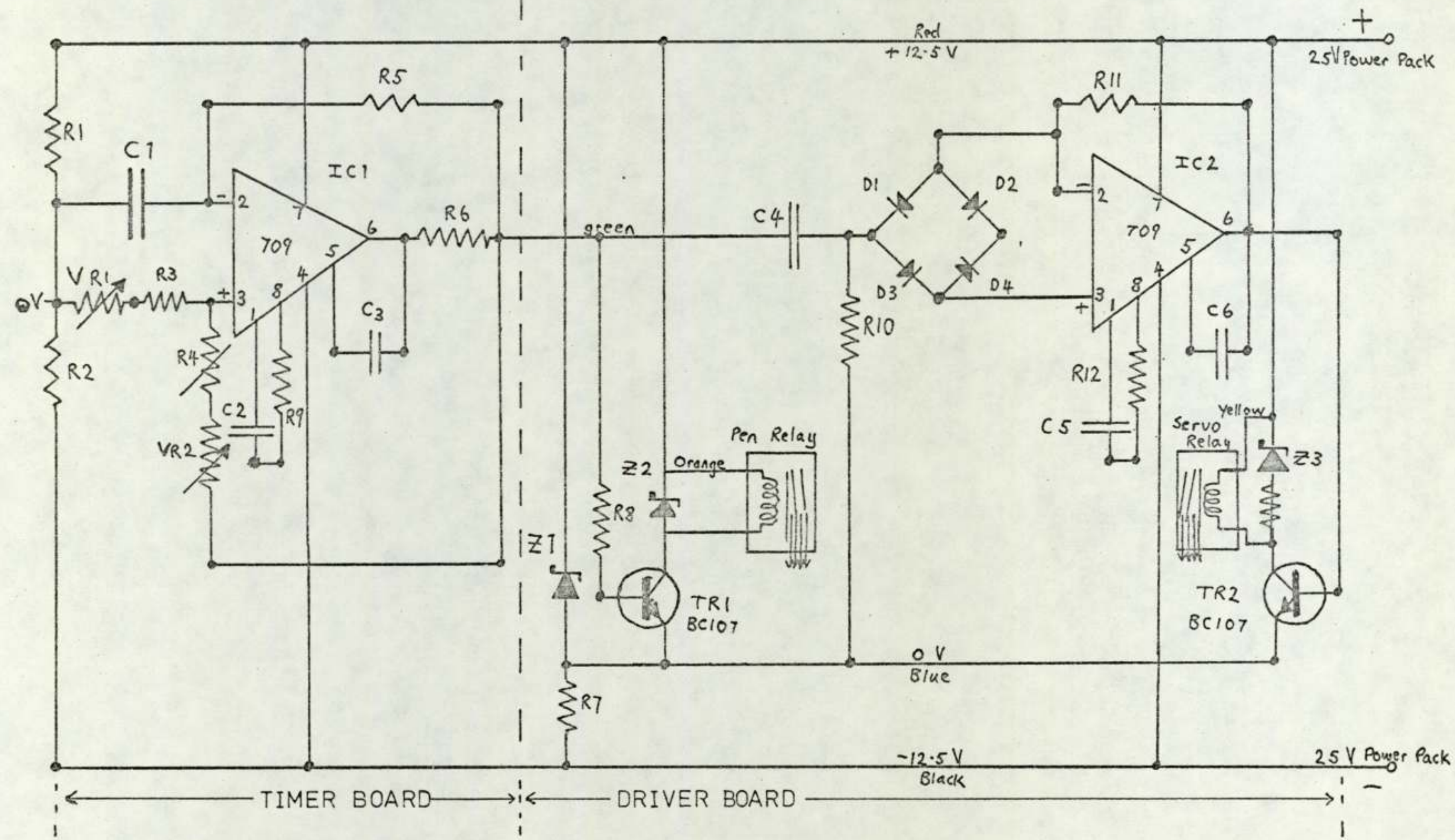

FIGURE 7.5 CIRCUIT FOR THE TIMER TO CONTROL VALVE AND PENS.

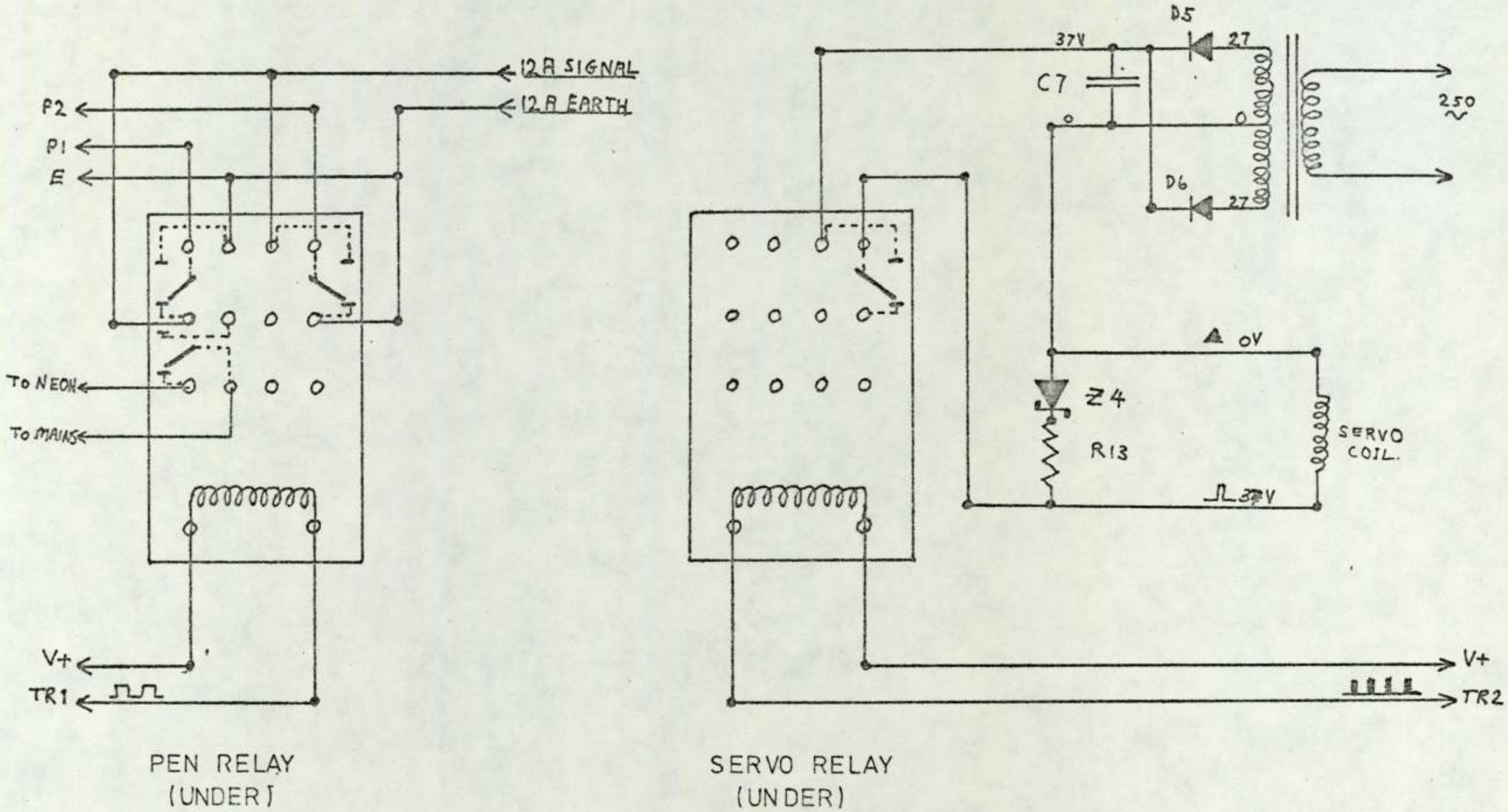

FIGURE 7.6 CONNECTIONS TO RELAYS IN TIMER.

TABLE 7.1

Components

IC1, IC2	SN72709		
TR1, TR2	BC107		
R1	3.3K Ω	C1	1000 μF, 25 UDC
R2	3.3K Ω	C2	100 pF polystyrene
R3	22K Ω	C3	3.3 pf
R4	22K Ω	C4	2 μF polystyrene
R5	330K Ω	C5	100 pF polystyrene
R6	51 Ω	C6	1000 pF polystyrene
R7	1.2K Ω	C7	1000 μF electrolytic
R8	15K Ω		
R9	1.5K Ω		
R10	120K Ω	D1)	
R11	1M Ω	D2)	Signal diodes, 15 PlV
R12	1.5K Ω	D3)	
R13	750 Ω	D4)	
VR1	2M Ω , log	D5	50 PlV, 1A
VR2	2M Ω , log	D6	50 PlV, 1A
		Z1	12V, 1 watt
Relays : GEC/MK		Z2	30V, 400 mw
M1492		Z3	30V, 400 mw
24V, 670		Z4	30V, 400 mw

transistor TR1 as a switch. TR1 controls the pen relay. Also, the multivibrator is differentiated by C4 and R10 (time constant C4.R10 $\sim$ 0.2 s) giving alternate positive and negative pulses at each state change. These pulses are relative to the OV rail. IC2 is used as a differential amplifier to amplify pulses occurring across the full wave rectifier (D1, D2, D3, D4). Positive pulses enter the non-inverting input, negative pulses the inverting input. The output is always a positive pulse and is used to drive transistor TR2 as switch. TR2 controls power through the relay from a 37V D.C. supply to the valve servocoil, (resistance 450 Ω) as in Figure 7.5. The combination of full wave rectifier and operational amplifier exploits the two inputs to prevent loss of pulses of one polarity to the negative rail as would occur with a single input amplifier. A feedback resistance (R11; 1MΩ) prevents IC2 acting as a Schmitt trigger. Inductive kicks on all coils are filtered by zenner diodes (Z2, Z3) thus avoiding transistor damage and preventing oscillatory feedback to IC2. A neon bulb wired to the mains through the pen relay is useful to check that the pens and valve keep in phase.

7.2.2 Valve and Servo

The valve face plate seats on the lapped surface of the brass valve body. The face plate is grooved to connect adjacent gas inlets in pairs (Figures 7.2, 7.7, 7.8). The flotation springs provide axial load to seat the face plate at all seating angles. The shaft peg carries the torque through to the face plate without disturbing the seating. This arrangement improves the gas seal over the valve surface. The photograph (Figure 7.8) shows how the weight on the string tends to

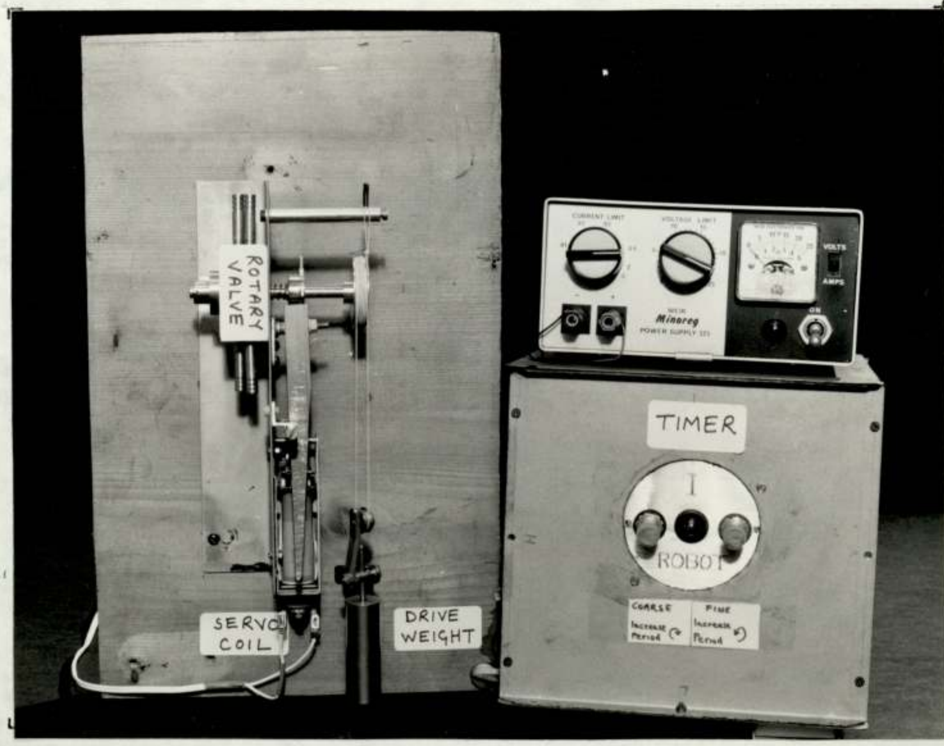

FIGURE 7.7 GENERAL VIEW OF THE TWO TUBES APPARATUS, WITH THE VALVE MECHANISM ON THE LEFT AND CONTROL ELECTRONICS ON THE RIGHT.

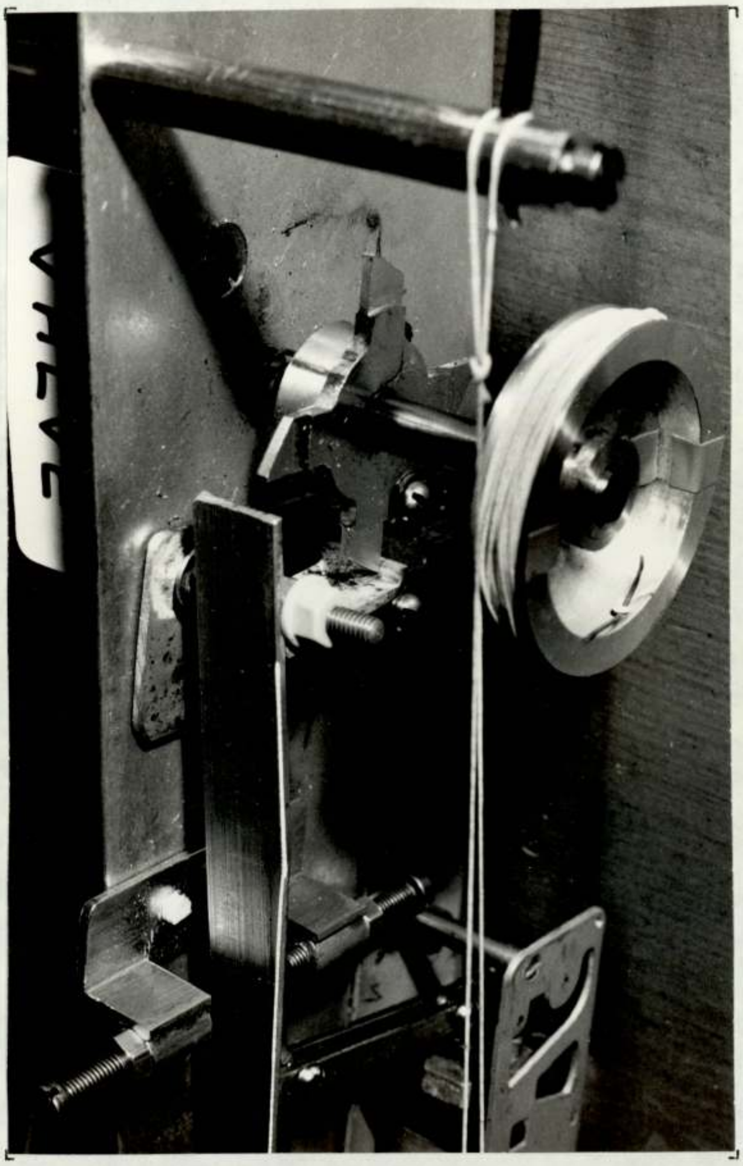

FIGURE 7.8 VALVE SERVO ASSEMBLY. THE WEIGHTED STRING GIVES TORQUE TO THE VALVE SHAFT, WHICH CAN ONLY ROTATE WHEN THE SOLENOID IS ENERGISED TO RELEAS THE SERVO. THE VALVE ROTATES NINETY DEGREES WITH EACH PULSE.

rotate the valve. When a voltage pulse is applied the solenoid moves the servo arm. The valve rotates through ninety degrees as the hook is released and caught again at the end of the pulse.

7.3 Laboratory Tests

7.3.1 The Valve

The flow system was set up to sample laboratory air, with the connections to the valve as in Figure 7.1. The electronic timer was not used, and the I2A was connected direct to the chart recorder. The I2A set to full scale deflection of 100ppm gave an insignificant reading on laboratory air. A source of 100ppm NO in N_2 was connected to the short tube. The valve was rotated into each position by hand. Any significant reading on the I2A when connected to the long tube would have been due to cross leaks but in fact no leak was observed.

The procedure was repeated with the air and NO inlets reversed, and no leak from the long tube to the short tube was seen. Leaks were obtained only when excessive NO/N_2 pressure was applied or an inlet was sealed. In the normal mode with both sides of the valve passing comparable flows of gas the leaks were insignificant.

7.3.2 Tube Flow Dynamics

The long tube finally used was a fifty six metre length of 0.48 cm i-d Teflon, sleeved in PVC. The down tube transit time as measured by pulse injection of NO was ninety seconds. The flow was $\sim$ 0.7 $l\,min^{-1}$. The Reynolds number is therefore $3.4.10^4$ and the flow probably laminar (Monin and Yaglom, 1971j).

In the long tube, viscous effects cause a gradient of longitudinal velocity across the tube, with the fastest flow in the centre. The resulting longitudinal mixing mixes adjacent elements of gas as they pass down the tube.

With an infinitely long tube, a point injection of material is dispersed along the axial direction into a Gaussian concentration distribution (Monin and Yaglom, 1971k).

This dilution effect, or non ideal plug flow, smooths the changes in concentration.

Let the smoothing to have a time constant τ. Then τ is the time taken for pollutant concentration, with a step input, to rise to $1/e$ of its final value (Bair, 1962) With step height Sm, and signal S_t at time t,

for a rising signal $S_t/Sm = 1 - \exp(-t/\tau)$, and

for a falling signal $S_t/Sm = \exp(-t/\tau)$

Thus for the former $-\log_e (S_t/Sm - 1) = t/\tau$, and for the latter $-\log_e (S_t/Sm) = t/\tau$. The results from an injection of 100 ppm NO into the air stream of the long tube are plotted in Figure 7.9. For the rise, τ = 2.1s, and for the fall τ = 1.4s. The model 12A has a time constant of $\sim$ 1s, on the 0.25ppm scale. The long tube therefore was causing only a slight smoothing effect. The close fit of the finer structure between the long and short tube traces when

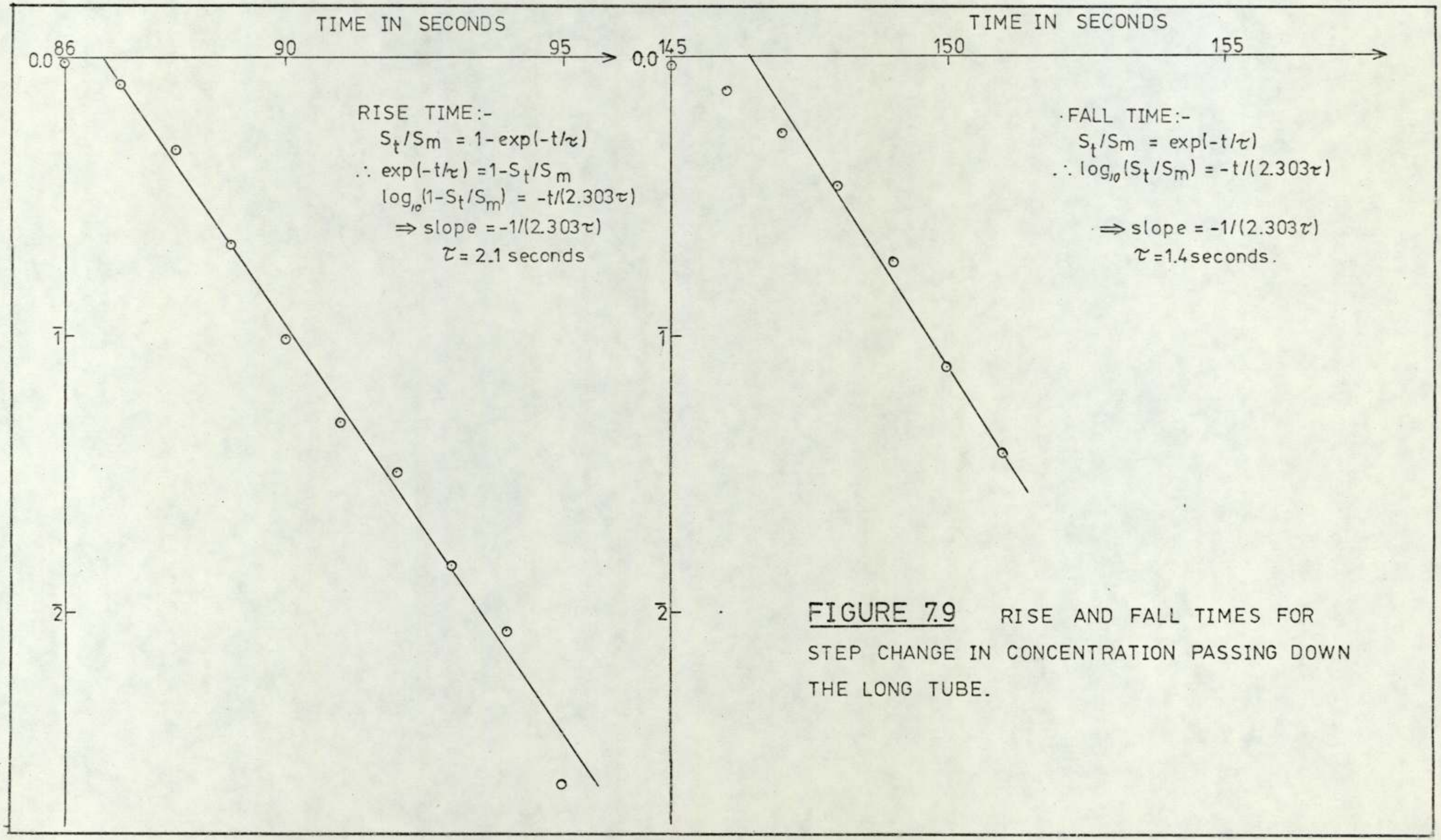

<u>FIGURE 7.9</u> RISE AND FALL TIMES FOR STEP CHANGE IN CONCENTRATION PASSING DOWN THE LONG TUBE.

sampling the same inlet, as in Figure 7.12, is typical of the results obtained.

7.3.3 Accuracy of the Long Tube Record

The equipment was run with the long and short tube inlets joined (Figure 7.10) at Y-(1). At Y-(2), ambient air entered when the cylinder supply of standard gas was closed. Pulses of pollutant were generated by briefly opening the cylinder: Y(2) kept the flow constant by allowing either excess pressure to escape or air to enter. An example pulse injection is shown in Figure 7.11; a comparison of long and short tube analyses for a common inlet of atmospheric air is shown in Figure 7.12. Table 7.2 gives a numerical comparison of analyses for three cycles: the means of the long and short tube analyses agree within three per cent. The superimposed traces also showed (Table 7.3) that the time error $e = d_2 - d_1$ was reasonably constant.

7.3.4 Summary of Testing

The long tube caused slight smoothing of the trace (two seconds for a ninety second flow-time down a fifty six metre tube). From superimposed tracings with joined inlets the time error e could be measured with good consistency ($\pm$ 1 second). Time scale expansion could be set to unity. Intercepts could therefore be read from each state and averaged: the means agreed to within three per cent.

The similarity of joined inlets results showed that the equipment

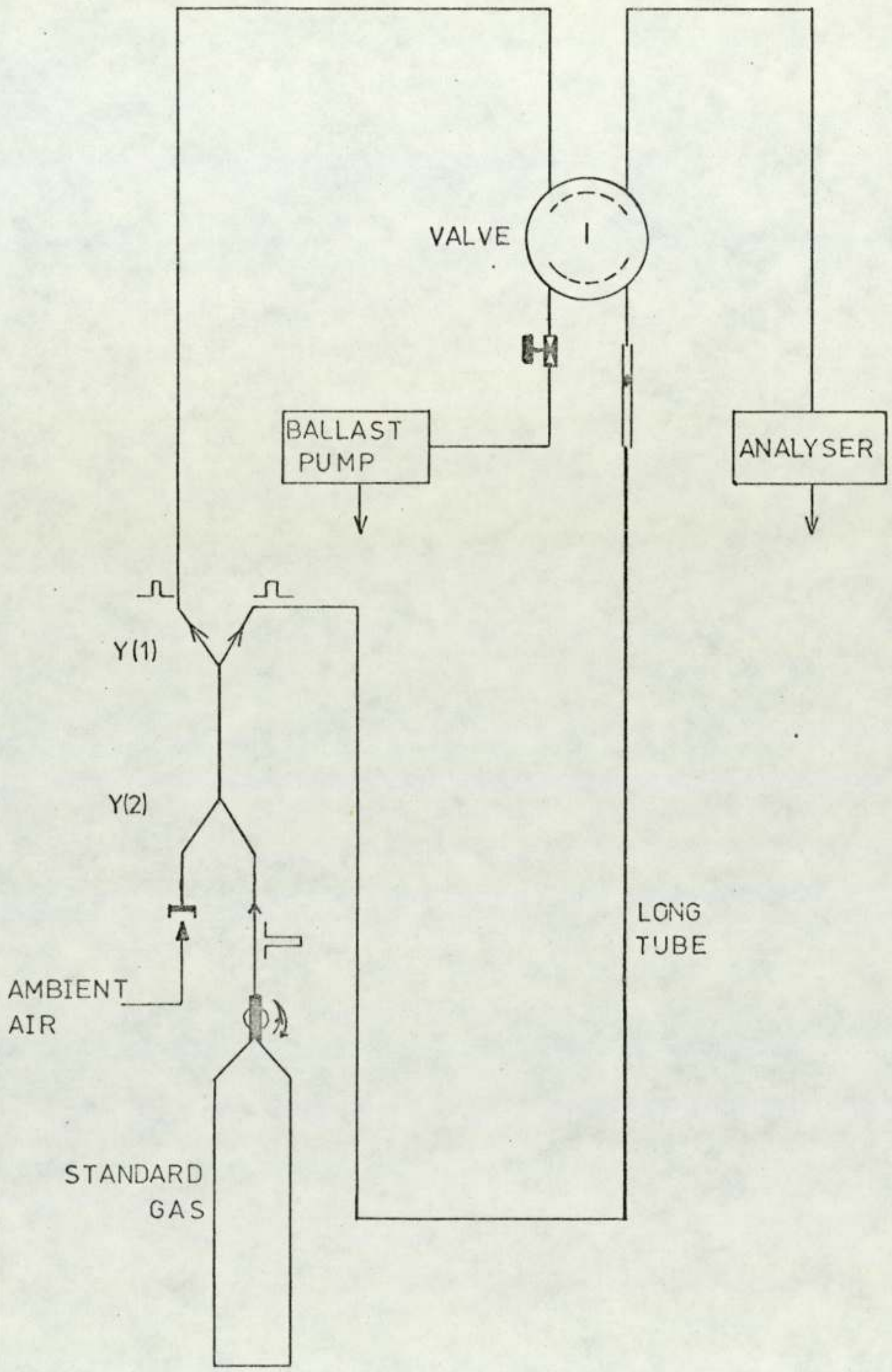

FIGURE 7.10 ARRANGEMENT OF INLETS FOR INJECTION OF IDENTICAL PULSES OF CONCENTRATION INTO BOTH TUBES AT THE SAME TIME. THE AMBIENT AIR INLET ACTS BOTH AS EXCESS PRESSURE RELEASE AND REFERENCE CONCENTRATION.

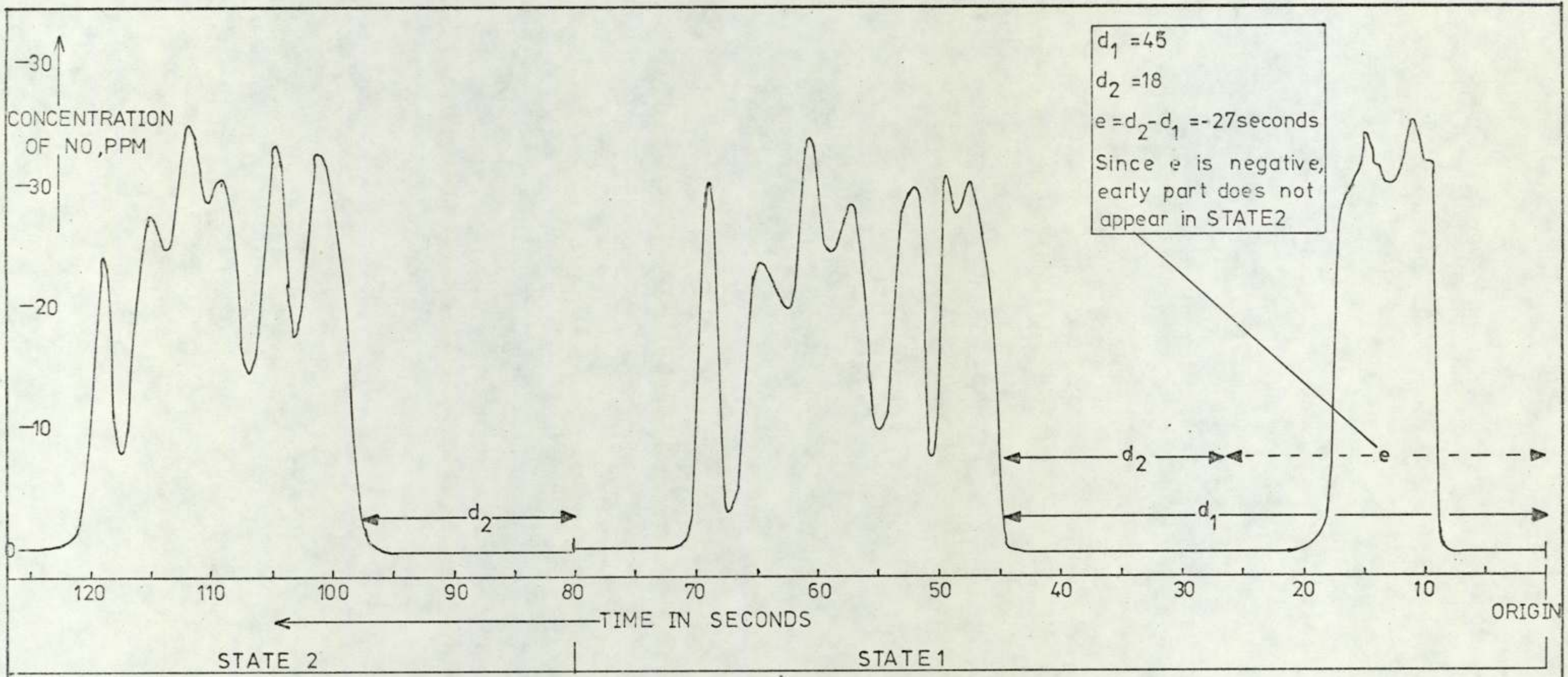

FIGURE 7.11 COMPARISON OF LONG AND SHORT TUBE ANALYSES OF CONCENTRATION PULSES GENERATED BY THE ARRANGEMENT SHOWN IN FIGURE 7.10.

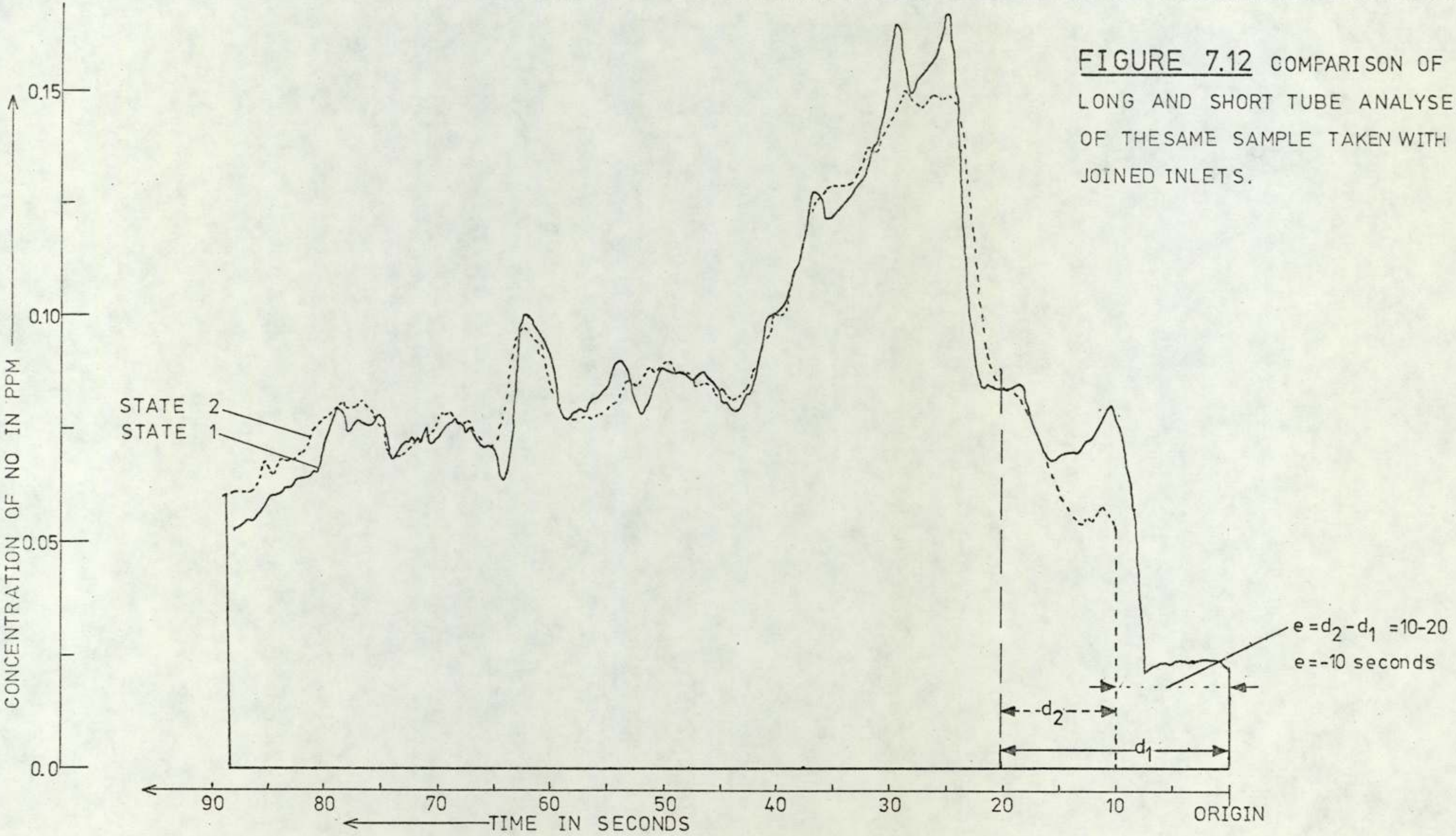

FIGURE 7.12 COMPARISON OF LONG AND SHORT TUBE ANALYSES OF THE SAME SAMPLE TAKEN WITH JOINED INLETS.

TABLE 7.2

Comparison of Long and Short Tube Traces

Cycle Number	Mean of 14 Intercepts, 5 seconds apart		Ratio
	Short Tube	Long Tube	
3	0.093212	0.090535	0.97
4	0.11750	0.11517	0.98
5	0.14125	0.14321	1.01

Source: 56m tube; 90 second flow time; ppm NO.

TABLE 7.3

Consistency of Time Error e (27-11-1974)

Cycle Number	Seconds		$e = d_2 - d_1$
	d_1	d_2	
5	17.5	12.5	5.0
6	15.0	10.0	5.0
7	14.0	9.0	5.0
8	14.0	9.0	4.5
9	14.5	10.0	4.5

as constructed could measure instantaneous analyses from two places using one pollutant analyser.

7.4 Application Beside M6 Motorway

7.4.1 Field Set-Up

The site was at the Perry Barr works entrance adjacent to the Police Motorway Control Centre. The Motorway runs through relatively open country at this point (Figure 7.13: Map). There are no other major roads nearby. The Bedford van containing the equipment was driven on to the grass by the sliproad; it was $\sim$ 25 metres from the Motorway. The site was not ideal: the sliproad passes under the Motorway here so an artificial valley and hill are present. The van was as far from the bridge as possible. When set up the Model J2A developed noise but since such experiments require special arrangement (e.g. with the police and for electricity) the run was made. The aim was to evaluate the application of the technique in the field.

The instrument noise (from a damp PM tube despite prior servicing) meant the joined inlets traces agreed to within $\pm$ fifteen percent; this is unusually large.

7.4.2 Results

Two positions of the long tube were used. For each cycle fifteen points were abstracted at five second intervals for both states. For each cycle, the averages of these are shown in Figure 7.14. The graph covers thirty cycles (each of 1.5 minutes) every three minutes: a total time of forty five minutes. The lower line is

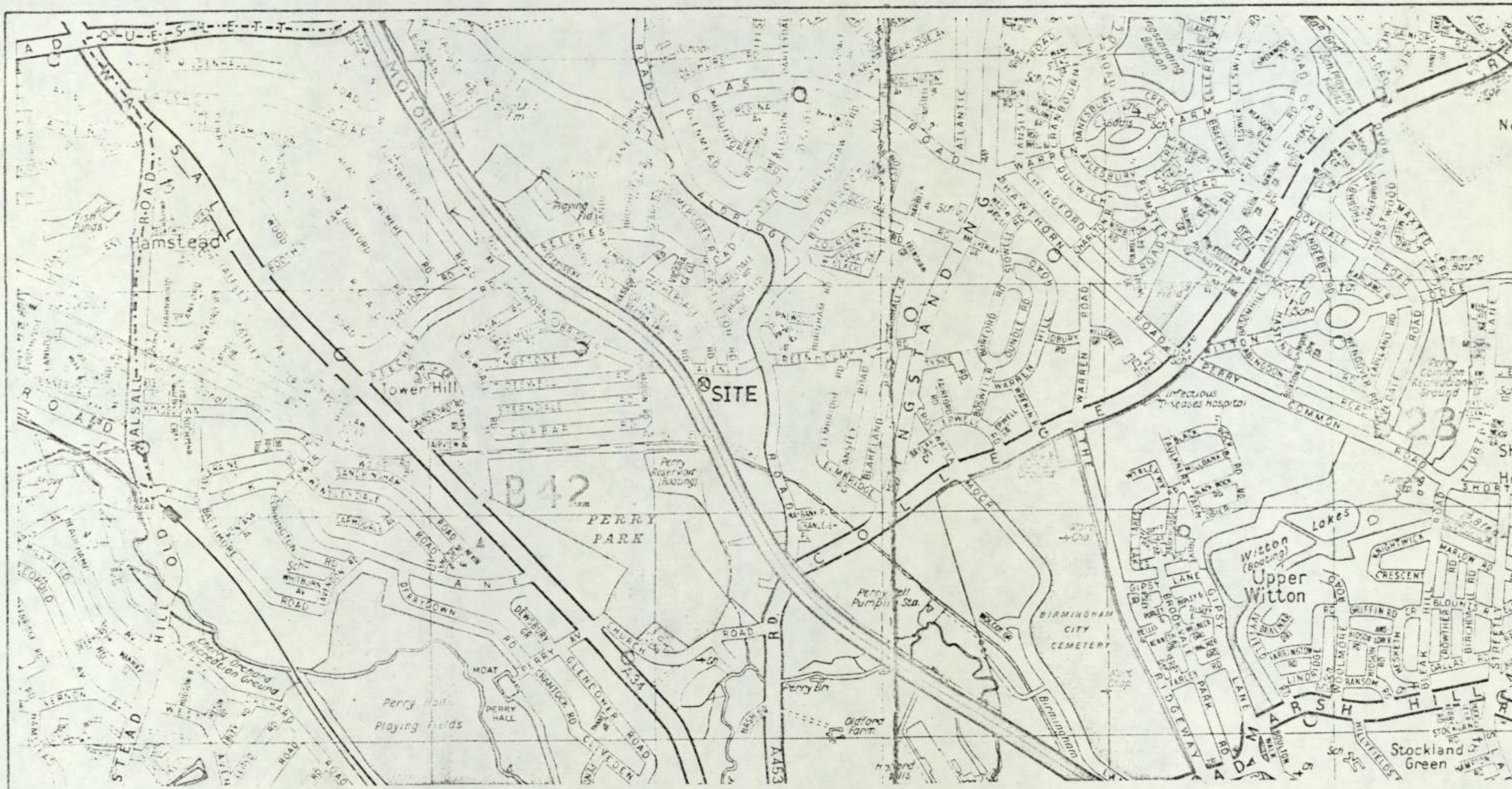

FIGURE 7.13 SITE OF THE TWO TUBES STUDY OF CONCENTRATION OF NO FROM M6 MOTORWAY.

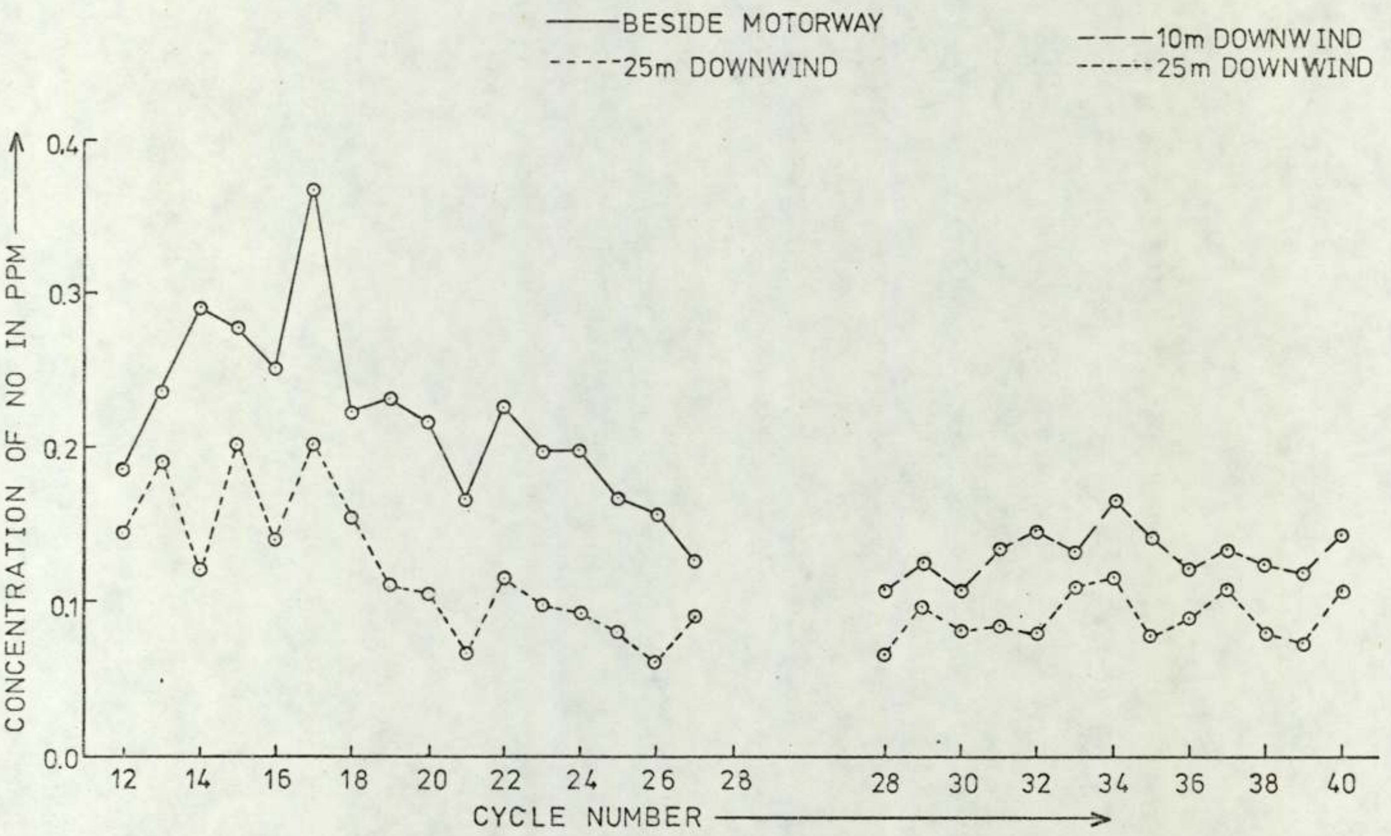

FIGURE 7.14 SIMULTANEOUS MEASUREMENTS OF NO CONCENTRATION AT TWO DISTANCES DOWNWIND FROM M6 MOTORWAY.

concentration for the short tube placed twenty five metres downwind; the upper, for the long tube at two positions.

The fluctuations in both the short-term concentration (averaging time $\sim$ 75 seconds) and the short-term concentration gradient (ratio of time coincident concentrations from two downwind positions) can be seen in Table 7.4, and Figures 7.15, 7.16. These changes are associated with fluctuations in traffic flow, wind-speed and atmospheric conditions.

7.4.3 Comparison With Theory

During the experiment the traffic-flow was 4,500 vehicles per hour, wind-speed was 13 knots and cloud 7 oktas so the stability was class D. The wind was perpendicular to the Motorway.

The programme described in Chapter 6 was used to predict the NO concentration from a straight ground-level road with these conditions and an NO source emission factor of $Q_{NO} = 4.7843.10^{-4}$ppm $m^2 s^{-1} (vh^{-1})^{-1}$ described in Chapter 6. The predictions made for a straight road 1,000 metres long with five metre steps extending equal distances to either side of the observer line (Figure 7.17) are shown in Table 7.5 and Figure 7.18.

The agreement is satisfactory considering the uncertainties in the readings (from instrument noise), emissions estimate and weather readings (from Elmdon Airport).

Concentrations were measured alongside a Motorway as sequential half-hour averages (Butler, MacMurdo, Middleton, 1974) on Thursday

TABLE 7.4

Concentrations recorded at Perry Barr alongside M6 Motorway.

Results have 0.08ppm background subtracted.

Cycle	Concentrations Short Tube	Concentrations Long Tube	Ratio Long ÷ Short
	25m downwind	at M6	
12	0.148	0.187	1.266
13	0.192	0.238	1.240
14	0.123	0.293	2.386
15	0.204	0.279	1.369
16	0.141	0.252	1.783
17	0.203	0.369	1.813
18	0.156	0.225	1.440
19	0.112	0.233	2.077
20	0.106	0.219	2.063
21	0.069	0.169	2.442
22	0.116	0.227	1.954
23	0.099	0.198	1.993
24	0.094	0.198	2.106
25	0.081	0.168	2.083
26	0.064	0.158	2.469
27	0.092	0.177	1.920
	25m downwind	10m downwind	
28	0.067	0.107	1.594
29	0.097	0.125	1.297
30	0.081	0.107	1.320
31	0.087	0.135	1.562
32	0.080	0.147	1.833
33	0.110	0.134	1.218

Continued/......

TABLE 7.4 (continued)

	25m downwind	10m downwind	
34	0.117	0.167	1.429
35	0.078	0.142	1.821
36	0.089	0.121	1.358
37	0.108	0.134	1.241
38	0.080	0.124	1.550
39	0.072	0.119	1.648
40	0.109	0.144	1.325

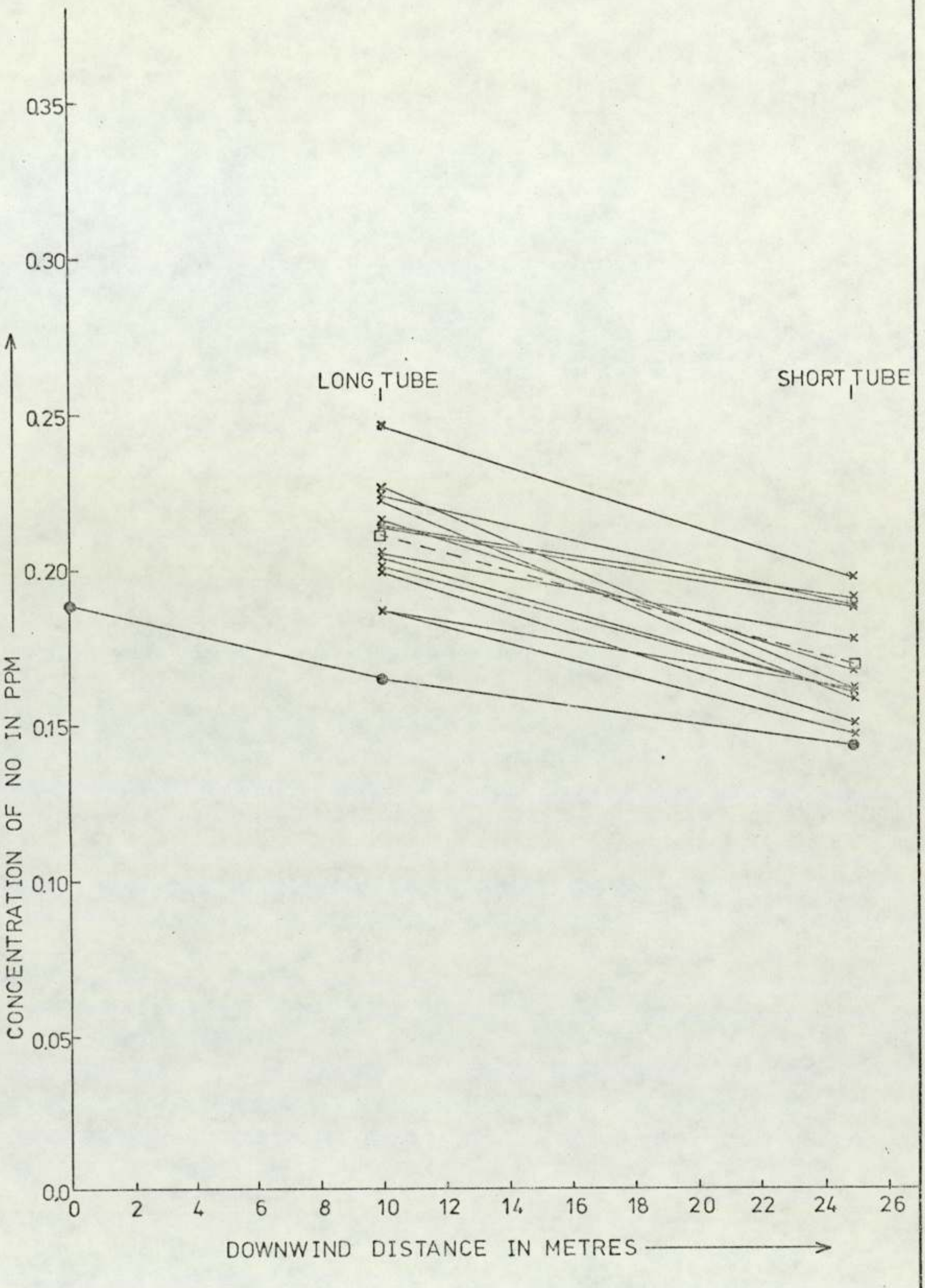

FIGURE 7.15 DECREASE IN CONCENTRATION OF NO WITH DISTANCE DOWNWIND FROM M6 MOTORWAY.

KEY :- ×—× EXPERIMENTAL (FOR A SINGLE CYCLE)

□- -□ MEAN OF ALL CYCLES

●—● CALCULATED USING PROGRAMME (SEE TEXT).

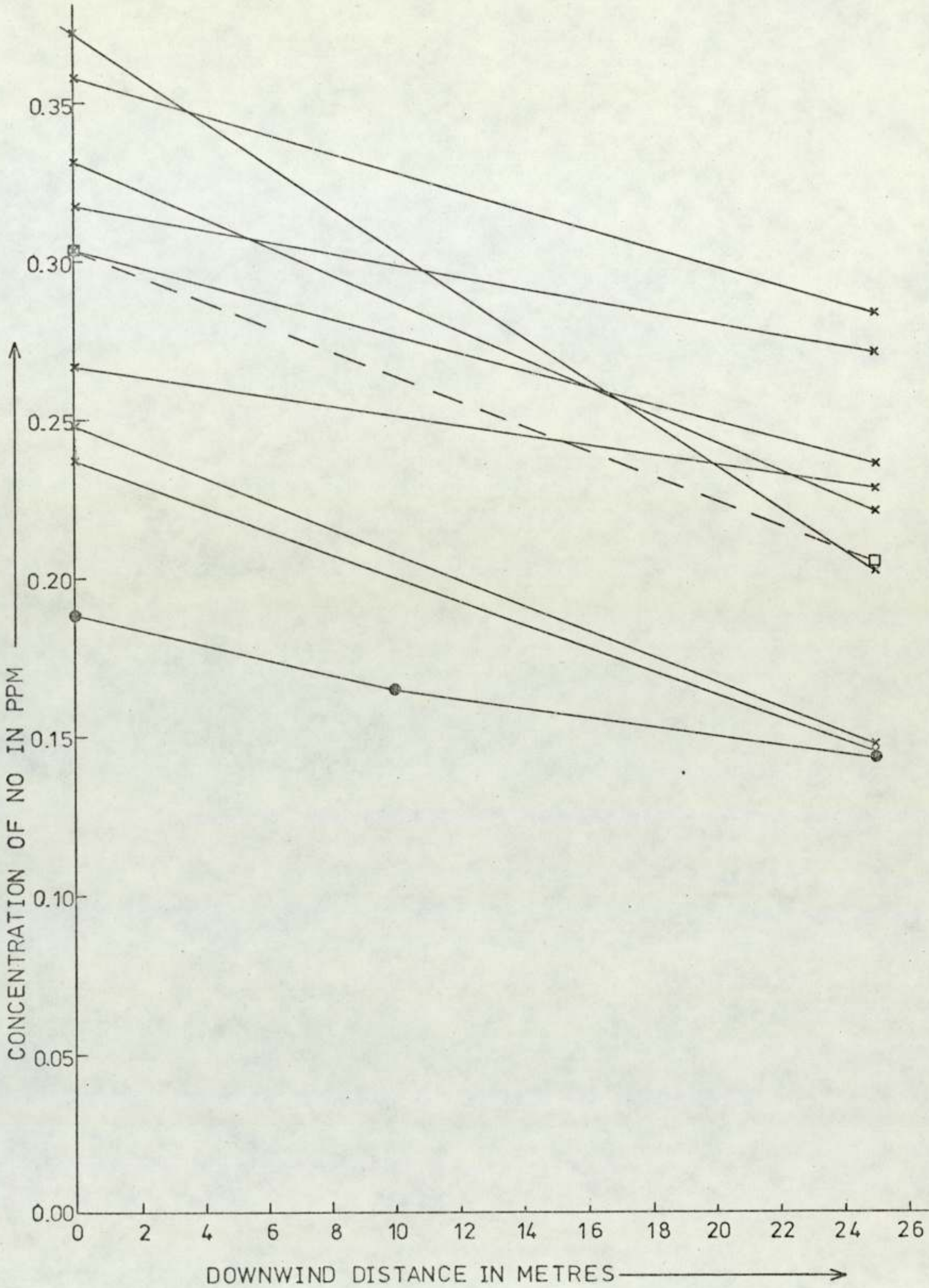

FIGURE 7.16 DECREASE IN CONCENTRATION OF NO WITH DISTANCE DOWNWIND FROM M6 MOTORWAY.

KEY:- ×—× EXPERIMENTAL (FOR A SINGLE CYCLE)

□- -□ MEAN OF ALL CYCLES

●—● CALCULATED USING PROGRAMME (SEE TEXT)

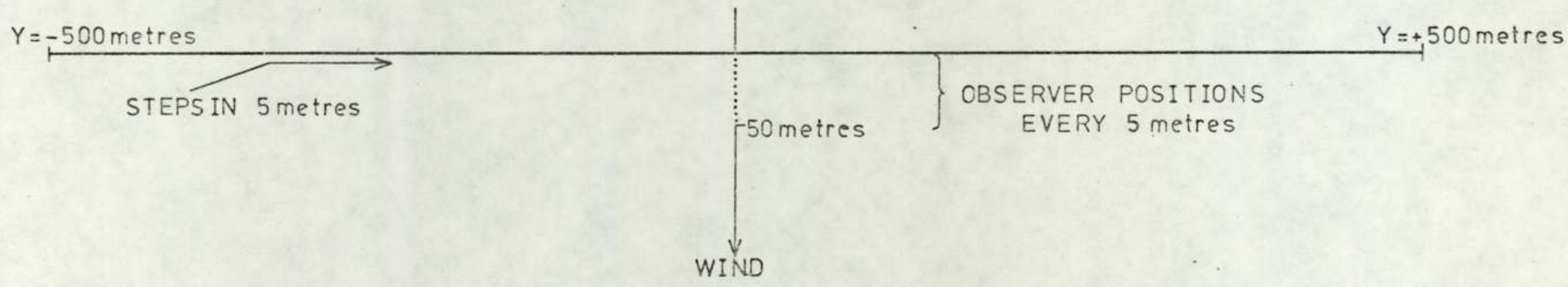

FIGURE 7.17 ROAD LAYOUT FOR THE CALCULATED RESULTS OF TABLE 7.5

TABLE 7.5

Average and Predicted Concentrations for Each Tube Position

Cycles	Mean concentrations[1], ppm NO, (measured)		
	Long Tube		Short Tube
	at road	10m downwind	
12 - 27	0.224	-	0.125
28 - 40	-	0.131	0.090
	Calculated concentrations		
Programme	0.164	0.125	0.094
Calder (1973)	0.173	0.133	0.099

Note 1: Zero level 0.08ppm measured in clean air blowing under the bridge was subtracted.

Note 2: Conditions:- 4500 vehicles h^{-1}, wind speed 13 knots, cloud 7 oktas.

Note 3: Discrepancy is due to slight differences in σ_z:
Programme uses $\sigma_z(0)=1.6$, $\sigma_z(10)=2.1$, $\sigma_z(25)=2.76$ while Calder uses 1.5, 1.95, 2.6 respectively.

$Q_{NO} = 0.00047843 \text{ppm } m^2 s^{-1} (vh^{-1})^{-1}$, $T = 4500$ vehicles h^{-1},
$u = 6.63\ m^2 s^{-1} (vh^{-1})^{-1}$, $Q_L = T.Q_{NO} = 2.1529\ m^2 s^{-1}$

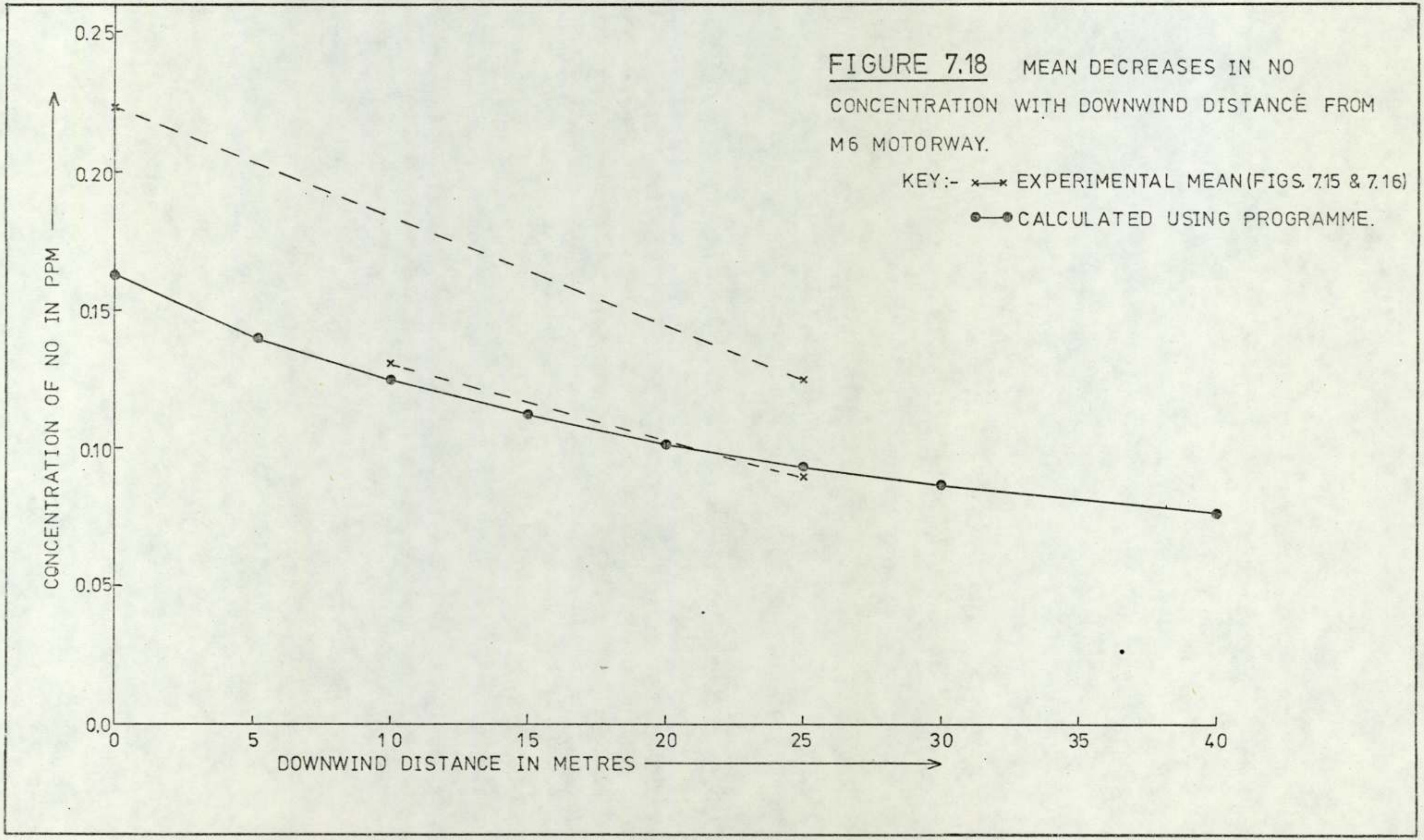

FIGURE 7.18 MEAN DECREASES IN NO CONCENTRATION WITH DOWNWIND DISTANCE FROM M6 MOTORWAY.

TABLE 7.6

Average and Predicted Concentrations -

for single inlet results

(Butler, MacMurdo, Middleton, 1974)

Source	Downwind Distance m	Concentration[1] NO, ppm
Butler et al.	0	0.257
	15	0.200
	27	0.155
Programme	0	0.164
	5	0.141
	10	0.125
	15	0.112
	20	0.102
	25	0.0940
	30	0.0871
	40	0.0762

Note 1: Zero of 0.037 subtracted

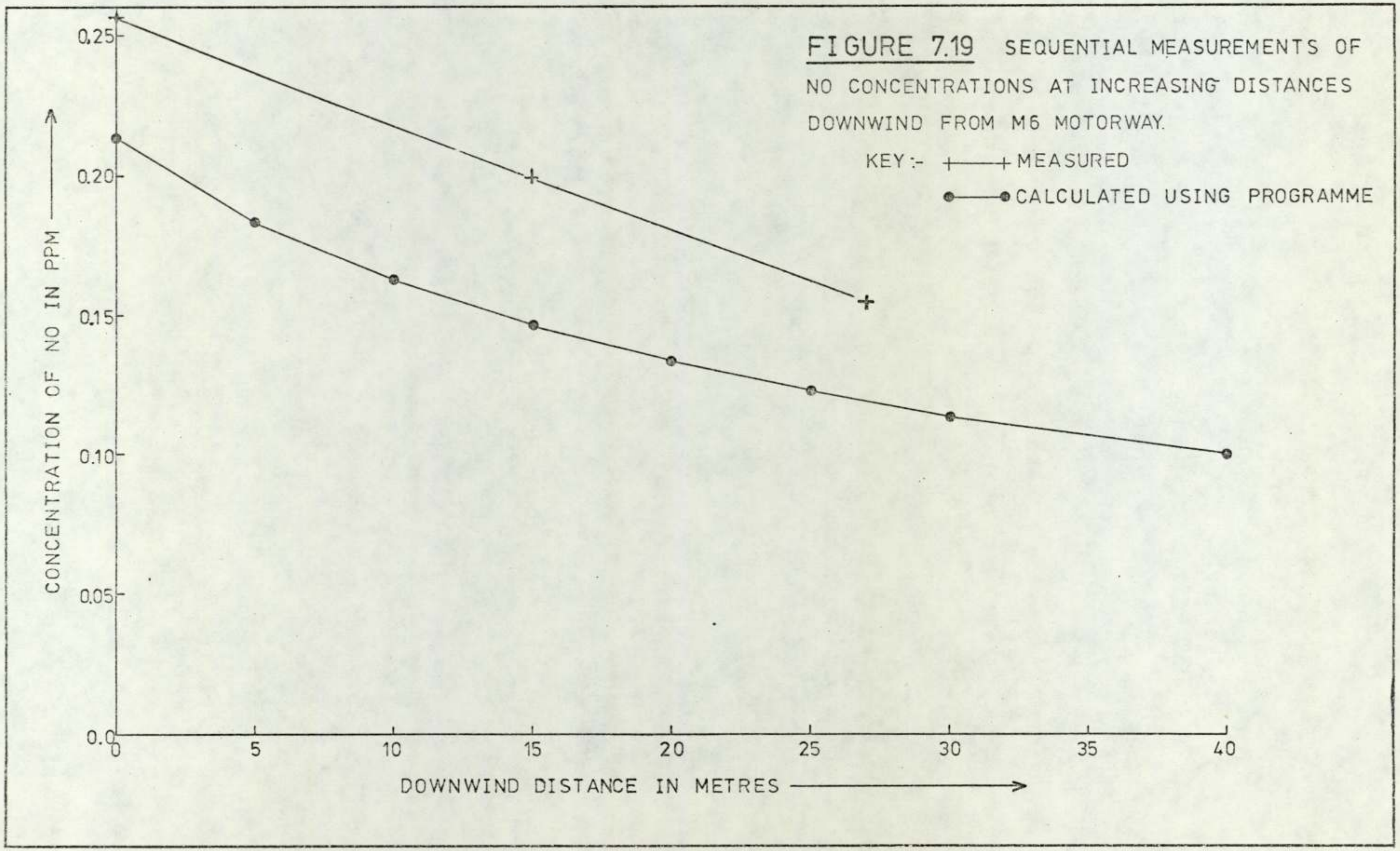

FIGURE 7.19 SEQUENTIAL MEASUREMENTS OF NO CONCENTRATIONS AT INCREASING DISTANCES DOWNWIND FROM M6 MOTORWAY.

03-05-1973. Conditions were 8 oktas cloud with wind-speed 4-5 ms^{-1}. The concentrations are compared in Table 7.6 and Figure 7.19 with similar predictions using a traffic-flow of 4,000 vehicles h^{-1}, a mean wind-speed of 4.5 ms^{-1} and class D stability. Figure 7.19 shows that the prediction is low.

7.5 Horizontal and Vertical Sampling at a Complex Site

The technique was used to measure concentrations across and vertically above the centre of the roundabout. The short tube inlet was placed on the roof of the toilets at the roundabout centre. For the vertical sampling a pulley was attached to the barrier at the side of the elevated section of road passing directly above the centre of the roundabout. A continuous loop of string over the pulley was attached to the long tube to raise and lower the inlet.

The concentrations fluctuated over a short time scale; average concentrations were calculated for each tube position (Table 7.7) and scaled to common units by dividing by the short tube result. The relative concentrations are plotted in Figures 7.20, 7.21 and 7.22, together with curves predicted using the programme SPAGSIMP, as described in Section 6.5. The concentration on 22-11-1974 and 25-11-1974 (Figures 7.21 and 7.22) decreased with downwind distance, across the roundabout: this is consistent with an effective increase in dilution distance. The concentration on 23-10-1974 (Figure 7.22) increased again at the far or downwind side: this unexpected increase at the far side is present in the calculated results also. This form of curve reflects the wind direction and source geometry. From Figures 7.20,

TABLE 7.7

Horizontal and Vertical Sampling at Salford Circus

Data and computer generated curves are shown in Figures 7.20, 7.21, 7.22 and 7.23 (Programme SPAGSIMP, using meteorological data and roundabout traffic count for the nearest hour on the day, and for simplicity, a 17.00 hours traffic (Friday) for the rest of the intersection). In the Table, numbers in brackets are ppm levels predicted by the programme (selected from the predictions used for the computer curves above).

SAMPLING	Set and Date	Number of Cycles	Short Tube Position	Long Tube Position	Mean Concentration for the set PPM		Ratio Long÷Short Normalised
					Short	Long	
HORIZONTAL	1 23.10.74	17	Centre: 40m	Upw 0	0.035 (.02866)	0.057 (.07195)	1.63
	2 23.10.74	10	Centre: 40m	Down 80	0.043 (.02866)	0.057 (.05680)	1.31
	3 22.11.74	14	Centre: 40m	Upw 0	0.350 (.08629)	0.502 (.1285)	1.43
	4 25.11.74	16	Centre: 40m	Upw 0	0.115 (.06342)	0.206 (.09203)	1.79

Continued/......

TABLE 7.7 (continued)

HORIZONTAL	5 25.11.74	12	Centre: 40m	Down 80	0.095 (.05035)	0.074 (.04291)	0.78
VERTICAL	6 27.11.74	9	Centre: 3m	H1: 13	0.117	0.105	0.90
	7 27.11.74	8	Centre: 3m	H2: 11	0.080	0.080	1.00
	8 27.11.74	8	Centre: 3m	H3: 8	0.086	0.078	0.90
	9 27.11.74	10	Centre: 3m	H4: 5	0.099	0.092	0.93

FIGURE 7.20 RELATIVE DECREASE IN NO CONCENTRATION ACROSS SALFORD CIRCUS ROUNDABOUT IN THE INTERSECTION.

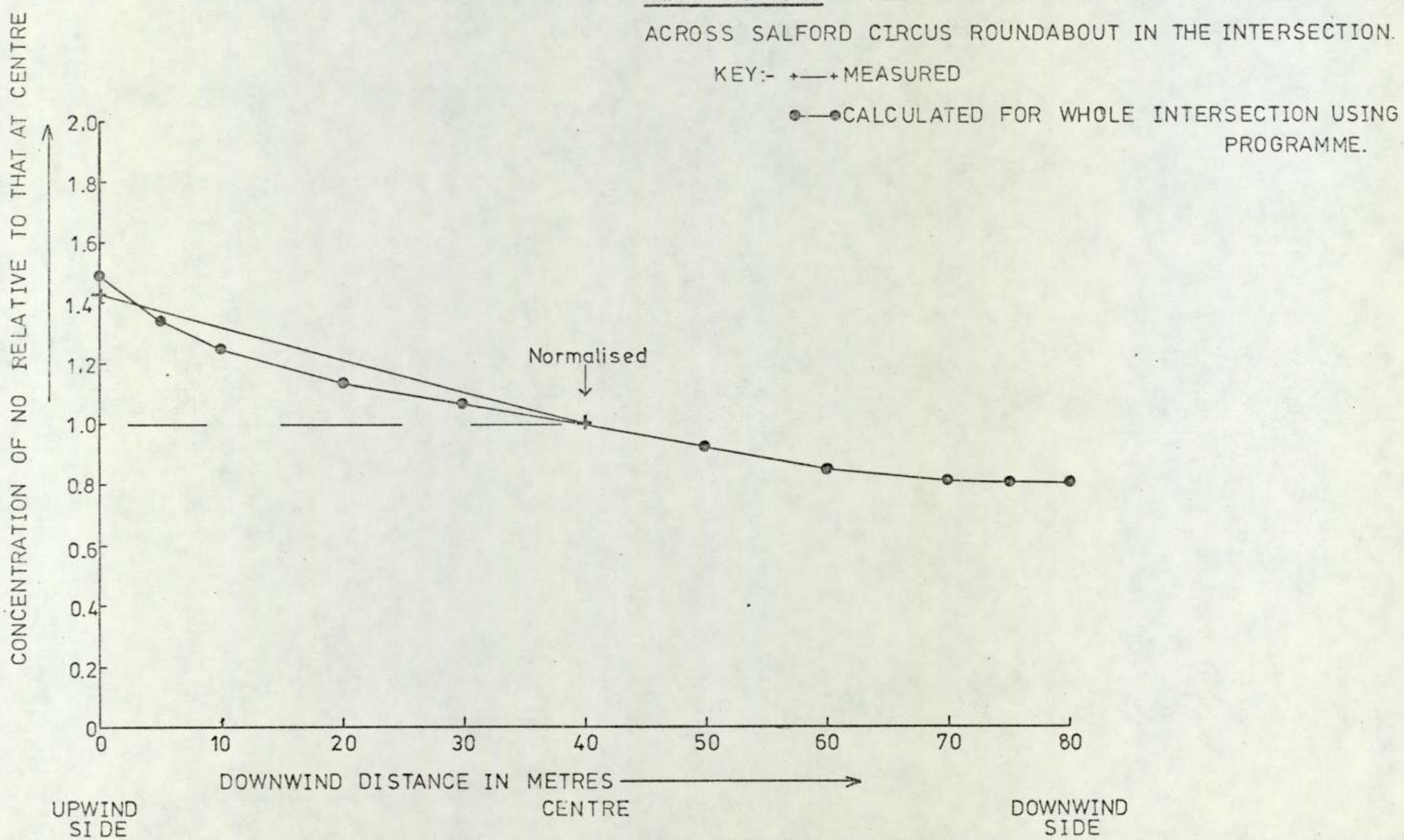

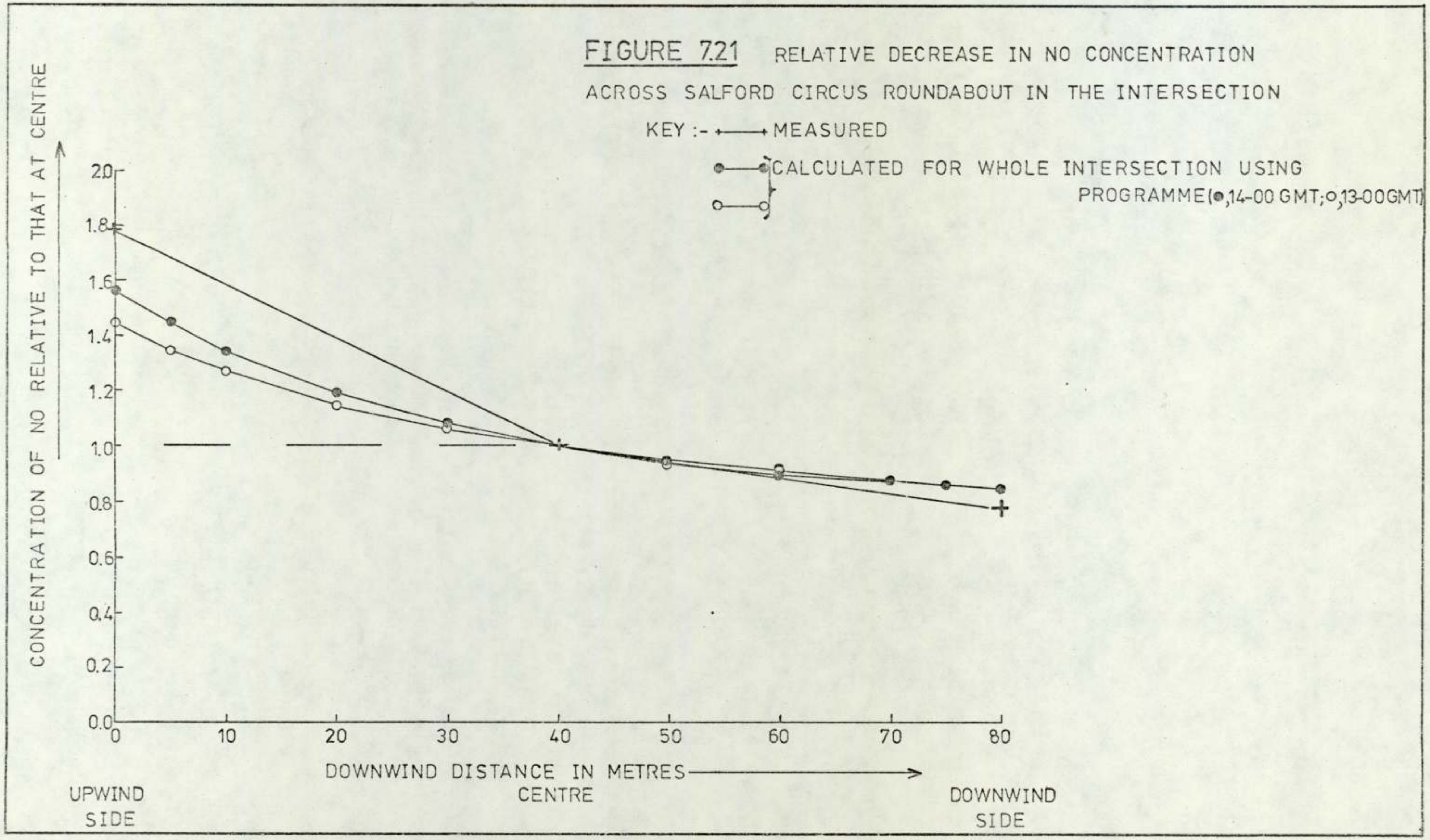

FIGURE 7.21 RELATIVE DECREASE IN NO CONCENTRATION ACROSS SALFORD CIRCUS ROUNDABOUT IN THE INTERSECTION

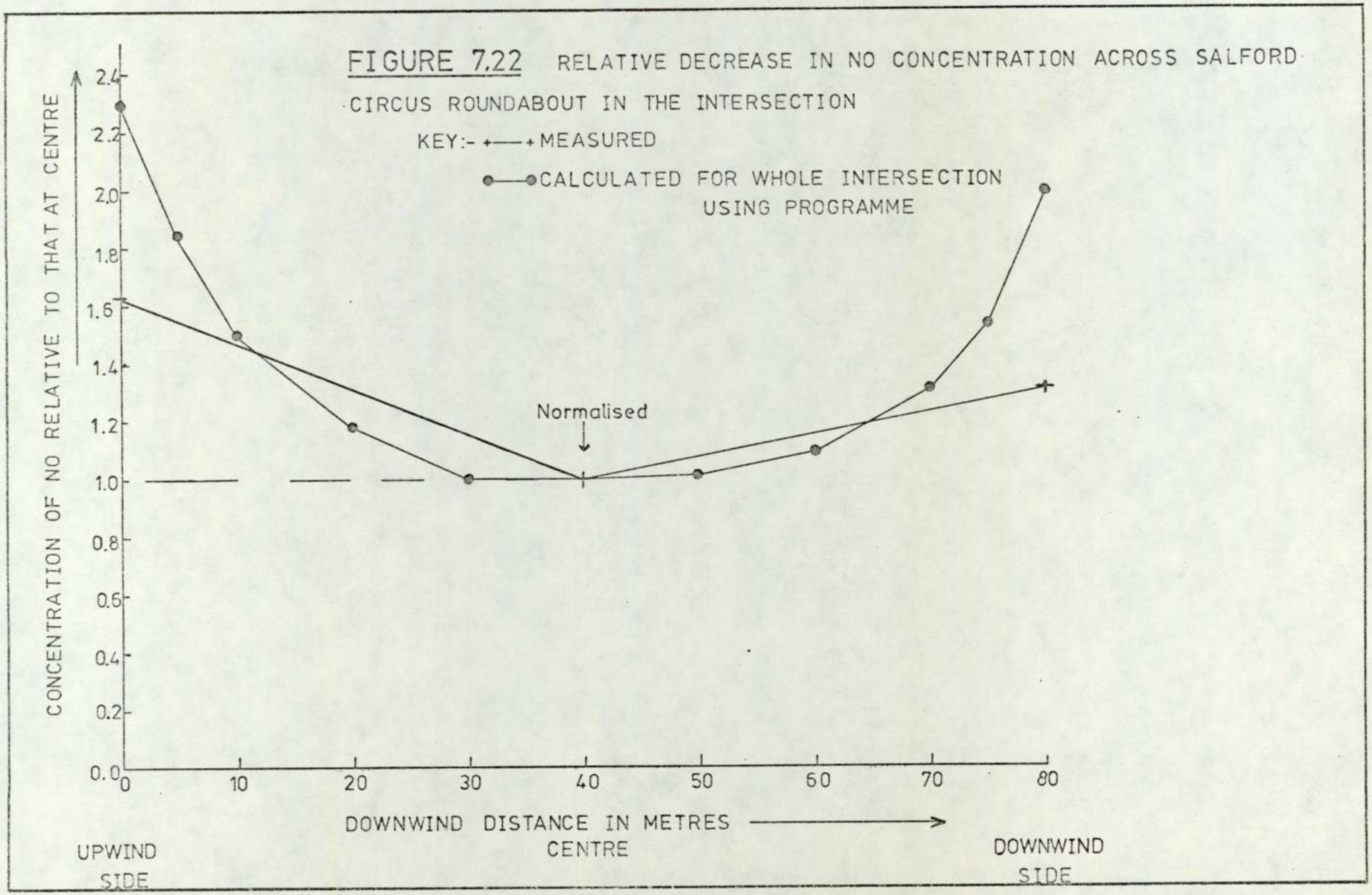

FIGURE 7.22 RELATIVE DECREASE IN NO CONCENTRATION ACROSS SALFORD CIRCUS ROUNDABOUT IN THE INTERSECTION

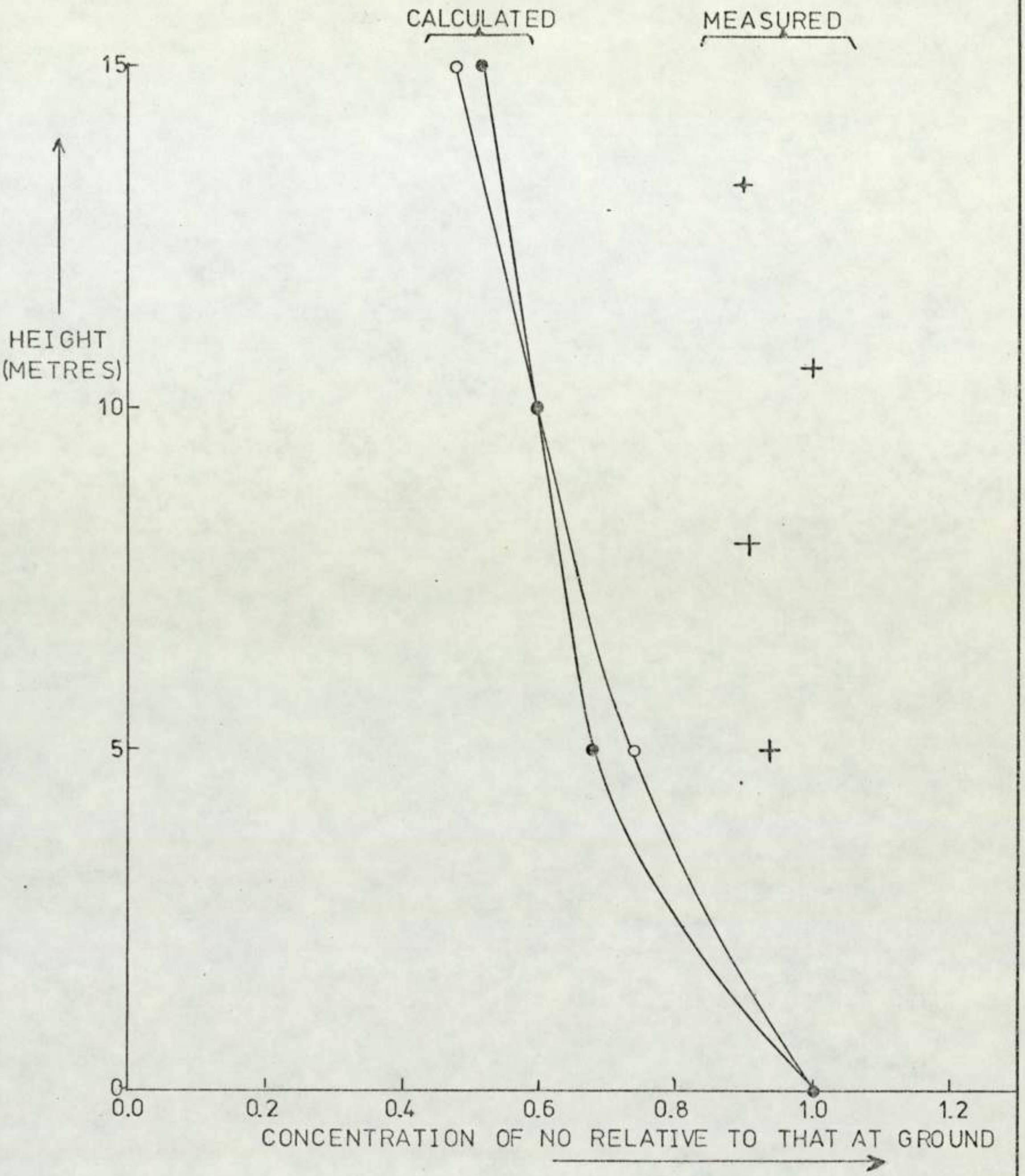

FIGURE 7.23 VERTICAL CHANGES IN NO CONCENTRATION AT SALFORD CIRCUS ROUNDABOUT IN THE INTERSECTION.

KEY:- +—+ MEASURED

●—● } CALCULATED USING PROGRAMME
○—○ }

7.21 and 7.22, the programme did give dilution curves of form consistent with the concentration gradients measured by the technique.

In Figure 7.23 a similar, though less satisfactory, comparison is made between the measured vertical gradient and programme curves. There was however much eddying, particularly when just below the elevated roads so the scatter present in the raw data and the poor agreement of Figure 7.23 was not surprising. The geometrical simplification present in the model, particularly the use of horizontal roads throughout, probably affects this comparison also: the roads above the sample tube do slope down, so there are pollutant contributions from all heights which would affect the programme curve.

7.6 Summary

A sampling technique to measure concentrations simultaneously at two different places, using only one analyser, has been described. The equipment was tested in part and then as an operating technique in the field: some measurements of pollutant plumes were presented.

The measurements were compared with predictions using the programme SPAGSIMP (Section 6.5, Paragraph 5); the same emissions estimate (per vehicle) was used for this work as for the analysis of the routine monitoring results (Chapter 6).

The results for horizontal sampling were consistent (both at the Motorway and in the roundabout) with the programme predictions: the vertical sampling was less conclusive and the weakness of the programme with regard to local eddying and road-slopes was suggested as responsible.

The general levels predicted by the programme for the roundabout were lower than as measured: this is consistent with the observations of Chapter 6. This lowness was less pronounced alongside the M6, where perhaps less acceleration occurs, and a more representative source description possible.

CHAPTER 8

CONCLUSIONS

As stated in the introduction (Chapter 1), the project studied the intersection as a source of pollution. We explained there that by the very nature of the problem, field monitoring would precede interpretation. Having described the work itself in previous Chapters, we now list the conclusions.

8.1 Calibrations

Dilution of NO and CO from 100% in two stages (Chapter 2) showed that calibrations using the commercial mixtures of standard gas would be accurate within an order of magnitude, but might be low. Concentrations reported for oxides of nitrogen could be $\sim$ 30% low, and for carbon monoxide, $\sim$ 40% low. Part of this uncertainty arises from experimental limitations and more sophisticated apparatus was referenced. Mixtures of standard gases can be unstable and should be treated with suspicion.

Single-stage dilution of standard mixtures showed that the analysers for oxides of nitrogen and carbon monoxide were linear to within 10% and 5% respectively.

A cross-check made by altering the hydrocarbon analyser to measure carbon monoxide as methane suggested that the standards for carbon monoxide and hydrocarbons were consistent.

Together, these results imply that, with regard to calibration, the concentrations recorded during the project were self-consistent. Some uncertainty remains as to their absolute magnitude.

8.2 Field Monitoring

This is an exercise in itself because instrument drift is more severe than in the laboratory. Ideally, automatic zero checks should be made, or failing that, daily visits. Chart recorders were very useful to watch both instrument performance and pollutant trends, but did make data abstraction lengthy.

The chemiluminescent analyser for oxides of nitrogen, NO and NO_x, was, with the automatic zero-checker added, quite adequate despite needing much maintenance. Measurement of nitrogen dioxide as $NO_2 = NO_x - NO$ was not satisfactory. The non-dispersive infra-red analyser for carbon monoxide was very reliable, but a 0-10ppm scale would have been useful. The flame ionisation detector for hydrocarbons was satisfactory, except that it was noisy at times. Ideally the zeroing of this instrument requires study as to whether an oxygen effect occurs.

Pollutant concentrations fluctuated widely and although several points were abstracted for each hour, there remains an uncertainty in the values quoted because of this fluctuation. This uncertainty and the selection of both instrument response-time and data-averaging time should be studied.

8.3 Data Processing

Monitoring generates large quantities of data (Chapters 3, 4). Errors and missing values occur. Thus data processing for this type of work must meet several requirements:-

1. Flexibility of data sequence and data set size.
2. Unique but efficient coding of information for time, date, year, site and identification of variables, followed by any number of observations. The use of pre-defined card-columns and a card character-search by the programme proved very helpful. The method could be made more efficient by greater use of header information (e.g. for year and site which may occur on every row in the set) to shorten each data row.
3. Ability to process incomplete data sets, either by deletion of incomplete rows, or by interpolation of occasional missing values if the data follow an understood pattern. This requirement is because simultaneous observations may be required for many variables, especially if modelling is to follow the observational study (in our case traffic on twenty four roads, five pollutant variables and three weather parameters).
4. Option to interpolate whole data sets from a smaller sample of real observations, where possible. E.g. we interpolated hourly traffic counts from twelve hourly photographs, thus drastically reducing the manhours in abstraction.
5. Correction for zero and calibration drifts, and averaging of pollutant levels, e.g. into hourly averages. This

requires complete flexibility in the numbers (from none upwards) and times of zeroes, calibrations and observations.

6. Ability to sort and manipulate the data easily, since errors are found in manually abstracted data.

8.4 Emissions - Dilution Model

A computer programme was developed (Chapter 6) to calculate the concentration of a gaseous pollutant at any site for any network of roads and traffic-flows. A simple map reference system based on the Ordnance Survey represents roads of any geometry (lines, curves or circles) and height. Any number of observer positions are similarly represented. Axes are rotated (X downwind) so that the distances of an observer downwind and crosswind from points along each road may be calculated. With these distances, if the element of road is upwind of the observer, the contribution of that element to pollution at the observer is calculated and added to that of previous elements. Pollutant concentrations for each element are represented by the continuous point-source or Gaussian plume formula, with plume widths and heights obtained by the Pasquill category method using windspeed, cloud cover and insolation (latter is estimated). The integral over the intersection is scaled by the constants, namely (windspeed)$^{-1}$ and the source strength, to give the calculated concentration. Source strength is, in effect, the product of road-length (m), traffic-flow (vehicle h^{-1}) and emission parameter (m^3 pollutant m^{-1} road (vehicle $h^{-1})^{-1} s^{-1}$. The programme thus calculates concentrations of pollutants with no reference to measured concentrations, relying on source geometry and literature values for plume dilution and emissions parameters.

8.5 Model Test: Dilution

For a simple line source, the concentration decay calculated by the programme was similar to that given in numerical form by Calder (1973).

A two-tubes sampling technique (Chapter 7) was tested to assess its use for the measurement of concentration gradients, and in so doing, obviate limitations arising from the restricted availability of monitoring sites and gas analysers. Concentrations recorded simultaneously at two separate places on the one analyser were converted to relative decreases in concentration. The latter were consistent in form with those calculated by the programme.

8.6 Model Test: Routine Monitoring

Routine monitoring results for the heart of the intersection were compared statistically with levels calculated by the programme from weather readings and traffic counts taken at the same time. With 236 hourly observations, the correlation coefficients between calculated and measured levels were, for NO_x and NO, 0.76; for CO, 0.67; for HC, 0.72; NO_2 was rejected. The model gave values lower than those observed.

New emissions estimates were calculated to see what was implied by the low nature of the calculated levels. For NO, the new emissions estimate was reasonable; for CO, rather high; for HC, extremely high. One should not use these without further thought for there are many deficiencies in the model - both in its representation of the intersection as a source (Chapter 6), and the possibility of sources not considered. For example, although the HC levels given by the model correlated well with the measured ones, they differed by two orders of magnitude. Nevertheless, with NO, and less so with CO, the behaviour of the model was encouraging. It appears that in the intersection, traffic was a significant source of nitric oxide and carbon monoxide.

The model was not used at the site outside the intersection because of an interfering chimney, but data were recorded for winds from the city. For all gases except HC, the concentrations in the city background at that site were noticeably lower than at the intersection.

A high background level of HC seen at both sites has not been explained.

8.7 Sensitivity Analysis

A simulation by the programme of the plume from the intersection revealed several points.

Pollutant concentration decreases rapidly with downwind distance at first (Figure 6.13), although this drop levels out at greater distances. With very unstable conditions (Class A, MST2 =1), the initial drop is very steep in comparison to that for neutral (Class D, MST2 =7) and stable (Class E, MST2 =8) conditions.

If the effect of wind speed on the choice of stability index is ignored, the concentration is proportional to the reciprocal of wind speed.

The concentration field from the intersection as modelled by the programme reflected the source density of the intersection (Figures 6.16 to 6.20), since a plume from the roundabout at Salford Circus was recognisable. Although exaggerated by the source representation employed, this does stress the need for as full a source representation as possible. It also implies that the downwind pollutant pattern depends on the layout of the intersection, consistent with "common sense".

Study of a line source showed that at small downwind distances, the concentration was very dependent on road height. Thus the elevated nature of the structure would tend to reduce ground-level concentrations in the immediate vicinity of the intersection; this would be less pronounced further away.

8.8 Summary

The use of continuously operating gas analysers in the field made it possible to obtain a set of hourly measurements of NO_x, NO, NO_2, CO and HC at a complex motorway intersection. Simultaneously, traffic counts and weather readings were obtained.

A programme was developed to use published models of turbulent diffusion to calculate pollution concentrations from the traffic and weather data for any layout of roads. The calculated concentrations had a high correlation with the measured concentrations, suggesting that the programme was adequately describing the fluctuations of pollutant concentrations even though it tended to give values that were low.

A further cross-check of the programme was provided by the measurements of concentration gradients. For this a sampling technique was designed to take simultaneous samples from two separate places for analysis on the one available analyser. These results, and those of the programme, were mutually consistent.

The previous sections in this Chapter describe main features of the work in order to outline further directions of study.

8.9 Perspective

It is not easy to draw a satisfying conclusion from this type of work, because of the many ways of looking at it. The project relates directly to the frequently asked question "Well, how bad is the pollution at the intersection?" This implies both questions of what pollutant concentrations occur, and how do they fluctuate, and questions of given these concentrations over a period of time, what was the exposure of people to them, and how might such an exposure affect their health in years to come. There is therefore a matter of defining the question to be answered.

This work aimed specifically at seeing if a contribution from traffic to the pollution could be recognised, which implied distinguishing the various contributions of surrounding sources. To facilitate the latter, we restricted work to a site near where the traffic-effect, if any, might be readily seen, and further away for comparison. This gave us a basic check on the calculations.

With many factors involved (Figure 1.3) and each either measured inaccurately (Figure 6.31) or not at all, we cannot expect too good a fit between calculations and experiment, particularly at greater distances where dilution has occurred. Thus the "ideal test-case" does not give an exact check on calculation, so extrapolation to practical problems of deciding transport policy (e.g. road versus rail, or both) will not give accurate figures for immediate debate.

Nevertheless public concern over pollution does demand some idea of the concentrations occurring, and what affects them, in the hope that then sensible decisions may be taken. In this study we have simply looked for an understanding of the dilution of gases emitted by road vehicles at the intersection, and do not attempt to define or answer these other important but difficult questions.

APPENDIX 1

CHART-DATA

PROCESSING PROGRAMME

This programme written in ICL Algol uses character handling procedures for the flexible data entry. The following numbered paragraphs outline the main features of the programme (Flow chart: Figure 3.8; example output: Figure 3.9).

1. Coding of Data

Numbers can be comma or space (2) separated. A slash, /, ends the data. Each card represents one hourly observation: the card end is recognised as a character marking the end of data for that particular hour. Each card is uniquely defined by the first eight columns as in Table A1.1. G ranges from 1 to 6 to represent the pollutant identity; Z, from 0 to 2 to represent a zero, observation or calibration card. For example input: see Figure A1.1.

2. Procedure Definitions

PMØNTH (YR, MTH, DINMTH) uses the year YR and month MTH to calculate the number of days in the month; the answer is returned as DINMTH. Due note is taken of leap years.

TIMELAPSE (DATA, G, Z, B1, B2, PMØNTH, DINMTH, PERIØD) is used to obtain the difference in hours between the times of two data-cards B1 and B2 for the observation of type G, Z. This procedure uses PMØNTH so that the cards B1 and B2 could be in different months (as might happen in data taken at the end of a month and beginning of the next). When the number of days between the two cards has been found as T1DAY,

CALIBRATIONS

```
2,2,4,15,04,11,74,100,100,80.5,
1,2,4,15,04,11,74,100,101,90.6,
5,2,4,15,04,11,74,50,50,35,
6,2,4,15,04,11,74,10,8,77.5,
```

ZEROES

```
1,0,4,12,04,11,74,1,1.0,
2,0,4,12,04,11,74,1,1.0,
1,0,4,14,04,11,74,1,0.2,
2,0,4,14,04,11,74,1,1.2,
```

OBSERVATIONS FOR OXIDESOF NITROGEN

```
1,1,4,13,04,11,74,1,07,06,05,10,12,10,11,14,14,39,20,10,11,12,10,
2,1,4,13,04,11,74,1,20,20,05,06,37,04,11,20,09,12,03,10,10,16,08,
1,1,4,14,04,11,74,1,17,35,23,07,11,11,09,11,11,11,
2,1,4,14,04,11,74,1,22,07,05,23,06,08,06,22,                07,12,11,
1,1,4,15,04,11,74,1,07,14,10,13,09,                 13,23,13,13,07,
2,1,4,15,04,11,74,1,03,             08,08,13,10,14,14,10,10,13,
1,1,4,16,04,11,74,1,10,27,09,10,11,37,18,19,15,10,09,10,10,10,11,
2,1,4,16,04,11,74,1,10,23,08,06,15,10,15,13,06,16,10,13,10,08,10,
1,1,4,17,04,11,74,1,12,13,17,13,25,15,26,16,18,22,13,09,11,15,15,
2,1,4,17,04,11,74,1,14,10,20,16,14,17,10,08,12,20,09,12,06,12,15,
1,1,4,18,04,11,74,1,10,13,19,17,12,16,11,16,12,15,15,20,17,11,15,
2,1,4,18,04,11,74,1,16,11,11,10,12,14,17,12,11,11,13,10,12,10,13,
1,1,4,19,04,11,74,1,14,15,16,14,09,
2,1,4,19,04,11,74,1,10,16,20,10,14,
1,1,4,20,04,11,74,1,10,09,15,14,09,14,10,13,29,11,09,10,09,18,08,
2,1,4,20,04,11,74,1,06,10,07,05,09,09,09,10,13,17,07,10,10,07,06,
1,1,4,21,04,11,74,1,10,11,10,20,12,10,08,11,08,09,09,12,09,19,07,
2,1,4,21,04,11,74,1,06,16,09,09,10,04,05,06,07,04,07,06,06,07,06,
1,1,4,22,04,11,74,1,08,10,10,10,09,10,10,08,09,59,07,13,12,12,12,
2,1,4,22,04,11,74,1,10,07,10,10,10,07,06,06,10,10,08,05,10,08,05,
1,1,4,23,04,11,74,1,07,07,10,10,08,07,09,39,06,35,06,10,07,06,07,
2,1,4,23,04,11,74,1,07,10,08,06,06,11,09,06,16,35,05,07,05,11,15,
1,1,4,24,04,11,74,1,13,09,08,06,09,08,07,11,11,10,06,09,07,06,05,
2,1,4,24,04,11,74,1,08,10,13,11,08,06,05,05,05,09,04,10,05,05,05,
1,0,4,19,04,11,74,1,0.6,
2,0,4,19,04,11,74,1,0.6,
```

SALFORD CIRCUS TRAFFIC COUNTS

```
4,1,4,01,04,11,74,0389,
4,1,4,02,04,11,74,0161,
4,1,4,03,04,11,74,0066,
4,1,4,04,04,11,74,0054,
4,1,4,05,04,11,74,0090,
4,1,4,06,04,11,74,0347,
4,1,4,07,04,11,74,0941,
4,1,4,08,04,11,74,2695,
4,1,4,09,04,11,74,2698,
4,1,4,10,04,11,74,2447,
4,1,4,11,04,11,74,2118,
4,1,4,12,04,11,74,2171,
4,1,4,13,04,11,74,2321,
4,1,4,14,04,11,74,2355,
4,1,4,15,04,11,74,2471,
4,1,4,16,04,11,74,2761,
4,1,4,17,04,11,74,3370,
4,1,4,18,04,11,74,3411,
4,1,4,19,04,11,74,2073,
4,1,4,20,04,11,74,1413,
4,1,4,21,04,11,74,1163,
4,1,4,22,04,11,74,1044,
4,1,4,23,04,11,74,0866,
4,1,4,24,04,11,74,0634,
```

OBSERVATIONS FOR CARBON MONOXIDE

```
5,1,4,12,04,11,74,50,17,16,17,17,12,14,15,15,
5,1,4,13,04,11,74,50,15,15,16,16,16,16,18,17,17,17,17,17,
5,1,4,14,04,11,74,50,17,17,18,17,17,17,17,18,18,16,20,17,
5,1,4,15,04,11,74,50,16,17,
5,1,4,16,04,11,74,50,06,07,09,08,06,11,07,07,06,07,06,08,
5,1,4,17,04,11,74,50,08,06,07,09,08,06,10,09,08,08,08,11,
5,1,4,18,04,11,74,50,06,09,07,08,09,07,06,06,12,09,06,07,
5,1,4,19,04,11,74,50,06,06,07,08,08,06,06,07,07,07,06,07,
5,1,4,20,04,11,74,50,07,07,09,08,07,07,08,08,07,07,07,06,
5,1,4,21,04,11,74,50,07,06,06,07,08,06,05,06,06,09,08,06,
5,1,4,22,04,11,74,50,07,08,07,08,08,07,06,06,06,08,07,06,
5,1,4,23,04,11,74,50,07,06,06,06,06,06,06,05,06,06,05,05,
5,1,4,24,04,11,74,50,10,08,07,08,06,07,06,06,05,05,05,05,
5,0,4,12,04,11,74,50,10.2,
5,0,4,15,04,11,74,50,11.0,
5,0,4,15,04,11,74,50,1.0,
```

OBSERVATIONS FOR HYDROCARBONS

```
6,0,4,12,04,11,74,100,03.0,
6,1,4,13,04,11,74,100,08.7,
6,1,4,14,04,11,74,100,06.7,
6,1,4,16,04,11,74,100,09.5,
6,1,4,17,04,11,74,100,09.8,
6,1,4,18,04,11,74,100,09.5,
6,1,4,19,04,11,74,100,09.3,
6,1,4,20,04,11,74,100,09.5,
6,1,4,21,04,11,74,100,09.3,
6,1,4,22,04,11,74,100,09.5,
6,1,4,23,04,11,74,100,09.5,
6,1,4,24,04,11,74,100,09.5,
6,0,4,15,04,11,74,100,02.8,
```

FIGURE A1.1 ROUTINE MONITORING RESULTS CODED FOR CALIBRATION AND ZERO CORRECTION, AS INPUT TO CHART50.

it is multiplied by 24 and the hours added. The result is PERIØD.

TIMECROS (DATA, G1, G2, Z1, Z2, B1, B2, PMØNTH, DINMTH, TIMDIF) is similar to TIMELAPSE. They differ only in that TIMECROS is a more general procedure: it compares the time of a card B2 of type G2, Z2 with that of B1 of G1, Z1. TIMECRØS is used to get all times relative to a common origin, the first NO_x card, by setting G1 =1, Z1 = 1 when the procedure is called.

3. Data Entry

G, Z are read from the card and a counter, CRDNUM [G,Z] , incremented (maximum value: 50) as cards of type G, Z are read. This provides serial counting of each card within its type and forms the subscript for storage by card number. The six numbers defining site, time and instrument fsd (nominal) are read into the elements of DATA[G, Z, CRDNUM [G,Z]] for J = 1 to 6. If the card were a traffic card, G = 4, no more need be read. If it is for a calibration, Z = 2, and control passes to CALREAD. If it is an observation, Z = 1, or zero, Z = 0, card, it is handled as follows: the characters on the card are checked for spaces (skipped), end-of-card (see below) or end-of-data (begin calculations). Failing these the next number is read. A second counter, MØNITR [G, Z, CRDNUM [G,Z]] is stepped to record how many observations are read off the card. Thus any number of observations can be put on a card as room allows, provided the last two characters are spaces to ensure correct character handling following use of the Algol procedure READ. Any order of card types is allowed, but all cards of the same type must be in chronological order. At the end of the card the points read in from the chart are averaged and multiplied by the nominal instrument fsd over 100. The result, DATA [G, Z,[CRDNUM [G,Z]],6] , is the hourly average (obtained from the chart average as a percentage of the nominal fsd) in ppm. This is calibrated later.

If the card were for a calibration (Z = 2), then the concentration GASCNC of the standard gas in ppm and the chart reading DIVS the instrument at nominal fsd DATA [G, Z, P, 6] showed are read. Then for the Pth calibration card, the nominal fsd was DATA [G, Z, P, 6], and ONEDIV [G, P] := (GASCNC*100)/(DATA [G, Z, P, 6] *DIVS), i.e. the factor by which the instrument readings must be multiplied to read true, e.g. if the 100 ppm gas reads 95 divisions on the 100ppm nominal sensitivity, ONEDIV = $\frac{100.100}{100.\ 95}$.

4. Calibration

When all cards have been read the hourly averages for zeroes and observations are calibration-corrected. For the Pth card (observation or zero), the average is multiplied by ONEDIV [G, CP]; DATA [G, Z, P, 6] := DATA [G, Z, P, 6] *ONEDIV [G, CP] where CP is the card number for the calibration card either coincident with or immediately before the hourly-average being calibrated. The appropriate calibration card is identified as card-number CP by comparison of the time of the Pth observation ØBSTIM [G, Z, P] with the times CALTIM [G, CP] of all calibrations CP = 1 to CRDNUM [G,2] for the gas G. For that card CP the correction factor ONEDIV G,[CP] is used in the above equation.

Where no calibration cards for gas G are read a correct instrument calibration is assumed.

5. Zero Correction

The calibrated zeroes are now subtracted from the calibrated observations. The times OBSTIM [G, O, Z] of the zero cards (numbered here as Z) are compared with the times ØBSTIM[G, 1, P] of the Pth observation. If a zero is coincident with the observation it is subtracted. If the zero occurs before the observation the next zero is tested until either a coincident zero is found for subtraction, or the zero immediately preceding and that immediately following the observation have been identified (using two card-numbers Z1, Z2 for the preceding and following zeroes). In the latter case the equation of the line joining these two zeroes is used to interpolate the (drifted) zero at the time of the observation. The interpolated value is subtracted. If no zero cards for gas G are present a true zero is assumed.

6. Traffic Storage

Streeter-Amet counts are included for ease of processing as a whole: their presence enables the output table to include all measurements made in the project except intersection counts (Chapter 4) and weather readings. The values need no calculation: they are merely read into DATA [4, 1, P, 6] and later stored in ANSWR [4, P] for traffic card P.

7. Procedure Call for CHEKTIM G,P

CHEKTIM[G, P] is the time in hours of all observations G, P measured in hours from the first NO_x or G = 1 card. This is so that, unlike OBSTIM [G, P] we have in the matrix CHEKTIM values for the times from a common origin, and therefore can sort the cards for each gas G according to whether an observation of one gas is coincident in time with that of another.

8. Card Sequence Checks

The data entry may have cards within a type G, Z not in correct chronological order: this may be due to wrong card sequencing or a data error. All cards are checked so that one programme run finds all the sequence errors in the data; if an error is found the programme quits.

9. Coincidence Sorting

Given correctly sequenced data the cards are sorted into rows: there is one row per hourly observation. Each row contains the value for each gas G at the time of the row. The table is created by a coincidence search of the times CHEKTIM [G, P] of each card. For G2 = 2, 4, 5, 6 a variable LØGIC [G2, B1] is set equal to 1 only if the card B2 of gas G2 is coincident with card B1 of gas G2 = 1. When all cards G2, B2 have been tried against the card B1 of gas G1 = 1 the variables LØGIC [G2, B1] are multiplied together.

LØGAL [Bl] = LØGIC [2,Bl] *LØGIC [4,Bl] *LØGIC [5,Bl]
*LØGIC [6,Bl]

The product, LØGAL [Bl] is unity only if all gases have an observation taken at the time of Gl, Bl. When such a coincidence has been found, the card numbers of each G2 card that had the same time as Gl, Bl, are stored as the value of the element CØØRD [ØCC,G2], where ØCC is a counter incremented at each coincidence. Thus for G+1 to 6 the six elements CØØRD [ØCC,G] equal the card numbers for those cards that are mutually coincident.

Also, if LØGIC [2,Bl] is unity then the coincident NO reading can be subtracted from the NO_x to estimate the NO_2.

10. Test Output

The results of the calibrations, zero abstractions and data sorting are output gas by gas for checking.

11. Results Output

The results are then output as a Table of hourly rows: each row contains the time and site, followed by the NO_x, NO, NO_2, traffic at Salford Circus, CO and HC levels for that time and site.

APPENDIX 2

DETAILS OF

THE TRAFFIC PROGRAMMES

The programmes perform tasks as outlined in Chapter 4 and Figure 4.1. The following paragraphs apply to the general flowchart (Figure A2.1). The roads are defined by Figure 4.1 and Tables A2.1, A2.2.

1. The numbered cards are read into DATA [I,J] . A counter M is increased whenever a value of -1 signifying a missing value is read. DATA [I,J] is split into TIME [I,J] which holds the six values defining the photograph's time, and CØUNT [I,J] which holds the counter-readings for all twenty eight counters in the Ith photograph.

2. The count of vehicles over the Jth counter during the period PERIØD [I] from TIME [I - 1, J] to TIME [I,J] is

   DIFF [I,J] = CØUNT [I,J] - CØUNT [I - 1, J]

   since the counts are cumulative. When a counter passes zero, DIFF [I,J] < 0 so 999999 is added.

3. If either CØUNT [I,J] or CØUNT [I - 1, J] is missing DIFF [I,J] is not obtainable directly. The subscripts I, J of the missing difference DIFF [I,J] are stored in MISSI [Q], MISSJ [Q] , where Q is a counter incremented for each missing difference.

4. PERIØD [I] is calculated using the procedures PMØNTH, to obtain the number of days in the month, and TIMELAPSE to give the period in hours and decimal fraction of the hour.

5. LØGIC [I,J] is 1 if DIFF [I,J] exists, else zero.

6. Missing differences are interpolated as follows:-

Each row I is scanned, and for each the columns J are scanned. If LØGIC [I,J] = 1, then DIFF [I,J] exists and may be added to those other differences existing for the Ith row.

$$RØWSUM[I] = \sum DIFF[I,J]$$

summed over J for which DIFF [I,J] exists

Also

$$SIGMAR[I] = \sum RJ[J]$$

summed over J for which DIFF [I,J] exists

where RJ [J] is the fraction of a complete twenty eight counter count that each counter contributed to that complete count. RJ [J] represents the relative proportions of traffic-flow over the various counters. The twenty eight values RJ [J] , J = 1.. ....28, were calculated using the programme TRRLRATGEN, a modified form of the first programme, i.e. based on 1 - 4 above, as it was before the missing value interpolation was inserted. Table A2.3 shows the values for RJ [J] .

RØWSUM [I] is the total of the available differences and is a fraction SIGMAR [I] of a full twenty eight counter count T that would exist were all the differences present.

Then

RØWSUM [I] = SIGMAR [I] *T

We redefine the value of RØWSUM to save storage as T.

RØWSUM [I] = T = RØWSUM [I] /SIGMAR [I]

This full count may be subdivided according to RJ [J] to estimate the missing differences.

If LØGIC [I,J] = O, then we interpolate

DIFF [I,J] = RJ [J] *RØWSUM [I]

to substitute for the missing value.

7. The counters in general read high (because of lane discipline) thus FAC [ ] in the programme holds the factors for correction.

FACDIF [I,J] := FAC [J] *DIFF [I,J]

8. Several counters contribute to one road.

The combinations of counters are defined for any numbered road by the alphabetic-groups as on the map, Figure 4.1 and as in Tables A2.1, A2.2. Thus the number of vehicles passing along any one road between the photographs I - 1, I and during PERIØD [I] is the summation of FACDIF [I,J] for those J relevant to the road. Some terms may be subtracted, dependent on the counter combinations.

E.g. $$\text{M6FLØW} [I] = \sum_{J = 1, 2, 3, 6, 7, 8} \text{FACDIF} [I,J]$$

9. The programmes output the total flow elapsed as above during PERIØD [I] , and the flow per hour as total flow divided by PERIØD [I] . These flows are printed for M6, A38(M), M6-South & North, A38(M)-North and A38(M)-South.

10. In addition TRRLRØFLØ gives the flow PBF [RD,I] for every road RD of the junction. This requires a full labelling of the roads as on the map (Figure 4.1), and two procedures to set up the complex set of counter combinations. The function procedure BØX becomes the traffic-flow elapsed for the alphabetic-group as

defined by a parameter K of the procedure. A switch is used to select those counters appropriate to the group (Table A2.1). Thus

$$BØX = \sum FACDIF [I,J]$$

summed according to those counters contributing to the Kth alphabetic-group. BØX is calculated for the Kth group using the Ith row of the matrix FACDIF by a call

Function := BØX (K,I,FACDIF).

The procedure RØFLØW has a similar use of switch to select those alphabetic-groups contributing to the desired road RD. The combinations are defined in Table A2.2.

E.g. for the M6 we need group A plus group B, to sum

FACDIF [I,J] for J = 1, 2, 3, 6, 7, 8

The procedure call RØFLØW (1, BØX, I, FACDIF, PBF) will set up the element

PBF [1,I] := BØX (1,I,FACDIF) + BØX (2,I,FACDIF).

The two calls of BØX give us

PBF [1,I] := FACDIF [I,1] + FACDIF [I,2] + FACDIF [I,3]
+ FACDIF [I,6] + FACDIF [I,7] + FACDIF [I,8]

for the M6. The programme will print

PBF [1,I] /PERIØD [I], the flow along the road in vehicles per hour.

11. TRRLBØX will interpolate hourly flows if the periods between the photographs exceed one hour.

The procedures RØFLØW and BØX are called as above to obtain the flow along each road. PBF [RD,I] is the number of vehicles which passed during PERIØD [I] ; PERIØD [I] might have been twelve hours. To subdivide this into hourly flows, we need the hourly traffic-pattern; this reflects the rise and fall with peak periods. We suppose the hourly traffic-pattern is different for every road and for each type of day. In practice Mondays, Tuesdays, Wednesdays, Thursdays are similar (Errors: Appendix 3), and Fridays, Saturdays and Sundays are distinct. A sample set of hourly photographs were abstracted (12-09-74 to 16-09-74) and used in the programme TRRLRØFLØ. The results were stored in a "standard" matrix STD which holds the traffic-flows for all roads of the junction for four day-types, where a Monday is denoted 1 and so on to Sunday, 7. The programme TRRLBØX uses this standard to interpolate hourly flows. STD [RD,I,J] is read for every road RD, and all twenty four hours I of the day, for day-types J = 5, 6, 7, 1. Then STD [RD,I,J] for J = 2, 3, 4 is set equal to STD [RD,I,1] making Tuesday, Wednesday and Thursday equivalent in pattern to Monday. The reading of STD is complex: crosschecks are made to be sure the proper data are read.

STD now has the flow for every road for every hour of each day-type throughout the week. We assume the total flow of vehicles may change, but that from the elements of STD scaled according to the total flow we may estimate hourly flows. The value of each hour between the Ith and I-1th photographs is calculated. Fig. A2.2 shows overlapped hours numbered for illustration and the photograph times. The variables A1, A2, H1, H2 are also defined on the Figure.

Define A1, the fractional time after photograph I-1, and before the first full hour.

A1 = 1 -(TIME [I-1,6])/60   i.e. minutes/60

A2, the fractional time after that last full hour still within the overlap period

A2 =(TIME [I-1,6])/60   i.e. minutes/60

(H1 + 1), the first full hour overlapped

H1 = TIME[I-1,5] + 1   hours

H2, the last full hour overlapped

H2 = TIME [I,5]   hours

We use an hour-subscript, HSUB, to step over the overlapped hours. HSUB is initially set equal to H1. The day-type D is required when calling the elements of STD.

D = TIME [I-1,4]

HSUB will be incremented as HSUB = HSUB + 1; the number of full hours overlapped is INTERV, which is related to PERIØD[I] . It is possible that the fractional times A1, A2 together account for over an hour, and since INTERV will be used to control the number of interpolations required it must be integral. Rounding errors must be avoided. Hence INTERV = ENTIER (PERIØD [I]) - ENTIER (A1 + A2) where ENTIER, an ALGØL procedure, rounds to the nearest integer below the function.

We now have the number of full hours overlapped and the start and end points of overlap.

HSUB is incremented: if midnight is passed HSUB is set to unity and day-type D reset to unity at the end of a week.

As J increases from unity to INTERV we increment HSUB and D as each hour is passed, and store them as HR [J] , DY [J]. The relevant elements of STD are retrieved and summed:

$$TØTSTD = \sum_{J=1}^{INTERV} STD[\,RD, D, HSUB\,]$$

(at present D = DY [J] , HSUB = HR[J])

At the end of summation TØTSTD is the total count present in the standard matrix for those hours in the day-types which are overlapped. The fractional terms from either end of the overlap are added

$$TØTSTD = TØTSTD + A1*STD[\,RD, TIME[\,I-1,4\,], H1\,] + A2*STD[\,RD, TIME[\,I, 4\,], H2 + 1\,]$$

For each overlapped hour the flows are estimated assuming the same traffic-pattern existed during PERIØD [I] as that represented by those elements of STD that were overlapped.

$$FLØW = \frac{STD[\,RD, DY[\,J\,], HR[\,J\,]\,]*PBF[\,RD, I\,]}{TØTSTD[\,RD\,]}$$

The interpolated FLØW is printed.

TABLE A2.1

Counter Numbers by Alphabetic Group

Alphabetic Group (Map: Figure 4.1)	Counters included[1] in the group (Values of J)	Calibration Factor (Measured: Section 4.2.4)
A	1, 2, 3	0.80
B	6, 7, 8	0.91
C	4, 5	0.97
D	9, 10	0.81
E	11, 16	0.96
F	21, 26	0.86
G	12	0.89
H	22, 27	0.76
I	13, 18	0.89
J	28	0.78
K	14, 15, 19, 20	0.90
L	24, 25	0.77

Note 1: Procedure BØX sums the matrix elements DIFF [I,J] for the Ith photograph over those counters or J values given by this Table.

TABLE A2.2

Alphabetic Counter-Groups contributing to Each Road

Road	Alphabetic group combination[1]
1	A + B
2	C + D + G + I + K + L - E - J
3	--- (Salford Circus)
4	I
5	C - E + F
6	H
7	C
8	F --- D - F
9	D
10	F
11	L
12	K
13	½(L)
14	½(L)
15	G
16	G - J
17	H - I
18	J
19	H - I + J
20	C - E + F --- E - F
21	½(K)
22	½(K)
23	G - J + I
24	E

<u>TABLE A2.2 (continued)</u>

Note 1: Procedure RØFLØW calls each combination of alphabetic groups: for each alphabetic group a call of the function BØX is made to select the counters as in Table A2.1.

TABLE A2.3

Values RJ[J] for interpolation of

Missing Values

J	RJ[J]	J	RJ[J]
1	0.006026	15	0.003828
2	0.003892	16	0.000001
3	0.006810	17	0.003150
4	0.005262	18	0.000608
5	0.003315	19	0.000104
6	0.004698	20	0.003531
7	0.008829	21	0.004241
8	0.003141	22	0.003716
9	0.001400	23	0.004094
10	0.003080	24	0.008776
11	0.000001	25	0.004102
12	0.001246	26	0.000692
13	0.003869	27	0.005944
14	0.005086	28	0.000560

FIGURE A2.1 OUTLINE FLOWCHART FOR THE COMPUTER PROGRAMMES TO CALCULATE TRAFFIC FLOWS FROM REGULAR PHOTOGRAPHS OF THE COUNTER READINGS.

PART 1: RELATIONSHIPS BETWEEN THE PROGRAMMES, AND PARTS THEY HAVE IN COMMON.

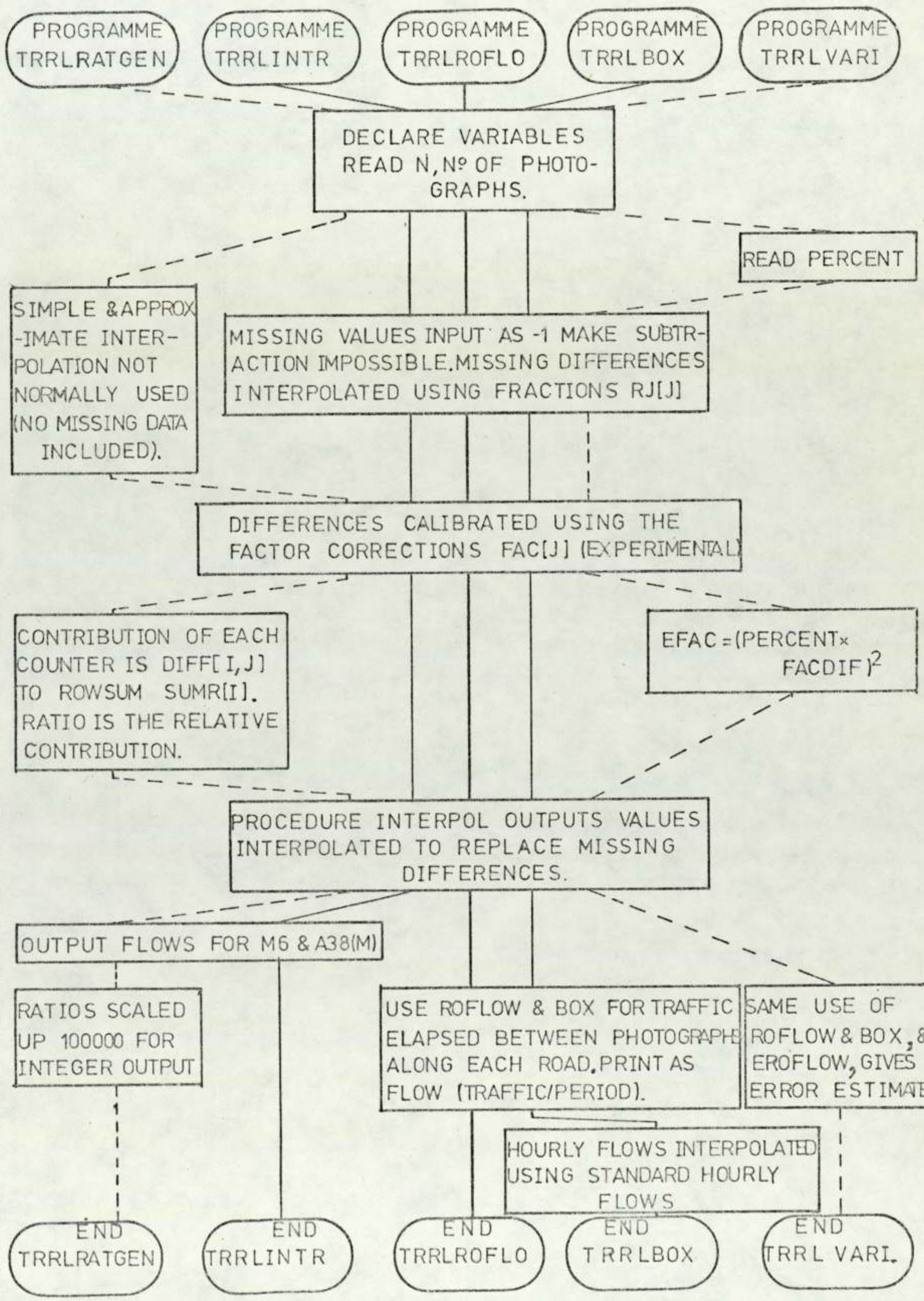

CONTINUED ON NEXT PAGES

FIGURE A2.1 (CONTINUED) 2

PART2: OUTLINE FLOWCHART

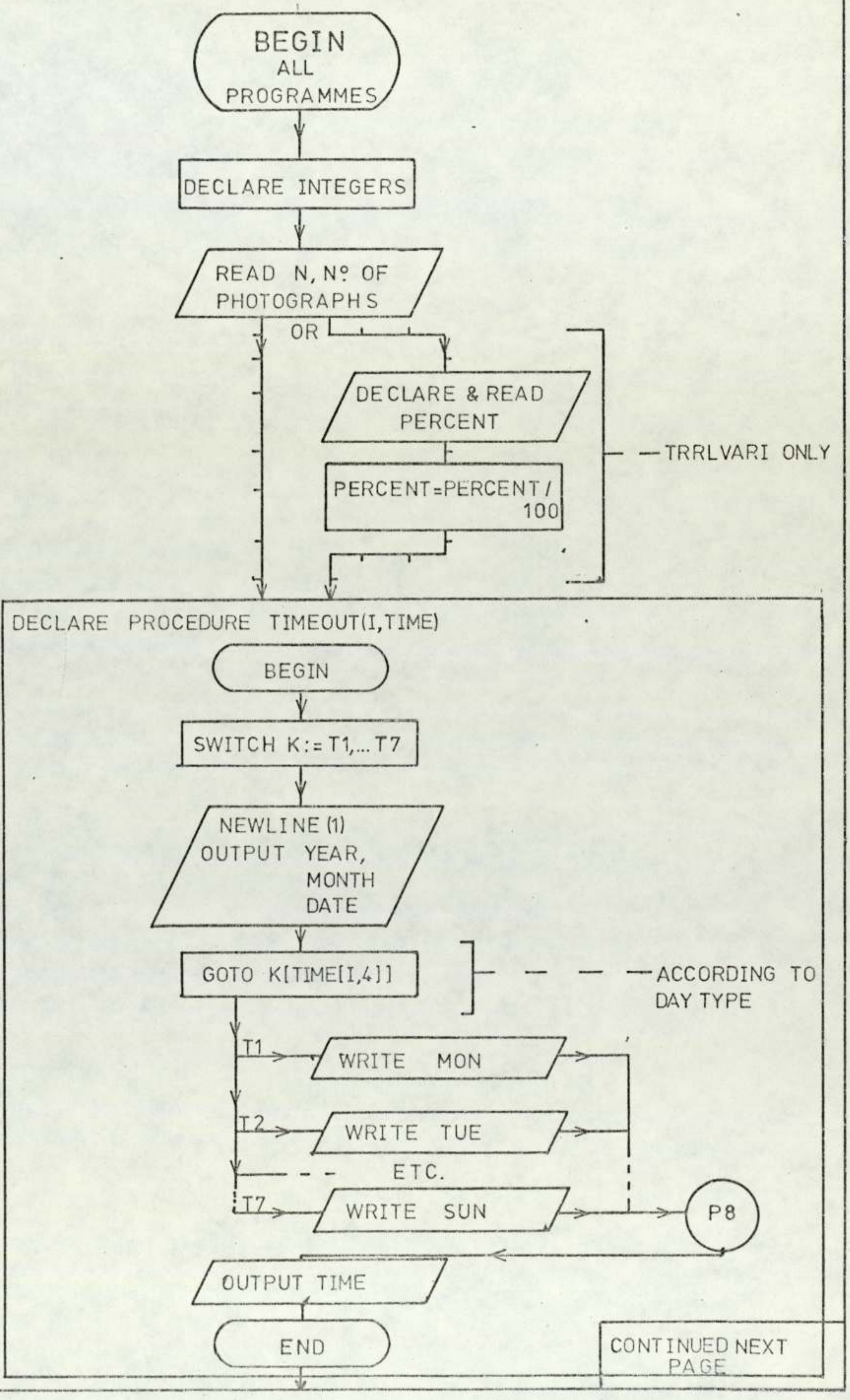

CONTINUED NEXT PAGE

FIGURE A2.1 (CONTINUED) 3

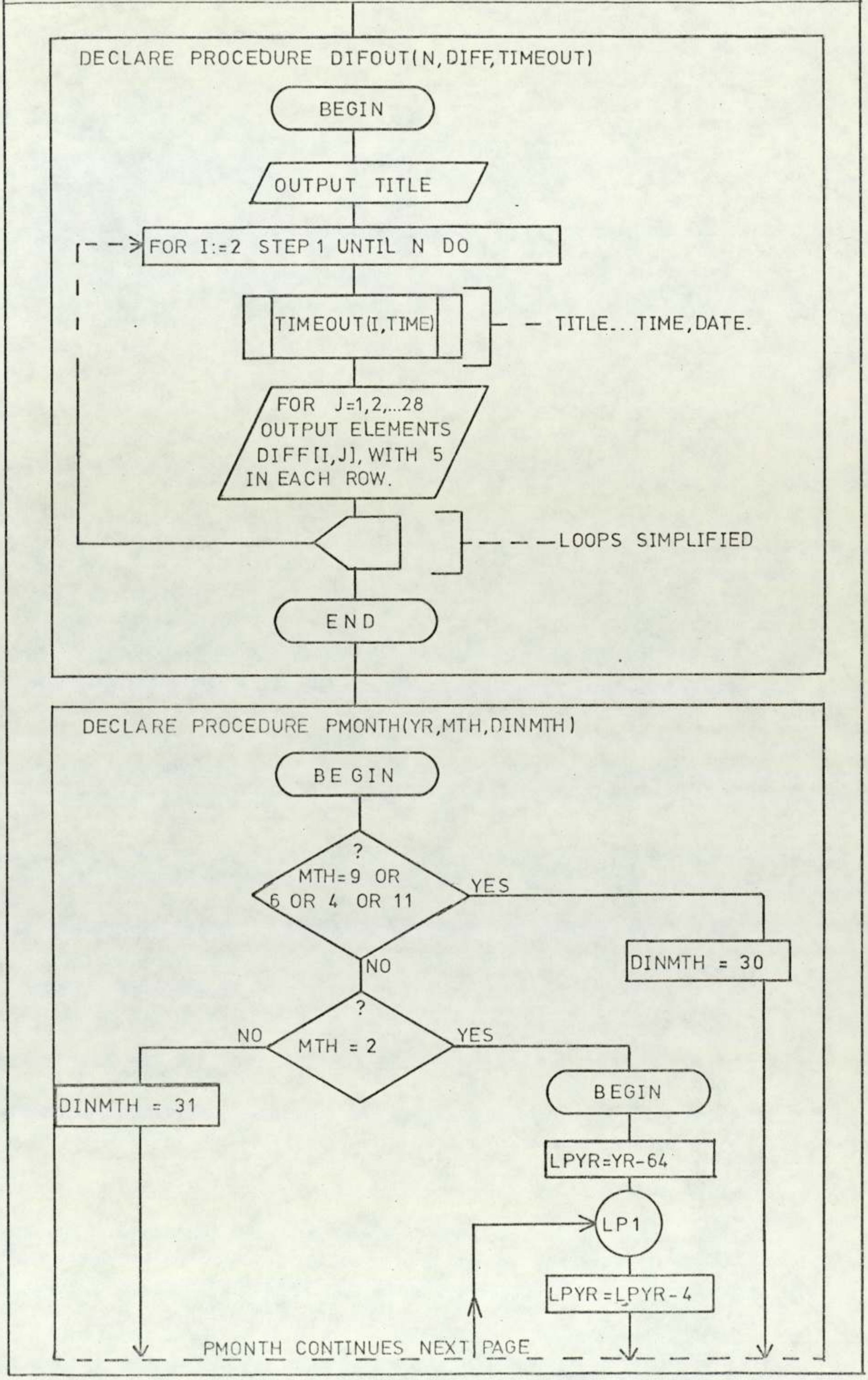

FIGURE A2.1 (CONTINUED) 4

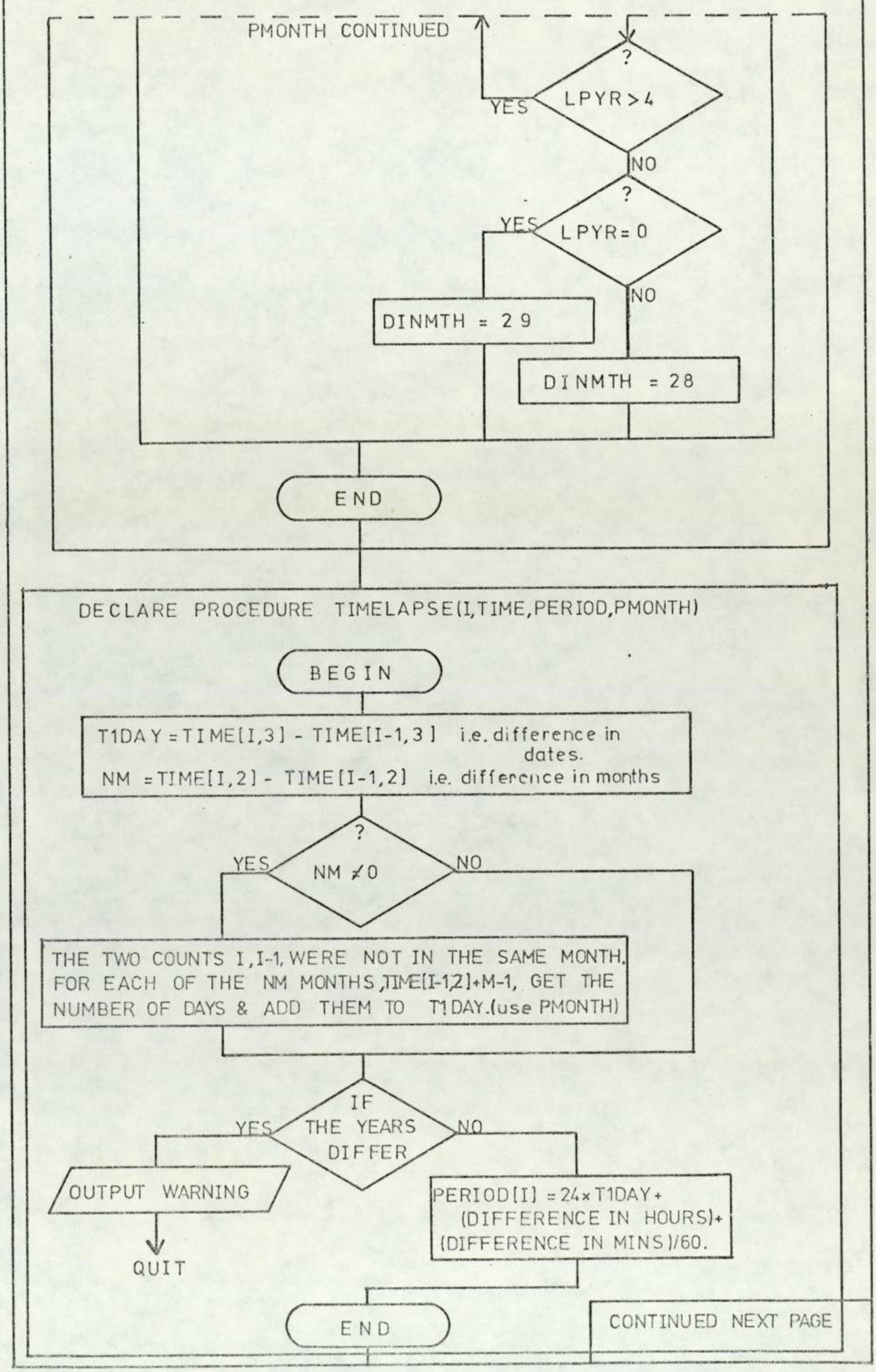

FIGURE A2.1 (CONTINUED) 5

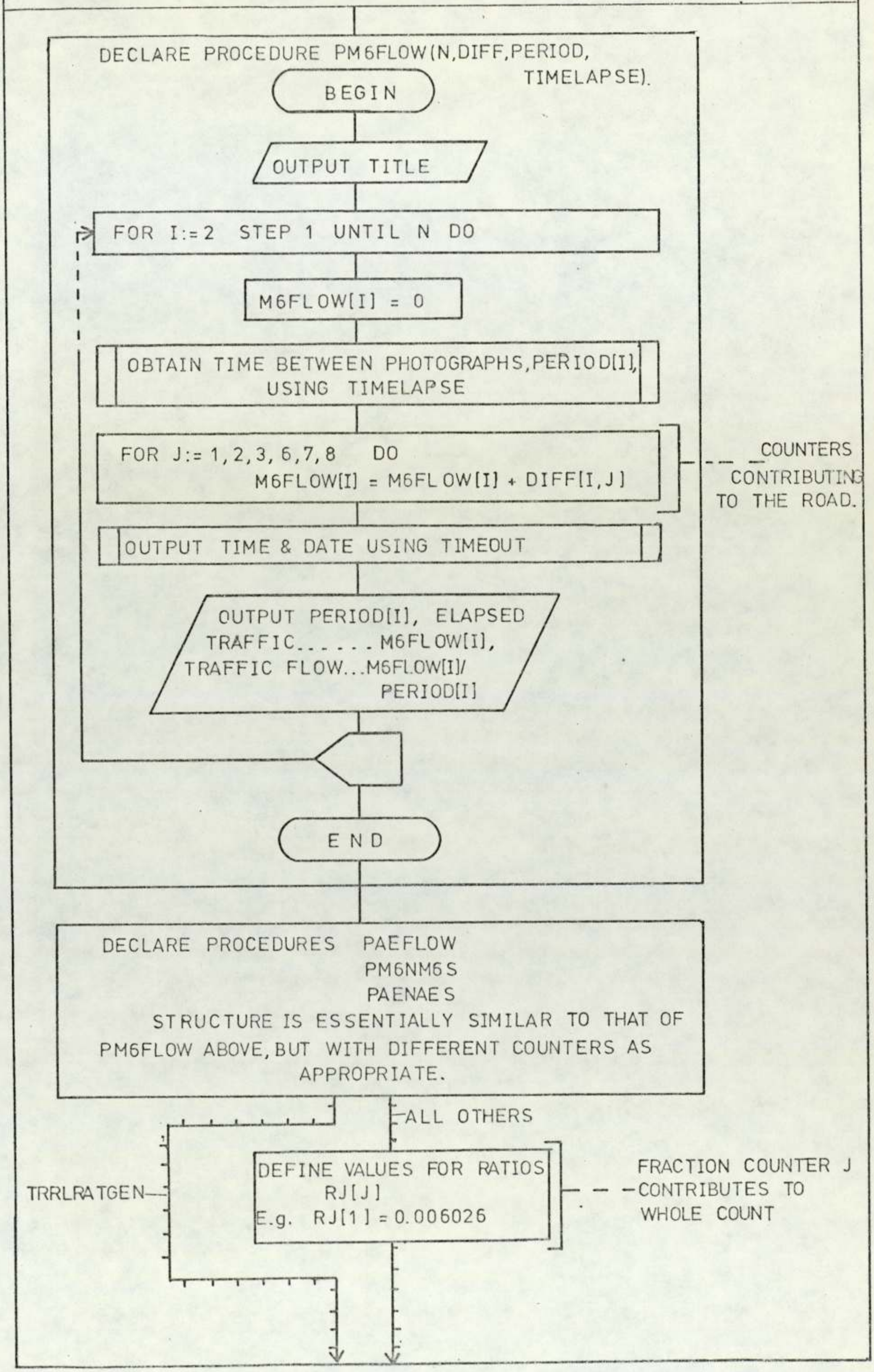

FIGURE A2.1 (CONTINUED) 6

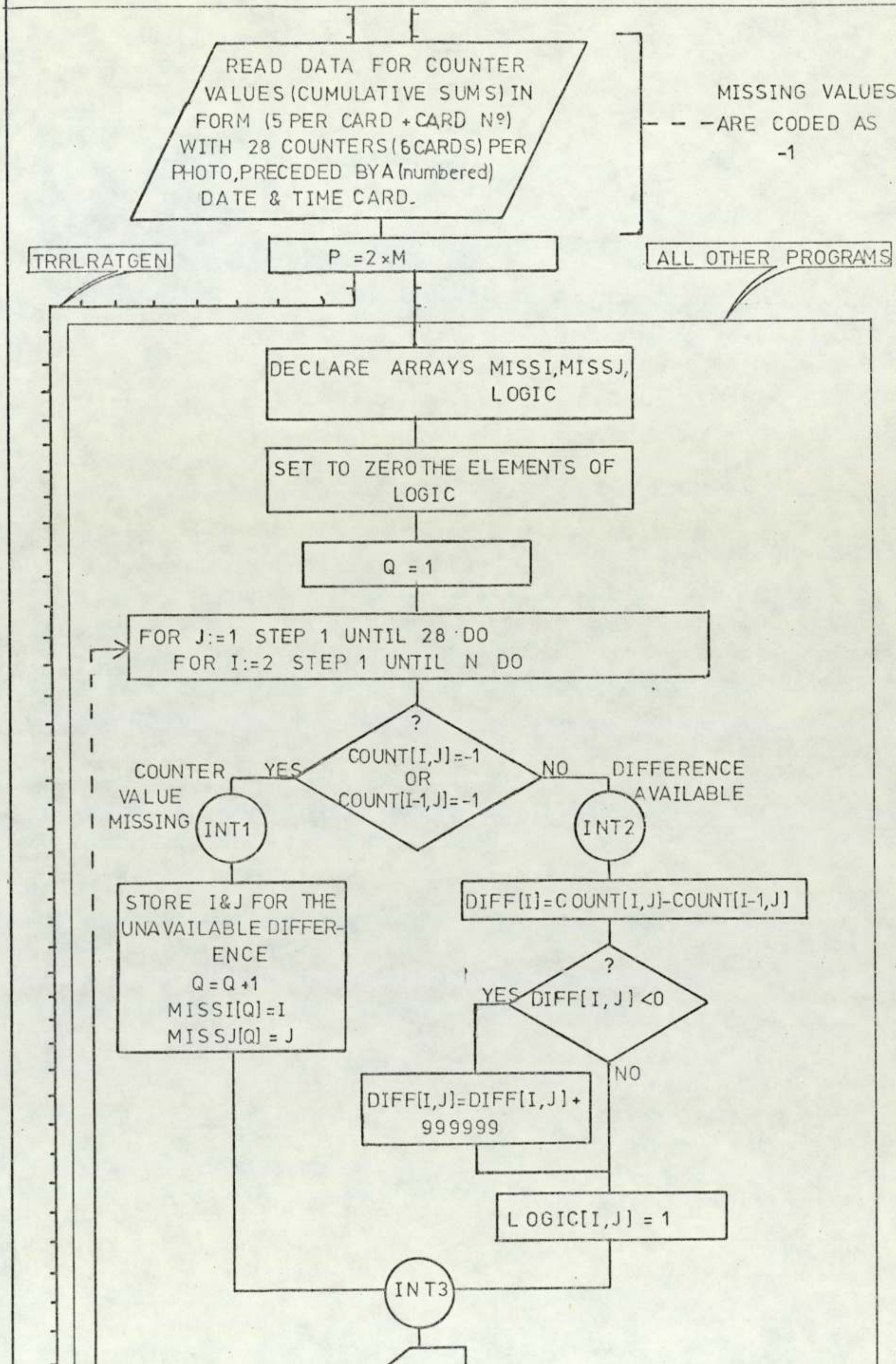

FIGURE A2.1 (CONTINUED) 7

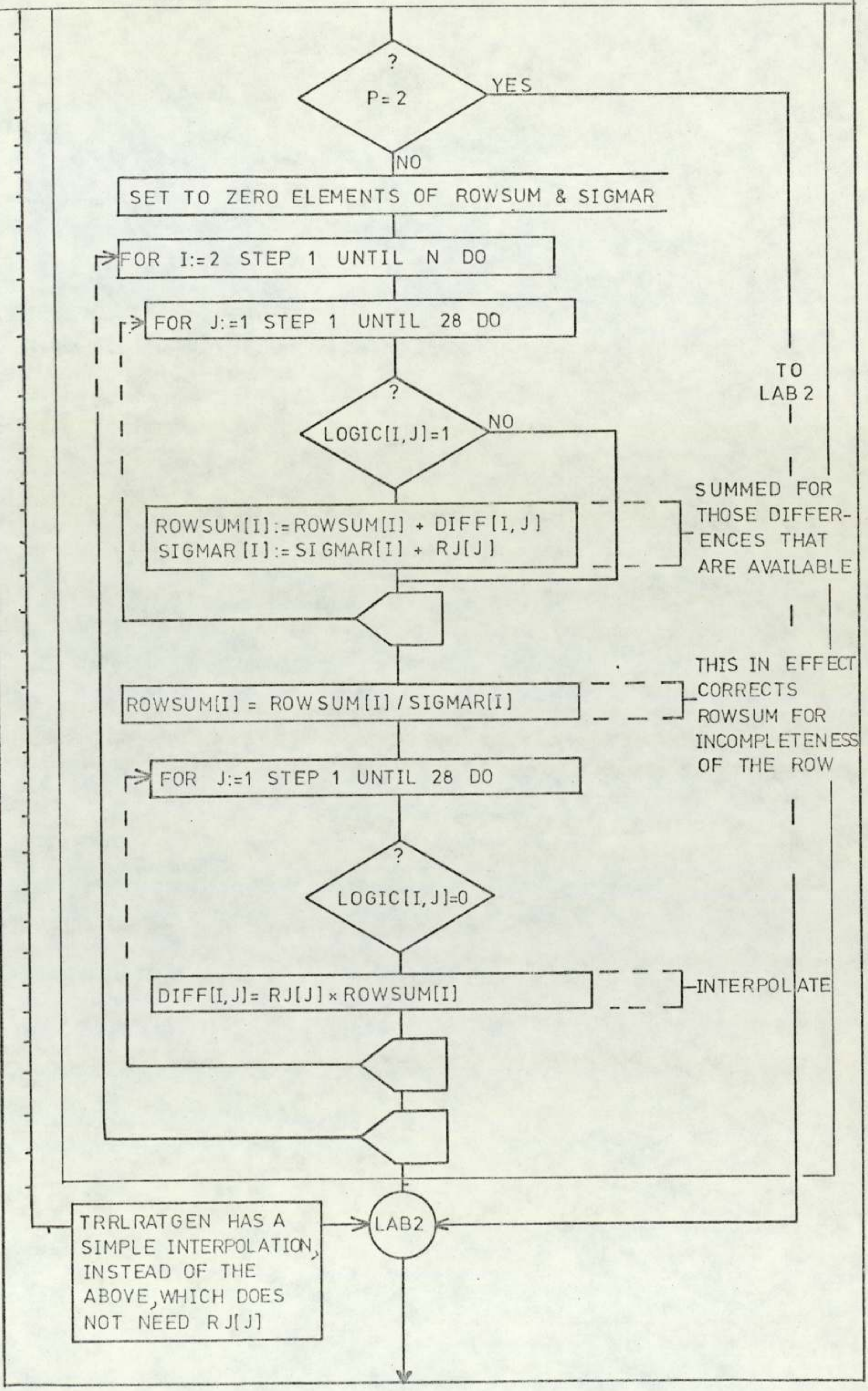

FIGURE A2.1 (CONTINUED)8

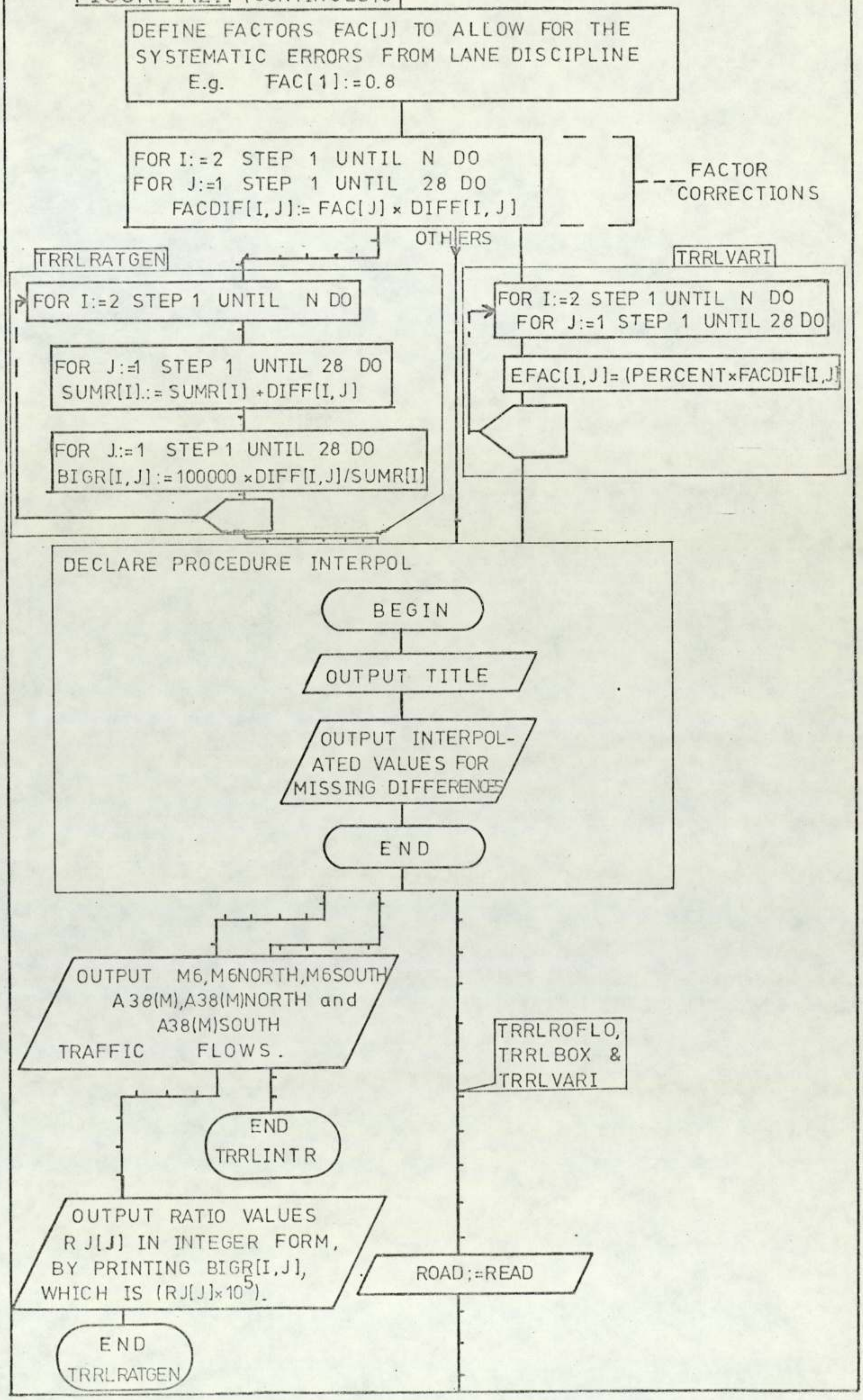

FIGURE A2.1 (CONTINUED) 9

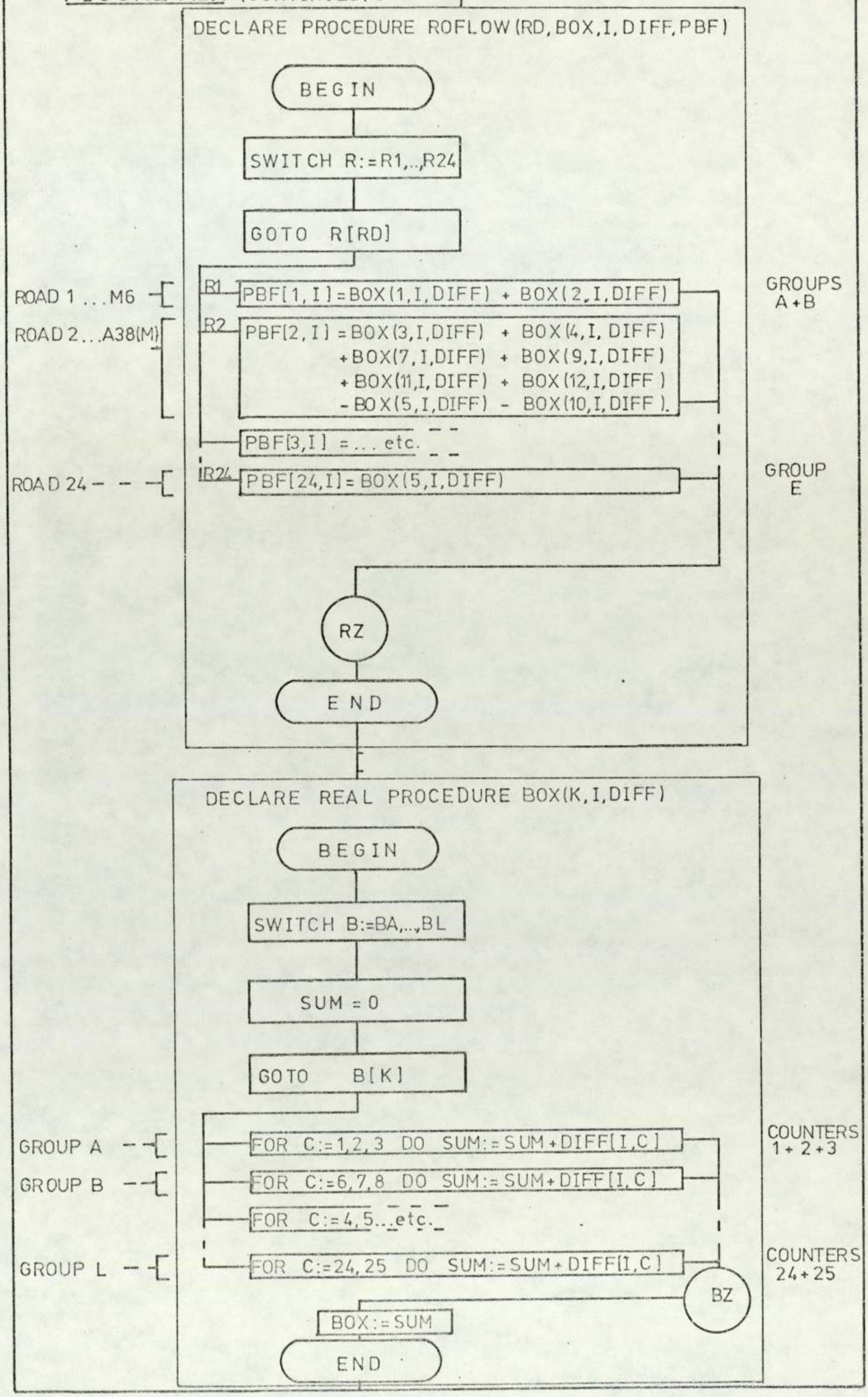

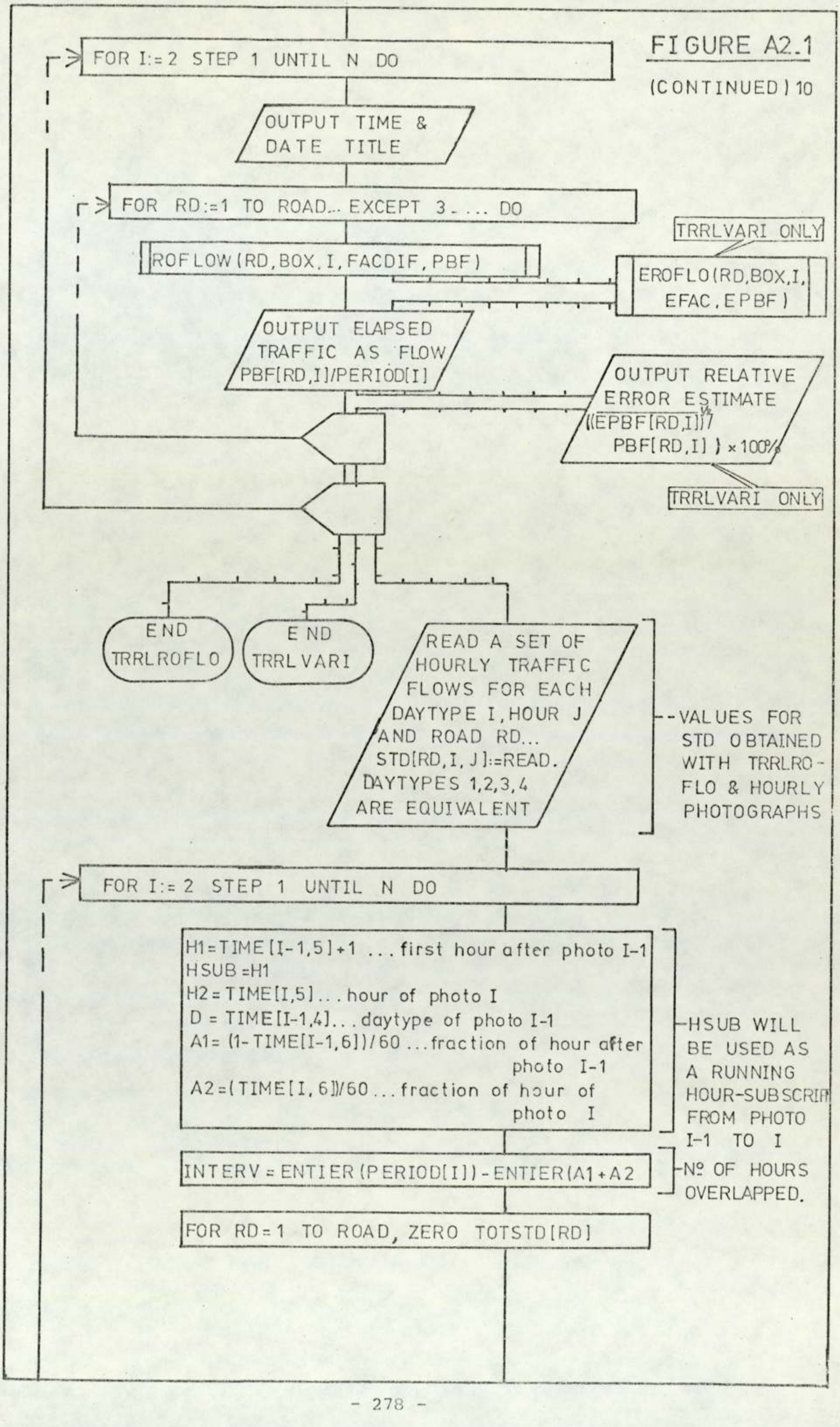

FIGURE A2.1

(CONTINUED) 10

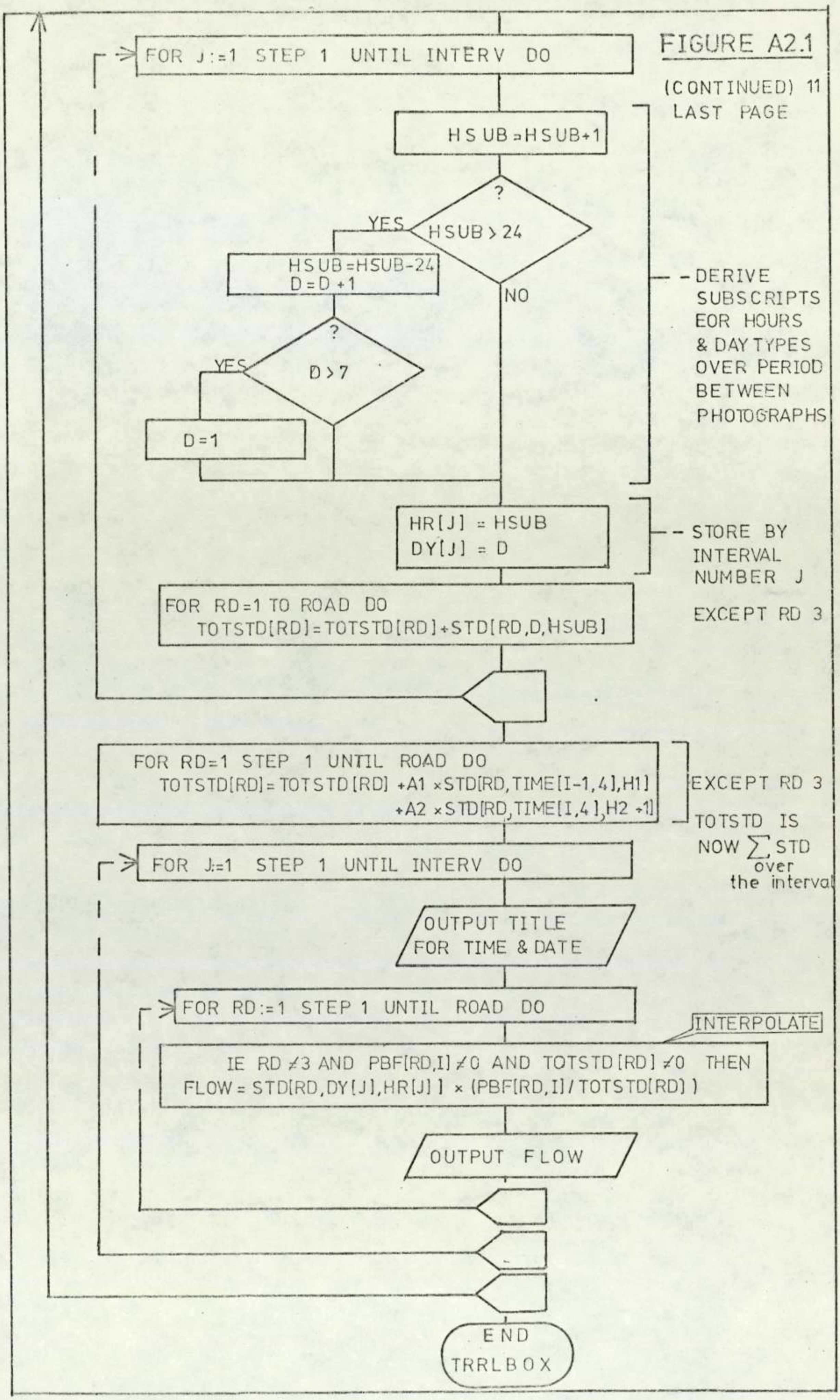
FIGURE A2.1
(CONTINUED) 11
LAST PAGE
FOR J:=1 STEP 1 UNTIL INTERV DO
HSUB=HSUB+1
?
HSUB > 24
YES
NO
HSUB=HSUB-24
D=D+1
?
D > 7
YES
D=1
- DERIVE SUBSCRIPTS EOR HOURS & DAY TYPES OVER PERIOD BETWEEN PHOTOGRAPHS
HR[J] = HSUB
DY[J] = D
- STORE BY INTERVAL NUMBER J
FOR RD=1 TO ROAD DO
TOTSTD[RD]=TOTSTD[RD]+STD[RD,D,HSUB]
EXCEPT RD 3
FOR RD=1 STEP 1 UNTIL ROAD DO
TOTSTD[RD]=TOTSTD[RD] +A1 ×STD[RD,TIME[I-1,4],H1]
+A2 ×STD[RD,TIME[I,4],H2 +1]
EXCEPT RD 3
TOTSTD IS NOW ∑ STD over the interval
FOR J:=1 STEP 1 UNTIL INTERV DO
OUTPUT TITLE
FOR TIME & DATE
FOR RD:=1 STEP 1 UNTIL ROAD DO
INTERPOLATE
IE RD ≠3 AND PBF[RD,I] ≠0 AND TOTSTD[RD] ≠0 THEN
FLOW = STD[RD,DY[J],HR[J]] × (PBF[RD,I]/TOTSTD[RD])
OUTPUT FLOW
END
TRRLBOX

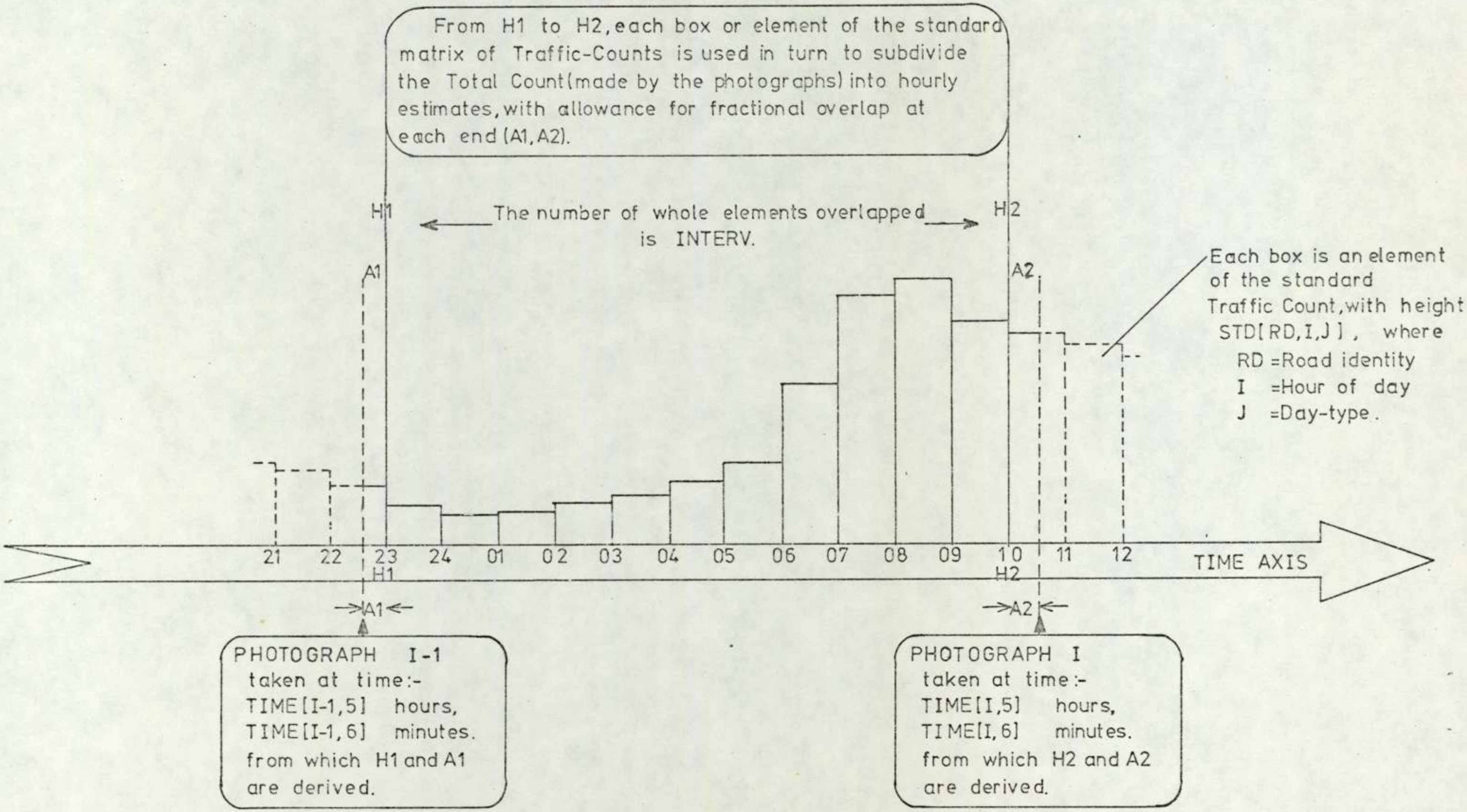

FIGURE A2.2 OVERLAP OF PHOTOGRAPHS WITH THE COINCIDENT PART OF THE STANDARD TRAFFIC PATTERN.

APPENDIX 3

ERRORS IN THE TRAFFIC-FLOW RESULTS

This appendix provides more detail than Section 4.3.3 could: it is the basis for the comments made in that Section. It is assumed that Appendix 2 has been read.

In the following numbered paragraphs we discuss sources of error and their separate effects. We then combine these errors to assess the accuracy of the calculated traffic-flows.

A3.1 Sources of Error

1. Record pulses:-

   Systematically high readings arise from poor lane discipline. The correction factors (from calibration: Section 4.2.4) were derived from a limited sample, so have probable error of say 5%, i.e. there is a loss in precision from the attempt to correct a systematic error (cf. Bevington, 1969

2. Abstract numbers; punch cards:-

   Observers may misread numbers: counts are in error occasionally. Gross errors seen from programme output are correctable while errors in less significant digits may escape detection. This type of error has been ignored: it is regarded as an occasionally wrong data-point, perhaps analagous to noise in the information.

3. Interpolate missing values:-

   The data for November 1974 had counter 13 missing, affecting block I and therefore roads 2, 4, 17, 19, 23 (Tables A2.1, A2.2). The error varies with the combination of counters that defines the flow of the road. Test runs on a count with counter 13 present and missing gave results as in Table A3.1.

4. Counter combinations:-

Propogation of errors through counter combinations:-

The traffic-flows for each road are sums and differences of (inaccurate) counter differences. Subtraction tends to increase the relative error of the calculated traffic-flow. The exact size of the error varies with the number of additions and subtractions, the sizes of the terms and the uncertainty in each term.

For addition of n equal functions f, each having relative error e, we have a result nf with absolute error $\sqrt{n}fe$. If these operations included s subtractions, the result is (n - s)f with absolute error $\sqrt{n}fe$. In this case the relative error is increased from e to $\sqrt{n}fe/((n - s)f)$, or $\sqrt{n}/(n - s)$ times. This simple argument indicates the effect expected. In practice there are varying numbers of terms with varying errors. An estimate was made as follows using a modified form of the programme TRRLRØFLØ.

We assume each counter error is a random error uncorrelated with any other errors. If, for example, $Z = X \pm Y$ we have $\sigma_Z^2 = \sigma_X^2 + \sigma_Y^2$ (Bevington, 1969 a) where σ_Z, σ_X, σ_Y are the standard deviations in the estimates of Z, X and Y respectively. In the programme TRRLVARI, derived from TRRLRØFLØ, a modified form of the procedure RØFLØW was used to call the counter combinations (through the use of function procedure BØX) in addition (subtractions in RØFLØW were changed to addition); the terms summed were elements of EFAC, where the element

EFAC [I,J] = (PERCENT*FACDIF [I,J] /100)^2 is equivalent to σ_J^2 for the variable FACDIF [I,J] . PERCENT was read in as 5. The procedure call ERØFLØ (RD,BØX,I,EFAC,EPBF) stores in the element EPBF [RD,I] the sum $\sum_J \sigma_J^2$ for those counters J contributing to the road RD. The square root E = (EPBF RD,I)$^{\frac{1}{2}}$ is printed as a percentage of the flow PBF [RD,I] existing in the road (E is shown in Table A3.2).

Comparison between roads of the error propagation due to the particular counter combination for each road can be seen in Table A3.2. The data used PERCENT = 5 and a twenty four hour count. The graph (Figure A3.1) shows a positive correlation between $\sqrt{n}/(n - s)$ and the relative increase in error E $\div$ PERCENT, due to the combining of counters. Thus the function $\sqrt{n}/(n - s)$ is a useful guide to the relative increase in error for n counters, of which s are subtracted. Typical effect is that the standard deviation of a road flow measured as a percentage of the road flow is ($\sqrt{n}/(n - s))(E_J)$, where E_J is the percentage error of the single counter J (measured as a percentage of the counter flow: E_J = PERCENT/100 here; in general a counter J has σ_J, so $E_J = \sigma_J$/FACDIF [J] .

In summary, the present traffic counts for each road have an error equal to $\sqrt{n}/(n - s)$ times the typical percentage error of the counters.

5. Timer Drift: Error in STD:-

The photograph time although not at the hour desired is known exactly. No error is incurred through use of PERIØD [I] to divide elapsed counts since PERIØD [I] is accurate to one minute. The resultant traffic-flow will be used to represent that existing on the hour H as the count in H - 1 to H. There is a phase-error between the times of photographs I, I - 1 which are not exactly on the hours H, H - 1.

This phase-error between the time at which the flow is measured, and the time H used to represent that time, is serious where the traffic-flow changes rapidly with time about the hour H. Figure A3.2 shows a histogram of actual counts; the circled points show how each box in the histogram is rounded to H as if it represented a period H - 1 to H. This particular plot is taken from the counts used to set up the matrix STD and by chance the effect of the phase-error is not severe for most of the time where the traffic-flow changes gradually. The phase-error can be half an hour: when the traffic rises from 700 h^{-1} at 07.00 to 1600 h^{-1} at 08.00 to 2900 h^{-1} at 09.00, $dT/dH \sim 1000\ h^{-2}$.

Assuming $dT/dH \sim \Delta T/\Delta H$, for $H = \frac{1}{2}^{h}$, $\Delta T = 500\ h^{-1}$. At 08.00 the count is 1600 ± 500 h^{-1}; an error of ~ 30%. Those elements of STD for this time (09.00 on a FRIDAY, day-type 5) have the worst error since in the rest of the elements of STD the error in timing is less than ± 10 minutes.

The morning rush-hour flows interpolated for Fridays have systematic error at 07.00 and 08.00 hours when the values are probably 30% low; otherwise the probable error due to timer drift (of ~ ± 10 minutes in the hour) is ~ ± 10%. These errors are additional to those discussed earlier.

6. Hourly Interpolation

The interpolation of hourly flows relies on the reproducibility of traffic patterns for each day-type, as stored in the matrix STD. These values in STD have error as in paragraphs 1 to 5 immediately above because of the method of measurement. We then assume the traffic pattern is constant. A series of hourly traffic-flows for Salford Circus and twelve hourly traffic-flows for the M6 were abstracted in groups according to time of day and day-type. Table A3.3 shows the variation derived from groups of Mondays; Table A3.4 that for day and night values.

This suggests the traffic pattern is constant to within 4%. The values in STD are thus an inaccurate (from measurement) single sample from a distribution of traffic patterns which themselves are scattered. To represent the traffic pattern by STD implies both a random measurement-error and a random sampling-error. We combine these to estimate the error in any element of STD as typically $\pm$ 14%. The fractions A1, A2 at the start and end of the overlapped period take into account the exact times of the two photographs which together form the twelve hourly count; the timer drift in twelve hourly photographs causes no additional error. For the overlapped period the appropriate elements of STD are summed into TØTSTD. Only summation is involved: the element TØTSTD [RD] has the same relative error as the elements for the road RD of STD [RD,D,H] from which it was derived; these errors have been discussed already at the beginning of this paragraph 6. The interpolation itself uses

$$\frac{\text{STD [RD, DY [J] , HR [J]] *PBF [RD,I]}}{\text{TØTSTD [RD]}}$$

to interpolate hourly subdivisions of PBF [RD,I] . Each element of PBF has errors as in paragraphs 1, 3, 4, but not 5 since the drift in twelve hourly photographs is slight. The elements of STD and TØTSTD have errors as discussed above in this paragraph 6. The interpolated answer has a combined error of $\sim \pm 18\%$.

For roads 2, 4, 17, 19, 23 the error (from missing values) is larger (Table A3.1). On a Friday morning rush-hour the value is low by $\sim 30\%$.

TABLE A3.1

Effect of Missing Counters:

Case Study for Counter 13 (missing during

November 1974 when monitoring at Salford Circus)

Road	Flow with true counter readings	Flow with reading for Counter 13 (missing) interpolated	Error
2	1460	1511	+ 4%
4	84	135	+ 60%
17	124	73	- 40%
19	145	93	- 35%
23	121	172	+ 42%

TABLE A3.2

Error Propagation due to the Combination of Inaccurate Counter Readings;

Results from a 5 per cent Fraction of the Flow recorded by Each Counter over Twenty

Four Hours (07.49 on 27-09-74 to 07.51 on 28-09-74)

Road	Counter Combinations			Mean Flow in Period	Error[1] $E=(EPBF[RD,I])^{\frac{1}{2}}$	E/5	$\sqrt{n}/(n - s)$
	n	s	n - s				
1	6	0	6	2218	2.2	0.44	0.408
2	16	3	13	2776	1.7	0.34	0.308
3	-	-	-	-	-	-	-
4	2	0	2	299	4.4	0.88	0.707
5	16	2	14	875	2.8	0.56	0.286
6	2	0	2	558	3.6	0.72	0.707
7	2	0	2	586	3.6	0.72	0.707
8	2	0	2	289	4.4	0.88	0.707
9	2	0	2	272	3.8	0.76	0.707
10	2	0	2	289	4.4	0.88	0.707
11	2	0	2	860	3.8	0.76	0.707

TABLE A3.2 (continued)

Road	Counter Combinations			Mean Flow in Period	Error[1] $E=(EPBF\,[RD,I])^{\frac{1}{2}}$	E/5	$\sqrt{n}/(n - s)$
	n	s	n - s				
12	4	0	4	716	2.9	0.58	0.500
13	2	0	2	430	5.3	1.06	0.707
14	2	0	2	430	5.3	1.06	0.707
15	1	0	1	80	5.0	1.00	1.00
16	2	1	1	43	10.4	2.08	1.414
17	4	2	2	259	9.3	1.86	1.00
18	1	0	1	38	5.0	1.00	1.00
19	5	2	3	297	8.1	1.62	0.745
20	6	2	4	875	2.8	0.56	0.612
21	4	0	4	358	4.1	0.82	0.500
22	4	0	4	358	4.1	0.82	0.500
23	4	1	3	342	4.0	0.80	0.667
24	2	0	2	0	-	-	0.707

Note 1: See text: paragraph 4 of Appendix 3.

TABLE A3.3

Variation of Traffic Pattern at Salford Circus.

Hourly Traffic-Flows at Time H for Each of Eight Mondays (28.10.74 to 16.12.74) were averaged and Standard Deviation Calculated

H	Mean Flow	Standard Deviation	Coefficient of Variation, %
08-00	2755	49	1.9
09-00	2783	60	2.4
12-00	2204	39	1.9
15-00	2379	46	2.0
17-00	3426	53	1.6
20-00	1423	75	5.6
		Mean	2.6%

TABLE A3.4

Variation of Twelve Hour Total of Traffic on M6 Motorway.

Traffic elapsed over Twelve Hours averaged in Groups of Three

Day (or Night) Time Values for Three Days of the Same Type

Day-type	Mean	Standard Deviation	Coefficient of Variation, %
THUR-DAY*	55671	861	1.9
THUR-NIGHT*	11518	248	2.6
FRI-DAY	59686	549	1.1
FRI-NIGHT	12040	912	9.3
SAT-DAY	29104	973	4.1
SAT-NIGHT	08009	1015	15.6
SUN-DAY	25216	287	1.4
SUN-NIGHT	15219	374	3.0
MON-DAY*	53949	441	1.0
MON-NIGHT*	10478	221	2.6
TUE-DAY*	53945	251	0.6
TUE-NIGHT*	11014	251	2.8
WED-DAY*	54247	296	0.7
WED-NIGHT*	11371	445	4.8
		Mean	3.7%

* These four days were grouped as one type, the Friday flow being somewhat higher.

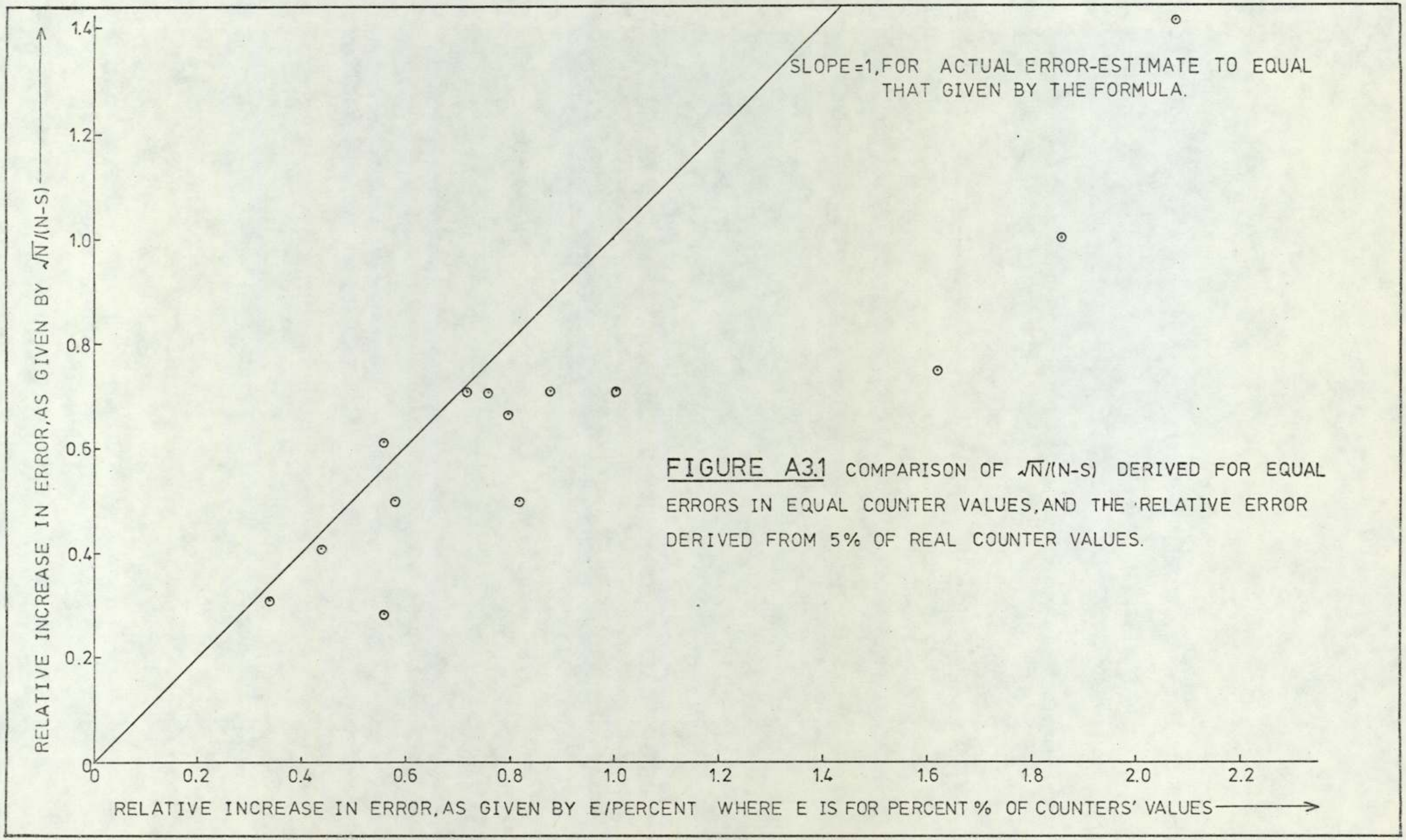

FIGURE A3.1 COMPARISON OF $\sqrt{N}/(N-S)$ DERIVED FOR EQUAL ERRORS IN EQUAL COUNTER VALUES, AND THE RELATIVE ERROR DERIVED FROM 5% OF REAL COUNTER VALUES.

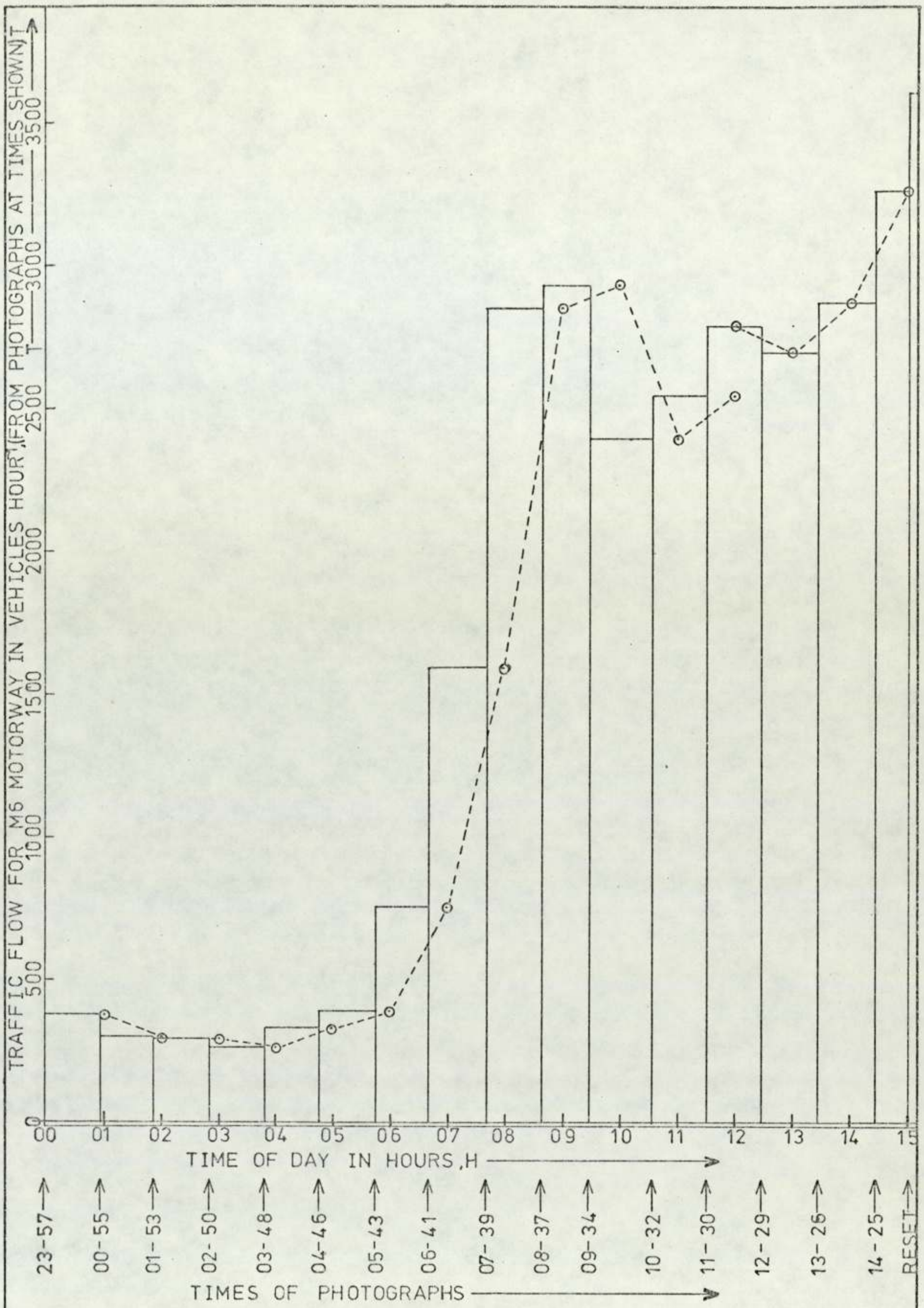

FIGURE A3.2 HISTOGRAM OF TRAFFIC-FLOWS AS RECORDED AND AS ROUNDED TO THE NEAREST WHOLE HOUR H.

KEY:- ⎍ AS RECORDED

-o- TIME ROUNDED TO H

APPENDIX 4

SEMI-EMPIRICAL DIFFUSION EQUATION

In this Appendix we give an outline understanding to the equation rather than a rigorous derivation.

For an element volume dV at location $\underline{P}$ downwind of a pollutant release. Concentration $C(\underline{P})$ is uniform over dV, and the mass of pollutant is either:

$C(\underline{P})dV$ if $C(\underline{P})$ is in mass volume^{-1} units

$\rho C(\underline{P})dV$ if $C(\underline{P})$ is in volume volume^{-1} units.

We use the former.

The transport wind is $U(\underline{P})$ along the X axis, and particles settle with a velocity S(P). (Figure A4.1). The concentration within the element changes with time:

$$\text{ACCUMULATION} = dV\left(\frac{\partial C(P)}{\partial t}\right) = \text{INPUT} - \text{OUTPUT}$$

Now transport, diffusion, settling and chemical reaction may all contribute to the right hand side.

1. Transport

Into face X by wind $U(P).C(P).dy.dz$

Out of face (X + dX) by wind $U(P).C(P).dy.dz + U(P).\left(\frac{\partial C(P)}{\partial x}.dx\right)dy.dz$

$\therefore$ Nett transport into face $= -U(P)\frac{\partial C(P)}{\partial x}.dV$

2. Diffusion: occurs by turbulent and molecular diffusion, conveniently defined by assuming a form similar to Fick's Law.

Diffusivity K is such that the flux F is proportional to concentration gradient.

$$F_x = -K_{xx} \frac{\partial C(P)}{\partial x} \quad , \quad F_y = -K_{yy} \frac{\partial C(P)}{\partial x} \quad , \quad F_z = -K_{zz} \frac{\partial C(P)}{\partial z}$$

where F_x, F_y, F_z are components of flux F(P) of particles or molecules at P.

We assume K_{xx} is constant in X, K_{yy} in Y, but K_{zz} varies with height.

$$\therefore \quad \frac{\partial F_x}{\partial x} = -K_{xx} \frac{\partial^2 C(P)}{\partial x^2} \quad , \quad \frac{\partial F_y}{\partial y} = -K_{yy} \frac{\partial^2 C(P)}{\partial y^2} \quad ,$$

$$\frac{\partial F_z}{\partial z} = \frac{-\partial}{\partial z} \left(K_{zz} \frac{\partial C(P)}{\partial z}\right)$$

Rate of flow of particles or molecules

Into the element = F.dy.dz across X face

Out of the element = $F.dy.dz + \frac{\partial F}{\partial x}(P).dx.dy.dz$ across X face.

Similar equations apply to the other faces.

Differencing,

Nett flow into element = $-\left(\frac{\partial F}{\partial x} + \frac{\partial F}{\partial y} + \frac{\partial F}{\partial z}\right) dxdydz$

$\therefore$ Nett diffusion into element =

$$\left[K_{xx} \frac{\partial^2 C(P)}{\partial x^2} + K_{yy} \frac{\partial^2 C(P)}{\partial y^2} + \frac{\partial}{\partial z} \left(K_{zz} \frac{\partial C(P)}{\partial z}\right) \right] dV$$

3. Sedimentation: this is defined to have the same sence as Z, as in Figure A4.2.

Particles settling across lower face in unit time =

$C(P).(-S).dxdy$

Particles settling across upper face in unit time =

$$C(P).(-S).dxdy + \left(\frac{\partial C(P)}{\partial z}.dz\right)(-S).dxdy$$

$$\text{Nett sedimentation} = \frac{-\partial C(P)}{\partial z}.S.dV$$

4. Chemical reaction: for simplicity, suppose a series of species R_i are reacting with rate constants K_i and orders of reaction m_i to produce C.

$$\text{Nett Accumulation} = -KC^N \prod_i (R_i^{m^i})dV$$

Thus combining,

$$\frac{\partial C(P)}{\partial t}dV = -U(P).\frac{\partial C(P)}{\partial x}dV + \left[K_{xx}\frac{\partial^2 C(P)}{\partial x^2} + K_{yy}\frac{\partial^2 C(P)}{\partial y^2} + \frac{\partial}{\partial z}\left(K_{zz}\frac{\partial C(P)}{\partial z}\right) \right]dV$$

$$- \frac{\partial C(P)}{\partial z}.S.dV - KC^N \prod_i (R_i^{m^i})dV.$$

Whence if no reaction or settling occur one has Equation 5.2, and otherwise

$$\frac{\partial C(P)}{\partial t} + U(P)\frac{\partial C(P)}{\partial x} + S\frac{\partial C(P)}{\partial z} + KC^N \prod_i R_i^{m^i}$$

$$= \left(K_{xx}\frac{\partial^2 C(P)}{\partial x^2} + K_{yy}\frac{\partial^2 C(P)}{\partial y^2} + \frac{\partial}{\partial z}\left(K_z\frac{\partial C(P)}{\partial z}\right)\right)$$

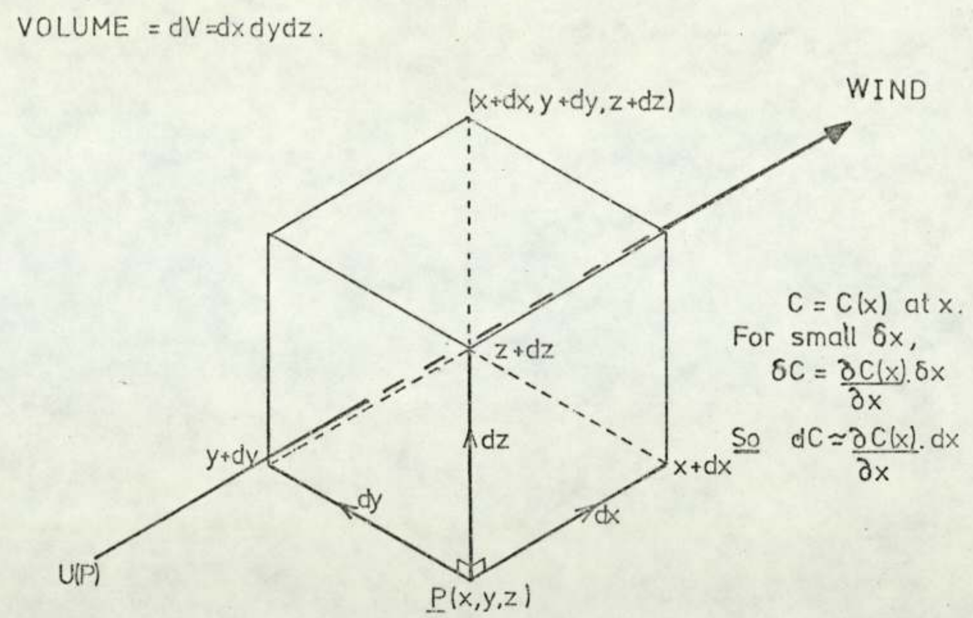

FIGURE A4.1 CO-ORDINATES FOR THE ELEMENT dV AT P.

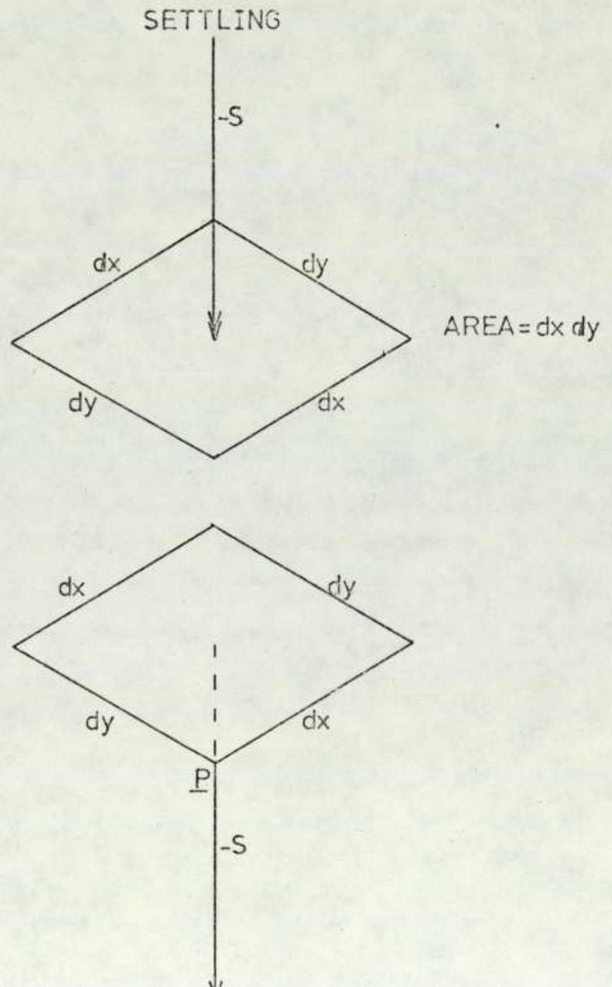

FIGURE A4.2 SETTLING OF MATERIAL THROUGH THE ELEMENT.

REFERENCES

REFERENCES

"Am. Conf. Govt. Hygienists" 4th Edition. 1972. Air Sampling instruments for evaluation of atmospheric contaminants. American Conference of Governmental Industrial Hygienists, P O Box 1937, Cincinnati, Ohio 45201.

Bair, E.J. 1962. Introduction to chemical instrumentation. 349 p. New York: McGraw-Hill Book Co.

Bendat, J.S. and A.G. Piersol. 1966. Measurement and analysis of random data. New York: John Wiley and Sons.

Bevington, P.R. 1969. Data reductions and error analysis for the physical sciences. 320 p. New York: McGraw-Hill Book Co.

Bevington, P.R. 1969a. Data reductions and error analysis for the physical sciences. New York: McGraw-Hill Book Co. P 7.

Bevington, P.R. 1969b. Data reductions and error analysis for the physical sciences. New York: McGraw-Hill Book Co. P 64.

Bibbero, R.J. and I.G. Young. 1974. Systems approach to air pollution control. 531 p. New York: John Wiley and Sons.

Bibbero, R.J. and I.G. Young. 1974a. Systems approach to air pollution control. New York: John Wiley and Sons. 20 - 21.

Butler, J.D., S.D. MacMurdo and D.R. Middleton. 1974. Motor vehicle generated pollution in urban areas. Assoc. Public Health Inspectors Environmental Health Congress and Exhibition, Torbay, U.K. 69 - 77.

Calder, K.L. 1970. Some miscellaneous aspects of current urban pollution models. Chapter 4 in Proc. Symposium on multiple-source urban diffusion models. Environmental Protection Agency, Research Triangle Park, N.C. AP 86. 416 P. Ed: A.C. Stern.

Calder, K.L. 1973. On estimating air pollution concentrations from a highway in an oblique wind. Atmospheric Environment 7: 863 - 868.

Chamberlain, A.C. 1974. Travel and deposition of lead aerosols. Atomic Energy Research Estab., Harwell, U.K. R7676.

Drivas, P.J. and F.H. Shair. 1974. Dispersion of an instantaneous cross-wind line source of tracer released from an urban highway. Atmospheric Environment 8: 475 - 485.

Derwent, R.G. and H.N.M. Stewart. 1973. Air pollution from the oxides of nitrogen in the United Kingdom. Atmospheric Environment 7: 385 - 401

Fontijn, A., A.J. Sabadell and R.J. Ronco. 1970. Homogeneous chemiluminescent measurement of nitric oxide with ozone-implications for continuous selective monitoring of gaseous air pollutants. Analytical Chemistry 42: 575 - 579

Fussel, D.R. 1970. Atmospheric pollution from petrol and diesel engined vehicles. Petrol. Rev. 24: 192 - 202.

Geomet Inc. 1971. Validation and Sensitivity Analysis of the Gaussian plume multiple-source urban diffusion model. R.C. Koch et al. Geomet EF-60. APTD 0935. CA 7094. 351 P. Nov 1971. FLD/GP 13B

Gifford, F.A. 1961. Use of routine meteorological observations for estimating atmospheric dispersion. Nuclear Safety 2 4: 47 - 51

Hay, J.S. and F. Pasquill. 1959. Diffusion from a continuous source in relation to the spectrum and scale of turbulence. Adv. in Geophysics 6: 345 - 365.

Hewson, E.W. and G.C. Gill. 1944. Air pollution survey trail, British Columbia, Canada. U.S. Bureau of Mines, Bulletin 453: 23, 138 - 149, 154, 167 - 172, 189, 289.

Hoffert, M.I. 1972. Atmospheric transport, dispersion, and chemical reactions in air pollution: a review. Amer. Inst. Aeronautic and Astronautics Journal. 10: 377 - 387.

Islitzer, N.F. 1961. Short range atmospheric-dispersion measurements from an elevated source. Jnl. Meteorology 18: 443 - 450

Johnson, W.B., W.F. Dabberdt, F.L. Ludwig and R.J. Allen. 1971. Field study for initial evaluation of an urban diffusion model for carbon monoxide. Stanford Research Instit., California, U.S. CRC APRAC - CAPA 3 68 2. 254 P
FLD/GP 4A 13B

Lamb, A.B., W.C. Bray and J.C.W. Frazer. 1920. The removal of carbon monoxide from air. Indus. Engineer. Chem. 12: 213 - 221.

Leahey, D.M. and J. Halitsky. 1973. Low wind turbulence statistics and related diffusion estimates from a site located in the Hudson River Valley. Atmospheric Environment 7: 49 - 61.

Linford, A. 1961. Flow measurement and meters. Pp. 143, 255 - 6. E. & F.N. Spon Ltd.

McElroy, J.L. 1969. A comparative study of urban and rural dispersion. Jour. Applied Meteorology 8: 19 - 31.

Monin, A.S. and A.M. Yaglom. 1971. Statistical Fluid Mechanics: mechanics of turbulence. Volume 1, 769 p. English translation (edited by J.L. Lumley) of Statisicheskaya gidromekhanika - Mekhanika Turbulentnosti, published in 1965 by Nauka Press, Moscow. Cambridge, Massachusetts: MIT Press.

Monin, A.S. and A.M. Yaglom. 1971a: above text, 579 - 580.

Monin, A.S. and A.M. Yaglom. 1971b: above text, 591 - 606.

Monin, A.S. and A.M. Yaglom. 1971c: above text, 604

Monin, A.S. and A.M. Yaglom. 1971d: above text, 606 - 614.

Monin, A.S. and A.M. Yaglom. 1971e: above text, 576, 607 - 9ff.

Monin, A.S. and A.M. Yaglom. 1971f: above text, 643 - 657.

Monin, A.S. and A.M. Yaglom. 1971g: above text, 644, 647.

Monin, A.S. and A.M. Yaglom. 1971h: above text, 650 - 651.

Monin, A.S. and A.M. Yaglom. 1971i: above text, 577.

Monin, A.S. and A.M. Yaglom. 1971j: above text, 618.

Monin, A.S. and A.M. Yaglom. 1971k: above text, 617 - 632.

Pasquill, F. 1961. The estimation of the dispersion of wind-borne material. The Meteorological Magazine, Meteorological Office, U.K. 90: 33 - 49

Pasquill, F. 1970. Prediction of diffusion over an urban area - current practice and future prospects. Chapter 3 in Proc. Symposium on multiple-source urban diffusion models. Environmental Protection Agency, Research Triangle Park, N.C. Ap 86. 416 P. Ed. A.C. Stern.

Pasquill, F. 1971. Atmospheric dispersion of pollution. Quart. Jour. Roy. Met. Soc. 97: 369 - 395

Pasquill, F. 1974. Atmospheric diffusion: the dispersion of windborne material from industrial and other sources. 2nd ed. Chichester: Horwood; New York; London: Distributed by Wiley. P. 373.

Pooler, F., JR. 1966. A tracer study of dispersion over a city. Jour. Air Pollution Control Assoc. 11: 677 - 681.

Porter, K. and D.H. Volman. 1962. Flame ionisation detection of carbon monoxide for gas chromatographic analysis. Analyt. Chem., 34: 748 - 749

Smith, F.B. 1972. A scheme for estimating the vertical dispersion of a plume from a source near ground-level (a first draft). Extended summary communicated personally by F.B. Smith, Department Met.O.14., Meteorological Office, Bracknell, Berkshire, England; closely related to Smith (1972a) and Pasquill (1974).

Smith, F.B. 1972a. A scheme for estimating the vertical dispersion of a plume from a source near ground level. Chapter 18 in Proc. Third Meeting Expert Panel on Air Pollution Modelling. NATO Committee on Challenges to Modern Society.

Stern, A.C. 1970. Proc. symposium on multiple-source urban diffusion models. Environmental Protection Agency, Research Triangle Park, N.C. AP 86. 416 P.

Turner, D.B. 1970. Workbook of atmospheric diffusion estimates. Public Health Service, Cincinnati, Ohio. Div. of air pollution. PHS PUB 999 AP 26. 88P.

Williams, O.T. 1974. Some considerations in the design and operation of multi-level interchanges. The Highway Engineer - Jour. Instit. Highway Engineers. 21 5: 12 - 20.

SUPPORTING DOCUMENTS

Listings for the following programmes will be found under separate cover.

CHART50	Chart data zero corrected, calibrated and averaged ... Chapter 3, Appendix 1.
TRRLINTR	Traffic flows for M6 and A38(M) ... Chapter 4, Appendices 2, 3.
TRRLRATGEN	Calculate RJ[J]for missing value interpolation by other traffic programmes ... Chapter 4, Appendices 2, 3.
TRRLROFLO	Calculate traffic flow for all roads - uses hourly photographs ... Chapter 4, Appendices 2, 3.
TRRLBOX	Calculate mean traffic flows between photographs, and interpolate hourly flows for all roads for each hour between photographs ... Chapter 4, Appendices 2, 3.
TRRLVARI	Error analysis for traffic programmes ... Chapter 4, Appendix 3.
SPAG68	Calculation of pollutant concentrations by integration over road geometry ... Chapter 6.
SPAGSIMP	As for SPAG68, using either same input format as SPAG68, or a simplified one with observer position to nearest metre. No field observations need be read ... Chapter 6.
SPAGSENS	Sensitivity analysis for SPAG68 ... Chapter 6.